345
3-7-85 JS (3)

DR-0833-8

DOE/ET/15020-1634(Vol.2)
(DE85004560)

PHASE II–PRIMARY HEATER MODULE

Final Report for the Period February 1980–November 1983

By
John Campbell

December 1983

Work Performed Under Contract No. AC21-80ET15020

For
U. S. Department of Energy
Morgantown Energy Technology Center
Morgantown, West Virginia

By
Rockwell International
Canoga Park, California

MASTER

Technical Information Center
Office of Scientific and Technical Information
United States Department of Energy

DISCLAIMER

This report was prepared as an account of work sponsored by an agency of the United States Government. Neither the United States Government nor any agency thereof, nor any of their employees, makes any warranty, express or implied, or assumes any legal liability or responsibility for the accuracy, completeness, or usefulness of any information, apparatus, product, or process disclosed, or represents that its use would not infringe privately owned rights. Reference herein to any specific commercial product, process, or service by trade name, trademark, manufacturer, or otherwise does not necessarily constitute or imply its endorsement, recommendation, or favoring by the United States Government or any agency thereof. The views and opinions of authors expressed herein do not necessarily state or reflect those of the United States Government or any agency thereof.

DISCLAIMER

Portions of this document may be illegible in electronic image products. Images are produced from the best available original document.

DISCLAIMER

This report was prepared as an account of work sponsored by an agency of the United States Government. Neither the United States Government nor any agency thereof, nor any of their employees, makes any warranty, express or implied, or assumes any legal liability or responsibility for the accuracy, completeness, or usefulness of any information, apparatus, product, or process disclosed, or represents that its use would not infringe privately owned rights. Reference herein to any specific commercial product, process, or service by trade name, trademark, manufacturer, or otherwise does not necessarily constitute or imply its endorsement, recommendation, or favoring by the United States Government or any agency thereof. The views and opinions of authors expressed herein do not necessarily state or reflect those of the United States Government or any agency thereof.

This report has been reproduced directly from the best available copy.

Available from the National Technical Information Service, U. S. Department of Commerce, Springfield, Virginia 22161.

Price: Printed Copy A99
Microfiche A01

Codes are used for pricing all publications. The code is determined by the number of pages in the publication. Information pertaining to the pricing codes can be found in the current issues of the following publications, which are generally available in most libraries: *Energy Research Abstracts (ERA); Government Reports Announcements* and Index *(GRA* and I); *Scientific and Technical Abstract Reports (STAR);* and publication NTIS-PR-360 available from NTIS at the above address.

DOE/ET/15020--1634-Vol.2

DE85 004560

PHASE II
PRIMARY HEATER MODULE

FINAL REPORT
FOR THE PERIOD
FEBRUARY 1980 - NOVEMBER 1983

VOLUME II

JOHN CAMPBELL

DECEMBER 1983

CONTRACT DE-AC21-80-ET15020

ROCKWELL INTERNATIONAL, ROCKETDYNE DIVISION
6633 CANOGA AVENUE
CANOGA PARK, CALIFORNIA 91304

FOREWORD

This program was conducted by the Rocketdyne Division of Rockwell International under Contract DE-AC21-80-ET15020 for the Department of Energy (DOE) during the period February 1980 through November 1983. Major subcontractors were the Battelle Columbus Laboratories and Burns and Roe Pacific, Inc. The DOE manager who initiated the program was Carey A. Kinney, Fossil Energy Division. The program was then transferred to the Morgantown Energy Technology Center in 1982, and the DOE manager was Larry K. Carpenter. Jerry M. Friefeld was the program manager at Rocketdyne. This final report is presented in several volumes:

RI/RD83-213 Executive Summary

RI/RD83-213A

- SECTION 1: Phase II Program
- SECTION 2: Summary
- SECTION 3: Program Organization

- RI/RD83-213B
  - SECTION 4: AFB Heat Exchanger Technology

RI/RD83-213C

- SECTION 5: PC Heat Exchanger Technology

RI/RD83-213D

- SECTION 6: Series Bed Heat Exchanger Technology
- SECTION 7: Working Fluid Corrosion Technology
- SECTION 8: Planning for Phase III
- SECTION 9: Interpretation of Program Results, Conclusions, and Recommendations

RI/RD83-213E

- APPENDIX A: 6' x 6' AFB Combustor/Heater Drawings
- APPENDIX B: CCGT Cogeneration System Performance

RI/RD83-213F

- APPENDIX C: 6' x 6' AFB Installation Photographs

ABSTRACT

Research was conducted on components and subassemblies of coal-fired heaters suitable to supply the heat input to closed-cycle gas turbine-based cogeneration systems of 25 to 50 MWe electrical output.

Three concepts were researched: (1) a dry bottom, pulverized coal-fired radiant furnace heater for 1450 to 1550 F turbine inlet temperature, (2) an atmospheric pressure fluidized bed fired heater for 1450 to 1550 F, and (3) a heater employing atmospheric pressure fluidized beds in series, for 1750 F turbine inlet temperature. The series beds concept employs ceramic heating surface in its high-temperature bed.

Both laboratory and field testing was conducted on heating surface materials durability in the pulverized coal and fluidized bed environments. Burner and furnace designs were researched for pulverized coal heaters employing large quantities of flue gas recirculation to moderate the furnace heat flux. A 6' by 6' fluidized bed was assembled and tested for materials and operational research on the 1450 to 1550 F heater concept. A ceramic-to-metal joint concept was devised, fabricated and made ready for test. The conceptual commercial heater concepts were refined.

The program results indicate that each of the three heater concepts is technically feasible. The fluidized bed concepts are judged most likely to be both technically and commercially feasible. Their continued development is recommended.

CONTENTS

4.0 AFB Heat Exchanger Technology 4-1

4.1 AFB Laboratory Metals Corrosion/Erosion Testing 4-3

4.2 24-Inch-Diameter Atmospheric Fluidized Bed Experimental Program . . 4-85

4.3 Material Specimen Analysis from 24-Inch AFB 250-Hour Tests . . . 4-247

4.4 Rocketdyne 6' x 6' AFB Research Test Bed Combustor System 4-345

4.5 6' x 6' AFB Advanced Heat Exchanger Metal Alloy Corrosion/Erosion Research Testing 4-440

References 4-610

ILLUSTRATIONS

4-1. Plot of Log P_{O2} and Log P_{S2} as Functions of the Stoichiometric Ratio of Combustion of 4% S Containing Illinois No. 6 Coal 4-6

4-2a. Experimental Apparatus (Schematic) 4-8

4-2b. Experimental Apparatus (Furnace for Mixed Gasesous Environments) 4-9

4-2c. Experimental Apparatus (Typical String of Specimens After Exposure) 4-10

4-3. Composite Phase Stability Diagrams for Fe-O-S, Ni-O-S, and Cr-O-S at 1650 F 4-11

4-4. Optical Micrographs of Inconel 617 Exposed to Environment A for 15 Minutes and 8 Hours 4-14

4-5. Inconel 617 Exposed to Environment A for 4 Hours 4-15

4-6. Optical Micrographs of Nimonic 86 Exposed to Environment A for 0.5 and 4 Hours 4-17

4-7. Nimonic 86 Exposed to Environment A for 0.5 Hour 4-18

4-8. Inconel 618E Exposed to Environment A for 0.5 Hour 4-20

4-9. Optical Micrographs of Hastelloy X Exposed to Environment A . . 4-21

4-10. Optical Micrograph of PE-13 Exposed to Environment A 4-22

4-11. Hastelloy X Exposed to Environment A for 0.5 Hour 4-23

4-12. Hastelloy X Exposed to Environment A for 23 Hours 4-24

4-13. Distribution of Elements in the Area Shown in Fig. 4-12B . . . 4-25

4-14. Distribution of Elements in the Needle Phase 4-26

4-15. Optical Micrographs of Alloys Exposed to Environment A 4-28

4-16. Schematic Representation of Growth of Corrosion Products on a Ni-Cr Alloy Exposed to an Environment Containing Oxygen and Sulfur 4-29

4-17. Optical Micrograhs of Incoloy 800H Exposed to Environment A . . 4-34

4-18. Semi-Micrographs of the Area Shown in Fig. 4-17(d) 4-36

4-19. AISI 347 Stainless Steel Exposed to Environment A for 0.5 Hour 4-37

4-20. AISI 304 Stainless Steel Exposed to Environment A for 0.5 Hour 4-38

4-21. Optical Micrographs of Fe-15 Cr-Al-Y (a) and Fe-25 Cr-Al-Y (b) Alloys Exposed to Environment A for 150 Hours 4-40

4-22. Fe-25Cr-Al-Y Alloy Exposed to Environment A for 23 Hours . . . 4-41
4-23. Fe-15Cr-Al-Y Alloy Exposed to Environment A for 23 Hours . . . 4-42
4-24. Optical Micrographs of Incoloy 800H Exposed to Environment B 4-43
4-25. Optical Micrographs of AISI 310 Stainless Steel Exposed to Environment B 4-44
4-26. Optical Micrographs of AISI 304 Stainless Steel Exposed to Environment B 4-46
4-27. Oxygen Partial Pressure Variations in an Operating AFB 4-49
4-28. Furnace Schematic 4-52
4-29. Oxygen Probe Voltage Output as a Function of Reaction Time . . . 4-54
4-30. Pit Formed on AISI 310 Stainless Steel During 15-Minute Low PO_2/15-Minute High PO_2 Cycle 4-55
4-31. Pit Formed on AISI 304 Stainless Steel During 15-Minute High PO_2/15-Minute Low PO_2 Cycles 4-57
4-32. Pit Formed on Hastelloy X During 15-Minute Low PO_2/15-Minute High PO_2 Cycle 4-57
4-33. Pit Formed on Inconel 617 During 15-Minute High PO_2/15-Minute Low PO_2 Cycles 4-59
4-34. Scaled Formed on Inconel 671 During 15-Minute Low PO_2/15-Minute High PO_2 Cycles 4-60
4-35. Pit Formed on Inconel 671 During 15-Minute Low PO_2/15-Minute High PO_2 Cycles 4-61
4-36. The Ca-O-S Phase Stability Diagram at 1650 F 4-66
4-37. Laboratory AFB Metals Testing Furnace for Exposure to Simulated Deposits 4-68
4-38a. Fe-25Cr-4Al-1.0 Y Exposed to the $CaO/CaSO_4$ Deposit for 320 Hours 4-69
4-38b. Fe-15Cr-4Al-0.5 Y Exposed to the CaS/CaO Deposit for 320 Hours 4-69
4-39. Inconel 617 Exposed to the CaS/CaO Deposit for 24 Hours
4-40a. Inconel 617 Exposed to the $CaO/CaSO_4$ Deposit for 50 Hours . . . 4-72
4-40b. Nimonic 86 Exposed tc the CaS/CaO Deposit for 24 Hours 4-73
4-41. Inconel 618E Exposed to the CaS/CaO Deposit for 50 Hours . . . 4-75
4-42. Inconel 618E Exposed for 120 Hours in the CaS/CaO Deposit . . . 4-76
4-43. Inconel 618E Exposed to the $CaS/CaSO_4$ Deposit for 320 Hours . . 4-77

4-44a. Hastelloy X Exposed to the CaS/CaO Deposit for 50 Hours 4-78
4-44b. Hastelloy X Exposed to the CaO/$CaSO_4$ Deposit for 50 Hours . . . 4-78
4-45. Incoloy 800 Exposed to the CaS/CaO Deposit for 120 Hours . . . 4-79
4-46. AISI 310 Stainless Steel Exposed to CaS/CaO Deposit for 120 Hours 4-81
4-47. AISI 304 Stainless Steel Exposed to the CaS/CaO Deposit for 50 Hours 4-82
4-48. Schematic of 24-Inch Combustor 4-87
4-49. 24-Inch Fluidized Bed Reactor 4-89
4-50. Distributor Plate 4-90
4-51. Coal Feed Port 4-91
4-52a. 24-Inch AFB Heat Exchanger (Side View) 4-92
4-52b. 24-Inch AFB Heat Exchanger (End View From Outside of Combustor) . 4-93
4-53. Coal and Limestone Feeder System 4-95
4-54. Flue Gas Sampling System 4-99
4-55. Modified Coal Feed Port 4-115
4-56. End View of Heat Exchanger Showing Location of Heat Exchanger Tubes 4-117
4-57. Top View of Heat Exchanger 4-118
4-58. Diagnostic Port 4-120
4-59. Temperature Distribution in Bed 4-134
4-60. Equilibrium Oxygen Partial Pressure in Flue Gas as a Function of the Initial Air-to-Fuel Ratio for the Combustion of Coal (Illinois No. 6) with Air 4-144
4-61. Schematic of Combined Oxygen Activity PO_2 and Gas-Sampling Probe 4-147
4-62. Assembly Drawing of Gas-Sampling/Oxygen Activity Probe Tip . . . 4-148
4-63. Photographs of PO_2/Gas-Sampling Probe 4-149
4-64. Schematic Diagram of PO_2/Gas-Sampling Measurement System and Support Apparatus 4-150
4-65. Tip Components, Including New and Used Ceramic Filters 4-152
4-66. Schematic of High-Temperature Galvanic Cell 4-155
4-67. Exhaust Oxygen Sensor Tip 4-156
4-68. Typical Voltage vs Time from PO_2 Sensor and Thermocouple . . . 4-161
4-69. Schematic of Probe Entry Port 4-163

4-70. PO_2 Sensor Calibration Data 4-167
4-71. Typical Oxygen Partial Pressure vs time Data and Corresponding Histogram and Numerical Data Analysis Results . . 4-168
4-72. Locations of Diagnostics Probe and Corrosion Sample Ports Relative to the Heat Exchanger Array 4-174
4-73. Location of Diagnostic Measurement Positions and Schematic of Original Coal Feed Port Design 4-175
4-74. Location of Diagnostic Measurement Positions and Schematic of New Coal Feed Port Design 4-176
4-75. Probability of Encountering Oxidizing or Reducing Conditions at Various Locations throughout the In-Bed Region for Base Conditions 4-178
4-76. Wall and Centerline Oxygen Concentration as a Function of Axial Location within the Bed 4-179
4-77. Wall and Centerline Carbon Dioxide Concentration as a Function of Axial Location without the Bed 4-180
4-78. Wall and Centerline Carbon Monoxide Concentration as a Function of Axial Location within the Bed 4-181
4-79. Average Oxygen Content Near the Combustor Wall Determined with Gas-Sampling and Time-Averaged Zirconia PO_2 Sensor Methods 4-182
4-80. Average Oxygen Content Near the Combustor Centerline Determined with Gas-Sampling and Time-Averaged Zirconia PO_2 Sensor Methods 4-183
4-81. Time-Average Oxygen Content Determined by the Zirconia Sensor for Various Locations throughout the Bed 4-185
4-82. Minimum Value of Measured Oxygen Partial Pressure for Various Locations within the Bed 4-186
4-83. Spatial Variation of Reducing Potential as a Function of Conveying Air 4-188
4-84. Spatial Variation of Reducing Potential as a Function of Conveying Air 4-189
4-85. Spatial Variation of Reduction Potential for Base Test Conditions as a Function of Port Design 4-190
4-86. Spatial Variation of Reducing Potential for 20% Conveying Air as a Function of Port Design 4-191
4-87. Spatial Variations of Reducing Potential as a Function of Various Coal Types 4-192

4-88. Spatial Variations of Reducing Potential as a Function of Superficial as Velocity 4-193
4-89. Spatial Variation of Reducing Potential as a Function of Superficial Gas Velocity 4-194
4-90. Spatial Variation of Reducing Potential as a Function of Excess Air 4-196
4-91. Spatial Variation of Reducing Potential as a Function of Excess Air 4-197
4-92. Temperature Variations within the Bed for Tests No. 1 and 10 . . 4-198
4-93. Overall View of Tube Array and Access Ports 4-227
4-94. Strain Gage Positions on Simulated Heat Exchanger Tubes 4-228
4-95. Fixture Used to Mount the 1-Inch-OD Simulated Heat Exchanger Tubes 4-229
4-96. Instrumented 1-Inch-OD Alumina Tube 4-231
4-97. Instrumented 1-Inch-OD Steel Tube 4-231
4-98. Deadweight Calibration Loading of the Simulated Heat Exchanger Tubes 4-232
4-99. Calibration Data Obtained for OD Tubes Mounted in Three Locations 4-233
4-100. Strain Gage Trace Obtained During Phase II for 1-Inch-OD Steel Tube Mounted in Location 83 4-237
4-101. Strain Gage Trace Obtained During Phase XII for 1-Inch-OD Steel Tube Mounted in Location 83 4-238
4-102. Assumed Loading Configuration During Operation of the Bed . . . 4-243
4-103. Metallic Materials to Operate at Working Fluid Temperatures . . 4-251
4-104. Inconel 617 Etched in 10% Oxalic Acid 4-261
4-105. Inconel 618E, Transverse Sections Etched in 10% Oxalic Acid . . 4-262
4-106. Inconel 618E, Longitudinal Sections Etched in 10% Oxalic Acid . . 4-263
4-107. Nimonic 86, Transverse Sections Etched in 98 HCL, 2 HNO_3 0.5 g $CuCl_2$ 4-264
4-108. Nimonic 86, Transverse Sections Etched in 98 HCL, 2 HNO_3 0.5 g $CuCl_2$ 4-265
4-109. Inconel 800H Etched in 10% Oxalic Acid 4-266
4-110. AISI 310, Etched in 98 HCL, 2 HNO_3, 0.5 g $CuCl_2$ 4-267
4-111. AISI 304 Etched in 98 HCL, 2 HNO_3, 0.5 g $CuCl_2$ 4-269

4-112. Incoclad FeCrAlY/617, Transverse Sections Showing Cladding Interface 4-270
4-113. Incoclad FeCrAlY/617, Transverse Section Showing Lack of Bonding 4-270
4-114. Incoclad 347/618E, Transverse Section Showing Cladding Interface 4-271
4-115. Typical Transverse Section of Seamless AISI 347 Tubing Etched in 98 HCL, 2 HNO_3, 0.5 g $CuCl_2$ 4-271
4-116. Schematic Diagram of BCL Corrosion Probe Installed in FBC . . . 4-273
4-117. Details of Corrosion Probe Specimen 4-274
4-118. Schematic Diagram of Combined Oxygen Activity (PO_2) and Gas-Sampling Probe 4-276
4-119. Schematic Diagram of 24-Inch-Diameter AFBC 4-276
4-120. Equilibrium Partial Pressure in Flue Gas as a Function of Air/Fuel Ratio 4-281
4-121. Oxygen Probe Output vs Time for Various Bed Locations During Third 250-Hour Run 4-282
4-122. Oxygen Probe Output vs Time for Various Bed Locations During First 250-Hour Run 4-284
4-123. Oxygen Probe Output vs Time for Various Bed Locations During Second 250-Hour Run 4-285
4-124. Summary of XS Air/Substoichiometric for the Various 250-Hour Runs as a Function of Bed Location 4-287
4-125. Phase Stability Diagrams for the Systems Fe-O-S, Ni-O-S, and Cr-O-S, at 1172 K, 1 ATM 4-290
4-126. Plots of Weight-Loss Data, Probabilities for XS Air/ Substoichiometric Conditions and Corrosion Probe Temperature vs Radial Distance into Fluidized Bed Combustor 50% Excess Air 4-293
4-127. Plots of Weight-Loss Data, Probabilities for XS Air/ Substoichiometric Conditions and Corrosion Probe Temperature vs Radial Distance into Fluidized Bed Combustor 50% Excess Air 4-294
4-128. Plots of Weight-Loss Data, Probabilities for XS Air/ Substoichiometric Conditions and Corrosion Probe Temperature vs Radial Distance into Fluidized Bed Combustor 50% Excess Air 4-295

4-129. Plots of Weight-Loss Data, Probabilities for XS Air/ Substoichiometric Conditions and Corrosion Probe Temperature vs Radial Distance into Fluidized Bed Combustor 50% Excess Air 4-296

4-130. Plots of Weight-Loss Data, Probabilities for XS Air/ Substoichiometric Conditions and Corrosion Probe Temperature vs Radial Distance into Fluidized Bed Combustor 20% Excess Air 4-297

4-131. Plots of Weight-Loss Data, Probabilities for XS Air/ Substoichiometric Conditions and Corrosion Probe Temperature vs Radial Distance into Fluidized Bed Combustor 20% Excess Air 4-298

4-132. Plots of Weight-Loss Data, Probabilities for XS Air/ Substoichiometric Conditions and Corrosion Probe Temperature vs Radial Distance into Fluidized Bed Combustor 20% Excess Air 4-299

4-133. Plots of Weight-Loss Data, Probabilities for XS Air/ Substoichiometric Conditions and Corrosion Probe Temperature vs Radial Distance into Fluidized Bed Combustor 20% Excess Air 4-300

4-134. Plots of Weight-Loss Data, Probabilities for XS Air/ Substoichiometric Conditions and Corrosion Probe Temperature vs Radial Distance into Fluidized Bed Combustor 20% Excess Air 4-301

4-135. Plots of Weight-Loss Data, Probabilities for XS Air/ Substoichiometric Conditions and Corrosion Probe Temperature vs Radial Distance into Fluidized Bed Combustor 0% Excess Air 4-302

4-136. Plots of Weight-Loss Data, Probabilities for XS Air/ Substoichiometric Conditions and Corrosion Probe Temperature vs Radial Distance into Fluidized Bed Combustor 0% Excess Air 4-303

4-137. Plots of Weight-Loss Data, Probabilities for XS Air/ Substoichiometric Conditions and Corrosion Probe Temperature vs Radial Distance into Fluidized Bed Combustor 0% Excess Air 4-304

4-138. Surface Appearance of Exposed Corrosion Probe 4-306

4-139. Fluidized Bed Combustor Data from the Literature for 300-Series Stainless Steels 4-309

4-140. BCL 24-Inch Bed Corrosion Data for 304H 4-310

4-141. Fluidized Bed Combustor Corrosion Data from the Literature for Incoloy 800 4-311

4-142. BCL 24-Inch Bed Corrosion Data for Incoloy 800H 4-312
4-143. Cross Sections of AISI 304H after 115 Hours in 50% XS Air Run 4-316
4-144. Cross Sections of Incoloy 800H after 115 Hours in 50% XS Air Run 4-317
4-145. Typical Cross Sections of Incoloy 800H; 115 Hours, 50% XS Air, Port 33, Middle of Probe 4-318
4-146. Schematic of Corrosion/Erosion Mechanism 4-320
4-147. Corrosion Morphologies on Top and Bottom Surfaces of AISI 304H, as a Function of Location on Probe, after 70-Hours Exposure in 0% XS Air 4-321
4-148. Corrosion Morphologies on Top and Bottom Surfaces of Incoloy 800H at 10-Inch and 18-Inch Locations on Probe, after 70-Hour Exposure in 0% XS Air 4-322
4-149. Cross Sections of Incoloy 800, Inconel 617, and Nimonic 86, 70 Hours, 0% XS Air, Port Number 83, Middle of Probe 4-324
4-150. Downstream Surface Corrosion Morphology on Inconel 618E After 70 Hours in 0% XS Air Run 4-325
4-151. Cross Sections After 70-Hours-Inch, 0% XS Air, Both from Middle of Probe 4-326
4-152. Corrosion Products Formed on Incoloy 800H 4-327
4-153. Cross Section of FeCrAlY Cladding and Corresponding PO_2 Data . . 4-328
4-154. Deposit from Probe No. 2 4-330
4-155. Deposit from Probe No. 3 4-330
4-156. Deposit from Probe No. 7 4-332
4-157. Outer Surface of Deposit from Probe No. 7 4-333
4-158. Inner Surface of Deposit from Probe No. 7 Showing Machining Marks from Alloy Surface, and Apparently a Joint Between Specimens 4-334
4-159. Detail of Inner Edge of Deposit from Probe No. 7, Showing Optical Image and Corresponding X-Ray Images for Cr, Fe, and S 4-335
4-160. Deposit from Probe No. 8 4-336
4-161. Phase Stability Diagram for Ca-O-S System at 1650 F, 1 Atm . . . 4-341
4-162. 6" x 6" AFB Experimental Facility 4-346

4-163. Overall Schematic 4-350
4-164. 6' x 6' CCGT/AFB Facility Plan 4-351
4-165. Conceptual Commercial CCGT Heater 4-356
4-166. 6' x 6' Overall Assembly 4-362
4-167. Distributor Assembly 4-369
4-168. Ash Recycles Ports 4-370
4-169. In-Bed Heat Exchanger 6' x 6' AFB 4-371
4-170. In-Bed Wall Penetration Detail, 6' x 6' AFB 4-376
4-171. Hanger Types 4-377
4-172. In-Bed Tube Support Locations 4-378
4-173. Convection Heat Exchanger 4-380
4-174. Typical Setting Construction 4-384
4-175. Diagnostic Probe Port 4-390
4-176. Materials Corrosion Probe, 6' x 6' AFB 4-392
4-177. Specimen Temperature vs Coolant Flow 4-395
4-178. Bosch Oxygen Sensor 4-399
4-179. Oxygen Partial Pressure Probe 4-401
4-180. 6' x 6' AFB Nominal Weights 4-404
4-181. 6' x 6' AFB Preparation for Transportation 4-405
4-182. Forced Draft Blower Operating Range 4-407
4-183. Hoffman Blower 4-408
4-184. Forced Draft Blower Estimated Performance Curve 4-409
4-185. Air Preheater Layout 4-411
4-186. Air Heater 4-413
4-187. Multiclone Dust Collector 4-415
4-188. Cyclone 4-416
4-189. Baghouse 4-418
4-190. Induced Draft Fan 4-420
4-191. In-Bed Ignition Burner 4-422
4-192. Combustion Air Duct Ignition Burner 4-423
4-193. Flue Gas Monitoring Console and Stack Probe 4-425
4-194. Coal Feed Schematic 4-428
4-195. Limestone and Bed Material Schematic 4-431

4-196. Ash Recycle Schematic 4-433
4-197. Combustion Control Unit 4-437
4-198. Dust Control Fabric Filter Baghouse 4-439
4-199. Run 001 Test Schedule 4-447
4-200. Run 002 Schedule of Events 4-450
4-201. Run 003 Schedule of Events 4-452
4-202. Run 004 Schedule of Events 4-455
4-203. Run 005 Chronology of Events 4-459
4-204. Summary of Run 006 Test Activities 4-466
4-205. Run 005 Coal Feed Port Modifications 4-495
4-206. Coal Plume Distributor Installed in Quadrant No. 1 Prior to Run 005 4-496
4-207. Run 005, Tuyere Cap Modification to Increase Air Flow Near Coal Port 4-498
4-208. Modifications to Quadrant No. 4 4-500
4-209. Augmented Air Supply Injected Over Coal Feed Port 4-501
4-210. Posttest Installation of Augmented Air Port 4-502
4-211. Ash Injection Needle with Extension and Turning Vanes 4-503
4-212. Distributor Area Configuration 4-506
4-213. Post-Run 006 Distributor 4-507
4-214. Distributor Area Configuration for Runs 007 and 008 4-509
4-215. Ash Recycle Schematic 4-516
4-216. Typical Bed Pressure/Height Plot 4-519
4-217. Coal Feed Schematic 4-521
4-218. Coal Eductor Configuration 4-522
4-219. Eductor Coal Flow 4-523
4-220. Four Coal Ports per Quadrant Configuration 4-529
4-221. Run 005 Ash Size Analysis 4-531
4-222. Acoustic Soot Blower 4-533
4-223. Air Heater Characteristics During Fouling - Run 005 4-535
4-224. Limestone Utilization and Sulfur Capture 4-547
4-225. Schematic of Material Specimen Probe 4-549
4-226. Analytical Material Probe Temperature Profile 4-550

4-227. Run 005 Material Specimen Probe Temperature Profile 4-551
4-228. Material Specimen Probe Temperature Profile with Heated Coolant 4-552
4-229. Circumferential Temperature Profile 4-554
4-230. Variations in Material Specimen Probe Wall Temperature with Bed Temperature 4-556
4-231. Temperature Rake Data - Run 007 4-558
4-232. ESG Coal Particle Size Distribution 4-562
4-233. PO_2 Probe Locations - Below Bed Heat Exchanger 4-568
4-234. PO_2 Probe Locations - Middle Lower Ports of Bed Heat Exchanger 4-569
4-235. PO_2 Probe Locations - Above Bed Heat Exchanger 4-570
4-236. Run 005 PO_2 Data (Coal Plume Distributor and Reference Port) 4-571
4-237. Run 005 PO_2 Data (Effect of Augmented Air on Reference Port) 4-573
4-238. Run 005 PO_2 Data (Effect of Augmented Air on Reference Port) 4-574
4-239. Run 005 PO_2 Data (Effect of Ash Recycle on Reference Port and Coal Plume Distributor) 4-575
4-240. Run 005 PO_2 Data (Effect of Ash Recycle on Augmented Air) . . . 4-577
4-241. Run 005 PO_2 Data (Effect of Ash Recycle on Augmented Air) . . . 4-578
4-242. Run 005 PO_2 Data (Four Coal Ports Per Quadrant) 4-579
4-243. Run 005 PO_2 Data (Four Coal Ports Per Quadrant and No Ash Recycle) 4-580
4-244. Probe Locations - Below Bed Heat Exchanger 4-581
4-245. Probe Locations - Middle Lower Ports of Bed Heat Exchanger 4-582
4-246. Probe Locations - Above Bed Heat Exchanger 4-583
4-247. Run 006 PO_2 Data (Augmented and Reference Ports) 4-584
4-248. Run 006 PO_2 Data (Effect of Various Quantities of Augmented Air) 4-586
4-249. Run 006 PO_2 Data (Effect of Various Quantities of Augmented Air) 4-587
4-250. Run 006 PO_2 Data (Effect of No Ash Recycle Air) 4-588
4-251. Run 006 PO_2 Data (Effect of 150% of Nominal Ash Conveying Air) 4-589

4-252. Run 006 PO_2 Data (Effect of Low Excess Air) 4-590
4-253. Run 006 PO_2 Data (Effect of Low Excess Air) 4-591
4-254. Run 006 PO_2 Data (Effect of PO_2 Probe Filter) 4-593
4-255. Run 006 PO_2 Data (Four Coal Ports Per Quadrant at Nominal Conditions) 4-594
4-256. Run 006 PO_2 Data (Effect of Low Excess Air (4%) on Four-Port Quadrant) 4-595
4-257. Run 006 PO_2 Data (Effect of Low Excess Air (-5%) on Four-Port Quadrant) 4-596
4-258. Run 007 PO_2 Data (Ash Recycle and 26% Excess Air) 4-597
4-259. Run 008 PO_2 Data (Ash Recycle and 28% Excess Air) 4-598
4-260. Run 007 PO_2 Data (Ash Recycle and 29% Excess Air) 4-600

TABLES

4-1. Nominal Compositions of the Selected Alloys 4-13
4-2. Nominal Composition of the Selected Alloys 4-33
4-3. Nominal Composition of the Heat Exchanger Alloys Selected for this Research 4-51
4-4. High-Temperature Equilibrium Partial Pressures for Gas Mixtures Used in This Research 4-52
4-5. Nominal Compositions of Alloys in Weight Percent 4-65
4-6. Corrosive Conditions 4-67
4-7. Run Summary 4-86
4-8. Air Paths Through Heat Exchanger 4-94
4-9. Coal Analysis 4-100
4-10. Limestone Analysis 4-100
4-11. Basic Data 4-103
4-12. Ash Analysis. 4-103
4-13. Heat-Transfer Data 4-104
4-14. Air Paths Through Heat Exchanger 4-118
4-15. Size Analysis of Coal, Coke, and Limestone. 4-121
4-16. Chemical Analysis of Fuels 4-122
4-17. Operational Data 4-125
4-18. Heat Transfer Data 4-129
4-19. Chemical Analysis of Fly Ash and Bed Material 4-130
4-20. Sieve Analysis of Ash and Bed Draining 4-131
4-21. Run Summary 4-133
4-22. Test Conditions During Characterization Experiments. 4-172
4-23. Coal Analyses 4-203
4-24. Chemical Analyses of Limestone and Ash 4-204
4-25. Sieve Analysis 4-205
4-26. Summary of Run Conditions 4-207
4-27. Log of 250-Hour Experiments 4-208
4-28. NO_x Experiments. 4-217
4-29. Air Flow 4-218
4-30. Bed Operating Conditions During Phases I Through XV 4-235
1-31. Results for 1-Inch-OD Seamless-Steel Tube Mounted in Location 83 4-239

4-32. Results for 1-Inch-OD Seamless-Steel Tube Mounted in Location 31 . 4-240
4-33. Results for 1-Inch-OD Seamless-Steel Tube Mounted in Location 32 . 4-241
4-34. Results for 1-Inch-OD Seamless-Steel Tube Mounted in Location 33 . 4-242
4-35. Dimensions and Material Properties of Simulated Heat Exchanger Tubes 4-245
4-36. Maximum Stress Values for High-Performance Alloys, ksi 4-252
4-37. Maximum Stress Values for Steels 4-253
4-38. Alloys Selected for Advanced CCGT Heat Exchanger Duty With Use Temperature Limits 4-258
4-39. Compositions of Alloys Used in FBC Corrosion Tests 4-260
4-40. Summary of Corrosion Probes 4-278
4-41. Summary of Combustion Conditions Used in Corrosion Runs 4-279
4-42. Index to Combustion Coonditions Used on Corrosion Runs. 4-313
4-43. Corrected X-Ray Fluorescence Analysis of Deposits 4-338
4-44. Possible Compositions of Deposits 4-339
4-45. 6" x 6" AFB Test Program Objective 4-347
4-46. Range of Test Capability 4-348
4-47. 6" x 6" AFB Nominal Design Parameters 4-352
4-48. 6" x 6" AFB Flow Profile at 8 ft/sec 4-353
4-49. CCGT Heater Technology Needs 4-354
4-50. Approach to 1450 to 1550 F AFB Fired Heaters 4-357
4-51. Objectives of 6' x 6" Experimental Combustor Design 4-358
4-52. 6' x 6' AFB Size and Performance Criteria 4-359
4-53. Structural Design Criteria 4-360
4-54. Testing Provisions 4-360
4-55. 6' x 6' AFB Overall Assembly Design Features 4-363
4-56. Combustion System Characteristics 4-365
4-57. Combustion System Design Features 4-367
4-58. Bed Bank Characteristics 4-372
4-59. Bed Bank Design Features 4-374
4-60. Convection Bank Characteristics 4-381
4-61. Convection Bank Design Features 4-383
4-62. Combustor Setting Characteristics 4-385
4-63. Setting Design Features 4-386
4-64. Ports, Probes, Instrumentation 4-389

4-65. In-Bed Corrosion Probe Characteristics 4-393
4-66. In-Bed Corrosion Probe Features 4-394
4-67. Convection Bank Probe Materials 4-397
4-68. Forced Draft Blower 4-410
4-69. Air Preheater 4-412
4-70. Cycline 4-417
4-71. Cyclone Expected Performance 4-417
4-72. Baghouse 4-419
4-73. Induced Draft Fan 4-421
4-74. Ignition Burners 4-424
4-75. Flue Gas Monitoring System 4-426
4-76. Coal Feed System Components 4-430
4-77. Limestone Feed System 4-432
4-78. Ash Recycle System 4-434
4-79. Control Functions 4-436
4-80. Dust Control Unit 4-438
4-81. Summary of the 6' x 6' AFBC Characterization Test Program . . . 4-443
4-82. Summary of Test Conditions 4-444
4-83. Run 005 General Run Conditions 4-457
4-84. Run 005 Chronology 4-458
4-85. Run 005 Expected (Actual) Operation 4-462
4-86. Run 006 Chronology 4-464
4-87. Ruin 006 Expected (Actual) Operation 4-467
4-88. General run Conditions Materrial Specimen Exposure Test Series . . 4-468
4-89. Run 007 Chronology 4-469
4-90. Run 008 Chronology 4-471
4-91. Tank Filling Procedures 4-475
4-92. Expected Operation 4-476
4-93. Operating Data 4-479
4-94. Run 005 Summary of Data 4-482
4-95. Run 006 Summary of Data 4-485
4-96. Run 007 Summary of Data 4-489
4-97. Run 008 Summary of Data 4-491
4-98. Run 005 Summary of Distributor Area Modifications 4-494
4-99. Run 006 Summary of Distributor Area Modifications 4-505

4-100. Summary of Distributor Area Modifications 4-510
4-101. Typical (Run 006) Coal Feed system Operating Parameters 4-527
4-102. Refractory Cure Schedule 4-537
4-103. System Heat Balance Without Ash Recycle 4-541
4-104. System Heat Balance 4-541
4-105. System Heat Balance 4-542
4-106. Estimated Carbon Burnup 4-543
4-107. Heat Exchanger Performance Comparison of Run 003 Data to Design Model 4-544
4-108. Limestone Utilization 4-546
4-109. Bed Temperature Profile 4-557
4-110. Solids Inventory 4-560
4-111. Coal Analysis 4-561
4-112. Size Distribution 4-563
4-113. Ash Chemical Analysis 4-564
4-114. Post Run 008 Comparison of Heat Exchanger Tube Measurements . . . 4-603

4.0 AFB HEAT EXCHANGER TECHNOLOGY

Atmospheric fluidized bed (AFB) combustion technology is one of the three major tasks in the Phase II Program. The AFB work consisted of evaluation of combustion and heat exchanger technology, both theoretically and experimentally, to provide CCGT/AFB design criteria. The work was performed both at Rocketdyne and at the Battelle Columbus Laboratories. This included controlled laboratory tests wherein accelerated corrosion was measured for determination of the mechanisms, and actual metal sample exposures were made in operating research AFB furnaces.

The purpose of the effort was to provide combustor and heat exchanger design criteria for CCGT/AFB systems with high efficiencies that compete favorably with existing technology by providing cost savings as well as reliability. The results of this work are presented in this section.

The Battelle effort included all the experimental laboratory corrosion research work, and the test AFB operations with their 24-inch research AFB furnace. The Rocketdyne work included the designing of the prototype commercial systems and the design, fabrication, erection, and operation of a 6' x 6' advanced AFB furnace for metallurgy research exposure of heat exchanger (HEX) wall metal alloy samples. The commercial systems designs are covered in another section of this final report. In this section, the BCL and Rocketdyne AFB testing results are presented in detail.

The primary improvement in the combustion process consisted of controlling the oxygen content throughout the combustion bed instead of the conventional control of average bed conditions as is now usually done in AFB furnaces. The local variations within the bed zone are suspected of providing the vast arena of contradictory data that has arisen and plagued the design of high-efficiency AFB furnaces in the past. To eliminate this, the combustion was designed and demonstrated to be controllable throughout the bed volume, temperature and oxygen content being the control variables. The corrosion of the heat exchanger alloy metal wall materials also was evaluated under specific controlled laboratory conditions so the effects were quantifiable for comparison to the results obtained in the operating AFB furnaces.

The high temperatures inherent in the high-efficiency, gas-cooled furnaces pushes the metal heat exchanger wall materials and designs to the limits of practical use. At the wall temperature of 1650 F, there are very limited choices of metal alloys under the constraints of the ASME Boiler Code-type strength criteria. The system design cooling fluid pressure drop requirements add another dimension of constraint to the problem. The available metals, generally, in descending order of maximum allowable stress, are Inconel 617, Inconel 618E, Nimonic 86, and Incoloy 800H. The design concept is to use a minimum of these high-cost alloys, probably not more than two of them at most, in the highest temperature working fluid outlet passes, with conventional 300 series stainless steels and low alloy steels used wherever the system pressures and temperatures allow. The nominal working fluid (air) pressure for the design considerations was taken as 600 psig.

The widespread experience of rapid, but sometimes seemingly unpredictable, corrosion of nickel-rich alloys in the fireside environment of coal-fired AFB combustion makes it essential to understand the behavior of nickel-base alloys. This will allow proper protective strategies of location and protection to be used to obtain reliable long service life and economical use of higher cost alloys. The need is to research the materials and control the combustion environment to provide for conditions that give long service life. Providing the research, understanding, application of information learned, and the design criteria for advanced heat exchangers with controlled combustion for a significant step forward in efficiency and reliability is the objective of the program effort. The results are intended for CCGT/AFB cogeneration and power-only systems attractive to industrial and institutional applications.

The results presented in this section are for the completed BCL AFB research and the continuing Rocketdyne 6' x 6' AFB research effort. Rocketdyne completed the contracted 250 hours duration of AFB HEX metal samples exposure testing. In addition, another 100 hours of testing was performed, to bring the total exposure to 350 hours. An add-on contract will provide for an additional 650 hours of

exposure testing, for a total of 1000 hours. One of the metal sample probes was removed, after the 350 hours of test exposure, for metallurgical analysis. The remaining samples will stay in the AFB combustor for the targeted 1000 hours of operating exposure.

4.1 AFB LABORATORY METALS CORROSION/EROSION TESTING

This task consisted of controlled laboratory tests in simulated AFB environments designed to facilitate the interpretation of corrosion data obtained from exposure of probes in the 24-inch diameter and the 6' x 6' fluidized bed combustor. Carefully machined and dimensionally measured metal coupon samples were prepared and exposed in high-temperature corrosive atmosphere furnaces to allow accelerated corrosion to occur under closely controlled and defined environments. From these test results, insight and understanding of corrosion mechanisms and rate-determining factors will be used to ellucidate and quantify the corrosion observed in the 24-inch AFB and the 6' x 6' AFB corrosion test results. The basic testing technology has been previously developed at Battelle Columbus Laboratories. The salt preparation and gas compositions used available laboratory equipment and technology.

The apparatus built for this task comprises two fairly standard furnaces, equipped to operate to 1800 F, $\pm$2 F, with accurate control of the gaseous environments. A vertical furnace was designed to allow specimens to be exposed in a controlled, mixed gas environment; by simultaneously exposing several strings of specimens, which can be separately withdrawn in the cool zone of the furnace, the progress of corrosion with time can be followed in a given gas mixture. This furnace also utilized a specially built Y_2O_3 stabilized ZrO_2 solid-state electrolyte cell to measure the prevailing oxygen partial pressure in the system. By using a known oxygen partial pressure (air on one side of the cell), the emf generated by the oxygen partial pressure difference across the cell can be used to reduce the unknown oxygen partial pressure.

4.1.1 Corrosion Behavior of Nickel-Base Alloys in Simulated Substoichiometric Combustion

Combusting coal in an air-fluidized bed of sulfur sorbent is a process offering considerable advantage over conventional methods of burning coal while satisfying constraints. Typically, the dense bed regime in an air-fluidized bed combustor consists of a mass of particles, usually of a sulfur absorber such as limestone or dolomite, expanded by air flow from beneath and containing approximately 1% combusting coal. The size of the particle is typically 20-60 mesh (250-850 μm), depending on the superficial air fluidizing velocity which ranges from about 328 ft/sec. Particle motion within the bed is complex but, in general, two distinct phases of motion prevail. These are the bubble phase which is characterized by low-density, high-velocity particle flow associated with slugs of air rising through the bed, and dense-bed phase, characterized by high-density, low-velocity flow.

The corrosive character of the dense bed is more complex than would at first appear. In spite of the inherent, good mixing characteristics of fluidizing beds, the oxygen partial pressure inside the bed is by no means uniform. Recent oxygen probe measurements (Ref. 4-1) indicated that in the BCL 24 inch-diameter bed (1650 F, 6 ft/sec), the oxygen partial pressure near the coal feed port, for 80% of the time, was roughly 10-14 volume percent oxygen, with excursions to 3 to 10 volume percent oxygen, even though the averaged exhaust gas analysis registered a constant 3% oxygen. This observed range of oxygen partial pressure is similar to that measured (Ref. 4-2) in a different, smaller fluidized-bed combustor, although the correspondence with location in the combustor is different.

The low level of oxygen in the gaseous phase near the coal feed port is thought to be associated either with the presence of a plume of volatiles emanating from the coal and limestone, or with the partial combustion of carbon to carbon monoxide. Additional combustion and oxygen partial pressure-monitoring experiments were performed (Ref. 4-3) in the BCL 24-inch-diameter bed (1650 F) in which the coal size, the level of excess air, the coal type and the fluidizing

velocity were varied. In all the tests, the oxygen partial pressures in the bed oscillated between about 10^{-1} and 10^{-16} atm, the percentage of time spent at each extreme depending on the particular bed operating condition, and location in the fluidized bed.

Thermodynamic combustion calculations using a computer code for Illinois No. 6 coal (4% S) and different levels of combustion air revealed that a reduction in the combustion stoichimetric ratio from the typical value of 1.2 (20% excess air) to 0.9 could substantially reduce the equilibrium oxygen partial pressure values from 10^{-1} atm to 10^{-16} atm (Fig. 4-1). Simultaneously, an increase in the sulfur partial pressure values occurred from 10^{-26} atm (at 20% excess air) to values as high 10^{-5} atm. These thermodynamically calculated oxygen partial pressure values are remarkably similar to those measured in the dynamic bed of a fluidized combustor and suggest that the fluctuating oxygen partial pressures are real, and could result from the passage of bubbles of combustion gases past the oxygen sensor. Additionally, these data suggest that in locations where low (10^{-11}) atm oxygen partial pressures are measured in the bed, a high sulfur partial pressure also is likely. Consideration of the thermodynamic stability of alloy phases in such environments suggests sulfidation attack of the metallic heat exchanger tubes in the bed is quite possible under such conditions. Whether real alloys undergo sulfidation attack in these environments is determined by the ability of the alloys to resist initiation of sulfidation attack and to resist propagation of the attack, once initiated.

Sulfidation attack, if initiated, can be quite harmful to the structured integrity of the HEX tube alloys, especially when the heat exchanger tubes are operating at close to the bed temperature (1650 F). Nickel-base alloys are extremely vulnerable to catastrophic sulfidation attack because of the possible formation of low melting Ni-Ni_3S_2 (MP 1170 F). Nickel-base alloys often have an advantage of high-temperature creep strength. Hence, it is essential the corrosion behavior of such advanced nickel-base alloys in the AFB combustor tube environment be understood so solutions, either metallurgical or environmental, can be developed to alleviate the corrosion problems. With this objective in mind, a laboratory research program was performed to investigate and obtain

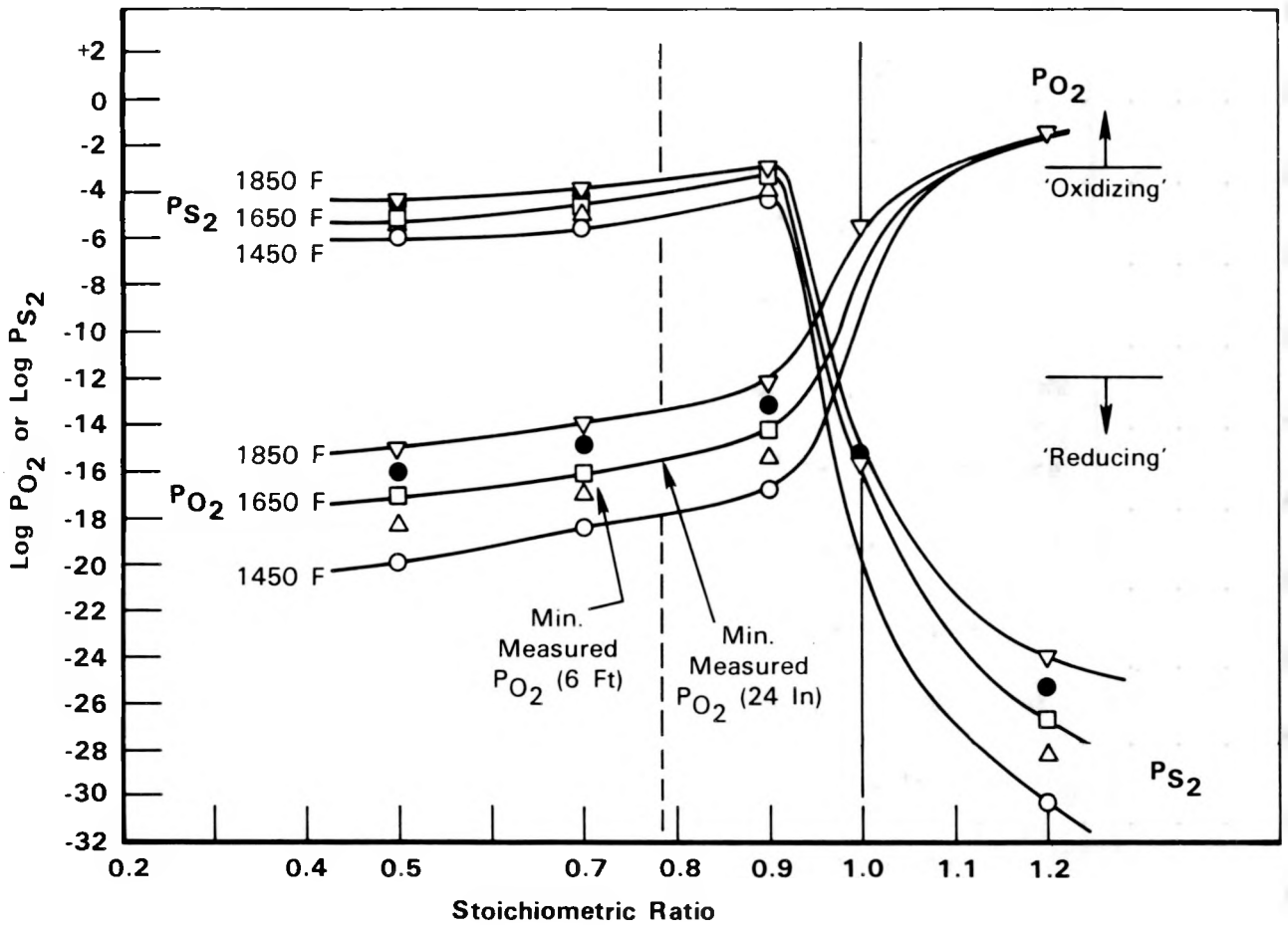


Figure 4-1. Plot of Log P_{O2} and Log P_{S2} as Functions of the Stoichiometric Ratio of Combustion of 4% S Containing Illinois No. 6 Coal

understanding of the susceptibility to initiation of sulfidation corrosion of a number of commercial nickel-base tube alloys.

Experimental Procedures. Five nickel-base tube alloys, Inconel 617, Inconel 618E, Hastelloy X, PE-13 and Nimonic 86, were selected for this laboratory investigation. The nominal compositions are listed in Table 4-1. The alloy selection rationale was previously discussed and is presented in Ref. 4.5. A vertical tube surface, shown in Fig. 4-2a and 4-2b was used to carry out the experiments at 1650 F. An yttria-stabilized zirconia cell, used as an oxygen probe, continuously monitored the oxygen partial pressure of the environment. The oxygen partial-pressure in the furnace was controlled by controlling the flowrates of CO and CO2 gases admitted into the reaction chamber. The sulfur partial pressure of the environment was controlled by accurately metering the SO_2 flow into the system. Thus, the laboratory corrosive environment consisted of a mixture of CO + CO_2 + SO_2 gases, which simplistically simulated the AFB combustion environment. Two exposure conditions were selected, both employed sulfur partial pressure of 10^{-5} atm, while the oxygen partial pressure was 10^{-11} (environment A) or 10^{-13} atmospheres (environment B). These conditions were intended to model environments where the coal would be combusting sub-stoichimetrically in the bed. Figure 4-3 shows the composite (Fe, Ni, Cr) oxygen-sulfur phase stability diagrams and in the chosen gas mixtures, the alloys are expected to form oxides of chromium and iron and nickel sulfide as stable surface corrosion products. Gas mixtures, simulating conditions where the PS_2 was 10^{-5} atm and the PO_2 was lower than 10^{-13} atm could not be obtained by the techniques used here since the required SO_2 flowrates were too small to accurately control with rotometers.

The typical experimental procedure consisted of maintaining the furnace at a constant temperature of 1650 F, admitting metered amounts of CO + CO_2 + SO_2 mixtures and introducing coupons of the alloys into the reaction zone. Coupons (Fig. 4-2) approximately 1 cm x 1 cm x 0.2 cm were prepared by grinding them to 6000 grit finish, cleaning them in alcohol, measuring their dimensions and weighing them. The coupons were suspended using platinum wires. After exposure, the specimens were quickly withdrawn from the furnace, metallographically mounted

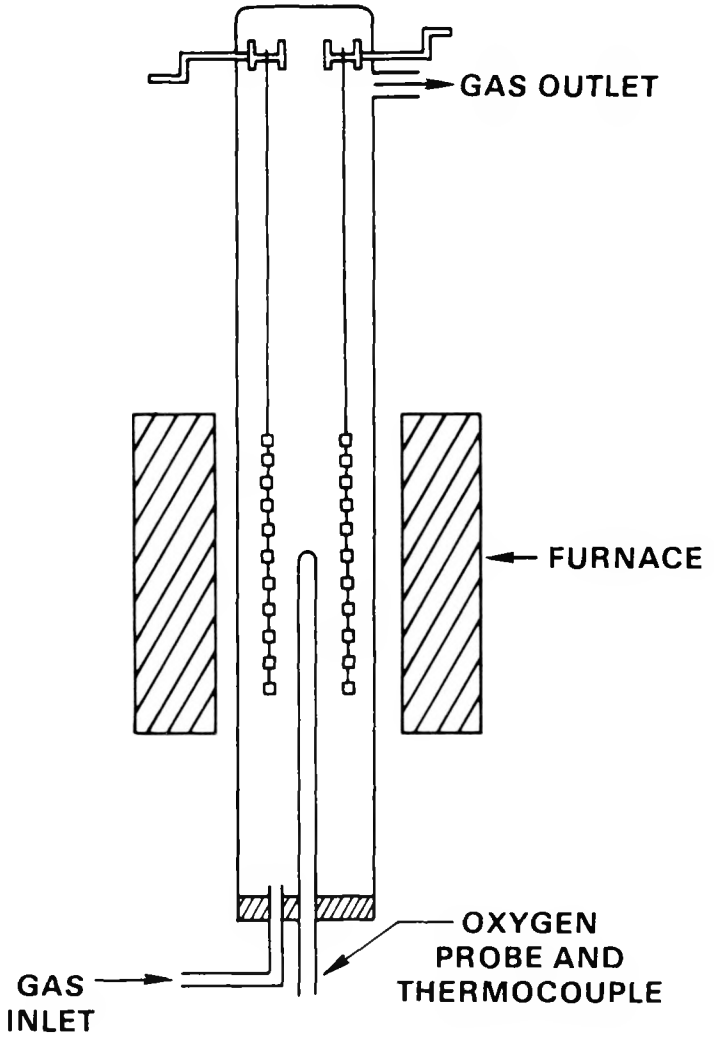


Figure 4-2a. Experimental Apparatus (Schematic)

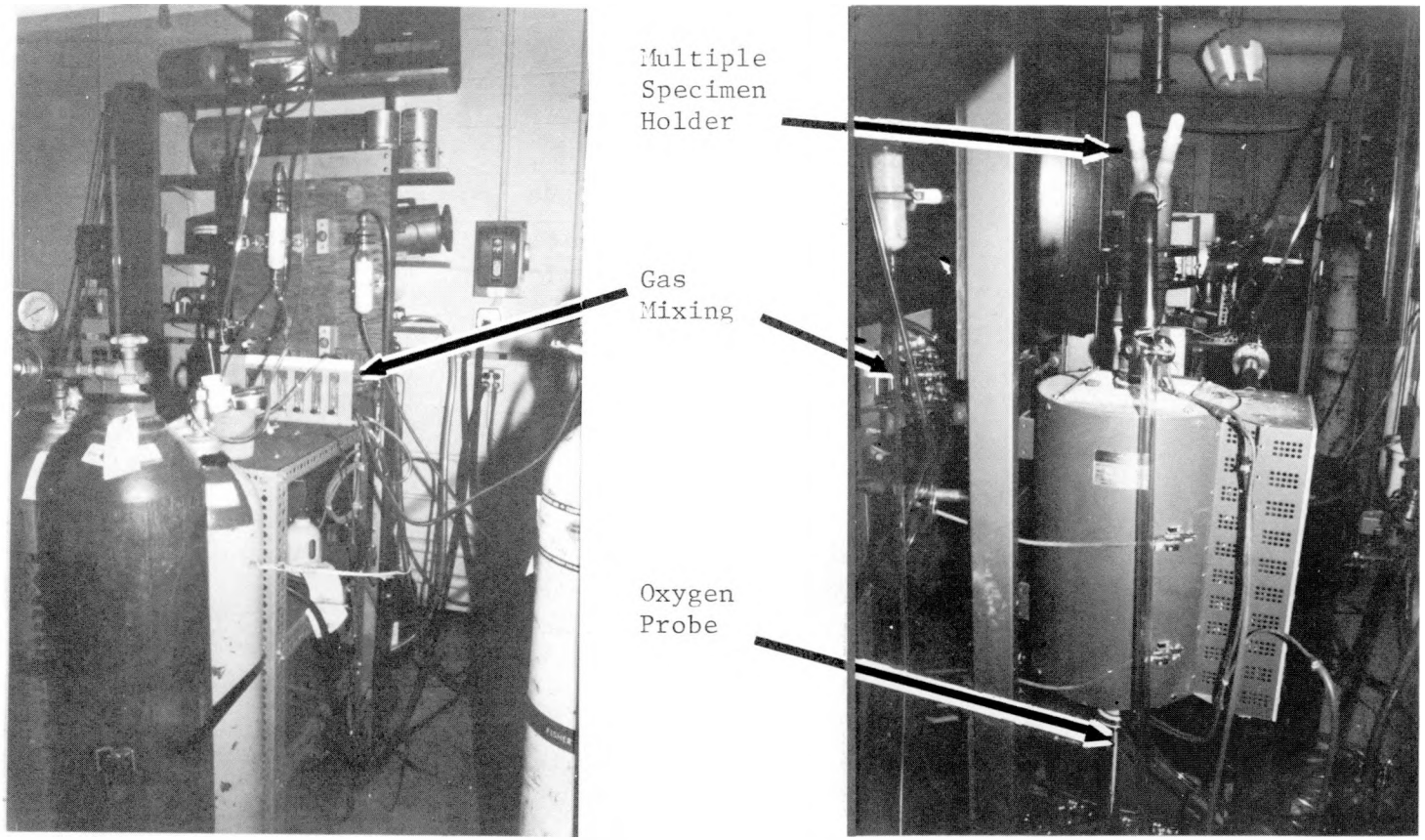


Figure 4-2b. Experimental Apparatus (Furnace for Mixed Gaseous Environments)

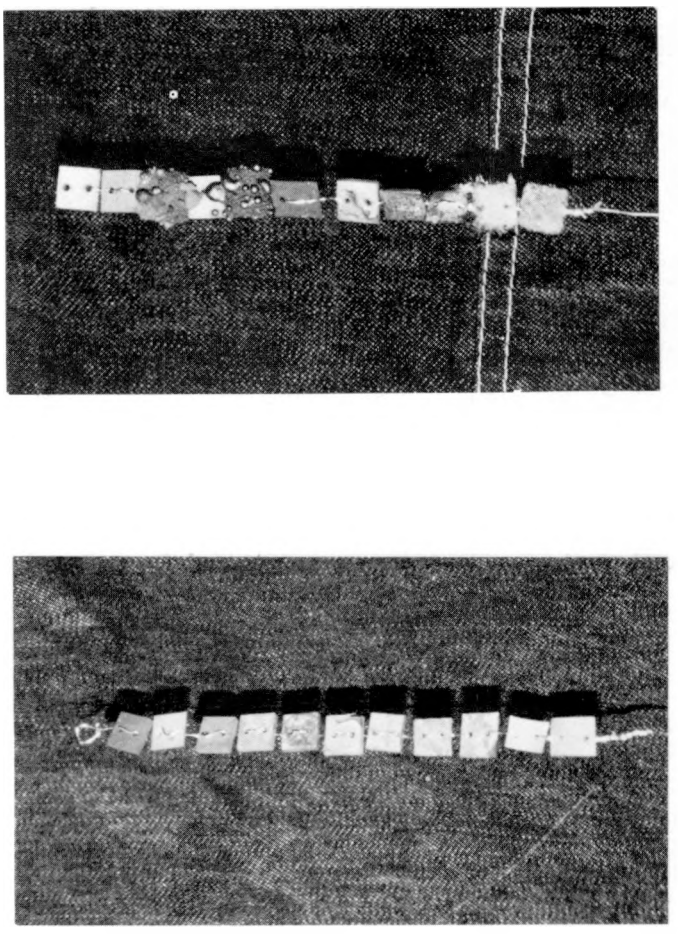


Figure 4-2c. Experimental Apparatus (Typical String of Specimens After Exposure)

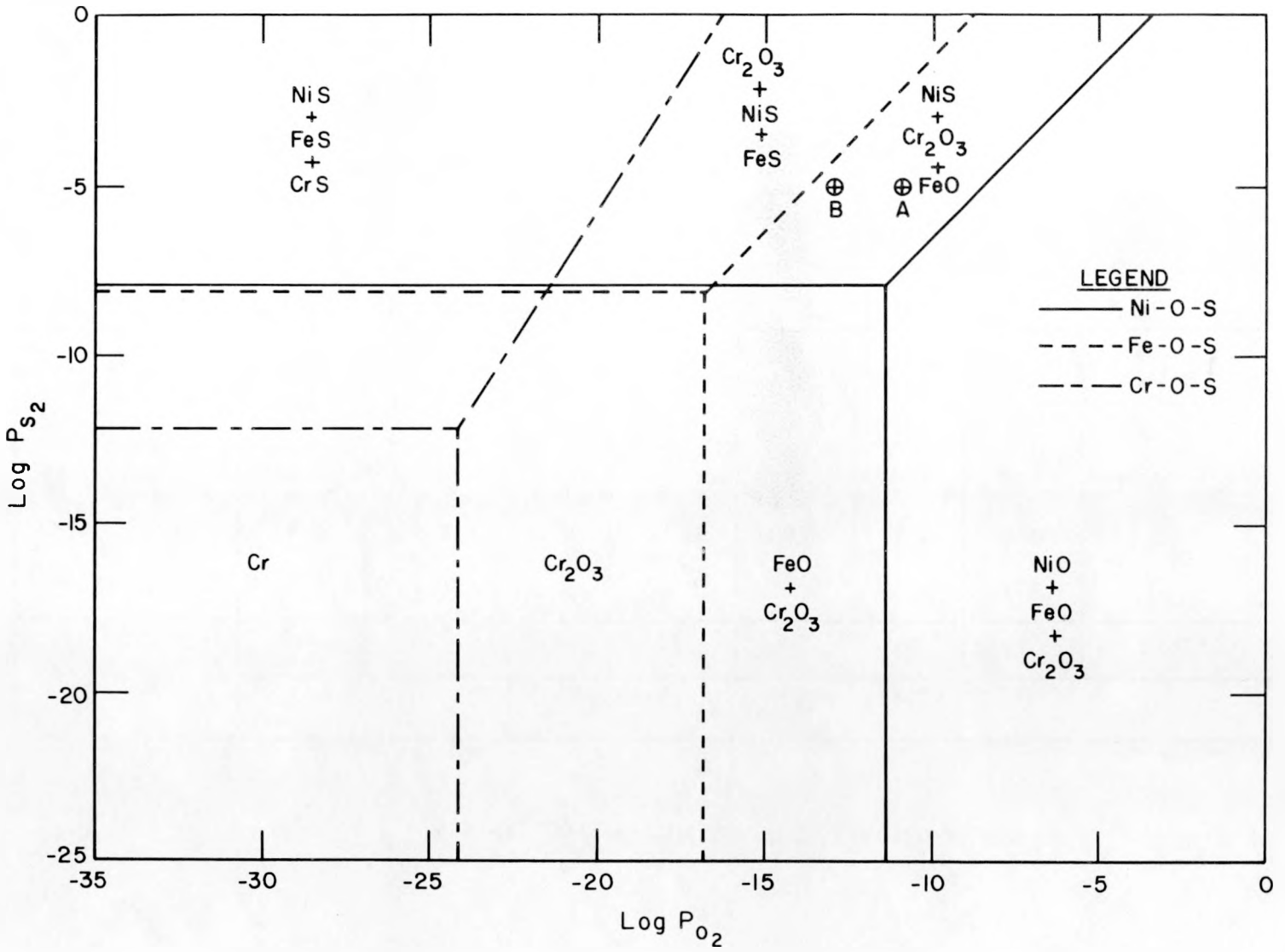


Figure 4-3. Composite Phase Stability Diagrams for Fe-O-S, Ni-O-S, and Cr-O-S at 1650 F (Points A and B represent the experimental conditions)

TABLE 4-1. NOMINAL COMPOSITIONS OF THE SELECTED ALLOYS

ALLOY	COMPOSITION IN WEIGHT PERCENT							
	Fe	Ni	Co	Cr	Mo	W	Al	OTHERS
INCONEL 618	0.0	54.0	12.5	22.0	9.0	0.0	1.0	
INCONEL 618E	16.0	55.0	0.0	23.0	0.0	6.0	0.0	
HASTELLOY X	18.5	46.0	2.5	22.0	9.0	0.6	0.0	1 Mn, 1 Si
PE-13	18.5	46.0	2.5	22.0	9.0	0.0	0.0	
NIMONIC 86	0.0	64.0	0.0	25.0	10.0	0.0	0.0	0.03 Ce

to retain all the corrosion scale in place, surface ground, and fine polished. Optical microscopy, scanning-electron microscopy (SEM), and electron microprobe analysis (EMPA) were performed to investigate the corrosion morphologies and to identify the various corrosion product phases.

Results. The detailed information on the corrosion morphologies of the specimens exposed to environment A is presented first, followed by the corrosion morphologies in environment B.

Environment A ($PO_2 = 10^{-11}$ atm, $PS_2 = 10^{-5}$ atm). All the alloys exposed in this environment were found to undergo sulfidation corrosion with noticeable corrosion being initiated within 15 minutes. Figures 4-4 and 4-5 show the optical micrographs of Inconel 617 subjected to corrosion for 15 minutes, 4 hours, and 9 hours in this environment. After 15 minutes, the specimen has formed an external corrosion product layer that consists of a thin, Cr_2O_3-rich scale and globules of nickel sulfide. Sulfur has penetrated the alloy to form dense chronium-rich sulfide precipitates in the substrate to a thickness of about 20-40 μm. The micrograph shown in Fig. 4-4b has similar features, except the depth of internal penetration by chromium-rich sulfides has increased to ~200μm, while the dimensions of the outer scale are little changed. A different area of the same 8-hour specimen is shown in Fig. 4-4c, and reveals more extensive outer scale formation that is primarily composed of a mixture of Cr_2O_3 and nickel sulfide (lighter phase), with a corresponding reduction in the depth of penetration of internal sulfides (~120μm).

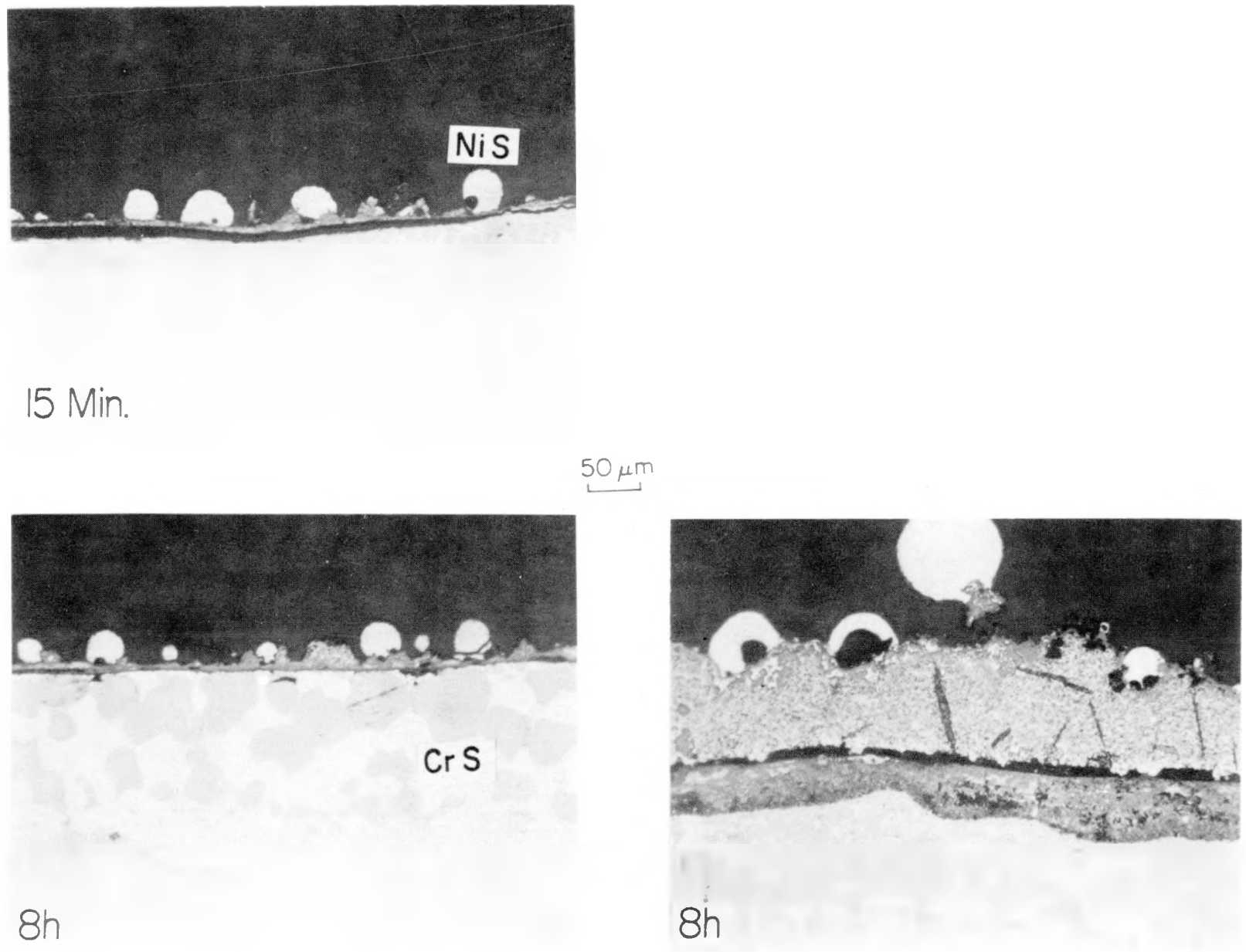


Figure 4-4. Optical Micrographs of Inconel 617 Exposed to Environment A for 15 Minutes and 8 Hours

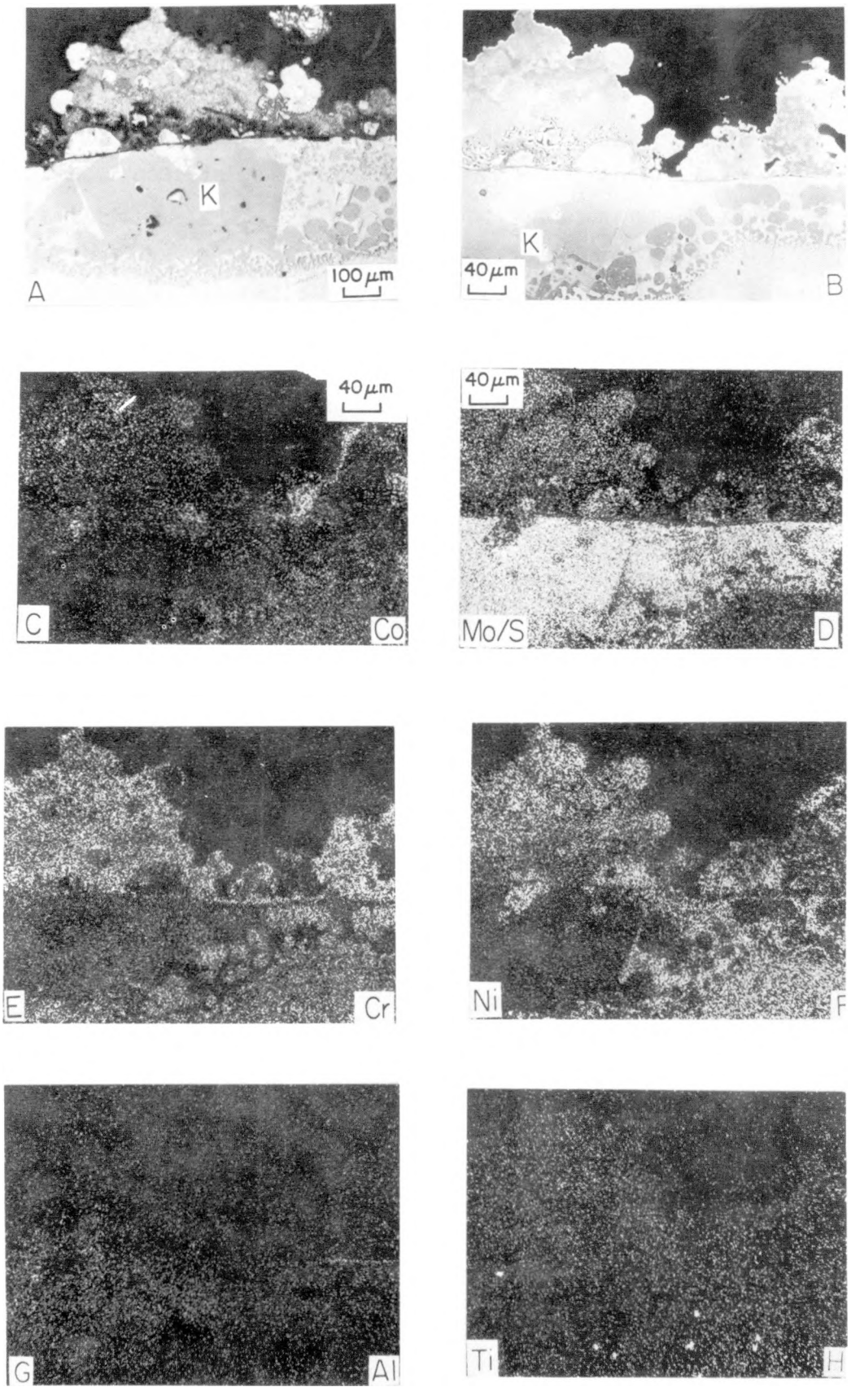


Figure 4-5. Inconel 617 Exposed to Environment A for 4 Hours

The details and extent of sulfidation of another specimen corroded for 4 hours are shown in Fig. 4-5. This illustrates the optical micrographs, the electron image, and the EDAX elemental maps for Co, Mo/S*, Cr, Ni, Al and Ti, respectively. Precipitates that are "blocky" in appearance (marked K in Fig. 4-5a and 4-5b) appear to be rich in Mo/S (Fig. 4-5d) but also contain some Cr and Al. These are probably Mo-rich complex sulfides; the exact reasons for this peculiar morphology are not known. Nickel and cobalt sulfide phases are present in the external scale as well as in the substrate. The chromium-rich phases appear to be predominantly Cr_2O_3 in the external scale and CrS_x in the substrate.

As the exposure time is increased, the extent of corrosion increases. A specimen approximately 2 mm thick was completely destroyed after 23 hours of exposure time.

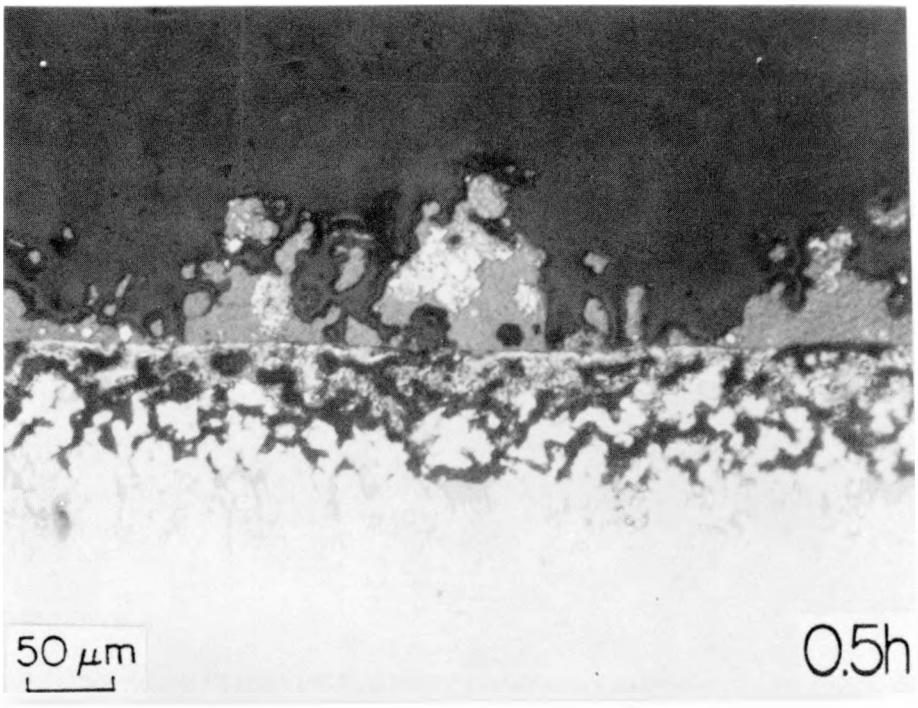
The corrosion behavior of Nimonic 86 was found to be quite similar to that of Inconel 617: sulfidation was initiated within 15 minutes and a specimen approximately 2 mm thick was completely destroyed after 23 hours. Figure 4-6 shows the optical micrographs of specimens exposed for 0.5 and 4 hours. The external scale consists of a mixture of Cr_2O_3 and globular nickel sulfide and the substrate is penetrated by sulfur which has resulted in the precipitation of CrS_x.

Figure 4-7 shows the electron image and the X-ray maps for Cr, S, Mo, Ni, and oxygen, respectively (obtained using an EMPA), of a different area of the specimen of Nimonic 86 exposed for 0.5 hour. The X-ray maps show what appears to be a mixture of Cr_2O_3 and nickel sulfide in the external scale layer. The specimen has been internally sulfidized; precipitates of CrS_x are evident.

The corrosion behavior of Inconel 618E, although similar to those of Inconel 617 and Nimonic 86, appears to proceed somewhat more slowly; however, sulfidation

---

*The EDAX peaks for Mo and S coincide and cannot be resolved.



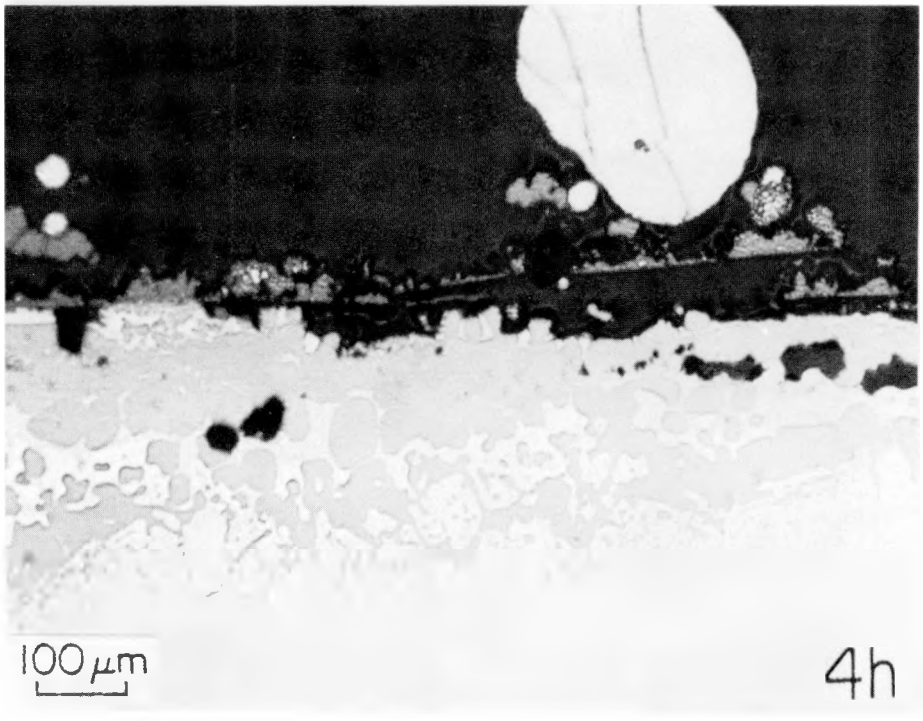


Figure 4-6. Optical Micrographs of Nimonic 86 Exposed to Environment A for 0.5 and 4 Hours

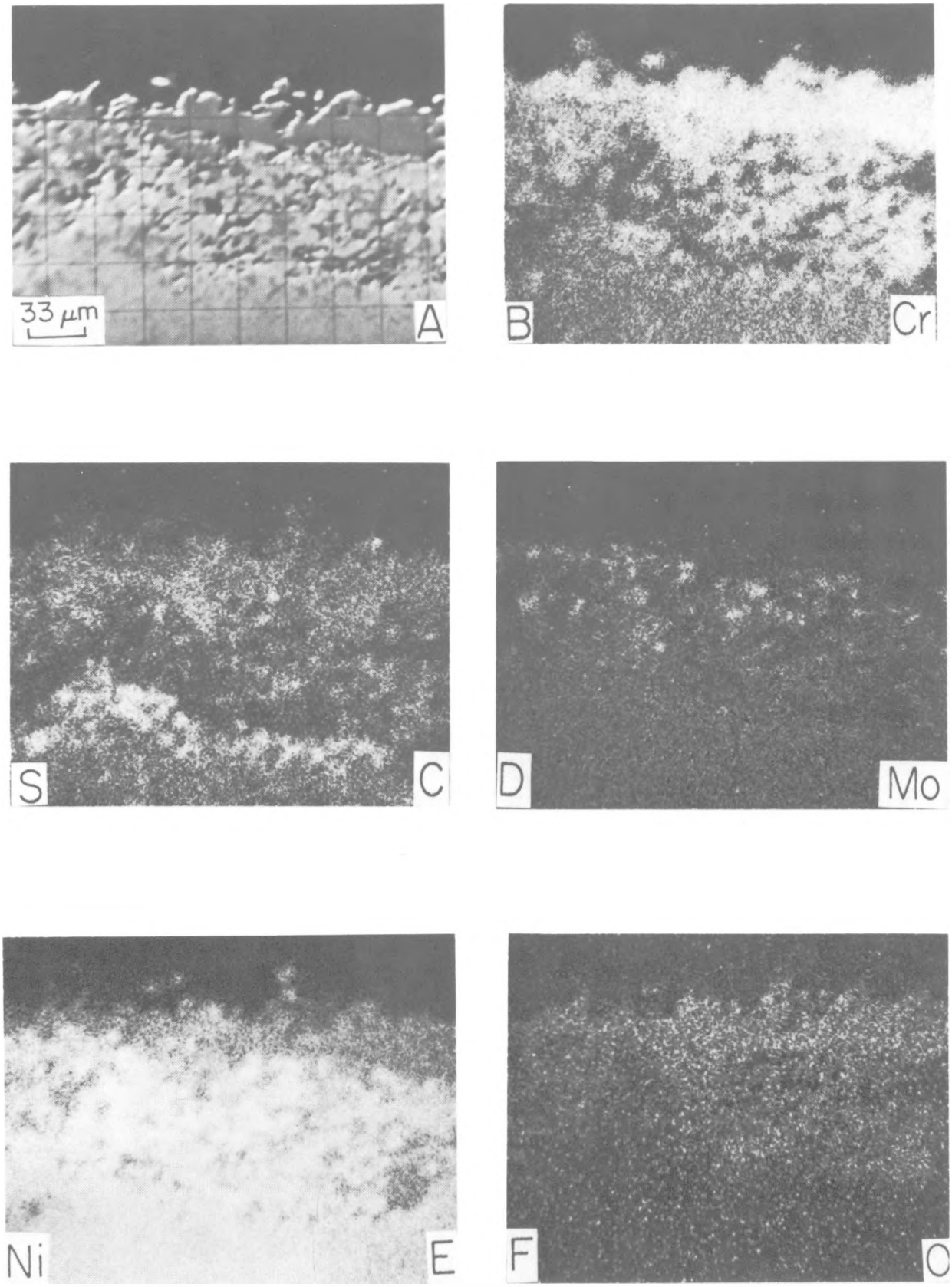


Figure 4-7. Nimonic 86 Exposed to Environment A for 0.5 Hour

could be initiated quite readily. Figure 4-8 shows the optical micrograph, the electron image, and the X-ray maps for Ni, S, O, Fe, and Cr, respectively, of a specimen exposed for 0.5 hour. A continuous external iron-rich oxide layer also has formed, below which a Cr_2O_3 layer has formed. The formation of nickel sulfide has apparently caused lifting and bulging of the iron + chromium oxide layers. Sulfur has penetrated the external oxide scale to form both nickel sulfide and chromium sulfide in the alloy matrix. Although sulfidation occurred within 0.5 hour, the propagation of attack was slow; a specimen 2 mm thick, exposed for 23 hours, suffered extensive sulfidation but was not completely penetrated. After 50 hours, the specimen was completely penetrated.

Hastelloy X and PE-13 are nickel-base alloys of almost identical chemical composition and show similar corrosion behavior. Of the five alloys examined, these two appear to corrode the slowest; Hastelloy X appears to corrode at a slightly slower rate than PE-13. Figure 4-9 shows the optical micrographs of Hastelloy X corroded for 0.5, 4, 23, and 50 hours; Fig. 4-10 shows the optical micrographs of PE-13 corroded for 0.5, 4, 8, and 23 hours. Although sulfidation can be initiated within 0.5 hour in both alloys, note that no external globular nickel sulfides had formed. The external scale layers shown in Fig. 4-9a and 4-9b and in Fig. 4-10a and 4-10b appear compact and duplex. The X-ray maps shown in Fig. 4-11 of a specimen of Hastelloy X corroded for 0.5 hour clearly show the presence of an iron-rich and chromium-rich oxide layer. However, sulfur seems to have penetrated this layer.

Increasing the exposure time caused further influx of sulfur through the external oxide layer and extensive internal sulfidation. Figure 4-12 shows a specimen of Hastelloy X exposed to the corrosive environment for 23 hours along with the electron image and the EDAX elemental maps for Mo/S, Cr, Fe, and Ni (obtained using an SEM). The external scale is absent and this is probably due to the scale spalling off during cooling of the specimen after the corrosion exposure. Sulfur penetration has resulted in the formation of globular chromium sulfides and needle-shaped, molybdenum-rich sulfides. Figures 4-13 and 4-14 show the distribution of the elements in the bulk and in the needle phase. The needle phase is essentially composed of Mo/S and is probably molybdenum sulfide.

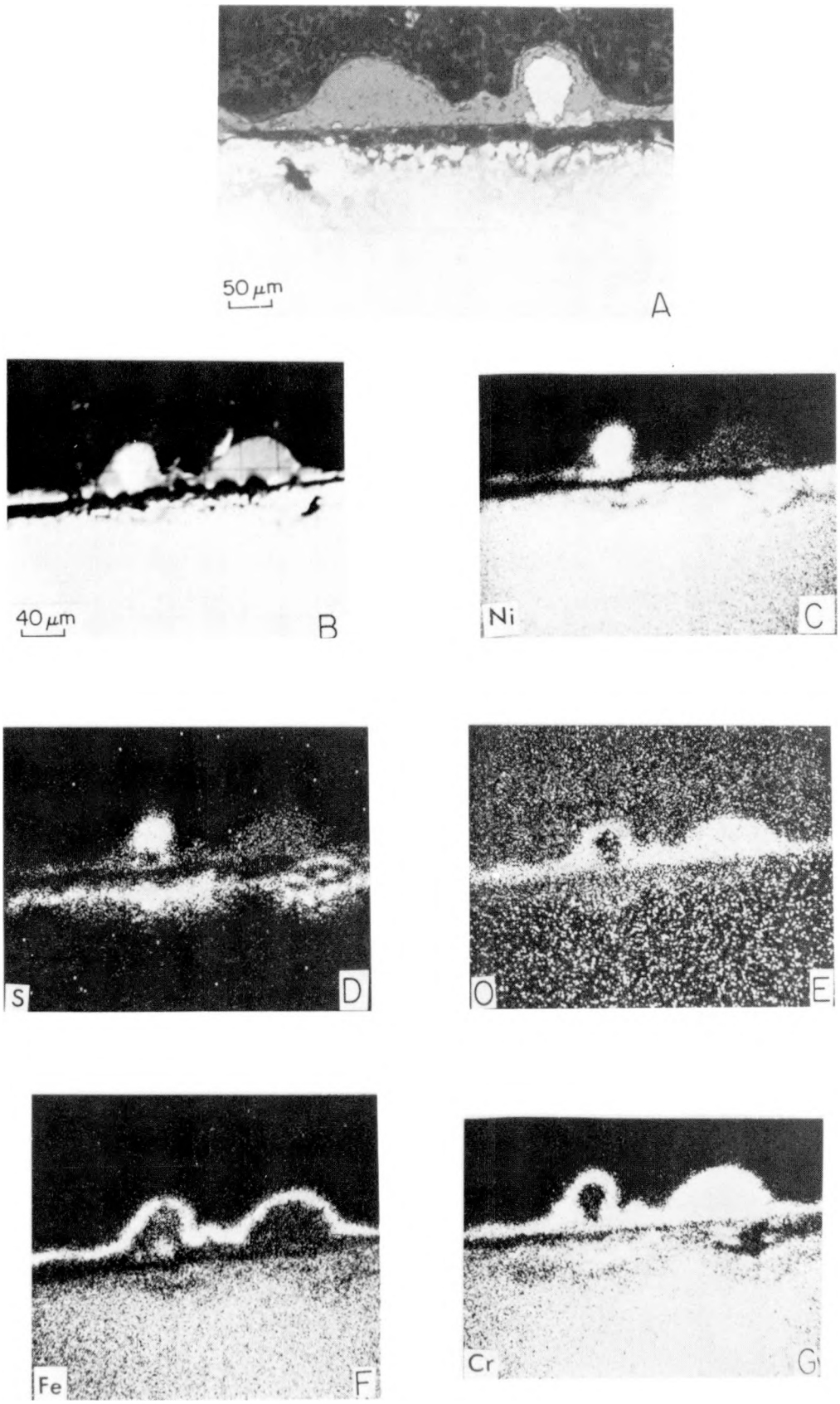


Figure 4-8. Inconel 618E Exposed to Environment A for 0.5 Hour

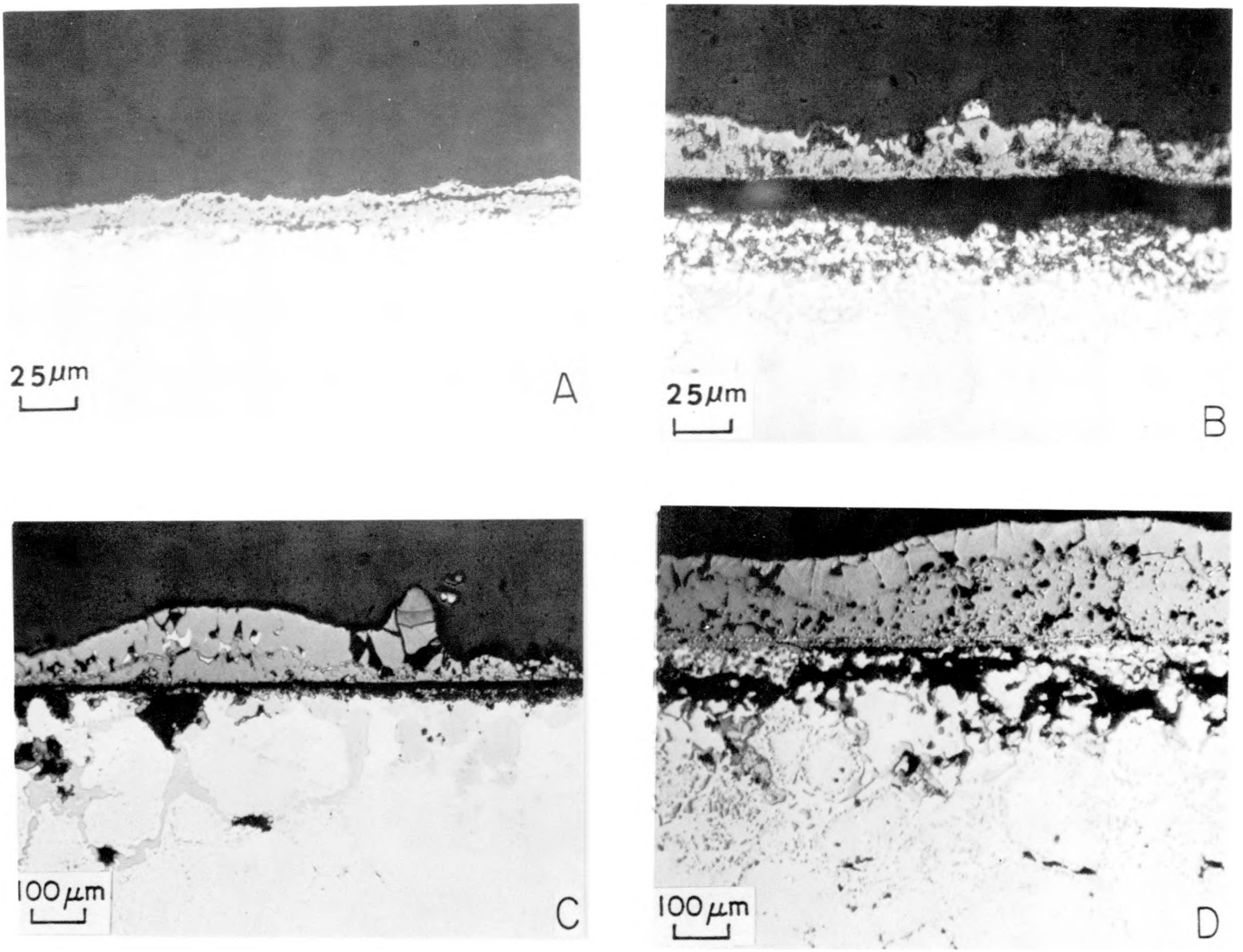


Figure 4-9. Optical Micrographs of Hastelloy X Exposed to Environment A

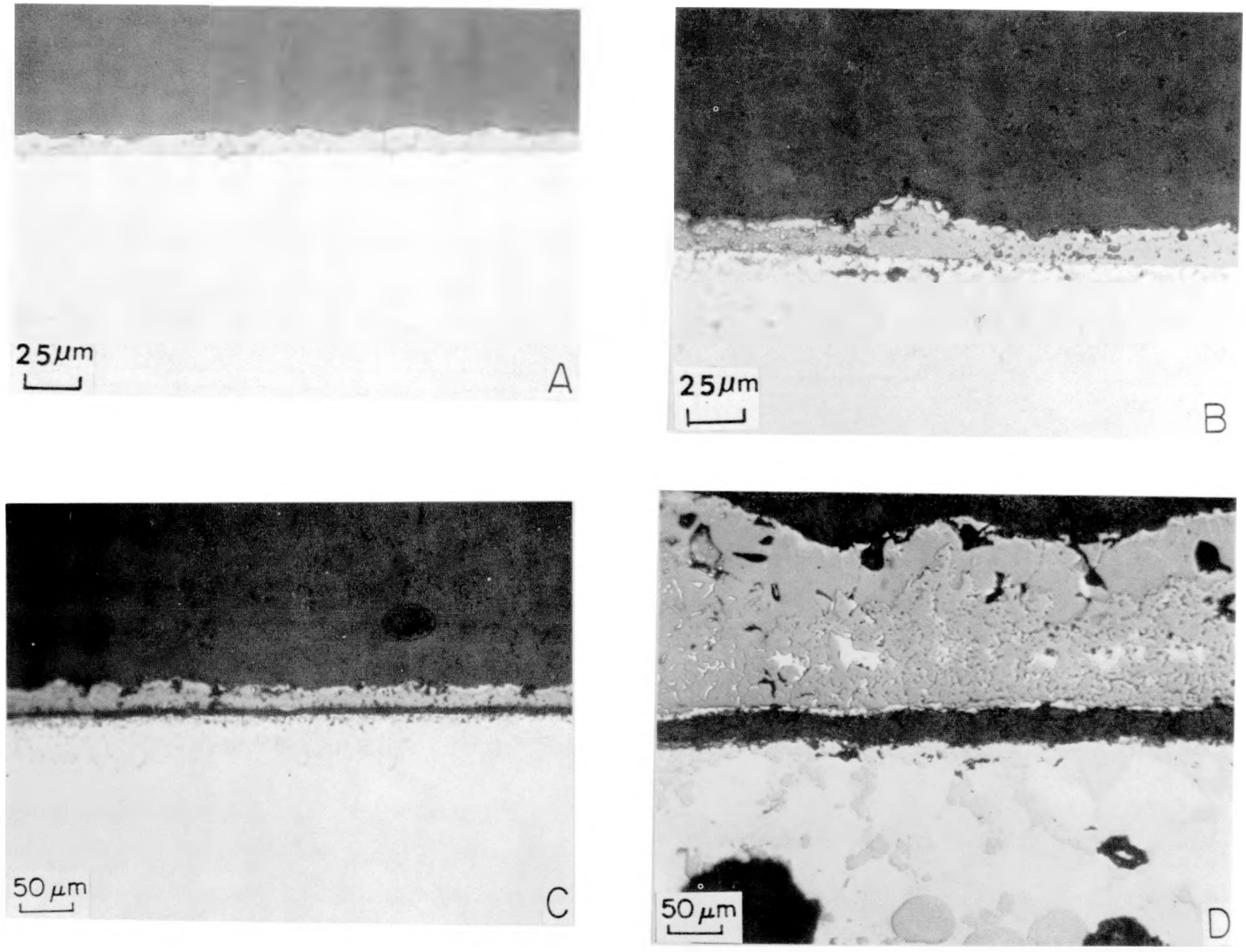


Figure 4-10. Optical Micrograph of PE-13 Exposed to Environment A

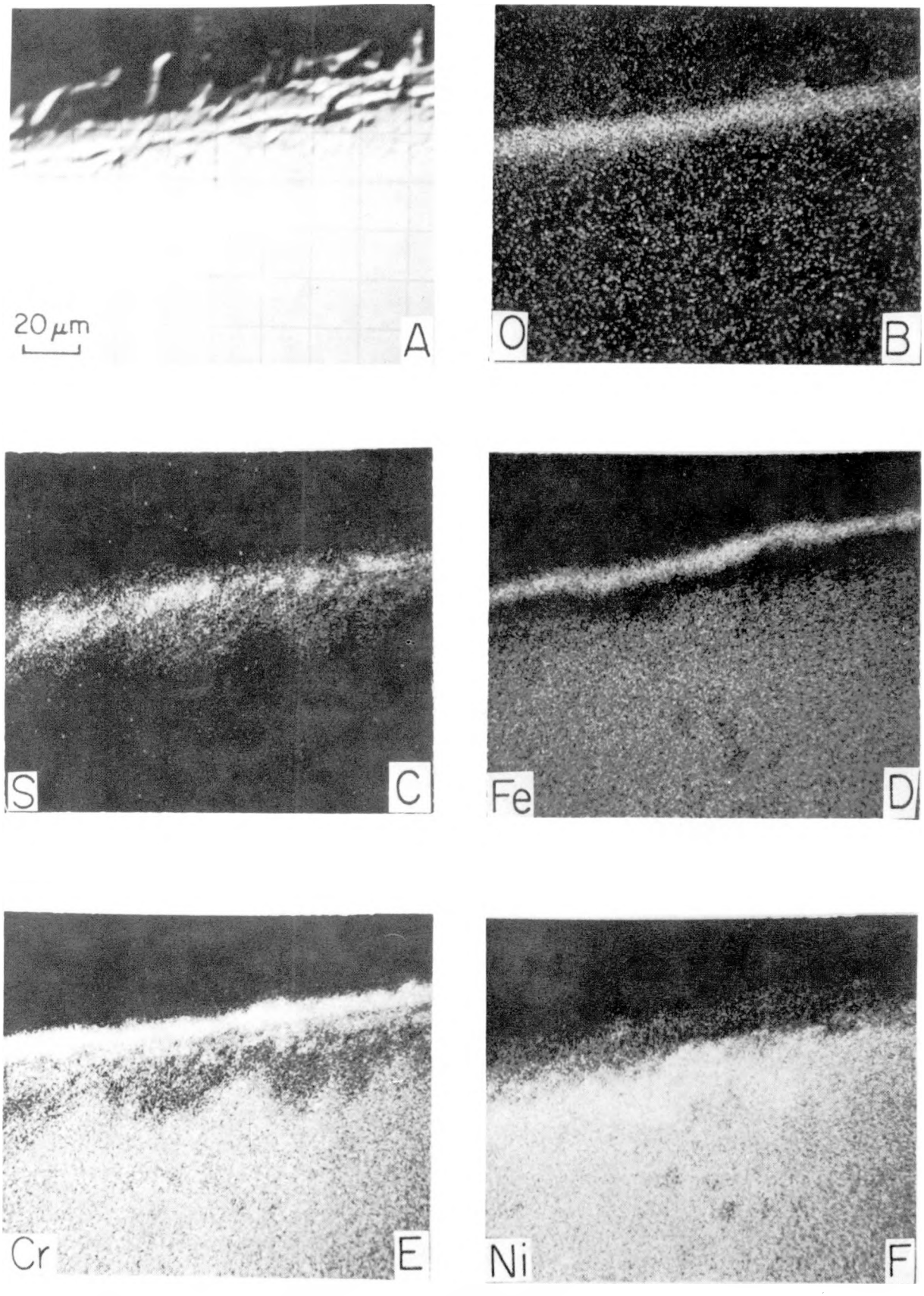


Figure 4-11. Hastelloy X Exposed to Environment A for 0.5 Hour

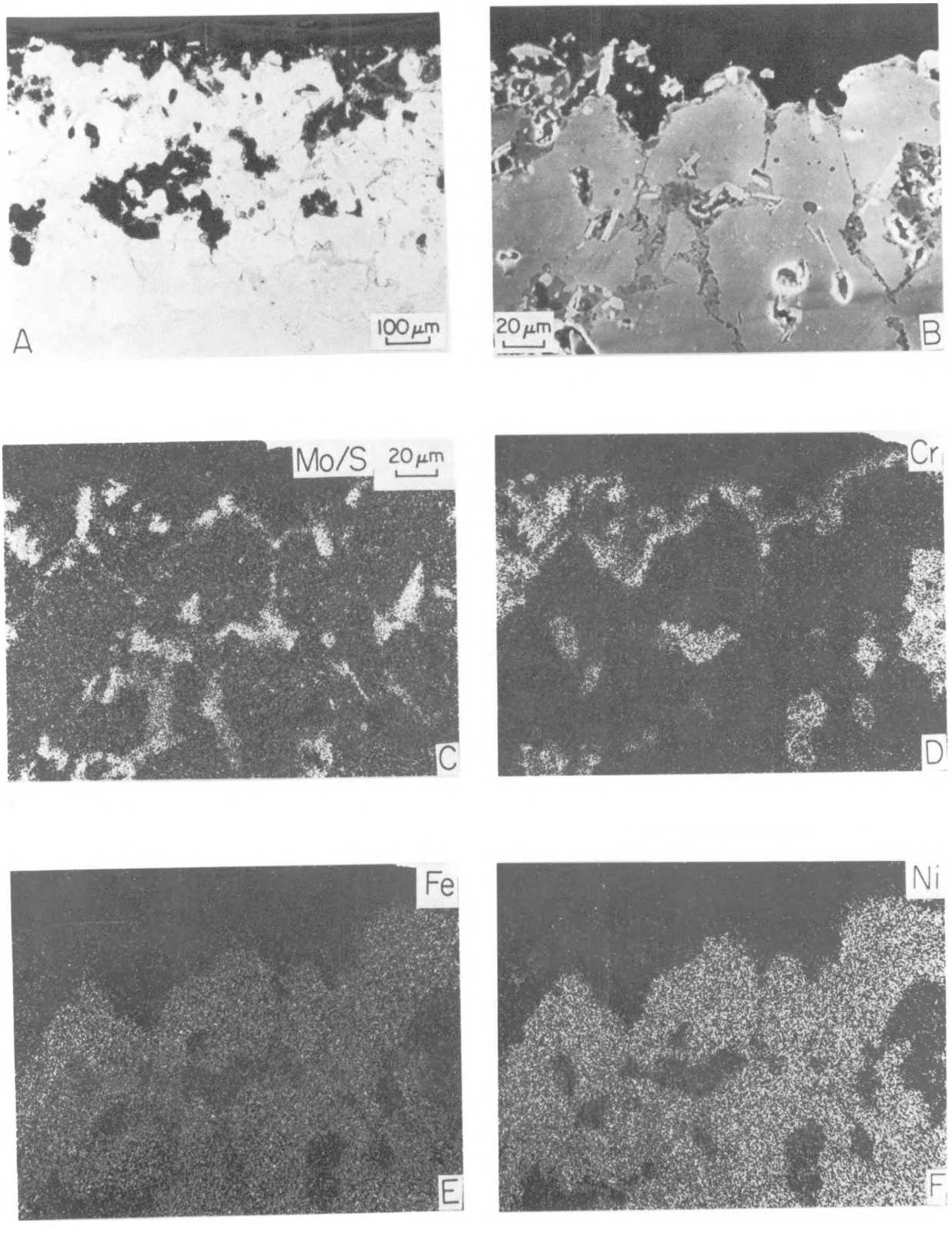


Figure 4-12. Hastelloy X Exposed to Environment A for 23 Hours

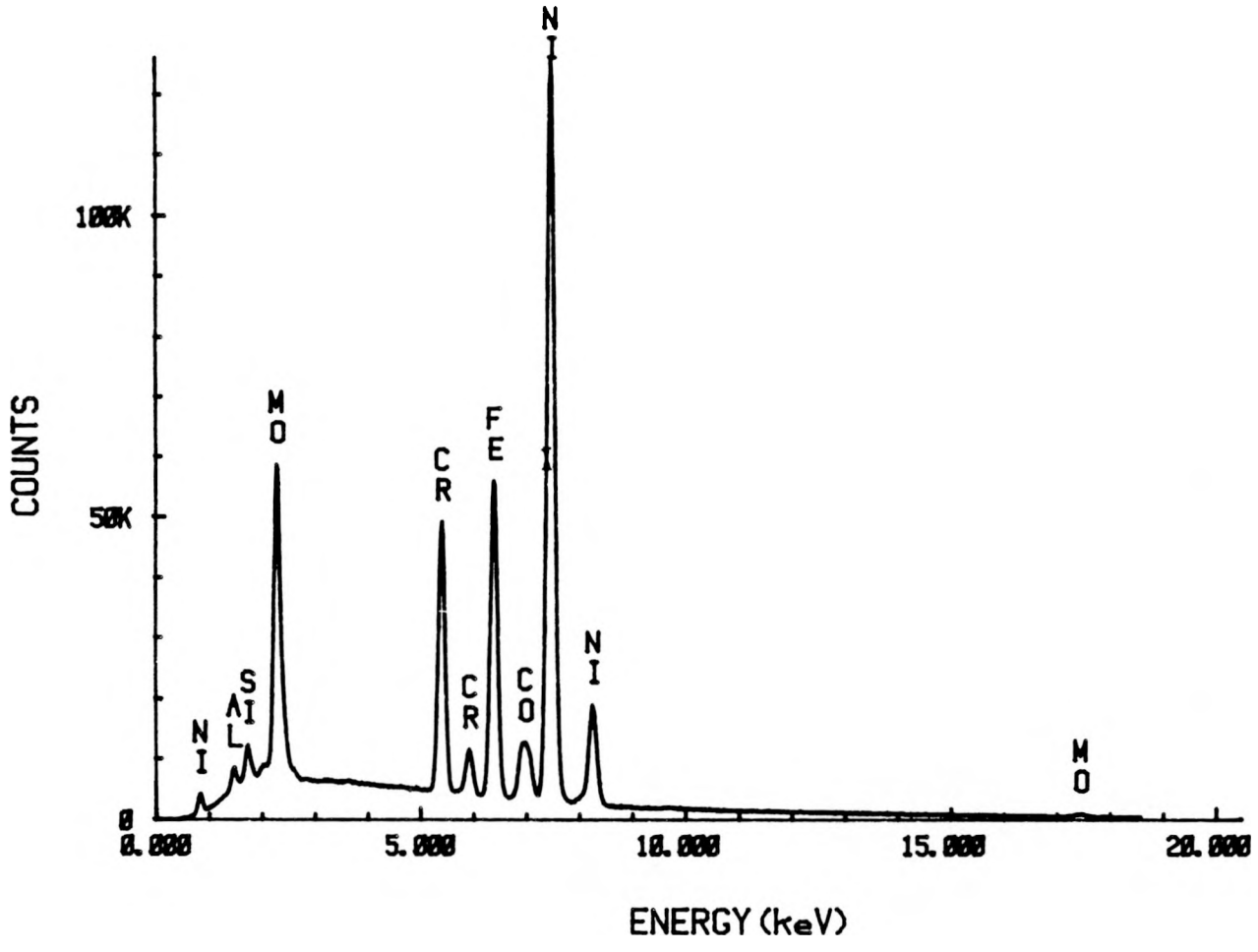


Figure 4-13. Distribution of Elements in the Area Shown in Fig. 4-12B

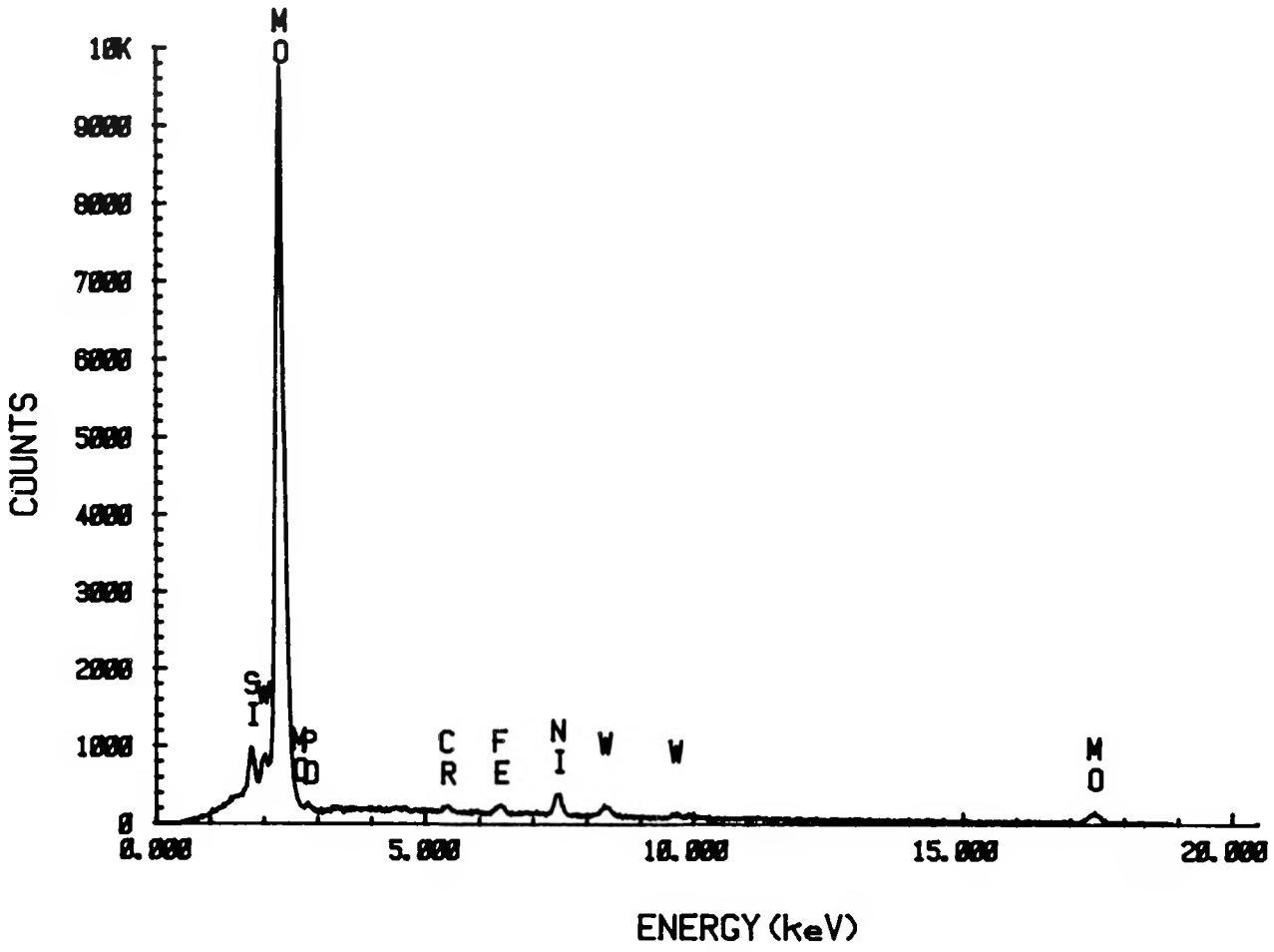


Figure 4-14. Distribution of Elements in the Needle Phase

Environment B (PO_2 = 10^{-13} atm, PS_2 = 10^{-5} atm). The corrosion behavior of all the five alloys in this enviroment is morphologically almost identical to that in environment A, but the rate of corrosion appears to be slower. Figure 4-15 shows the optical micrographs of Inconels 617 and 618E and Hastelloy X corroded for 2 hours and 70 hours, respectively. Although sulfidation was observed to be initiated within 2 hours, and the attack after 70 hours was extensive, the specimens were not completely penetrated. It took 150 hours for 2 mm-thick specimens of Nimonic 86 and Inconel 617 to be completely penetrated by sulfur and oxygen. After 250 hours, a specimen (2 mm thick) of Inconel 618E was completely penetrated by sulfur (but not by oxygen): specimens of Hastelloy X and PE-13 were not completely penetrated by sulfur in this exposure time.

Discussion. The results presented so far indicate that initiation of sulfidation occurs in all the alloys; however, the chemistries of both the alloy and the environment affect the initiation and to some extent the propagation of sulfidation.

Scale Growth Model. The mechanism of initiation of corrosion of a binary Ni-Cr alloy in an oxygen- and sulfur-containing gaseous environment where the thermodynamically stable phases on the surface of the alloy are nickel sulfide and chromium oxide can be schematically represented, as shown in Fig. 4-16. As soon as a fresh surface of the Ni-Cr alloy is exposed to the corrosive gas, nuclei of Cr_2O_3 form (Stage I in Fig. 4-16). At this stage, although nickel sulfide is thermodynamically stable on pure nickel, in a binary Ni-Cr alloy, it cannot nucleate in regions of the alloy containing chromium. However, formation of Cr_2O_3 nuclei causes depletion of chromium from the alloy (Stage I in Fig. 4-16) and, in such regions, nickel sulfide can nucleate (Stage II in Fig. 4-16). The rate of growth of nickel sulfide is high compared to the rate of growth of Cr_2O_3. Hence, the nickel sulfide nuclei can outgrow the Cr_2O_3 nuclei (Stage III). Since the nickel sulfide is a liquid at this temperature, transport of sulfur and oxygen through the growing nickel sulfide can be rapid. Hence, at the advancing nickel sulfide alloy interface, inwardly migrating sulfur and oxygen can react with outwardly migrating chromium in the alloy to form either

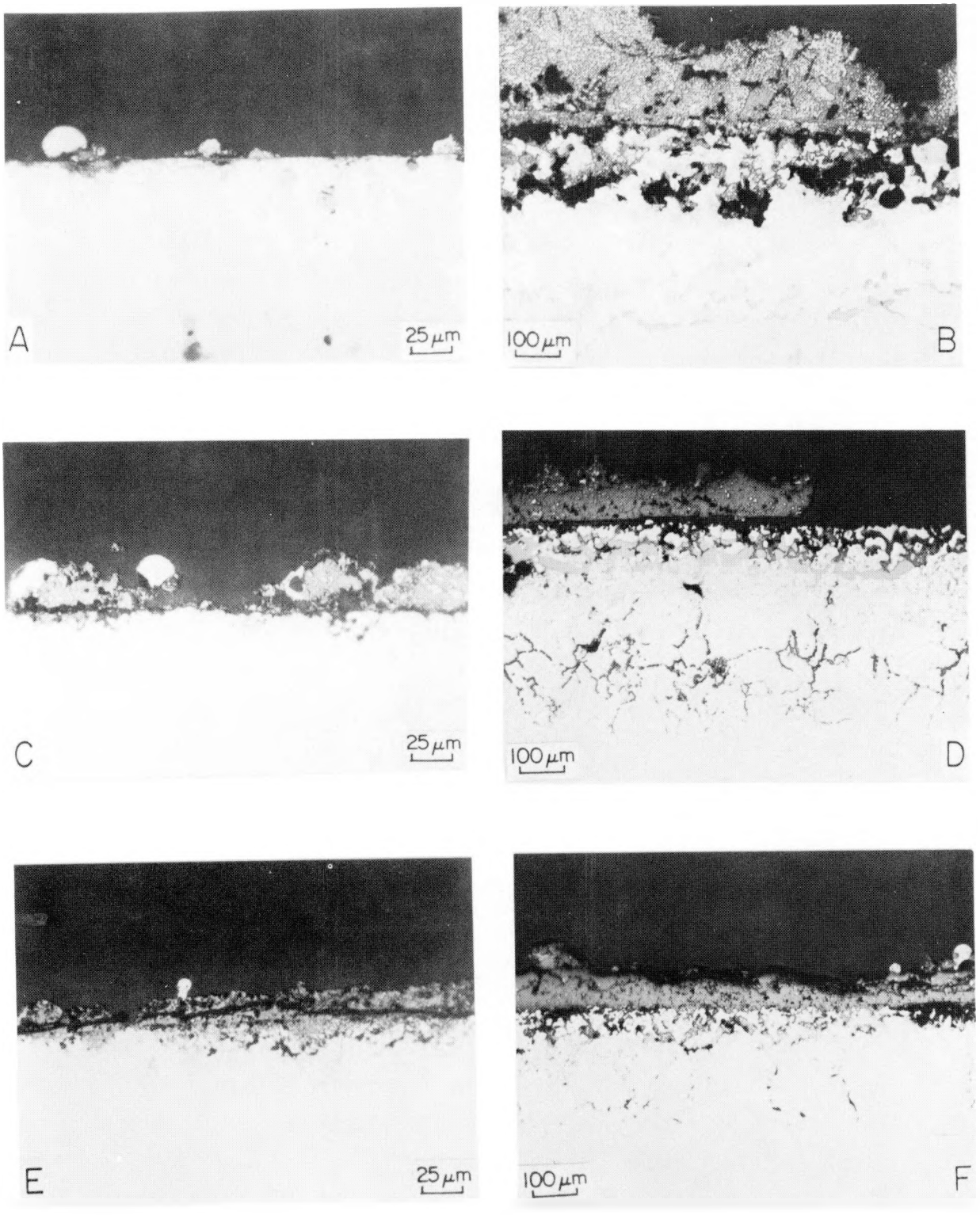


Figure 4-15. Optical Micrographs of Alloys Exposed to Environment A

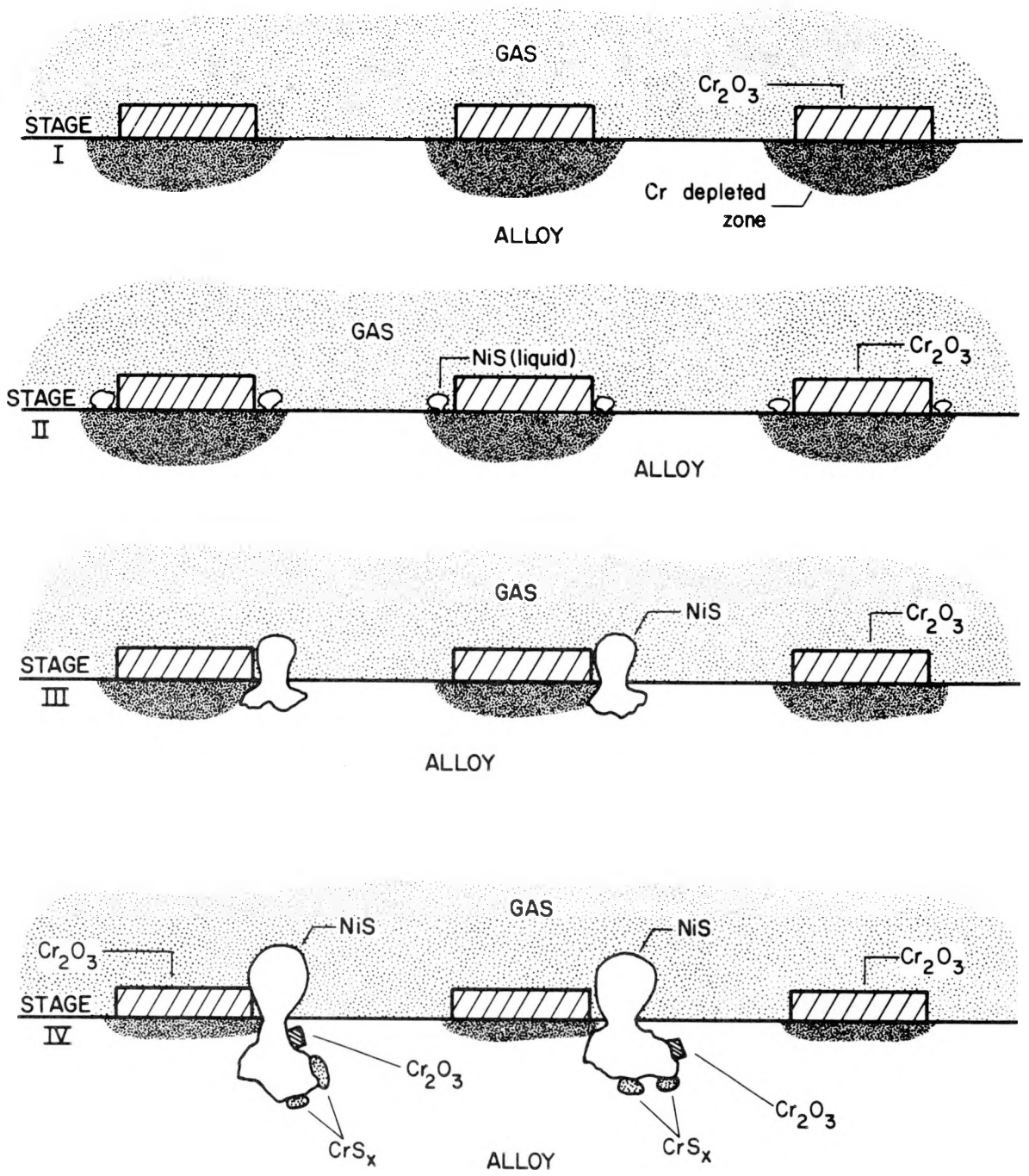


Figure 4-16. Schematic Representation of Growth of Corrosion Products on a Ni-Cr Alloy Exposed to an Environment Containing Oxygen and Sulfur

chromium sulfide or chromium oxide depending on the PS_2/PO_2 ratio available at that interface. Such a development is represented in Stage IV. The net result of these early stages of scale development is that the alloy surface gets covered with:

- Solid Cr_2O_3 which is not present as a continuous layer covering the entire surface
- Liquid nickel sulfide droplets on the surface
- Internal precipitates of CrS_x and/or Cr_2O_3

Essentially, the binary alloy does not develop a protective scale because of the presence of nickel sulfide channels in the scale. Formation of internal precipitates of Cr_2O_3 and CrS_x causes wastage of chromium which otherwise would have participitated in the formation of external protective scale.

Effect Of Alloying Additions. In commercial alloys, the presence of other elements such as iron and cobalt, etc., can alter the reactions occuring during initiation, described in Fig. 4-16. Iron oxide is a stable phase in these environments and, hence, alloys containing iron will nucleate iron oxide in addition to Cr_2O_3 during Stage I. Since iron oxide grows rapidly, the number of physical sites available for formation of nickel sulfide during Stage II is probably reduced. Hence, the resultant scale would be expected to contain fewer nickel sulfide channels and, hence, propagation of corrosion will be slower. In fact, in alloys containing iron (Inconel 618E, Hastelloy X and PE-13), the growth of iron oxide is so predominant that the alloys develop an outer iron oxide scale within 0.5 hour (see Fig. 4-8); these alloys corrode at slower rates than iron-free alloys (Inconel 617 and Nimonic 86).

In both the environments, cobalt sulfide is a stable phase and it forms a liquid solution with nickel sulfide. Hence, the presence of cobalt in the alloy does not significantly modify the events described in Fig. 4-16, and the corrosion behavior of the alloy remains unaffected.

Molybdenum does not appear to play a role during the initiation stage. It may be participating in the propagation stage; Fig. 4-5 and 4-12 show the formation of internal molybdenum sulfides. However, its effect on the corrosion rate is unclear.

Effect of Environment. The results indicate that the rate of corrosion in the lower oxygen partial pressure environment (B) is lower than the rate of corrosion in the higher oxygen partial pressure environment (A). This is somewhat unexpected since the lower oxygen partial pressure environment is thermodynamically more conducive to sulfidation attack. It appears that kinetic considerations may be more important than thermodynamic considerations in this case. For this experiment, both the environments are maintained at the same sulfur partial pressure but differ only in their oxygen partial pressures. The sulfur partial pressure is controlled by the SO_2 flowrate and by the reaction:

$$SO_2 = 1/2\ S_2 + O_2$$

Reduction of the oxygen partial pressure by nearly 2 orders of magnitude necessitates reduction of the SO_2 partial pressure (the flowrate of SO_2) by nearly 2 orders of magnitude to maintain the same sulfur partial pressure. The PSO_2 in environment A was 10^{-2} atm and the PSO_2 in environment B was 10^{-4} atm. The reduction in the "flux" of sulfur-carrying species (SO_2) seems to slow down the propagation of sulfidation.

Finally, experiments performed with probe specimens in a 24-inch AFB (Ref. 4-8) showed the morphologies of corrosion of these alloys were quite similar to those observed here for the shortest term exposures, indicating that the simple laboratory experiments can serve as an accelerated test and provide information on the expected mode of corrosion of the field specimens experience.

Conclusions. In the two specific environments studied here, analysis of the corrosion morphologies produced leads to the following conclusions:

- Sulfidation corrosion can be initiated in all alloys within 0.25 hours in both the environments.
- The presence of iron in the alloys appears to be beneficial since iron-containing alloys (Inconel 618E, Hastelloy X and PE-13) corroded significantly slower. Iron may be slowing down the initiation of sulfidation attack by forming a continuous oxide layer.
- The presence of cobalt does not seem to alter the corrosion reaction.
- The presence of molybdenum does not seem to affect the initiation of sulfidation. However, molybdenum seems to take part in the "propagation stage".
- Kinetic factors and the flux of sulfur dioxide, rather than thermodynamic factors and the partial pressure of oxygen in the environment, appear to be dominant factors in influencing the corrosion reaction.

4.1.2 Corrosion Behavior of Iron-Base Alloys in Simulated Substoichiometric Combustion Gases

The susceptibility to initiation of sulfidation attack of a series of nickel-base alloys in a simulated substoichiometric combustion environment of a fluidized bed combustor (AFB) was examined in Section 4.1.1. The experimental results indicated sulfidation attack could be initiated within 15 minutes in most of the alloys, mainly because nickel sulfide could form as a stable phase in these environments. The alloys formed external scales containing mixtures of oxides of chromium and iron, and nickel sulfide. It was postulated that the external scales were defective due to the presence of channels of nickel sulfide which permitted easy diffusion of sulfur and oxygen into the alloy, causing further internal sulfidation attack. The presence of iron in the alloys was found to be beneficial since an outer layer of iron oxide formed, which appeared to slow down the ingress of sulfidation. This section examines the corrosion behavior of a series of iron-base alloys intended for the construction of a heat exchanger loop in an advanced closed-cycle gas turbine air heater fired by a fluidized bed combustor.

Alloy Selection. The rationale for alloy selection (Ref. 4-9) was presented in Section 4.1. The heat exchanger alloys for the construction of the advanced air heaters were selected primarily on the basis of their strength. High-strength nickel-base alloys were selected for the construction of the hotter segment of the heat exchanger loop, and the medium- and low-strength iron-base alloys were selected for the construction of the relatively cooler segment of the loop. The FeCrAlY alloys were selected for use as claddings since these alloys are believed to have good corrosion resistance (Ref. 4-10). Table 4-2 lists the nominal compositions of the selected alloys.

TABLE 4-2. NOMINAL COMPOSITION OF THE SELECTED ALLOYS

ALLOY	COMPOSITION IN WEIGHT PERCENT				
	Fe	Ni	Cr	Al	OTHER
INCOLOY 800 H	44	33	21	0.35	0.35 Ti 0.75 Mn 0.5 Si
AISI 310	52	20	25	0.00	1.5 Mn 0.5 Si
AISI 347	BAL	10	18.0	0.00	(Nb+Ta)
AISI 304	BAL	8	18.0	0.00	
FeCrAlY	BAL	0	15	4	0.5Y
FeCrAlY	BAL	0	25	4	1.0Y

The experimental procedure (Ref. 4-5) was described in the previous section. The corrosive environments consisted of gaseous mixtures of CO + CO_2 + SO_2. The ratios of the gases were such that the PS_2 of the environments was 10^{-5} atm. The PO_2 of the environments was changed from 10^{-11} atm (environment A) to 10^{-13} atm (environment B). The temperature of exposure was 1650 F and the exposure time was varied from 15 minutes to 250 hours.

Results.

Environment A: (PO_2 = 10^{-11} atm, PS_2 = 10^{-5} atm). Incoloy 800H was susceptible to initiation of sulfidation attack. Fig. 4-17 shows the optical

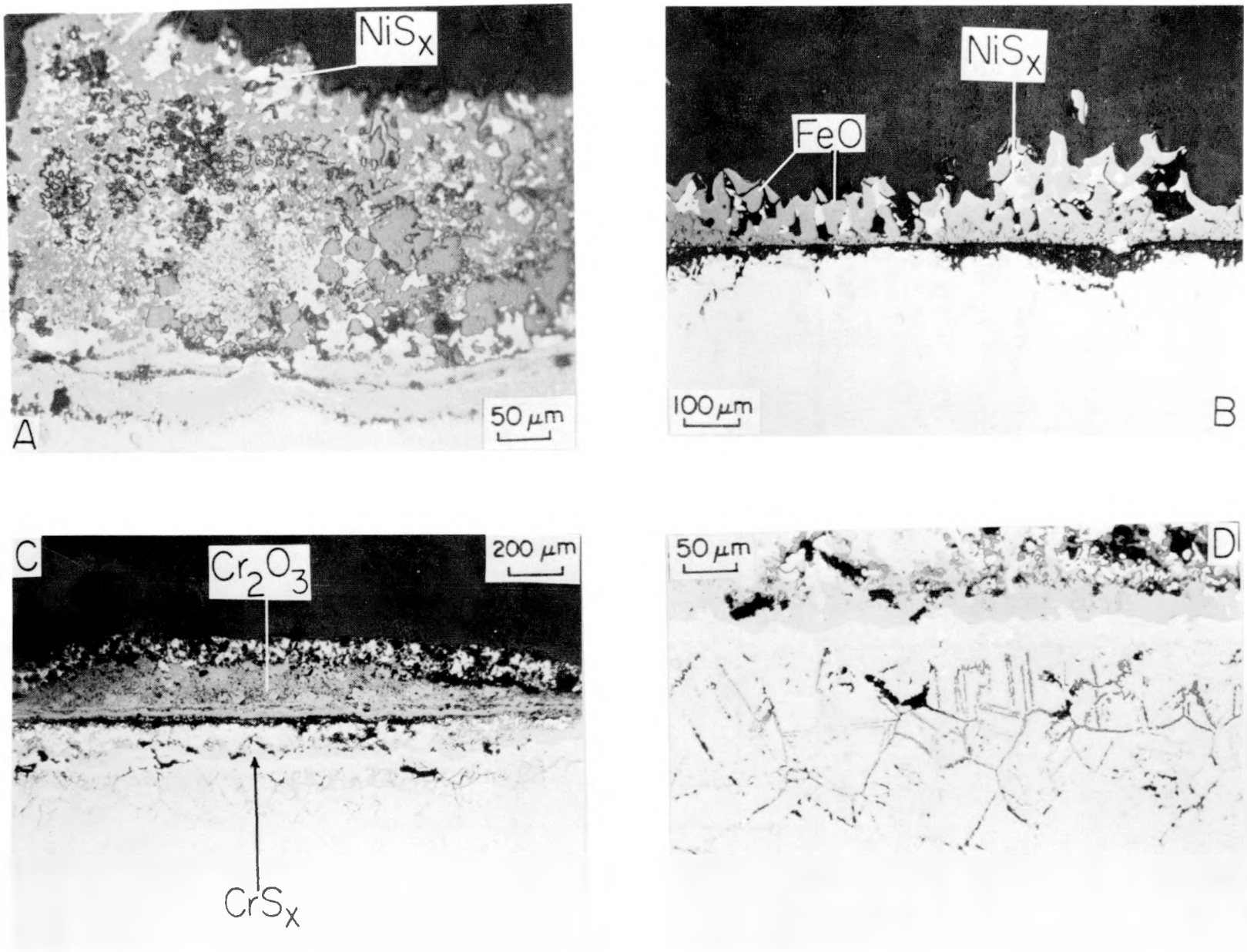


Figure 4-17. Optical Micrographs of Incoloy 800H Exposed to Environment A

micrographs of the alloy exposed for 15 minutes, 8 hours, and 100 hours. Sulfidation was initiated within 15 minutes (Fig. 4-17a), and the external scale after 8 hours consisted of iron oxide (darker looking phase) and nickel sulfide (lighter looking phase). On increasing the exposure time, the external scale thickened and consisted of an outer iron-rich oxide layer and an inner chromium-rich oxide layer. Sulfur penetrated the alloy and formed a thick bank of chromium-rich sulfides. Figure 4 18 shows the electron image and EDAX-elemental maps for Fe, Cr, Ni and S, respectively, of the specimen shown in Fig. 4-17c and 4-17d. The external scale, in addition to oxides of iron and chromium, contains a layer of iron sulfide (beneath the outermost iron oxide layer).

AISI 310 stainless steel shows a similar behavior to that of Incoloy 800H. The morphological features are almost identical to those observed on Incoloy 800. However, AISI 310 stainless steel corrodes at a slightly slower rate.

AISI 347 stainless steel, in contrast to Incoloy 800H and AISI 310 stainless steel exhibited a tendency to form corrosion pits. Figure 4-19 shows the optical micrograph, the electron image, and the X-ray maps for Ni, S, Fe, Cr and oxygen, respectively, of a pit on a specimen exposed for 0.5 hour. A broken iron oxide layer is evident and the specimen has developed copious chromium oxide and chromium sulfide. Areas away from the pit are protected by a thin Cr_2O_3-rich scale. In increasing the time of exposure, more pits developed and covered the entire specimen.

The behavior of AISI 304 stainless steel was almost identical to that of AISI 347 stainless steel. Figure 4-20 shows the optical micrograph, the electron image, and the X-ray maps for Nr, S, Fe, Cr, and oxygen, respectively, of a specimen exposed for 0.5 hour. (Note the similarities between Fig. 4-19 and Fig. 4-20.) On increasing the exposure time, the number of pits increased and this alloy appeared to corrode somewhat faster than AISI 347. A specimen of AISI 304 stainless steel approximately 2 mm thick, exposed for 50 hours, was completely destroyed while a similar specimen of AISI 347 lasted up to 150 hours.

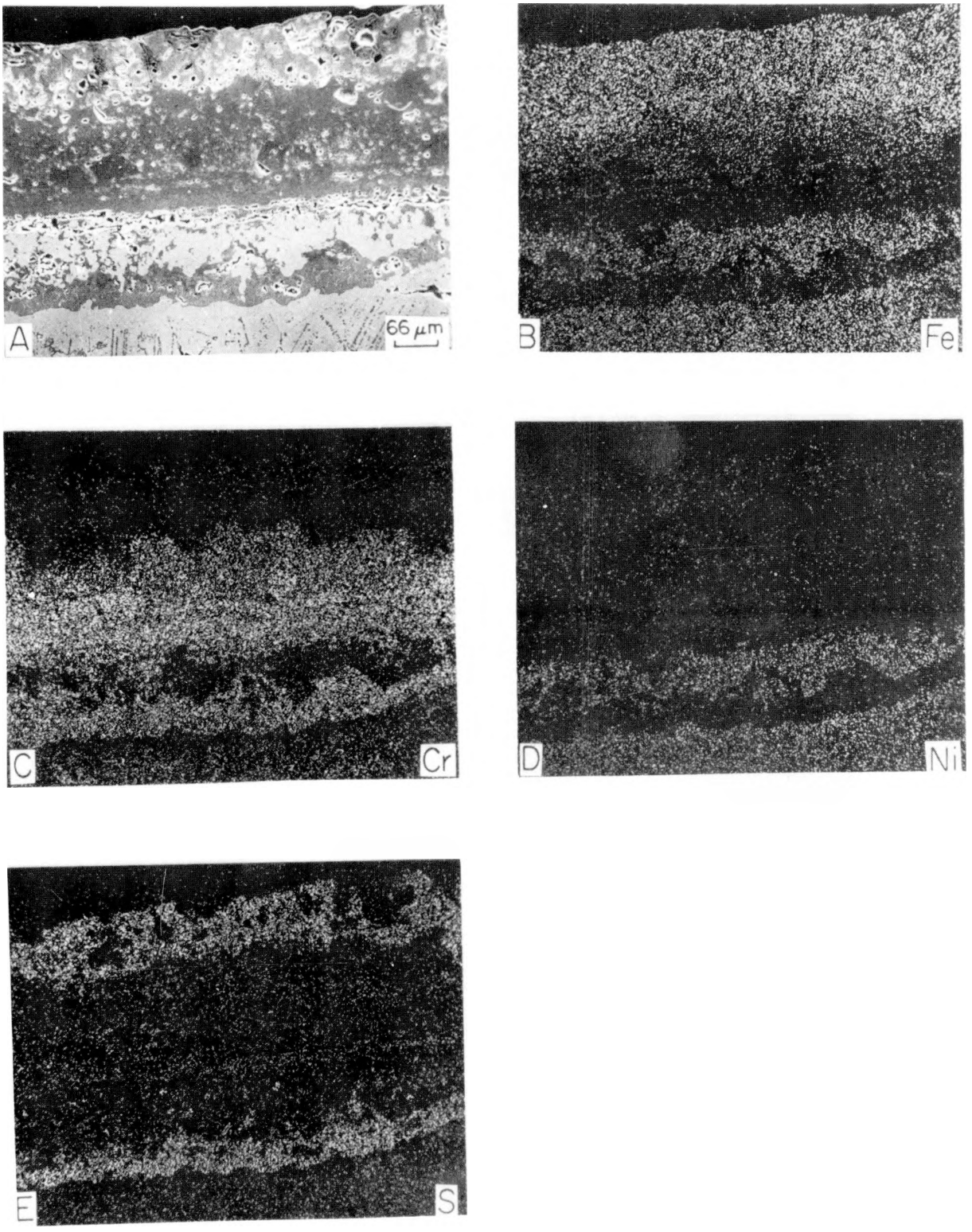


Figure 4-18. Semi-Micrographs of the Area Shown in Fig. 4-17(d)

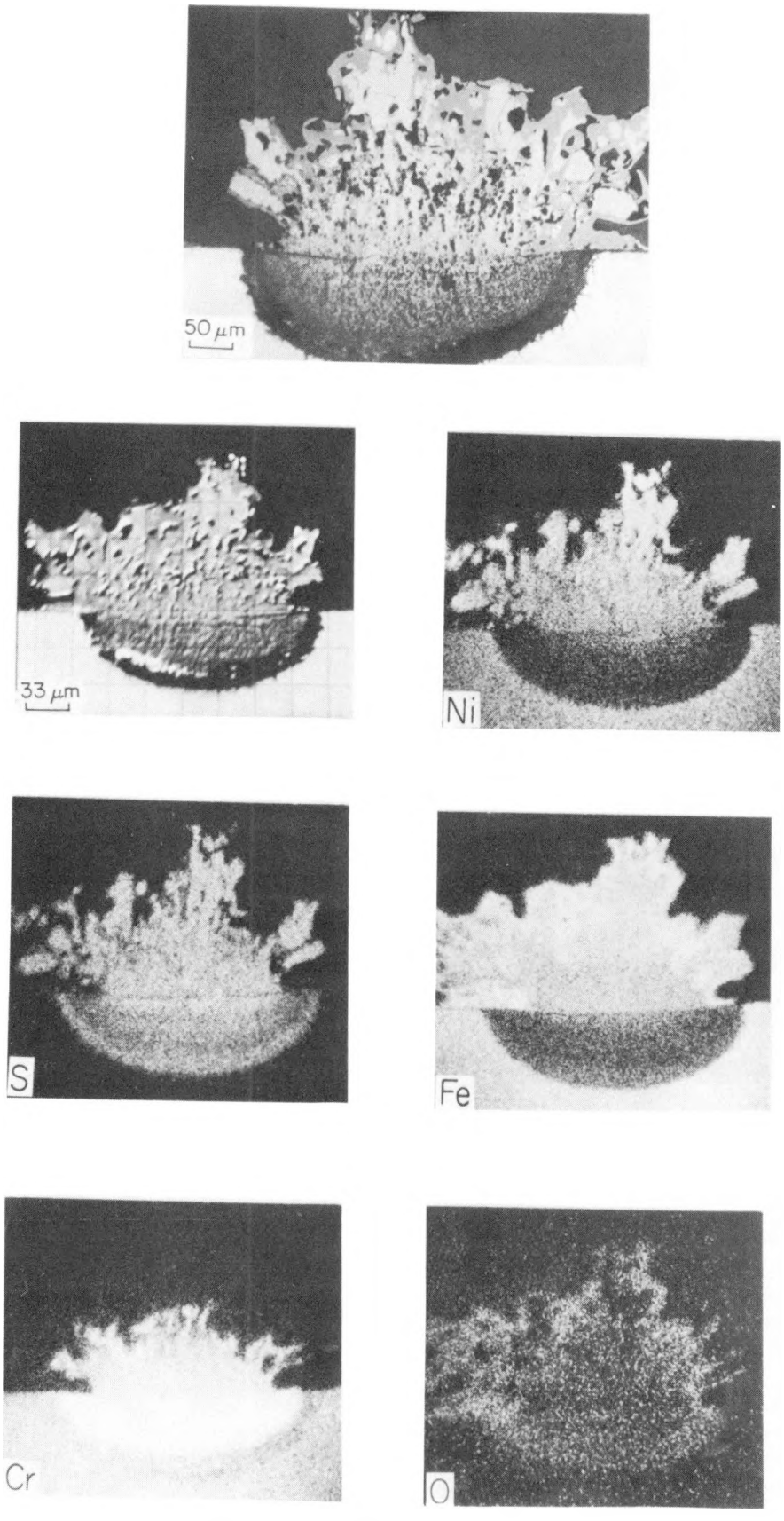
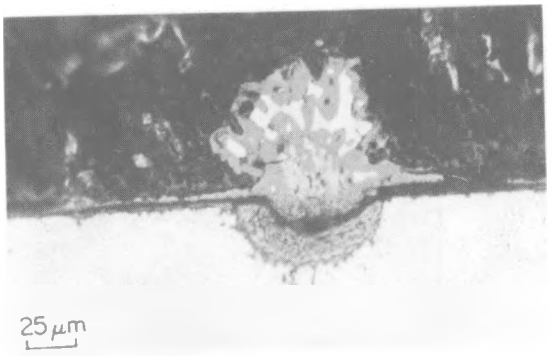
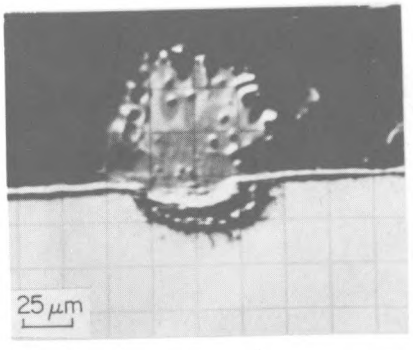
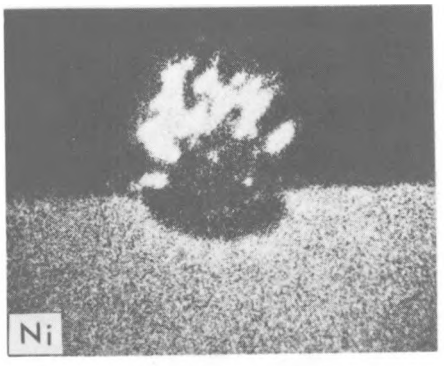


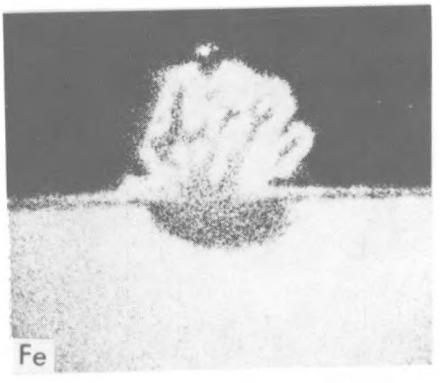
Figure 4-19. AISI 347 Stainless Steel Exposed to Environment A for 0.5 Hour

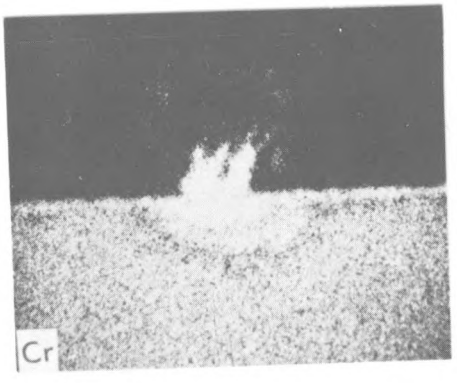












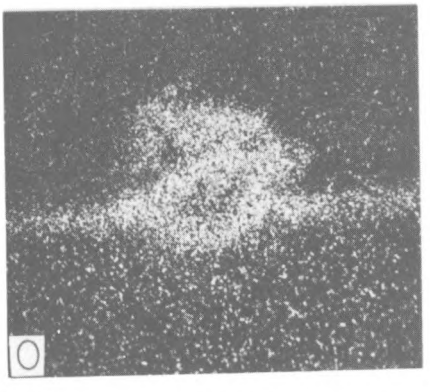


Figure 4-20. AISI 304 Stainless Steel Exposed to Environment A for 0.5 Hour

The two FeCrAlY alloys, on the other hand, did not suffer any initiation of sulfidation, even after 250 hours. Figure 4-21 shows the optical micrographs of specimens of Fe-15Cr-4Al-0.5Y alloy and Fe-25Cr-4Al-1Y alloy exposed for 150 hours. The alloys have formed thin oxide scales with no internal sulfidation attack. Figure 4-22 shows the electron image, and the EDAX-elemental maps for Fe, Cr and Al respectively, of a specimen of Fe-25Cr-4Al-1Y alloy exposed for 23 hours. A continuous aluminum oxide layer is present beneath an iron + chromium oxide layer. Figure 4-23 shows the electron image, and the EDAX-elemental maps for Fe, Cr and Al of a specimen of Fe-15Cr-4Al-0.5Y alloy exposed for 23 hours. Again, a protective aluminum oxide layer is evident.

Environment B: ($PO_2 = 10^{-13}$ atm, $PS_2 = 10^{-5}$ atm). The corrosion behavior of all the alloys in this enviroment was found to be similar to that observed in environment A. However, the extent of corrosion was much less. Figure 4-24 shows the optical micrographs of Incoloy 800H specimen exposed for 0.5, 4, 23 and 70 hours. The outer scale of the specimen exposed for 0.5 hour consisted of a mixture of oxides of iron and chromium and liquid nickel sulfide. Internal precipitates of chromium sulfides have already formed. After 4 hours, the extent of internal sulfidation has increased.

However, the outer scale appears more compact, and nickel sulfide regions seem to have coalesced. After 23 and 70 hours of exposure, the alloy matrix reveals extensive carbide precipitation and internal sulfidation. The outer scale is compact and consists of an outer layer of iron oxide and an inner layer of iron + chromium oxides. Nickel sulfide does not appear to be present. It is likely that the stresses generated due to the growth of iron oxide have resulted in squeezing out the liquid nickel sulfide. Figure 4-25 shows the progress of corrosion on AISI 310 stainless steel exposed for 0.5, 2, 4 and 23 hours. Corrosion initiates in the form of pits (Fig. 4-25a) which then appear to spread laterally producing internal precipitates of chromium sulfide. The external scale consists of an outer iron oxide layer and an inner iron + chromium oxide layer. Unlike the specimens exposed in environment A, nickel sulfide in significant quantities does not appear to form.

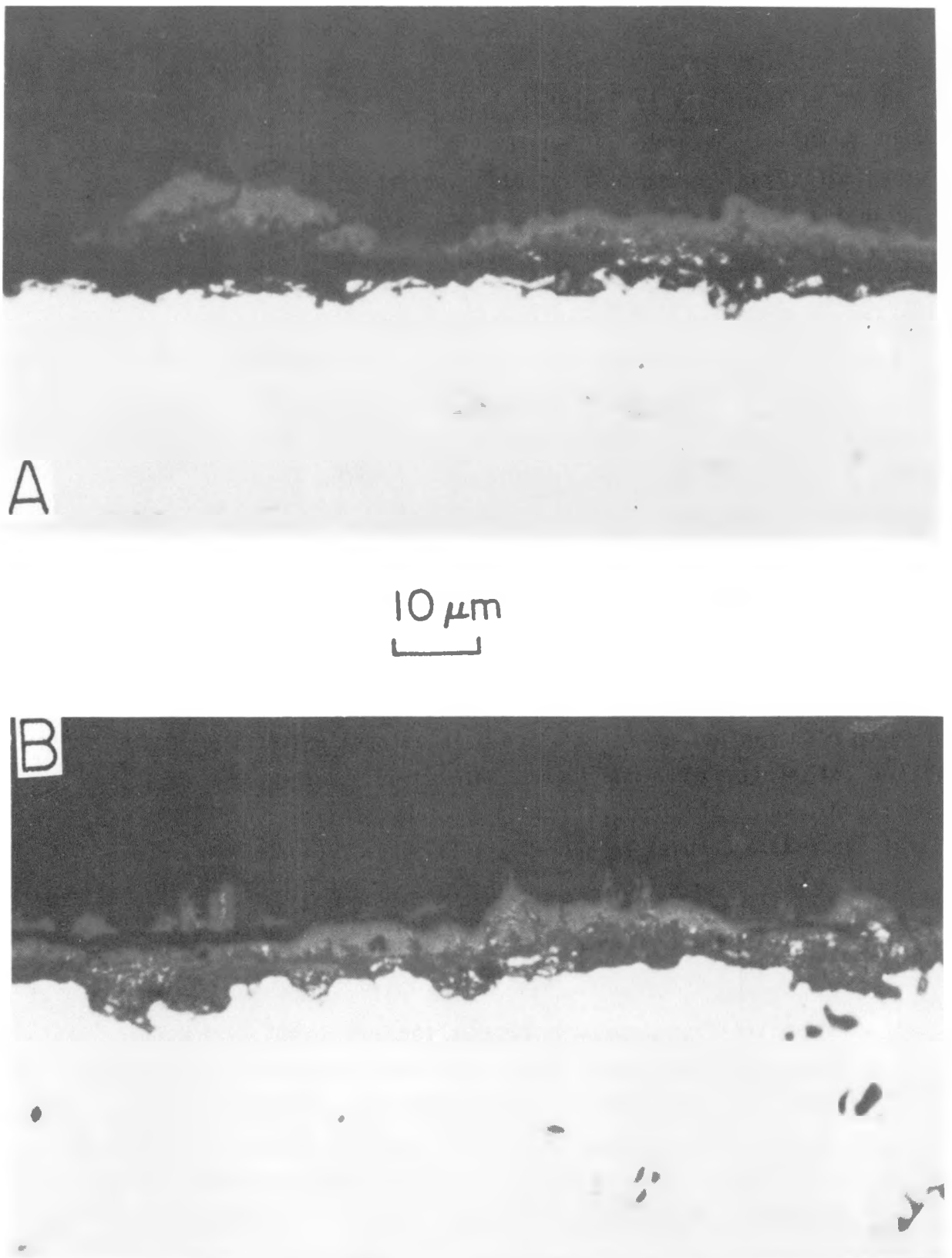


Figure 4-21. Optical Micrographs of Fe-15 Cr-Al-Y (a) and Fe-25 Cr-Al-Y (b) Alloys Exposed to Environment A for 150 Hours

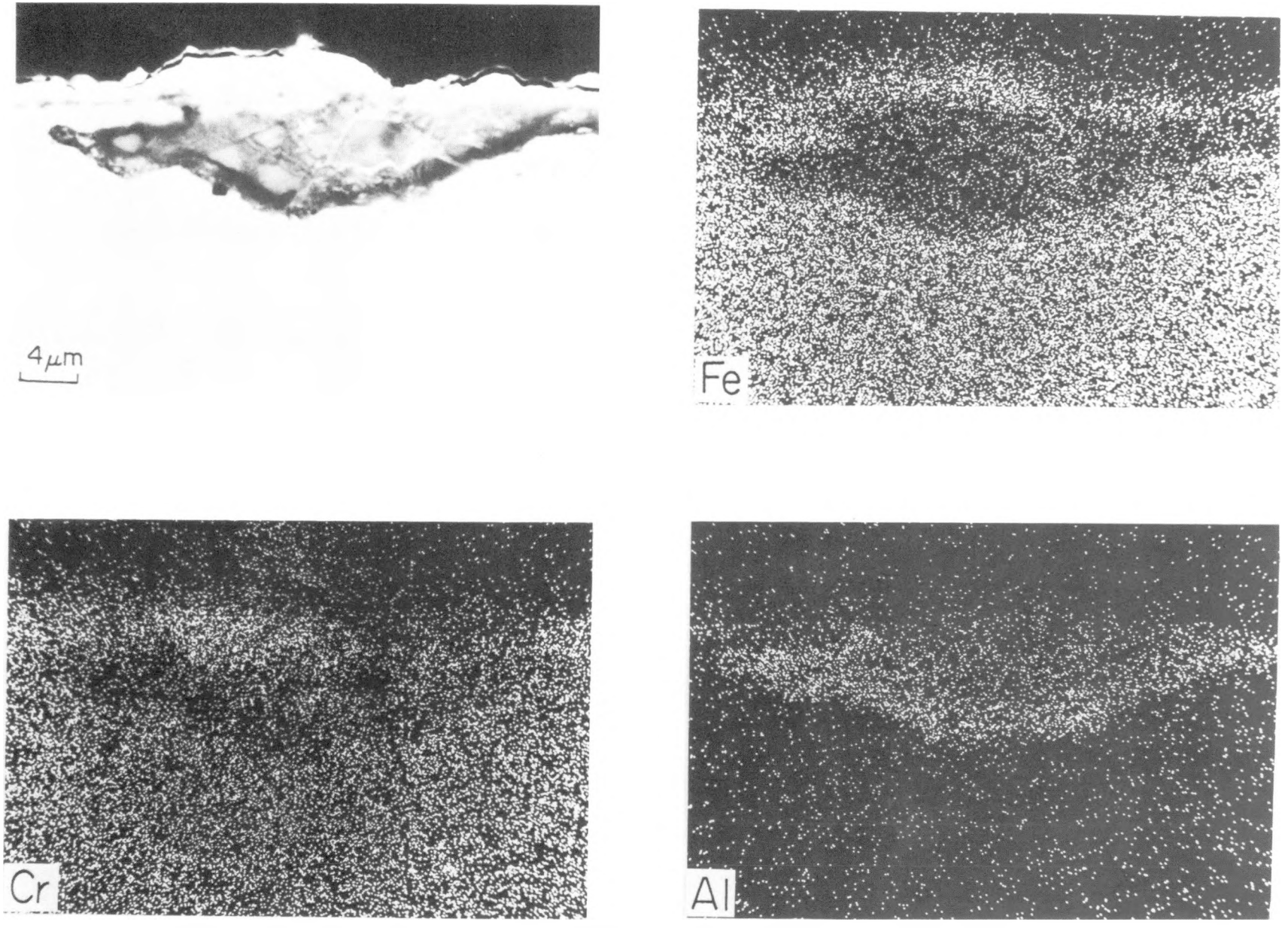


Figure 4-22. Fe-25Cr-Al-Y Alloy Exposed to Environment A for 23 Hours

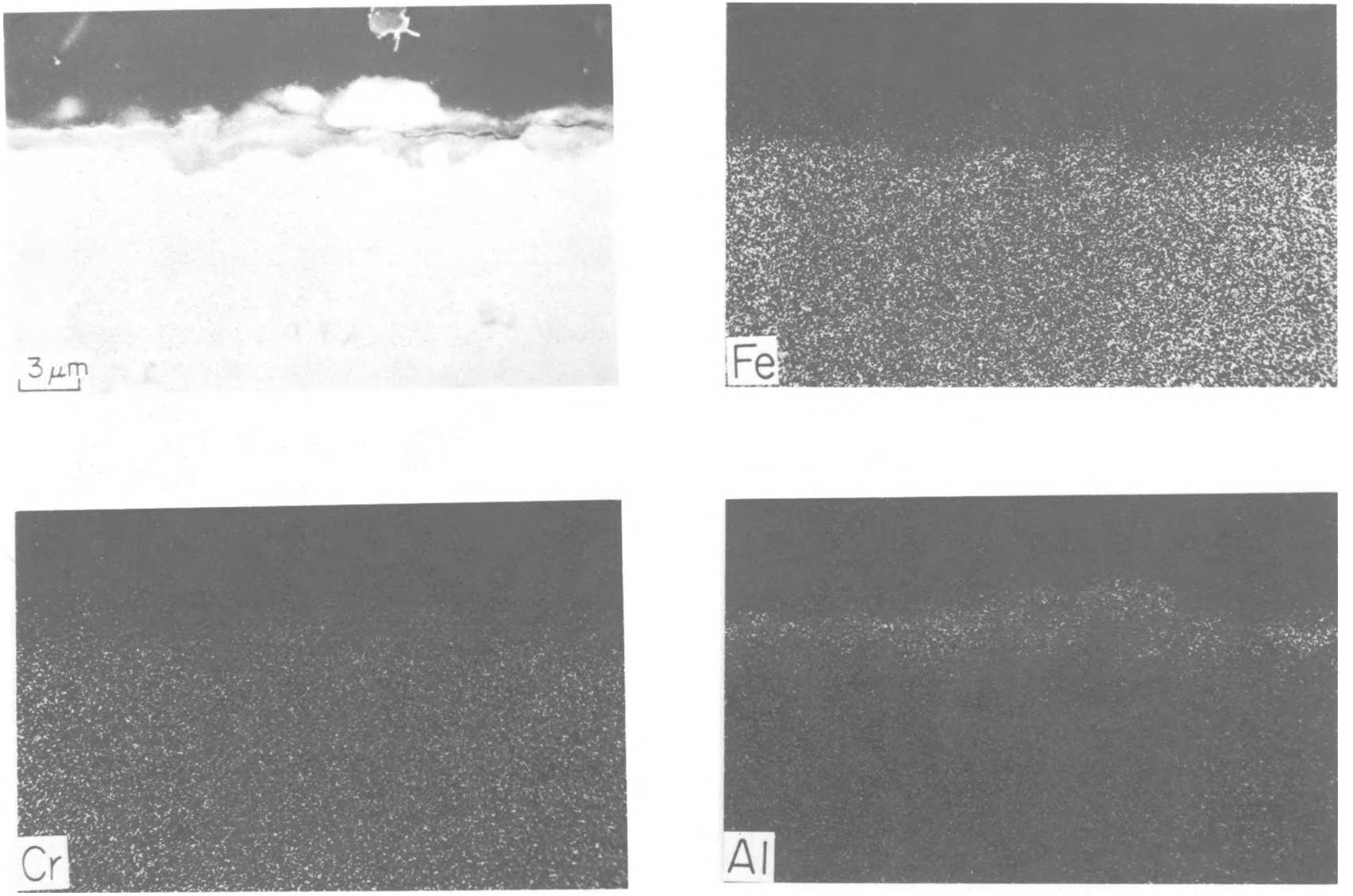


Figure 4-23. Fe-15Cr-Al-Y Alloy Exposed to Environment A for 23 Hours

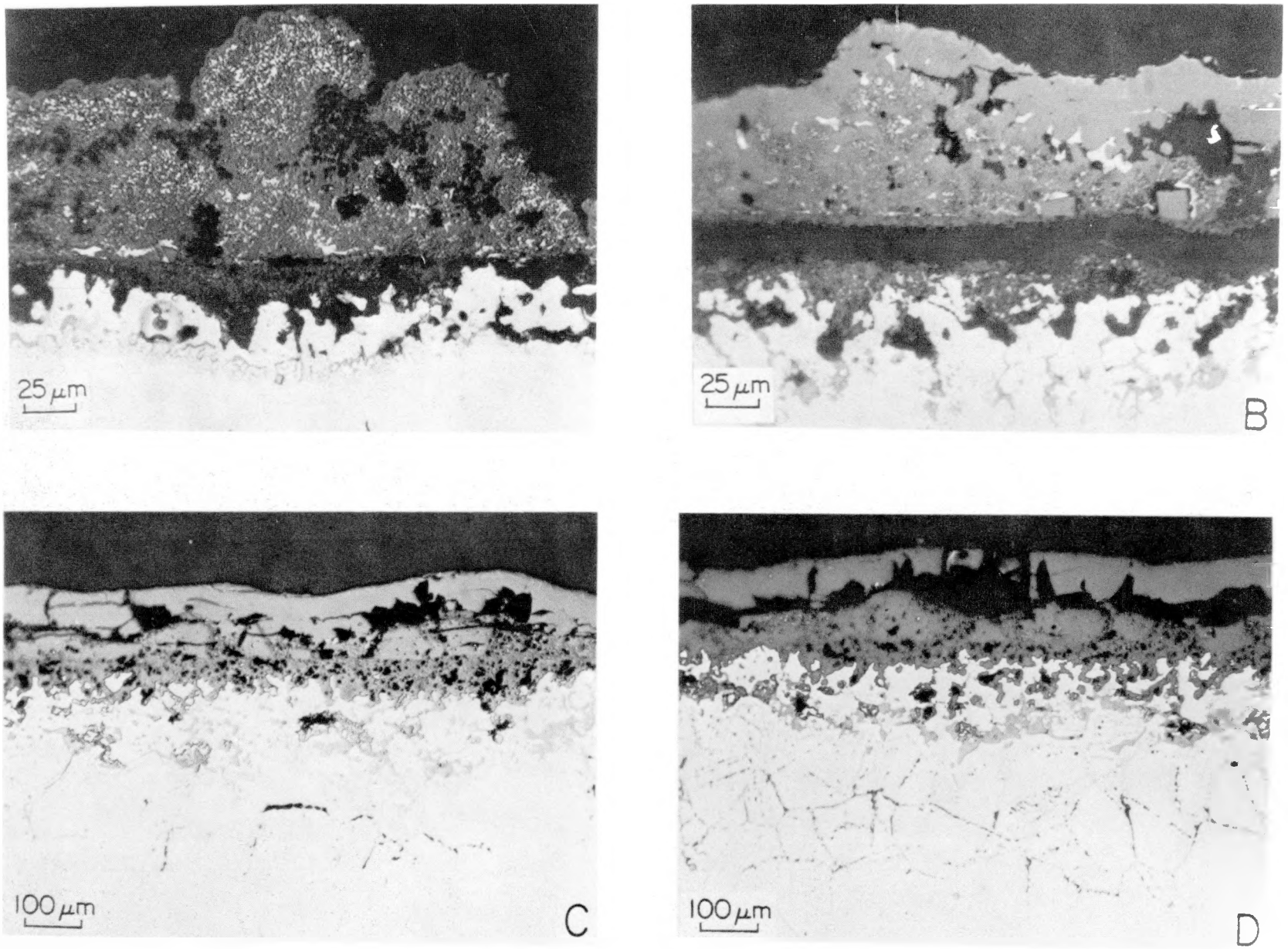


Figure 4-24. Optical Micrographs of Incoloy 800H Exposed to Environment B

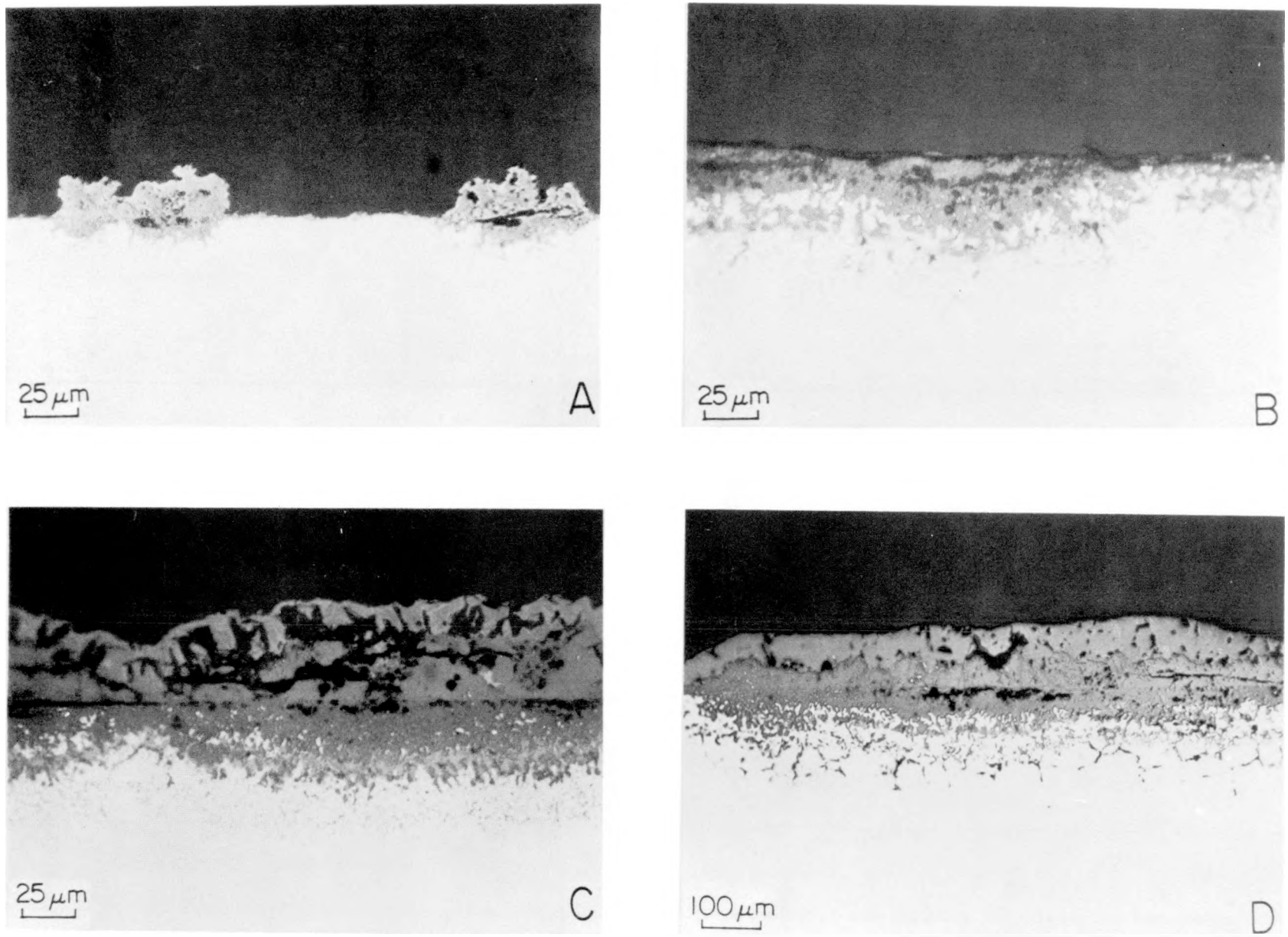


Figure 4-25. Optical Micrographs of AISI 310 Stainless Steel Exposed to Environment B

AISI 304 and 347 stainless steels appeared to be very resistant to sulfidation attack in this environment. However, corrosion occurred in the form of accelerated oxidation. Figure 4-26 shows the optical micrographs of specimens of AISI 304 exposed for 0.5, 4, 23 and 70 hours. Corrosion occurred in the form of pits, which grew in size and number as the exposure time was increased, but there was no evidence of sulfidation attack even after 250 hours. The pits were composed of an external layer of iron oxide and an internal layer of iron + chromium oxide.

The two FeCrAlY alloys did not suffer any initiaiton of sulfidation attack, even after 250 hours of exposure. The alloys formed compact and protective alumina-rich external scales.

Discussion. The corrosion behavior of all the alloys in environments A and B is consistent with the hypothesis proposed earlier regarding the "flux" of SO_2 in the environment which controls the rate of corrosion. Hence it is not surprising that all the alloys corrode more readily in environment A than in environment B.

The results also agree with the scale growth model proposed in Section 4-11. The nickel-containing alloys are susceptible to sulfidation, while the nickel-free FeCrAlY alloys are not susceptible since they form an external scale containing only oxides of Fe, Cr and Al (and no nickel sulfide).

In the nickel-containing alloys, the amount of nickel sulfide formed in the external scale will depend on (1) the nickel content of the alloys as well as (2) the "flux" of sulfur-carrying species in the environment. In other words, the total probability (P) for nickel sulfide formation would be a product of the concentration of nickel (P_1) in the alloy and the concentration of SO_2 in the environment (P_2). Simplistically, $P = P_1 P_2$.

In environment B, where the value of P_2 would be small (since the concentration of SO_2 is low), the value of P would be greatly influenced by P_1 (the concentration of nickel in the alloy). The measured results clearly indicate that while sulfidation occurs within 0.5 hour in the high nickel-containing

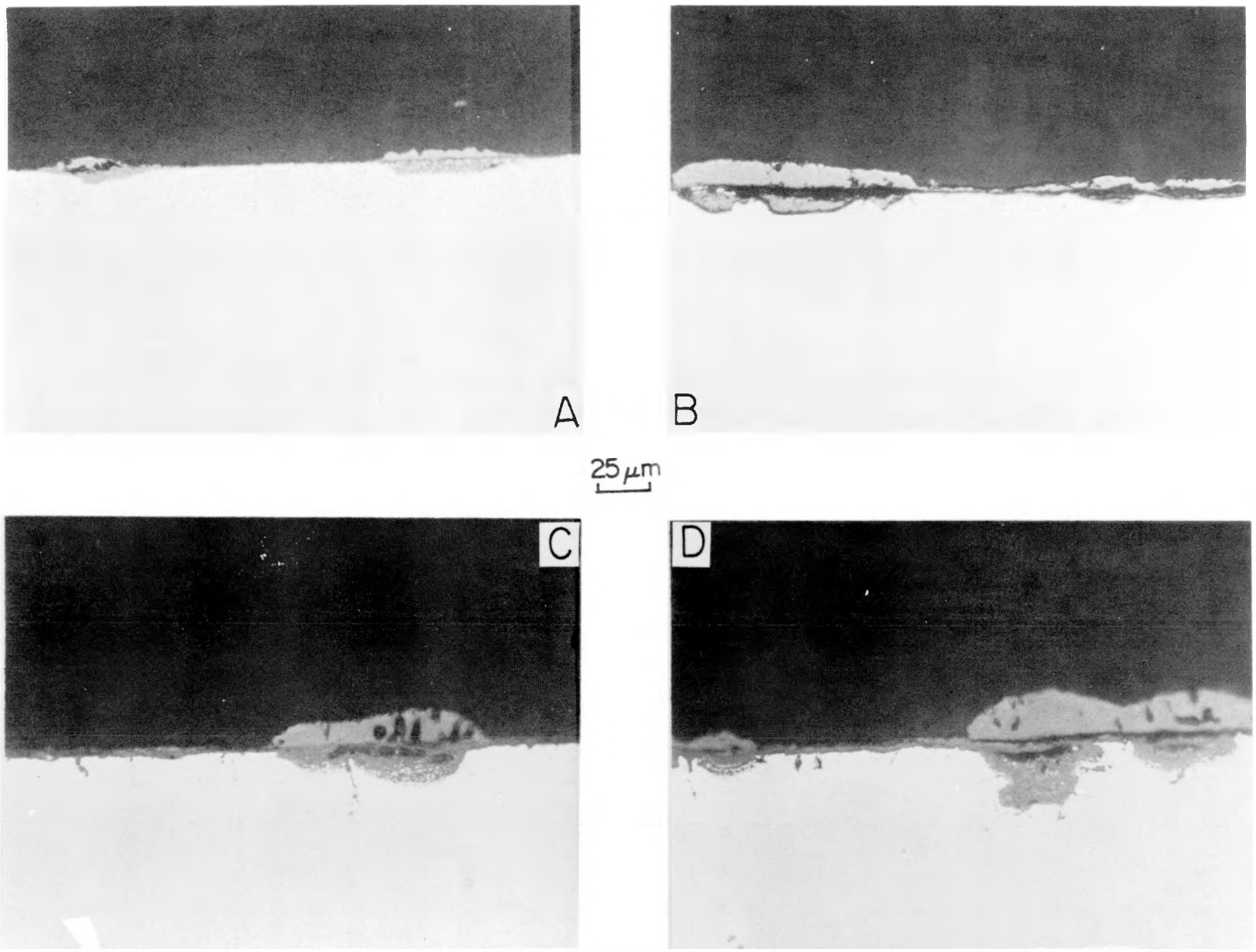


Figure 4-26. Optical Micrographs of AISI 304 Stainless Steel Exposed to Environment B

Incoloy 800H, sulfidation does not occur, even after 250 hours in the low nickel-containing AISI 304 stainless steel. In environment A where the value of P_2 is high (the contraction of SO_2 is high), the value of P would not be expected to be influenced by P_1 (the concentration of nickel in the alloy). The results clearly indicate such a trend: all the nickel-containing alloys sulfidize within 0.5 hour, and the nickel content only affects the rate at which sulfidation attack covers the surface. In high-nickel-containing alloys, the coverage occurs more rapidly than in the low-nickel-containing alloys.

Once sulfidation is initiated, propagation occurs by the classical "sulfidation-oxidation" mechanism (Ref. 4-6). The rate of propagation appears to depend on the amount of sulfur that enters the alloy during initiation.

Conclusions. In the two specific environments studied here, detailed analyses of the corrosion morphologies produced lead to the following conclusions:

- Sulfidation corrosion cannot be initiated in nickel-free alloys, such as the FeCrAlYs, even after 250 hours of exposure.
- Sulfidation corrosion can be initiated in nickel-containing alloys. However, the extent of corrosion depends on the "flux" of SO_2 in the environment and the nickel content of the alloys.
- In the low SO_2-containing environment, higher nickel-containing alloys, Incoloy 800H and AISI 310 stainless steel, suffer sulfidation corrosion while the low nickel-containing alloys AISI 304 and 347 stainless steels do not corrode.
- In the high SO_2-containing environment, all the nickel-containing alloys undergo initiation of sulfidation corrosion.

Hence, the recommended alloys for corrosion protection in these environments are the FeCrAlYs as claddings on stronger substrate alloys and AISI 304 and 347 either as claddings or as tubes.

4.1.3 Sulfidation Corrosion in Oscillating Oxygen and Sulfur Partial Pressure Environments

Measurements have shown that the combustion environment in the fluidized bed can have oscillating oxygen and sulfur partial pressures environments. An experimental program was undertaken to investigate the effects of the oscillating environment on selected heat exchanger materials, and the results were used to develop a morphology of sulfidation corrosion in the oscillating fluidized bed environment.

Background. The in-bed environment of a fluidized bed coal combustor (AFB) is comprised of a well-mixed dense phase of solid particles and a bubble phase which may contain air and/or products of combustion (Ref. 4-11). Recent measurements (Ref. 4-1) of the oxygen content of the in-bed environment of a 24-inch-diameter atmospheric AFB indicate the presence of three distinct regions of fluctuating oxygen composition:

- A region in which the average oxygen content was 3 volume percent with periodic excursions to low levels to 10^{-14} volume percent (at a frequency of approximately 2 Hz).
- A region in which the average oxygen content was 0.3 volume percent, but where the prevailing oxygen content was around 10^{-14} volume percent with periodic excursions to 10 volume percent (again at approximately 2 Hz).
- A region near the walls of the combustor where the oxygen content was found to oscillate between the extreme conditions observed in the two previous regions.

Figure 4-27 illustrates graphically the oxygen partial pressure variation with time in the three regions of the bed, respectively (Ref. 4-1). Similar oxygen partial pressure measurements have been made elsewhere, with similar results (Ref. 4-2 and 4-12).

Despite the general experience of satisfactory corrosion resistance of boiler/heat exchanger tube materials in operating fluidized bed combustors, instances of

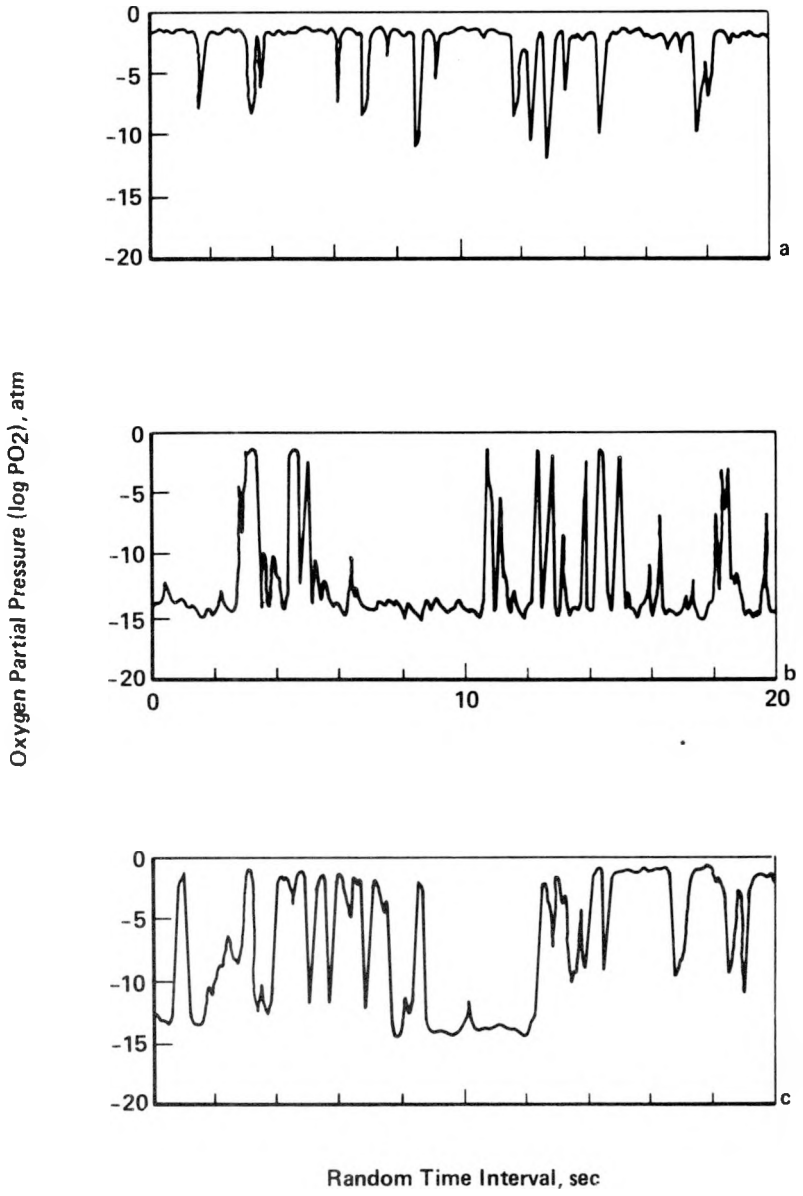


Figure 4-27. Oxygen Partial Pressure Variations in an Operating AFB

severe, local sulfidation-related attack have been reported for nickel-base and iron-base alloys (Ref. 4-13 and 4-14). Such sulfidation-related attack is thought to occur due to the low oxygen content prevailing in the environment. Laboratory studies (Ref. 4-5) simulating such environments have shown that sulfidation can be initiated quite readily (often within 15 minutes of exposure) in most of the nickel- and iron-base alloys. The alloys, during the initial stages of exposure, formed external corrosion-product layers containing mixtures of chromium oxide, iron oxide, and nickel sulfide. Such layers are not protective since rapid diffusion of sulfur (and oxygen) occur through the nickel sulfide. Alloys that do not nucleate nickel sulfide during the initial stages form protective oxide scales. In other words, the events that occur during the early stages of scale development influence the subsequent corrosion behavior.

Since the environment in the AFB is dynamic and fluctuating with respect to its oxygen content, the heat-exchanger tubes in the AFB may initially be exposed, either to the low oxygen content environment or to the high oxygen content environment. If the alloy is initially exposed to the low oxygen content environment, the corrosion product layer would consist of a mixture of chromium oxide, iron oxide, and nickel sulfide. As the oxygen content fluctuates to the high value, thermodynamically, nickel sulfide should get converted into nickel oxide, and the corrosion product layer should consist of a mixture of oxides of chromium, iron, and nickel. It is not known whether such a layer would offer protection as the oxygen content fluctuates back to the lower value. Hence, the issue is whether the "re-oxidized corrosion product layer" offers protection as the oxygen content fluctuates back to the low value. On the other hand, if the alloy is initially exposed to the high oxygen content environment, the corrosion product layer would consist of a mixture of oxides of chromium, iron, and nickel. As the oxygen content fluctuates to the low value, thermodynamically, the nickel oxide can get converted into nickel sulfide. If such a conversion reaction occurred, the critical issue then is whether the "initially formed oxide" layer remains protective as the oxygen content fluctuates to the low value.

To answer these questions, a research program was undertaken and this section describes the results of the findings.

Experimental Procedures. The alloys selected for these experiments are listed in Table 4-3 and represent candidates for high-temperature heat exchanger tubes, and/or tube support structures. Coupons of the alloys (approximately 1 cm x 1 cm x 0.2 cm) were ground to a 600 grit finish, measured, cleaned, degreased and weighed. The coupons were suspended vertically in an airtight ceramic reaction chamber using platinum wire and heated to temperature with a cylindrical tube furnace. The experimental apparatus is illustrated schematically in Fig. 4-28. All of the experiments were conducted at 1650 F, essentially the operating temperature of a typical fluidized bed combustor, and the maximum metal temperature expected in the advanced heat exchanger designs.

The compositions of the gaseous environments used in the corrosion studies are summarized in Table 4-4. These high-temperature equilibrium gas partial pressures were calculated using the initial inlet compositions and the appropriate thermodynamic data. Rotometers and needle valves were used to control the flowrates of the gases, which were mixed and dried at room temperature. Two different gas mixtures, as described in Section 4.1.1, were used to simulate the low PO_2 environment. A mixture of CO_2 and air was used to simulate the high PO_2 environment.

TABLE 4-3. NOMINAL COMPOSITION OF THE HEAT EXCHANGER ALLOYS SELECTED FOR THIS RESEARCH

ALLOY	NOMINAL COMPOSITION, W/O				
	Fe	Ni	Co	Cr	Mo
AISI 304	70	9	0	18	0
AISI 347	70	10	0	18	0
AISI 310	53	20	0	25	0
INCOLOY 800	44	33	0	21	0
HASTELLOY X	19	45	2.5	22	9
INCONEL 617	0	54	12	22	9
INCONEL 671	0	50	0	48	0

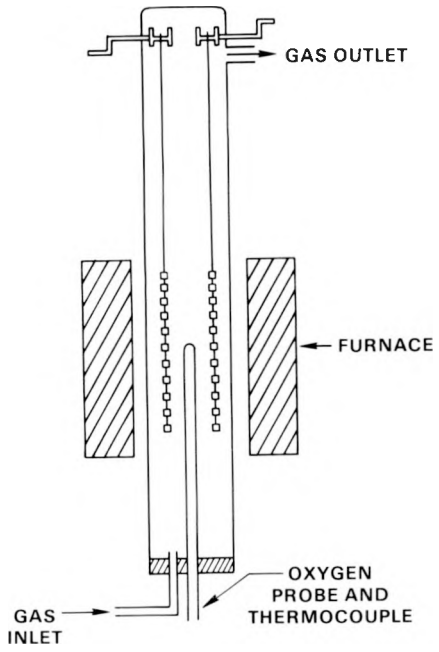


Figure 4-28. Furnace Schematic

TABLE 4-4. HIGH-TEMPERATURE EQUILIBRIUM PARTIAL PRESSURES FOR GAS MIXTURES USED IN THIS RESEARCH (T = 1650 F)

TYPE	INITIAL MIXTURE	PO_2 ATM	PS_2 ATM	PSO_2 ATM
HIGH PO_2 MIXTURE	CO_2 + AIR	10^{-2}	0	0
LOW PO_2 MIXTURE NO. 1	CO_2 + CO + SO_2 + AR	10^{-13}	10^{-5}	10^{-4}
LOW PO_2 MIXTURE NO. 2	CO_2 + CO + SO_2	10^{-11}	10^{-5}	10^{-2}

Oxygen partial pressure measurements in fluidized bed combustors indicate that the ratio of the time spent in the high PO_2 environment to the time spent in the low PO_2 environment varies from 50/50% to 85/15% (Ref. 4-11).

Based on these "time-at-PO_2 ratios", two types of PO_2 cycles were used in the corrosion studies, i.e., 15 minutes high PO /15 minutes low PO_2 and 25 minutes high PO_2/5 minutes low PO_2. The time-at-PO_2 values (5, 15, and 25 minutes) were selected to give PO_2 oscillation frequencies that could be accurately controlled experimentally (PO_2 oscillation frequencies of a few cycles per second are difficult to simulate experimentally.) Also, two different cycling procedures were employed. In the first procedure (low PO_2/high PO_2), the specimens were exposed first to the low PO_2 environment. In the second procedure, the exposure cycles were reversed.

A calcia-stabilized zirconia probe, located in the middle of the hot zone, was used to monitor the oxygen partial pressure of the various gas mixtures. The voltage output from the zirconia probe was plotted with a strip chart recorder for the duration of the experiment. The total exposure time (number of cycles x 30 minutes per cycle) was varied from 30 minutes (1 cycle) to 8 hours (16 cycles). A typical voltage versus time plot is illustrated in Fig. 4-29, indicating a total exposure time of 60 minutes and consisting of two 15-minute low PO_2/15-minute high PO_2cycles.

The experimental procedure consisted of starting the gas flows, adjusting the flowmeters to the required flowrates and PO_2 values, lowering the specimens into the hot zone of the furnace, cycling the gas mixtures at the desired time intervals, and withdrawing the specimens at the end of the desired total exposure time. After exposure, the specimens were reweighed, mounted in epoxy, surface polished, and examined using optical and electron microscopic techniques.

Results.

AISI 310 and Incoloy 800H. These two alloys exhibited essentially identical corrosion behavior during all of the experiments. When they were exposed first

in the high PO_2 environment, they developed an adherent, protective Cr_2O_3 scale. Good protection was maintained throughout all of the low PO_2 exposures at both SO_2 pressures. A few small, isolated pits were usually observed.

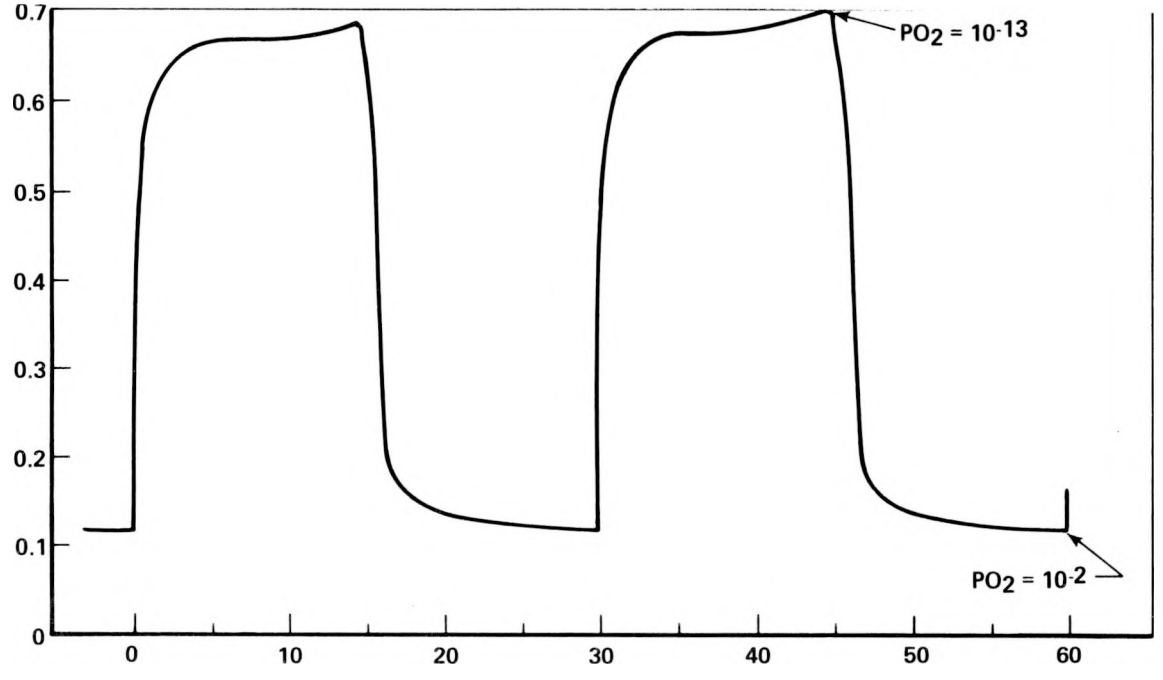


Figure 4-29. Oxygen Probe Voltage Output as a Function of Reaction Time

When these alloys were exposed first to the low PO2 environments, they were severely attacked. Figure 4-30a illustrates the characteristic pit morphology observed on these alloys. Figure 4-30b is the secondary electron image. Figure 4-30c through 4-30f shows the elemental maps for Fe, Cr, Ni, and S, respectively. These maps suggest that the outermost layers are oxides of iron. The innermost layer is a mixed oxide of iron and chromium (presumably $FeCr_2O_4$). Beneath this mixed iron-chromium oxide are internal, intergranular precipitates of chromium-rich sulfides. The number and size of the pits and the amount of internal sulfides increased with increased SO_2 pressure and increased exposure time.

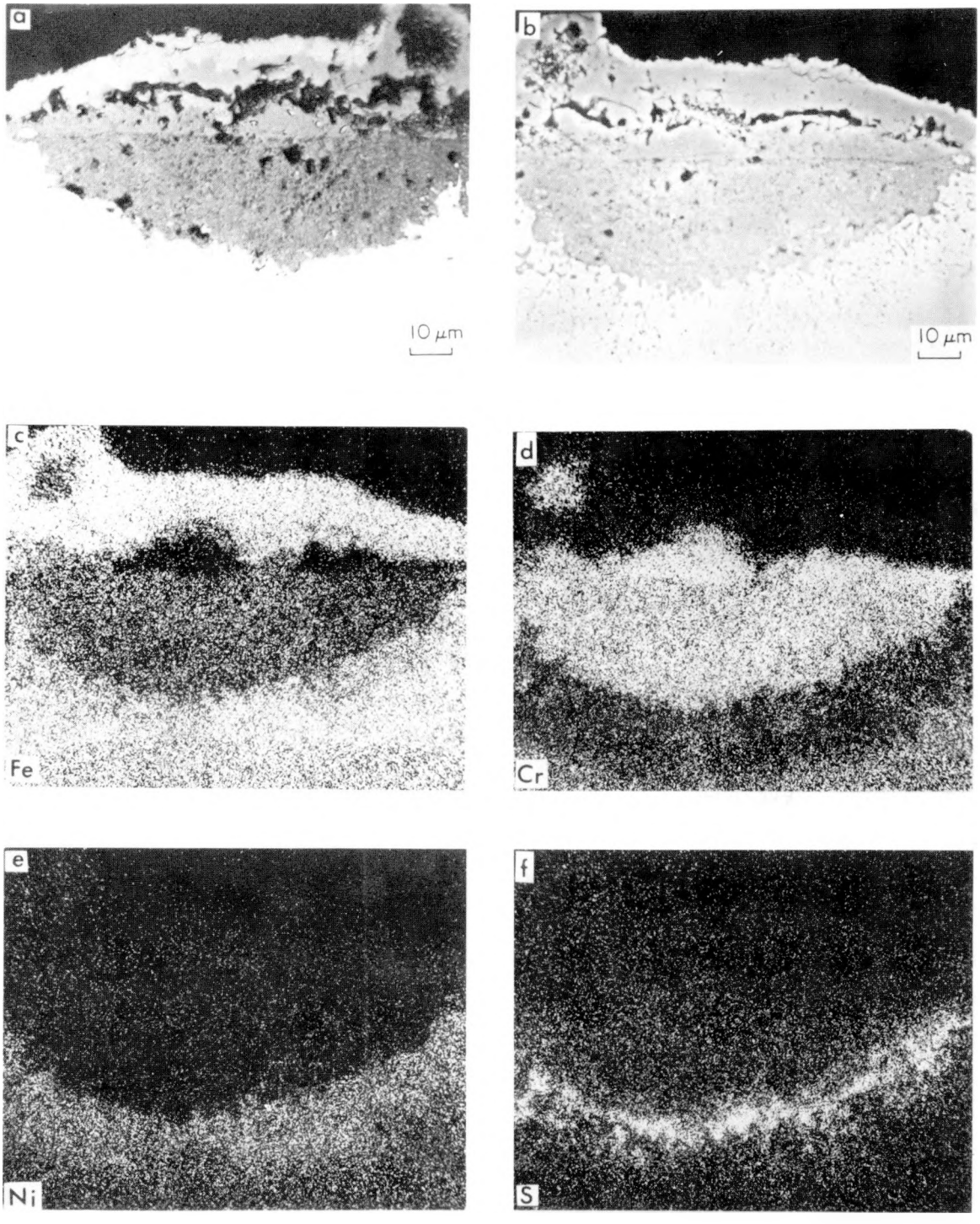


Figure 4-30. Pit Formed on AISI 310 Stainless Steel During 15-Minute Low PO_2/15-Minute High PO_2 Cycle (Total exposure time = 30 minutes)

AISI 304 and 347. These two alloys exhibited almost identical corrosion behavior during all of the experiments. When exposed first in the high PO_2 environment, they developed a thin Cr_2O_3 scale. However, both the 5-minute and 15-minute low PO_2 exposures provided sufficient time to initiate pits in this Cr_2O_3 scale. The number and size of the pits increased with increased SO_2 pressure, and increased exposure time. Figure 4-31 illustrates the characteristic pit morphology observed on these alloys. The corrosion products were very similar to those observed on alloys 310 and 800 (Fig. 4-30a through 4-30f). However, alloys 304 and 347 had extremely small amounts of internally precipitated sulfides, and often none at all.

When these alloys were exposed first to the low PO_2 environments, they developed the same pit morphology, as illustrated in Fig. 4-31. However, the number and size of the pits were greater in these experiments, and again increased with increased SO_2 pressure and increased exposure time and on the external surface) increased with increased SO_2 pressure and increased exposure time.

Hastelloy X. When this alloy was exposed first in the high PO_2 environment, it always developed an adherent, protective Cr_2O_3 scale. Excellent protection was maintained throughout all of the low PO_2 exposures at both SO_2 pressures. A few small, isolated pits were usually observed.

When this alloy was exposed first to the low PO_2 environments, it was severely attacked. The characteristic pit morphology is illustrated in Fig. 4-32. The corrosion product consisted primarily of a mixed oxide of iron and chromium beneath a very thin iron oxide outer layer. Once again, chromium-rich sulfides were precipitated internally at the alloy grain boundaries. The number and size of the pits and the amount of internal sulfides increased with increased SO_2 pressure and increased exposure time.

Inconel 617. The only time this alloy developed and maintained a protective Cr_2O_3 scale was when it was exposed first for 25 minutes in the high PO_2 environment. During the 15-minute high PO_2 exposures, this alloy did no

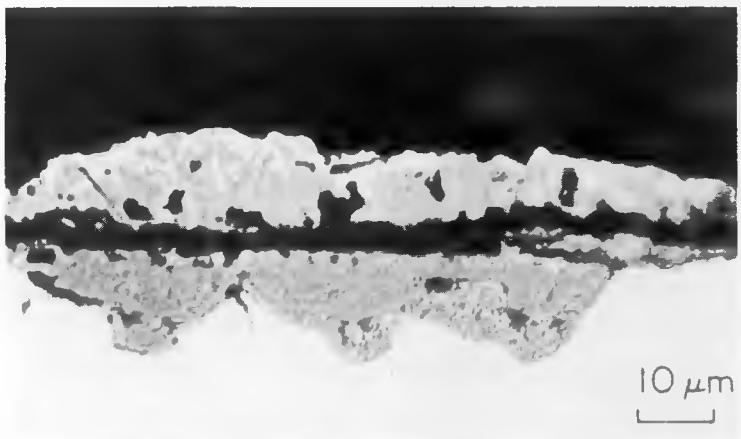


Figure 4-31. Pit Formed on AISI 304 Stainless Steel During 15-Minute High PO_2/15-Minute Low PO_2 Cycles (total exposure time = 2 hours)

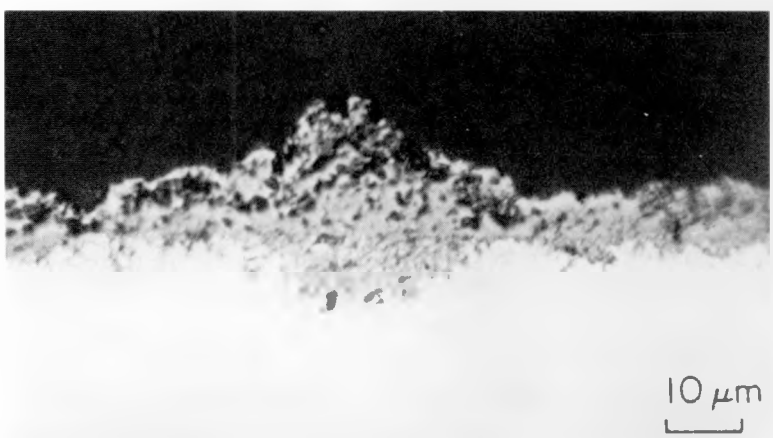


Figure 4-32. Pit Formed on Hastelloy X During 15-Minute Low PO_2/15-Minute High PO_2 Cycle (total exposure time ≤ 30 minutes)

develop a protective scale which could withstand the low PO_2 exposures. The alloy was severely attacked in every experiment. Figure 4-33a illustrates the characteristic pit morphology observed on this alloy. Figure 4-33b is the secondary electron image. Figure 4-33c through 4-33f shows the elemental maps for Ni, Cr, Co, and S, respectively. Based on these maps, the thin outermost layer of the pit is a mixture of nickel and cobalt oxide. The white area under the thin oxide layer is nickel sulfide, which would have been molten at the reaction temperature, resulting in the spherical or "droplet" morphology observed. Beneath the sulfide droplet is a chromium oxide phase (presumably Cr_2O_3), and a mixed oxide plus nickel sulfide region. Once again, chromium-rich sulfides have precipitated at the bottom of the pit along the grain boundaries of the alloy. The same pit morphology was observed on all the specimens, regardless of the cycle procedure. The number and size of the pits, and the amount of sulfide formation (both internal and on the external surface) increased with increased SO_2 pressure and increased exposure time.

Inconel 671. When this alloy was exposed first to the high PO_2 environment, it always developed and maintained a protective Cr_2O_3 scale. When it was exposed first to the low PO_2 environment, very inconsistent behavior was observed. Sometimes a thick, protective Cr_2O_3 scale was developed, as illustrated in Fig. 4-34. In other cases, very severe attack was observed, particularly at the higher SO_2 pressure. Figure 4-35a illustrates the corrosion products observed on this alloy when exposed first to the low PO_2 environment with the higher SO_2 pressure. Figure 4-35b is the secondary electron image of the right-hand portion of Fig. 4-35a. Figure 4-35c through 4-35e shows the elemental maps for Cr, Ni and S. The corrosion product consists primarily of sulfides of nickel and chromium. The external layer is nickel sulfide with some chromium sulfide and long stringers of chromium oxide. The internal layer is predominantly chromium sulfide.

Discussion. The following summarizes the cyclic elevated temperatures results.

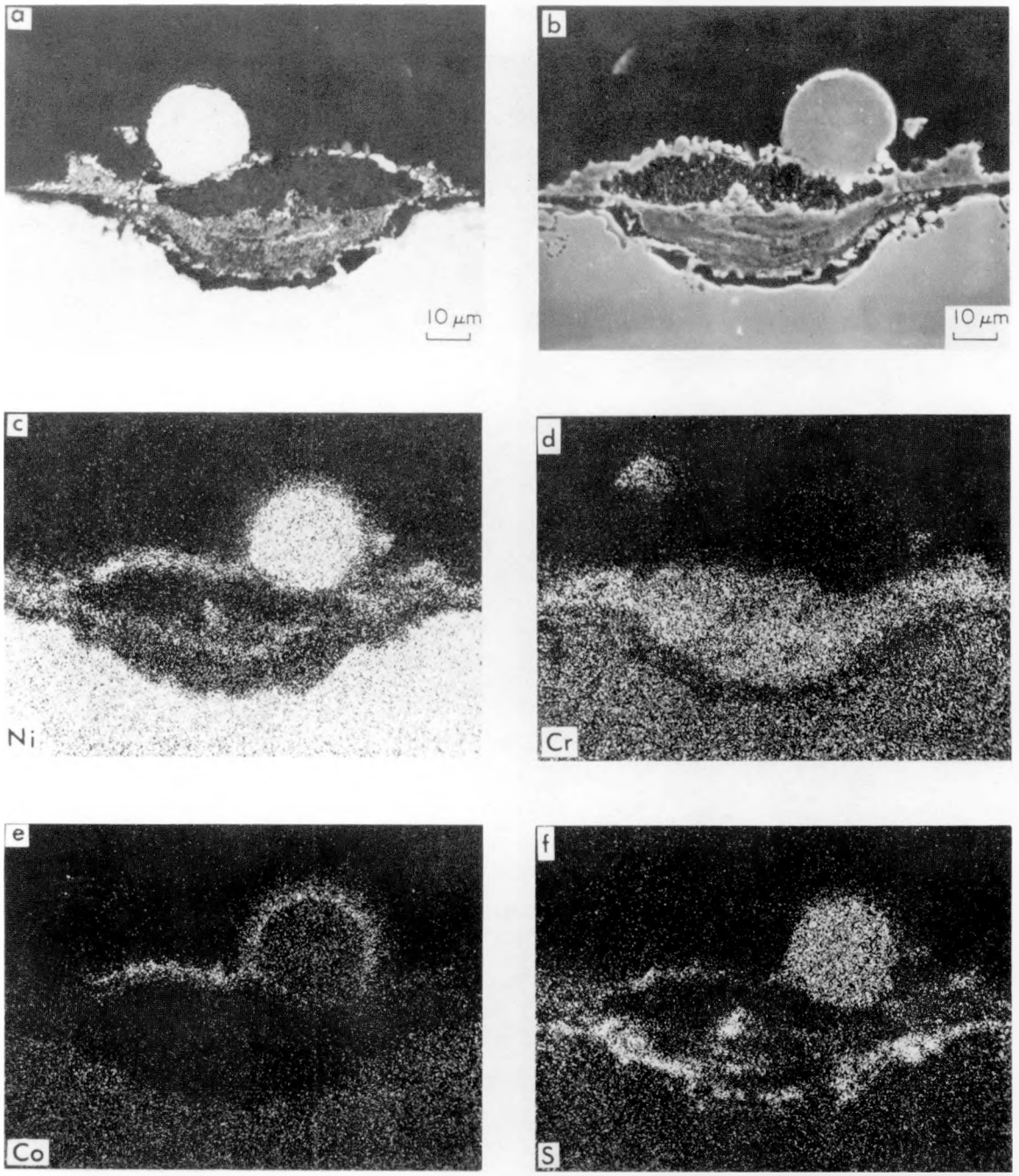


Figure 4-33. Pit Formed on Inconel 617 During 15-Minute High PO_2/15-Minute Low PO_2 Cycles (total exposure time = 1 hour)

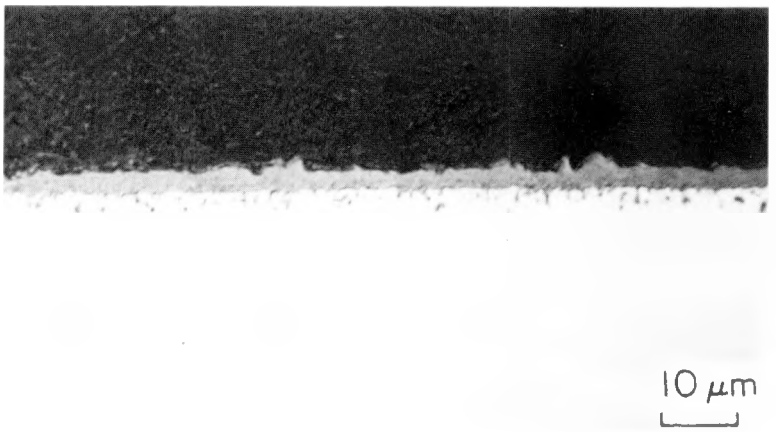


Figure 4-34. Scaled Formed on Inconel 671 During 15-Minute Low PO_2/ 15-Minute High PO_2 Cycles (total exposure time = 1 hour)

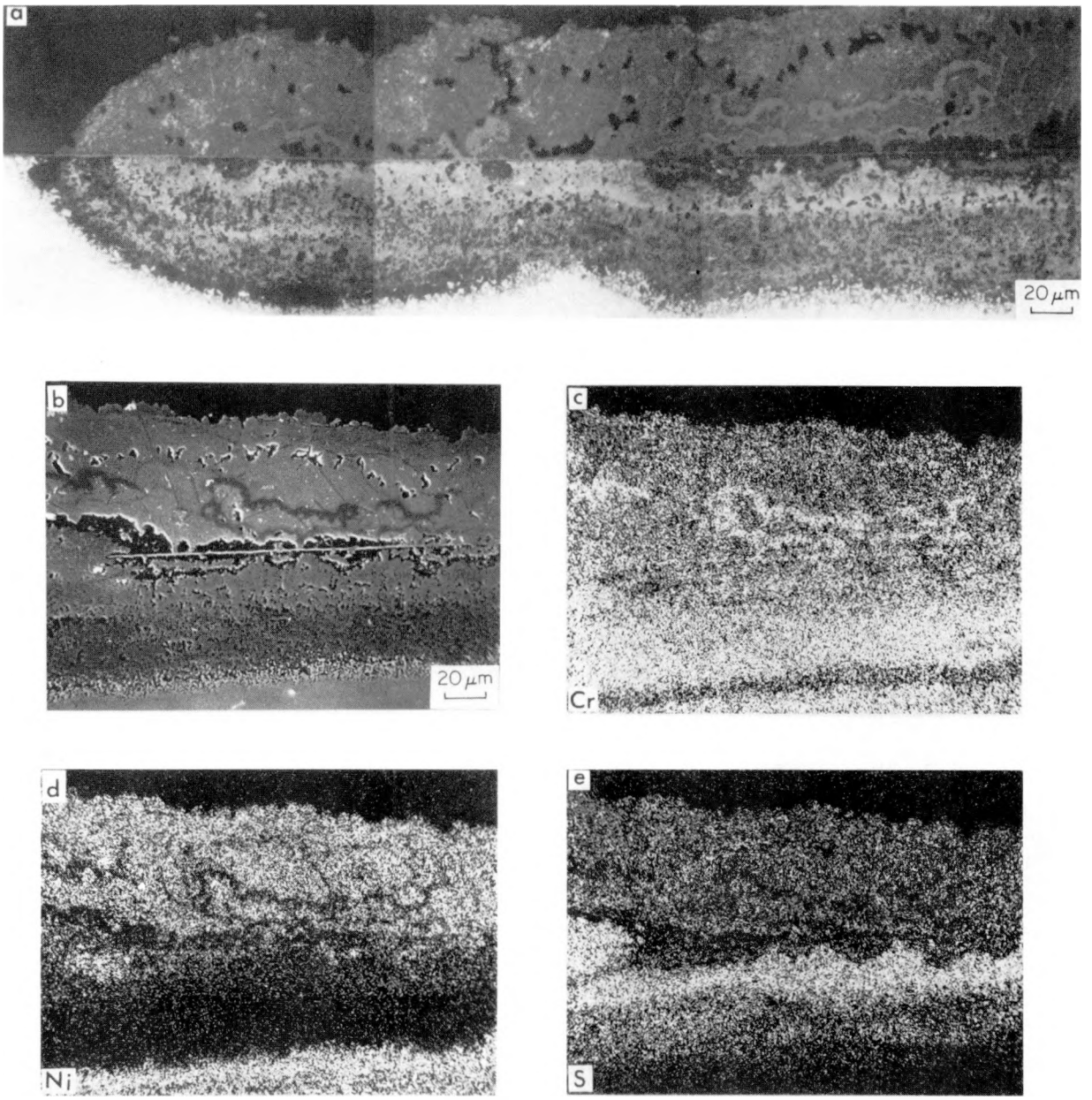


Figure 4-35. Pit Formed on Inconel 671 During 15-Minute Low PO_2/15-Minute High PO_2 Cycles (total exposure time = 2 hours)

High PO_2/Low PO_2 Experiments. When exposed first in the high PO_2 environment, all of the alloys developed a Cr_2O_3-rich scale. In general, the protective nature of this "initially formed oxide" scale in the low PO_2 environments depended on two factors: the initial chromium content of the alloy and the amount and type of other "active" alloying elements. The other active metals (Fe, Co, Ni) form oxides during the initial stages of oxidation, which can be beneficial or harmful during the subsequent low PO_2 exposures.

The first effect, chromium content, is easily understood and well documented (Ref. 4-15). Generally, alloys that rely on an adherent, protective Cr_2O_3 scale for high-temperature oxidation resistance require a certain minimum chromium content, which varies with alloy system, temperature and, to some extent, alloy structure. At the temperature of interest, the minimum chromium content lies in the region of 20% for Ni-Cr alloys, and somewhat less for Fe-Cr alloys, apparently because of the wide range of stoichiometry of $FeCr_2O_4$. The alloys containing less than 20% Cr (304 and 347) exhibited fair to poor resistance to pitting during the low PO_2 exposures. However, alloys containing greater than 20% Cr (310, 800, Hastelloy X, and 671) exhibited good resistance to pitting during the low PO_2 exposures.

The only exception was Inconel 617, which exhibited very poor resistance to pitting and internal attack during the low PO_2 exposures. This is attributed to the second factor, the harmful effects of transient metal oxides. When initially oxidized in the high PO_2 environment, the surface of the alloy is expected to be covered with nuclei of all the oxidizable elements in the alloy, probably in proportion to their content in the alloy. The fast-growing transient oxide nuclei soon cover the slower growing Cr_2O_3 nuclei. If protective behavior is to be established, the Cr_2O_3 nuclei will have to grow laterally and impinge to form a continuous Cr_2O_3 scale beneath the transient oxides, which stop growing. When this layered scale is exposed to the low PO_2 environments, the transient oxides may convert to the more stable sulfides, depending on thermodynamic considerations.

In the case of 617, the transient oxides will consist essentially of NiO and CoO. At the reaction temperature and oxygen/sulfur partial pressures in the low PO_2 exposures, the sulfides of Co and Ni are the stable species (the oxides of Fe are still stable, however). The sulfides CoS and NiS will melt, possibly penetrating grain boundaries and cracks in the Cr_2O_3 scale and providing paths for rapid sulfur penetration into the base alloy. This could result in the formation of chromium-rich sulfides in the grain boundaries of the alloy. This process would result in the morphology observed in Fig. 4-32. All of the other alloys (except 671) contained enough iron to form a somewhat continuous iron oxide layer on top of the Cr_2O_3 scale during the initial stages of oxidation. This iron oxide layer would remain stable (i.e., would not convert to a sulfide) during the low PO_2 exposures, and the Cr_2O_3 scale would remain protective.

The pitting of the relatively low chromium alloys (304 and 347) during the low PO_2 exposures appears to be caused by the formation of a mixed oxide of iron and chromium beneath the transient oxide, as opposed to the desired Cr_2O_3 scale. This is illustrated in Fig. 4-31. The formation and continued growth of this mixed oxide would leave the affected areas of the alloy unprotected and susceptible to deep pitting.

Low PO2/High PO2 Experiments. When exposed first in the low PO_2 environment, all the alloys developed external scales consisting of a mixture of Cr_2O_3, iron oxide (in iron-containing alloys) and NiS (along with CoS in the cobalt-containing alloy). These scales were not protective and all the alloys exhibited corrosion. The extent of corrosion depended on the alloy type, the exposure time, and the partial pressure of SO_2 in the environment. The 15-minute exposure cycle and the higher PSO_2 environment produced greater corrosion.

As the environment was changed to the high PO_2 gas, nickel sulfide (formed during exposure to the low PO_2 gas) did not appear to be rapidly converted into nickel oxide. A thin film of nickel oxide covering the liquid nickel sulfide droplet as seen in Fig. 4-33, might have been acting as a barrier between the

gaseous environment and the nickel sulfide, thus slowing down the conversion reaction. The fact that corrosion persists after exposure to the high PO_2 environment is a clear indication that the "re-oxidized corrosion product layer" is not protective.

Conclusions.

1. All the alloys tested are susceptible to accelerated attack when exposed to the simulated oscillating oxygen partial pressure environments encountered in fluidized bed combustors.
2. When exposed to the high PO_2 environments first:
   a. AISI 310, Incoloy 800, Hastelloy X, and Inconel 671 developed protective Cr_2O_3 scales which exhibited good pitting resistance in the low PO_2 environments.
   b. AISI 304, AISI 347, and Inconel 617 developed Cr_2O_3 scales which exhibited fair to poor resistance to pitting in the low PO_2 environments.
3. When exposed to the low PO_2 environments first, all of the alloys were severely attacked.
4. In general, the iron-base alloys (or alloys containing greater than 20% Fe) exhibited better resistance to attack than the nickel-base alloys, apparently because of the formation of solid iron oxides in the former, compared to molten nickel sulfides in the latter, which reduced the flux of sulfur into the alloy.
5. The morphology of attack for a given alloy was similar under both conditions of low PO_2/high PS_2, but the severity of attack increased with increased SO_2 partial pressure and increased exposure time.

4.1.4 Corrosion of Advanced Materials in Simulated AFB Deposits

The corrosion behavior of a number of candidate heat exchanger tube alloys (Table 4-3) in the substoichiometric combustion enviroments of a fluidized bed combustor (AFB) was discussed in Sections 4.1.1 to 4.1.3. The susceptibility to sulfidation attack was related to the ease of formation of nickel sulfide on the

surface of the alloys, which were in intimate contact with the combustion gases. However, in actual fluidized bed combustors, the alloys are not in intimate contact with the combustion gases because of the formation of a dense deposit of the bed materials on the alloy surfaces. It has been suggested that the quasi-equilibrium conditions established between the deposit and the gaseous equipment might influence the corrosion reactions (Ref. 4-16). Hence, a laboratory research program was undertaken to investigate the influence of the bed materials on the overall corrosion behavior of the selected alloys (Table 4-5).

TABLE 4-5. NOMINAL COMPOSITIONS OF ALLOYS IN WEIGHT PERCENT

ALLOY	Fe	Ni	Cr	Co	Al	OTHERS
INCONEL 617	0	BAL	22	12	1	9 Mo
INCONEL 618E	16	BAL	23	0	0	6 W
HASTELLOY X	19	BAL	22	2.5	0	9 Mo
PE-13	19	BAL	22	2.5	0	9 Mo
NIMONIC 86	0	BAL	25	0	0	10 Mo
INCOLOY 800	44	33	21	0	0.5	
AISI 310	BAL	20	25	0	0	
AISI 304	BAL	8	18	0	0	
AISI 347	BAL	10	18	0	0	Nb + Ta
FeCrAlY - TYPE 1	BAL	0	25	0	4	1 Y
FeCrAlY - TYPE 2	BAL	0	15	0	4	0.5 Y

Rationale for the Corrosion Experiments. Results of a recent study (Ref. 4-17) where a number of iron and nickel-base alloys were exposed in air, to mixtures of bed materials (CaO and $CaSO_4$), indicated that sulfidation-related corrosion did not occur even after 1000 hours of exposure. It was proposed that the equilibrium sulfur pressure that could be generated by the interaction of the bed materials with the gaseous enviroment (PO_2 = 0.2 atm) was so low (PS_2 = 10^{-30} atm) that sulfidation-related corrosion could not occur. However, the equilibrium sulfur partial pressures that can be generated by the interaction of

the bed materials with the substoichiometric combustion gases can be high enough to cause serious sulfidation-related corrosion problems.

Figure 4-36 shows the Ca-O-S phase stability diagram plotted at 1650 F in which the two selected test conditions are represented by points A and B. The oxygen partial pressure corresponding to point A is approximately 10^{-11} atm. If equilibrium prevails between the bed materials (CaO and $CaSO_4$) and the gaseous enviroment (CO and CO_2), the sulphur partial pressure in the environment will be approximately 10^{-5} atm. The phase stability diagram also reveals that if the oxygen partial pressure in the enviroment is below 10^{-12} atm, $CaSO_4$ can no longer be stable. Instead, CaS becomes a stable compound and the bed materials should consist of a mixture of CaS and CaO. Hence, point B represents an environment where the gaseous mixture, CO and CO_2, is in contact with CaO and CaS and, if equilibrium is maintained, the sulfur partial pressure will be approximately 10^{-5} atm. Both conditions represent environments where rapid sulfidation attack of heat exchanger tube alloys can occur quite readily. Furthermore, the selected conditions represent environments which are close to the enviroment represented by the triple point in the phase stability diagram (corresponding to the CaS-CaO-$CaSO_4$ equilibrium in the Ca-O-S phase stability diagram), whose sulfur partial pressure, thermodynamically, is the maximum that is attainable with the bed materials in the combustor.

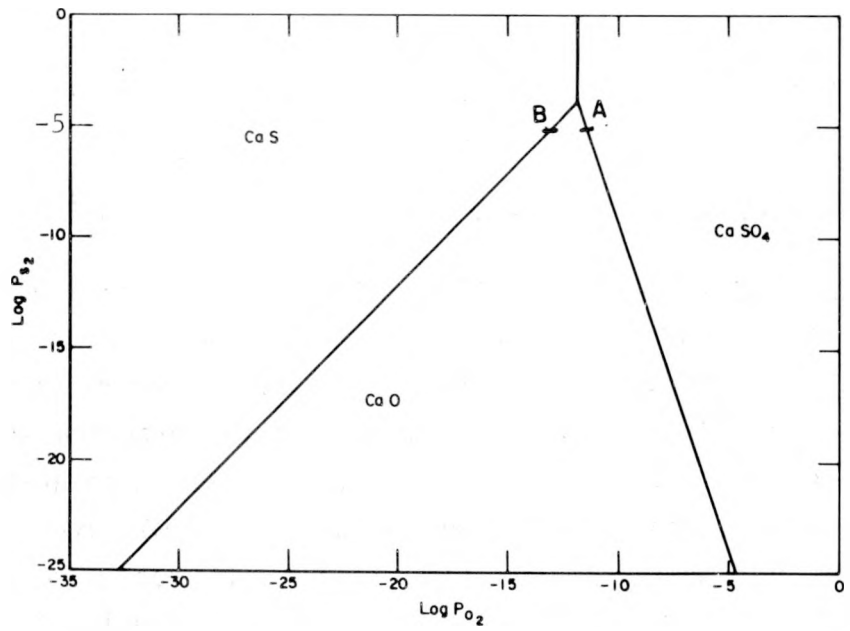


Figure 4-36. The Ca-O-S Phase Stability Diagram at 1650 F

Experimental Procedure. A laboratory tube furnace (as shown in Fig. 4-37) with a constant temperature zone was used to carry out the experiments and was equipped with a calcia-stabilized zirconia tube, which was used to measure the oxygen partial pressure of the furnace enviroment. Metered amounts of CO and CO_2 were used to control the PO_2 of the environment and the total flowrate of the gases was approximately 1000 cc/min.

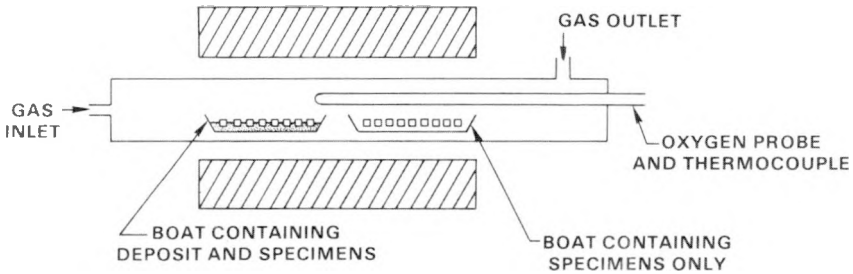
The corrosive conditions employed for the experiments are listed in Table 4-6. All the experiments were conducted at 1650 F, the typical bed temperature, for times of 24, 50, 120, and 320 hours.

TABLE 4-6. CORROSIVE CONDITIONS

ENVIRONMENT	DEPOSIT	GASES	CONTROLLED PO_2 ATM	ANTICIPATED EQUILIBRIUM PS_2, ATM
A	CaS/CaO	CO, CO_2	10^{-13}	10^{-5}
B	CaO/$CaSO_4$	CO, CO_2	10^{-11}	10^{-5}

The deposit mixtures were prepared by blending equimolar mixtures of CaS and CaO, and CaO and $CaSO_4$. Alumina boats were filled with the synthetic deposit mixtures and coupons (1 cm x 1 cm x 0.2 cm) of the alloys, surface ground to 600 grit finish, were immersed vertically in the deposit. The boats were then introduced into the hot zone of the tube furnace and the gas flow was initiated. After the completion of each run, the boats were quickly withdrawn from the hot zone of the furnace and were allowed to cool. The specimens were reweighed after exposure and then were mounted for metallographic examination. The polished cross sections were analyzed using an optical microscope; electron microprobe analysis was carried out on selected specimens to identify the corrosion products.

Results. Of the alloys investigated, the two FeCrAlY claddings did not suffer any initiation of sulfidation attack. Instead, these alloys formed protective oxide scales, as shown in Fig. 4-38. The other alloys showed various indications of sulfidation attack, with the extent of sulfidation depending on alloy and deposit chemistry.



SCHEMATIC OF THE LABORATORY EXPERIMENTAL ARRANGEMENT

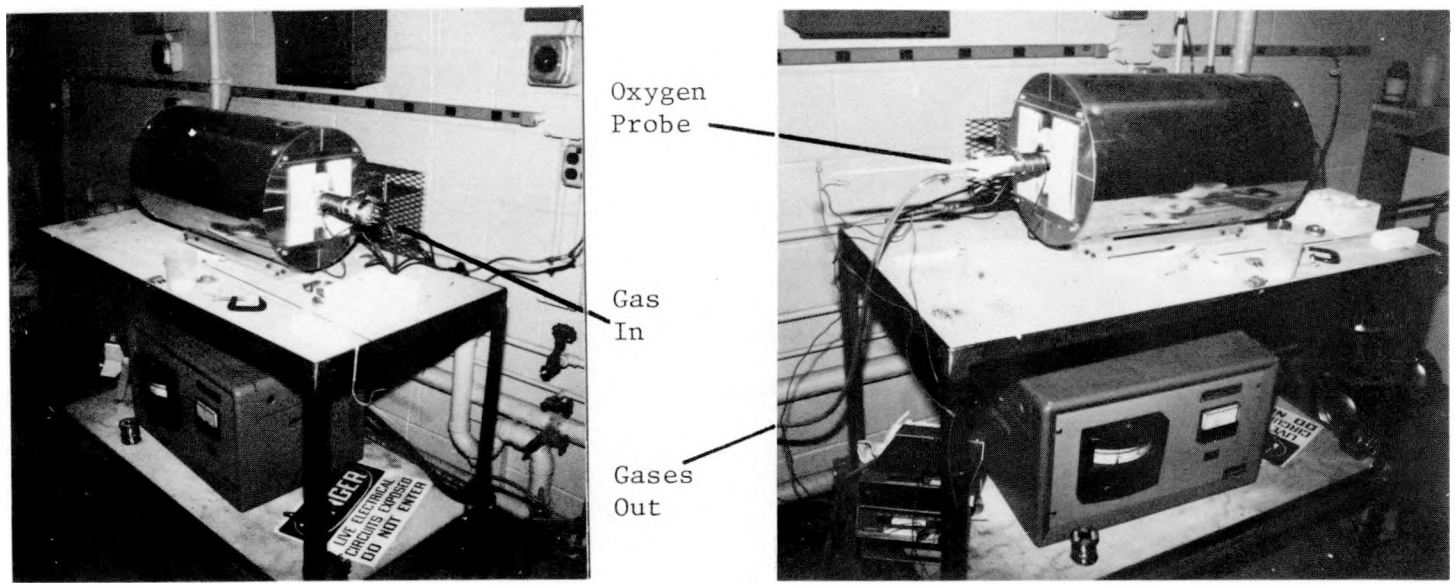


Figure 4-37. Laboratory AFB Metals Testing Furnace for Exposure to Simulated Deposits



Figure 4-38a. Fe-25Cr-4Al-1.0 Y Exposed to the $CaO/CaSO_4$ Deposit for 320 Hours

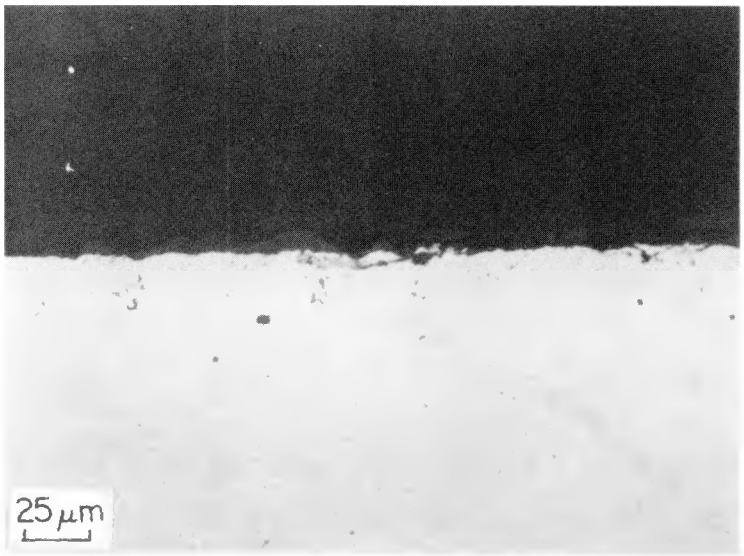


Figure 4-38b. Fe-15Cr-4Al-0.5 Y Exposed to the CaS/CaO Deposit for 320 Hours

The high-strength nickel-base alloy, Inconel 617, was found to undergo sulfidation corrosion in both deposits, producing similar morphological features in each case. However, in the CaS-containing deposit, the rate of corrosion appeared to be faster than in the $CaSO_4$-containing deposit. A specimen exposed for 24 hours in the CaS/CaO deposit showed extensive corrosion and was completely destroyed after 50 hours; in the $CaO/CaSO_4$ deposit, no signs of the onset of sulfidation were evident after 24 hours and, even after 320 hours, the specimen had not been completely penetrated by sulfur. Figure 4-39 shows an optical micrograph of a specimen exposed for 24 hours in the CaS/CaO deposit, along with the secondary electron image and the EDAX-elemental maps for sulfur, chromium, nickel, and cobalt. The outer scale consists of a mixture of compounds containing mainly nickel, sulfur, and chromium (from the maps), and the optical micrograph shows the presence of two phases in the outer scale. From thermodynamic phase stability diagrams, it is known that chromium can only form the Cr_2O_3 phase near the outer surface, while nickel can only form the sulfide. Hence, it appears that the outer scale consists of a mixture of Cr_2O_3 and nickel sulfide. Furthermore, nickel sulfide is a liquid phase at this temperature, and the morphology of the external scale suggests the existence of a liquid corrosion product. The inner scale consists mainly of a mixture of Cr_2O_3 and chromium sulfide, while the alloy beneath the inner scale is depleted in chromium.

Figure 4-40a shows the optical micrograph of a specimen exposed to the $CaO/CaSO_4$ deposit for 50 hours. The morphology of corrosion is very similar to that shown in Fig. 4-39: the outer scale consists of a mixture of nickel sulfide and Cr_2O_3 and the inner scale consists of chromium sulfide and Cr_2O_3. However, an initially formed cobalt oxide layer is still present as the outermost layer.

Nimonic 86, an alloy similar in composition in Inconel 617, showed a similar kinetic behavior in the deposits, with similar morphological features (Fig. 4-40b).

Inconel 618E, an alloy analogous to 617, but strengthened by W + Fe instead of Mo + Co, formed an initial external oxide scale containing iron and chromium in the

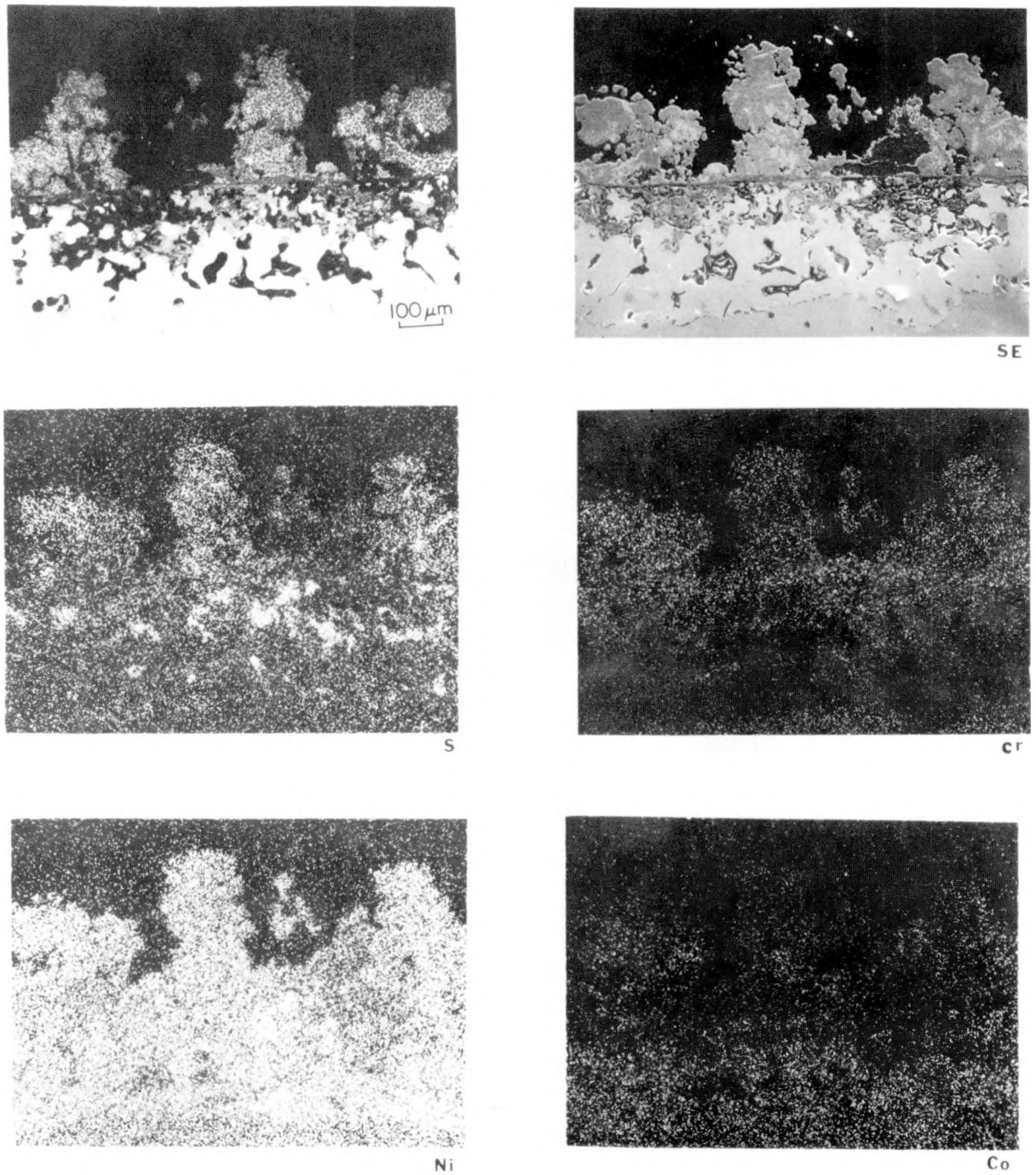


Figure 4-39. Inconel 617 Exposed to the CaS/CaO Deposit for 24 Hours (optical micrograph, secondary electron image, S-map, Cr-map, Ni-map, and Co-map)



Figure 4-40a. Inconel 617 Exposed to the $CaO/CaSO_4$ Deposit for 50 Hours

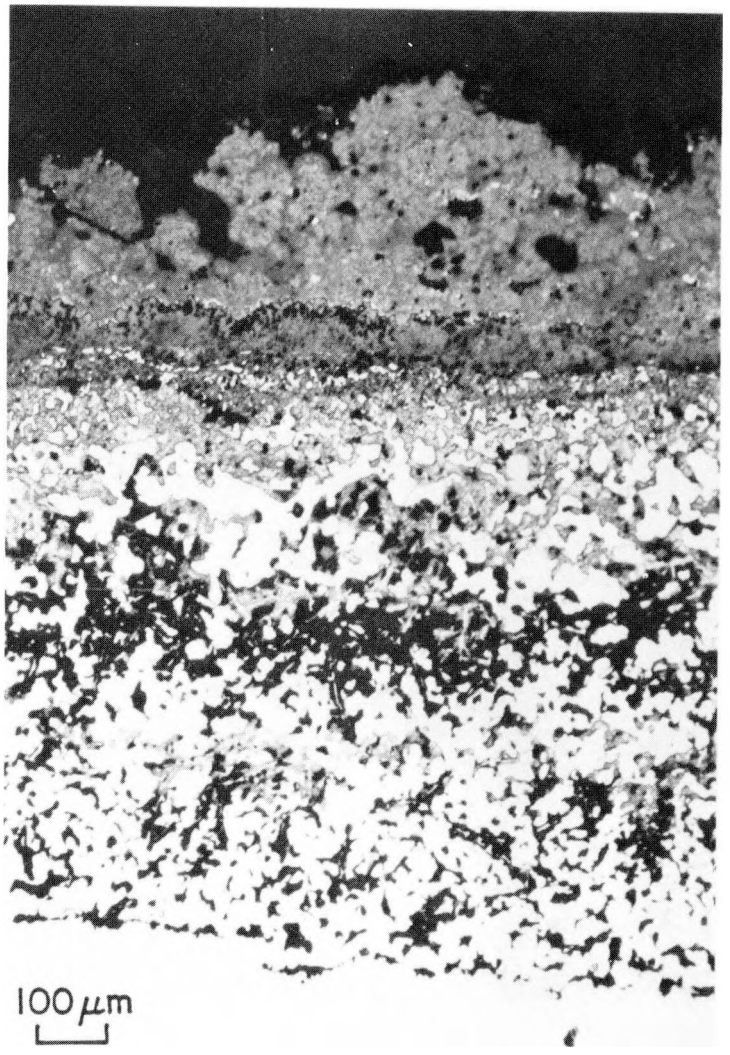


Figure 4-40b. Nimonic 86 Exposed to the CaS/CaO Deposit for 24 Hours

deposit exposures. Figure 4-41 shows an optical micrograph of a specimen of 618E exposed for 50 hours in the CaS/CO deposit along with the secondary electron image and the EDAX-elemental maps for iron, chromium, nickel and sulfur. The iron and chromium maps show the presence of these elements in the external scale: the concentration of iron is high near the scale/gas interface. Nickel sulfide is present in the external scale, and the inner scale is composed mainly of a mixture of oxides and sulfides of chromium. However, a specimen exposed for 120 hours did not show sulfidation attack. Figure 4-42 shows the electron image and the X-ray maps for Ni, Ca, and Cr (sulfur was not detected). The maps reveal that the alloy had formed a protective Cr_2O_3 scale which had been reacted with CaO in the deposit to provide a solid reaction product (possibly $CaCr_2O_4$).

On exposure to the $CaO/CaSO_4$ deposit, the alloy sulfidized and Fig. 4-43 shows a specimen exposed for 320 hours. The morphology of corrosion is similar to that observed in the CaS/CaO deposit, but the extent of corrosion appears to be less: the weight gain of the specimen exposed for 320 hours to the $CaO/CaSO_4$ deposit was found to be less than 50% of a similar specimen exposed to the CaS/CaO deposit.

The behavior of Hastelloy X and PE-13 was similar to that of Inconel 618E. Figure 4-44 shows the optical micrographs of a specimen of Hastelloy X exposed for 50 hours to the CaS/CaO and $CaO/CaSO_4$ deposits. The presence of iron in the alloy appears to facilitate the establishment of an initial iron-rich oxide layer which seems to delay the onset of sulfidation corrosion.

Increase in the iron content to over 40%, as in Incoloy 800, resulted in a slow-down in the rate of corrosion in both the deposits. Figure 4 45 shows an optical micrograph of a specimen of Incoloy 800 exposed to the CaS/CaO deposit for 120 hours along with the secondary electron image, and the EDAX-elemental maps for chromium, iron, nickel and sulfur. Corrosion often occurred in the form of isolated pits: the corrosion products were mainly oxides of iron and chromium,

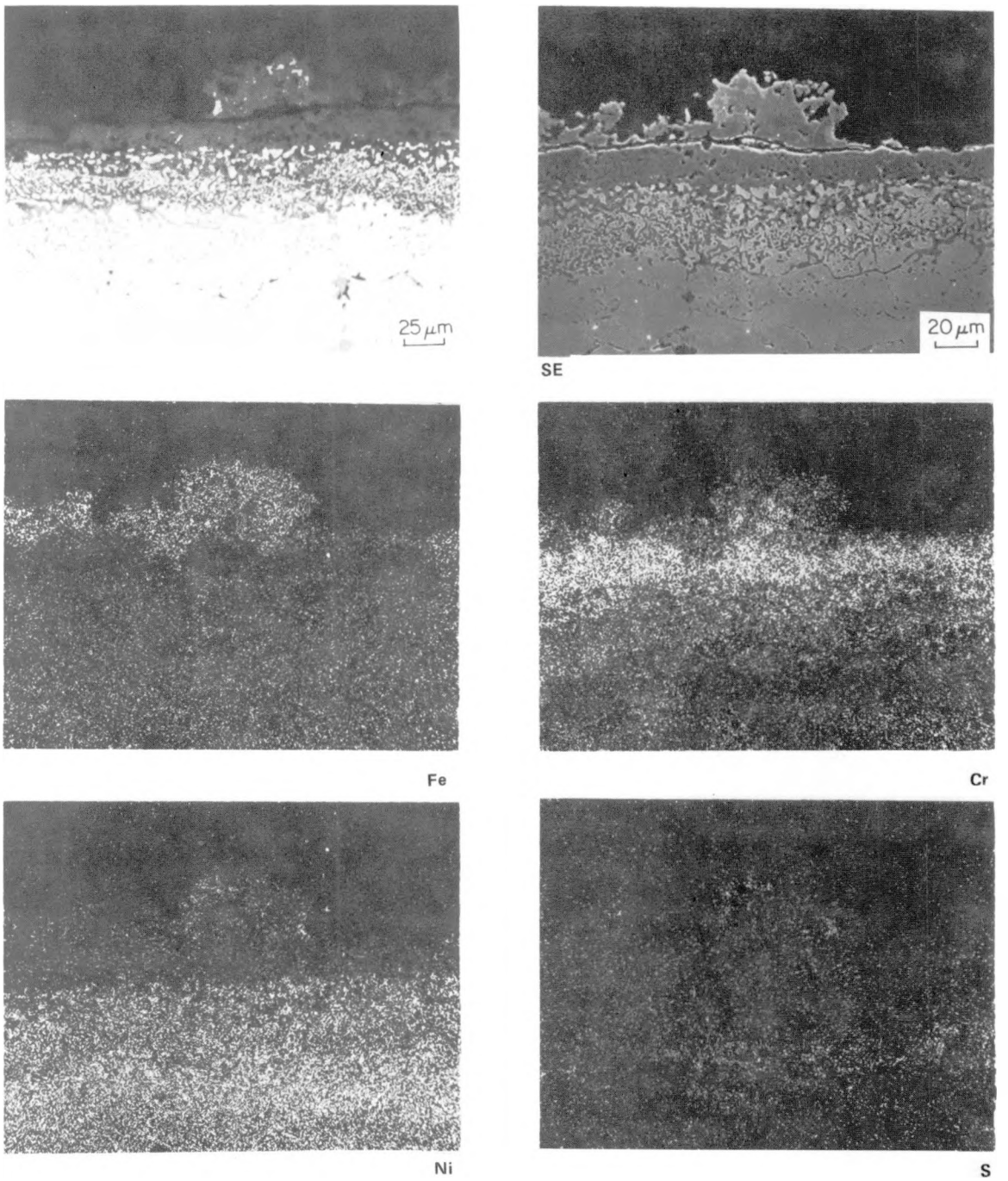


Figure 4-41. Inconel 618E Exposed to the CaS/CaO Deposit for 50 Hours (optical micrograph, secondary electron image, Fe-map, Cr-map, Ni-map, and S-map)

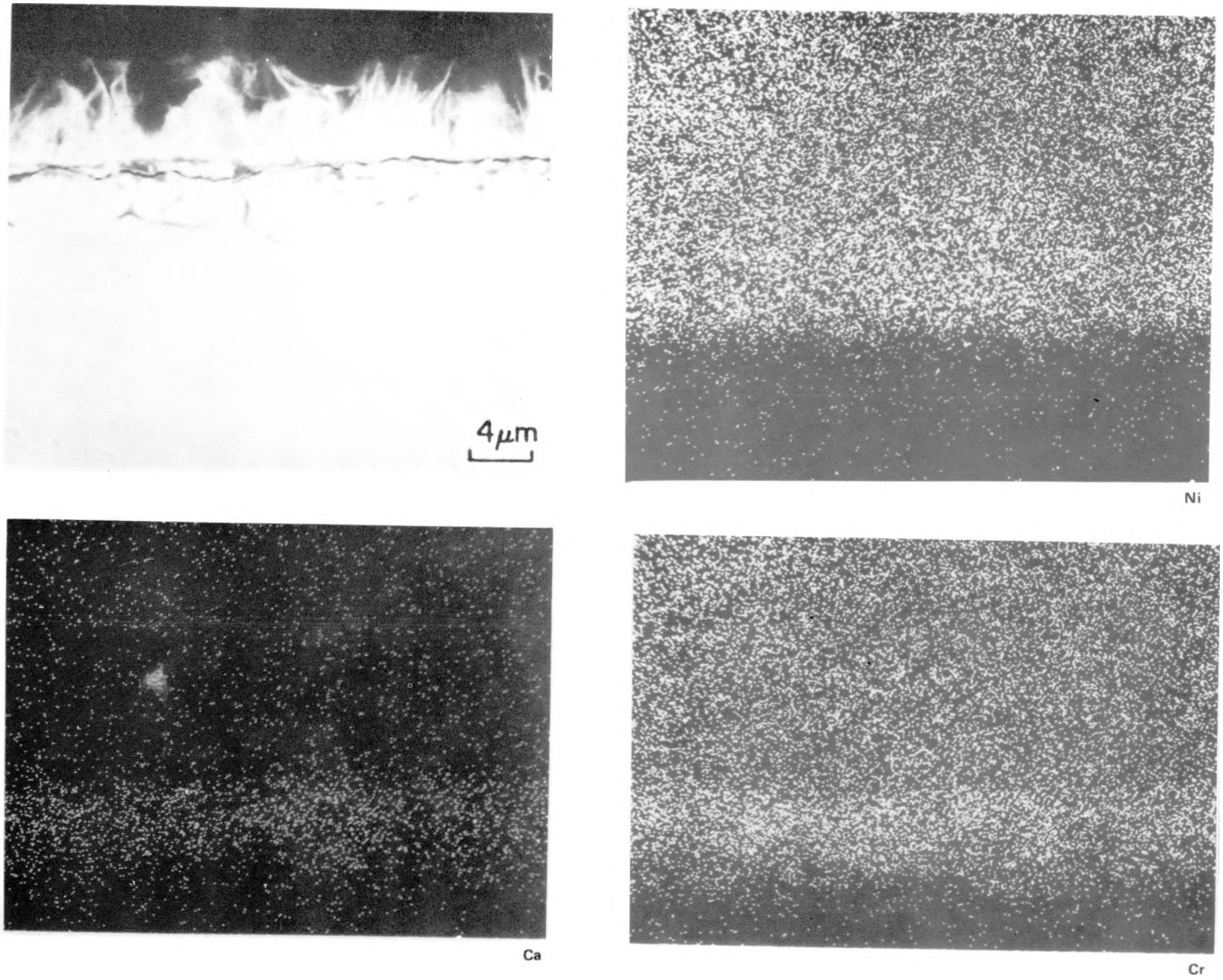


Figure 4-42. Inconel 618E Exposed for 120 Hours in the CaS/CaO Deposit (electron image, Ni-map, Ca-map, and Cr-map)

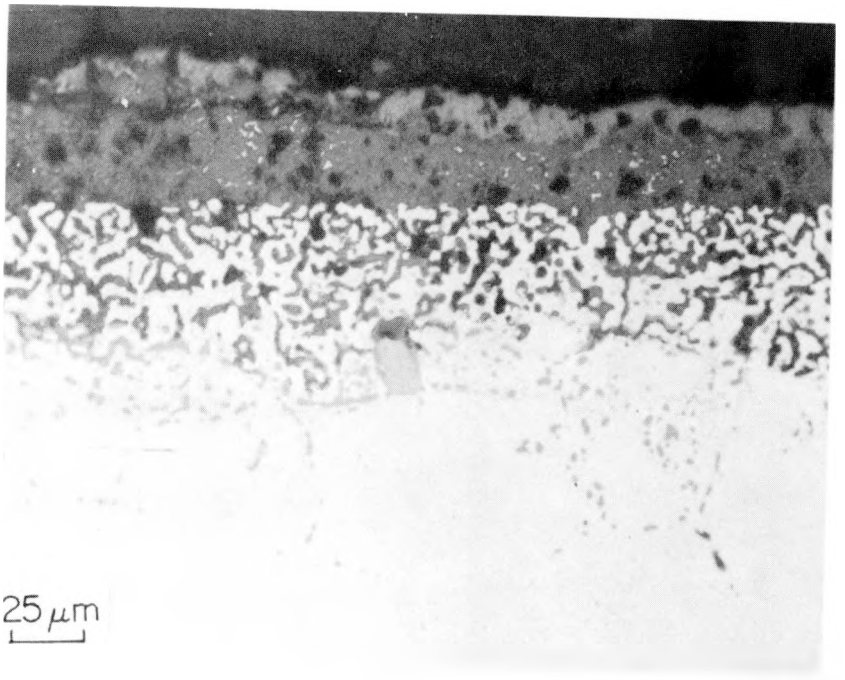


Figure 4-43. Inconel 618E Exposed to the $CaS/CaSO_4$ Deposit for 320 Hours

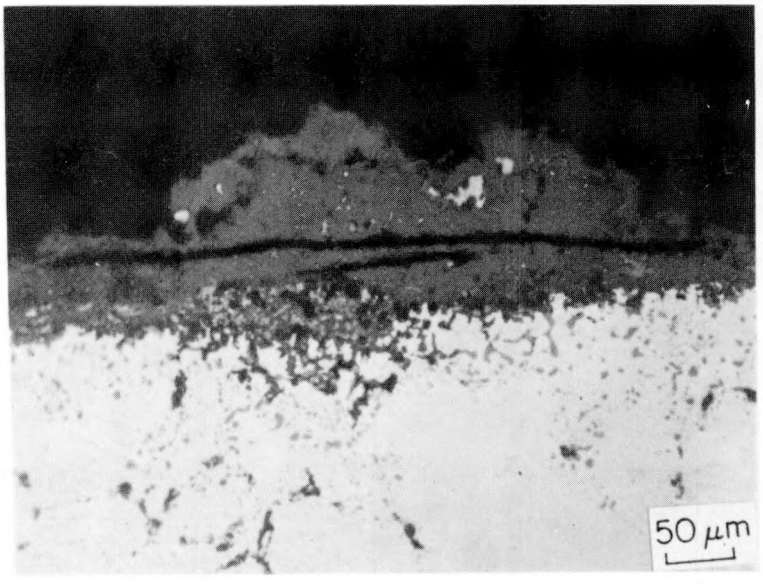


Figure 4-44a. Hastelloy X Exposed to the CaS/CaO Deposit for 50 Hours

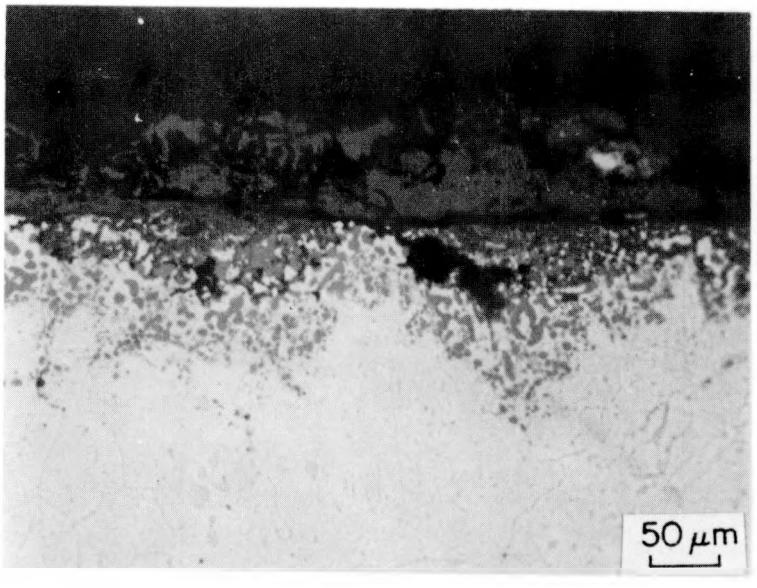


Figure 4-44b. Hastelloy X Exposed to the $CaO/CaSO_4$ Deposit for 50 Hours

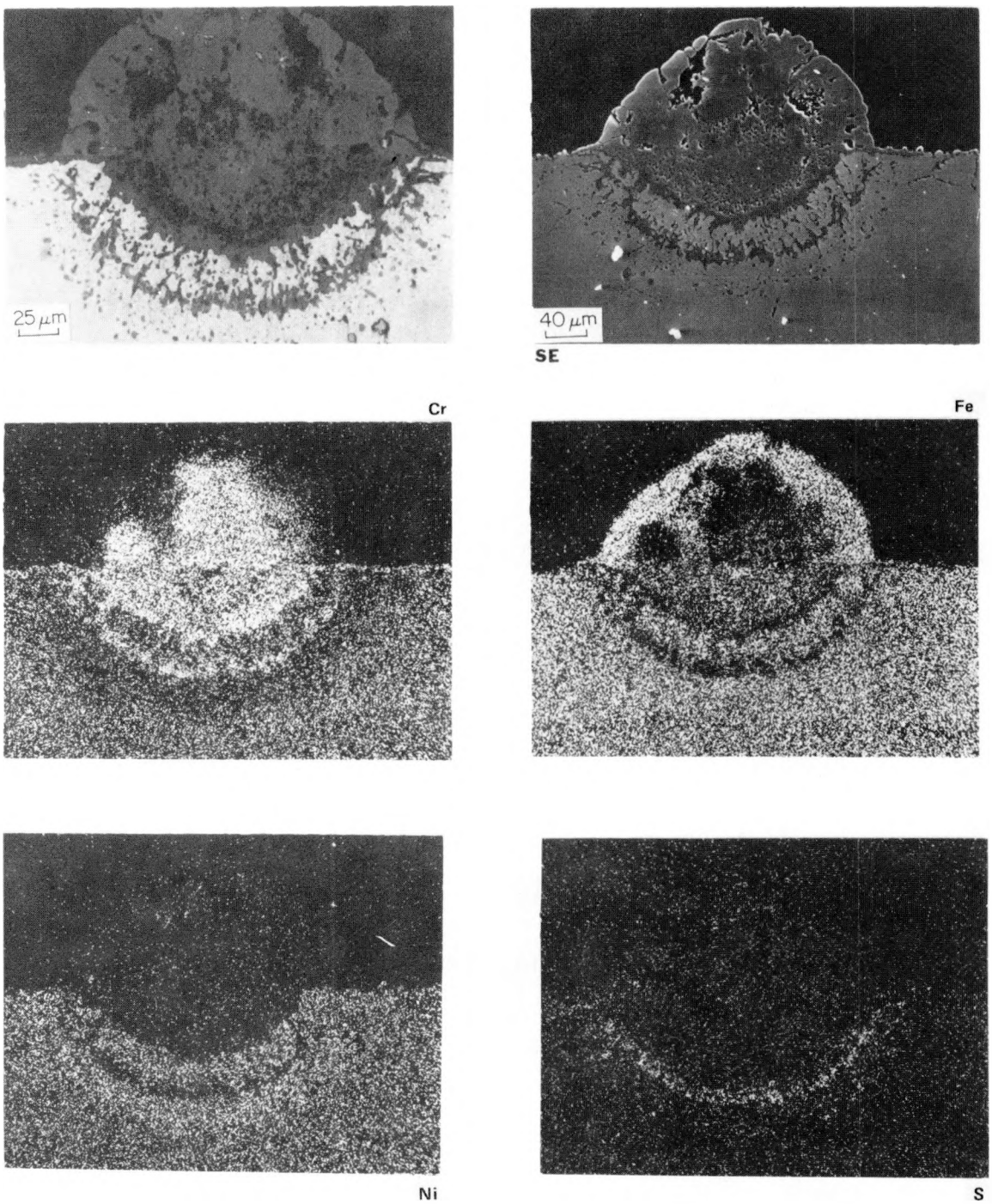


Figure 4-45. Incoloy 800 Exposed to the CaS/CaO Deposit for 120 Hours (optical micrograph, secondary electron image, Cr-map, Fe-map, Ni-map, and S-map)

along with a few precipitates of internal sulfides of chromium. In the CaO/$CaSO_4$ deposit, the specimen exposed up to 320 hours had essentially a protective oxide layer with no internal sulfides.

AISI 310 stainless steel, which contains over 50% iron, underwent sulfidation in the CaS/CaO deposit but not in the CaO/$CaSO_4$ deposit even after 320 hours of exposure. Figure 4-46 shows the electron image and EDAX-elemental maps for Ca, Fe, Ni, S, and Cr of a specimen exposed for 120 hours in CaS/CaO deposit. A region of the outermost layer contained both Ca and S and this was probably the deposit. The rest of the layer was enriched in iron and Ca and this was probably a product formed by the reaction between CaO in the deposit and the iron oxide layer formed on the alloy. A few nickel sulfide precipitates were also evident. A thick, chromium-rich layer formed underneath the external layer. However, this layer was penetrated by sulfur to form internal precipitates of chromium sulfide along the grain boundaries of the alloy.

Increase in the iron content to still higher levels (70%), as in AISI 304 and 347 stainless steels, resulted in a further improvement in resistance, with the absence of internal sulfidation even up to 320 hours in both the deposits. Figure 4-47 shows an optical micrograph, the electron image, and the EDAX-elemental maps for iron, chromium, nickel, and sulfur of a specimen of AISI 304 stainless steel exposed to CaS/CaO deposit for 24 hours. The micrographs show a pit, but a protective Cr_2O_3 layer has formed at the base of the pit. Similar features were observed on the specimen exposed to the $CaSO_4$/CaO deposit.

Summary and Discussion. The results of these experiments are summarized as follows:

- Sulfidation of some of the alloys, especially the nickel-base alloys, occurs in the presence of bed material, when the PO_2 of the environment is in the range of 10^{-11} to 10^{-13} atm
- Calcium sulfide, at its dissociation oxygen partial pressure, appears to be more aggressive than calcium sulfate at its dissociation oxygen partial pressure.

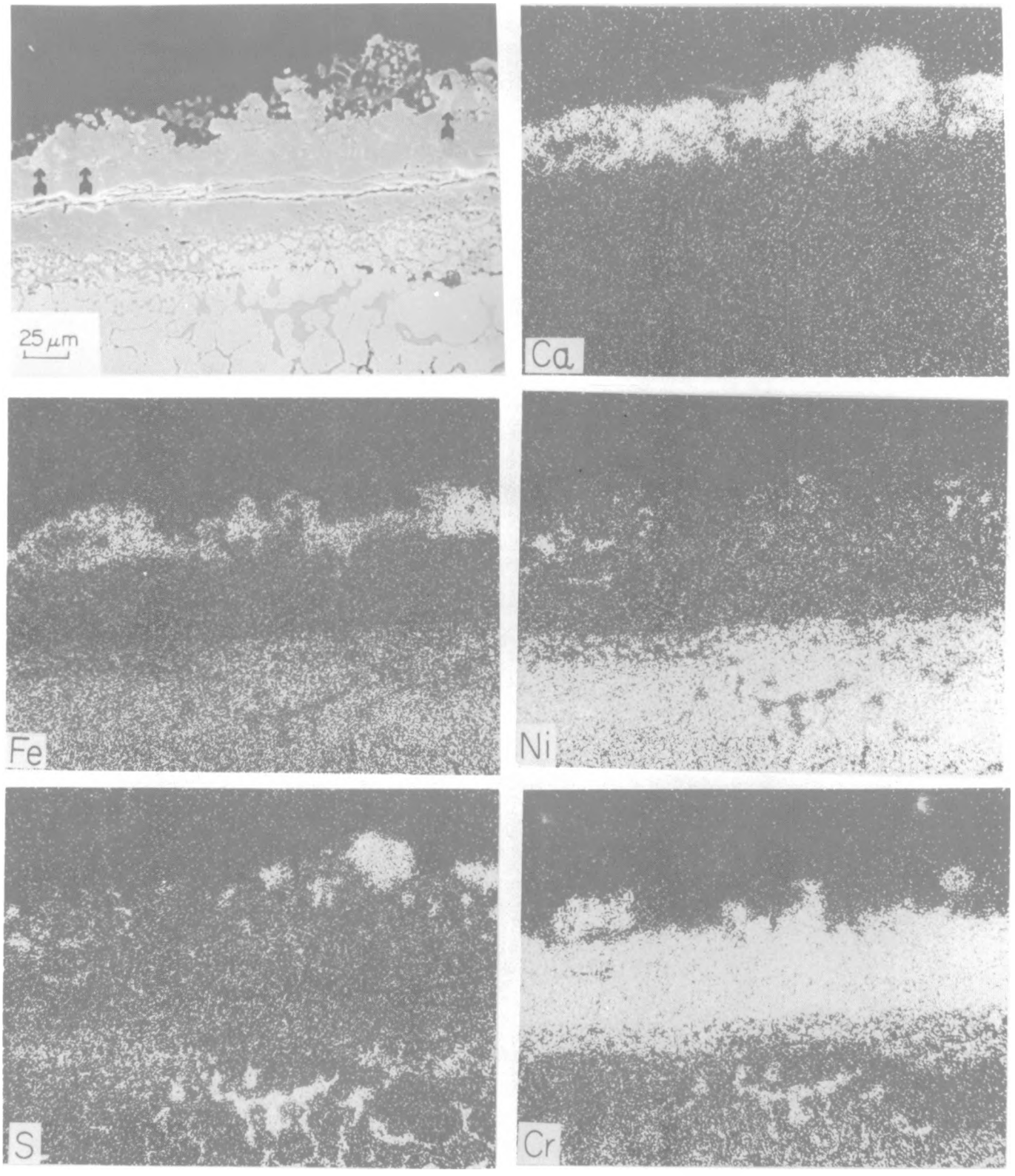


Figure 4-46. AISI 310 Stainless Steel Exposed to CaS/CaO Deposit for 120 Hours (electron image, Ca-map, Fe-map, Ni-map, S-map, and Cr-map)

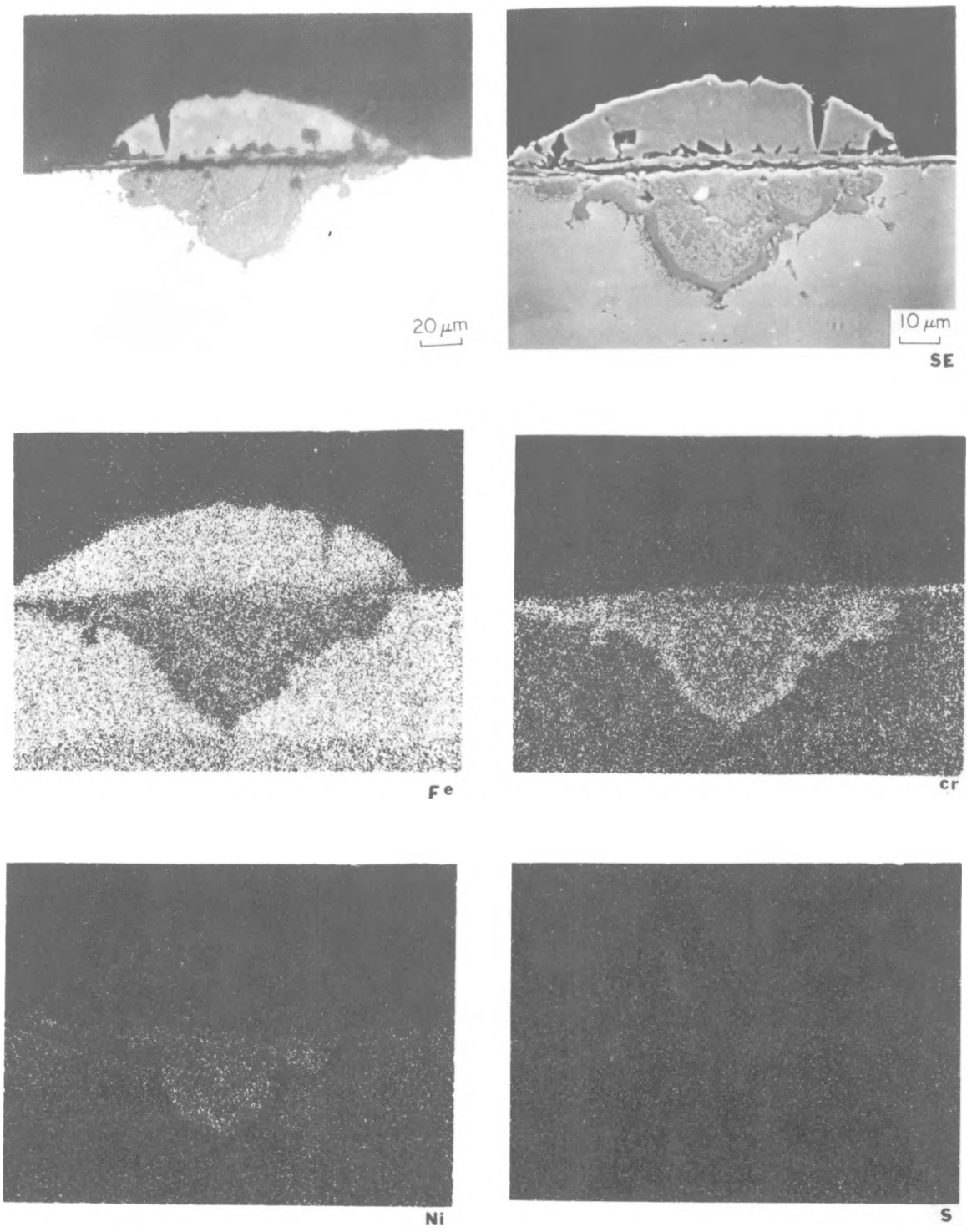


Figure 4-47. AISI 304 Stainless Steel Exposed to the CaS/CaO Deposit for 50 Hours (optical micrograph, secondary electron image, Fe-map, Cr-map, Ni-map, S-map)

- Nickel-base alloys, in general, appear to be susceptible to sulfidation-related accelerated attack. However, the presence of other elements, such as cobalt and, in particular, iron, may delay the onset of sulfidation.
- Iron-base alloys, in general, appear to be less susceptible to sulfidation, although increasing the nickel content may increase this susceptibility.
- The FeCrAlYs are extremely resistant in these environments.

The release of sulfur from the deposits probably occurs by the reactions:

$$CaSO_4 = CaO + 1/2\ S_2 + 1\text{-}1/2\ O_2$$

and

$$CaS + 1/2\ O_2 = CaO + 1/2\ S_2$$

Reaction (1) is a decomposition reaction while reaction (2) is a displacement reaction. The observed corrosion behaviors suggest that the displacement reaction is occurring at a faster rate than the decomposition reaction.

These results suggest that accelerated corrosion of heat exchanger alloys may occur beneath deposits of bed material where conditions are such that the local oxygen and sulfur partial pressures are set by the equilibium established between $CaS/CaO/CaSO_4$. Under nominally normal operating conditions of a fluidized-bed coal combustor, using approximately 20% excess air, the deposit found on in-bed tubes has been observed to be mainly $CaSO_4$ (Ref. 4-18), with other major phases being Fe_2O_3, $Ca_3Fe_2Si_3O_{12}$, and SiO_2. Calcium sulfide has not been reported as a major constituent of such deposits, but does occur under conditions of substoichiometric combustion (Referece 4-19), and so must be considered a possible constituent at specific locations where persistent low oxygen partial pressures have been measured in AFBs.

However, accelerated sulfidation-related corrosion was consistently observed in a series of in-bed corrosion tests (Ref. 4-9) in regions where metal specimens overlapped to form traps for bed material, even though the prevailing oxygen partial pressure varied among the tests. The extent of the corrosion observed in

250 hours in these tests was, however, much more extensive than found in the laboratory tests in $CaO/CaSO_4$ mixtures described here, and involved massive sulfidation of alloys like Inconel 617 and 618E, with morphologies similar to those formed in CaO/CaS mixtures. The implications are that CaS may have been present in the trapped deposits in these actual bed tests. We suggest that one way in which alloy corrosion behavior is influenced by the prevailing local oxygen partial pressure in an AFB may be through its effect on the $CaO-CaSO_4$-CaS equilibrium at a given location, and, hence on the different proportions of these constituents incorporated in the tube deposits.

The interaction between CaO in the deposit and oxides (of chromium and iron) in the protective scale can have a major influence on the retention of the protective oxide scale on the alloys. Although, in this investigation, only a few specimens showed interaction between CaO in the deposit and the oxide scale layer on the alloys (Fig. 4-42 and 4-46), a previous investigation with deposits in air (Ref. 4-17) had shown ample evidence for interaction between CaO and the protective oxide scales. The product of such a reaction is a solid compound at these temperatures and could spall off quite readily. In fact, deposits formed on heat exchanger tubes from operating AFBs readily spall off along with the protective oxide scale. The protective oxide scale appears more adherent to the deposit than to the substrate alloy and this may be due to the interaction between CaO and the protective oxide scale, as seen in this investigation.

4.2 24-INCH-DIAMETER ATMOSPHERIC FLUIDIZED BED EXPERIMENTAL PROGRAM

An experimental program was conducted in the Battelle Columbus Laboratories (BCL) atmospheric fluidized bed (AFB) unit. This was an existing unit that was modified for this program to provide experimental results early in the program. Results from this program were used in the design and operation of the larger 6' x 6' AFB program (described in Sections 4.4 and 4.5) as well as providing data useful in the heat exchanger material studies.

The experimental program on the 24-inch AFB consisted of characterization and material specimen exposure test series. The characterization testing was conducted in two phases where (1) the unit's operation was characterized and developed, (2) the influence of various parameters on the bed environment were investigated, and (3) the oxygen partial pressure probe design and operation were verified as well as used to measure the fluidized bed environment. The material specimen exposure test series consisted of three series of 250-hour tests to expose various heat exchanger material specimens to operation at various conditions of excess air from 50% to stoichiometric. Additionally, the bed forces, as exerted on the heat exchanger tubes, were measured during the course of the 24-inch AFB test program.

This section describes the two phases of the characterization experimental program followed by a separate discussion of the oxygen partial pressure results. The material specimen exposure experimental program is then presented, and the analysis of the material specimens is presented in a separate section (4.3). The results of the bed force experiments are then presented.

4.2.1 24-Inch AFB Characterization (Runs 1-7)

A series of experiments was performed using the BCL 24-inch-diameter research AFB furnace to define operating conditions and design parameters for the 6' x 6' bed at Rocketdyne. Since these experiments covered a wider range than the experiments performed with the 6' x 6' bed, the results will also have impact on the conditions and designs for future prototype fluidized beds. The experiments also aided

in selecting conditions for the subsequent erosion-corrosion experiments. During some of these experiments, diagnostic probes were inserted into the bed to measure bed characteristics.

These experiments were the first operational use of the basic furnace equipment since major modification made for this program. Operational techniques, modified because of information obtained, were used during the erosion-corrosion experiments.

This section reports on the first seven runs on the 24-inch fluidized bed operated to characterize the AFB combustion conditions in it. The main purpose of these runs was to define conditions for later runs, and to define operational parameters for the 6' x 6' fluidized bed and for prototype beds. Table 4-7 is a summary of the results and operating conditions.

TABLE 4-7. RUN SUMMARY

RUN NO.	1	2	3	4	5	6	7
BED TEMPERATURE, F	1584	1623	1574	1580	1600	1628	1656
SUPERFICIAL VELOCITY, FT/SEC	6.1	7.9	3.5	6.1	6.4	6.3	6.5
EXCESS AIR, %	16	22	25	52	22	13	22
SO_2, LB/10^6 BTU	0.94	0.99	1.30	1.20	0.42	1.20	1.10
LENGTH OF RUN, HOURS	8	4	4	4	4	4	4
COMBUSTION EFFICIENCY, %	96.5	93.6	96.4	97.0	97.9	97.8	98.9
Ca/S	1.8	2.1	2.2	2.0	3.8	2.1	3.9

These results indicated the bed would operate satisfactorily over a wide range of conditions. This indicates the recommended operating conditions for larger units can be determined primarily by erosion-corrosion data, rather than operability limits, as operability and combustion are satisfactory over a wide range.

Equipment. The Battelle studies were carried out in the 24-inch fluidized bed system shown in Fig. 4-48. The system consists of the fluidized bed itself, an in-bed heat exchanger, the coal and limestone feed system, a fly ash collection

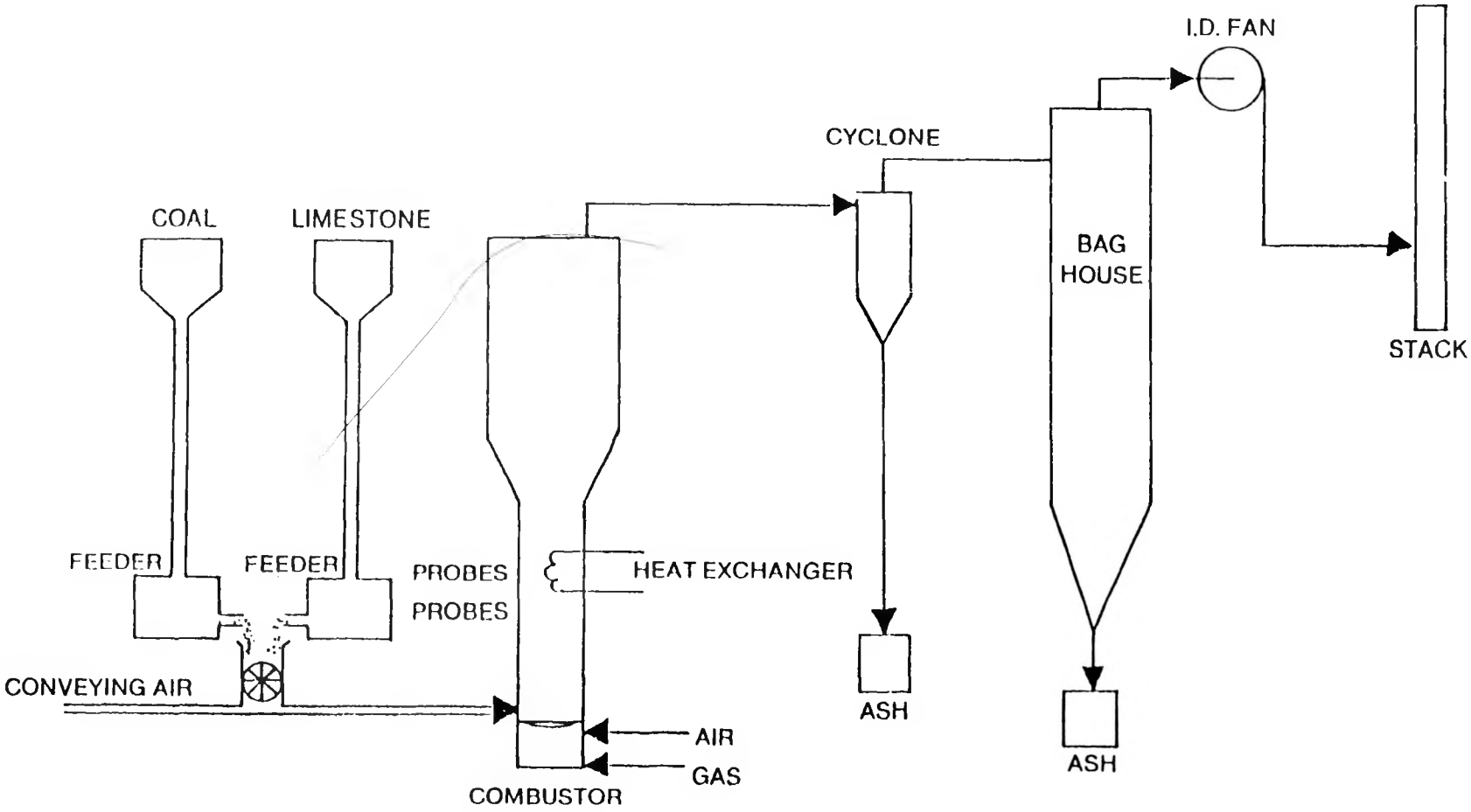


Figure 4-48. Schematic of 24-Inch Combustor

system, a preheater to heat the bed to ignition temperature, and the required instrumentations. In addition to the equipment used directly, supporting equipment was used for coal and limestone preparation and for chemical analyses.

Fluidized Bed Unit. A sketch of the fluid bed is shown in Fig. 4-49 where the locations of the feed port and pressure taps are indicated. Thirteen thermocouples are located throughout the bed about 2 inches in from the wall, and an additional four are located in the freeboard.

Geometry. The fluidized bed is a 2-foot-ID cylinder, 64 inches high. On top, it expands via a conical section to a freeboard which has an ID of 3 feet and is 8 feet high. The inside is lined with a mullite lining 4 inches thick, backed by 5 inches of cast insulating refractory with a thermal conductivity of 1.3 Btu-in./hr-ft^2-F. The refractory covers the inside of a steel shell. A bed material drain port is located in the wall 28 inches above the bottom of the bed.

Distributor Plate. Figure 4-50 is a sketch of the distributor plate. This design is similar to that used in the B&W Alliance unit. Each distributor cap has 16 holes that are 1/8 inch in diameter, except the caps next to the wall have omitted the five holes that would point at the wall. The 11 remaining holes were increased in size so the total open area was the same as if 16 holes had been drilled.

When the feed port was modified, about one-third of the combustion air was admitted through it. Therefore, the six distributor caps in the center were plugged.

Feed Port. Figure 4-51 is a sketch of the feed port. A cap over the top acts to spread the coal and to prevent bed material from draining into the port. This port is a minor modification of the design used at Alliance.

Heat Exchanger. An air-cooled heat exchanger is placed in the combusting bed to remove heat for control of bed temperature, to simulate the bed geometry in prototype units, and for measurement of operational heat transfer rates. Figure 4-52 is a sketch of the heat exchanger. The entire heat exchanger can be

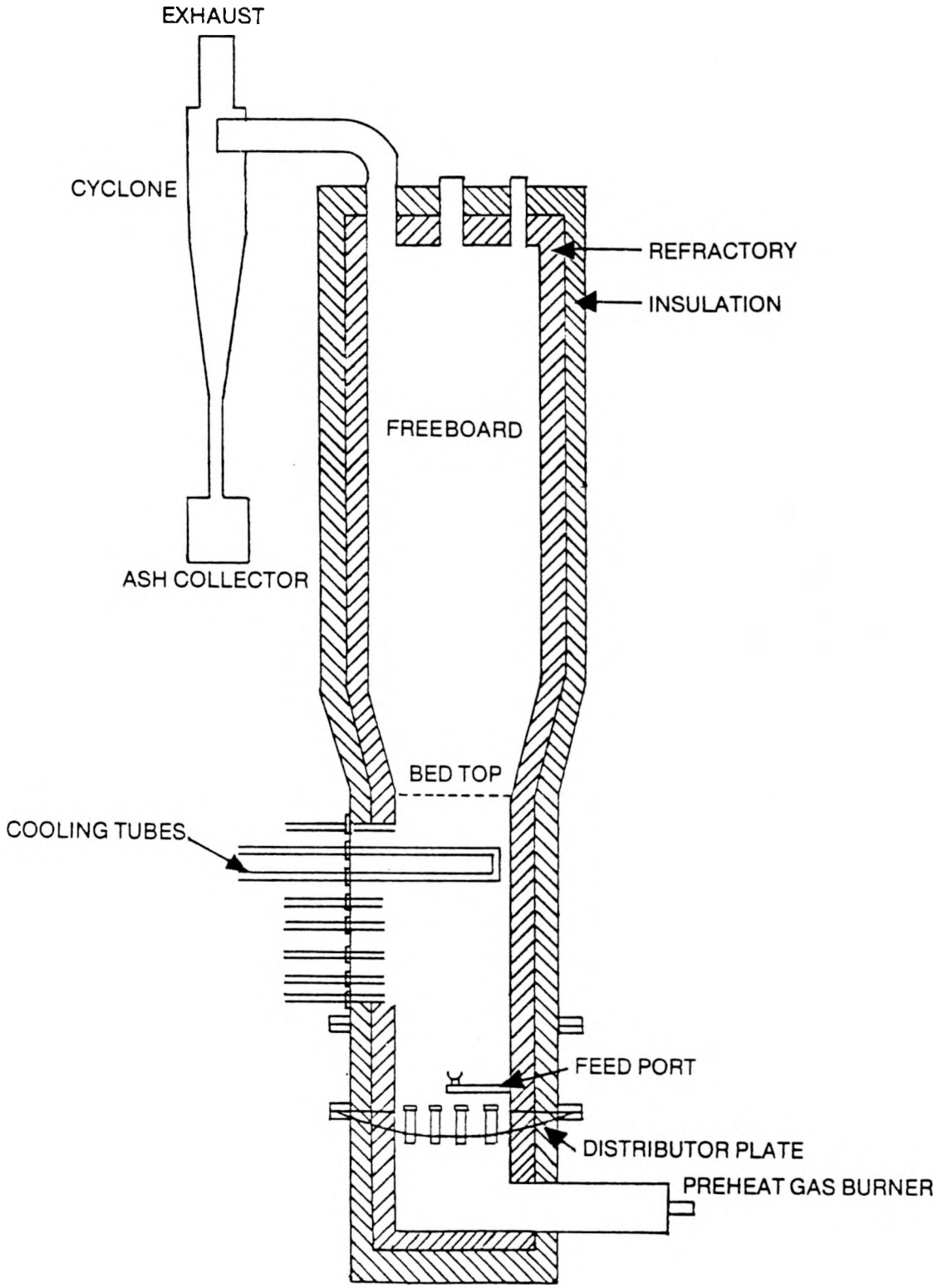
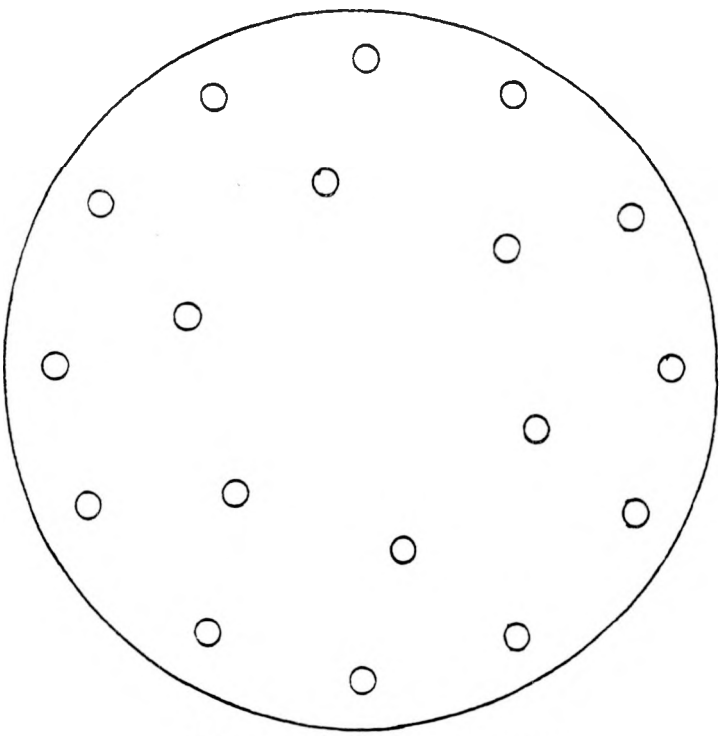


Figure 4-49. 24-Inch Fluidized Bed Reactor



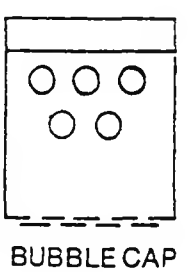


Figure 4-50. Distributor Plate

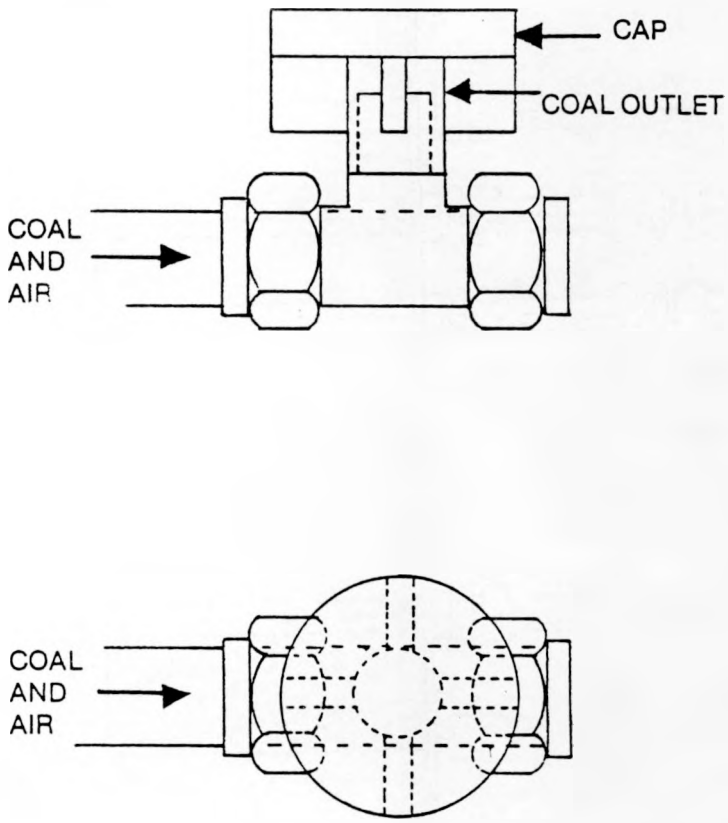


Figure 4-51. Coal Feed Port

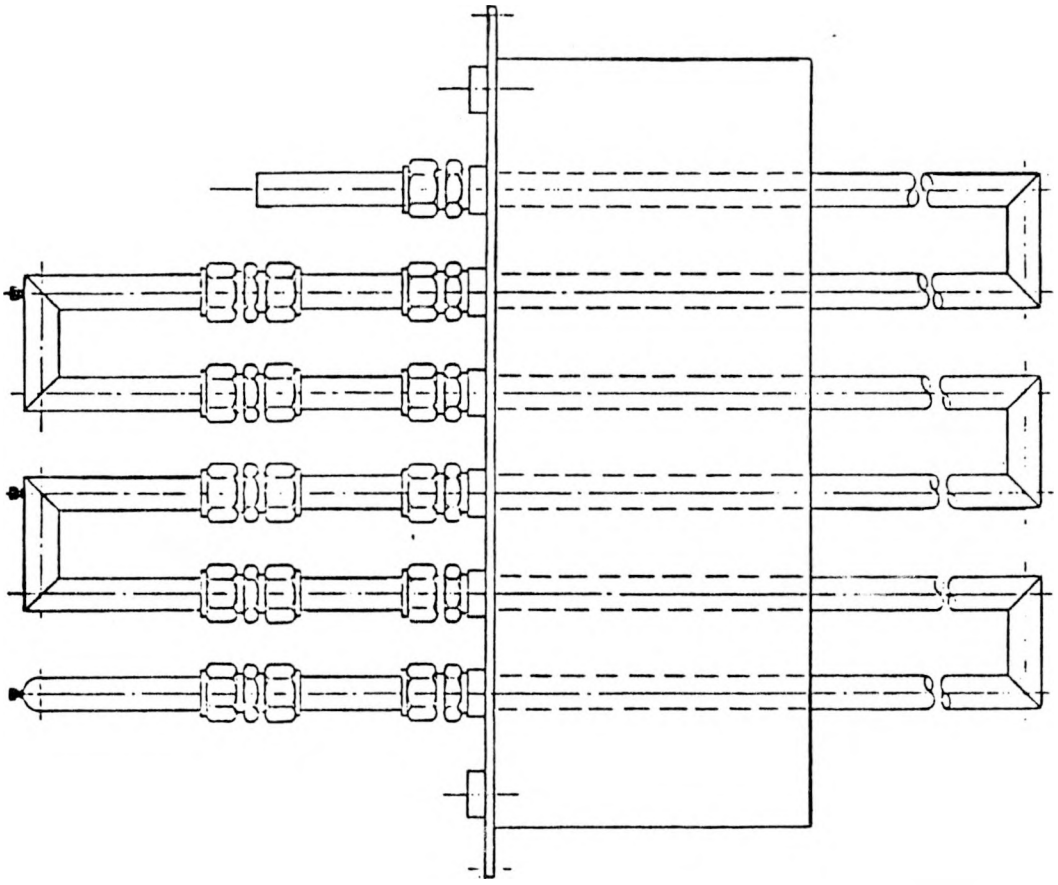


Figure 4-52a. 24-Inch AFB Heat Exchanger (Side View)

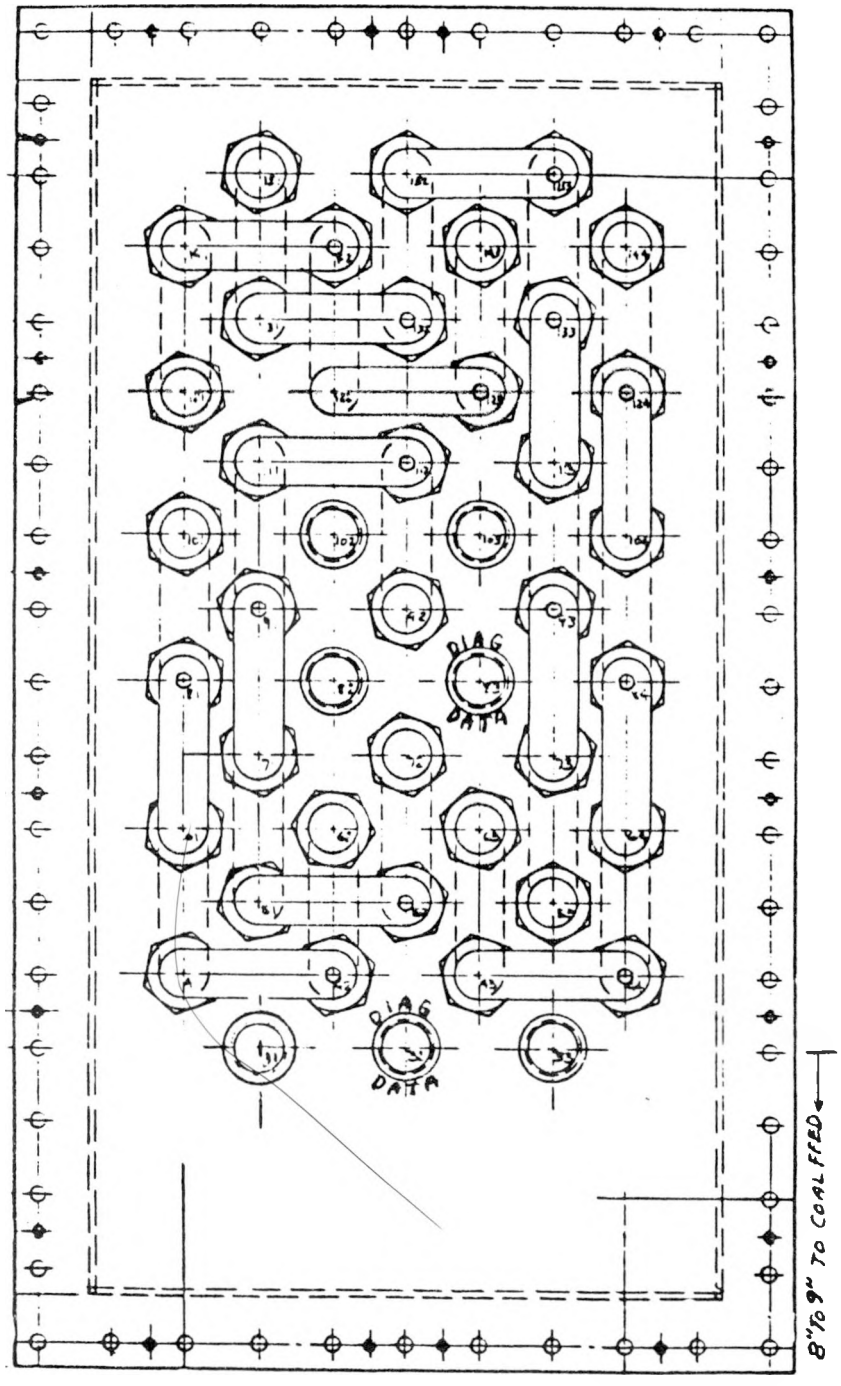


Figure 4-52b. 24-Inch AFB Heat Exchanger (End View From Outside of Combustor)

removed as a unit from the fluidized bed. Fifty-three 2-inch pipes penetrate the refractory, and air-cooled U-bends can be placed to connect any adjacent penetrations. Each penetration is identified by a reference number.

The heat exchanger was installed so air passed through the heat exchanger in five parallel paths, with three, four, or five U-tubes in each path. Five paths were needed to pass the required cooling air, and several U-tubes were needed in series so heat transfer coefficients could be determined at several temperatures. Table 4-8 lists the penetrations used by the U-tubes in each pass. Between experiments 4 and 5, uncooled straight tubes were added in positions 82, 83, and 102 to complete the tube bank for better simulation of the prototype heat exchanger conditions.

TABLE 4-8. AIR PATHS THROUGH HEAT EXCHANGER

PASS NO.	1	2	3	4	5
NO. 1 U-TUBE	151-131	101-81	121-141	63-43	92-112
NO. 2 U-TUBE	132-152	61-41	142-122	44-64	111-91
NO. 3 U-TUBE	153-133	42-62	123-143	84-104	71-51
NO. 4 U-TUBE	113-93	-	-	124-144	52-72
NO. 5 U-TUBE	73-53	-	-	-	-

Air Supply. The cooling air to the heat exchanger was supplied by the same 1600 cfm, 8 psi blower that supplied the combustion air. The air warmed to about 200 F in the blower and was cooled to about 110 F in a water-cooled heat exchanger before it entered the fluidized bed heat exchanger. The flow through each parallel path was controlled by a gate valve.

Coal and Limestone Feeders. The coal and limestone feeder system is shown in Fig. 4-53. Before the shakedown tests, L-valve feeders had been installed, but the minimum capacity of the L-valve feeders (300-500 lb/hr) was found to be greater than the system requirements (30-150 lb/hr). The L-valve feeders, therefore, were replaced with Acrison feeders.

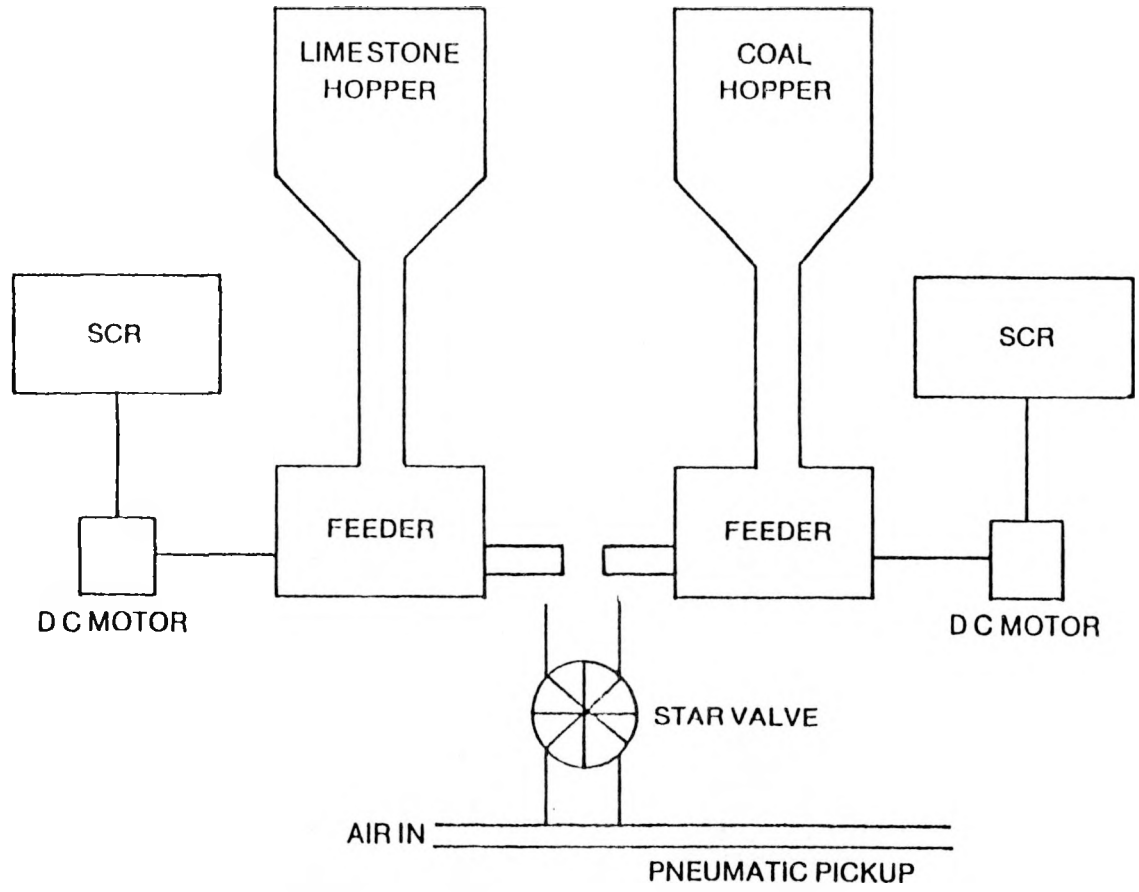


Figure 4-53. Coal and Limestone Feeder System

The Acrison feeders as used are volumetric feeders with a helical screw feeding through a 2-inch tube. The screw is driven by a d-c motor through an SCR controller. The feed rate is calibrated against the controller setting. The Acrison feeder for limestone stripped a gear between runs 6 and 7 and it was replaced with a vibrating feeder for run 7. The Acrison feeder was repaired and used for the erosion-corrosion experiments.

The coal and limestone ash dropped through a funnel into a Penberthy GL-1 ejector where they were entrained in air so the bed pressure was overcome. These solids were then air conveyed into the bed.

Ash Collection. Ash was collected at three points: drainings from bed, cyclone ash, and baghouse ash. The bed was drained every 4 to 12 hours to maintain a constant bed level. The cyclone ash and baghouse ash were continually removed, generated, and collected in hoppers or barrels.

Ignition. A Maxon gas burner fired into the lower (Dutch oven) section of the fluidized bed unit. It fired at a maximum rate of about 600,000 Btu/hr. Combustion air was supplied by a 100-psi compressor (which supplied all of the house air). During the initial stages of startup, the burner was used with high excess air to control the temperature rise. During the remainder of the startup time, the burner was operated at capacity with only a small amount of excess air. The hot gas from the burner was diluted with air from the 8-psi blower to provide fluidization velocity and control of the temperature in the Dutch oven. The Dutch oven temperature was limited to about 1650 F by the operators. When the fluidized bed temperature reached about 1050 F, the coal feed into the bed was started at a slow rate and increased as the temperature rose. At a bed temperature of 1450 F, the igniter was turned off and coal only was burned to heat the bed to 1650 F.

Temperature. The temperature was measured with chromel-alumel thermocouples. The temperatures were read using a digital electronic readout and recorded in a notebook. In addition, a 24-point recorder was used to record most of the bed temperatures once every 2 minutes. In addition to the electronic digital indicator, an indicator-controller was used to measure baghouse temperature.

The thermocouple wells in the combustor extended about 2 inches through the refractory into the bed, and thus measured temperatures near the outside edge of the bed. The bed temperature listed in this report is the average of the readings of all the thermocouples in the bed.

The thermocouples in the heat exchanger were placed in the external U-bends of the heat exchanger tube. They were 1/8-inch sheathed thermocouples and were not in wells. They extended about 6 inches into the U-tube. The external U-tubes were not insulated. Similar thermocouples measured temperatures at the baghouse.

Air and Gas Flows. The air flows to the five heat exchanger passages were determined using 1.60-inch-diameter orifices in a 3-inch pipe. The main combustion air flow was determined using a 2.16-inch orifice in a 4-inch pipe. The pressure differences across the orifice plates were measured with water manometers. The upstream pressure, as measured with a 0-30 psi Bourdon tube gage and with a mercury manometer, was always the rated 8-psi output of the blower. The gas flow to the coal injector was measured with a rotometer corrected for pressure. During warmup for run 5, the rotometer broke and the flow was recorded the same as previously calibrated and measured at that nozzle pressure (30-70 psig). The air aspirated into the system with the coal and limestone was not measured, but was estimated at 2-5 cfm.

The gas flow to the ignition burner was not recorded. Up to 7 cfm of gas was used as indicated by a rotometer. There was no meter in the air line. The flow to the ignition burner was used only during warmup to about 1350 F. It was off for more than 4 hours before an experiment was started.

Pressure. Pressures in the air lines were measured with Bourdon tube gages. The pressures between the distributor plate and the freeboard, and the bed bottom and the freeboard, were measured with mercury manometers. A pressure tap was located 44 inches above the distributor plate to measure bed depth, and the pressure between this tap and the freeboard was measured with a water manometer. Additional water manometers measured the freeboard pressure and the pressure drop across the baghouse.

Flue Gas. The flue gas sampling system is shown in Fig. 4-54. The flue gas was taken from the top of the combustor through a port next to the flue and flowed through a stainless-steel tube to a set of traps. The gas cooled in the tube, and the first trap caught water that condensed in the tube. The second and third traps used ice to dry the gas. The last trap was a glass wool filter to remove particulates. The gas was pumped to about 1 psi by a bellows pump, the pressure being controlled by a bypass on the pump. The gas was then passed through an O^2 meter and SO^2 meter in parallel. The oxygen meter had a built-in pressure relief. Instrument air was used for SO^2 zero gas and oxygen span gas. SO^2 (873 ppm in N^2) was used to span the SO^2 meter. The oxygen meter works on a paramagnetic principle and is zeroed by removing the magnet from the instrument. The SO^2 meter is a Faristor type and, since excessive pressure can damage the meter, individual rotometers were supplied for span, calibrate, and run gage modes. Operating experience has shown that this is necessary to prevent damage to the meter.

Materials. Illinois No. 6 coal was used for the fuel and Grove limestone was used as the sorbent. Their chemical analyses are presented in Tables 4-9 and 4-10. The coal had been ground to -8 mesh. During experiments 1 to 4, the -100 mesh coal fraction had been removed. The limestone was purchased as an 8 x 20 mesh material. It was screened through 4 mesh hardware cloth before use to protect the feed system from trash in the stone.

Operating Procedure. The bed was ignited by heating the bed with a gas flame. The bed was then brought to equilibrium conditions before the data reported were taken.

To prevent damage to the new refractory, the fluid bed was warmed at a rate of about 250-300 F by burning gas in the Dutch oven under the reactor. To accomplish this, the gas burner was ignited and operated with a lean flame until the bed temperature reached about 300 F. Then, the main combustion air was turned on until the bed temperature reached about 600 F. At this point, the baghouse fan was turned on and the flue gas started through the baghouse. About one-half of the bed was added at this time. When the bed temperature reached 1000 F, cooling air was started through the heat exchanger at a rate to maintain about 1000 F exit cooling air.

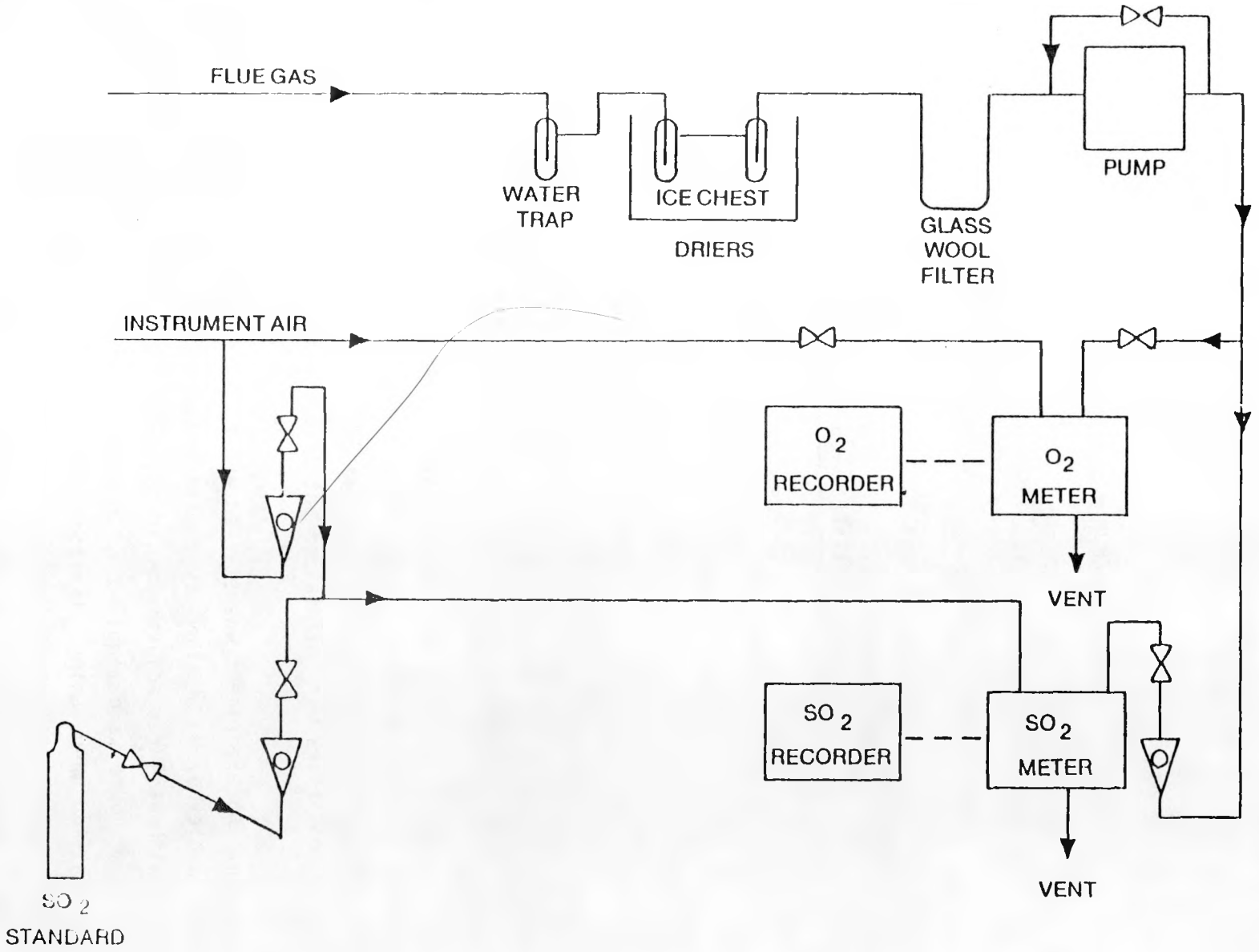


Figure 4-54. Flue Gas Sampling System

TABLE 4-9. COAL ANALYSIS
(Weight Percent as Burned)

MOISTURE	10.0
ASH	10.8
VOLATILE	36.2
FIXED CARBON	43.0
SULFUR	4.76
CARBON	62.19
HYDROGEN	4.38
NITROGEN	0.78
CHLORIDE	0.18
OXYGEN (BY DIFFERENCE)	6.91

TABLE 4-10. LIMESTONE ANALYSIS
(Weight Percent)

	DRY BASIS
$CaCO_3$	98.06
REMAINING Ca AS CaO	1.26
CO_2	43.12
CaO	56.20

At about 1100 F, coal feed was started at a slow rate. When the bed reached 1350 F, limestone was added to bring the bed level up to operating conditions. At about 1400 F, the gas burner was turned off. When the operating temperature was reached, conditions were maintained until steady state was reached.

Operation. An experiment was started about an hour after steady-state conditions were achieved, as defined by constant temperature and SO_2 flue gas concentration, without large adjustments in coal rate, limestone rate or cooling air rate. About 3 hours were required to achieve steady state between experiments, or after ignition when using limestone bed. About 12 hours was required to achieve steady state after heatup using a new limestone bed. A chemical analysis, which showed unsintered limestone in the bed during runs 1 and 2, appeared tc indicate that 12 hours is too short if good Ca/S data are required.

During the experiment, the air flow was held constant. The coal rate was varied to control excess air, the limestone rate was varied to control SO_2 concentration in the flue gas, and cooling air flow was controlled to maintain temperature. The cooling air to the different air paths was controlled to maintain approximately the same air outlet temperatures in the different paths. If any of these control changes were large, the run was aborted and restarted.

At the start and end of the experiment, the fly ash collection drum was changed. The collected fly ash provided a fly ash sample for analysis and the weight of fly ash collected determined the fly ash rate. At the end of the run before conditions changed, the bed was sampled. The bed was usually drained to maintain bed level between experiments. The bed depth reading was not accurate enough to obtain a rate of bed buildup during a 4-hour experiment. Measurement of bed drains covering all operating time indicated that the amount of bed buildup is about equal to the fly ash collected.

During all operating times, the flue gas oxygen and SO2 concentration, and the bed temperatures were continuously recorded. Every hour, these numbers were entered in a notebook along with the pressures, flows, and cooling air temperatures. The numbers used in this report are the average of the five readings taken during the 4-hour experiment.

The coal and limestone feed rates were determined by calibration of the feeders. However, in the flowing test phase, samples were taken and weighed each hour to determine rate more accurately.

The heat transfer coefficient between bed and tubes, calculated from the data obtained, was not accurate because the major temperature drop was between tube and cooling air. In future experiments, one air channel at a time will be operated at high air flow to reduce the tube-to-air temperature drop and, thus, permit a more accurate determination of the tube-to-bed heat transfer coefficient.

Operability. The system was operable over the entire planned test range, except that the minimum fluidization velocity was found to be 3.5 ft/sec, rather than the planned 3 ft/sec. (The minimum velocity is determined by increases of temperature differences within the bed, and a change in the pattern of pressure

fluctuations across the bed.) From the operator's standpoint, all of the conditions (except 3 ft/sec superficial velocity) were easily reached, indicating that scaleup should not be a problem. If a lower superficial velocity is desired, a finer limestone might be used. Finer limestone also may be a more effective sorbent. For fluidized bed operation, the preferred limestone size is that which will just maintain bed level at maximum overload superficial velocity. The 8 x 20 mesh stone used in these experiments is larger than preferred. The preferred size depends on the limestone source and may vary with stone from the same source. The preferred size also depends on bed geometry and the Battelle bed may be capable of using a finer stone than the Rocketdyne bed.

Data and Results. Table 4-11 presents the basic data for the experiments. The pressure tap on the bed depth gage was plugged for the first 4 runs; therefore, depth was estimated from total bed pressure drop rather than the pressure above the upper bed pressure tap. Table 4-12 presents the analysis of the ash. Table 4-13 presents the heat transfer data. A dash (-) in the table indicates the calculated rate by Dittus-Boelter equation (convective heat transfer inside tubes) was less than the measured overall coefficient.

Effect of Temperature. The temperature was not deliberately varied in these experiments. The last run was at a slightly higher temperature than the others and more limestone was required to keep the SO_2 level at the desired level. In this short run, this change may be only a normal variation, as the sulfur content of the ash was not significantly different from other experiments. The carbon content of the fly ash in the last run was down indicating a slightly higher combustion efficiency at the higher temperature. Neither of these effects is large enough to indicate a temperature other than 1650 F should be considered because of fluidized characteristics.

Effect of Superficial Velocity. The designed 6 ft/sec superficial velocity is satisfactory for the operation of the fluidized bed. The combustion efficiency was about 3% less at 8 ft/sec. The 8 ft/sec velocity would be satisfactory for an overload condition, but this should be avoided as a design condition because of reduced combustion efficiency. The maximum turndown was only 58% of design, which may not be adequate for some applications. A finer limestone should b selected for greater turndown.

TABLE 4-11. BASIC DATA

RUN NO.	1	2	3	4	5	6	7
COAL RATE, LB/HR	125	140	70	103	123	160	136
LIMESTONE RATE, LB/HR	36	46	24	32	74	52	74
FLUIDIZING AIR, SCFM	141	180	63	142	141	129	138
COAL CONVEYING AIR, SCFM	35	35	35	34	50	66	48
TOTAL AIR, SCFM	176	215	98	176	191	195	186
FLY ASH RATE, LB/HR	40	60	29	34	29	32	27
BED DEPTH, INCHES	46	46	58	50	63	56	56
DISTRIBUTOR PLATE ΔP, Hg	2.0	3.0	0.8	2.0	2.0	1.6	1.8
O_2 IN FLUE GAS, %	2.9	3.8	4.3	7.2	3.8	2.4	3.8
SO_2 IN FLUE GAS, PPM	472	474	611	475	201	652	525
LENGTH OF RUN, HOURS	8	4	4	4	4	4	4

TABLE 4-12. ASH ANALYSES
(Weight Percent)

	FLY ASH				BED DRAININGS			
RUN	C	S	Ca	CO_3	C	S	Ca	CO_3
1	9.0	6.3	29.0	1.07	3.1	7.6	45.5	14.8
2	7.1	6.8	28.4	0.95	1.27	9.2	46.9	6.8
3	7.1	5.5	25.3	0.79	0.14	8.5	52.2	0.37
4	7.3	8.2	27.0	0.86	0.22	8.7	53.0	0.19
5	7.5	5.8	30.5	1.80	0.47	7.4	52.2	0.18
6	9.0	4.5	16.9	0.88	1.2	9.3	49.9	0.16
7	6.5	7.2	26.2	0.84	1.9	8.2	50.8	0.18

TABLE 4-13. HEAT-TRANSFER DATA

Run No.	1	2	3	4	5	6	7
T-Bed F	1587	1626	1575	1582	1602	1632	1658
			Circuit No. 1				
Air flow rate, scfm	144	140	145	136	139	137	135
			U-Tube 151-131				
Air temp in, F	108	108	103	103	108	103	108
Air temp out, F	450	460	559	444	458	466	463
U, Btu/ft^{2}hr F	21.7	21.2	9.6	20	21	21	20
h-Air-tube,Btu/ft^{2}hr F	28	26.8	11.5	26	26	27	27
h-Bed-tube,Btu/ft^{2}hr F	180	208	179	182	230	181	129
			U-Tube 132-152				
Air flow rate, scfm	144	140	45	136	139	137	135
Air temp in, F	450	460	559	444	458	466	463
Air temp out, F	731	750	871	724	746	762	766
U,Btu/ft^{2}hr F	20	19	8	19	20	19	19
h-Air-tube,Btu/ft^{2}hr F	29	29	12	28	29	29	28
h-Bed-tube,Btu/ft^{2}hr F	85	78	30	76	82	86	81
			U-Tube 153-133				
Air flow rate, scfm	144	140	45	136	139	137	135
Air temp in, F	731	750	871	724	746	762	766
Air temp out, F	880	914	1055	889	933	934	959
U, Btu/ft^{2}hr F	15.8	16.7	7.8	16.7	19.7	17.3	18.9
h-Air-tube,Btu/ft^{2}hr F	30.6	30.1	12.4	29.9	31.0	30.7	29.8
h-Bed-tube,Btu/ft^{2}hr F	38.3	44.9	27.8	45.7	70.4	48.4	67.9
			U-Tube 113-93				
Air flow rate, scfm	144	140	45	136	139	137	135
Air temp in, F	880	914	1055	889	933	934	959
Air temp out, F	1036	1061	1113	1028	1046	1066	1076
U, Btu/ft^{2}hr F	21	18	3	17	14.8	16.5	142
h-Air-tube,Btu/ft^{2}hr F	32	30	12	30	30.5	30.9	29.7
h-Bed-tube,Btu/ft^{2}hr F	81	60	4	51	32.8	41.9	31.3

(Continued)

TABLE 4-13. (Continued)

Circuit No. 1							
Run No.	1	2	3	4	5	6	7
T-Bed F	1587	1626	1575	1582	1602	1632	1658
		U-Tube	73-53				
Air flow rate, scfm	144	140	45	136	139	137	135
Air temp in, F	1036	1061	1113	1028	1046	1066	1076
Air temp out, F	-	-	-	-	1110	1130	1140
U, Btu/ft^{2}hr°F	-	-	-	-	9.8	9.4	9.0
h-Air-tube,Btu/ft^{2}hr F	-	-	-	-	30.6	30.3	30.7
h-Bed-tube,Btu/ft^{2}hr F	-	-	-	-	15.3	14.6	13.6

(Continued)

- = No data

TABLE 4-13. (Continued)

	Circuit 2						
Run No.	1	2	3	4	5	6	7
T-Bed F	1587	1626	1575	1582	1602	1632	1658
	U-Tube 101-81						
Air flow rate, scfm	52	52	35	34	87	91	75
Air temp in, F	108	108	103	105	108	103	108
Air temp out, F	530	543	576	400	482	433	507
U, Btu/ft^{2}hr F	12.4	12	9.5	9.7	17.5	15.5	15.6
h-Air-tube,Btu/ft^{2}hr F	12.9	13	9.5	9.1	19.3	19.7	16.9
h-Bed-tube,Btu/ft^{2}hr F	-	-	-	-	-	148	-
	U-Tube 61-41						
Air flow rate, scfm	52	52	35	34	87	91	75
Air temp in, F	530	543	576	600	482	433	507
Air temp out, F	304	823	832	855	747	681	785
U, Btu/ft^{2}hr F	11	10.9	7.2	7.1	16.4	14.8	14.5
h-Air-tube,Btu/ft^{2}hr F	13	13.8	10.0	10	20.1	20.2	18.1
h-Bed-tube,Btu/ft^{2}hr F	157	107	40	38	238	86.5	167
	U-Tube 42-62						
Air flow rate, scfm	52	52	35	34	81	91	75
Air temp in, F	804	823	832	855	747	681	785
Air temp out, F	-	-	-	-	951	899	990
U, Btu/ft^{2}hr F	-	-	-	-	12.2	12.2	10
h-Air-tube,Btu/ft^{2}hr F	-	-	-	-	20.9	20.9	18
h-Bed-tube,Btu/ft^{2}hr F	-	-	-	-	36.3	36	28.6

Continued

TABLE 4-13. (Continued)

	Circuit No. 3						
Run No.	1	2	3	4	5	6	7
T-Bed F	1587	1626	1575	1582	1602	1632	1658
	U-Tube 121-141						
Air flow rate, scfm	47	77	35	63	94	151	104
Air temp in, F	108	108	103	105	108	103	108
Air temp out, F	551	502	526	504	473	420	458
U,Btu/ft^{2}hr f	11.7	16.2	8.3	13.9	18.5	24.6	18.7
h-Air-tube,Btu/ft^{2}hr F	11.9	17.4	9.1	14.8	20.8	29.9	21.9
h-Bed-tube,Btu/ft^{2}hr F	-	-	-	-	-	380.9	588
	U-Tube 142-122						
Air flow rate, scfm	47	77	35	63	94	151	104
Air temp in, F	551	502	526	504	473	420	458
Air temp out, F	735	755	955	952	740	752	756
U, Btu/ft^{2}hr F	4.7	10.1	9.5	17.5	13.1	25.9	15.3
h-Air-tube,Btu/ft^{2}hr F	12.0	18.2	9.8	15.7	21.4	32.3	23.2
h-Bed-tube,Btu/ft^{2}hr F	8.6	27.4	-	-	42.8	196	61.1
	U-Tube 123						
Air flow rate, scfm	47	77	35	63	94	151	104
Air temp in, F	735	755	955	952	740	752	756
Air temp out, F	-	-	-	-	983	928	989
U, Btu/ft^{2}hr F	-	-	-	-	16.1	17.4	16.0
h-Air-tube,Btu/ft^{2}hr F	-	-	-	-	22.1	31.9	23.9
h-Bed-tube,Btu/ft^{2}hr F	-	-	-	-	92.3	45.6	67

(Continued)

TABLE 4-13. (Continued)

Run No.	1	2	3	4	5	6	7
			Circuit No. 4				
T-Bed F	1587	1626	1575	1582	1602	1632	1658
			U-Tube 63-43				
Air flow rate, scfm	111	110	35	34	35	121	35
Air temp in, F	108	108	103	105	108	103	108
Air temp out, F	528	542	678	698	706	537	696
U, Btu/ft^{2}hr F	19.3	19.1	8.9	9.0	9.2	20.8	8.6
h-Air-tube,Btu/ft^{2}hr F	22.7	22.5	9.8	9.5	9.7	24.3	9.7
h-Bed-tube,Btu/ft^{2}hr F	551.8	532	-	-	-	809.6	-
			U-Tube 44-64				
Air flow rate, scfm	111	110	35	34	35	121	35
Air temp in, F	528	542	678	698	706	537	696
Air temp out, F	739	762	859	876	891	760	898
U,Btu/ft^{2}gr F	17.5	17.5	5.5	5.4	5.7	19.3	5.8
h-Air-tube,Btu/ft^{2}hr F	24.4	24.3	9.9	9.6	10	26.2	10
h-Bed-tube,Btu/ft^{2}hr F	93	97.1	15.3	14.6	16	120	17
			U-Tube 84-104				
Air flow rate, scfm	111	110	35	34	35	121	35
Air temp in, F	739	762	859	876	891	760	898
Air temp out, F	859	882	862	884	915	887	915
U, Btu/ft^{2}hr F	12.0	11.5	0.1	0.3	0.8	13.4	0.6
h-Air-tube,Btu/ft^{2}h F	24.8	24.7	9.9	9.6	10	27.0	10.0
h-Bed-tube,Btu/ft^{2}h F	26.7	24.7	0.1	0.3	0.9	30.5	0.6
			U-Tube 124-144				
Air flow rate, scfm	111	110	35	34	35	121	35
Air temp in, F	859	882	862	884	915	887	915
Air temp out, F							
U, Btu/ft^{2}hr F	-	-	-	-	-	-	-
h-Air-tube,Btu/ft^{2}hr F	-	-	-	-	-	-	-
h-Bed-tube,Btu/ft^{2}hr F	-	-	-	-	-	-	-

(Continued)

TABLE 4-13. (Concluded)

	Circuit No. 5						
Run No.	1	2	3	4	5	6	7
T-Bed F	1587	1626	1575	1582	1602	1631	1658
	U-Tube 92-112						
Air flow rate, scfm	153	150	35	36	156	157	155
Air temp in, F	108	108	103	105	108	103	108
Air temp out, F	484	498	646	648	485	493	489
U, Btu/ft^{2}hr F	22	22	8	8	22	22	21
h-Air-tube,Btu/ft^{2}hr F	30	29	9	10	31	31	31
h-Bed-tube,Btu/ft^{2}hr F	123.4	129	111	120	117	127	100
	U-Tube 111-91						
Air flow rate, scfm	153	150	35	36	156	157	155
Air temp in, F	484	498	646	648	485	493	489
Air temp out, F	854	813	872	810	775	710	770
U,Btu/ft-hr F	36	28	6	4	27	19	24
h-Air-tube,Btu/ft^{2}hr F	32	31	10	10	33	32	32
h-Bed-tube,Btu/ft^{2}hr F	-	-	16	7.2	393	60	203
	U-Tube 71-51						
Air flow rate, scfm	153	150	35	36	156	157	155
Air temp in, F	854	813	872	810	775	710	770
Air temp out, F	852	871	888	895	862	872	880
U, Btu/ft^{2}hr F	-	6.4	0.5	2.4	10	17.4	11.8
h-Air-tube,Btu/ft^{2}hr F	32	31.6	9.9	10.1	32.6	32.8	32.5
h-Bed-tube,Btu/ft^{2}hr F	-	8.3	0.5	3.3	15.2	44	20
	U-Tube 52-72						
Air flow rate, scfm	153	150	35	36	156	157	155
Air temp in, F	852	871	888	895	862	872	880
Air temp out, F	-	-	-	-	991	1004	1014
U,Btu/ft^{2}hr F	-	-	-	-	14.5	14.6	14.2
h-Air-tube,Btu/ft^{2}hr F	-	-	-	-	33.1	33.0	34.0
h-Bed-tube,Btu/ft^{2}hr F	-	-	-	-	28.9	28.9	27.4

Effect of Excess Air. The major effect of changing air is in the change in design heat output rating of a unit of a specific size. Excess air did not affect combustion efficiency and had a minor effect on limestone utilization. Since fluidized bed units are designed for a specific area and superficial velocity, the air rate at design conditions is fixed. More fuel can be burned at low excess air and, thus, the heat rating of a fluidized bed combustor is higher if a low excess air is specified. The combustion efficiency at 13% excess air was not significantly different than when using 50% excess air (see run 6 versus run 4).

The limestone usage for runs 4 and 6 were not significantly different. However, the sulfur distribution in the ash was different with 13% excess air, the sulfur content of the bed drainipgs was the greatest of all runs, and the sulfur content of the fly ash was the least of all runs. The limestone would be expected to be used more efficiently at low excess air, since the allowable SO_2 concentration is higher. (SO_2 emission regulations limit the amount of SO_2 emitted per M Btu of fuel fed). Since less flue gas is exhausted per unit of fuel at low excess air, the actual allowable concentration of SO_2 in ppm is greater).

The lower limit of excess air was not determined in this series of runs. It probably is about 10% since with less excess air, normal local bed variation may cause momentary substoichiometric conditions that would reduce efficiency. A 10-15% excess air level is recommended because a smaller (and, therefore, less expensive) unit can be used.

Effect of Limestone Rate. The SO_2 concentration in the flue gas could be readily controlled by changing the limestone rate. With the Grove limestone used, the stone was active only for a short time after it was fed into the bed (perhaps 15-30 minutes). After this time, it appeared to be inert. This is contrary to Battelle experience with Greer limestone which remained active for many hours after feeding and with the Greer limestone changes in limestone feed rate, did not affect the SO_2 concentration in the flue gas for several hours.

Heat Transfer Coefficient. The heat transfer coefficient data are not as accurate as desired, and the experimental technique was modified for later tests to obtain more accurate data. The internal resistance to heat transfer between the air and the tube was too large to permit accurate calculations of the bed-to-tube heat transfer coefficient.

Recommendations. For the 6' x 6' Rocketdyne bed:

1. A limestone finer than 8 mesh should be used to improve turndown
2. The design superficial velocity of 6 ft/sec is satisfactory
3. The design operating temperature of 1650 F is satisfactory
4. The minimum excess air should be 10-15%

4.2.2 24-Inch Characterization (Runs 8-16)

The 24-inch fluidized bed described in the previous section was operated for runs 8 through 16 to characterize its combustion conditions. The main purpose was to define conditions for later metal heat exchanger alloy sample exposure, and to define operational parameters for the 6' x 6' fluidized bed and for prototype beds. Considering all 16 runs, the bed operated satisfactorily over a wide range of conditions. The recommended operating conditions for larger units can be determined primarily by erosion/corrosion considerations rather than operability limits.

The oxygen probe measurements made in the operating bed during the first tests showed, when burning coal, oxygen concentrations of 10^{-13} atm were present most of the time over the coal feed port, and for very short but frequent time intervals in the rest of the bed. This reducing (fuel rich) atmosphere may rapidly corrode high nickel alloys by a sulfidation reaction. To reduce the potential for corrosion, the distance between the coal feed port and the heat exchanger tubes was increased by 10 inches and another set of characterization experiments made (tests 8 through 10). Then, for tests 11 through 16, the coal feed port was modified to spread the coal over a larger area of the bed, and some of the experiments were repeated. This change had a significant effect on the measured oxygen levels in the bed, but no effect on the operability or bed operating parameters.

Heat transfer measurements were made and the measured heat transfer coefficients were about 60 Btu/hr-ft^2-F. Several other experiments were performed to examine bed conditions under unusual conditions. In a future advanced AFB concept, two fluidized beds would operate in series. The first bed would operate at about 1850 F, at a temperature where limestone does not efficiently absorb SO_2 The flue gas from this bed would be cooled and mixed with combustion air inserted into a second bed operating at 1650 F. One experiment (run No. 6) was to determine if SO_2 from the first bed would efficiently be removed in the second bed.

In another experiment (run No. 16), the conditions of the B&W 6' x 6' bed were duplicated so oxygen measurements for that bed condition could be correlated with the other measurements made in the 24 inch bed. Run No. 9 was made using coke for fuel eliminating the volatiles from the combustion process.

Equipment Changes. During the shutdown between operation in January 1981, which was reported in the previous section, and the August 1981 operation reported in this section, several changes described below were made in the equipment. These were used for tests 8 through 16, except the feed port was modified as indicated for tests 11 through 16.

Combustor. A 10-inch-high section was added to the combustor just above the distributor plate. The coal feed port was relocated into this 10-inch section. Two of the combustor thermocouples were placed in this section as was a pressure tap measuring pressure just above the distributor plate. The depth of the bed was increased 10 inches by this change.

Feed Systems. A star valve replaced the Penberthy ejector previously used to feed coal and limestone into the bed. The ejector was used in January after the L-valves designed into the system failed and no other immediate replacement was available. The ejector's performance was marginal, and with the deeper bed installed between January and August (and, thus, higher pressure differential), an ejector may not have been usable. The star valve was known to work well but has a short life because the seals quickly wear out. This partially satisfactory feed system was used because no satisfactory feed system was available.

With the star valve, the ratio of primary to total air can be controlled. Such control was not possible using the ejector, but some error in the overall combustor air flow measurement is introduced by both methods. The ejector aspirated unmeasured air into the system, while some unmeasured air leaked out of the system through the star valve. The unmeasured air in either case was probably less than 5 cfm.

The air metering system for the coal injection has been changed. A different rotormeter was installed for more accurate reading. The coal and limestone rates were determined by feeder calibration and now are obtained by weighing a timed sample.

Feed Port. The feed port was modified as sketched in Fig. 4-55 for experiments 11-16. The coal enters from behind and is blown just under the 6-inch-diameter top plate. Combustion air enters from the plenum through the two tubes on the bottom. Four holes in the bottom of the port blow air into this coal stream and carry it out to the periphery. At this point, 12 additional jets entrain the coal and disperse it into the bed. The 16 air ports are 5/16-inch diameter to obtain good penetration. The air flow through the coal distributor is the same as it had been through the six bubble caps on the inner diameter of the distributor plate. These bubble caps were welded shut when the new coal port was installed.

Distributor Plate. When the feed port was modified, about one third of the combustion air was admitted through it. Therefore, as indicated above, the six distributor caps in the center were plugs.

Igniter. The Dutch oven under the combustor, described in the previous section (Fig. 4-49) was removed and replaced by a completely new ignition system that used a can heater to replace the old Maxon burner. A new safety system for turning off rhe gas if flame is lost was installed. The thermocouples and pressure tap from the Dutch oven were installed in the new plenum. The new ignition system can burner (jet engine-type) was fired by natural gas at rates up to 1,000 Btu/hr. The hot combustion gases from the burner flowed into the plenum under the bed. The gas temperature could be regulated from about 900 F to 1700 F over a wide range of flow conditions. All the combustion air for the fluidized bed passed through the burner, even when gas is not being burned.

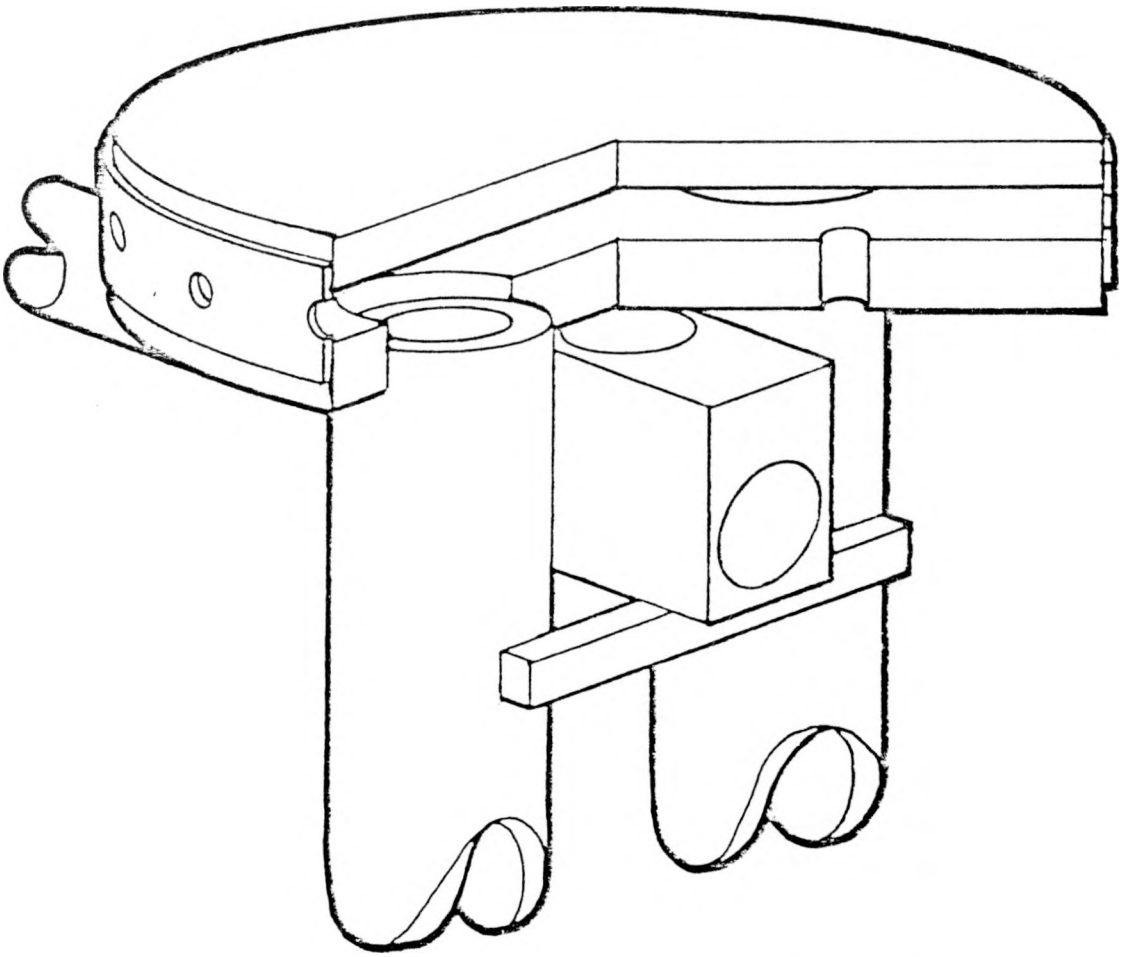


Figure 4-55. Modified Coal Feed Port

Heat Exchanger. An air-cooled heat exchanger was placed in the bed to remove heat for control of bed temperature to simulate the bed geometry in prototype units and for measurement of heat-transfer rates. Figures 4-52a and b, 4-56 and 4-57 show the heat exchanger configuration. The entire heat exchanger could be removed as a unit from the fluidized bed. Fifty-three 2-inch pipes penetrate the refractory and air-cooled U-bends could be placed between any two adjacent penetrations. Each penetration was numbered for reference. The penetrations are on 6-inch centers and the rows are 3 inches apart. The tubes are 2 inches OD by 0.120-inch wall thickness. Uncooled 2-inch tubes were placed in positions 72, 83, 103, 131, and 151. In the 250-hour experiments, metal or ceramic specimens were placed in these positions. The air passed through the heat exchanger in five parallel paths and two, three, or four U-tubes were in each path. Five paths were needed to pass the required cooling air and several U-tubes were needed in series so heat transfer coefficients could be determined at several temperatures. Table 4-14 lists the penetrations used by the U-tubes in each pass.

Two U-tubes (131-151 and 52-72) were removed from the heat exchanger bundle because these positions were used for diagnostics or to expose ceramic samples. U-tube 131-151 was replaced with uncooled tubes as was the part of the U-tube in Position 72. Position 52 was used for diagnostics. The heat exchanger external passes were replumbed. External insulation was placed on the heat exchanger at the location of the thermocouples to reduce radiation effects on temperature measurements.

Diagnostic Ports. Figure 4-56 shows the location of diagnostic ports as they relate to the heat exchanger bank. The centerline of the lowest diagnostic test port is 16 inches above the air bubble caps and 13 inches above the coal feed port. The diagnostic and metal exposure ports enter from the side opposite the heat exchanger tubes. The ports for ceramic exposure are identical to the ports for heat exchanger and enter from the heat exchanger side. The ceramic and metallic exposure ports above row 40 were filled with uncooled 2-inch tubes to simulate heat-exchanger tubes in the fluidized bed during these experiments. The lowest row of exposure ports simulate the lowest row of heat exchanger tubes in

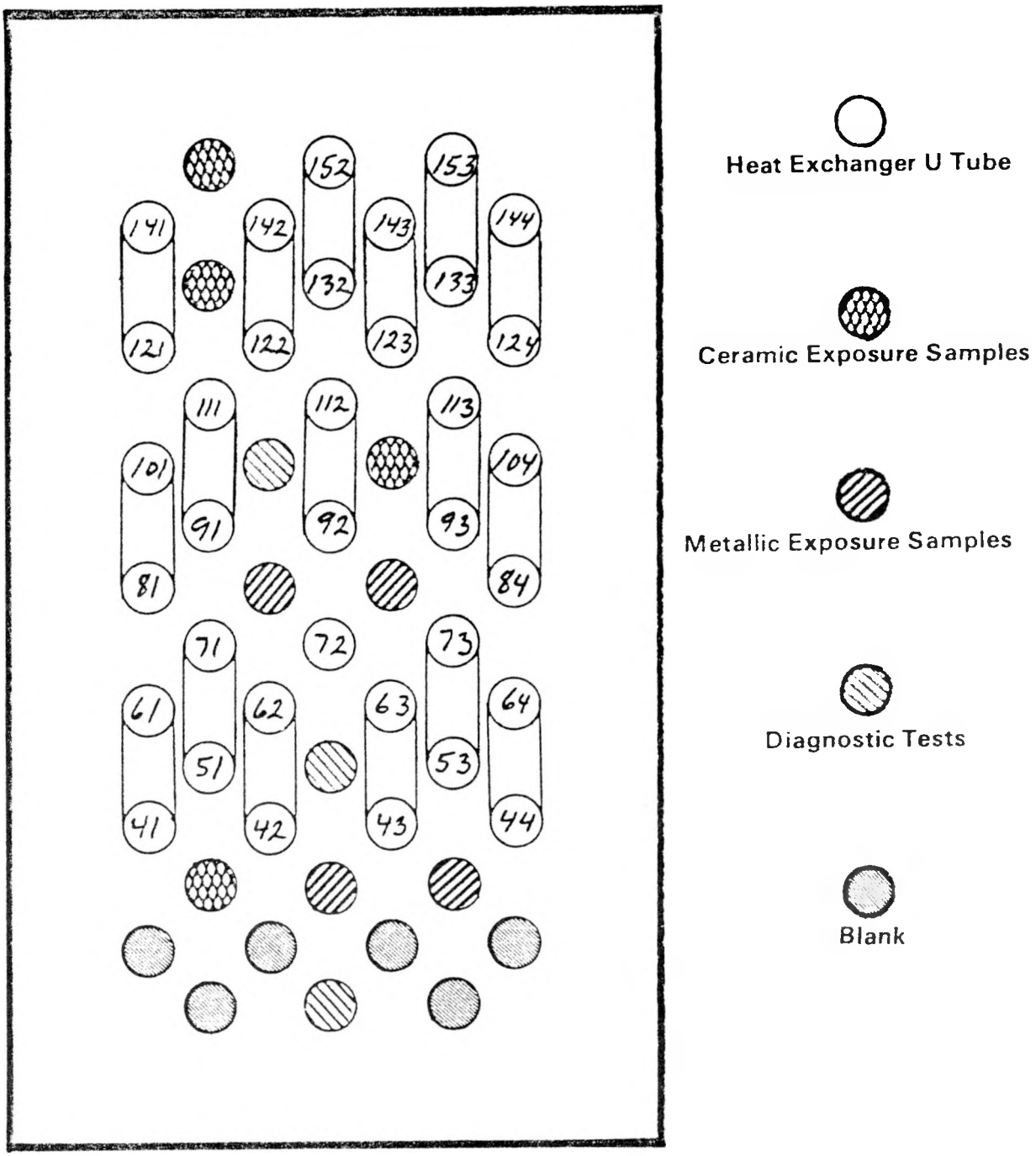


Figure 4-56. End View of Heat Exchanger Showing Location of Heat Exchanger Tubes

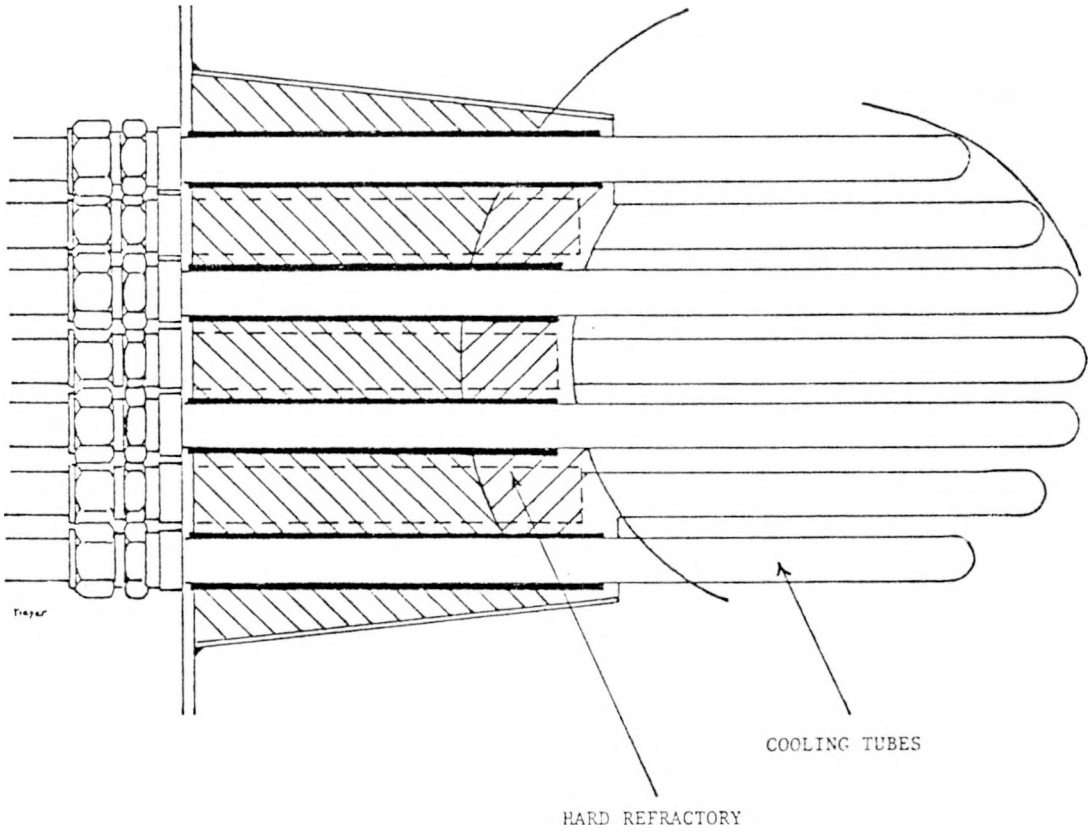


Figure 4-57. Top View of Heat Exchanger

TABLE 4-14. AIR PATHS THROUGH HEAT EXCHANGER

	1	2	3	4	5
NO. 1 U-TUBE	141-121	142-122	53-73	63-43	92-112
NO. 2 U-TUBE	101-81	123-143	93-113	44-64	111-91
NO. 3 U-TUBE	61-41		133-153	84-104	71-51
NO. 3 U-TUBE	42-62		152-132	124-144	

the prototype. The other exposure ports simulate the other tubes. The blank positions are placed where heat-transfer tubes may be inserted into the bed, but were not used during these experiments.

Fig. 4-58 is a sketch of a diagnostic port. When not in use, the ball valve seals the port from the bed. Air from the side entrance is used to blow bed material from the port into the bed just before insertion of the probes. Additional probes/diagnostic ports were installed at positions 12 and 52.

Coal and Limestone Feeders. The coal and limestone feeder system (Fig. 4-53 includes screw feeders which are volumetric feeders with a helical screw feeding through a 2-inch tube.

The screw is driven by a d-c motor through an SCR controller. A rough calibration of the feeders was made before operation. During operation, the coal and limestone rates were determined by collecting the coal or limestone for a predetermined time (7.9 seconds) and weighing the material collected.

The coal drops from the feeder into a Meyer abrasion-resistant 6- by 6-inch rotary valve. The valve is sealed with polyurethane seal strips. These seal strips wear out in about 250 hours and need replacement. The purpose of the valve is to seal the 3 or 4 psi presssure in the feed line from the atmospheric pressure at the feeders. A little air bleeds back through the valve when the seal is good and an excessive quantity blows back when the seal is worn. This air is very dirty and a small hood (not shown) collected this dust.

The coal pickup under the rotary valve consisted of a homemade ejector to suspend the solids in the air. The ejector was made to avoid plugging rather than to overcome the bed pressure. It may reduce the pressure across the rotary air seal by 1 psi. A 1-inch pipe is used to pneumatically convey the coal to the bed. Just outside of the bed, the size is reduced to a 3/4-inch ID tube.

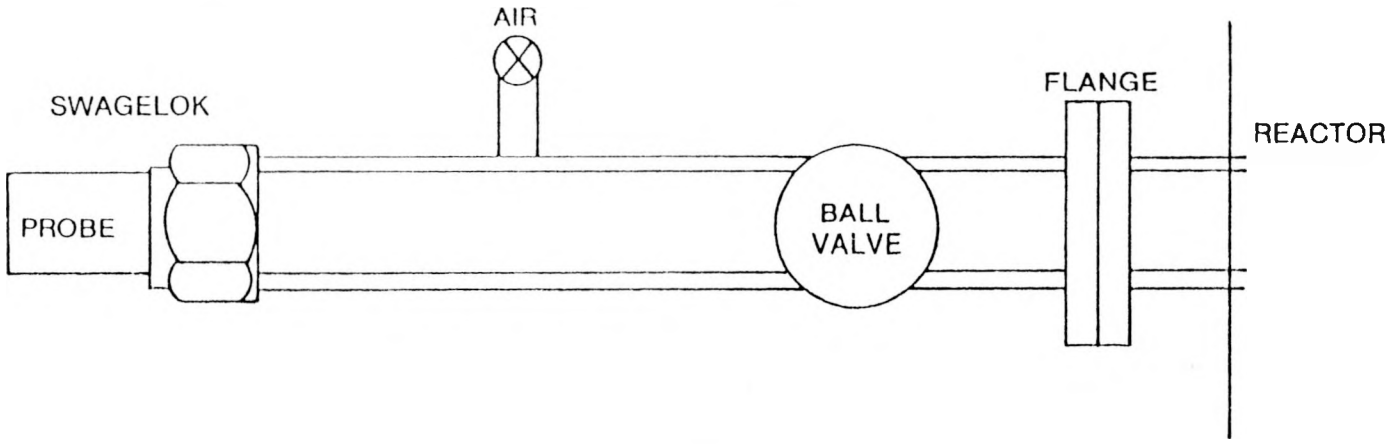


Figure 4-58. Diagnostic Port

Miscellaneous. Other changes that improve operations, but which did not affect experimental results, included lowering of a platform because the old one interfered with probe insertion at position 12, adding an air filtration system at the feeder to make a cleaner operation, and installing permanent electrical wiring for the feeders (required by Safety).

Materials.

Fuel. Coal from Illinois No. 6 seam was used as fuel. It was dried, ground, and sieved. For most experiments, a -8 mesh grind was used. For use in experiments designed to determine the effect of coal size, the -8 mesh grind was sieved into an 8 x 30 mesh fraction and a -30 mesh fraction. The chemical analysis of the -8 mesh grind used for experiments 1-10, 11-16, the 8 x 30 mesh fraction, and the -30 mesh fraction are presented in Table 4-16. The sieve analyses are given in Table 4-15. Getty fluid petroleum coke was used in experiment 9. It was sieved through 8 mesh before using and the oversize discarded. The chemical and sieve analyses are presented in Tables 4-15 and 4-16.

TABLE 4-15. SIZE ANALYSIS OF COAL, COKE, AND LIMESTONE

NOMINAL SIZE MATERIAL (MESH)	WEIGHT, PERCENT				
	-8 MESH COAL	8 X 30 MESH COAL	-30 MESH COAL	-8 MESH COKE	8 x 20 MESH LIMESTONE
+12	20.5	20.1	0.2	0.5	31.5
-12 +20	27.0	37.7	0.4	1.7	48.7
-20 +40	17.0	29.6	14.8	2.4	14.1
-40 +100	15.9	6.9	48.6	47.7	3.4
-100 +200	9.3	1.4	20.7	42.9	1.2
-200 +325	7.8	1.9	12.8	4.2	0.8
-325	2.5	2.4	2.5	0.6	0.3

TABLE 4-16. CHEMICAL ANALYSES OF FUELS

Sample Run	-8 mesh 1-10		-8 mesh 11-16		8 x 30 mesh 7		-30 mesh 8		Coke 9	
	as Burned	Dry	as Burned	Dry	as Burned	Dry	as Burned	Dry	as Burned	Dry
Proximate										
Moisture	9.88	--	11.06	--	10.21	--	8.47	--	1.92	--
Ash	11.38	12.63	10.02	11.27	10.53	11.73	12.07	13.19	0.58	0.59
Volatile	35.32	39.19	35.30	39.69	35.51	39.55	35.09	38.34	5.71	5.82
Fixed Carbon	43.42	48.18	43.62	49.04	43.75	48.72	44.37	48.47	91.79	93.59
Btu/lb	10947	12147	10995	12362	11071	12330	11054	12077	13819	14090
Ultimate										
Moisture	9.88	--	11.06	--	10.21	--	8.47	--	1.92	--
Carbon	60.88	67.55	61.40	69.03	61.49	68.48	61.48	67.17	85.69	87.37
Hydrogen	4.33	4.80	4.42	4.97	4.49	5.00	4.44	4.85	1.89	1.93
Nitrogen	1.04	1.15	1.09	1.23	1.03	1.15	1.09	1.19	0.89	0.91
Chlorine	0.19	0.21	0.15	0.17	0.16	0.18	0.12	0.13	0.03	0.03
Sulfur	4.07	4.52	3.74	4.20	3.97	4.42	4.02	4.39	5.45	6.08
Ash	11.38	12.63	10.02	11.27	10.53	11.73	12.07	13.19	0.58	0.59
Oxygen	8.23	9.14	8.12	9.13	8.12	9.04	8.31	9.08	3.04	3.09

Coal analyses are a set of standardized procedures that give the results listed in Table 4-16. The fixed carbon in the Proximate analysis and the oxygen in the Ultimate analysis are not necessarily related to the carbon and oxygen contents of the coal, as both are obtained by difference rather than by analysis. The analyses were designed for medium to high volatile coal and the analysis of Illinois No. 6 coal should represent physical reality. However, the coke analysis is less meaningful. The volatile fraction is probably reported high. The sulfur in the coke as well as carbon is reported as fixed carbon.

Limestone. Grove limestone was the same as used in January. The size analysis is presented in Table 4-15 and the chemical analysis in Table 4-16.

Sulfur Dioxide. Commercial grade sulfur dioxide was added to the fluidizing gas in one experiment (No. 6). The initial bed material was spent bed from the January experiments. It was approximately the same size and composition as the spent bed from these experiments.

Ignition and Warmup. To ignite the fluidized bed, the gas burner is turned on at as low a temperature as possible, with stable combustion. Bed material is added to bring the bed level to about 20 inches. The low 20-inch level is needed to limit heat extraction by the heat exchanger. When the bed reaches about 1000 F (4-5 hours), coal feed is started. When the bed reaches 1400 F, bed material is added to increase the bed level to the operating level. When 1500 F is reached, the gas to the burner is shut off and prescribed conditions are set. Prescribed conditions can be reached within 1 hour, but about 8 hours are needed to reach thermal equilibrium. Chemical equilibrium is attained at about the same time if a previously used bed material was loaded into the bed. Twelve to 24 hours are needed to sulfate a bed of limestone if no spent bed material is available, and about 48 hours is needed to complete the calcination of the limestone.

Data.

Operability. One to 3 hours were needed to reach steady state after changing conditions, depending on the severity of the change. The first experiment was started about 10 hours after temperature was reached; five hours probably would have been adequate.

The system was operable over the entire planned test range and, from the operator's standpoint, all of the conditions using coal, except for the high rate in run No. 16, were reached easily. The conditions were changed easily between experiments.

Air flow was regulated with a control valve. The coal flow was set by an uncalibrated controller. Since the O_2 reading was delayed 1-2 minutes (time for the sample gas to pass through the sample line), 5-10 minutes were needed to adjust the coal rate. The limestone rate took about 10-15 minutes to adjust.

The prescribed conditions (same as experiment 1, except for fuel) were not attained when burning coke (run 9). When the operator set new conditions, the bed temperature dropped and the freeboard temperature rose. However, it was found possible to operate with a bed temperature of 1700 F and a slightly reduced air flow.

In run No. 16, the prescribed conditions were not attained because of inadequate bed cooling. Additional heat exchanger tubes or a change in cooling air flow pattern to permit more cooling would be necessary before the 8-ft/sec velocity at 1550 F and 15% excess air can be attained. Run 16 was made at a 7.2 ft/sec superficial velocity while maintaining the prescribed temperature and excess air.

Chemical, Temperature and Flow Data. Table 4-17 presents the operational data for the experiments. In the table, the run condition describes the parameter varied for each experiment. The base case is the best estimate of conditions under full load in a prototype fluid bed. The first 10 runs were made with the coal feed port of Fig. 4-51, and the next 6 used the feed port of Fig. 4-55. The numbers in Table 4-17 were obtained by averaging hourly readings. The coal and limestone rates were obtained by taking 7.9 second samples and weighing. The samples were then used for sieve and chemical analyses.

TABLE 4-17. OPERATIONAL DATA

Run No.	1	2	3	4	5	6
Run Condition	Base Condition	High Primary Air	Low Primary Air	High Excess Air	Low Rate	Series Bed
Coal Rate lb/hr	139	136	134	112	81	111
Limestone lb/hr	37	64	53	50	33	75
Bed Temp, °F	1635	1640	1650	1640	1645	1640
Fluidizing air scfm	260	236	280	264	140	264
Coal conv air scfm	28	56	16	28	28	29
Total air scfm	288	292	296	292	168	293
Flyash rate lb/hr	20	22	22	17	2.6	13
Bed drain ash lb/hr	12	25	15	14	30	14
Bed depth, in.	67	68	67	66	66	71
Dist. plate Δp in. Hg	1.5	1.5	1.5	1.5	.7	2.5
O_2 in flue gas %	3.5	3.4	3.4	7.2	3.2	3.1
SO_2 in flue gas, ppm by vol	592	522	522	421	739	530
Length of run, hr	8-1/2	3	3	3	3	3

TABLE 4-17. (Continued)

Run No.	7	8	9	10	11	12
Run Condition	Coarse Coal	Fine Coal	Getty Coke	Base Condition	Base Condition	High Primary Air
Coal Rate lb/hr	133	124	104	139	132	139
Limestone lb/hr	46	63	0	60	50	54.6
Bed Temp, °F	1640	1630	1695	1630	1650	1655
Fluidizing air scfm	270	264	224	270	272	236
Coal conv air scfm	28	29	29	29	28	56
Total air scfm	298	293	253	299	300	292
Flyash rate lb/hr	31	14	20	28	19.5	26
Bed drain ash lb/hr	14	25	0	30	25	40
Bed depth, in.	67	68	70	69	68	60
Dist. plate Δp in. Hg	1.5	1.5	1.1	1.5	1.5	1.5
O_2 in flue gas %	2.8	4.2	2.7	3.4	3.3	3.3
SO_2 in flue gas, ppm by vol	428	586	-	496	567	567
Length of run, hr	3	4	3	3	4	3

TABLE 4-17. (Concluded)

Run No.	13	14	15	16
Run Condition	Low Excess Air	High Excess Air	Low Rate	B&W Condition
Coal Rate lb/hr	139	107	82.0	144
Limestone lb/hr	57	40	36	47
Bed Temp, °F	1650	1655	1650	1540
Fluidizing air scfm	238	236	152	322
Coal conv air scfm	56	56	28	31
Total air scfm	294	292	180	353
Flyash rate lb/hr	26	28	10	22
Bed drain ash lb/hr	20	30	25	25
Bed depth, in.	67	69	68	65
Dist. plate Δp in. Hg	1.2	1.2	.5	1.5
O_2 in flue gas %	2.2	7.1	3.2	3.0
SO_2 in flue gas, ppm by vol	432	470	622	600
Length of run, hr	3	3	4	3

Heat Transfer Data. The heat transfer coefficient between the bed and tubes was determined under the conditions of run No. 1 before that run was started. The coefficient in each U-tube was calculated from data obtained with maximum air flow through the U-tube. The air through the other U-tubes was reduced to control bed temperature. An additional set of data was taken during run No. 16 when all of the heat exchanger tubes were using air at near the maximum rate to maintain bed temperature. The heat transfer data obtained from the other experiments were not reduced to heat transfer coefficients because the coefficients would not be sufficiently accurate.

Table 4-18 presents the heat transfer data. The data for experiment No. 1 were taken before the diagnostic data. The cooling air flow was increased to maximum through the passage where measurements were made and reduced in the other four parallel passages to maintain a heat balance. The superficial velocity was 6.2 ft/sec. During experiment No. 16, the cooling was almost maximum during the experiment and the flow shown was maintained throughout the experiment. The superficial velocity was 7.2 ft/sec.

The temperature was measured 10 places in the bed and 2 places in the freeboard. The temperature reported is the average of three thermocouples below the heat exchanger tubes and one above the heat exchanger tubes.

The fluidizing air rate was calculated from an orifice pressure drop and pressure reading. The coal conveying air is from a rotometer reading. No correction for leakage through the star valve was made. It probably was zero for the first few experiments (starting with run No. 8) and increased to about 5 cfm for the last run, No. 16. The fly ash rate was obtained by weighing the fly ash collected for the entire run. The rate for bed drainings was obtained from the weight drained during and after the experiment. The time between runs was included.

Ash Analyses. Table 4-19 presents the chemical analyses and Table 4-20 presents the sieve analyses of the fly ash and bed material. The fly ash was collected in both a cyclone and a baghouse and the samples were combined for chemical analyses. Ten to 20% of the fly ash was collected in the baghouse. The siz did not change significantly between experiments.

TABLE 4-18. HEAT TRANSFER DATA

U-Tube	Air flow Rate SCFM	Air Temp °F in	Air Temp °F out	Air Temp °F Bed	Heat Transfer Coefficient Btu/hr ft^2°F Overall	Heat Transfer Coefficient Btu/hr ft^2°F Air-Tube	Heat Transfer Coefficient Btu/hr ft^2°F Bed-Tube
			Experiment 1				
142-122	200	113	458	1644	26.3	37.3	62
123-143	200	458	726	1644	26.4	39.3	58
53-73	156	116	470	1654	23.4	30.4	63
93-113	156	470	736	1654	22.8	32.3	54
133-153	156	736	937	1654	22.1	33.4	48
152-132	156	937	1040	1654	11.8	33.4	17
141-121	162	116	410	1650	24.2	31.0	67
101-81	162	410	644	1650	23.8	32.5	59
61-41	162	644	832	1650	23.6	34.3	54
42-62	162	832	996	1650	18 7	34.3	34
63-43	155	113	498	1652	23.0	31.2	58
44-64	155	498	694	1652	20.3	30.6	44
84-104	155	694	856	1652	20.2	33.5	40
124-144	155	856	990	1652	20.1	32.9	40
92-112	186	111	474	1643	24.4	34.1	59
111-91	186	474	710	1643	24.1	35.2	55
71-51	186	710	888	1643	22.6	37.4	45
			Experiment 16				
142-122	165	117	466	1540	23.9	31.8	62
123-143	165	466	726	1540	23.6	33.3	56
53-73	150	117	455	1540	23.3	29.0	68
93-113	150	455	701	1540	22.1	30.8	53
133-153	150	701	886	1540	21.5	31.1	49
152-132	150	886	977	1540	10.9	32.4	15
141-121	150	117	349	1540	18.7	31.3	37
101-81	150	349	625	1540	27.8	30.4	110
61-41	150	625	788	1540	20.7	30.9	46
42-62	150	788	943	1540	17.9	31.9	33
63-43	152	117	484	1540	23.4	29.4	67
44-64	152	484	666	1540	20.2	29.6	46
84-104	152	666	822	1540	21.3	32.0	47
124-144	152	822	945	1540	20.0	32.2	41
92-112	158	117	472	1540	22.0	30.7	53
111-91	158	472	698	1540	21.6	32.2	48
71-51	158	698	858	1540	19.1	33.3	37

TABLE 4-19. CHEMICAL ANALYSIS OF FLY ASH AND BED MATERIAL

Run No.	Fly Ash					Bed Material		
	Ca	S	C	CO_3	Ca/S	Ca	S	Ca/S
	Wt. Percent							
1	14.1	3.5	11.5	0.83	3.2	49.6	8.5	4.7
2	28.0	6.6	5.5	1.53	3.4	51.4	9.5	4.3
3	29.2	10.6	6.0	2.51	2.2	53.9	7.6	5.6
4	21.7	5.6	5.1	1.05	3.1	46.8	10.4	3.6
5	14.2	4.3	6.8	1.04	2.6	50.7	9.7	4.2
6	30.8	6.5	5.7	1.02	3.8	47.7	10.4	3.7
7	15.6	4.7	8.4	1.03	2.6	48.1	10.4	3.7
8	19.0	4.6	8.5	1.25	3.3	50.0	9.6	4.2
9	7.0	6.8	74.3	0.22	0.8	46.7	11.3	3.3
10	25.3	5.6	8.8	1.00	3.6	48.5	9.6	4.0
11	19.0	4.6	11.1	1.01	3.3	48.8	10.3	3.8
12	33.6	7.7	6.5	0.88	3.4	48.3	10.8	3.6
13	21.4	5.1	7.8	1.00	3.3	53.9	8.3	5.2
14	27.3	7.0	5.0	0.97	3.1	54.5	7.7	5.7
15	19.6	5.0	5.8	0.58	3.1	48.2	10.7	3.6
16	25.1	7.0	9.6	1.33	2.9	48.2	9.8	3.9

TABLE 4-20. SIEVE ANALYSIS OF ASH AND BED DRAINING

Sieve Size	Cyclone Ash	Baghouse Ash	Bed Draining
+12	1.9	*	16.3
-12 + 20	7.2		47.5
-20 +40	6.1		28.7
-40 +100	11.2		7.5
-100 +200	12.7		0
-200 +325	8.9		0
-325	51.7		0

* Baghouse ash could not be sieved. Appears to be all -325 mesh.

The baghouse ash could not be sieved because of severe agglomeration. Severe agglomeration is typical of solids without particle sizes of less than 20 microns. The solids captured in the baghouse should be less than 10 microns because larger particles are caught in the cyclone.

Discussion of Data. Table 4-21 is a summary of the results of each experiment. The superficial velocity, excess air, sulfur dioxide emission, combustion efficiency, ratio of primary to total air, and bed depth are calculated from the raw data.

Temperature. Figure 4-59 shows typical temperature variations measured at one time with different thermocouples in the bed. All thermocouples were located about 1 inch from the reactor wall. Multiple thermocouples at the same elevation were at different points on the circumference.

Run No. 10 was an experiment at base conditions and is typical of most experiments. In run No. 9, coke was the fuel and freeboard burning was extreme as noted by the temperature rise in the freeboard. Run No. 16 was made at high velocity and low temperature. A small amount of freeboard burning took place as deduced from the rise in freeboard temperature and poorer combustion efficiency.

At the very bottom of the reactor, one of the thermocouples read lower than the other because it did not extend quite as far into the bed as it should have. The thermocouples in the heat exchanger section also read lower, possibly because of the influence of the heat exchanger tubes.

The time variation of temperature during a run was related to the oxygen probe measurements. The oxygen probe was water cooled and when fully inserted into the bed, absorbed about 5% of the heat in the coal feed. The bed temperature usually dropped about 20 degrees as the oxygen was read at one port and then it rose the same 20 degrees after the probe was withdrawn to insert into another port. When oxygen measurements were not being made, the temperature could be kept constant.

TABLE 4-21. RUN SUMMARY

Run No.	Bed Temp, °F	Superficial Velocity ft/sec	Excess Air Percent	SO_2 lb/10^6Btu	Length of Run, hr	Combustion Efficiency Percent	Ca/S Ratio	Fuel	Fuel Size Mesh	Primary Total Air Ratio Percent	Bed Depth in.
1	1635	6.2	19	1.44	8.5	97.8	2.1	Coal	-8	10	67
2	1640	6.3	19	1.27	3	98.8	3.7	Coal	-8	19	68
3	1650	6.4	19	1.33	3	98.8	3.1	Coal	-8	5	67
4	1640	6.3	51	0.81	3	99.0	3.5	Coal	-8	10	66
5	1645	3.6	18	1.82	3	98.6	3.2	Coal	-8	17	66
6	1640	6.3	17	1.3	3	99.1	4.1	Coal + gas	-8	10	71
7	1640	6.4	15	1.08	3	97.4	2.7	Coal	-8 +30	9	67
8	1630	6.3	25	1.36	4	98.8	4.0	Coal	-30	10	68
9	1695	5.6	15	--	3	85.7	--	Coke	-8	11	70
10	1630	6.4	19	1.21	3	97.7	3.4	Coal	-8	10	69
11	1650	6.5	18	1.40	4	97.8	3.0	Coal	-8	9	68
12	1655	6.3	18	1.40	3	98.4	3.1	Coal	-8	19	69
13	1650	6.3	11	1.13	3	97.9	3.2	Coal	-8	19	67
14	1655	6.3	50	0.91	3	98.3	3.9	Coal	-8	19	69
15	1650	3.9	18	1.53	4	99.1	3.4	Coal	-8	16	68
16	1540	7.2	16	1.50	3	98.1	2.6	Coal	-8	9	65

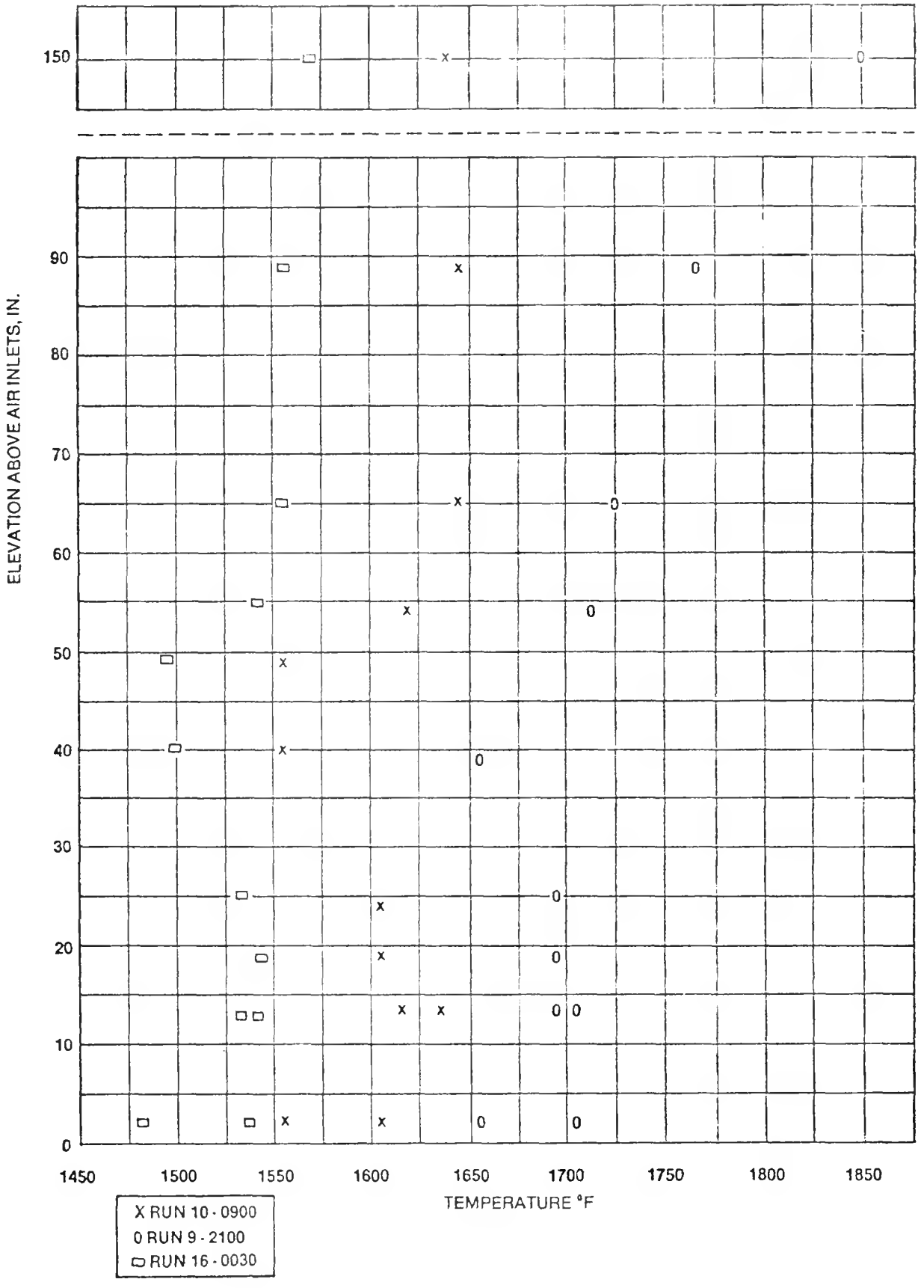


Figure 4-59. Temperature Distribution in Bed

The temperature rise to the 150-inch high point in the freeboard gives an indication of burning in the freeboard. In the low-temperature run (Run No. 16), the freeboard temperature was higher than the bed temperature, indicating poorer combustion in the bed.

The bed temperature was changed only for run No. 9 and 16, and, in those runs, other variables were changed so that the effect of temperature could not be obtained. Data from other experiments indicate that at temperatures above 1650 F sulfur capture is poor and at temperatures below 1400 F combustion efficiency is poor. The operators reported that sulfur capture was better at the lower bed temperatures as the temperature varied during an experiment.

Effect of Superficial Velocity. The superficial velocity was varied in run No. 5 and 15. Except for operating at a reduced rate, no significant changes were observed. While the total amount of ash decreased as expected, almost all of the decrease was in fly ash. The amount of bed drainings was similar to operation at a higher rate.

Effect of Primary (Conveying) Air Rate. The base case (runs No. 1, 10, and 11) used 10% primary air. In run No. 3, the primary air was reduced to 5% of the total air and in run No. 2 and 12, the primary air was 20% of the total air. The base case was 10% of the total air. Ihe oxygen level as measured with the oxygen probe in the bed was higher with the greater primary air flow and this appears desirable. Runs No. 13 and 14 also were made with 20% primary air. Changing the amount of primary air did not affect the operation of the fluid bed, the combustion efficiency, or the sulfur capture.

Effect of Excess Air. In the base condition, 20% excess air was used. The excess air was increased to 50% in runs No. 4 and 14 and reduced to 10% in Run No. 13.

The combustion efficiency was marginally improved with the higher excess air. Sulfur capture may have improved, but the improvement, if any, is less than the data scatter. Operationally, excess air was changed by changing coal rate. At constant fluidization velocity, less heat is generated and removed at high excess air.

Effect of Coal Size. Most of the experiments were made with a -8 mesh coal. For one experiment, the -30 mesh was screened out and used. For another experiment, the 8 x 30 mesh coal from the same screening operation was used. The combustion efficiency was best and sulfur capture poorest with the -30 mesh coal. Also, the freeboard temperature was about 20 F above the bed temperature when using -30 mesh coal as compared with about 5 degrees when using 8 x 30 mesh coal. These data indicate that more fine coal burns in the freeboard than coarse coal. The sulfur released in the freeboard is not captured as readily as the sulfur released in the bed. Also, the char from the coarse coal blows out to the bed and does not burn completely in the freeboard.

Effect of Coal Feed Port Design. The coal feed port was changed between runs No. 10 and 11 from the design of Fig. 4-51 to the design of Fig. 4-55. The oxygen concentrations in the bed as reported in another report changed slightly. Because the oxygen level was more uniform and more controllable, the use of the new port was recommended for the 250-hour metal exposure experiments. No effect was noted on operability, combustion efficiency, or sulfur capture.

Limestone. As previously indicated, the SO_2 concentration in the flue gas could be readily controlled by changing the limestone rate. The limestone used (Grove limestone) was only active for a short time after it was fed into the bed (perhaps 15-30 minutes). After this time, it appeared to be almost inert. This is contrasted with the Battelle experience with Greer limestone, which remained active for many hours after feeding. However, when using the Greer limestone, changes in limestone feed rate did not affect the SO_2 concentration in the flue gas for several hours and control of SO_2 concentration in the flue gas was difficult.

The control of SO_2 emission at 1.2 $lb/10^6$ Btu was still difficult, as indicated by the wide variation in emission shown in Table 4-21. This was because variations in coal rate, air rate, limestone rate, heating value of coal, sulfur content of coa", and reactivity of the limestone all affected SO_2 emission.

The size of the limestone theoretically should significantly affect the design and operation of the fluidized bed. The heat transfer coefficient should be inversely proportional to particle size. Therefore, with a finer limestone, the heat exchanger could be smaller. The calcium-to-sulfur ratio in the fly ash is lower than in the bed drainings. Thus, if more of the limestone were lost as fly ash, less limestone might be required to control sulfur. The size of the limestone affects the minimum fluidization velocity and, thus, the maximum turndown possible. All of these considerations indicate that finer limestone should be used.

The small size limit is determined by the size needed to maintain a bed. With too fine a stone, more unexpended calcium is lost as fly ash, increasing the rate of feed into the bed needed for sulfur capture. A 12 x 40 mesh Grove limestone should be more satisfactory than the 8 x 20 mesh stone used. The size needed will depend on the specific limestone used because different source stone has different attrition rates.

Series Bed (Experiment 6). The series bed experiment was to determine feasibility of using two beds in series where a small first bed would operate at about 1850 F using a ceramic heat exchanger. Because the high-temperature bed would not capture sulfur, its flue gas would be passed through a second, lower temperature bed for sulfur removal. The flue gas from the first bed would be cooled and, if necessary, the particulates removed; then it would be mixed with the fluidizing air for the second bed. The second bed would operate at 1650 F, and about 80% of the fuel would be burned in it.

To simulate the downstream bed, a sulfur containing flue gas was synthesized by adding SO_2 to the plenum under the reactor with the ignition burner in operation. The ignition burner heated the incoming air to 940 F as read by the thermocouple in the burner outlet. At a 940 F temperature rise, about 4.0 scfm of gas was used. This is the equivalent of 22 lb/hr of coal. Sulfur dioxide was added at the rate of 2.6 lb/hr to the plenum.

The Ca/S ratio required was 4.1, the highest of any experiment, indicating that about 20% more limestone is required using the series bed. This experiment shows that the two beds in series can be used, but that somewhat more limestone is required to control sulfur emission.

B&W Conditions. To compare the existing B&W bed and the Battelle 24-inch bed, an experiment (run No. 16) was made duplicating the expected conditions in that bed. The fluidizing velocity scheduled was not reached because the cooling coils were not adequate to remove the extra heat associated with the high superficial velocity. At the low temperature, the limestone was used efficiently, and the lowest Ca/S ratio of any experiment was attained. The combustion efficiency was not reduced by either the lower temperature or the higher velocity.

Effect of Burning Coke. In run No. 9, coke was burned to determine the effect of lack of volatiles on the oxygen content of the bed. Operationally, base conditions could not be attained. When they were set up, the bed temperature dropped rapidly and the freeboard temperature increased, indicating the coke was burning in the freeboard rather than in the bed. The bed temperature was raised to 1700 F and the fluidizing velocity was reduced to 5.6 ft/sec so that combustion could be maintained in the bed. No limestone was added to eliminate the heat requirement for calcining the limestone. The sulfur dioxide content of the flue gas was off scale (greater than 1000 ppm) on the meter. Even under these conditions, the combustion efficiency was only 85% and the temperature rose 150 F in the freeboard. About 5% of the coke burned above the bed. The combustion efficiency in the bed was about 80%. The Getty fluid petroleum coke used would not be a satisfactory fuel for a conventional fluid bed combustor operating at 1700 F or less.

Effect of Bed Depth. The bed depth was not deliberately varied for these experiments. The top of the heat exchanger is about 62 inches above the bottom of the bed. The bed depth was chosen to keep the tubes covered. The bed was about 10 inches deeper than in January and combustion efficiency was marginally better.

Heat Transfer. The heat transfer calculations were made assuming all heat transfer was in the bed and no heat transfer outside. The overall heat transfer coefficient was calculated by the equation:

$$U = Q/A\Delta T$$

This Q was calculated from the temperature rise in the air and the quantity of flowing air. "A" is based on the outside area of the tube in the bed, including the vertical section; ΔT is the log mean temperature difference between the bed and the tube. The tube-to-air heat transfer was calculated from the Colburn equation for straight tubes reduced by 12.4% because of the difference in inside and outside areas of the tube and increased by 40% because of the U-return bend. The temperature drop across the metal was neglected. The tube-to-bed heat transfer coefficient was calculated from the overall coefficient and the tube-to-air coefficient.

Errors are introduced into the calculated bed-tube coefficient from at least four sources, external heat losses, bends in the tubes, a vertical section in the bed, and determining coefficients by taking a small difference between two numbers. The coefficient is insensitive to small errors in air flow measurements. External heat losses become more serious at the higher cooling air temperatures and are probably the reason that the coefficient drops at the higher temperatures. They should not be large for the first U-tube in a pass. The bend in the U-tube increases the internal heat transfer coefficient over that predicted by the Colburn equation. Literature data (Ref. 4-20, -21, and -22) suggest that the coefficient is increased by about 80% after the return bend. To correct for this effect, the heat transfer coefficient predicted by the Colburn equation was increased by 40% (the average of 80 and zero). The vertical section may not have much effect as the horizontal sections, but their heat transfer coefficients should be about the same.

As part of the calculation, the difference between the reciprocals of the measured overall coefficient and the inside coefficient calculated by the Colburn equation is used. When these reciprocals are close, the error in the bed-to-tube coefficient becomes large. Thus, the accuracy of any large coefficient is poor. The accuracy of the 60 reading is probably about ±40%.

The temperature reading on the outlet of tube 121 appears to be in error; however, no cause for error is known and the number was not misread.

Theory. Textbooks on heat transfer in a fluid bed list many heat transfer equations. However, most data are from small beds operating at low temperature with fine particles at low fluidization velocities. The few data that are available from fluidized bed combustors were taken using water or boiling water for the cooling media in the tubes. Therefore, the metal temperature was much lower than the temperature in an air-cooled heater. From these published data, a heat transfer coefficient of about 40 was chosen for the preliminary design.

The B&W (Ref. 4-23) 6' x 6' bed most closely approximates our system. They recommend dividing the heat transfer coefficient into two parts: a convective part and a radiative part. The convective part is estimated by a modified Vreedenberg correlation (Ref. 4-24):

$$h = \frac{900(NPr)^{0.3}Kg}{d_t}\ (1 - e)\ \left(\frac{Gd_t}{\rho'_g\, d_p\, {}^3\rho_g}\right)^{0.326}$$

where

h = heat-transfer coefficient, Btu/hr-ft^2-F
(NPr) = Prandtl No. = 0.7 for air and flue gas
d_t = diameter of tube, feet
Kg = Thermal conductivity of gas, Btu/hr-ft^2-F/ft
e = bed voidage
G = mass velocity of gas, lb/hr-ft^2
ρg = density of gas
ρp = density of particle
u = viscosity of gas lb/hr ft
g = 32.2 ft/sec

In flue gas at 6 ft sec superficial velocity, 75% voids, a 2-inch tube, 0.03-inch particles, and 1650 F, the calculated convective heat transfer coefficient is 41. The radiant heat transfer coefficient, assuming an emissivity of 0.6 of a 1650 F bed to a 1000 F tube, is 24. Summing the two coefficients, the overall coefficient is 65.

In another paper (Ref. 4-25), the heat transfer variation around the tube circumference is reported. At 45 degrees from the top, the coefficient is 1.5 times the average rate. On the entire 180-degree bottom half of the tube, the heat transfer rate is about 80% of the average value.

Recommendations and Conclusions.

Recommended Heat Transfer Coefficient. Since the experimental data are very close to the values predicted by the modified Vreedenberg equation corrected for radiation, the values predicted by that equation are recommended. At the prototype conditions, 1650 bed, the average heat transfer coefficient is 66, with a metal temperature of 1000 F and 76 at a metal temperature of 1500 F.

Conclusions. The combustion and operational characteristics of the fluidized bed are satisfactory when operated anywhere within the test conditions used for these experiments. Therefore, the design point may be selected from considerations other than operation.

4.2.3 Design and Operation of the Oxygen Partial Pressure Probe

Fluidized bed combustion (AFB) units are expensive to build and modify. Performance data are costly to obtain, especially if materials erosion/corrosion results are needed. Maximum information must be obtained from each test run to minimize overall test time and to optimize efforts to modify bed characteristics. The need for detailed information is especially critical for the in-bed transient fluid, thermal and chemical environment about which little is known. One realistic and cost-effective approach to providing this capability is to develop advanced in-bed measuring devices to provide maximum localized characterization of the AFB in-bed environment.

The chemical environment, as described in the previous sections, has a major effect on the corrosion of in-bed materials, especially at elevated temperatures. For example, sulfidation attack occurs in regions of low oxygen partial pressure and corresponding high sulfur partial pressure.

In this section, a stabilized zirconium diagnostic probe is described which was designed and developed by BCL to determine details concerning gaseous chemistry in the localized vicinity of in-bed heat exchanger tubes. A detailed description of each probe element is provided, with comments on auxiliary equipment necessary to support the measurement efforts. Probe calibration procedures and diagnostic system operation during in-bed measurements are discussed, along with data reduction methodology. Finally, data presentation procedures are presented.

The available literature concerning the theories and applications for stabilized zirconia electrolytes is quite voluminous. Since the introduction of the calcia-stabilized zirconia electrolyte by Kiukkola and Wagner (Ref. 4-26), it has been used in hundreds of high temperature galvanic cell, fuel cell, and oxygen pressure gauge investigations. The excellent results obtained with stabilized zirconia oxygen pressure gauges led to a variety of successful industrial applications. Of particular current importance is the use of these oxygen sensors for combustion diagnostic and control technology. While the accuracy of oxygen measurements obtained with the zirconia atmospheric electrolyte sensor in an

atmospheric fluidized bed (AFB) environment remains under discussion, the validity and usefulness has been demonstrated amply. The following discussion, briefly introduces the major evidence related to measurement accuracy.

Excellent agreement ($\pm$2%) between predicted values and experimental results have been reported when the sensor was used to monitor the oxygen partial pressure (10^{-6} atm $<PO_2<1$ atm) in pure oxygen (Ref. 4-27) and in O_2 - inert diluent gas mixtures (Ref. 4-3). The stabilized zirconia oxygen sensor also has been used to monitor the oxygen partial pressure in $CO-CO_2$ (Ref. 4-28), H_2-H_2O (Ref. 4-12), and $CO-CO_2-H_2-H_2O$ (Ref. 4-29) gas mixtures. The calcu- lated oxygen partial pressure in these gas mixtures was between 10^{-6} atm and 10^{-23} atm, based on the assumption that all constituent phases were in thermo- dynamic equilibrium. Excellent agreement between these equilibrium calculations and experimental results have been reported provided the test gas mixtures were equilibriated, either by a precatalyst or because of the catalytic nature of the platinum electrode.

Although the accuracy of the zirconia oxygen sensor has been demonstrated by many researchers, as indicated above and in BCL calibration tests, the question still remains as to its validity in an AFB environment. If the oxygen probe data shown in Fig. 4-77 near the end of this section are, in fact, accurate, then what causes the excursions to the low measured oxygen partial pressures? One argument is that incomplete combustion occurs within the AFB environment due to insufficient mixing of the fuel and air. This lack of mixing could result in local substoichiometric combustion with a resultant gas phase that had a low equilibrium PO_2. Figure 4-60 illustrates graphically how the equilibrium oxygen partial pressure varies with the air-to-fuel ratio (A/F) for the combus- tion of pure carbon with air. These calculations show that even small deviations from stoichiometry (A/F = 1) result in a gas phase with low-equilibrium PO_2 of the same order of magnitude as those measured in Fig. 4-77 of the text.

Another explanation of the low PO_2 measurements is that the bed material itself determines the in-bed oxygen partial pressure. The fact that 99% of the bed is a

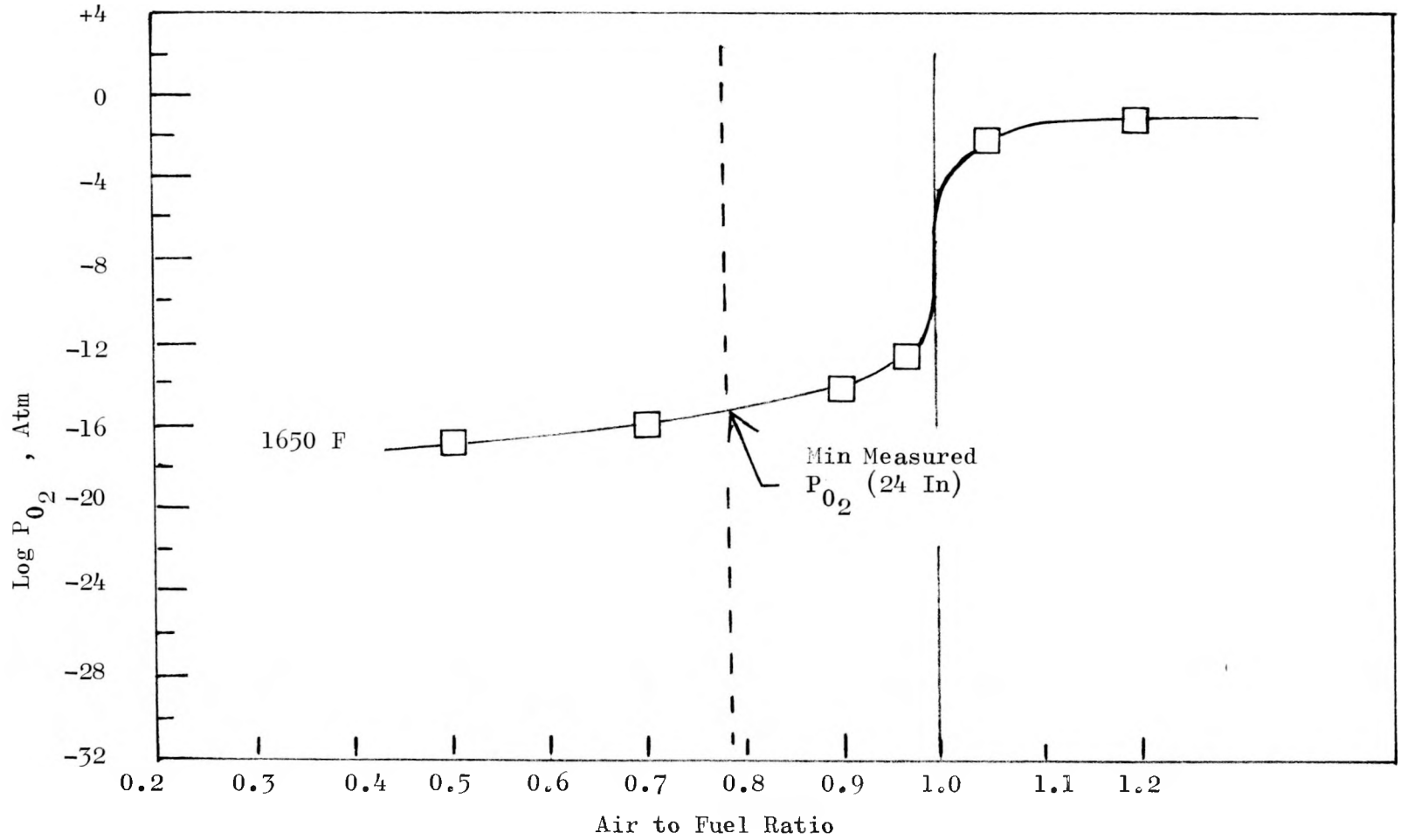


Figure 4-60. Equilibrium Oxygen Partial Pressure in Flue Gas as a Function of the Initial Air-to-Fuel Ratio for the Combustion of Coal (Illinois No. 6) with Air

mixture of CaO and $CaSO_4$, which has an equilibrium CO existent PO_2 the same order of magnitude as measured in the AFB environment, tends to support this hypothesis.

Description of Main Probe Components. To examine the corrosive potential at given locations within a fluidized combustion bed, a special probe was designed to obtain in situ measurements of fluctuating oxygen concentration (i.e., PO_2). In addition, the probe could be designed to simultaneously extract a time-averaged sample of in-bed gases for external analysis.

A schematic of the probe is shown in Fig. 4-61, and an assembly drawing of the probe tip is shown in Fig. 4-62. Photographs of the tip components identified in these figures are shown in Fig. 4-63. Finally, components of the overall probe system are shown in Fig. 4-64. A general description and comments related to the purpose of components labeled in these four figures are given below:

Component	Purpose/Description
• Probe Body	Eight-foot-long, 2-inch-diameter, water-cooled shaft that provides for measurement at points within the AFB environment.
• Porous Ceramic Filter	Separates in-bed gaseous and solid materials and protects PO_2 sensor.
• PO_2 Sensor (Exhaust Oxygen Sensor)	Located inside filter, it monitors fluctuating PO_2 by providing a voltage output proportional to log PO_2.
• Sampling/Purge Line	Provides for extraction of gas sample for external analysis and purging of filter with argon for protection during insertion.
• Water Supply	Cooling for probe body.
• Alarms	Water flow and temperature protection for probe.
• Air Supply	Standard low-pressure compressed air provides reference oxygen for sensor.

Component	Purpose/Description
• Argon Supply	Bottled argon used during probe insertion/ retraction, to minimize thermal shock to filters.
• Cold Trap/Particle Filter	Particle filter and ice bath to remove water vapor and tar residue from gas sample.
• Pump	Extracts gas sample from bed through filter and pumps sample to analysis station.
• Flow Monitor	Monitors sample line flowrate and pressure.
• T/C Instrumentation	Monitors PO_2 sensor temperature and provides appropriate analog signal proportional to temperature.
• Data Collection/Analysis Instrument	Provides for recording of analog PO_2 sensor voltage and sensor temperature. Digitizes and stores raw voltage data, converts raw data to PO_2 values, and plots/prints results.

Probe Body. The water-cooled probe body is an 8-foot long, 2-inch-OD hollow cylinder that provides for insertion of the probe measurement tip into the AFB environment. This probe body geometry was chosen to simulate presence of a single tube within the in-bed heat exchanger (HEX) network. The probe body inside diameter is 1-1/8 inches and provides for passage of various connections from the probe tip to the ambient environment outside the AFB unit. The annulus of this probe contains two water passages (Fig. 4-61 and 4-62). A cylindrical inner passage brings cool water to the probe tip, and a spiral return passage provides for uniform cooling and minimizes hot spots that could cause an undesirable condition of water flashing to steam within the cooling channels. The spiral passage is made of aluminum, while the remainder of the probe body is stainless steel. Quick disconnect water fittings are used to provide convenient detachment of the probe from the water-cooling system.

At the probe body tip (Fig. 4-61 and 4-62), a threaded section is provided for installation of the measurement apparatus (i.e., sensor/sensor retaining ring/gas sampling and purge line). A large nut (i.e., end cap in Fig. 4-62.And 4-63) held the measurement apparatus and the porous ceramic filter in place. "Neverseize"

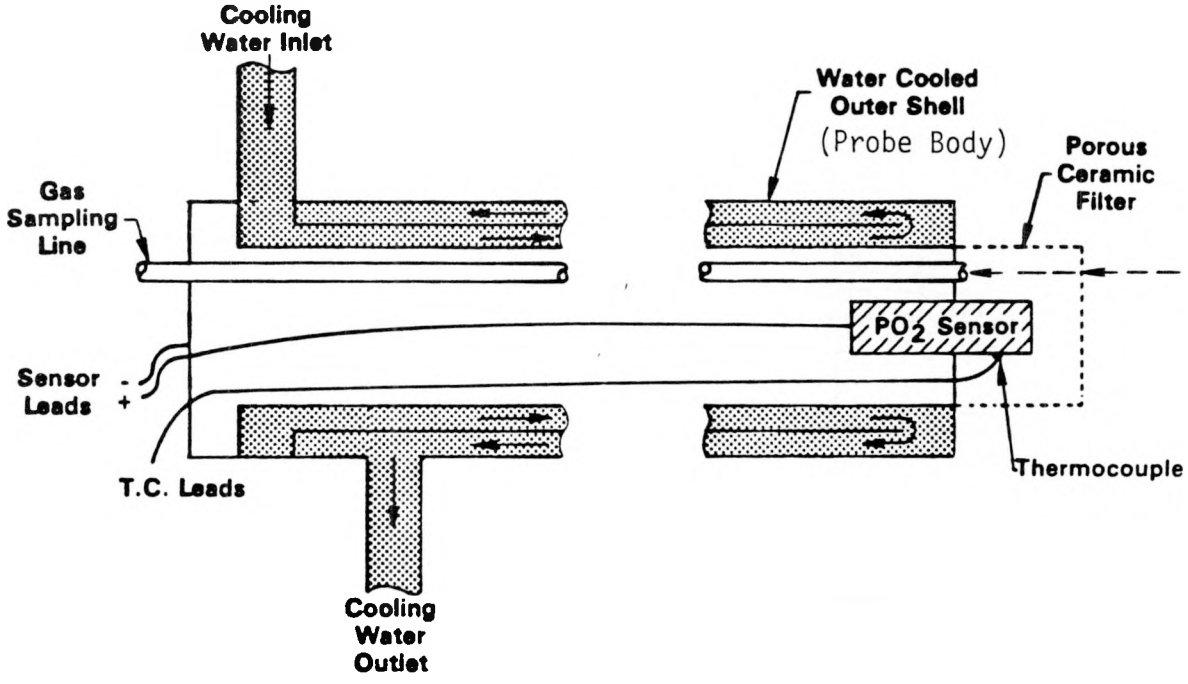


Figure 4-61. Schematic of Combined Oxygen Activity PO_2 and Gas-Sampling Probe

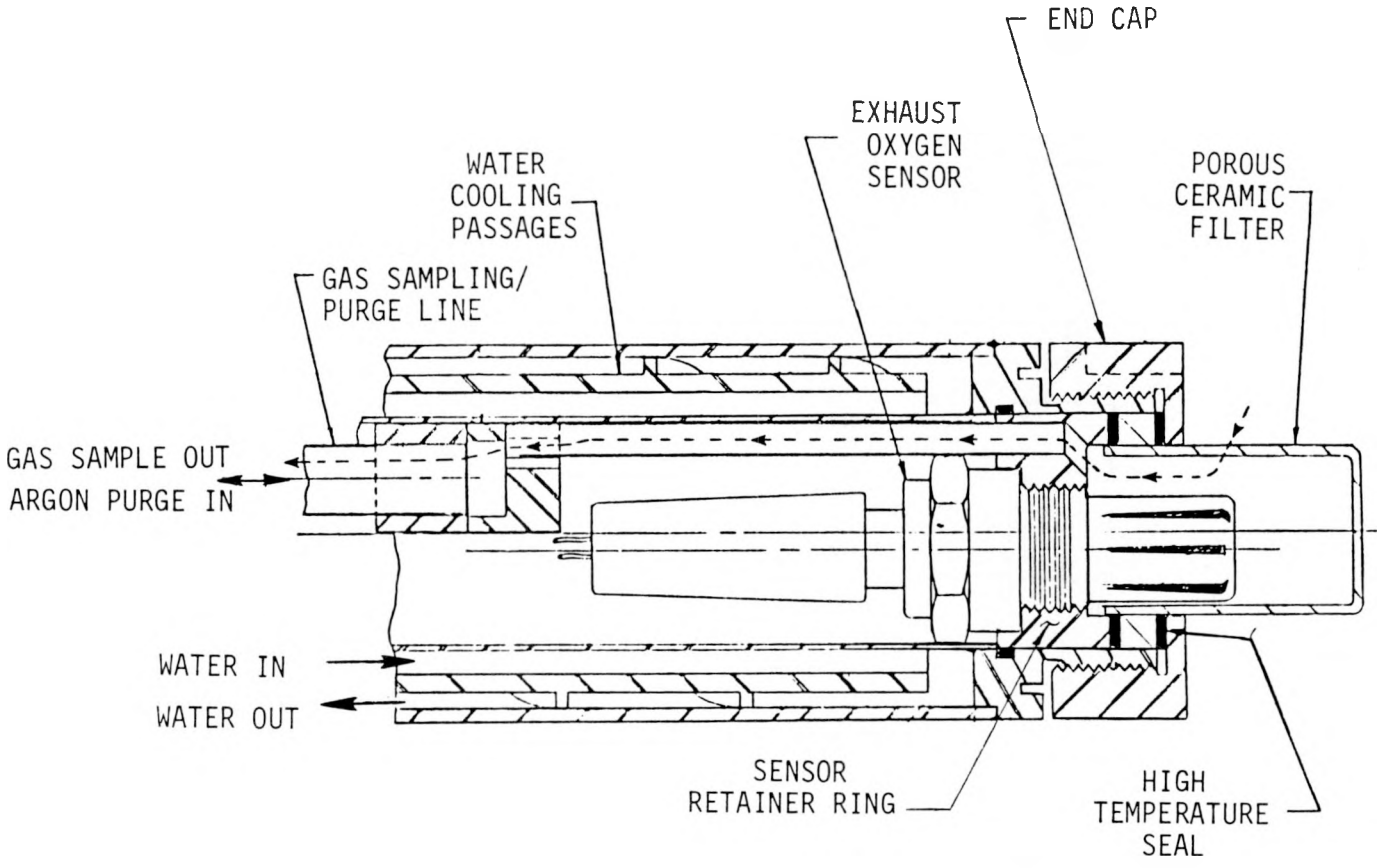


Figure 4-62. Assembly Drawing of Gas-Sampling/Oxygen Activity Probe Tip

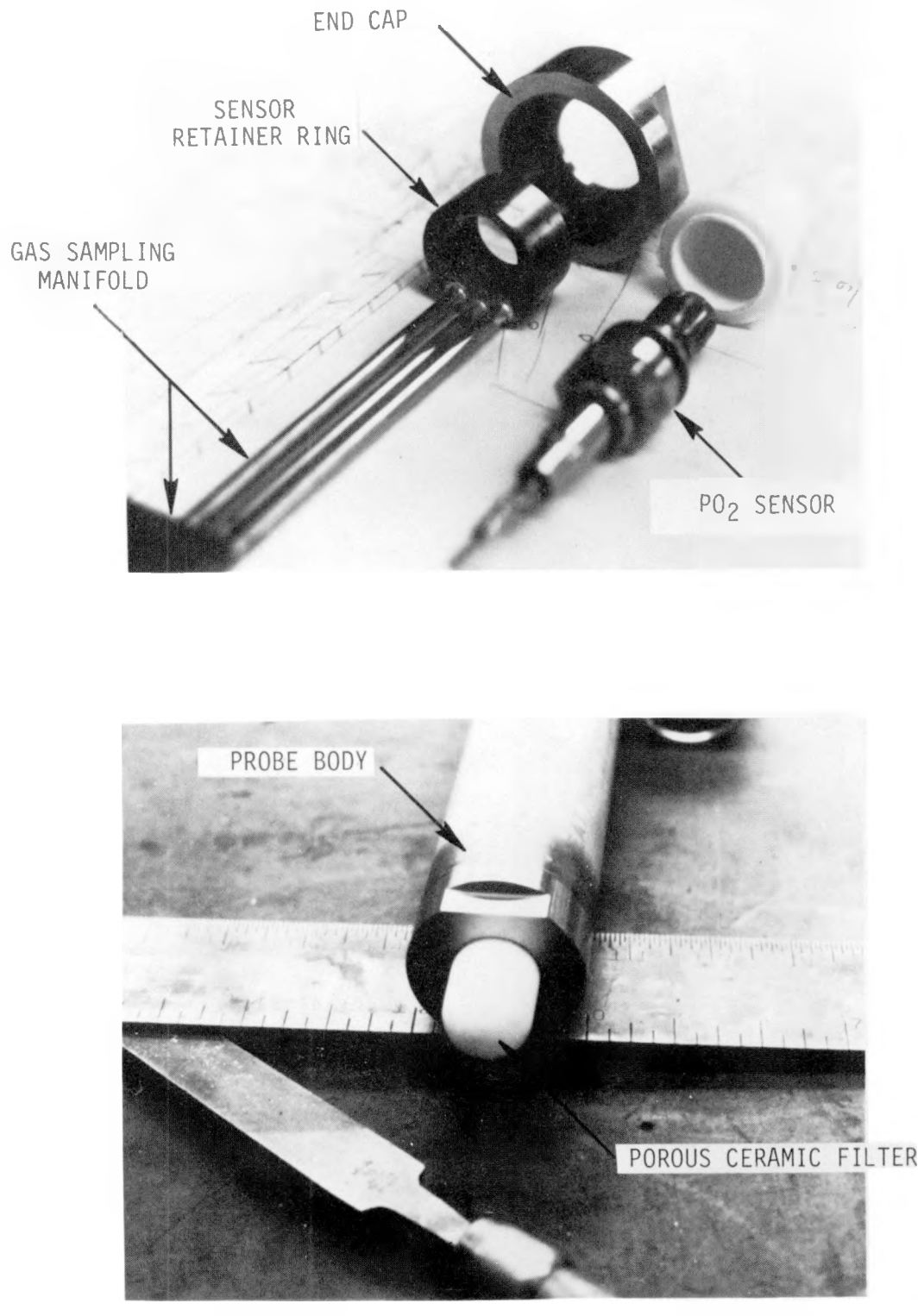


Figure 4-63. Photographs of PO_2/Gas-Sampling Probe

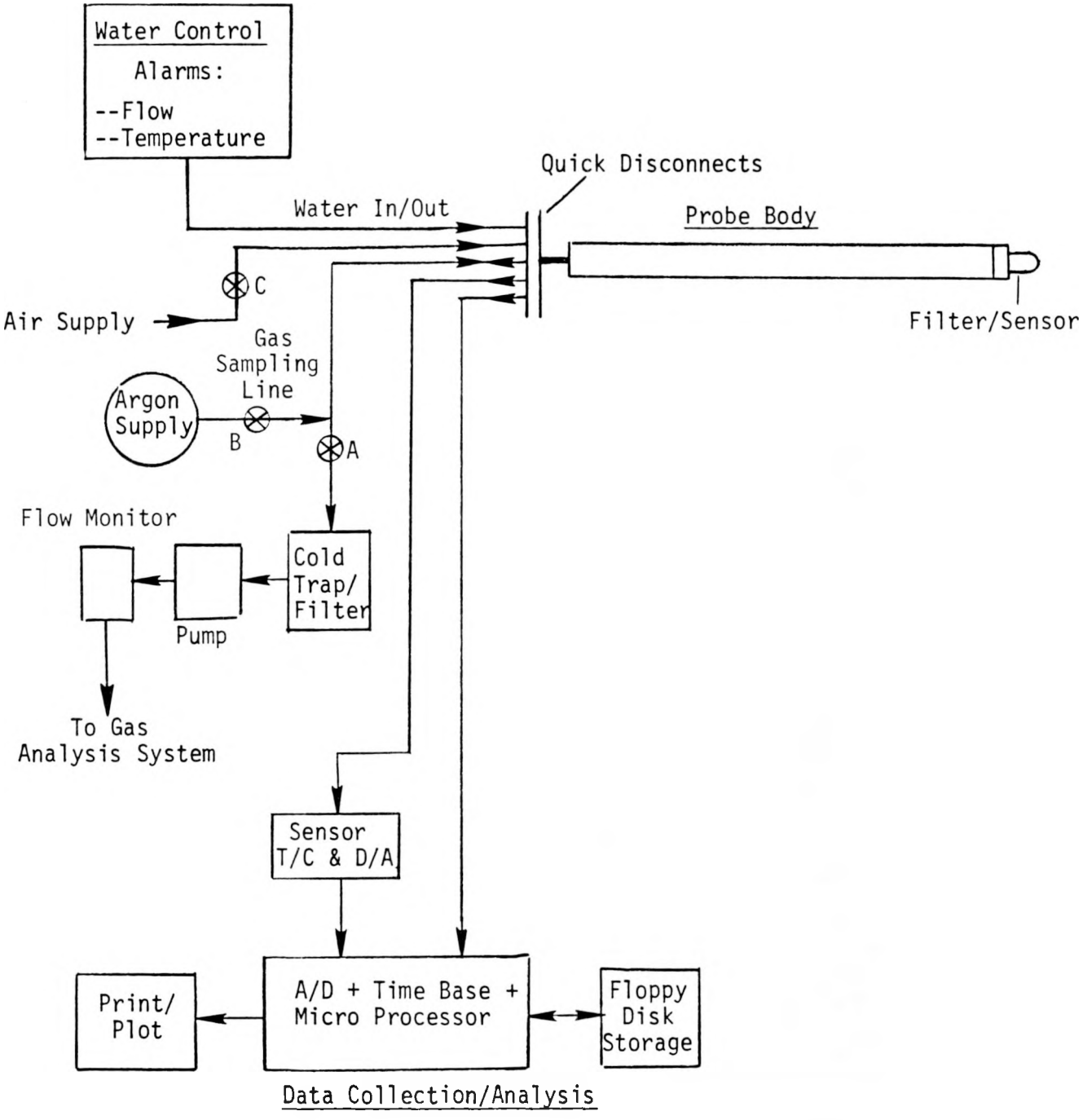


Figure 4-64. Schematic Diagram of PO_2/Gas-Sampling Measurement System and Support Apparatus

compound was painted on the threads of the nut each time it was removed to prevent seizing at high temperatures.

Porous Ceramic Filter. A 2-inch-long, thin-walled, porous ceramic (Alundum) cylinder with one closed end was used as a filter at the probe tip. One purpose of this thimbleshaped filter was to allow in-bed gases to be sampled through a sampling line (Fig. 4-61 and 4-62) connected to the filter cavity at a rate of approximately 5 scfh (standard cubic feet per hour). In-bed solids, which would plug the line, were prevented from entering by the small filter pore size. Another purpose for this filter was to protect the PO_2 sensor from damage due to impact by hot bed particles.

Photographs of a new filter and one that has been exposed to an AFB environment for approximately 20 minutes are shown in Fig. 4-65. Note from the photograph and drawing in Fig. 4-62.that a high density alumina ring was fastened onto the open end of the filter using high temperature Sauerizen cement. This ring provided a means for holding the filter in place and also sealing to prevent high temperature fine particulate material from entering into the gas sample. Fiberfrax cloth material 0.020-inch-thick was used to make this high-temperature seal. Washers were made from the cloth sheet (Fig. 4-65), and four to five washers were stacked on each side of the alumina ring to form the required seal. This cloth seal also served to cushion the ceramic material against physical shock of installation and thermal shock of insertion into the AFB environment. It should be noted that this high-temperature seal does not prevent bed gases from entering into the air reference region at the back of the sensor. This latter seal is accomplished with a high-temperature O-ring located between the sensor retainer ring and the inside wall of the probe body (Fig. 4-62).

Both the filters (Alundum Thimbles) and the alumina rings were ordered through the L.H. Marshall Company of Columbus, OH. The filters were manufactured and cut to size by McDanel Company and cost approximately $2 per unit. The filters operated satisfactorily for approximately 20 minutes within the AFB environment. Upon insertion into the bed, the sampling line pressure was noted to decrease relatively rapidly from 0 to approximately -3 psig where it remained relatively

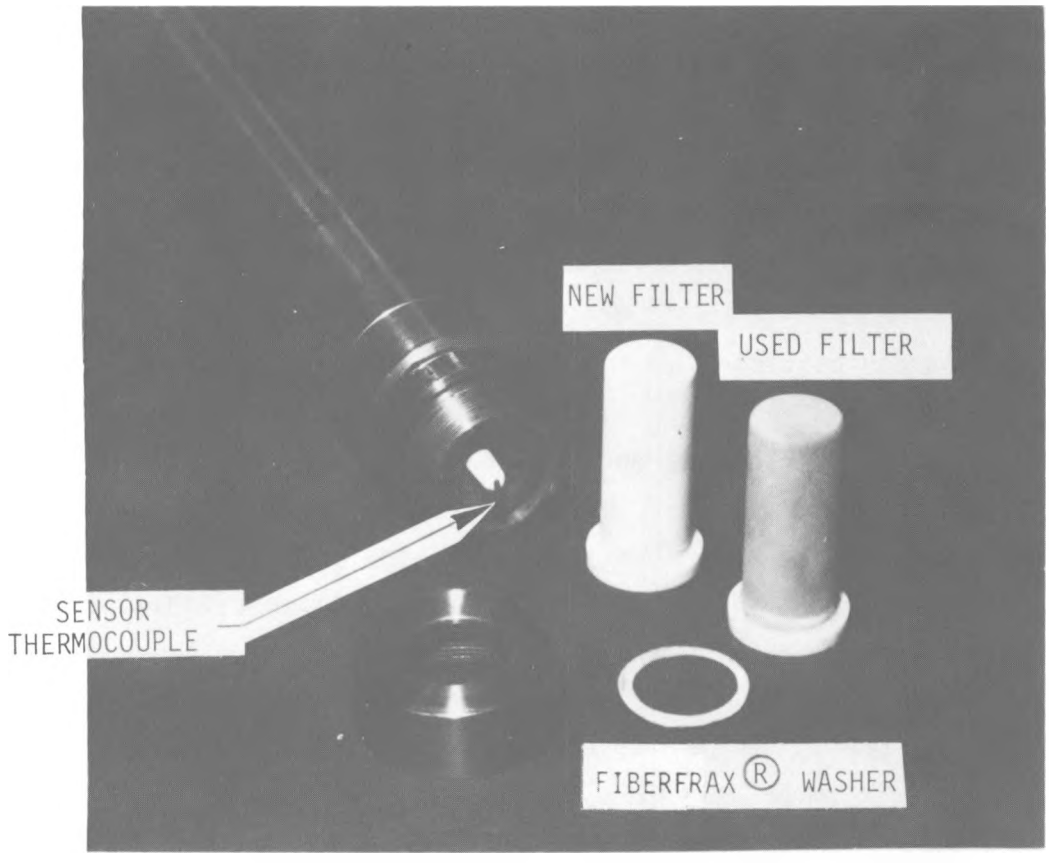


Figure 4-65. Tip Components, Including New and Used Ceramic Filters

constant for the 20-minute period of filter life. Slight adjustments were continually made to maintain the sampling rate of 5 scfh by adjusting the pump volume control valve. After this period of time, rapid plugging of the filter was noted by monitoring the relatively rapid decrease in sampling line pressure to a value of approximately -8 psig.

Filter plugging was primarily due to tar-like material buildup on the filter surface in addition to clogging of the filter pores by fine particulates. For this reason, back purging at elevated pressure with argon gas had little effect on extending filter life.

On several occasions, the filter broke off near the point where it entered the hole in the retaining nut (end cap in Fig. 4-62 and 4-63). This occurred usually during extraction of the probe from the AFB unit, so it was attributed to thermal shock effects during filter cooling. However, a few times the filter broke off during measurements within the bed. These breakages were attributed to physical impact of in-bed solids on the filter itself. Breakage was identified quickly by noting the rapid return of the sampling line pressure to near 0 psig. When filter breakage occurred during measurements, the sampling line had to be cleaned of bed material by backflowing high pressure air through the lines.

The filter was replaced quickly by removing the end cap with a large wrench and putting in a new filter with associated sealing washers. The end cap was then replaced, but no wrenches were used to tighten this cap for fear of over tightening and physically breaking the filter. Instead, the nut was handtightened using gloves to handle the nut if the probe had just been removed from the bed.

In general, the filters performed adequately. A longer-lasting filter design would be desirable. Also, a filter through which gas could be drawn at a higher rate (i.e., 15 scfh) for an extended period of time would be advantageous. The present filter life would have been reduced severely if higher sampling rates were employed.

PO_2 Sensor. Inside the filter body, an oxygen partial pressure, PO_2 sensor was positioned to measure the local, in situ fluctuating oxygen content of the bed. To accomplish this measurement from within the porous ceramic filter, some of the bed gases must be drawn into the filter cavity so these gases come in contact with the sensor surface. Therefore, the sampling pump was operative during PO_2 sensing as well as gas sampling in order to provide an in situ sample of in-bed gases for the sensor to analyze. The dependence of sensor output to variation in sampling flowrate through the filter was presented in the introduction.

The sensor itself is a platinum/zirconia (Y_2O_3 stabilized)/platinum high-temperature galvanic cell that has been used in the field of chemistry for many years to monitor oxygen (Ref. 4-30). A schematic diagram of the cell is shown in Fig. 4-66.

A miniature version (i.e., size of spark plug) of this cell, called a Lamda-Sensor, was developed by the automobile industry (Ref. 4-31 and 4-32) to monitor exhaust oxygen content (Fig. 4-62 and 4-63). In fact, the device used in the present work was manufactured by Bosch of Robert Bosch Gmblt (West Germany) and it costs approximately $60. It is used in the Volvo automobile and can be obtained from most Volvo dealers using the following designation:

464901-8 Volvo Exhaust Gas Oxygen Sensor, "LAMDASOND"

A close-up photograph of the sensor tip is shown in Fig. 4-67. The slotted metal, protective shield provided by the manufacturer, which is shown in Fig. 4-62 and 4-63, has been removed in this photograph. In all cases for the present study, this metal shield was removed prior to using the sensor in AFB diagnostics.

In essence, the zirconia-based electrolyte material of which this sensor is composed exhibits a predominant oxygen ion, $O^{=}$, conduction over a wide range of oxygen pressures (10^{-20} atm $<PO_2<1$ atm) and a wide range of temperatures (500 C to 1400 C). At the platinum anode and cathode, respectively, the loss or

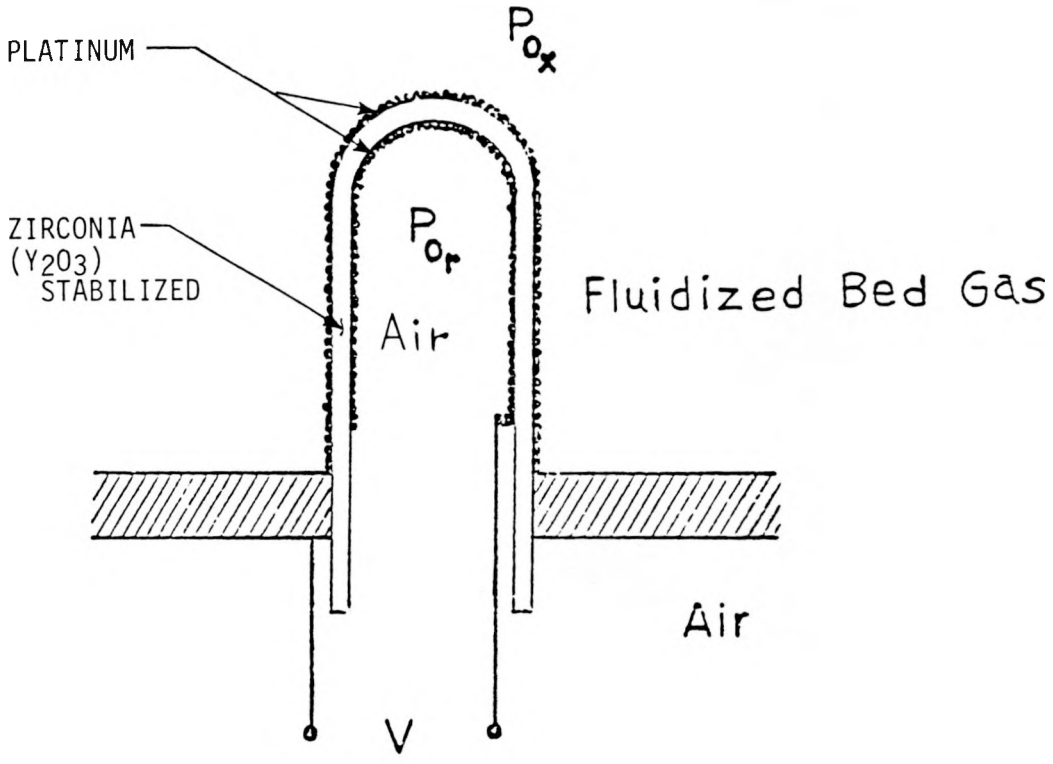


Figure 4-66. Schematic of High-Temperature Galvanic Cell

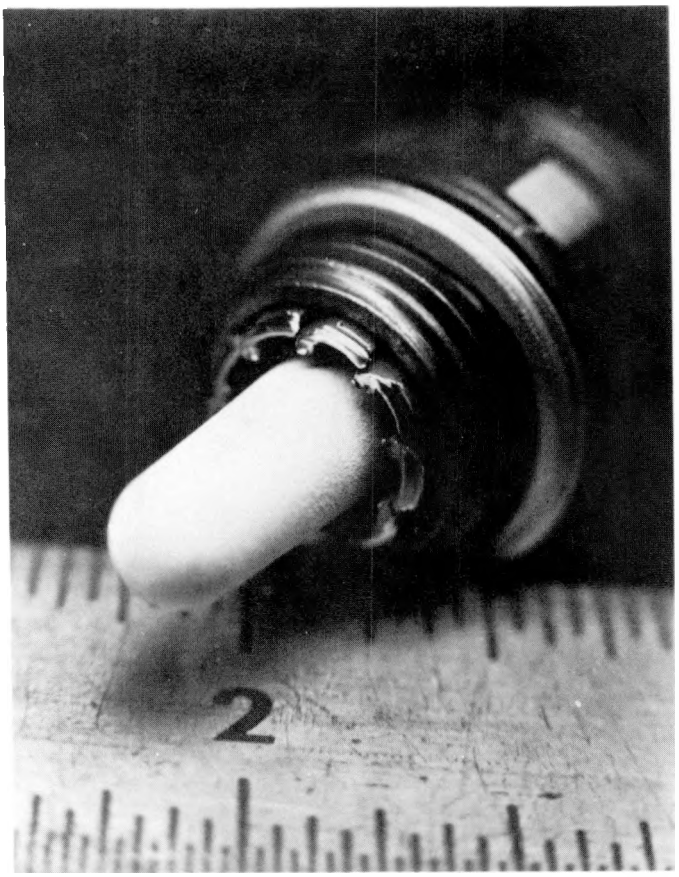


Figure 4-67. Exhaust Oxygen Sensor Tip (Protective Cover Removed)

gain of electrons from the external circuit accomplishes the formation or disassociation of oxygen molecules according to the relation:

$$O_2 + 4e^- \underset{\text{anode}}{\overset{\text{cathode}}{\rightleftharpoons}} 2O^= \qquad (1)$$

where $O^=$ denotes an oxygen ion found in the zirconia anion sublattice. The cell voltage, E_C, is normally associated with the ratio of oxygen chemical potentials at the electrodes according to the equation:

$$E_C = \frac{kT}{4e} \ln \frac{PO_2^r}{PO_2^x} \qquad (2)$$

where k, T, and e are Boltzmann's constant (1.38044×10^{-22} Joules/K), cell temperature (K), and electron charge (1.60206×10^{-19} Volts/Joule) respectively. The quantities PO_2^r and PO_2^x represent the oxygen partial pressure at the cathode (i.e., reference electrode) and anode (i.e., measurement zone), respectively.

Substituting the above constants into Eq. 2 results in the following equation for cell voltage:

$$E_C = 2.1542 \times 10^{-5}\ T \ln (PO_2^r/PO_2^x) \qquad (3)$$

E_C = Volts

T = K

Further, assuming $PO_2^r = 0.209$ atm (i.e., 1 atm air), Eq. 3 may be written as follows for log notation to obtain:

$$E_C = 4.9602 \times 10^{-5}\ T\ (-\log PO_2^x - 0.6799) \qquad (4)$$

E_C = Volts

T = K

PO_2^x = atm

From Eq. 4 it can be noted that for PO_2 = 1 atm air (i.e.,.209 atm O_2), no voltage is generated by the cell (i.e., E_C = 0). For 3% oxygen content (i.e., PO_2 = 0.03 atm), which is typical of many AFB exhaust conditions, and a cell temperature of 1172 K (1650 F), the voltage is E_C = 49.0 millivolts. Finally, for a low oxygen partial pressure, PO_2 = 10^{-14} atm, and identical cell temperature, E_C = 774.3 millivolts (i.e., .7743 volts). Hence, the greater the differential oxygen partial pressure across the cell, the greater the voltage; and the greater the cell temperature, the greater the voltage.

It should be made clear that oxygen gas does not actually diffuse through the zirconia cell material itself. Rather, electrons move through the cell lattice based upon the differential PO_2 across the cell. Therefore, the response time of this sensor is quite fast (i.e., typical measurements indicate that it is less than 0.01 seconds). However, physical presence of the porous Alundum filter acts analogous to a capacitor in an electrical circuit so that the sensor/filter response time is reduced. Actual measurements in an AFB environment indicated that the sensor/filter response time was of the order of 0.1 seconds.

It also should be emphasized that Eq. 2 (the Nernst equation) is valid only for the case that all constituent phases (test gas, metal electrode, and solid electrolyte) are in thermodynamic equilibrium. In fact, the platinum electrode itself tends to catalyze any nonequilibrium composition to produce chemical equilibrium at the anode surface. Hence, nonequilibrium in-bed gas compositions will not be measured accurately using the zirconia cell sensor. It should be

noted, however, that hot metal tubes in the bed also tend to catalyze chemical reactions, so it is highly likely that PO_2 sensor results are applicable to in-bed tube corrosion diagnostics (i.e., chemistry at the surface of in-bed materials) even though they may not be applicable, in all cases, to defining the actual in-bed gaseous environment.

In general, the oxygen sensor worked admirably and one sensor was used for the majority of AFB experiments in the present effort. Even though the protective filter broke several times, the sensor survived direct contact with in-bed solids for short periods of time (i.e., several minutes) without deleterious effects on sensor performance. It was determined that the sensors were very accurate for measuring PO_2 in laboratory calibration experiments (see Calibration Discussion to follow) over a wide range of oxygen potential.

The sensor was installed in the sensor retaining ring (Fig. 4-62) using the spark plug threads and compression fitting provided (Fig. 4-67). A small amount of Neverseize compound was used on the sensor threads to prevent high temperature thread joint-seizing problems.

From Eq. 2 it can be noted that the cell temperature also must be measured along with cell output voltage in order to infer oxygen partial pressure at the cell anode surface. Therefore, a thermocouple was located near the cell outside surface (Fig. 4-61 and 4-65) to measure this required temperature value.

Reference Air Supply. Standard, low-pressure, filtered, compressed air (i.e., shop air) was used to ensure that the oxygen sensor received an adequate atmospheric reference air supply on the back side (cathode surface) of the sensor. This reference supply was provided by bringing an 1/8-inch-O/D copper tube up through the center of the probe body to a position approximately 2 inches from the sensor. Air then was allowed to bleed into the sensor region by opening a needle valve (i.e., valve C in Fig. 4-64). Very low air flowrates are required to provide a sufficient air reference during in-bed operation of the probe. Without the reference supply, it was possible for the reference oxygen content at the probe cathode to be altered by small leaks in the sensor retainer ring, "O"

ring seal, or the sensor threads/compression washer. The existence of such leak and associated effect on the sensor output were noted early in the program and corrected with the use of the reference air supply.

Argon Supply. As noted above, argon gas was used during insertion and retraction of the probe to mitigate thermal shock effects on the porous ceramic filter. Standard bottled argon was utilized and was connected to the sampling line to valve B using 1/4-inch-OD polyethylene tubing. The bottle pressure was regulated down to provide an ordinary sampling line pressure of approximately 10 psig for these insertion and retraction sequences. Higher line pressure (approximately 30 psig) conditions were introduccd several times to attempt to unplug particle and tar-fouled filters. However, this procedure was generally unsuccessful.

Data Collection/Analysis System. In the present data collection system, two quantities are recorded simultaneously as a function of time. These are voltage output from the exhaust oxygen sensor tip and sensor temperature.

Due to the rapid variations of PO_2 as a function of time within an AFB combustor, sensor voltage data must be obtained at a high data rate (i.e., short response time of approximately 0.01 seconds). Typical outputs are shown in Fig. 4-68. Furthermore, since the AFB environment is quasi-steady in nature, enough data must be obtained to be statistically meaningful. Therefore, approximately 20 seconds of time-varying data were obtained. These requirements imply that a large amount of data (approximately 4000 points) must be collected, stored and analyzed. It also was determined during the course of this investigation that the sampling line pressure, as well as sensor temperature, should be recorded either manually or automatically. So, requirements even beyond those mentioned are likely. Therefore, a high volume, permanent storage, computer-based data acquisition/analysis system was mandatory if data were to be obtained at more than only a few measurement locations.

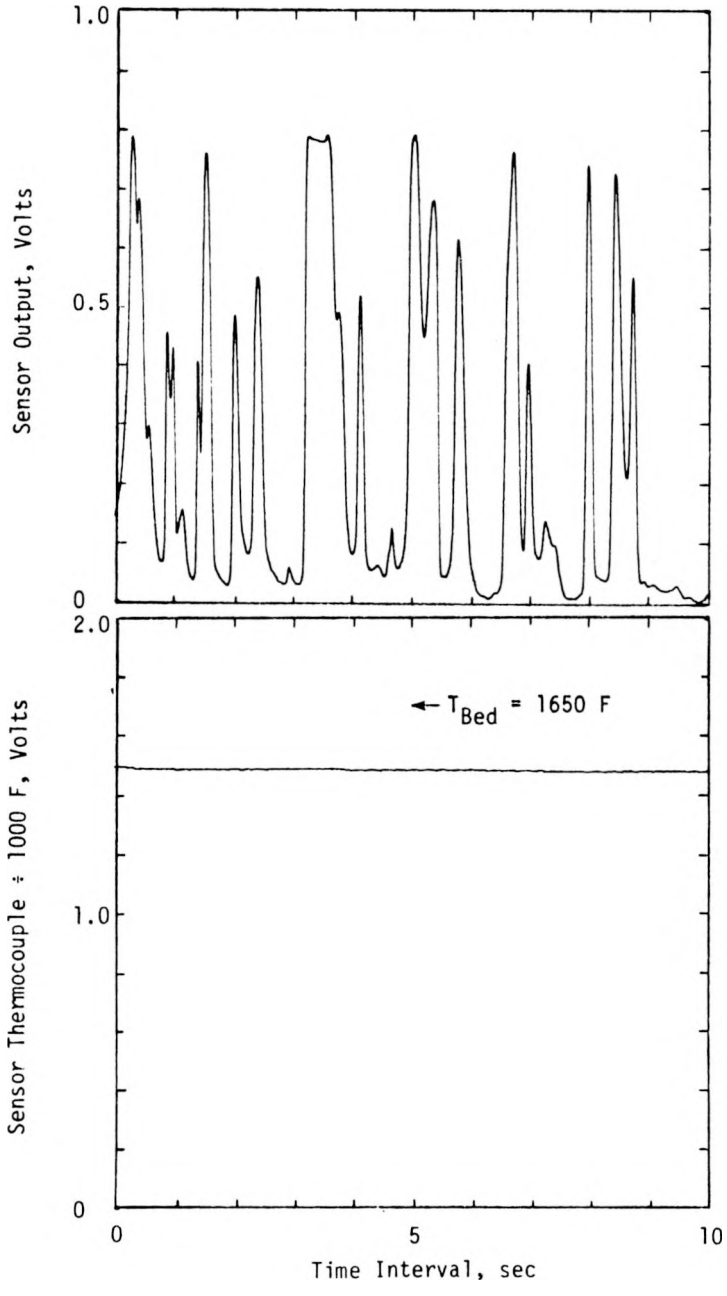


Figure 4-68. Typical Voltage Versus Time From PO_2 Sensor and Thermocouple (Oxidizing Environment)

Auxiliary Equipment. In addition to those items mentioned above, several associated components also were required for in-bed probing within an operating AFB unit. These components include:

Component	Purpose
Entry Port	Port through which probe enters the bed. It supports the probe during measurements and consists of a valve, fitting, and flange as integral parts.
Ram Tube	Cooled tube of same diameter as probe. It provides for a means of clearing bed particles out of the entry port so the probe may pass freely.

Entry Port. An entry port must be provided at each vertical (i.e., axial) location within the bed at which data are to be obtained to provide for entry and support during probe measurements. A schematic drawing of an entry port is shown in Fig. 4-69 for use in an atmospheric AFB unit. By inserting the probe to various positions within these ports, data could be obtained at many radial positions across the bed for various axial port locations.

Ram Tube. A separate, 2-inch-OD stainless steel tube was fabricated to clean agglomorated particles from the probe entry port prior to insertion of the PO_2/gas sampling probe. This device was water cooled using a simple double chamber design. In most instances, cooling was not necessary, especially if port cleaning was done quickly. But, occasionally, cooling was required if the agglomorated material was difficult to remove (i.e., after initial startup or restart).

Normally, the tube was inserted and simply pushed into the entry port until it just entered the bed, then it was retracted quickly. However, for the more difficult situations, the ram tube entry was inhibited by agglomorated material and cleaning could only be accomplished by rotating the tube using two handles provided at the proximal end. A sawtooth arrangement on the distal tip of the probe provided some assistance in boring through any well-packed material.

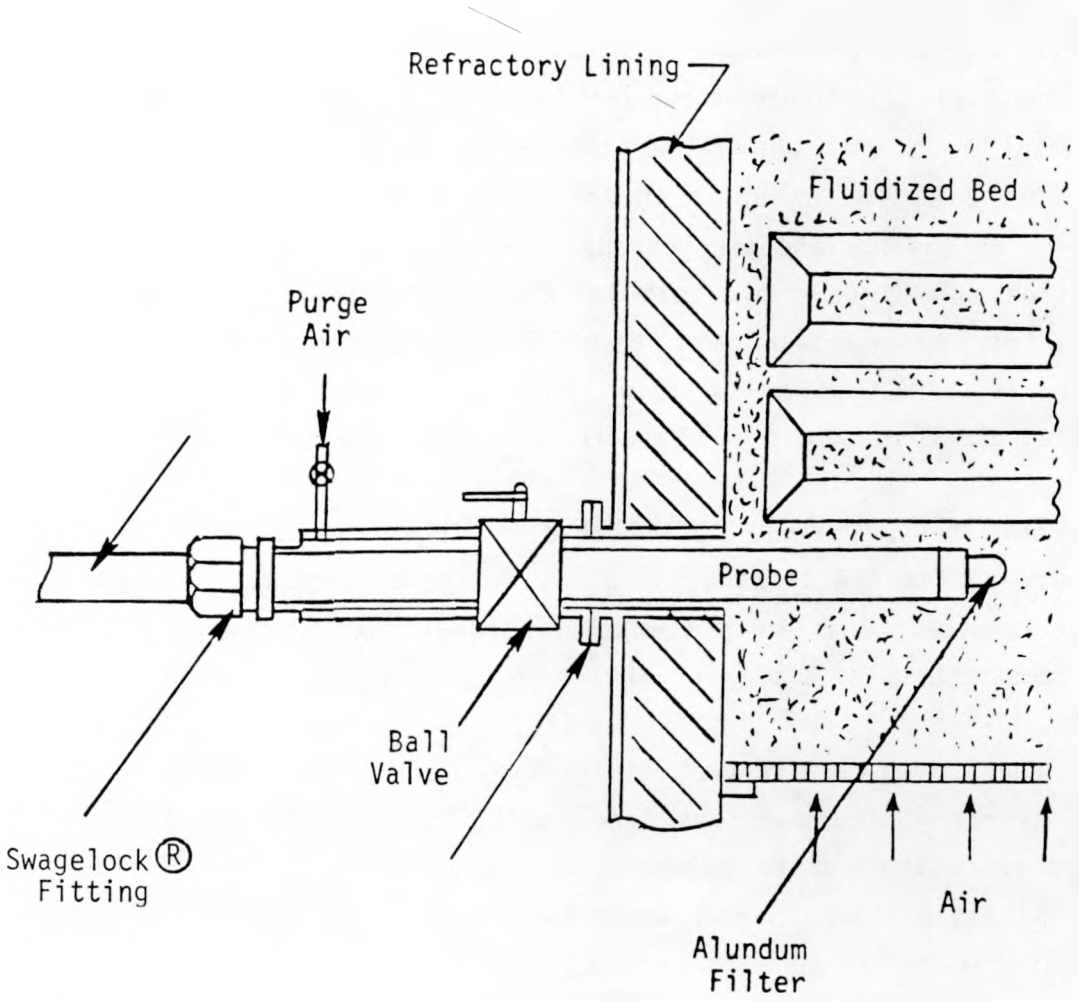


Figure 4-69. Schematic of Probe Entry Port

Calibration Procedure. Several items required calibration checks prior to use in the PO_2/gas sampling probe system. The PO_2 sensor voltage and temperature had to be accurately measured in order to obtain accurate PO_2 values because of the exponential dependence shown in Eq. 2. In fact, sensitivity calculations showed that a 1% error in either the sensor voltage or temperature measurement resulted in a 60 to 70% error in the measured PO_2 value. Therefore, the input amplifiers on the Norland were checked periodically using an internally generated calibration square wave provided by the manufacturer. The gain was adjusted appropriately to maintain less than 1% voltage measurement error. Also, the thermocouple, which measured sensor temperature, was checked prior to installation to ensure that it was accurate to less than 1% error.

The zirconia sensor itself was checked by inserting the end of the entire PO_2 probe, as used in AFB testing, into a 2.5-inch-ID electric resistance, cylindrical tube furnace. This furnace was operated at maximum power to produce zirconia sensor temperatures of the order of 1200 F.

A small quartz, thimble-shaped, calibration chamber was fabricated with open-end outside geometry of the porous ceramic filter that ordinarily fit at the probe tip. However, the quartz cylinder was longer (i.e., approximately 6 inches). Hence, the calibration chamber was inserted over the sensor and sealed with the probe end cap in a manner identical to the installation of a porous ceramic filter. A smaller diameter quartz tube was attached to the closed end of the quartz cylinder. This tube passes outside the furnace and allowed gases to be passed over the sensor from an external supply. The gases exited the sensor zone via the ordinary gas sampling lines in the probe. In this manner, the sensor could be exposed to a flow of known composition gases at elevated temperatures. By controlling the inlet pressure and the exit flowrate to this chamber, a slightly positive gas pressure was maintained inside the chamber to mitigate air leaks from the ambient environment.

Several different gases were introduced into the calibration chamber either singly or in combinations of two gases to produce know PO_2 levels for the required calibration. If a single gas was used, only pressure regulation wa

required and a direct hookup from the gas supply cylinder via a pressure regulator. If mixtures of gases were necessary, these gases were mixed dynamically prior to entry into the chamber. Rotometers and a steel wool-filled mixing chamber were used to provide the required dynamic mixing at various ratios of input gases.

The following bottled laboratory gases were used singly or two were dynamically mixed in the present calibration experiments:

1. Standard air (% = 20.9)
2. Argon with 200 ppm O_2 impurity (% O_2 = 0.02)
3. Nitrogen/oxygen mixture provided by Matheson (% O_2 = 3.0)
4. Carbon dioxide
5. Carbon monoxide

Gases No. 2 and 3 above were used either singly or mixed to produce PO_2 levels from $10^{-1.5}$ to 10^{-4} atmospheres. These known levels were calculated using standard ratios of mixture flowrates and known cylinder composition.

For the calibration range from 10^{-15} to 10^{-20} atm of O_2, mixtures of gases No. 4 and 5 were utilized. At elevated temperatures, inside the quartz calibration chamber, these gases reacted to produce oxygen according to the following:

$$2CO_2 \rightleftharpoons 2CO + O_2 \tag{5}$$

Equilibrium calculations indicated that the partial pressure of oxygen, PO_2, was given by

$$PO_2 = \left[\frac{\left(\frac{PCO_2}{PCO}\right)}{Kp(T)}\right]^2 \tag{6}$$

where (PCO_2/PCO) is equivalent the ratio of flowrates of CO_2 and CO gas, respectively. The equilibrium constant Kp(T) can be expressed as:

$$\log[Kp(T)] = 1.475 \frac{10^4}{T} - 4.523 \quad (7)$$

Therefore, by measuring the test chamber temperature, T in deg K, the input flow-rates, the expected partial pressure of oxygen for CO_2/CO mixture was computed using Eq. 6 and 7.

The computed values of the PO_2 then were compared to the measured partial pressure obtained the millivolt output of the zirconia cell, exhaust oxygen sensor.

The calibration results are presented in graphical form in Fig. 4-70. Note that, although some data scatter exists, the measured oxygen partial pressure agreed well with the calculated values. It was assumed that data scattered noted in Fig. 4-70 was likely due to small errors in measuring the temperature or the cell output voltage. It should be noted that less data scatter was obtained if alumina beads were placed in the calibration chamber to help catalyze the reaction in Eq. 5.

Results given in this figure show that calibration data brackets the region of interest in expected PO_2 within the bed (i.e., 10^{-16} atm $<PO_2<.21$ atm). Oxygen concentrations in the midrange could not be generated using the existing CO_2/CO calibration. setup that was limited to providing chamber temperatures of only 1200 F. However, the present calibration indicated that the exhaust oxygen sensors were accurate devices for measuring oxygen partial pressures over a wide range of values.

Data Presentation. The type of in-bed zirconia sensor data shown in the plots of Fig. 4-71 are informative, and such presentations should be obtained for various selected in-bed positions (i.e., along centerline or walls) at given test conditions. Note from the PO_2 versus time plot in this figure that large fluctuations in oxygen partial pressure were measured at frequencies near 1 Hz using the zirconia sensor. As shown in Fig. 4-71, oxygen content oscillated between values near 3% (i.e., log PO_2 = -1.5), which was indicative of the combustor exhaust

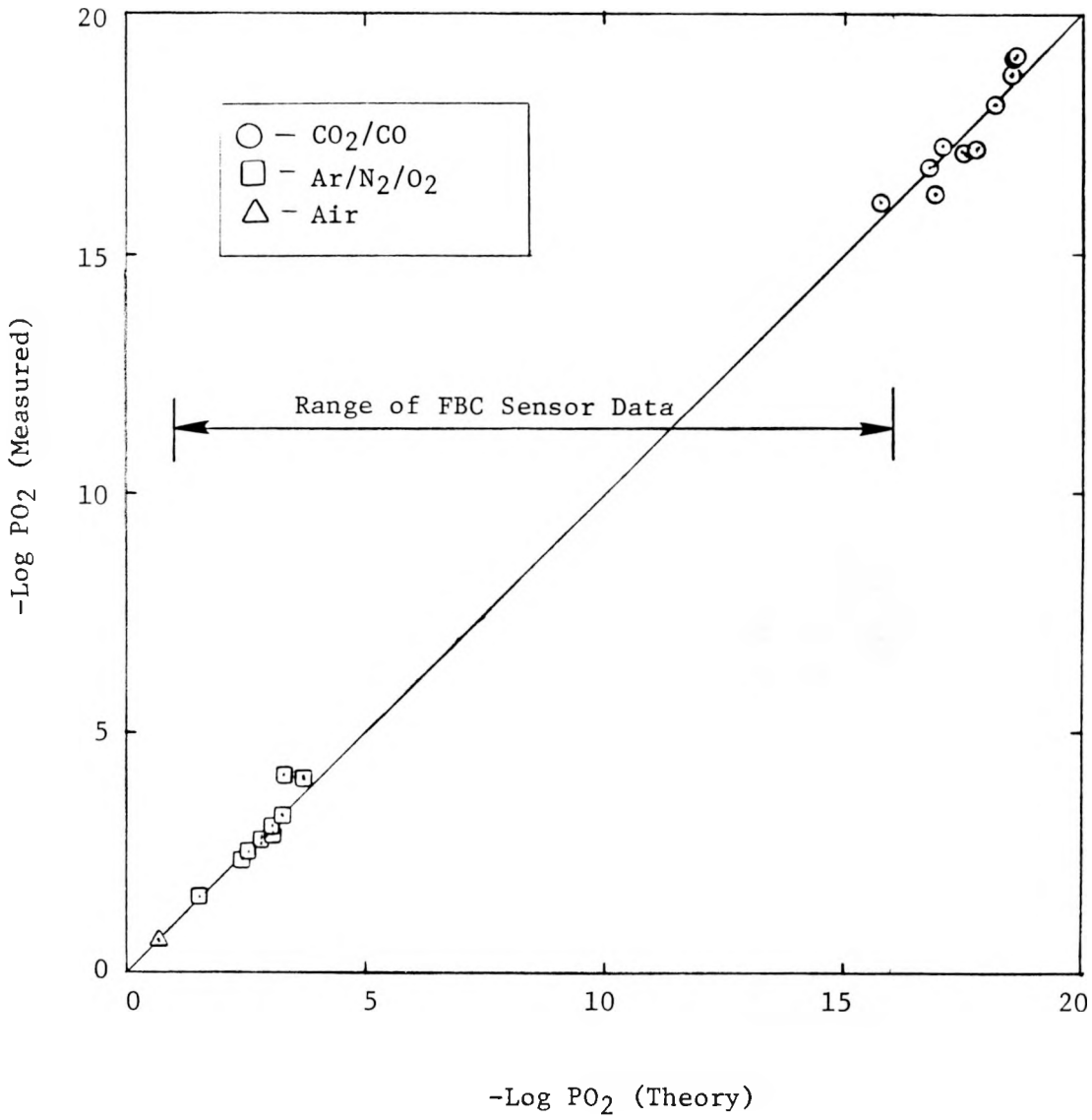


Figure 4-70. PO_2 Sensor Calibration Data

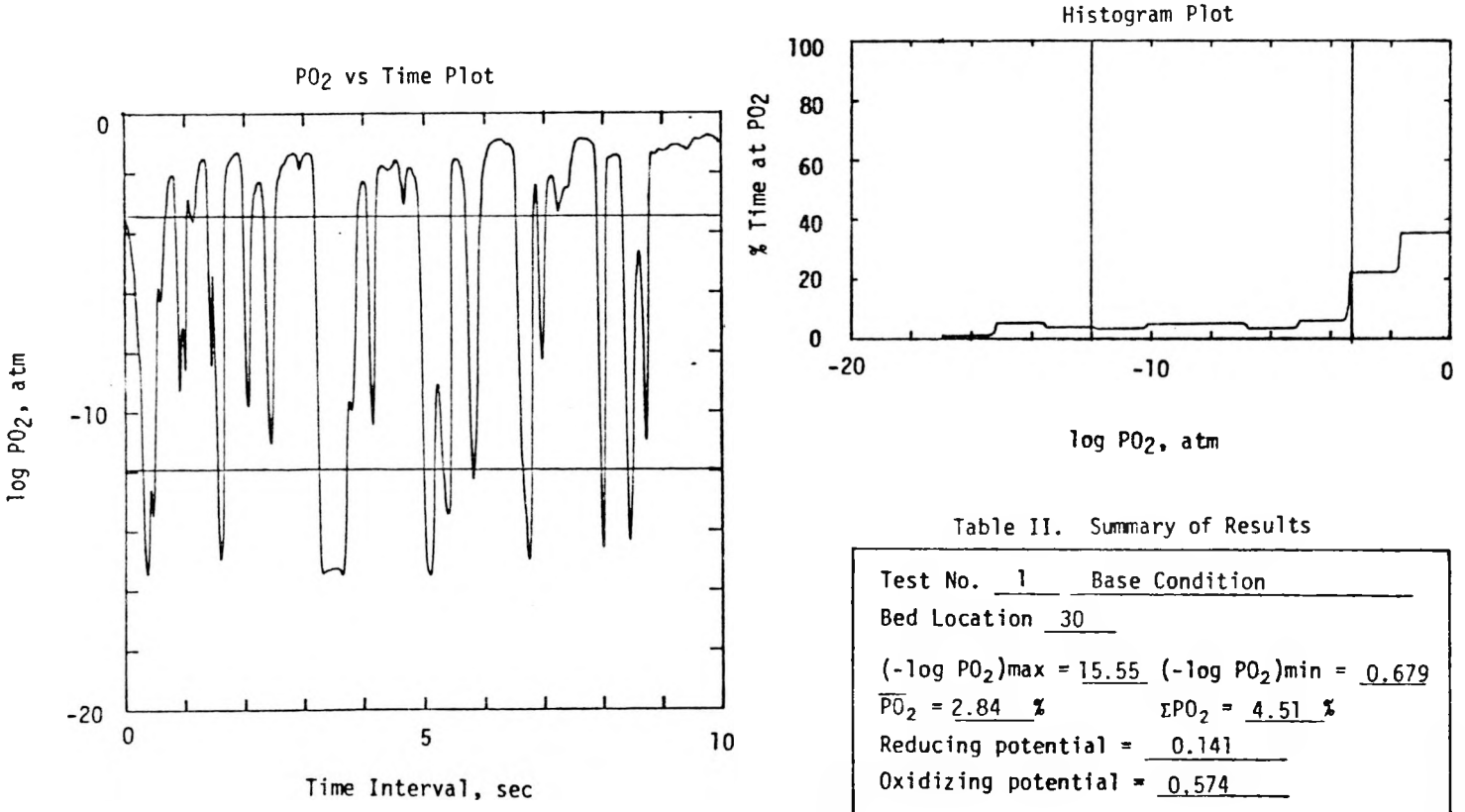


Table II. Summary of Results

Test No.	1 Base Condition
Bed Location	30
$(-\log PO_2)_{max}$	15.55
$(-\log PO_2)_{min}$	0.679
$\overline{PO_2}$	2.84 %
ΣPO_2	4.51 %
Reducing potential	0.141
Oxidizing potential	0.574

Figure 4-71. Typical Oxygen Partial Pressure Versus Time Data and Corresponding Histogram and Numerical Data Analysis Results (Oxiding Environment)

to very low concentrations (i.e., PO_2 10^{-16} atm). Histogram results in Fig. 4-78 show that 57% of the time, however, the oxygen partial pressure was greater than 0.04% (log PO_2 -3.4). During other tests, more extreme conditions were noted with sensor data indicating that more or less time was spent at the two extremes of the log PO_2 range shown in Fig. 4-60.

Although informative, PO_2 versus time is difficult to display and thereby comprehend for locations throughout the combustor.

In order to simplify the data presentation, and yet preserve the indication of oxidizing or reducing conditions, it was decided to represent the PO_2 versus time by two numbers only. These numbers are indicative of the oxidizing and reducing potential at a particular bed location.

The meaning of the above parameters is illustrated in the plot of Fig. 4-71 where the horizontal lines in the PO_2 versus time plot and vertical lines in the histogram plot at the appropriate PO_2 levels. These two PO_2 levels tend to bound the PO_2 measurements in that oxidizing conditions result in PO_2 values above the 10^{-34} atm level and reducing conditions result in PO_2 conditions below the 10^{-12} level. The above parameters also are related to the histogram data given in Fig. 4-71. Oxidizing potential (Op) is a sum of the first two histogram values, while reducing potential (Rp) is the sum of the last three. Obviously, if a given location had a value of Op near 1.0 and a value of Rp near zero, this could be considered an oxidizing environment, while if the reverse were true, a reducing environment would exist. Op and Rp values determined for the data are listed in Table I included in Fig. 4-71 (i.e., Op = .57, Rp = .14).

Time-varying PO_2 data were analyzed at various in-bed radial points located 3 inches apart for each of several axial locations above the coal feed port to determine Op and Rp values in several AFB combustors. The other values shown in Fig. 4-71 also were determined throughout the in-bed environment. These specific, single-valued data for each measurement location are more easily presented for various positions throughout the combustor.

Conclusions and Recommendations.

1. A probe employing the zirconia-platinum cell oxygen sensor can be successfully used to obtain in-bed, fluctuating oxygen partial pressure, PO_2, data in a variety of combustors, and for a variety of operating conditions
2. Although possible measurement errors caused by the sensor surface effects are not known quantitatively, the sensor output should still be usable to predict corrosion on hot metallic tubes in the bed
3. Zirconia sensor data should be obtained in a variety of AFB environments, especially larger units to understand the significance of the probe results on overall bed operation. These data also should be obtained over a variety of AFB operating conditions
4. Zirconia sensor data should be obtained at or near the location of in-bed material samples during short- and long-term materials test to further ascertain what correlations exist between local sensor-indicated oxidizing/reducing zones and material performance
5. A new type of in-bed porous ceramic filter should be developed to provide higher sampling life rates and longer service life.

4.2.4 Characterization of the 24-Inch Fluidized Bed Environment

The initial objective of in-bed diagnostic efforts was to define the environment which material samples would experience during corrosion testing in the AFB bed. This objective continually broadened to encompass the characterization of in-bed conditions as a function of operating parameters and geometric changes. It is believed this characterization data will assist AFB designers in tailoring bed conditions to avoid highly reducing zones within the bed, shown in Section 4.1 to be detrimental to the heat exchange alloy materials.

In situ oxygen partial pressure measurements obtained in January 1981 indicated that a severe reducing zone existed at the bottom of the 24-inch fluidized bed unit just above the coal feed port. Based upon these results, the bed depth below the heat exchanger (HEX) array was increased and a new coal feel port was constructed to eliminate this deleterious region.

In this report, the results of all 16 tests described in Sections 4.2.1 and 4.2.2 are presented as bed characterization experiments used to verify whether the modifications were successful in removing the detected localized reducing environments, and to investigate the severity of reducing zones as a function of various operating parameters. Furthermore, these data were used to assist in the choice of test conditions for three 250-hour material tests to follow in the near future. The data examined were obtained using the PO_2 probe described in Section 4.2.3.

Characterization Experiments. The combined fluctuating oxygen partial pressure (PO_2)/gas sampling probe was used to define the in-bed chemistry environment during AFB operation at 16 test conditions. A description of these conditions is presented in Table 4-22 as a variation from the base conditions also given in this table.

TABLE 4-22. TEST CONDITIONS DURING CHARACTERIZATION EXPERIMENTS

Test No.	Date	Port Type	Description
1	Jan 81	Original	Base Conditions*
2		Original	High Conveying Air (20%)
3		Original	Low Conveying Air (5%)
4		Original	High Excess Air (50%)
5		Original	Low Superficial Gas Velocity (3.5 FPS)
6		Original	Series Bed Case
7		Original	Coarse Coal (-4 + 30 mesh)
8	Aug 81	Original	Fine Coal (-30 mesh)
9		Original**	Coke
10		Original**	Base Conditions Repeated
11		New Design**	Base Conditions
12		New Design**	High Conveying Air (20%)
13		New Design**	Low Excess Air (10%)/High Conveying Air
14		New Design**	High Excess Air (50%)/High Conveying Air
15		New Design**	Low Superficial Gas Velocity (3.5 FPS)
16		New Design**	Babcock and Wilcox Conditions

* Temperature = 1650 F
Superficial Velocity = 6 FPS
Excess Air = 20%
Conveying Air = 10% of total
SO_2 in Flue = 1.2 lb/mm Btu
Bed Depth = 58 inches
Fuel: Ill. No. 6 coal
Coal Size: -8 mesh
Limestone Size: -8 + 20 mesh

** Deeper Bed

For these test conditions, extensive PO_2 and some gas sampling data were obtained at four axial positions above the coal feed port. These positions were located below and within the HEX array as shown in Fig. 4-72. Also shown in this figure are the in-bed positions where corrosion samples will be placed during the 250-hour material tests. Note that the diagnostic locations are at or near the corrosion sample locations to ensure that diagnostic results will aid in defining the chemistry environment experienced by test materials.

At each of the axial positions shown in Fig. 4-72, PO_2 and gas sampling data were obtained at various radial locations by inserting the probe at different depths into the bed from the wall of the combustor. The specific radial locations at which diagnostic data were obtained are shown in Fig. 4-73. Note that 21 locations were selected for PO_2 data acquisition while only 7 locations were used to define the chemistry of other gases of interest (i.e., CO_2 and CO). Furthermore, gas sampling chemistry data were obtained only for the base condition because of the inordinate amount of time required to obtain this less-critical data.

A schematic diagram of the original coal feed port design is shown also in Fig. 4-73. Note that two concentric sets of air tuyeres and a small cap are used in this feed port design. Figure 4-74 show a schematic of the new coal feed port design. The inner tuyere air has been rerouted through the coal feed port and exits the port radially rather than axially as in the original design. The feed port cap is also larger in this new design. It is evident from the schematics in Fig. 4-73 and 4-74 that a significant alteration in bed dynamics can possibly exist for the two different coal feed port designs.

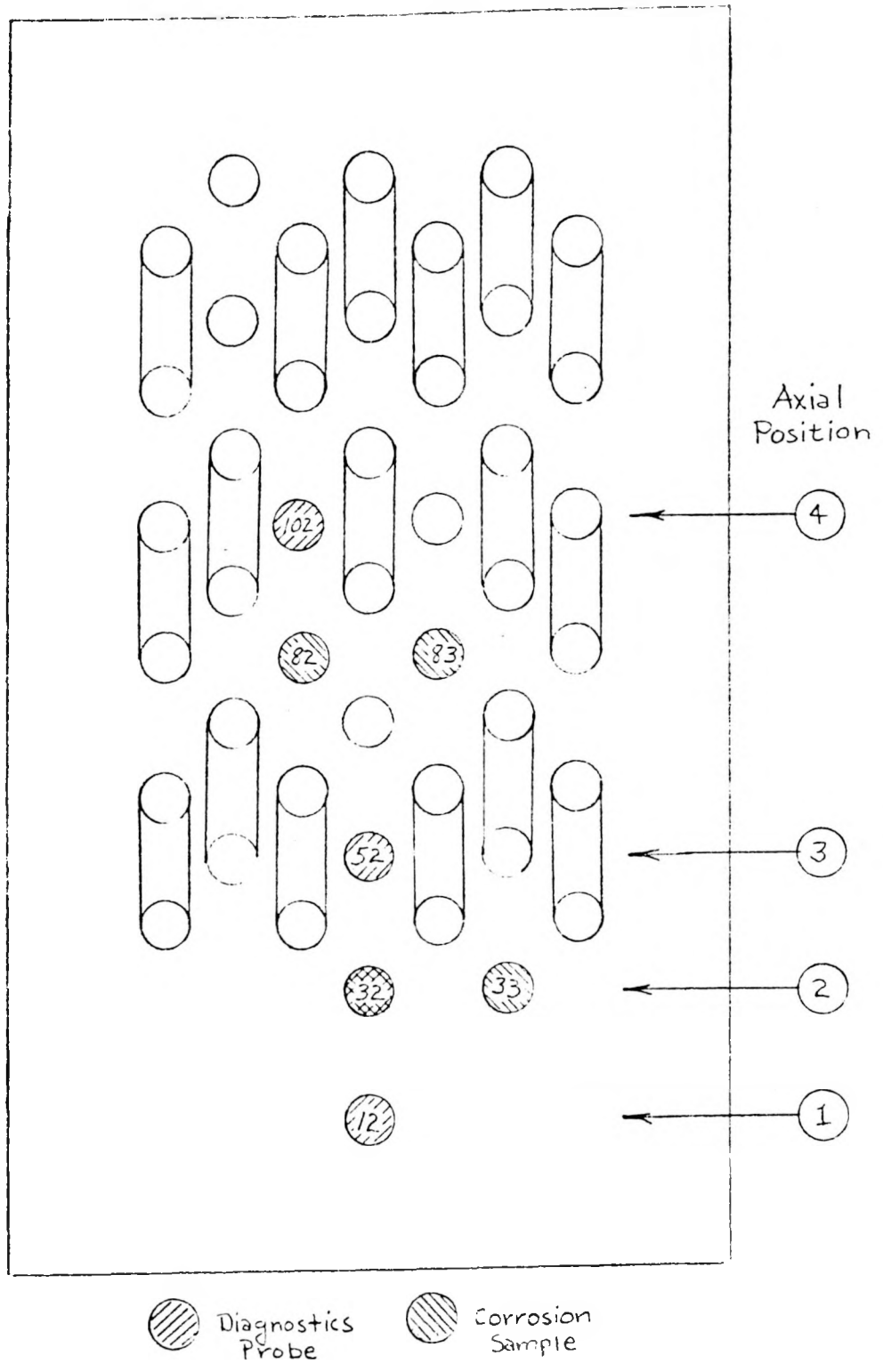


Figure 4-72. Locations of Diagnostic Probe and Corrosion Sample Ports Relative to the Heat Exchanger Array

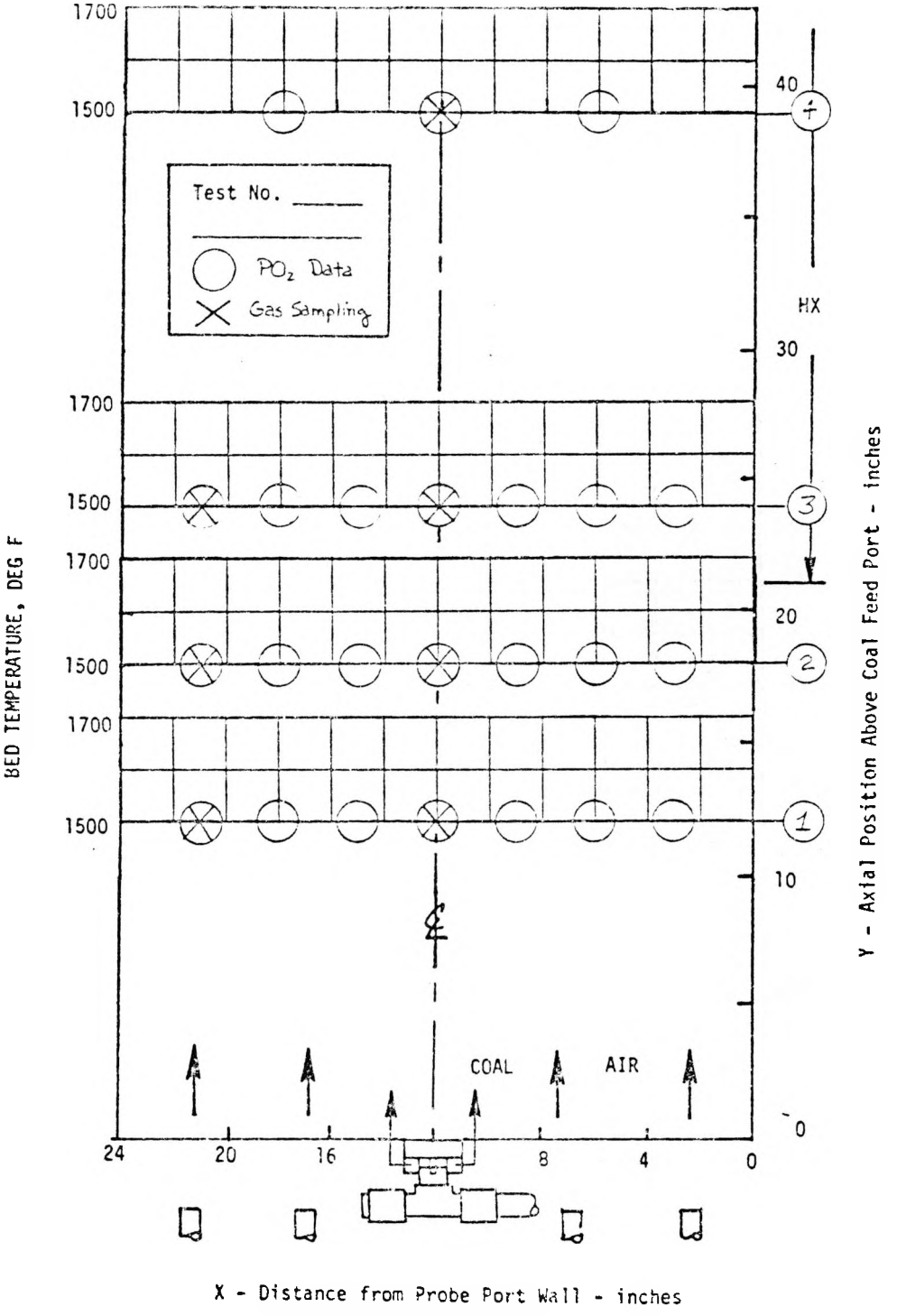


Figure 4-73. Location of Diagnostic Measurement Positions and Schematic of Original Coal Feed Port Design

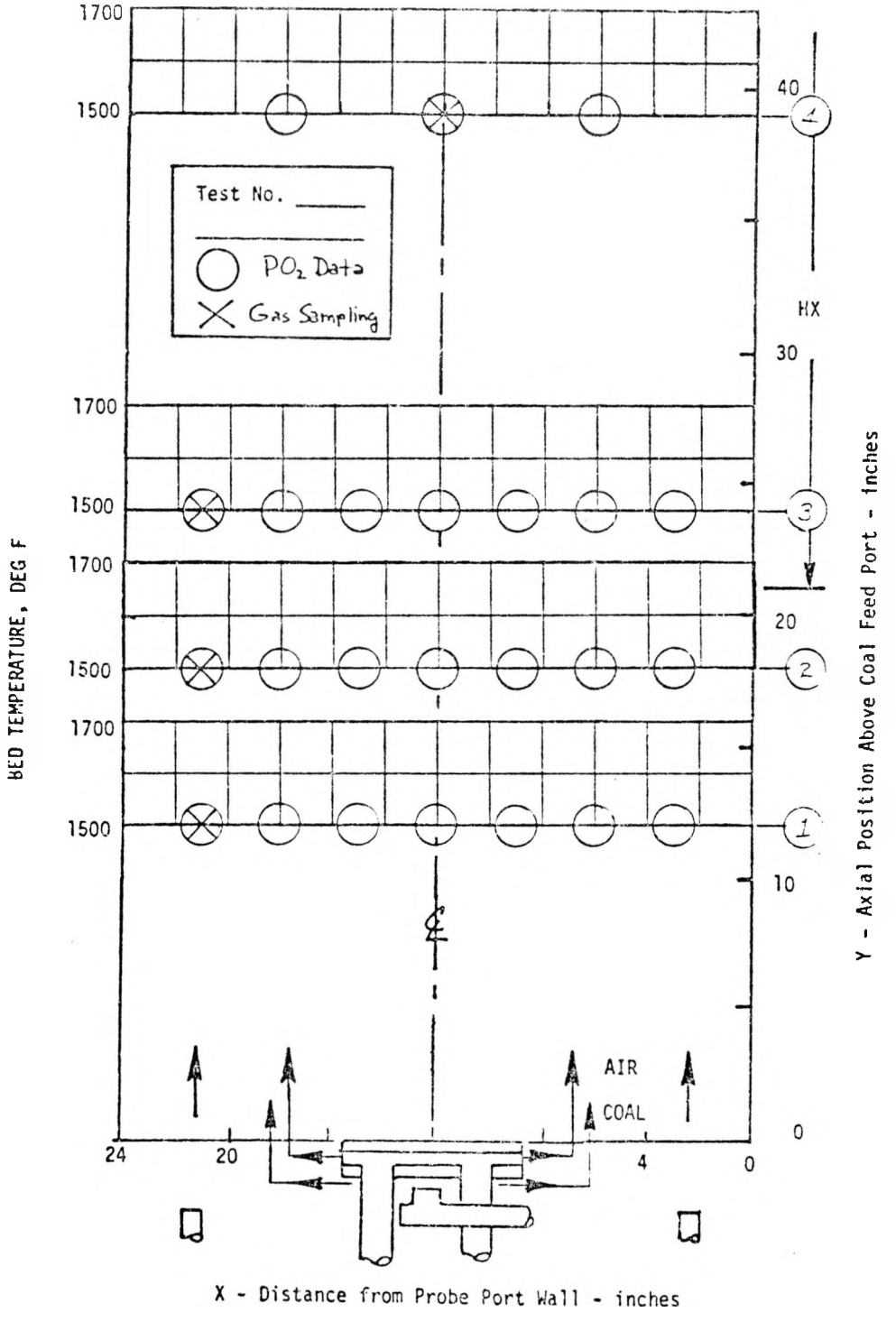


Figure 4-74. Location of Diagnostic Measurement Positions and Schematic of New Coal Feed Port Design

Base Conditions. More detailed data was obtained during tests 8 through 10 for the base test condition using the original coal feed port design. Furthermore, these data were analyzed to a higher degree of detail in order to validate the entire measurement sequence. As previously discussed, the oxidizing (O) and reducing (R) potentials were determined from recorded fluctuating PO_2 data for locations of interest in the bed. Results of these data reduction are shown plotted in Fig. 4-75 for base condition tests 1 and 10. A high O coupled with a corresponding low R indicates an oxidizing environment, since

$$O + R \cong 1 \tag{1}$$

Conversely, a high value of R coupled with a corresponding low O indicates that reducing conditions exist. Note that for the base condition, O/R data indicate that a shift from moderate oxidizing to moderate reducing conditions exist radially across the bed 12 inches above the coal feed port. However, at the 18-inch axial location, relatively severe reducing zones can be found near the combustor walls while near the centerline an oxidizing environment exists. Note that these wall-reducing zones still persist at the 24-inch location. Finally, within the midbed region (30 inches above the coal feed port), moderately oxidizing conditions exist across the entire bed.

The indication of reducing zones at combustor walls near the bottom of the HEX array was corroborated by gas-sampling data as shown in Fig. 4-76, 4-77, and 4-78. These data indicate that higher quantities of CO and CO_2 (i.e., higher volatile coal species) exist near the walls than at the combustor centerline, but less oxygen is present in the wall region (i.e., higher wall-reducing potential).

A comparison was made also of oxygen gas-sampling data to time-averaged data obtained from the instantaneous zirconia sensor probe output. Results of this comparison are shown in Fig. 4-79 and 4-80 where average oxygen content at the wall and centerline, respectively, are plotted as a function of axial distance above the coal feed port. Note that trends in increasing and decreasing average oxygen content were identically shown by both methods. This agreement further

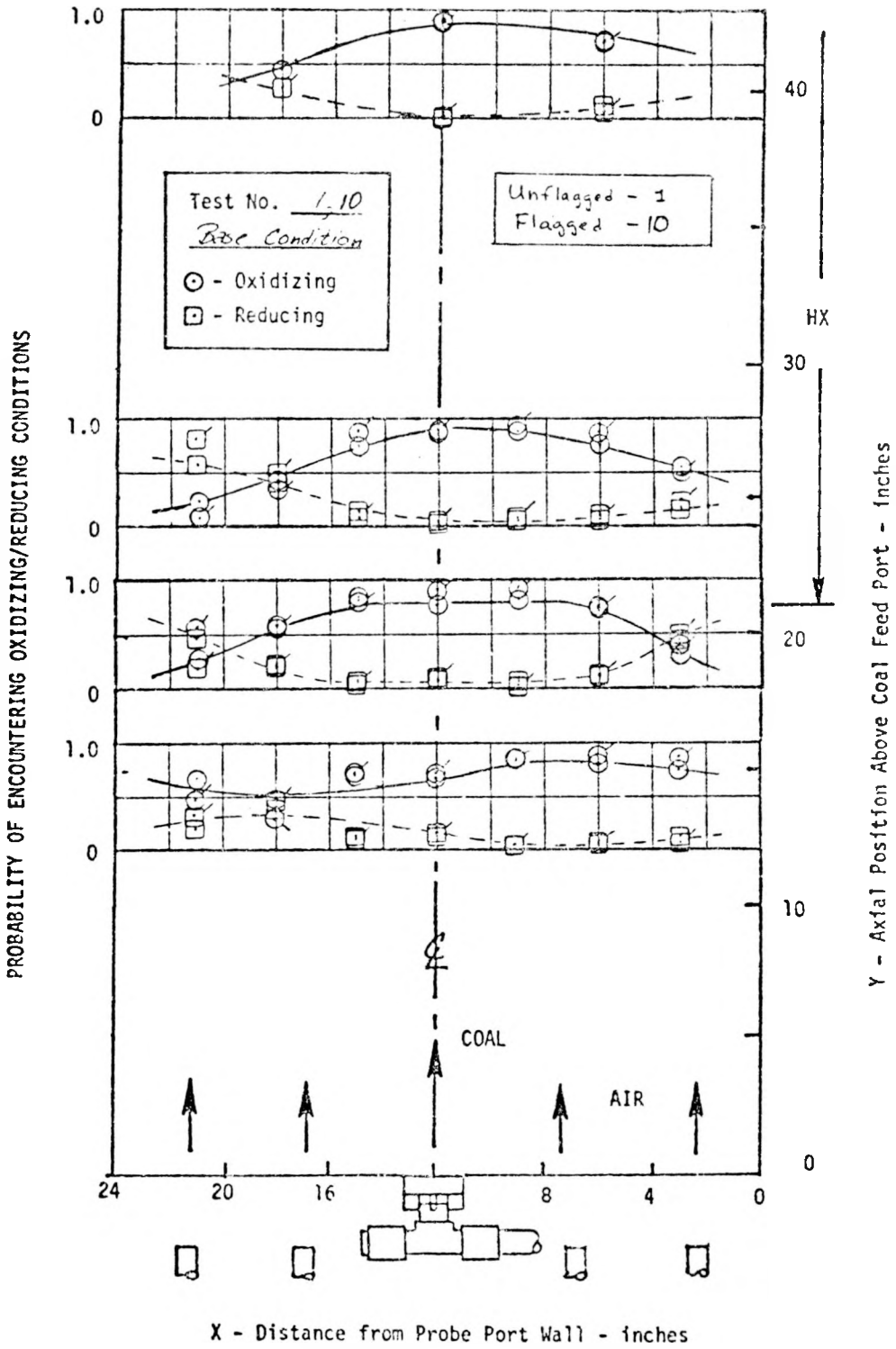


Figure 4-75. Probability of Encountering Oxidizing or Reducing Conditions at Various Locations throughout the In-Bed Region for Base Conditions (i.e., Test No. 1 and 10)

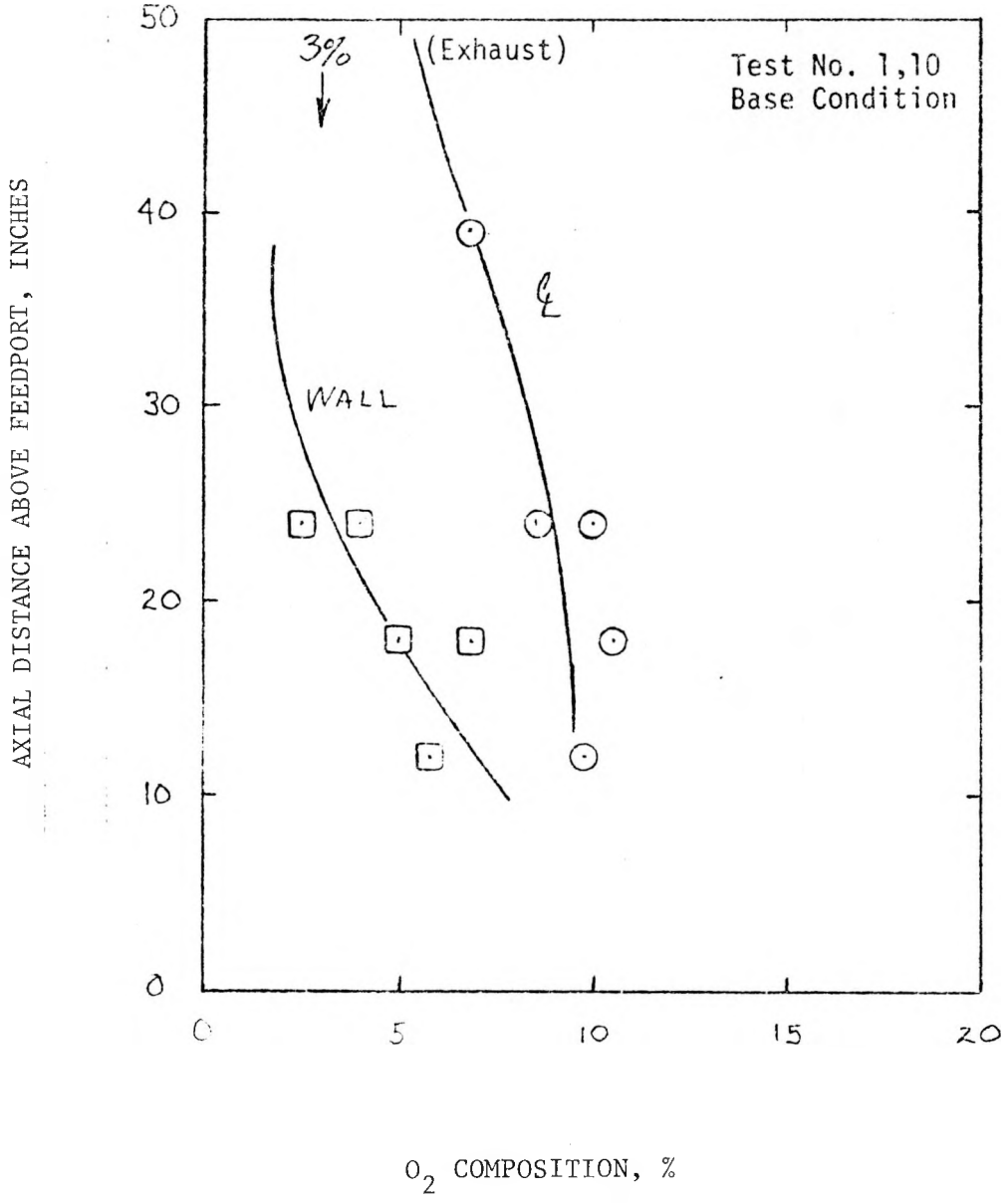


Figure 4-76. Wall and Centerline Oxygen Concentration as a Function of Axial Location within the Bed (Gas-Sampling Data)

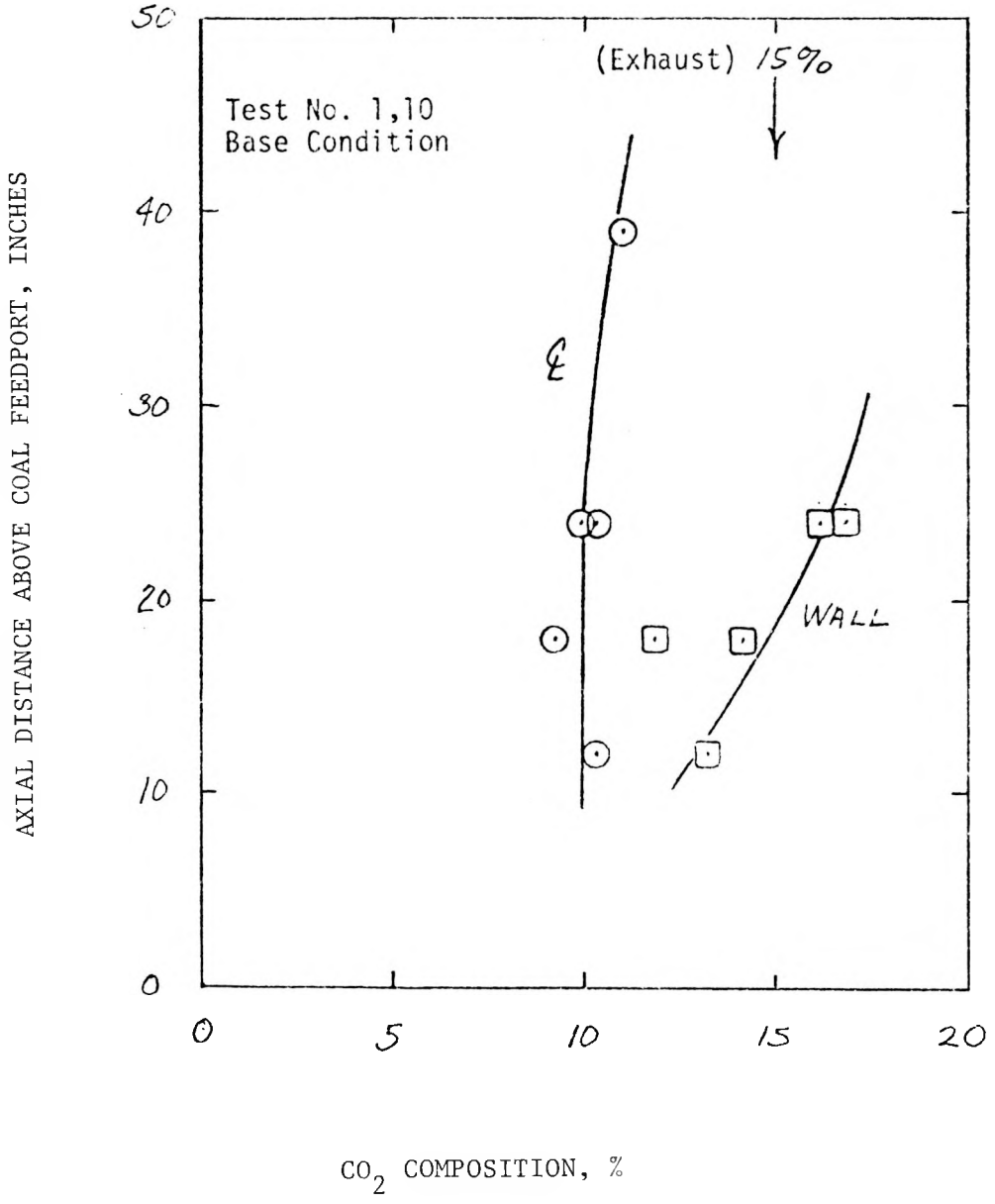


Figure 4-77. Wall and Centerline Carbon Dioxide Concentration as a Function of Axial Location without the Bed (Gas-Sampling Data)

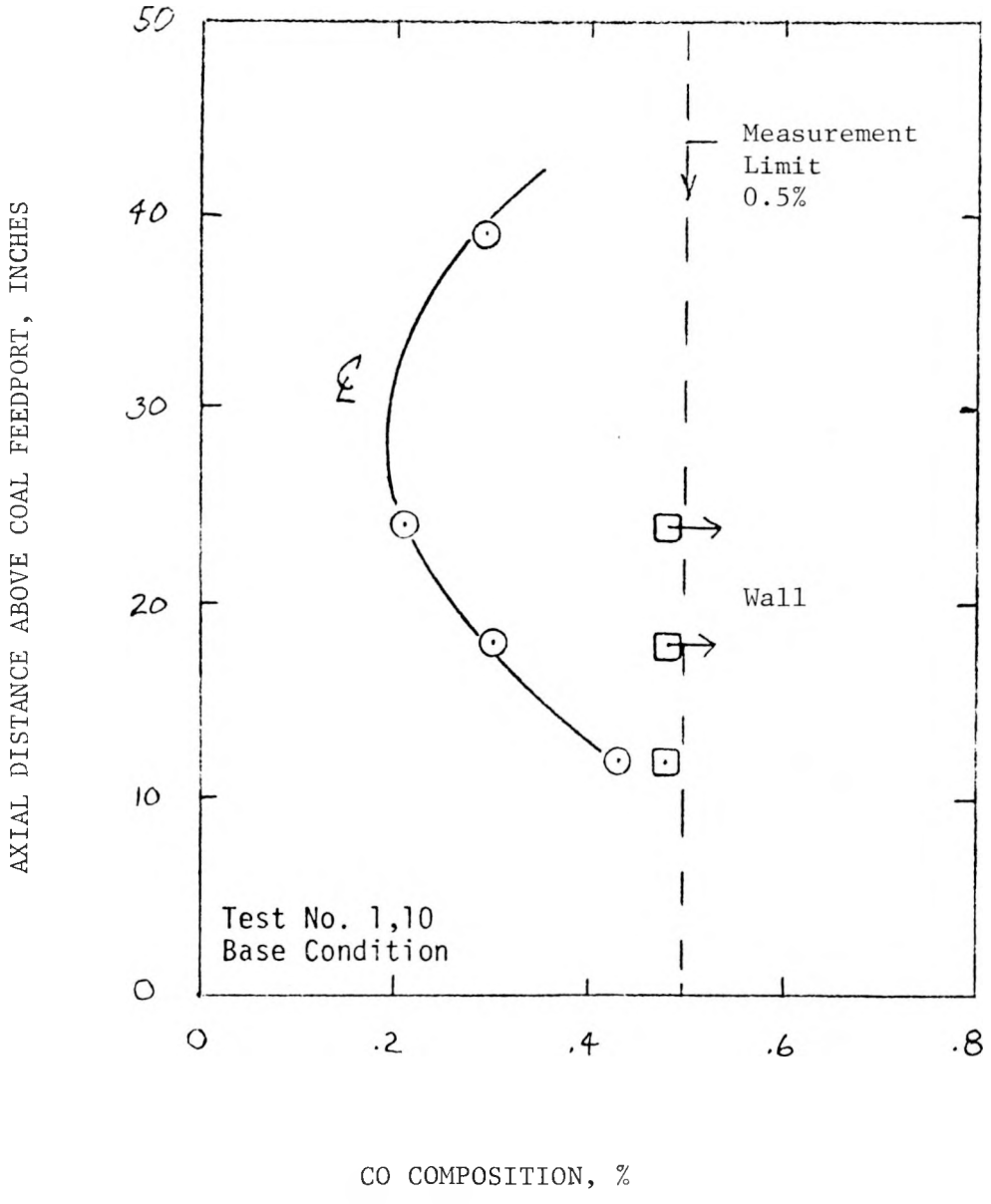


Figure 4-78. Wall and Centerline Carbon Monoxide Concentration as a Function of Axial Location within the Bed (Gas-Sampling Data)

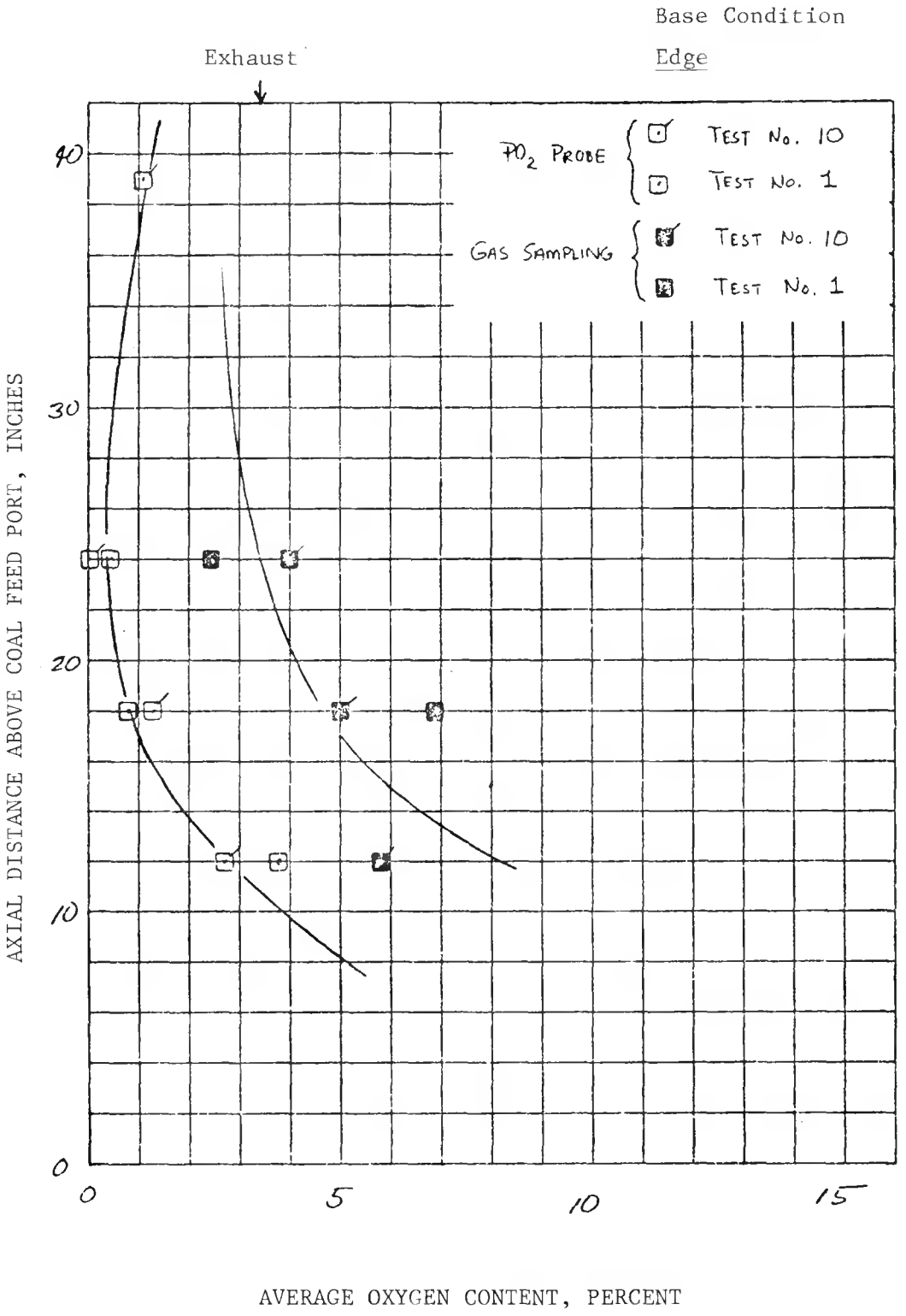


Figure 4-79. Average Oxygen Content Near the Combustor Wall Determined with Gas-Sampling and Time-Averaged Zirconia PO_2 Sensor Methods (Base Conditions)

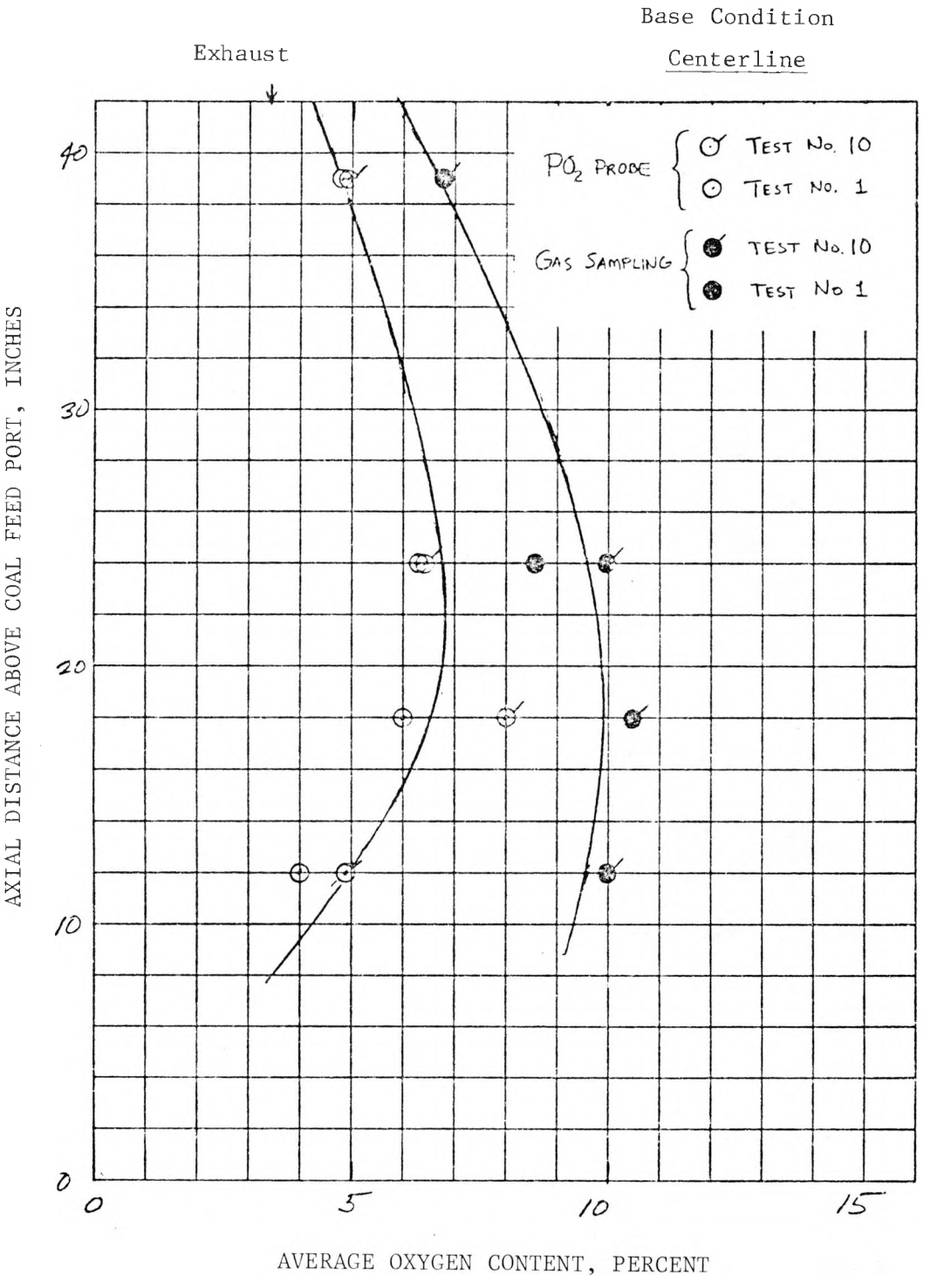


Figure 4-80. Average Oxygen Content Near the Combustor Centerline Determined with Gas-Sampling and Time-Averaged Zirconia PO_2 Sensor Methods (Base Conditions)

corroborates the zirconia sensor results. The 2 to 5% higher oxygen content determined by gas sampling techniques was due to experimental errors induced in both methods. At low-oxygen content, the gas sampling results are affected by small air leaks in the sampling lines that tend to increase the sampled O_2 content. At concentrations above 5%, the PO_2 sensor results are affected by the presence of the porous alundum filter that tends to cause lower average oxygen content to be indicated due to inadequate time response of the filtered zirconia sensor.

Based upon the relatively good comparison of average PO_2 content using both time-averaged sensor and gas-sampling data, the time-averaged PO_2 sensor data, PO_2, were plotted as a function of position throughout the bed for base test conditions as shown in Fig. 4-81. Comparing the results in Fig. 4-81 and 4-75, it can be noted that the log of average oxygen content (log PO_2) correlates with the oxidizing potential, O. In fact, all data from the 16 tests were statistically analyzed to determine the form of this correlation. It was discovered that to within a 94% coefficient of determination the following correlation exists:

$$O = 0.54 \log PO_2 + 0.390 \tag{2}$$

or

$$PO_2 = 10^{1.85\,(O\,-0.39)} \tag{3}$$

Hence, oxidizing potential, O, is related to the average oxygen content of the bed.

Using Eq. 3, we find

O = 0, reducing conditions, PO_2 = 0.19%
O = 1, oxidizing conditions, PO_2 = 13.4%
O = 0.65 exhaust conditions, PO_2 = 3.0%

Another property of the fluctuating PO_2 probe data examined for the base test condition was the minimum value of measured PO_2 at a given location within the bed. A plot of these data are shown in Fig. 4-82. Comparing Fig. 4-82 with Fig. 4-75, it can be noted that oxidizing conditions produce lower measured minimum PO_2 values for a given axial position. It also can be noted that the

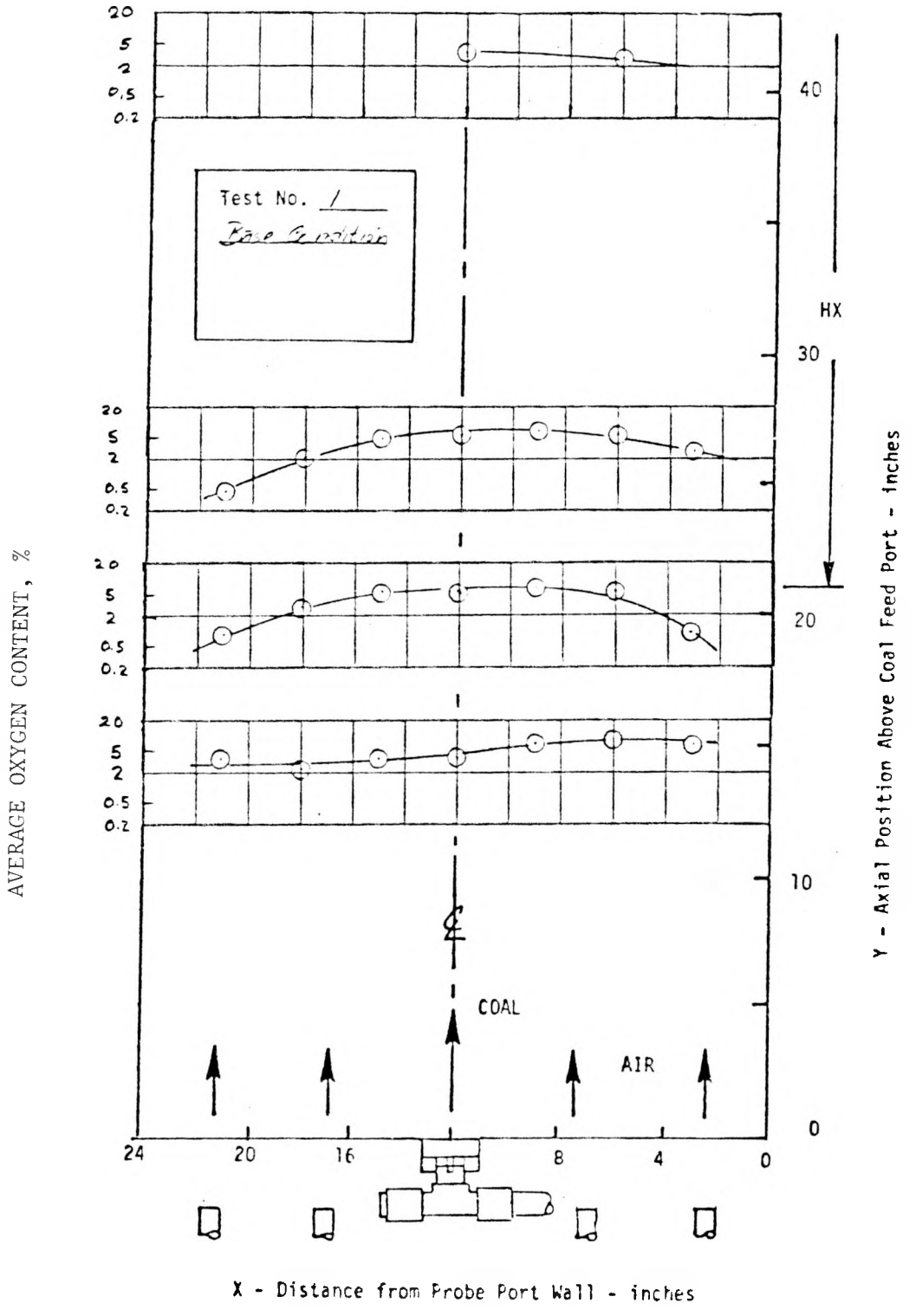


Figure 4-81. Time-Average Oxygen Content Determined by the Zirconia Sensor for Various Locations throughout the Bed (Base Test Conditions)

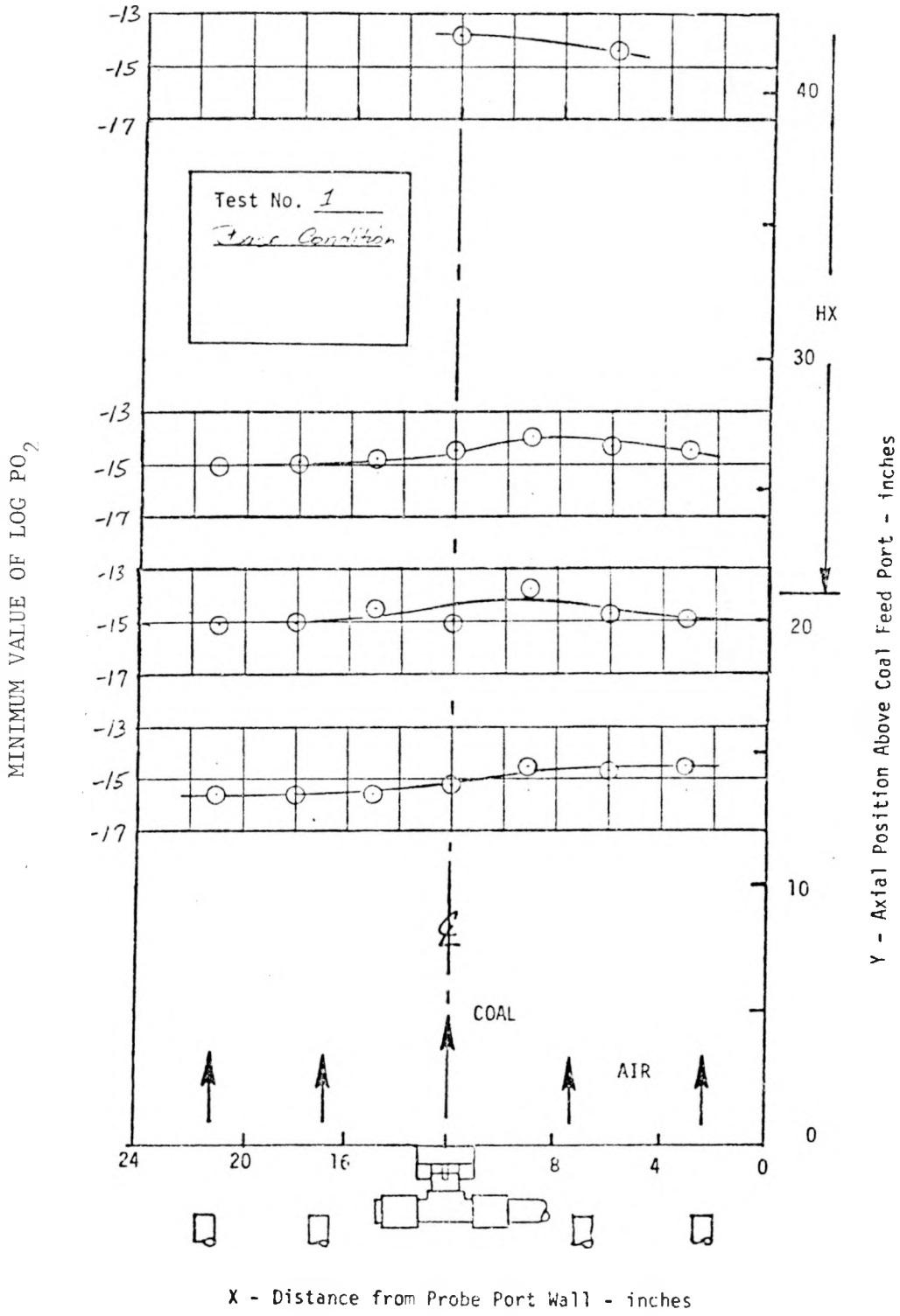


Figure 4-82. Minimum Value of Measured Oxygen Partial Pressure for Various Locations within the Bed (Base Test Conditions)

minimum value decreases with increasing position above the coal feed port from values near 10^{-16} atm at the 12-inch location to 10^{-14} atm near the midbed position (i.e., 39 inches above the coal feed port).

Oxidizing/Reducing Potential Results. The oxidizing and reducing potential data were analyzed by preparation of plots similar to Fig. 4-75 for the variations in port design and bed-operating conditions. To compare changes in the fluidized bed environment with variations in port or operating conditions, the individual plots were combined on summary plots.

In Fig. 4-83 and 4-84, the data for variations in conveying air are presented for the original and new port designs, respectively. It can be noted that the new port is much more sensitive to conveying air variations than the original port design. In fact, for 10% conveying air, the new design appears to produce higher reducing potential regions than the original (Fig. 4-90). However, for 20% conveying air, the reverse is true, as shown in Fig. 4-86, so that the new design is superior to the original. These figures (Fig. 4-85 and 4-86) indicate the advantage of utilizing the PO_2 probe to quickly optimize performance of a new feed port design.

In Fig. 4-87, the spatial variation of reducing potential is given as a function of various coal types. Both size and volatile matter variations are presented. It can be noted that in general, the fine (i.e., -30 mesh) and coarse coal (-4 + 30 mesh) produce slightly less severe reducing potential zones than the base coal size (i.e., -8 mesh). It also can be noted that the coal type that is nearly devoid of volatile matter (i.e., coke) produces a nearly total oxidizing environment within the fluidized bed.

The variations of reducing potential within the in-bed region as a function of superficial gas velocity are given in Fig. 4-88 and 4-89 for the original and new port designs, respectively. In both cases, lowering the velocity moderates the severity of reducing zones near the combustor walls.

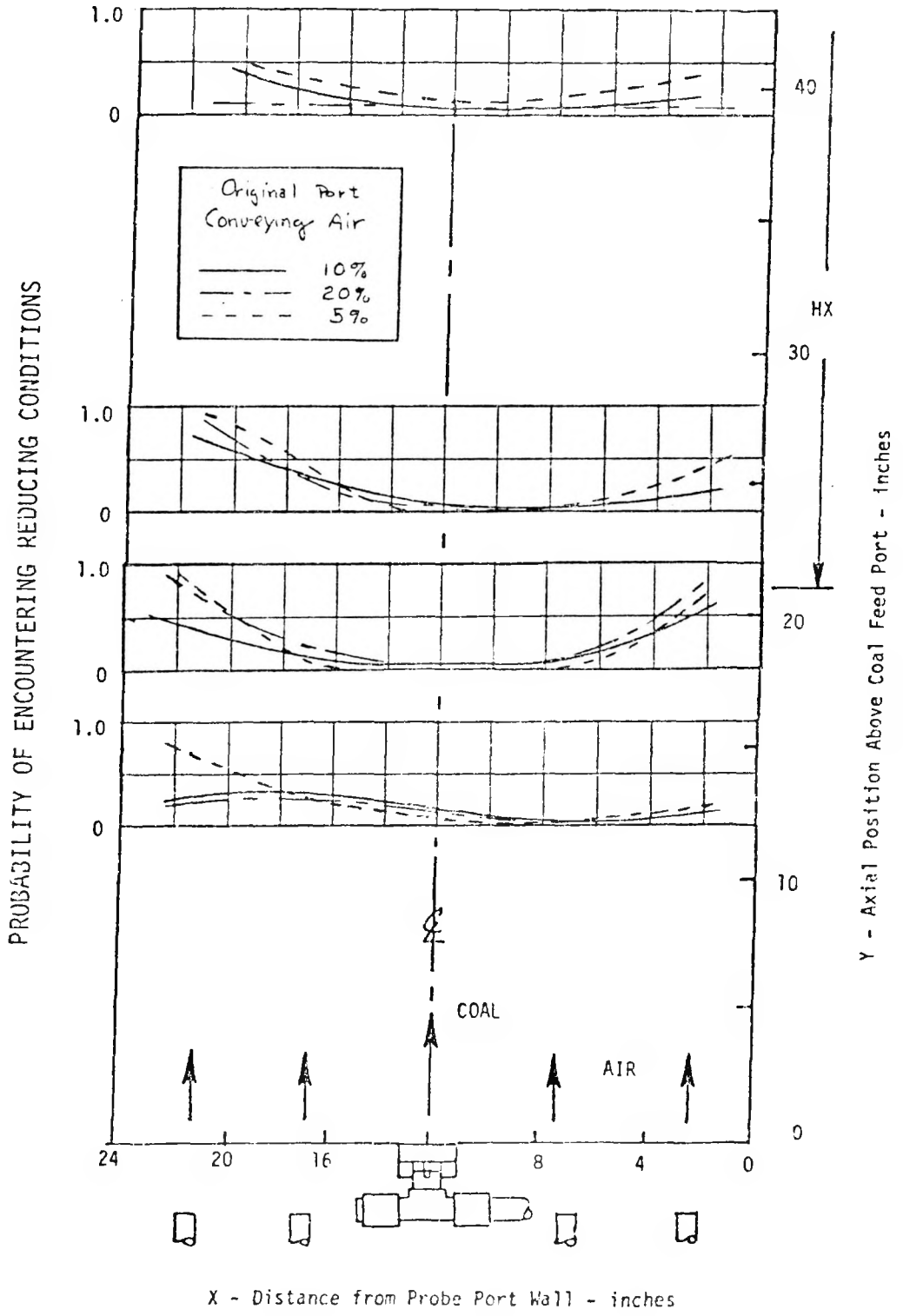


Figure 4-83. Spatial Variation of Reducing Potential as a Function of Conveying Air (Original Port Design)

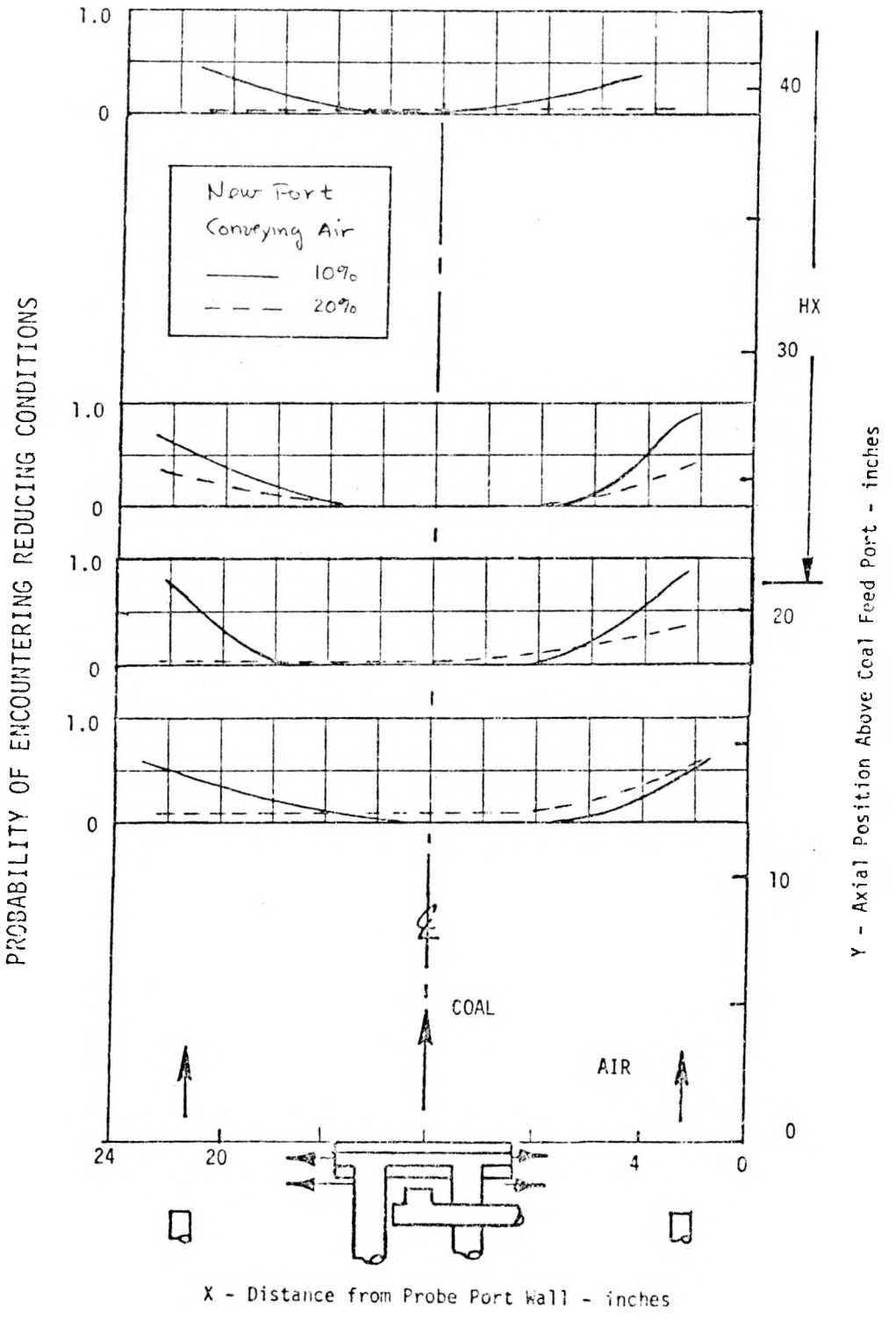


Figure 4-84. Spatial Variation of Reducing Potential as a Function of Conveying Air (New Port Design)

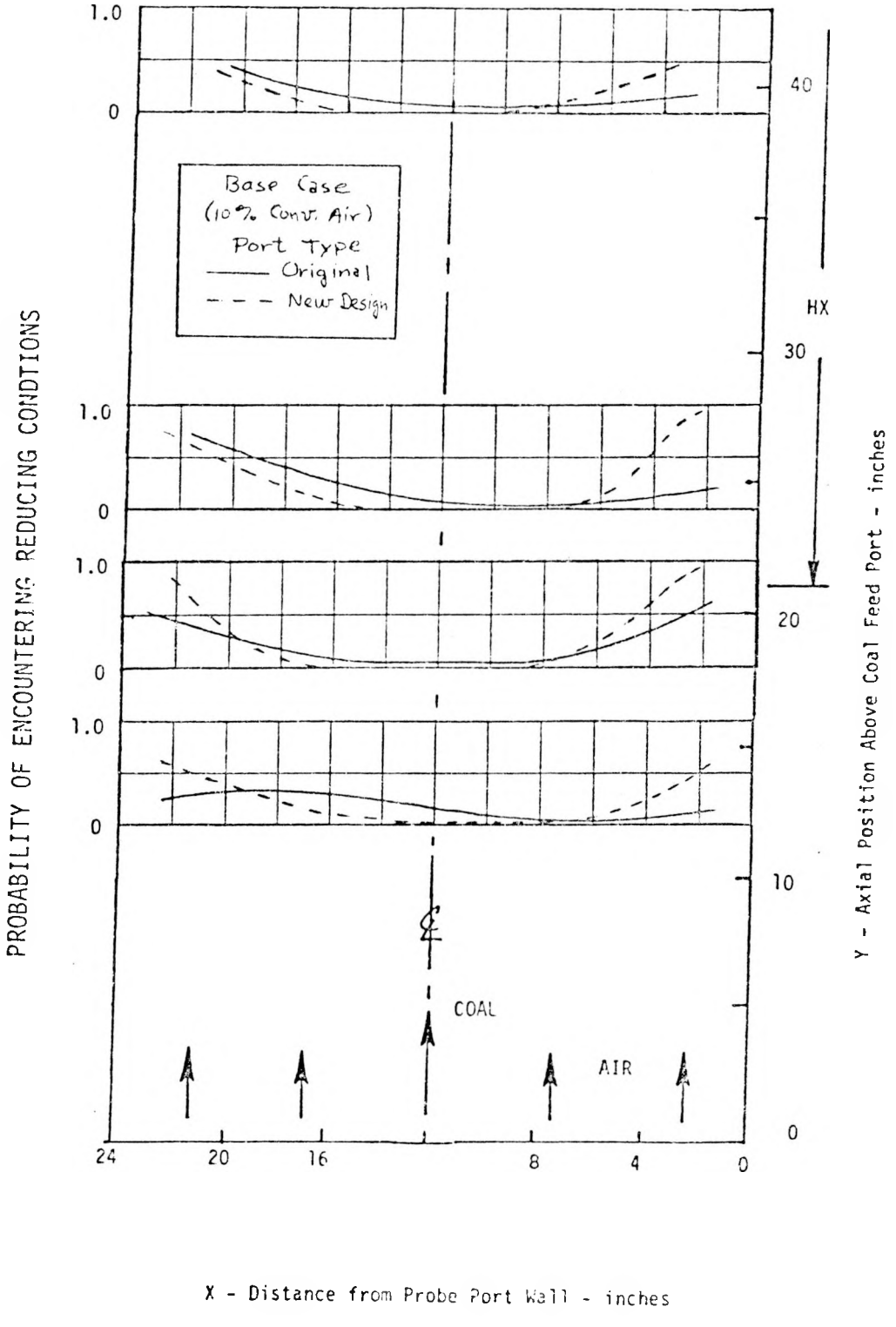


Figure 4-85. Spatial Variation of Reduction Potential for Base Test Conditions as a Function of Port Design

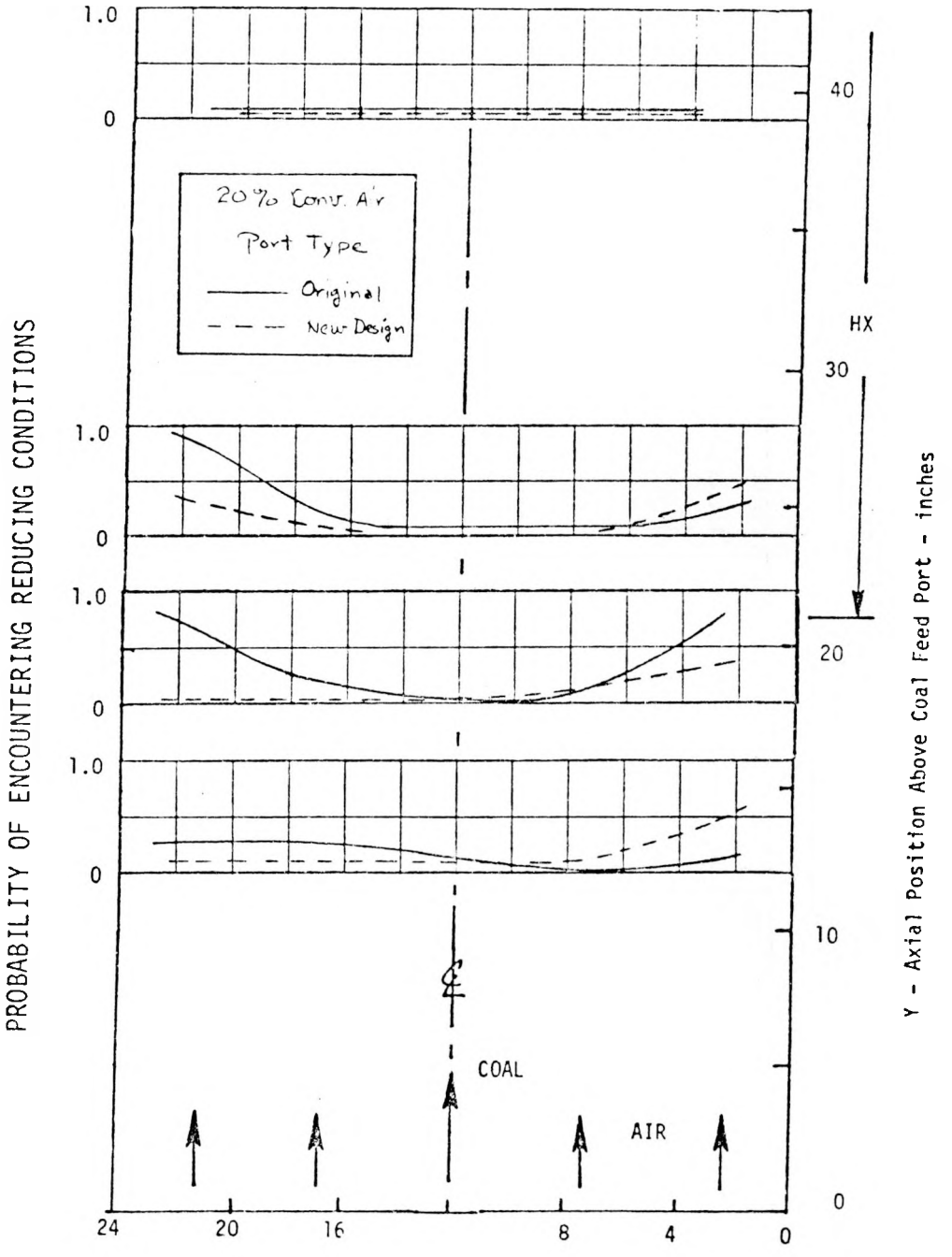


Figure 4-86. Spatial Variation of Reducing Potential for 20% Conveying Air as a Function of Port Design

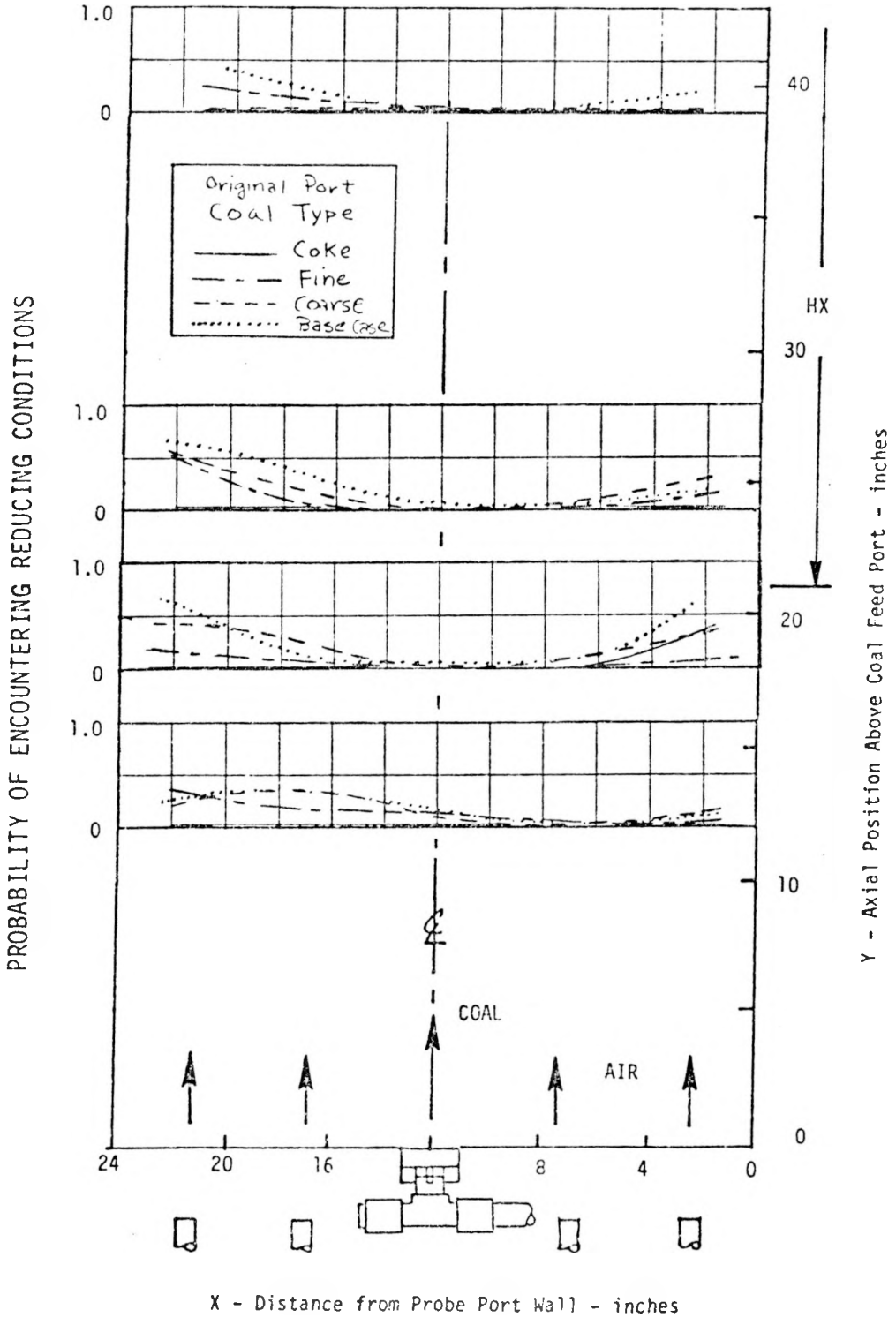


Figure 4-87. Spatial Variation of Reducing Potential as a Function of Various Coal Types (Original Port Design)

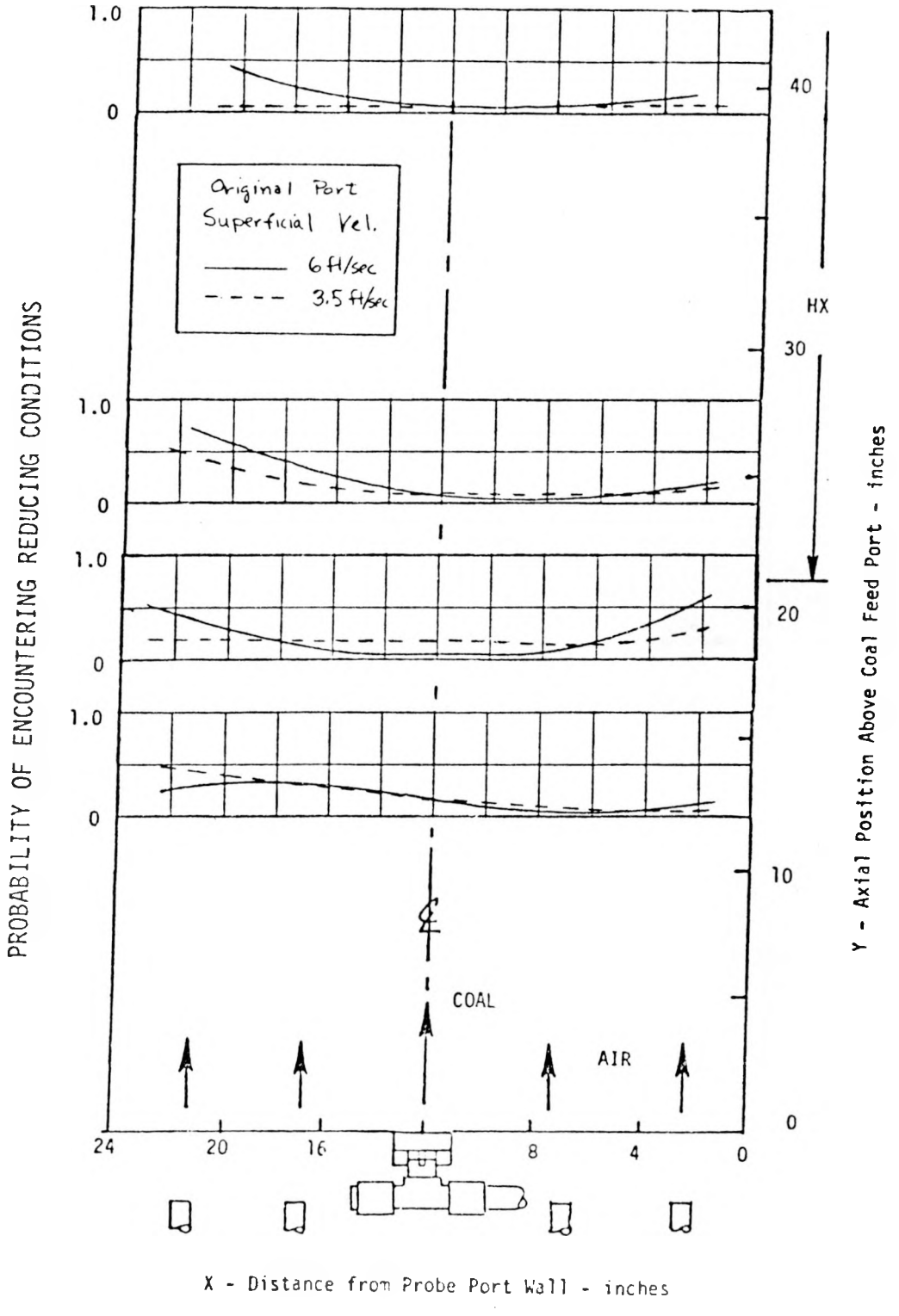


Figure 4-88. Spatial Variation of Reducing Potential as a Function of Superficial as Velocity (Original Port Design)

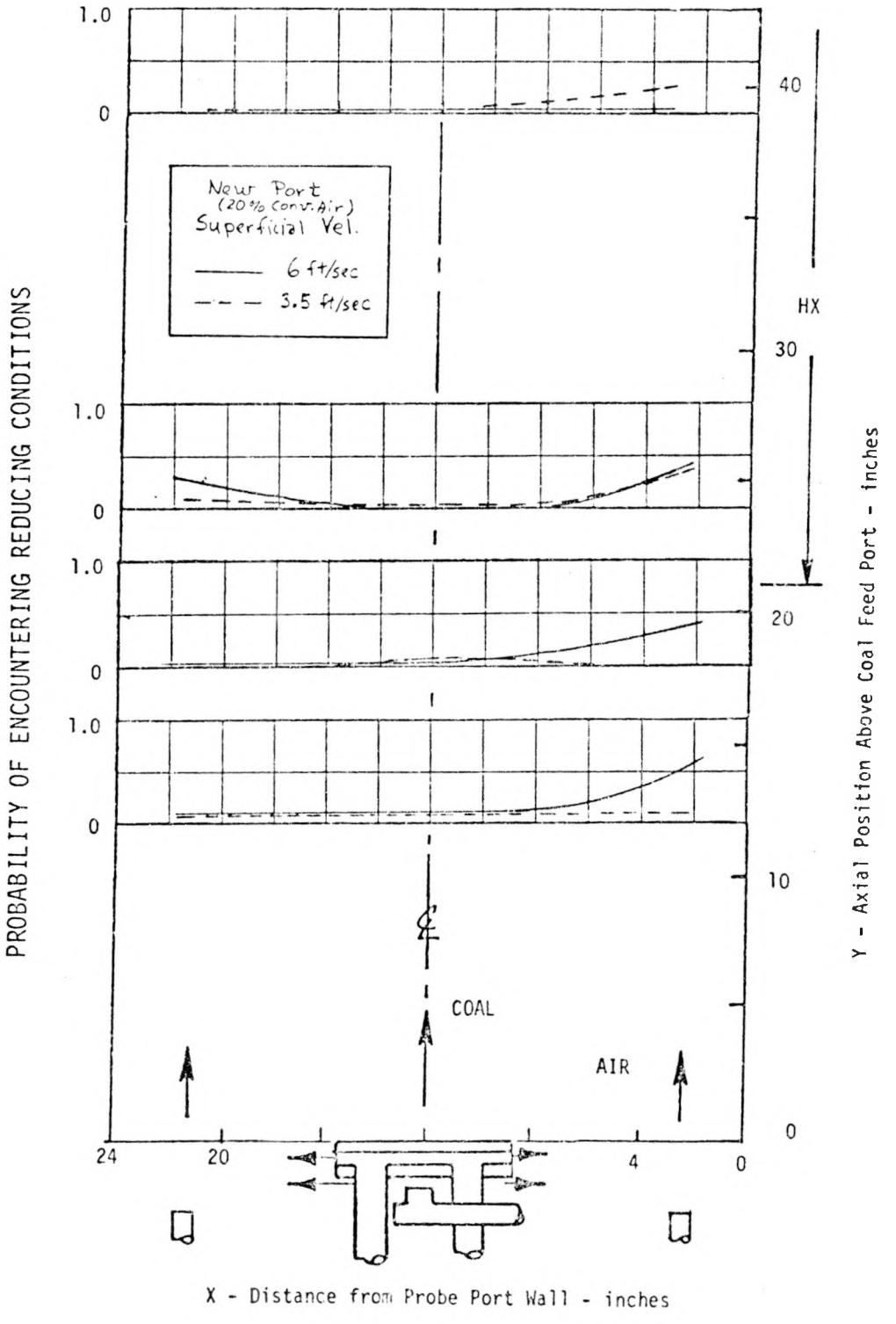


Figure 4-89. Spatial Variation of Reducing Potential as a Function of Superficial Gas Velocity (New Port Design)

Finally, the effect of excess air on reducing potential variation within the bed is given in Fig. 4-90 and 4-91 (original and new port design, respectively). In general, an increase in excess air results in a moderation of the reducing potential severity as would be expected.

Bed Temperature Variations. A thermocouple was mounted within the porous alundum filter to monitor temperature of the zirconia sensor. These sensor temperature data were used to convert output voltage of the sensor to PO_2 versus time data.

However, it was discovered that the measured temperature values were approximately 100 F less than the bed temperature itself. Therefore, these data were used to infer bed temperature variations throughout the lower-to-midbed region. The corrected values of temperature (i.e., measured data plus 100 F) are shown plotted in Fig. 4-92 for the base condition. Note that some asymmetry exists in the temperature measurements. Also, in most cases, wall values were found to be 50 to 100 F cooler than the centerline region. It also can be noted that no correlation exists between measured temperature and the existence of oxidizing or reducing zones within the bed.

DISCUSSION. Extensive fluctuating oxygen partial pressure data were obtained at a variety of in-bed locations to characterize the corrosion environment within Battelle's 24-inch fluidized bed unit. These data were recorded for 16 run conditions.

Some gas sampling data also were obtained for the base operating case.

In general, the characterization was very successful in identifying reducing zones within the bed and examining the changes in reducing potential as a function of changes in bed geometry and operating conditions. It was found that increasing the distance between the bottom of the heat exchanger and the top of the coal feed port altered the flow of solids so that reducing conditions were shifted from the centerline region to zones near the combustor walls. A new coal feed port design also was found to produce a less severe overall corrosion environment. Increases in excess air, lowering of superficial gas velocity and increasing conveying air also were found to reduce the severity of wall reducing zones.

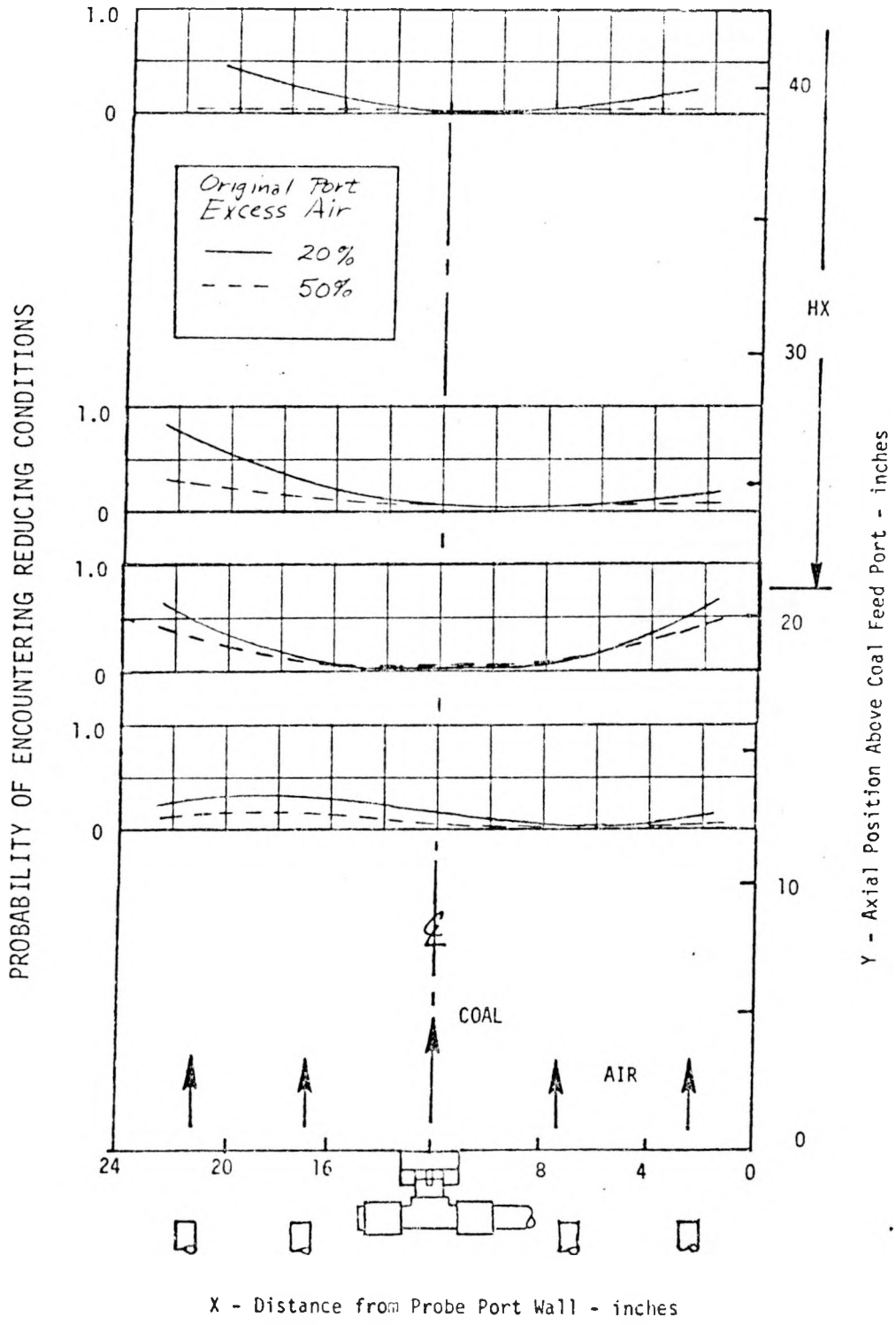


Figure 4-90. Spatial Variation of Reducing Potential as a Function of Excess Air (Original Port Design)

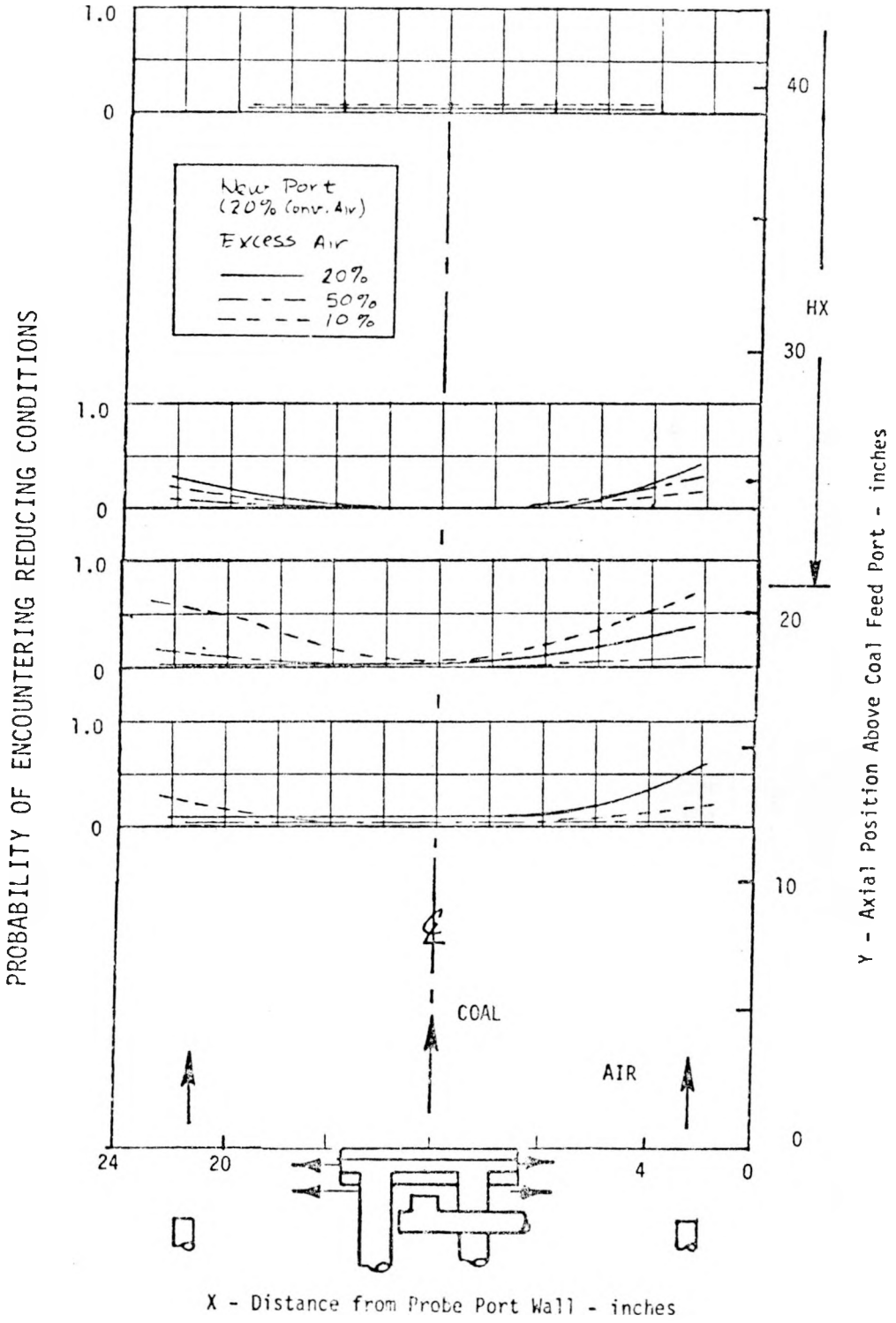


Figure 4-91. Spatial Variation of Reducing Potential as a Function of Excess Air (New Port Design)

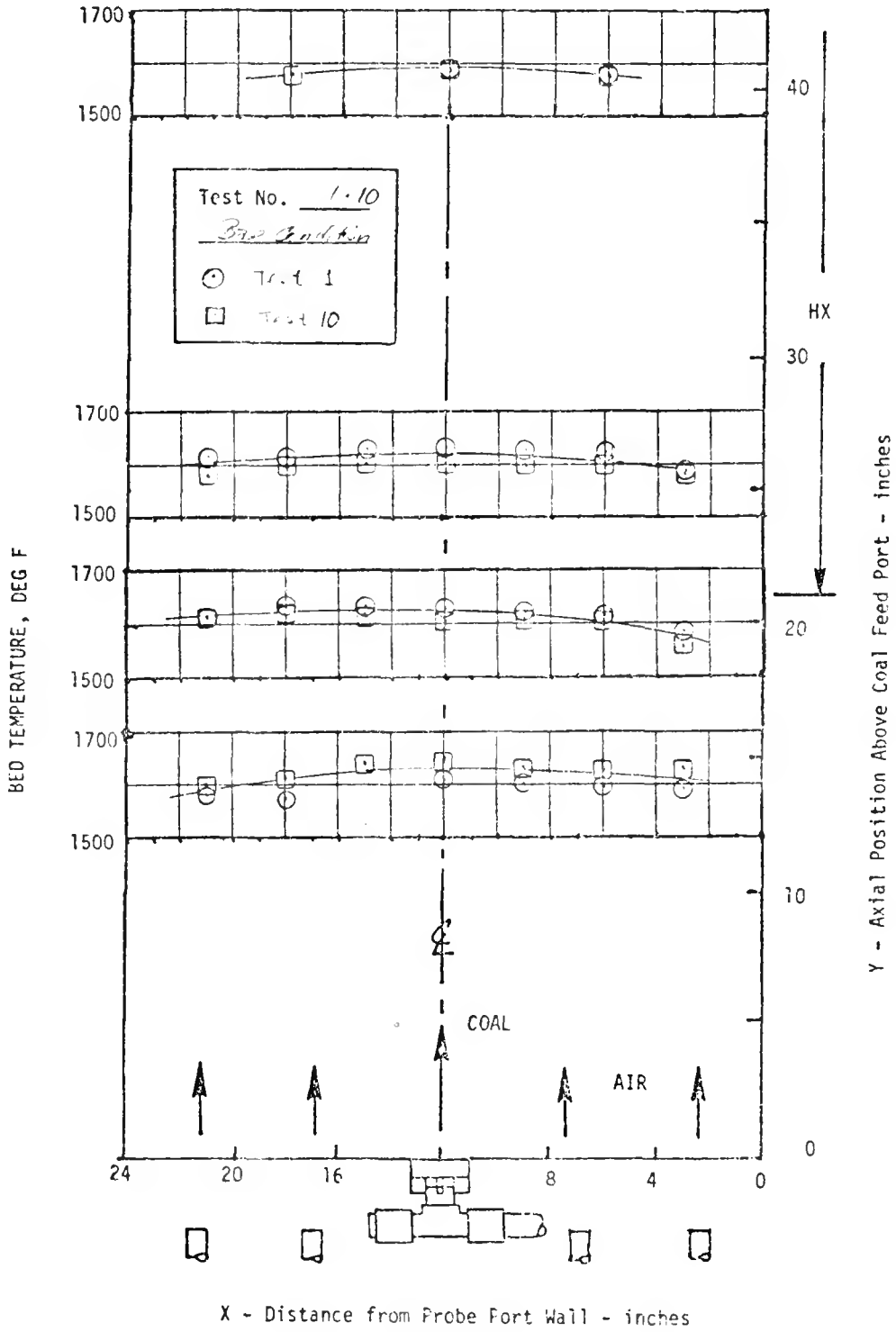


Figure 4-92. Temperature Variations Within the Bed for Tests No. 1 and 10

Conclusions. The probe demonstrated conclusively that obtaining in situ PO_2 data is a valuable and cost effective method of minimizing the corrosive environment within the heat exchanger array. The discovery, via probe data, that conveying air was a critical parameter with regard to the new coal feed port provided a means of demonstrating the improvement of this new port design. Further study of the reducing potential data also will be used to select conditions for the 250 hours of corrosion specimen tests to follow in the near future.

The diagnostic data presented in this section are limited to specific utilization only in Battelle's 24-inch unit. However, these data emphasize the requirement to measure the oxidizing/reducing environments within any AFB combustor to ascertain the corrosion potential variation with specimen position within the bed and bed operating parameter variations. The included data might be generalized to assist designers in predicting and thereby tailoring corrosive environments in other AFB units, provided a more accurate fluid mechanic and chemical model of in-bed processes were developed.

4.2.5 24-Inch AFB 250-Hour Material Specimen Exposure Test Series

The Battelle 24-inch fluidized bed combustor was used to expose metal and ceramic specimens to a fluidized bed environment. As discussed in the previous sections, the bed had been characterized at about 20 different conditions, and these characterization experiments indicated the major difference in bed environment under various operating conditions was the frequency and duration of local extremes of reducing conditions. Various locations in the bed had different environments so that specimens placed in different parts of the bed would have different exposure histories.

To obtain a maximum variation in exposure, three experiments were planned: one under normal operating conditions, one under reducing conditions, and one under conditions with high excess air. In addition, four experiments were to be made to determine nitrogen oxide in the flue gas. The metal specimens had been removed before these experiments, but the ceramic specimens were still in place.

The Battelle 24-inch fluidized bed combustor was operated for three 250-hour experiments to expose metal and ceramic specimens to a fluidized bed environment. The experiments were made at (1) 20% excess air to simulate normal bed operation; (2) stoichiometric air to simulate a corrosive environment, and (3) 50% excess air to simulate a benign environment. The bed was operated at 1650 F and superficial fluidization velocities of 5 to 6 ft/sec. The combustor operated at a combustion efficiency of 98 to 99%. A 4% sulfur, Illinois No. 6 coal was burned, and the sulfur emission was controlled to about 1.0 lb/mm Btu with a Ca/S (based on feed) ratio of 3.1 to 1.

At the end of the third 250-hour run, NOx was measured at four conditions. It was about 400 ppm when using normal (20 to 50%) excess air and dropped to 85 ppm when using stoichiometric air at 1650 F. When the temperature was increased to 1850 F, the NO_x concentration in the flue gas increased to 550 ppm with 20% excess air.

Equipment. The equipment has been described in the preceding sections. The modified coal feed port used in characterization runs 11 through 16 was used for all three erosion-corrosion runs.

Two-inch-OD bayonet-type cooling tubes were inserted in heat exchanger positions 52 and 103, when those positions were not being used for PO_2 probing to characterize the bed, to simulate a complete heat exchanger bank. A vacant tube position when the characterization probes were not in place might have changed the bed fluid dynamics. These tubes were air cooled with the cold air flowing in along the outside wall and the hot air exiting through a central tube. The air flow was about 20 scfm through each tube.

The erosion-corrosion and characterization probes are described in Sections 4.3. An unmeasured quantity of air, estimated at 40 scfm, flowed into the bed from the erosion-corrosion probes. During the third run, some (15 lb/hr) bed material was blown out of the reactor through the cooling air exit of one of the erosion-corrosion probes.

The Meyer 6-vane rotary valve used to feed the coal and limestone into the conveying air stream was replaced with an 8-vane valve between runs 1 and 2.

Test Materials. Illinois No. 6 coal and Grove limestone were used for these experiments. About one truckload (20 tons) of coal was used for each experiment. The coal from the several truckloads was not segregated. Some coal ground before the first experiment was set aside as an emergency reserve and used for the third experiment. The coal was received wet in a 1-1/4 x 1/4-inch size. It was dried and ground to -8 mesh before use. A new load of limestone was received during the second 250-hour run and used thereafter. The first load of limestone was received in October 1980 and stored outside in 55-gallon drums. The limestone in many drums was wet with rainwater when used for the 250-hour runs in the autumn of 1981. The wet limestone was dried by storing open drums near the hot fluidized bed exhaust system. Except for drying and screening for tramp metal, the limestone was used as received.

Samples of coal and limestone were taken daily at 8 a.m. and mixed into composite samples. The chemical and size analyses of these composite samples are presented in Tables 4-23, 4-24, and 4-25. The chemical analyses were consistent and average values were used for all computations. The size analysis of the coal for run 3 showed the coal was ground slightly finer for run 3 than for runs 1 or 2. This was not intentional.

Ash. Ash was collected at three places: a bed drain, a cyclone drain and a bag-house drain. The chemical and size analyses from composites of daily samples are presented in Tables 4-24 and 4-25.

The bed material was drained periodically, perhaps 12 times per day, to maintain bed level. Forty to 50 pounds of ash was normally drained at one time and up to 100 pounds of ash was drained occasionally. Fifty pounds of ash drained reduced the bed level by 2 to 3 inches. The bed material was at bed temperature (1650 F) when drained. Residual carbon in the drained bed burned during draining because of the high temperature. No analysis for combustible carbon was made for this reason. The bed drainings were expected to be less than 0.5% combustible as indicated by a new bright sparks of burning coal flowing into the ash barrel.

The calcium and sulfur analyses of the bed material showed about 20% of the lime in the limestone was converted to calcium sulfate. The resulting material was about 55 to 65% CaO, 25 to 30% $CaSO_4$, and 10 to 20% ash.

The size of the bed material was more uniform than the limestone feed material; the large limestone particles were ground and the small particles were elutriated from the bed. The bulk density of this ash was 5 lb/cu ft.

The cyclone collected ash was material blown from the bed. Chemically, it was similar to the bed material except that it was diluted with 50 to 60% ash and 6 to 7% free carbon. The coarser material (+70 mesh) looked as if it were a low density ash. The finer material looked as if it were ground limestone mixed with carbon and ash. The bulk density of this ash was 55 to 70 lb/cu ft.

TABLE 4-23. COAL ANALYSES

	Run 1		Run 2		Run 3	
	1st Half	2nd Half	1st Half	2nd Half	1st Half	2nd Half
Proximate as Burned						
Moisture, %	9.94	10.42	10.09	10.45	10.71	10.57
Ash, %	10.49	10.41	9.73	9.35	10.78	11.01
Volatile, %	35.81	35.21	35.78	35.82	35.58	35.54
Fixed Carbon, %	43.94	43.96	44.40	44.38	42.93	42.88
Sulfur, %	3.82	3.78	3.97	3.82	3.97	4.03
Btu/lb	11195	10909	11070	11028	11011	10893
Dry Basis						
Ash, %	11.45	11.62	10.82	10.44	12.07	12.31
Volatile, %	39.76	39.31	39.80	40.00	39.85	39.74
Fixed Carbon, %	48.79	49.07	49.38	49.56	48.08	47.95
Sulfur, %	4.24	4.22	4.41	4.27	4.55	4.51
Btu/lb	12431	12178	12312	12315	12332	12180
Ultimate as Burned						
Carbon, %	62.56	60.65	61.71	61.36	61.24	60.97
Hydrogen, %	4.24	4.34	4.34	4.34	4.30	4.30
Nitrogen, %	1.01	1.09	1.17	1.04	0.87	1.07
Chlorine, %	0.23	0.14	0.11	0.15	0.18	0.17
Oxygen (diff) %	7.89	9.17	8.88	9.49	7.95	7.88
Dry Basis						
Carbon, %	69.46	67.70	68.64	68.52	68.58	68.18
Hydrogen, %	4.71	4.85	4.83	4.85	4.82	4.81
Nitrogen, %	1.12	1.22	1.30	1.16	0.97	1.20
Chlorine, %	0.25	0.16	0.12	0.17	0.20	0.19
Oxygen (diff) %	8.77	10.23	9.89	10.59	8.91	8.80

TABLE 4-24. CHEMICAL ANALYSES OF LIMESTONE AND ASH

	Run 1		Run 2		Run 3	
	1st Half	2nd Half	1st Half	2nd Half	1st Half	2nd Half
Limestone						
Ca, %	39.0	38.7	39.1	39.0	38.9	38.7
CO_3, %	58.4	58.5	59.0	58.9	59.0	59.1
Bed Draining						
Ca, %	49.4	52.0	54.2	55.6	50.9	51.7
S, %	8.22	7.89	7.31	6.62	9.28	8.46
CO_3, %	2.69	0.84	0.96	0.73	1.00	0.87
Ca/S, mole ratio	4.8	5.2	5.9	6.7	4.4	4.9
Cyclone Ash						
Ca, %	21.2	23.9	22.8	18.7	27.5	28.1
S, %	3.85	3.51	2.50	2.38	3.53	3.69
Total C, %	8.1	8.0	23.9	27.9	6.0	6.4
CO_3, %	1.46	1.32	1.56	1.54	1.76	1.48
Ca/S, mole ratio	4.4	5.4	7.3	5.4	6.3	6.1
Baghouse Ash						
Ca, %	15.7	17.8	18.7	24.0	14.9	25.8
S, %	6.14	7.16	3.52	3.38	4.61	3.77
Total C, %	5.1	6.3	14.3	14.1	7.4	5.5
CO_3, %	0.49	0.56	2.12	3.20	1.25	1.41
Ca/S, mole ratio	2.0	2.0	4.2	5.7	2.6	5.6

TABLE 4-25. SIEVE ANALYSIS

	GOAL			Limestone			Bed			Cyclone Ash		
Run	1	2	3	1	2	3	1	2	3	1	2	3
Size Mesh												
+ 10	9.6	9.2	6.4	34.7	29.6	35.3	14.1	14.9	12.8	--	--	--
10 x 20	--	--	--	--	--	--	53.3	56.2	44.2	3.15	4.6	1.2
10 x 30	38.6	42.2	29.9	57.0	60.0	56.4	--	--	--	--	--	--
20 x 30	--	--	--	--	--	--	16.2	12.3	16.2	2.0	5.3	1.6
30 x 50	19.2	14.5	11.1	4.3	6.4	6.1	11.2	10.3	14.2	3.2	9.3	3.3
50 x 70	8.7	9.5	12.7	1.0	1.8	1.0	3.2	4.8	7.4	5.2	9.1	2.6
70 x 140	9.1	9.3	10.3	1.0	1.2	0.9	1.0	0.5	3.4	18.3	16.5	11.8
- 140	--	--	--	--	--	--	1.0	1.0	1.8	--	--	--
140 x 325	5.6	4.7	11.2	1.0	0.5	0.3	--	--	--	--	--	--
- 325	9.2	10.6	18.4	1.0	0.5	0.0	--	--	--	--	--	--
140 x 200	--	--		--	--	--	--	--	--	13.5	15.7	23.3
- 200	--	--		--	--	--	--	--	--	54.0	39.5	56.2

The baghouse collected the ash that passed through the cyclone. The cyclone was almost 100% efficient on +10 micron particles and about 50% efficient on 5 micron particles. Thus, the baghouse ash was essentially all particles smaller than 10 microns. The material was mainly coal ash. It contained 5 to 6% free carbon. The little calcium in it was converted to $CaSO_4$ to a greater extent than the other ash fractions. This ash had a very low bulk density of about 20 to 25 lb/cu ft.

Test Conditions. Table 4-26 is a summary of the test conditions. Each entry is an average over the run period. During run 2 when the bed was operated sub-stoichiometric, the SO_2 meter was disconnected because oxygen was needed for one type of meter (pulsed fluorescent), and the H_2S, which was present under reducing conditions would damage the other type of meter (Faristor). The CO concentration in the flue gas was measured during that experiment and averaged 0.4%.

Test Log. The test logs (Table 4-27) describe startup, probing, shutdown, and upsets that occurred during the experiments. The unit was at the nominal conditions (within control capabilities) when no entry appears in the log. Note that run 2 was started at 10% excess air and after about 36 hours, the operating conditions were changed. Stoichiometric air was used thereafter.

Discussion of Test Conditions. The test conditions were maintained by manual control through the experiments. The rates were fairly consistent except for the SO_2 concentration which varied by about 25% during the experiments.

Air Flow Rate. The fluidizing air flowrate was measured with an orifice meter and controlled within 2% of a value determined before the experiment. The blower pressure varied with ambient temperature (outside) and small corrections to the flow valve setting were made two to four times per day to compensate for the pressure change. The flow indication also varied about 5%, several times per second because of fluctuations in pressure drop across the bed.

TABLE 4-26. SUMMARY OF RUN CONDITIONS

Run No.	1	2	3
Coal rate lb/hr	158 ±6	175 ±5	139 ±7
Limestone rate, lb/hr	59 ±9	68 ±2	58 ±6
Bed temp. ^{o}F	1645 ±7	1650 ±7	1645 ±7
Fluidizing air, SCFM	236 ±5	212 ±5	236 ±5
Conveying air, SCFM	56	28	56
Total air, SCFM	292 ±5	240 ±5	292 ±5
Bed drain, lb/hr(1)	28	28	26
Cyclone ash, lb/hr	21	35	20
Baghouse ash, lb/hr	3	5	4
Bed depth, expanded, in.	65	65	64
O_2 in flue gas %	3.4 ±0.2	0	7.0 ±0.2
SO_2 in flue gas, PPM	550 ±200	*	470 ±50
SO_2 emitted, lb/MMBtu	0.8	*	0.9
Superficial velocity, ft/sec	6.3	5.2	6.3
Excess air, %	17	0	50
Combustion efficiency, %	98.6	93	98.7
Ca/S ratio as-fed	3.14	3.19	3.24
Number of startups	2	2	6

(1) Average rate, bed drained in approximately 50 lb batches.

* SO_2 meter inoperative because of reducing conditions.

± Indicates range of conditions during the test.

TABLE 4-27. LOG OF 250-HOUR EXPERIMENTS

Run 1

10-26-81	
1255	Ignition - Bed Empty. Erosion-corrosion probes in place
1400	Add 500 lb used bed
1900	Start coal feed
2030	Add bed material for 60-in. deep bed
2138	Gas ignition burner off
2230	Reached nominal conditions
10-27-81	
0315	Rotary valve plugged - system off 5 minutes
0335	Back at conditions
10-28-81	
1130-1345	Characterize bed
11-2-81	
0915-1235	Characterize bed
1100-1200	Remove erosion-corrosion probes and replace (33 and 83)
11-5-81	
0900-0100	Characterize bed
11-6-81	
0915-1020	Remove erosion corrosion probes
1035	Coal and limestone feed off, drain bed

TABLE 4-27. (Continued)

Run 2

1-9-81	
1700	Ignition - 500 lb bed in place
2300	Started coal feed
11-10-81	
0121	Ignition gas off
0300	At nominal conditions
1000-1200	Characterization probing
1200	Material probes in place
1430	Off because of hole in coal feed line Bed cooled to 1450°F
1450	On again
1510	At condition
11-11-81	
1445	Reduced combustion air to 236 SCFM to establish reducing condition in bed
1530	Reduced combustion air, 212 SCFM
1600	New reducing conditions established
11-12-81	
1206-1210	Limestone feeder off - line plugged
11-15-81	
0600	Shut bed off - hole in coal feeder
0700	Turn on ignition burner
0825	Ignition burner off
1000	Steady-state again
11-16-81	
1200-1315	Characterization probng
11-17-81	
1000	Replace materials probes 33 and 83, characterize at 83
11-20-81	
1500	Characterization probing
1530	Turn off coal and limestone feeders

TABLE 4-27. (Continued)

Run 3

11-30-81	
1700	Burner gas on, 500 lb of material in bed
12-1-81	
0100	Start coal feed
0530	Gas ignition burner off
0830	At conditions
1030-1115	Materials probes installed
1330	Material Probe 83 removed
1430	Coal and limestone off - drain bed
1630	Ignition burner on - Probe 83 reinstalled
2130	Coal feeder started
12-2-81	
0000	Bed material added to bring bed up
0215	Gas off
0230	At steady tate
12-6-81	
0330	Plug in coal feed line. Temperature dropped to 1620^{o}F before repair made
1200	Power failure. All power off 2 minutes. Bed temperature dropped 35^{o}F
12-7-81	
1000-1400	Characterization probing
1120-1400	Change material Probes 32 and 82
1430	Shutdown to remove broken materials Probe 32
1630	Ignition burner on
1750	Coal feed started

TABLE 4-27. (Concluded)

Run 3 (Continued)

12-7-81	
2000	Bed added to bring level up
2120	Ignition burner off
2310	At steady state
12-8-81	
0950	Replacement materials probe installed (32)
12-10-81	
0350	Power failure
0408	Power on. Temp. 1550°F
0410	Off. Conveying air compressor failed to start
0450	Start-up again. Temp. 1525°F
0515	Steady-state reached
12-12-81	
0830-0930	Materials probes removed
0930	NO_x Experiment 1 -380 ppm - 50% excess air
1000	NO_x Experiment 2 420 ppm - 20% excess air
1050	NO_x Experiment 3 85 ppm - stoichiometric air
1100	NO_x Experiment 4 540 ppm - 20% excess air 1845°F
1115	Shutdown

The coal conveying air flow was obtained from a 100 psi compressor. A pressure regulator reduced the pressure to 60 psi at the measuring rotometer and a needle valve was used to control flow. During the experiments, the flow was never observed to be different from the desired value.

As discussed later under Material Balance, unmeasured air enters the bed through leaks in the erosion-corrosion probes and possibly other places. This air acts to increase the superficial velocity at points above the leak. The characterization tests also indicated local oxidizing conditions above the probes at the side of the bed opposite of where the probe was installed, indicating that some or all of the leaks were local rather than diffused over the entire probe. Thus, this leak could cause increased local velocity as well as a general increase in superficial velocity. The erosion-corrosion specimens lowest in the bed should be exposed to the desired 6 ft/sec. Tubes at a higher level are exposed to a higher velocity (under 9 ft/sec), the exact value depending upon the location of the leaks. Presumably, erosion would increase with bed height because of the increased superficial velocity.

The superficial velocity was calculated from the air flowrates corrected for temperature. No correction was made for the combustion gas evolved by burning coal. This correction is small (less than 3%) and is related to the hydrogen content of coal. The area used to calculate superficial velocity was the open area of the bed without tubes. Since 2-inch tubes were used on 6-inch centers, the actual area between tubes is 2/3 of the open area and the net vertical velocity there would be 9 ft/sec.

In a commercial system, the air flowrate would not be set at a fixed value as in these experiments, but would be keyed to system output, either directly or indirectly. This would cause the air flow to vary more than in this system. The short-term (1 sec) variation in a commercial system also would be greater because the effect on flow of changes in bed pressure is less with a high-pressure blower. Battelle used an 8-psi blower. A commercial unit probably would use a 4 or 5-psi blower to reduce operating costs.

Coal Rate and Excess Air. The coal rate was set manually to maintain the desired excess air. As the excess air changed, the coal flowrate was adjusted. Only minor adjustments to the feedrate were needed, perhaps due to moisture content of the coal. The insertion and removal of the erosion-corrosion probes also caused changes in coal feed rate because of changing the air flow.

The coal rate was measured by taking an 8-second sample each hour and weighing the sample. During the sampling time, the oxygen content of the flue gas changed from a reading of 3.5 to 7% during the first experiment and made equivalent changes during the other experiments. Since backmixing occurred in the freeboard and sampling lines, the measured change in oxygen level was certainly less than that which occurred in the fluidized bed. This rapid change indicated that the coal burned very rapidly and little combustibles were in the bed.

In a commercial installation, the coal feed rate would probably be set by the system load demand and the combustion air would be supplied in proportion to the coal rate. The excess air would be controlled manually or automatically by setting the ratio of air to coal, based on the coal feed rate and monitoring the exhaust gas oxygen contents.

Limestone Rate and SO2 Concentration. The limestone rate was set manually to control the SO_2 concentration in the flue gas. During the first experiment, the SO_2 meter failed twice, the symptom being slow response to changes in SO_2 concentration. This slow meter response caused larger-than-normal variations in both SO_2 concentration and limestone flowrate. In the second run, the limestone rate was set and the setting was not changed. The SO_2 concentration was not measured because the Faristor SO_2 meter would be damaged by H_2S which, under the target test conditions, was undoubtedly in the flue gas. The other available meter, a pulse fluorescent meter, does not read accurately in the absence of oxygen. In the third experiment, the SO_2 meter was operating satisfactorily. The indicated control of 10% in SO_2 concentration was representative of what can be attained in fluidbed combustion.

The SO_2 concentration responded slowly to changes in limestone feed rate, indicating the limestone was active in the bed for a considerable length of time. An increase in limestone feed rate reduces the SO_2 concentration rapidly, but when the limestone feed rate was reduced or turned off, the SO_2 concentration increased slowly. Limestone feed rate was determined by taking an 8-second sample at the same time as taking the coal sample. The SO_2 concentration decreased by about 200 ppm momentarily because of the decrease in coal feed rate. If a limestone sample was taken when not taking a coal sample, no change in SO_2 concentration was observed. These observations would indicate that the limestone is moderately active when fed and the activity slowly decreases for several hours until the stone becomes inert.

The limestone efficiency did not appear to change with the normal fluctuations in bed temperature. When the temperature was increased to 1850 F, the SO_2 concentration was 1100 ppm, indicating that 50 to 60% of the SO_2 was being absorbed even at the high temperature.

In a commercial unit the limestone rate would probably be ratioed to coal rate. The ratio would be adjusted manually to control the SO_2 emission. SO_2 sensors do not appear to have sufficient reliability to be included in a control loop.

Bed Temperature. The bed temperature was controlled by manually setting cooling air flow. During the run, the temperature was controlled within 5 degrees. The temperature reported was an average of four readings at several points in the bed. These readings varied by about 15 degrees. The cooling air was adjusted almost hourly. The temperature sometimes dropped 20 to 30 degrees during installation of the erosion-corrosion probes and during the characterization studies. The insertion and removal of the specimen probes caused a short time upset in that they changed air flow which in turn caused a change in coal rate and heat release. The characterization probe was water cooled and its insertion into the bed absorbed heat and cooled the bed. The changes in probe position were made so frequently that the cooling air could not be adjusted manually to follow load changes. Generally, the bed temperature dropped to about

1620 F when measurements were being taken at one probe position and then rose to 1660 F when the probe was removed from the bed and placed in a different port.

In a commercial unit, the bed temperature could probably be allowed to vary. Load deviations could be detected by changes in the working fluid turbine discharge and process heat exchanger discharge temperatures rather than in the bed temperature. Assuming a constant working fluid temperature of 1550 F the bed would vary from 1550 F at light load to a design 1650 F at full load to about 1700 F under maximum overload condition. However, the thermal inertia of the bed and heat exchanger would be so large, no immediate response in bed temperature would be evident from changing loads.

Bed Depth and Ash Rates. The bed depth was measured by the pressure differential (water manometer) between a pressure tap 54 inches above the distributor plate and the freeboard. The bed density was assumed to be the same as water. Thus, a 10-inch water pressure reading was reported as a 64-inch-deep bed. On the short-term seconds, the pressure reading fluctuated by about 5 inches. This fluctuation was dampened by a pair of 30-foot-long 1/4-inch-OD copper tube lines between the ports and the manometer. The bed was level and was maintained by draining at a reading of 12 or 13 inches, to bring the level down to 9 or 10 inches. A 5-gallon bucket was filled during each draining and the ash weighed about 50 pounds.

The ash rates from the cyclone and baghouse were determined from the total ash drained during the experiment. The ash barrels were changed when they were full, about once a day for the cyclone ash and every second day for the baghouse ash. The time between changes of ash barrels was relatively constant for each run. Therefore, the ash rate was fairly consistent.

Shutdown - Startup. The system was shut down and started up at least once during each experiment. In run 1, the coal feed plugged and was unplugged in about 5 minutes. In run 2, the coal and limestone were turned off for 20 minutes to repair the feeder. In run 3, the coal in the coal hopper bridged and interrupted the feed for a few minutes. In each of these events, the fluidizing air

was not turned off and the bed temperature was raised back to operating temperature by reducing cooling air flow.

In run 3, a materials probe broke at two different times. Each time, the bed was drained, but not cooled, and the broken probe was removed. Ignition gas was used to heat the bed to operating conditions. The bed was refilled with bed drainings from several days before the incident, as the bed drained at shutdown was too hot to handle at startup.

Also, the power failed twice during run 3; once for 2 minutes and once for 18 minutes. The 18-minute downtime was prolonged to 1 hour when the conveying air compressor failed to restart and the motor starter on it required repair. The bed was slumped. The combustor was restarted by turning on the coal, air, and limestone. Temperature was raised by reducing cooling air flow.

NO_x Results. Table 4-28 shows the NO_x concentration in the flue gas at four combustion conditions. The concentrations are shown both as measured and as normalized to 18% excess air to eliminate the effect of air dilution.

At the temperature of combustion (1650 to 1850 F), all of the nitrogen in the flue gas should come from oxidation of fuel nitrogen as temperatures of 2400 F or above are required to oxidize air nitrogen. The Illinois No. 6 coal used had a low-nitrogen (1.0%) content, and if all of the fuel nitrogen were oxidized, the NOx concentration in the flue gas would be 1000 to 1200 ppm. Since typically 1/3 of the fuel nitrogen was released as NO_x, the 400 ppm concentration with 20 and 50% excess air was as expected. Since the NO_x concentration is usually reduced greatly at stoichiometric or substoichiometric combustion, the 85 ppm at stoichiometric again was about the value expected. The one experiment at 1850 F showed that NOx emissions increased by about 25% as the combustion temperature was increased from 1650 to 1850 F.

TABLE 4-28. NO_x EXPERIMENTS

NO_x ppm READING	NORMALIZED*	TEMPERATURE, F	EXCESS AIR, %	VELOCITY, FT/SEC
380	485	1650	50	6
20	25	1650	20	6
85	72	1650	0	6
540	550	1650	20	6.6
*NORMALIZED TO 18% EXCESS AIR.				

Mass Balance. The amount of gas flowing through the system can be calculated by two independent methods: directly from air flow and from coal rate and oxygen in the flue gas. During the characterization experiments, the two methods agreed within about 5%. However, during the 250-hour experiments, the gas flow calculated by the two methods differed by up to 30%. This discussion explores possible reasons for this difference.

Table 4-29 compares the air flow calculated by the two methods for the three 250-hour experiments and also for characterization run 12, which duplicated the 250-hour run 1 and for characterization run 14, which duplicated the 250-hour run 3. No characterization run duplicated the 250-hour run 2. The flowrates calculated by the two methods are close to the same for the characterization experiment, but for the 250-hour experiments, the flow calculated by coal rate was about 30% higher than measured. The following are several possible reasons for this discrepancy:

1. Air leakage into the bed through the erosion-corrosion probes
2. Air leakage through rotary valve
3. Combustion after gas sampling port
4. Air infiltration into combustor
5. Manometer pressure taps leaking
6. Lack of measurement sensitivity

The major change between the characterization experiments and the 250-hour experiments was the addition of the metallic and ceramic specimen probes. Since the metallic probes were known to be leaking while operating, the leakage was assumed to be the major cause of the material balance discrepancy. Consequently, the other possibilities were not investigated during operation. The third experiment was started without the metallic probes in place. The coal rate was 124 lb/hr, indicating an air flow of 350 scfm. When the probes were inserted, the coal rate increased to 139 lb/hr indicating a flow of 390 scfm. Thus, about 40 scfm can be attributed to the metallic corrosion probes. This is most of the discrepancy in run 1 but only about 1/2 of the discrepancy in runs 2 and 3. The cooling air flow to the erosion-corrosion probes is estimated at 10 scfm for each of four probes. Thus, 40 scfm in leakage appears high. However, the flow was not measured. Each of the four probes contained 24 specimens. The specimens were lathe machined flat and nested together, making 100 joints. The specimens had a circumference of more than 6 inches. Thus, a metal-to-metal ungasketed seam 600 inches or 50 feet long was in the bed. The pressure inside the probes was about 10 psi. Some leakage would be expected along this seam. The air exhausted from the probes through a tube about 18 inches long that fit into a pipe on the bed outlet. Bed material in the annular space between the pipe and the tube should seal the bed. However, the flow of gas leaving the vent was observed to vary with bed pressure fluctuation. Therefore, some of the cooling air must have been vented into the combustor.

TABLE 4-29 AIR FLOW

RUN NUMBER	MEASURED	CALCULATED FROM COAL RATE
250-HOUR NO. 1	292	352
CHARACTERIZAION NO. 12	292	309
250-HOUR NO. 2	292	308
250-HOUR NO. 3	292	392
CHARACTERIZATION NO. 14	292	303

The rotary valves leak air from the conveying air line to atmosphere. If the seal is tight, air at 3 or 4 psi enters the high-pressure side of the valve and

expands when the valve rotates to the atmospheric pressure side. This type of leakage is less than 1 cfm. When the seals wore, perhaps 10 to 15 cfm leaked through them. In the 250-hour runs 2 and 3, the seal was tight throughout the runs. In 250-hour run 1, the seal was tight at the beginning of the run, but a substantial leak developed between 150 and 200 hours and was repaired. In the characterization runs, the seal was tight for run 1, and gradually developed leaks until it was leaking substantially for run 16. These leaks would introduce an error in the mass balance indicating more air was injected than actually was injected. This error is opposite the direction of the observed error.

If some coal burned after the gas sampling port, the mass balance would be as observed. The cyclone was a region of high turbulence at combustion temperature and some burning probably took place in it. In the mass balance, the carbon in the ash was subtracted from the carbon fed to determine the carbon burned and the air used in burning coal. If a significant quantity of carbon had burned in the cyclone, it would have overheated, thus the amount burned in the cyclone was assumed to be small and should not affect the mass balance.

Air may infiltrate into the combustor and not be measured. The pressure in the freeboard was not measured, but probably was about 4 inches of water negative. It varied considerably, perhaps 10 inches from the average value. The pressure in the bed on the average depends upon bed depth and the pressure increases about 1 inch of water for each inch of bed depth. However, the pressure fluctuated perhaps 20 inches of water. Thus, negative pressure fluctuations occur deep into the bed. Alternating leakage in and out will increase the air rate as calculated from coal rate as fresh air leaks in and is available for combustion while flue gas leaks out.

Five large gaskets (three 48 inch diameter, one 60 inch diameter, and one 26 inch x 52 inch rectangular) and many small penetrations were potential leaks. Infiltration could cause a substantial part of the difference between air flow calculated from air measurement and from coal measurements. Because of design and operation of the baghouse system, the negative pressure in the combustor would be expected to be greater when the weather is cold than when the weather is hot.

Since the discrepancy between the material balances was greater in December than in August, some of the discrepancy could be from infiltration.

Air leakage through a heat exchanger tube could cause the observed discrepancy in air rates. The cooling tubes are difficult to inspect and have not been inspected since the start of the characterization experiments.

Instrument sensitivity affects the mass balance. The coal was measured by collecting the feed for 7.9 seconds and weighing. Assuming timing within 0.4 seconds, the coal flow was accurate within 5%. Coal rate readings were observed to be repeatable within 2%. Orifice meters are normally accurate within 5% and repeatable within 2%. Minor changes in air temperature and pressure were not corrected and could cause another 2% error. The sum of these errors indicates the air flow should be correct to within 7% error. Oxygen was measured on a 21% meter calibrated at zero (by removing the magnet from a paramagnetic meter) and at 21% with ambient air.

Assuming 5% of full-scale accuracy, the oxygen could be misread by 5% of the observed reading, equivalent to a 5% error in air flowrate. Thus, instrument sensitivity could cause a 12% discrepancy between the two air flowrates.

The connections to the manometers measuring air flow were found to be leaking after the characterization runs. While they were occasionally checked during operations, a leak could have opened and caused an erroneous reading.

From this discussion, about 1/2 of the difference in air flowrate, calculated by the two methods, could be attributed to the probes. The cause of the other half could not be determined. Either air in leakage or instrument error could account for the remaining error.

Equipment Operability. The equipment operated well during the experiments. The main air blower, the coal feeder and the baghouse operated with essentially no attention. The other units required some attention in addition to normal

maintenance. The feed system and instrumentation required the most attention. Each unit is discussed in the following paragraphs.

Main Air Blower. The main air blower (Hoffman Model 383B 8PSI, 1600 SCFM) operated without attention. Normal maintenance was to clean the air filter and lubricate every 2 weeks. Neither maintenance procedure required a blower shutdown.

Air Cooler. The blower supplies air at about 200 F. The air was passed through a cooler (36,000 Btu air conditioning "A" frame modified for water cooling). The cooler was used for about 3000 hours without attention, but required cleaning at shutdown. The outlet air temperature was almost 120 F at the end of the experiments, compared to 95 F observed when the cooler was new.

Coal and Limestone Preparation and Feed System. The coal was prepared by drying, grinding, and sieving to -8 mesh. The mechanical handling systems in the coal preparation unit, occasionally failed, shut down the preparation unit, and required repair. The system in general was difficult to operate in bad weather. Wet, rained-on coal was difficult to dry and frozen coal was very difficult to handle. Normally, 7 to 10 tons of prepared coal was on hand and this supply was ample to operate the combustor while the preparation unit was down for repair or because of bad weather. The coal feeder was an Acrison feeder with SCR control. No problems were encountered.

The limestone was bought sized. It was stored outside in 55-gallon drums and became wet in storage. It was dried by storing drums for a few days next to the hot cyclone on the combustor exhaust system. The limestone feeder was an Acrison feeder with a helical screw. The screw jammed once during early operations. A stronger screw is needed for limestone service in future runs.

The coal and limestone dropped from the feeders through a Meyer rotary valve into the pneumatic conveying line. A 6-vane valve was used during the characterization runs and the first 250-hour run. It developed significant leaks through the polyurethane seal strips in less than 200 hours. The valve was replaced after

the characterization experiments. Eight-vane valves were used for the second and third 250-hour runs. The valve was replaced between the two runs because of our poor experience with the 6-vane valves. However, the 8-vane valves did not leak.

A vacuum pickup for dust control was mounted over the rotary valve. The duct design caused some problems as the duct filled with coal dust after 3 or 4 days and plugged. Cleaning the duct did not interfere with system operation.

The pneumatic pickup under the rotary valve was a homemade injector. Air left a high-velocity nozzle aimed at the downstream pipe to act as an ejector and reduce the pressure differential across the rotary valve. The wide clearances used to prevent plugging reduced the efficiency of the ejector so that only about 1 psi was developed. A second smaller air jet was aimed toward the rotary valve to prevent coal from piling up behind the nozzle and to positive pressure any plug in the ejector. This air jet was difficult to aim and, when aimed at the side of the pickup, it quickly wore a hold through the pickup. This caused two shut-downs. With the new 8-vane valve, the ejector pickup probably is not needed.

Combustor. The combustor was almost troublefree. The flange bolts required tightening on the day following startup if the flange had been taken apart between runs.

Cyclone. The cyclone on the combustor outlet wore through during the first 250-hour experiment was temporarily patched for the second experiment and was replaced for the third run. The cyclones were made of 304 stainless steel, 20 gage, and lasted about 3000 hours.

Baghouse. The baghouse operated almost without problems. The differential pressure measurement lines collected condensed water that froze during winter operation. This prevented reading of the pressure across the bags. The ash is difficult to remove completely from the baghouse because it was very light and fluffy. However, in time it sets into cement. This cement formed between the

January and August experiments, and the rotary valve on the baghouse discharge required disassembly to remove the cement before the August experiments could be started.

Instrumentation. The instrumentation caused most of the operating problems. Because the system was operated manually, instrumentation failure did not result in system shutdown. The Faristor SO_2 meter failed several times because of poor cell response and was replaced. It had previously operated 5000 hours without problems. The gas-sampling pump, which had a 500- to 1000-hour life, failed and was replaced. The gas-sampling lines occasionally plugged. The filter in the gas sampling line required replacement every 2 to 4 hours. Thermocouples failed occasionally, but since redundancy was built into the system, these failures caused no problems. A more reliable instrumentation system, especially the gas analysis sensors, is needed for commercial development.

Conclusions. The fluidized bed was operated at conditions that should simulate practical commercial bed.

The equipment performed well and the other upsets should not affect the erosion-corrosion results.

4.2.6 Evaluation of Mechanical Pressures on Fluidized Bed Heat Exchanger Tubes

Heat exchanger tubes and other surfaces immersed into fluidized beds are subject to buffeting forces due to the motion of the bed solids and gas. Therefore, before immersing the ceramic heat exchanger tubes into the 24-inch AFB for evaluation, it was necessary to determine the nature and intensity of such forces so the ceramic tubes could be designed properly to prevent premature failure.

The nature and intensity of the forces acting on various lengths of 2-inch-OD metallic heat exchanger tubes immersed horizontally in gas-fluidized beds have been evaluated by Kennedy (Ref. 4-38). The measurements were made in 1 x 1, 3 x 3, and 8 x 1-ft sq beds at ambient temperatures. It was determined that these forces are comprised of both a verticle and horizontal component and, in general, the magnitude of the verticle component is about twice that of the horizontal component. It also was determined that the magnitude of the forces acting on a given heat exchanger tube is strongly dependent upon both the geometry of the heat exchanger array--i.e., the spacing and the arrangement of the tubes within the array--and upon the location of the tube within the array as well as on the length of the tube. The location of the maximum force intensity within a heat exchanger array was found to be dependent on the distance between the array and the gas distributor plate. Other factors found to have strong effect on the magnitude of the forces, but less than those discussed above, include superficial gas velocity, particle size, bed depth and, to a lesser extent, particle density.

Instantaneous measurement on each tube indicated that the forces consisted of a series of pulses occurring at a rate of 2 to 3 per second and having durations of 0.2 to 0.3 second. The force pulses have been found to be related to the bubble motion; the pulses result from the impacting of a front of solids against the tubes immediately after the passage of a bubble.

Limited number of experiments conducted by Kennedy (Ref. 4-33) in a high-temperature bed at 1500 F indicate that there were no significant differences in the character of tube forces at elevated temperatures compared to those observed at low temperatures.

Because of the fact that the intensity of the forces on heat exchanger tubes depends a great deal on the geometry and location of the tube in the array as well as on the location of the heat exchanger array with respect to the distributor plate (in addition to the various other factors discussed above) it is necessary to determine the forces experimentally on 1-inch-OD tubes in Battelle's 24-inch AFB (Atmospheric Fluidized Bed) for proper design of the silicon carbide ceramic tubes to be evaluated at high temperatures. Since Kennedy's findings indicated the nature of the forces at higher temperatures were not substantially different than those at room temperature, it was decided to measure the strains induced on simulated heat exchanger tubes when fluidized bed operated at ambient temperature. The distributed maximum pressure levels present in the bed during operation that exert forces on the tubes, then, can be inferred through these strain measurements.

The mechanical pressures exerted on simulated heat exchanger tubes were experimentally evaluated using Battelle's 24-inch-diameter atmospheric fluidized bed facility. The evaluations were made using strain gaged tubes at ambient temperatures and as a function of superficial air velocity. With the available equipment, however, the maximum superficial air velocities that could be achieved were 4.8 feet per second due to operating the bed at ambient temperatures. The maximum pressures exerted on the tubes during steady-state operations varied considerably depending on the location of the tube within the heat exchanger array and specific operating conditions. The pressures calculated from the strain measurements ranged from about 0.20 to 1.35 psi in vertical direction and from about 0.08 to 0.45 psi in the horizontal direction. The pressures on the tubes occur as a series of pulses at a rate of 2 to 3 per second.

Such transient operating conditions as suddenly turning on or off the fluidizing air did not produce any higher pressures than those produced during the steady-state operating conditions. During loading of the bed with limestone, the strain-gaged tubes oscillated at their fundamental frequency and behaved as pinned-end beans. This resonance condition could be detrimental to ceramic heat exchanger tubes located in a top row of a heat exchanger array where the tubes would be directly hit with the fluidized bed material during the filling of the bed. The experimental procedure and test results are presented in detail below.

Experimental Procedures. Battelle's 24-inch-diameter AFB was used to evaluat the forces on 1-inch-OD simulated heat exchanger tubes. The AFB combustor contains a heat exchanger array fabricated from 2-inch-OD stainless-steel tubings through which compressed air is circulated to maintain a constant bed temperature. The array also contains a number of access ports for inserting probes to characterize the bed or test and evaluate materials. Figure 4-93 shows the overall view of the heat exchanger array. The access ports identified by No. 31, 32, 33, and 83 were used to measure and evaluate the forces on simulated heat exchanger tubes. Details regarding the construction and instrumentation of the tubes, calibration of the tubes, and data reduction techniques are presented in the following discussion.

Construction and Instrumentation of the Tubes. Four simulated heat exchanger tubes were fabricated and instrumented, using the following tube materials:

- 1-inch-OD seamless-steel tubing (for locations 31 and 83)
- 2-inch-OD seamless-steel tubing (for location 32)
- Approximately 1-inch-OD alumina tube (for location 33)

It was originally intended to use a SiC tube for location 33. However, the SiC tube procured for this purpose was damaged during calibration, and a new SiC tube could not be obtained in time for testing. Therefore, an alumina tube was used in lieu of the SiC tube.

Four strain gages (Micro-Measurement EA-06-125AC 350) 90 degrees apart were mounted to each tube, as shown in Fig. 4-94. In all cases, strain gages 1 and 3 were used to measure strains produced in the vertical plane by operation of the bed, while gages 2 and 4 were used to measure strains produced in the hoizontal plane. The strain gage pairs were wired in adjacent arms of a conventional Wheatstone bridge, providing both high-signal output and thermal compensation of the gage output.

The three 1-inch-OD tubes were mounted in the bed chamber using the mounting fixture shown schematically in Fig. 4-95. This fixture was designed speciall

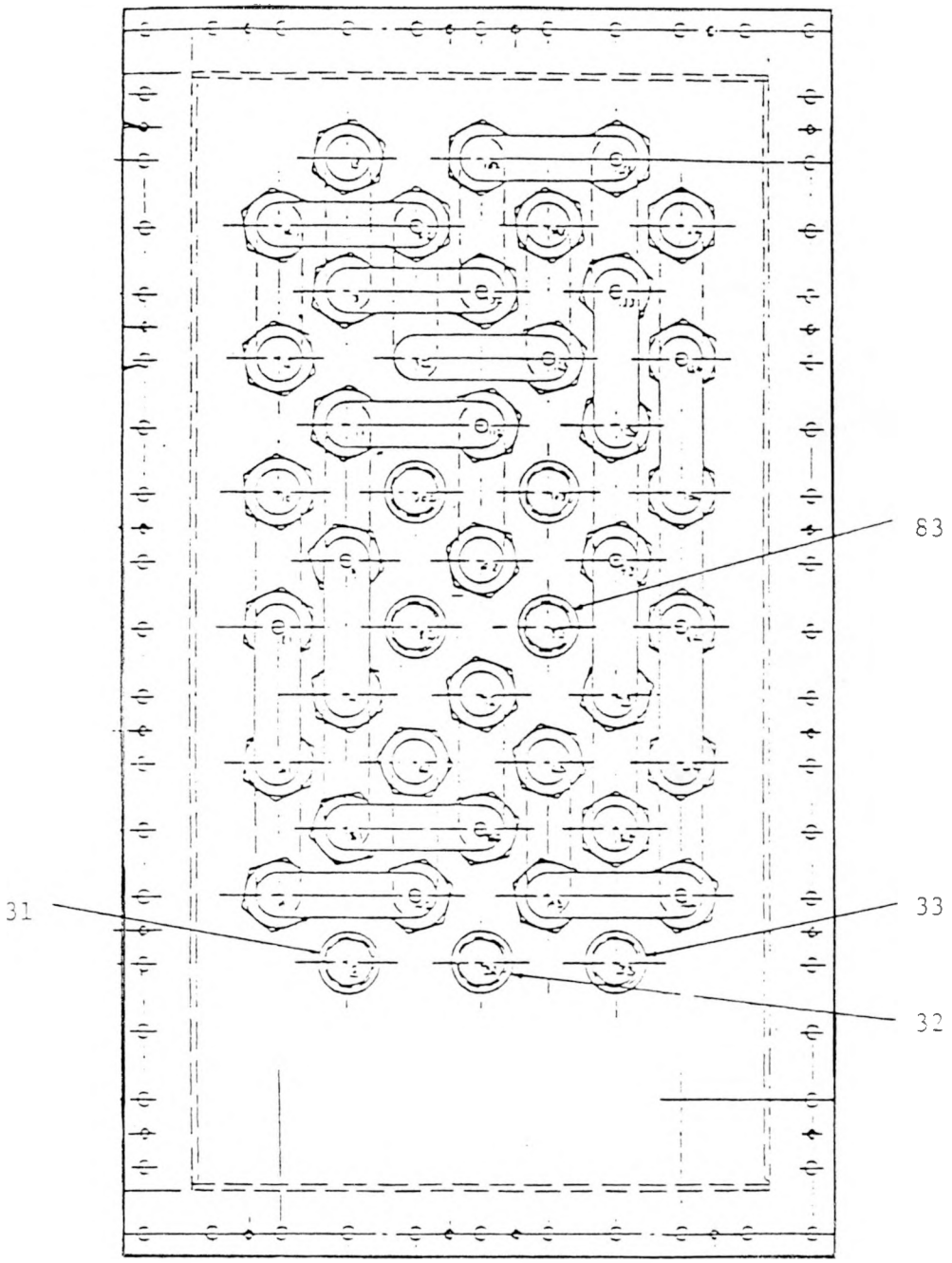


Figure 4-93. Overall View of Tube Array and Access Ports

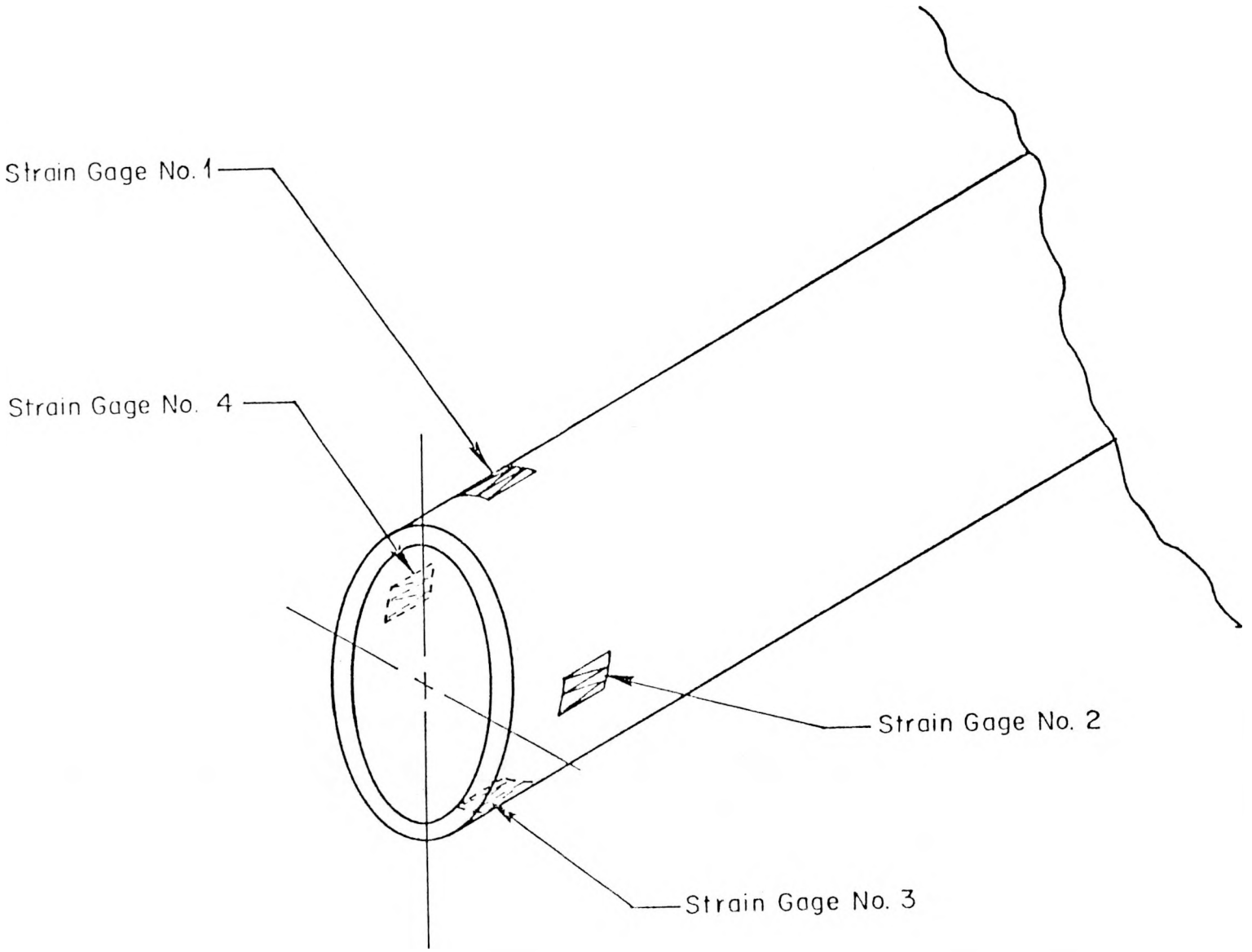


Figure 4-94. Strain Gage Positions on Simulated Heat Exchanger Tubes

1. OUTER MOUNTING TUBE 52-INCH LONG AND 2-INCH DIAMETER
2. INNER MOUNTING TUBE
3. SPACER TUBE
4. COMPRESSION TUBE
5. HIGH TEMPERATURE CERAMIC PACKING
6. CERAMIC HEAT EXCHANGER TUBE
7. COVER PLATE

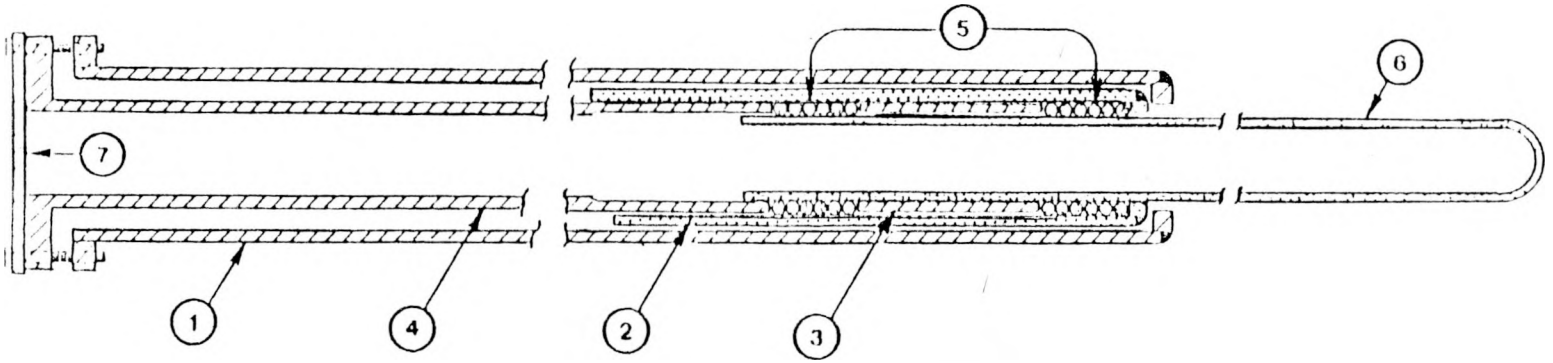


Figure 4-95. Fixture Used to Mount the 1-Inch-OD Simulated Heat Exchanger Tubes

for use with ceramic tubes and securely clamps the tubes while avoiding poin loads that would be potentially damaging to ceramic tubes. Since the tests were conducted at room temperature, Teflon packing material was used instead of high-temperature ceramic packing. A photograph of the instrumented alumina tube is shown in Fig. 4-96, and a fully instrumented and assembled 1-inch-OD steel tube is shown in Fig. 4-97.

The four simulated heat exchanger tubes were held in place in the bed chamber using 2-inch swage locks. Each tube was inserted into the bed so that the tip of the tube was approximately 1.5 inches away from the opposite wall of the bed chamber.

Calibration of the Tubes. The three steel tubes were calibrated in the laboratory prior to installation in the field. Simulation of the expected pressure loading could not be achieved easily, and so the tubes were calibrated by simply applying a deadweight load to the end of the tube. The loading configuration is shown in Fig. 4-98. The strain levels expected at the strain-gaged locations for this type of loading are given by

$$\varepsilon = \frac{P\ell c}{IE}$$

where

ε = expected strain levels, in./in.
P = deadweight load, lbf
ℓ = distance from load to strain gage, in.
c = distance from neutral axis to strain gage, in.
I = area moment of inertia, $in.^4$
E = modulus of elasticity, $lbf/in.^2$

Calibration results for each of the three steel tubes are presented in Fig. 4-99. As can be seen, all three tubes performed as expected.

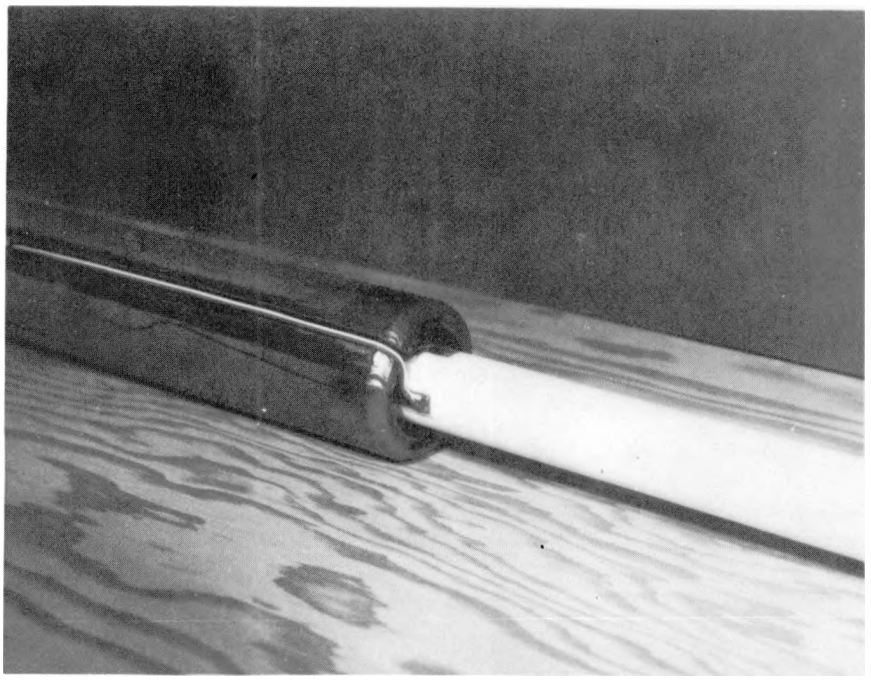


Figure 4-96. Instrumented 1-Inch-OD Alumina Tube

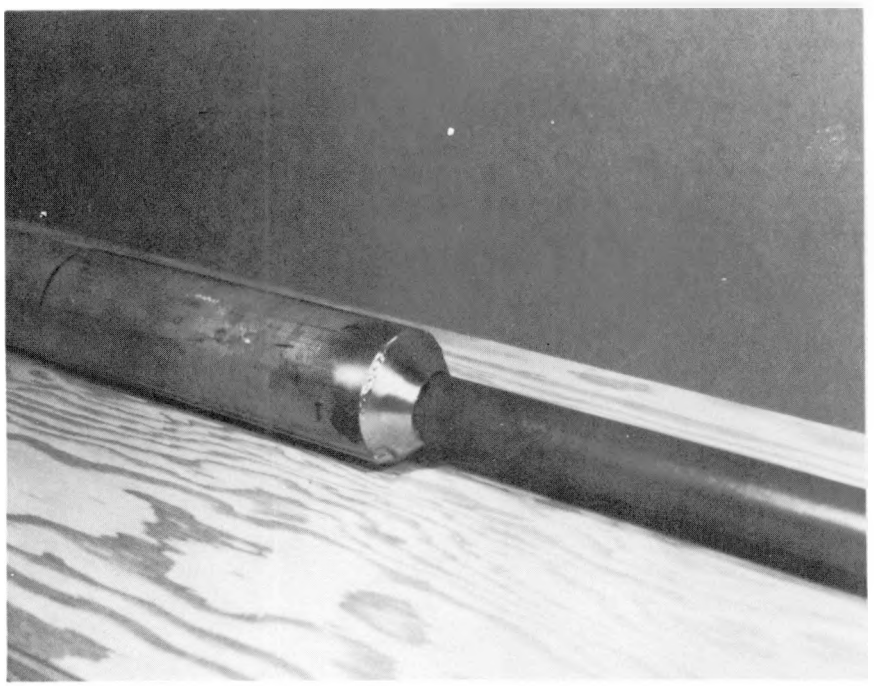


Figure 4-97. Instrumented 1-Inch-OD Steel Tube

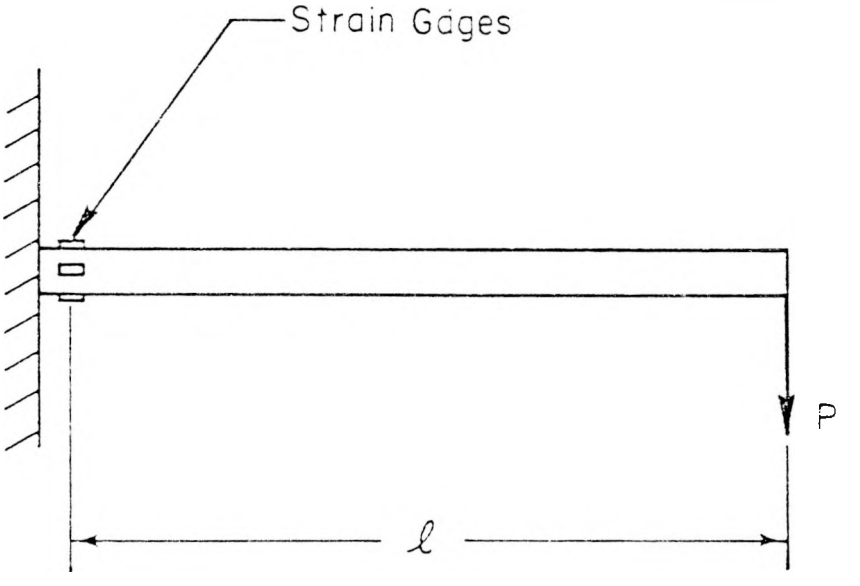


Figure 4-98. Deadweight Calibration Loading of the Simulated Heat Exchanger Tubes

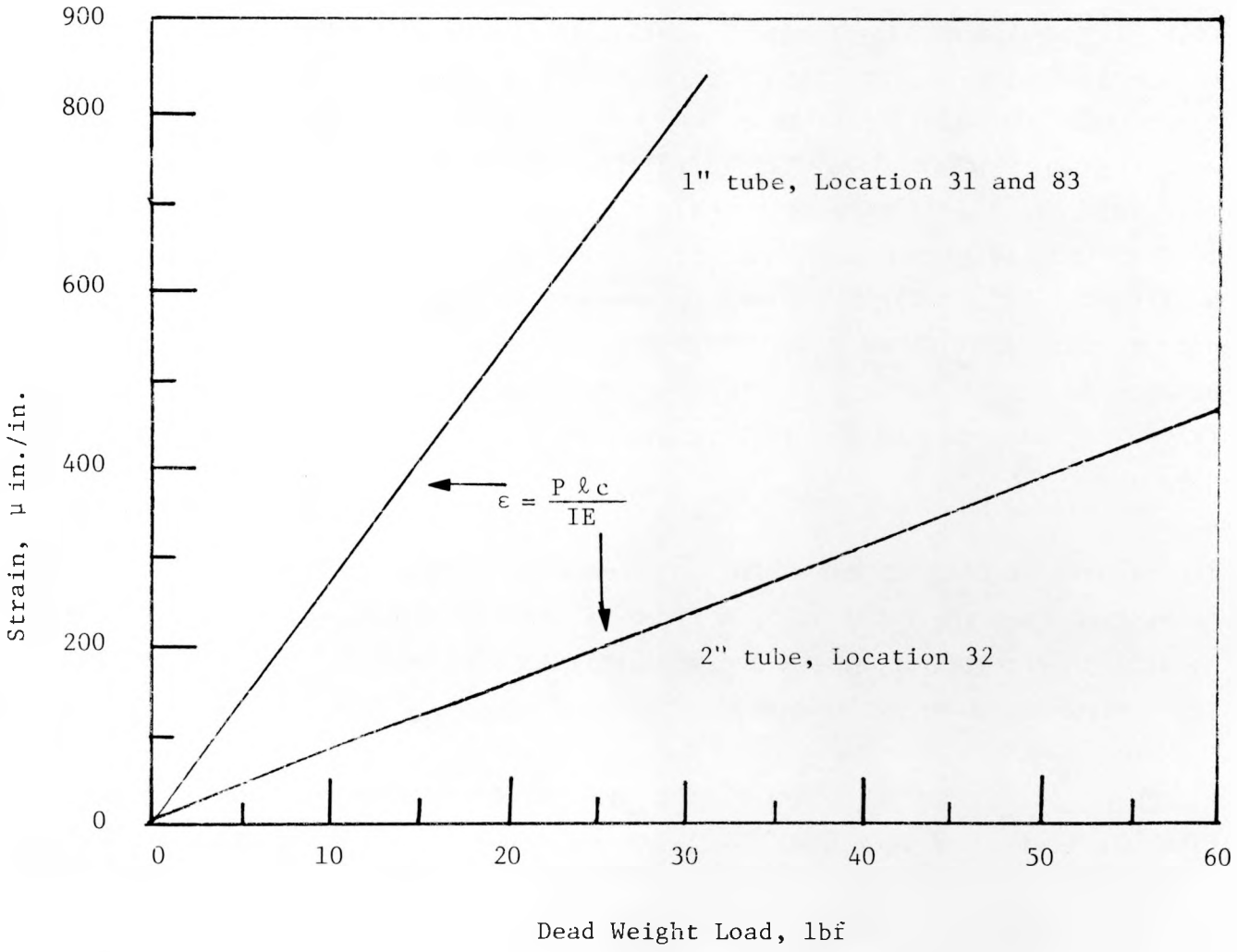


Figure 4-99. Calibration Data Obtained for OD Tubes Mounted in Three Locations

Results. The strain-gaged heat exchanger tubes were mounted into the bed at the locations identified in Fig. 49-3, using 2-inch swage locks. The strain levels induced in each tube were monitored and recorded using a high-speed chart recorder during all phases of the bed operation.

The bed was fluidized using a large capacity Hoffmann air compressor. However, with this equipment, the maximum superficial air velocity that could be attained by operating the bed at room temperature was only 3.7 ft/sec. To increase the superficial air velocity further, an auxiliary air ejector was utilized. In this way, the superficial air velocity could be increased up to 4.8 ft/sec. Although this value is still lower than the normal operating superficial air velocity (6 to 7 ft/sec) at higher temperatures, the bed was fully fluidized. Previous work by Kennedy (Ref. 4-33) has shown the mechanical forces exerted on the tubes did not increase significantly by operating the bed at superficial air velocities between 5 and 11 ft/sec. Therefore, increasing the superficial velocity to 7 ft/sec is not expected to increase the bending stresses much beyond the values determined.

The strains induced on each tube were measured under a variety of bed operating conditions that are essentially defined by the superficial air velocity. To aid in data interpretation, these bed operating conditions have been divided into 15 test phases as shown in Table 4-30.

Phase I. During this phase, the bed was being prepared for loading. Air flow was kept at a very low level, and no discernible strain measurements were recorded. Since the noise level associated with the strain measurement system was about 10 in./in., the strain levels induced in the tubes during this phase were below this level.

Phase II - Loading Bed. During this phase of operation, approximately 700 pounds of Grove limestone were loaded into the bed chamber. The limestone was loaded through an access port located at the top of the chamber. As each portion was allowed to fall into the chamber, the limestone would impact the tubes, caus-

TABLE 4-30. BED OPERATING CONDITIONS DURING PHASES I THROUGH XV

Phase	Bed Differential (inch Hg)	Plate Differential (inch Hg)	Orifice Differential (inch H_2O)	Superficial Air Velocity 9ft/sec)	Comments
I	0.0	0.6	0.1	∿ 0	Start Hoffman
II	0.0	0.6	0.1	∿ 0	Loading bed with 700 lbm Grove limestone
III	0.0	0.6	0.1	∿ 0	Bed fully loaded
IV	2.4	6.8	9.2	3.24	
V	2.3	6.3	8.0	3.00	
VI	2.4	7.8	10.0	3.38	
VII	2.5	8.6	12.0	3.70	
VIII	2.5	8.6	12.0	3.70	
IX	2.5	8.6	12.0	3.70	
X	2.4	8.5	11.7	3.90	Start ejector air - 58 psi
XI	2.4	10.5	15.8	4.45	Increase air flow to 15 in. Hg
XII	2.4	10.5	15.8	4.45	Disconnect Hoffmann by-pass
XIII	2.4	12.4	18.5	4.80	Maximum possible air flow setting
XIV	2.4	12.4	18.5	4.80	
XV	2.4	12.4	18.5	4.80	Hoffman off

causing oscillation of the tubes at their fundamental frequency. As would be expected. the highest stresses caused by this impact were induced in the 1-inch-OD tube mounted at location 83, which is closest to the top of the bed chamber. Figure 4-100 shows a strain gage trace obtained for this tube during loading of the bed. The tube exhibited a nearly perfect sinusoidal oscillation in both the vertical and horizontal planes. The cyclic frequency in the vertical plane was measured as 36.4 Hz, and for the horizontal plane as 36.6 Hz.

Phases III through XV. During these phases, the bed was operated under a variety of operating condition which were defined in Table 4-30. Figure 4-101 shows a typical trace obtained for the 1-inch-OD steel tube mounted in location 83. This trace was obtained during Phase XII. Deflection for this tube was characterized by vertical movement in one direction only, and horizontal movement in both directions. Similar deflection patterns also were observed for the remaining tubes.

Data Reduction. The maximum stress induced at the strain-gaged locations for each tube were calculated by multiplying the elastic modulus of the material with the maximum strains measured from the strain gage traces. The results obtained for each tube are summarized in Tables 4-31 through 4 34. The calculated maximum vertical and horizontal stresses are shown in the fourth and fifth columns of the tables. The second and third columns show the "dominant" frequencies also determined from the strain gage traces by averaging over several loading cycles (typically 7 to 10 loading cycles).

Since the ultimate goal of these efforts was to provide experimental data with which to properly size and design the ceramic heat exchanger tubes, the strain levels measured during this program are of less interest than the forces or operating pressures that produced them. That is, the maximum transient pressure levels present during operation of the bed will ultimately be used to design the heat exchanger tubes.

To facilitate data reduction, the tube loading configuration shown in Fig. 4-102 was assumed is that length of the tube that extended into the bed chamber proper,

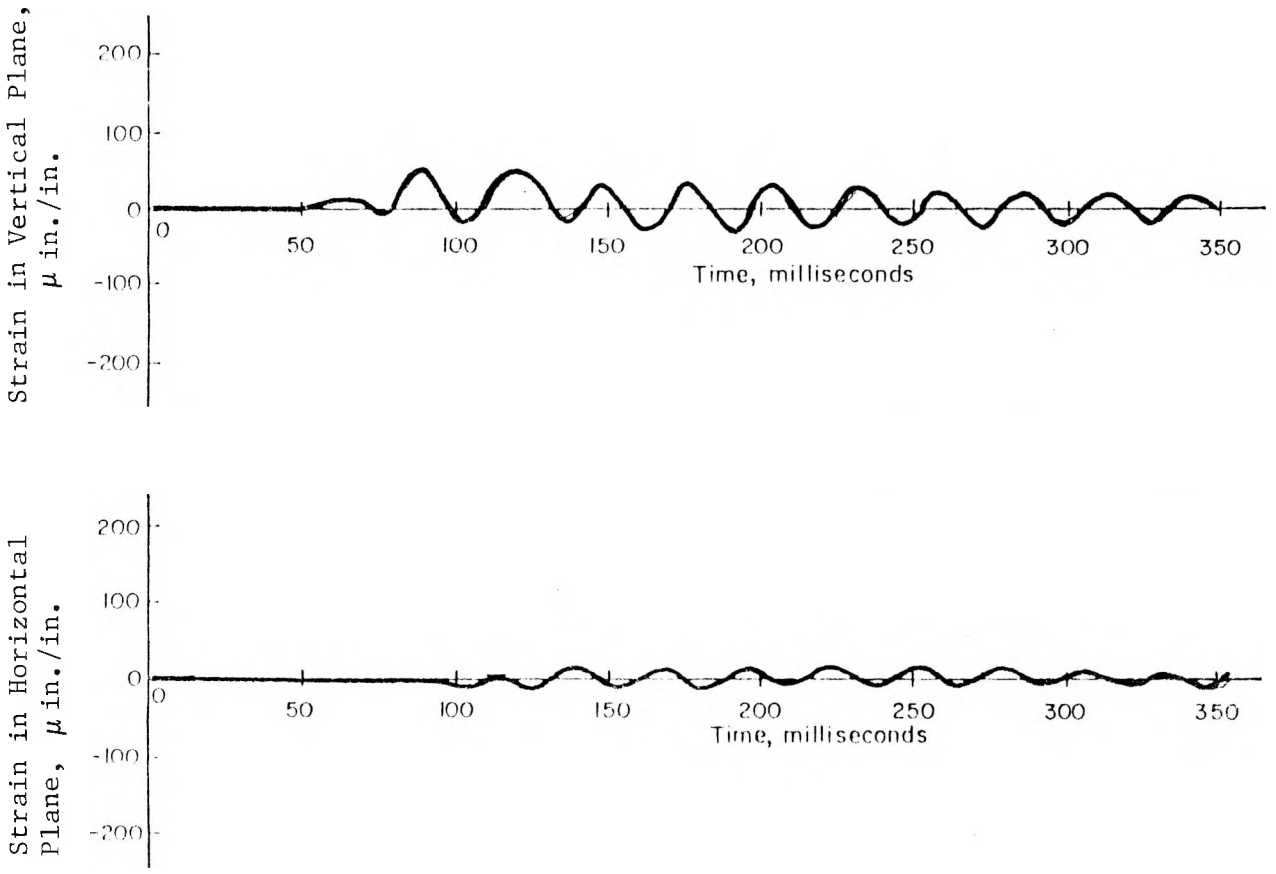


Figure 4-100. Strain Gage Trace Obtained During Phase II for 1-Inch-OD Steel Tube Mounted in Location 83



Figure 4-101. Strain Gage Trace Obtained During Phase XII for 1-Inch-OD Steel Tube Mounted in Location 83

TABLE 4-31. RESULTS FOR 1-INCH-OD SEAMLESS-STEEL TUBE MOUNTED IN LOCATION 83

Phase	Dominant Frequency (Hz)		Maximum Stress (psi)		Average Pressure (psi)		Comments
	Vertical	Horizontal	Vertical	Horizontal	Vertical	Horizontal	
I	--	--	<300	<300	<0.03	< 0.03	Strain reading below noise level
II	36.4	36.6	3,300	900	< 0.03	< 0.03	Loading bed
III	2.3	2.3	8,400	4,620	0.770	0.424	
IV	1.9	1.9	3,240	1,920	0.297	0.176	Vertical and horizontal frequencies in phase
V	1.7 to 1.9	1.5	2,700	960	0.248	0.089	Horizontal frequency irregular
VI	1.9	1.8	4,080	1,200	0.374	0.111	
VII	2.0	1.6	5,640	3,180	0.518	0.292	
VIII	2.4	2.4	6,600	1,560	0.606	0.143	Horizontal frequency irregular
IX	2.3	2.3	6,000	2,640	0.551	0.242	Horizontal frequency irregular
X	2.2	2.3	7,320	2,640	0.72	0.242	
XI	2.3	2.2	7,200	3,540	0.661	0.325	
XII	2.2	2.0	10,320	2 520	0.948	0.231	
XIII	2.4	2.4	12,600	3,060	1.156	0.281	
XIV	2.5	2.5	7,800	1,920	0.716	0.176	
XV	2.0	2.0	13,080	2,040	1.200	0.188	

TABLE 4-32. RESULTS FOR 1-INCH-OD SEAMLESS-STEEL TUBE MOUNTED IN LOCATION 31

Phase	Dominant Frequency (Hz)		Maximum Stress (psi)		Average Pressure (psi)		Comments
	Vertical	Horizontal	Vertical	Horizontal	Vertical	Horizontal	
I	--	--	< 300	< 300	< 0.03	< 0.03	Strain reading below noise level
II	--	--	2,400	600	< 0.03	< 0.03	Loading bed
III	2.4	2.3	9.180	3,000	0.885	0.289	
IV	1.6	--	3,600	1,680	0.346	0.162	Horizontal frequency not efined
V	1.8	2.2	2,520	780	0.243	0.075	Horizontal frequency irregular
VI	2.0	2.0	5,400	1,920	0.520	0.185	
VII	2.0	1.8	6,480	2,400	0.623	0.232	
VIII	2.1	2.1	4,560	1,440	0.440	0.139	
IX	2.1	1.6	7,200	1,800	0.694	0.173	Horizontal frequency irregular
X	2.3	2.7	7,800	2,040	0.752	0.197	
XI	2.1	2.5	8,040	3,120	0.775	0.300	
XII	2.4	--	9.360	2,880	0.902	0.277	Horizontal frequency not defined
XIII	2.6	2.6	13,920	3,960	1.338	0.382	
XIV	1.6	1.6	9,360	3,240	0.902	0.312	
XV	2.7	2.7	8,520	3,000	0.821	0.289	

TABLE 4-33. RESULTS FOR 1-INCH-OD SEAMLESS-STEEL TUBE MOUNTED IN LOCATION 32

Phase	Dominant Frequency (Hz)		Maximum Stress (psi)		Average Pressure (psi)		Comments
	Vertical	Horizontal	Vertical	Horizontal	Vertical	Horizontal	
I	--	--	<300	<300	< 0.02	< 0.02	Reading below noise level
II	--	--	900	600	< 0.02	< 0.02	Loading bed
III	2.2	2.2	3,600	1,110	0.950	0.293	Horizontal frequency irregular
IV	1.7 to 2.0	--	1,800	600	0.237	0.080	Horizontal frequency not defined
V	1.9	2.1	1,380	840	0.181	0.112	Vertical and horizontal frequencies irregular
VI	2.1	--	2,400	1,080	0.317	0.143	Horizontal frequency not defined
VII	2.0	2.6	3,720	840	0.492	0.112	Horizontal frequency irregular
VIII	2.5	--	3,720	840	0.492	0.112	Vertical and horizontal frequencies irregular
IX	2.2	2.1	2,760	1.080	0.365	0.143	Horizontal frequency irregular
X	2.4	2.4	3,960	840	0.522	0.112	
XI	2.3	2.4	2,760	1,920	0.365	0.253	
XII	2.3	--	5,040	2,400	0.665	0.317	Horizontal frequency not defined
XIII	2.8	2.4	6,240	960	0.825	0.127	
XIV	2.7	2.7	4,080	2,040	0.538	0.269	
XV	2.7	2.7	5,520	720	0.729	0.096	

TABLE 4-34. RESULTS FOR 1-INCH-OD SEAMLESS-STEEL TUBE MOUNTED IN LOCATION 33

Phase	Dominant Frequency (Hz)		Maximum Stress (psi)		Average Pressure (psi)		Comments
	Vertical	Horizontal	Vertical	Horizontal	Vertical	Horizontal	
I	--	--	<450	<450	< .08	< .08	Reading below noise level
II	--	--	<450	<450	< .08	< .08	Loading bed
III	2.3	2.5	1,800	1,100	.329	.201	
IV	1.5 to 2.3	1.5 to 2.3	900	900	.165	.165	Vertical and horizontal frequencies irregular
V	2.2	2.2	720	720	.132	.132	
VI	2.1	2.0	1,440	450	.263	.082	
VII	2.0	2.0	1,620	1,260	.296	.230	
VIII	1.7	1.6	2,340	1,260	.428	.230	Vertical and horizontal frequencies irregular
IX	1.9	1.9	1,800	1,440	.329	.263	
X	2.4	2.4	2,160	1,080	.395	.197	
XI	2.2	2.4	3,420	1,620	.625	.296	
XII	2.4	2.4	3,420	1,350	.625	.247	
XIII	2.6	2.6	3,600	1,350	.658	.247	
XIV	2.4	2.4	3,240	720	.592	.132	
XV	2.6	2.6	3,600	1,080	.658	.197	

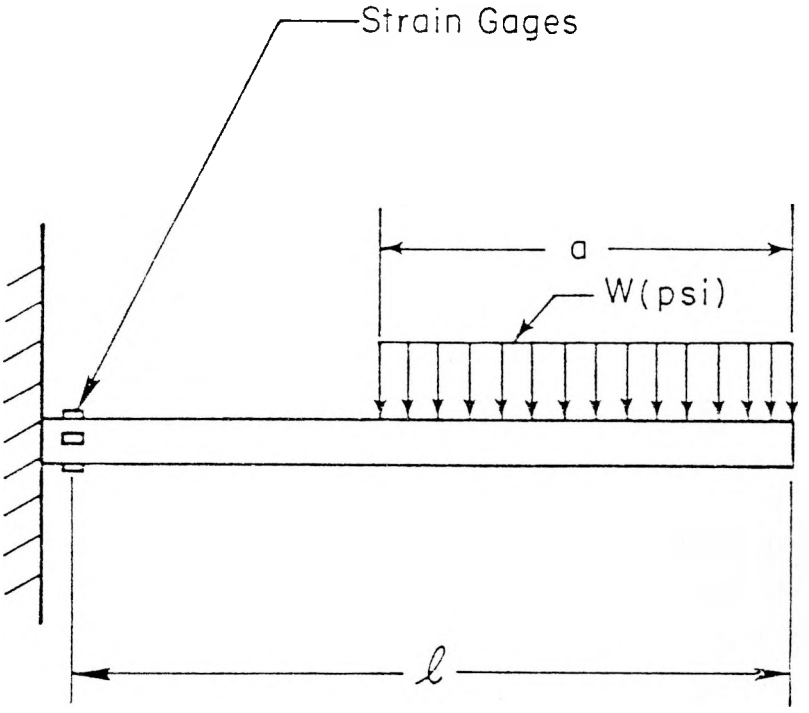


Figure 4-102. Assumed Loading Configuration During Operation of the Bed

and the loading pressure "W" was assumed to be constant, acting over the tube length "a". For this loading configuration, the pressure "W" is related to the measured strain ε by:

$$W = \frac{\varepsilon IE}{ac^2 (2\ell - a)}$$

The numerical values used for the above variables for each of the four tubes are itemized in Table 4-35.

The maximum stress (δ= E X E) values are taken from Tables 4-31 through 4-34. The resulting calculated average pressures W producing the maximum measured strains are presented in the sixth and seventh columns of Tables 4-31 through 4-34.

Discussion. The results show that the magnitude of the maximum pressure to be expected is approximately 1.35 psi, acting at about 2 to 3 Hz. In general, the higher the pressure drop across the orifice (or the superficial air velocity), the higher the operating pressures encountered by the heat exchanger tubes. Recent studies (Ref. 4-35) also showed that the vertical force on heat exchanger tubes increase rather rapidly with increasing superficial air velocity, then begin to level off at about 4.9 ft/sec. The horizontal forces increase much less rapidly and level off at lower superficial air velocities. Since the earlier work by Kennedy (Ref. 4-33) has shown the forces on heat exchanger tubes do not change substantially for the superficial air velocities between 5 and 11 ft/sec, the maximum pressure, 1.35 psi determined on the tubes in this study for 4.8 ft/sec superficial gas velocity should not increase much above this value at normal operating superficial gas velocities (6 to 7 ft/sec) of Batelle's AFB. Kennedy's work also showed that the nature and intensity of the forces measured at higher temperatures (1500 F) were not substantially different than those measured at ambient temperatures. Therefore, the maximum pressure exerted on the tubes at higher temperatures (1650 F) in Battelle's AFB should not be much different than that determined in this study.

TABLE 4-35. DIMENSIONS AND MATERIAL PROPERTIES OF SIMULATED HEAT EXCHANGER TUBES

TUBE TYPE	TUBE LOCATION NUMBER	I, $in.^4$	E, psi	ℓ, in.	a, in.	c, in.
1-INCH-OD STEEL TUBE	83	16.59×10^{-3}	30×10^6	27.50	21.74	0.50
1-INCH-OD STEEL TUBE	31	16.59×10^{-3}	30×10^6	27.50	19.28	0.50
2-INCH-OD STEEL TUBE	32	172.20×10^{-3}	30×10^6	40.25	22.50	1.000
0.975-INCH-OD ALUMINA TUBE	33	29.92×10^{-3}	45×10^6	27.50	19.28	0.49

The loading frequencies showed slight increase with increasing superficial air velocity and a small degree of random variability. These loading frequencies, as determined by averaging over 7 to 10 loading cycles, were between 2 to 3 Hz when the bed was fully fluidized. As previously noted, when the bed was being loaded with limestone, the loading frequency on the tube at location 83 increased substantially. The tube exhibited a nearly perfect sinusoidal oscillation in both the vertical and horizontal planes. The cyclic frequency in the vertical plane was measured as 36.4 Hz, and for the horizontal plane as 36.6 Hz. This is a somewhat surprising result, since a clamped beam with the dimensions given in Table 4-35 should exhibit a fundamental and second natural frequency of 8.0 Hz and 50.3 Hz, respectively (Ref. 4-34). However, a beam of the same physical dimensions with a pinned-end connection should exhibit a fundamental frequency of 35.2 Hz (Ref. 4-34). It, therefore, appears that the mounting fixture used during this program will behave as a pinned-end connection when the tubes are subjected to dynamic loadings of high frequency (frequencies approaching 35Hz), and as clamped-end connection when tubes are subjected to static or low-frequency dynamic loadings. Such oscillations of the tubes at their natural frequencies could induce fractures if the amplitudes of the oscillations were sufficiently high. Because of this condition, if the ceramic tube were mounted in the top row of the heat exchanger array rather than at location 83, i.e., in the middle of the array, it could have fractured due to the falling limestone fluidized bed material.

Therefore, sufficient care must be exercised during filling a fluidized bed that contains ceramic heat exchanger.

During the measurements, various other transient conditions also were examined. These included suddenly turning on and off the fluidizing air. The strain measurements during these conditions were less than those of the fully fluidized bed conditions (steady-state conditions).

Conclusions. The conclusions reached during the course of this research were as follows:

- The maximum operating pressures present within the bed during steady-state operation vary considerably depending upon location within the chamber and the specific operating conditions. The pressures calculated from the strain measurements range from about 0.20 to 1.35 psi in the vertical direction, and from about 0.08 to 0.45 psi in the horizontal direction.
- The frequencies of the cyclic pressure loading remain relatively constant over the entire bed operating range. Loading frequencies at low air flow levels are about 1.5 to 2.0 Hz, increasing to about 2.0 to 2.8 Hz at higher air flow levels.
- Transient operating conditions do not produce discernible changes in the pressure loading produced during steady-state operation of the bed.
- The fixtures used to mount the 1-inch-OD heat exchanger tubes in the bed chamber behave as clamped-end connections when subjected to static or low-frequency loadings, and as pinned-end connections when subjected to high-frequency (greater than about 35 Hz) loadings.

3 MATERIAL SPECIMEN ANALYSIS FROM 24-INCH AFB 250-HOUR TESTS

The major problem confronting materials selection for heat transfer materials for use in an atmospheric fluidized-bed combustor (AFB) is that there is no information available from practical experience of running such a combustor under real power generation conditions. This lack of data is especially true of materials operating in the metal temperature range of 1200 to 1650 F, since most of the long-term subscale tests have been run for steam-cycle materials, which have heat transfer surfaces exposed to maximum temperatures of 1200 F. Uncooled specimens run in these tests were chosen as candidates for tube support materials, not heat transfer materials.

Background

The longest operating AFBs are apparently in China, where large steam generating units have been in operation since 1969 (Ref. 4-35 through 4-38). Probably, the 5,000 to 6,000 hours running of the Alliance 6' x 6' AFB is the longest operation of an AFB in this country. During this time, some corrosion tests have been run, but the main thrust of the operation has been for combustion studies. Also during this period, the complete tube-bank has been changed at least once for engineering reasons. Plans made to examine the removed tubes apparently were shelved because of a lack of funds. Comments have been made about some observations of tubes being "polished," but no data have been forthcoming. Corrosion tests at the bottom of the tube bank in this bed indicated that dramatic sulfidation of uncooled nickel-base alloys, and of steels in contact with these alloys, occurred in the vicinity of the coal feed ports in 294 hours of exposure (Ref. 4-1). In zones of the bed away from the coal feed ports, only limited corrosion occurred of the same nickel-base alloys (with exception of Inconel 671).

These differences in behavior were attributed to anticipated gross differences in the prevailing oxygen partial pressures in the two locations. Over the coal feed ports, zones of low-oxygen activity were expected, along with high sulfur activities. In situ oxygen probe measurements made in a similar location in this bed, at a later date and under somewhat different operating conditions, indicated that low-oxygen partial pressures existed not only in the vicinity of the coal feed ort, but from the feed port inward to the center of the bed, and outward to the wall (Ref. 4-39). Hence, some substantiation was provided for Daniel and

Stringer's reasoning for accelerated attack, but not for the variation of corr sion behavior with location.

A Foster-Wheeler designed AFB steam at Georgetown University reportedly has suffered erosion losses from heat exchanger tubes "subjected to localized jetting in the bed" (Ref. 4-40). Aluminized coating has been tried, apparently with little success. No photomicrographs have been released, so no judgment can be made whether erosion or corrosion or both are involved, nor how general this behavior is.

The major AFB test programs designed to produce corrosion data have been funded by the Department of Energy (Fluidyne-Ref. 4-41), Battelle-Columbus (Ref. 4-42), Exxon (Ref. 4-43) and by EPRI (BCURA-Ref. 4-44), CURL (Ref. 4-29 and 4-45) and CERL (Ref. 4-46). The DOE programs ran for 4000 (four runs of 1000), 1500, and 1000 hours, respectively, while the EPRI programs ran four times up to 2000 hours (two runs of 1000 hours), with much of the work concentrated in 250-hour runs. Detailed comparison of results from these tests cannot be properly made, since each result has to be qualified by statements concerning metal temperature, bed temperature, location in the bed, superficial velocity, and so on. However, the most systematic of these studies was the series of 10 250-hour parametric runs funded by EPRI. Data from these particular runs are examined in some detail later in this report.

In general, very variable behavior, especially for nickel-base alloys, was noted in many of these tests, with some instances of very rapid sulfidation attack. While much of the sulfidation has been rationalized by proximity to coal feed ports, some observations were not understood until more recently. In particular, the unexpected corrosion observed in the Fluidyne work occurred away from the coal feed port at a location where in situ oxygen probes, used in later work, indicated a zone of low-oxygen partial pressure persisted. The 300 series stainless steels have, in general, exhibited acceptable corrosion behavior to temperatures up to about 1500 F, although AISI 304 is close to its oxidation limit at this temperature. Uncertainties still exist for the application of these alloys in crevice areas. In addition, they can corrode rapidly at points of contact with nickel-base alloys exposed in conditions of low-oxygen partial pressure. Carbon and low-alloy steels appear to corrode at a faster rate than observed ir

or instance, conventionally coal-fired steam boilers. As a result, the temperature limit for these alloys in AFB applications should be 50 to 100 F lower than in PC boiler applications.

A class of FeCrAlY alloys has been investigated quite extensively in the EPRI sponsored work, since these are potentially the most corrosion-resistant alloys available (although they have poor strength), and are prime candidates for use as protective claddings. Results have been surprisingly variable, with unexpected occurrences of corrosion in some compositions. Part of the reason apparently lies with manufacturing peculiarities. Overall, an FeCrAlY composition containing 25% Cr appears to give the best chance of achieving the promised corrosion resistance.

Unfortunately, at the time that most of these corrosion runs were made, the stabilized zirconia oxygen probe was in the early stages of being adapted for use in dirty environments, so that little characterization of the in-bed environments was possible. Routine analyses of extracted gas samples were made in the Alliance 6' x 6' bed for combustion studies, but were not very applicable to the corrosion studies. Some gas sampling made during the 1500-hour corrosion test in the Battelle-Columbus AFB did, in fact, reveal wide swings in CO and hydrocarbon contents, but again could not be related to the corrosion results. In situ oxygen probe measurements have been made in the later EPRI sponsored studies and used to rationalize corrosion behavior with bed operation.

In the work described in this report, in situ oxygen analysis was a major priority. Emphasis was placed on determining the characteristic oxygen partial pressure existing in the bed as a function of location, bed operating conditions, and to a limited extent, to combustion configuration. In addition, knowledge of the oxygen partial pressures prevailing in the vicinity of the in-bed corrosion probes was considered vital. The work described here is the most extensive and systematic attempt to date to use the oxygen probe as a tool to diagnose variations in the environment with location in the bed and with changes in bed operating variables and to interpret its output (Ref. 4-3, 4-47 and 4-48).

The signals obtained from in situ oxygen probes in different AFBs have exhibited ne same characteristic forms, which typically show oxygen partial pressures oscillating between about 10^{-2} and 10^{-13} to 10^{-16} atm. Analysis at the Battelle Columbus Laboratories suggests the equilibrium oxygen partial pressure

of flue gas from coal combustion in an AFB would range from ~10^{-2} to 10^{-1} atm. as the air/fuel ratio passed from excess air to substoichiometric air conditions. Hence, the oxygen probe signals may be interpreted to show the status and location of the combustion process in the AFB.

Experimental Program

Selection of Heat Exchanger Tube Materials. The advanced heat exchanger designs under consideration in this program contain segments that require metallic materials to operate at working fluid temperatures up to a nominal 1550 F, which implies that in practice excursions to metal temperatures of the order, of 1650 F can probably be expected. As indicated in Fig. 4-103 taken from the literature (Ref. 4-49), the choice of materials with sufficient strength in this temperature range is very limited. In addition, the metallic materials must possess a combination of strength and corrosion resistance to the fireside gases and to the working fluid, so alloy selection is rendered more difficult since optimum high-temperature strength and maximum hightemperature corrosion resistance are not always compatible. Because of the high temperatures and the novel corrosive environment (AFB and hot air working fluid) in part of the advanced heat exchanger loop, specific corrosion rate information is insufficiently developed to allow materials selection with great confidence. This is the reason for the current work. The alloys have been chosen, therefore, primarily for their mechanical properties, with emphasis on adequate strength at 1300 to 1650 F, leaving the corrosion resistance as a secondary consideration that may be taken care of by cladding, for instance, if necessary.

Alloys that have been candidates because of their combination of high-temperature strength and corrosion resistance are listed in Tables 4-36 and 4-37. The strength criterion was used based on the ASME Boiler and Pressure Vessel Code Safety factor guidelines for temperatures in the creep range, which states that the maximum allowable stress value shall not exceed the lowest of:

- 100% of the average stress for a creep rate of 0.01%/1000 hours
- 67% of the average stress for rupture at the end of 100,000 hours
- 80% of the minimum stress for rupture at the end of 100,000 hours

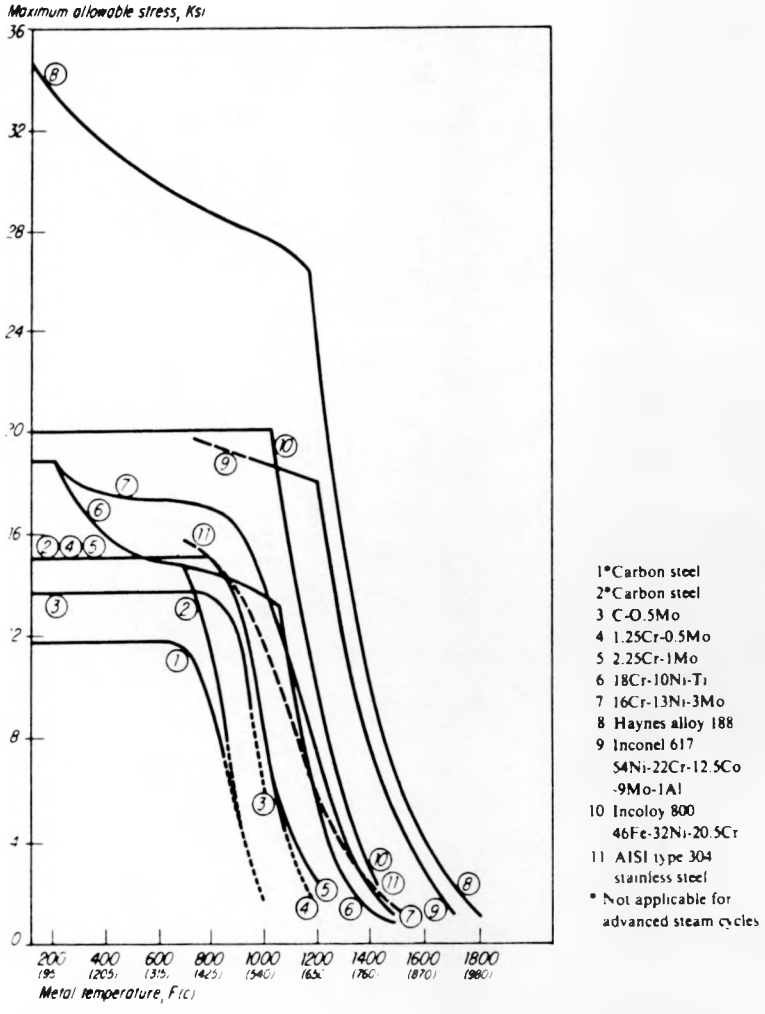


Figure 4-103. Metallic Materials to Operate at Working Fluid Temperatures

TABLE 4-36. MAXIMUM STRESS VALUES FOR HIGH-PERFORMANCE ALLOYS, ksi

Temperature	Haynes 188[A]	Inconel 617	Inconel 618 E[A]	Nimonic 86[A]	Hastelloy X (case 1321-2)	556[A]	Incoloy 800H (case 1325-9)	Hastelloy C (case 1324)	HK 40[C]
1800 F	1.3	1.0[B]	0.87	0.64	--	--	--	--	0.5
1700 F	1.9	1.8[B]	1.3	1.0	1.0[B]	--	0.87[B]	--	0.8
1600 F	2.5	2.7	1.9	1.8	2.4	2.0	1.6[B]	--	1.2
1500 F	4.4	4.2	3.0	3.1	4.0	3.4	2.5	--	1.7
1400 F	7.4	8.5	4.5	5.8	6.5	6.7	3.6	8.0[B]	2.6
1300 F	--	12.5	6.7	--	9.5	10.5	5.4	12.0[B]	4.3
1200 F	--	12.5	10.0	--	12.5	15.4	8.4	16.0[B]	6.1
					max 1650 F, 1.7)				

A: All data were estimated from manufacturer's and other published literature.

B: Specific data points estimated from published literature, other points from published code literature

C; Calculated from Battelle-Columbus data.

TABLE 4-37. MAXIMUM STRESS VALUES FOR STEELS (kpsi)
(Published Boiler Code Data)

TEMPERATURE	304-H (SA-213)	310	316 H (SA-213)	347 H (SA-213)	2 1/4 Cr - 1 Mo T 22 (SA-213)	1/2 Cr - 1/2 Mo T-2 (SA-213)	C-steel A-1 (SA-210)	5 CR - 1 Mo T-5 (SA-213)	9 Cr - 1 Mo T-9 (SA-213)	12 Cr - 1 A Tp 405 (SA-268)
1500 F	1.4	0.7[A]/0.2[B]	1.3	1.3	-	-	-	-	-	-
1400 F	2.3	1.2 /0.35[B]	2.3	2.5	-	-	-	-	-	-
1300 F	3.7	1.7 /0.75[B]	4.1	4.4	-	-	-	-	-	-
1200 F	6.1	2.7 /2.5[B]	7.4	7.9	-	-	-	-	-	-
1150 F	7.7	3.4	9.8	10.5	-	-	-	--	-	-
1100 F	9.8	4.1 /5.0[B]	12.4	13.0	4.2	-	-	3.1	3.3	-
1050 F	12.2	-	14.5	-	5.8	-	-	4.2	5.5	-
1000 F	13.8	- /11[B]	15.3	-	7.8			5.6	8.5	4.9
900 F	14.7	-	15.6	-	13.1	12.5		10.4	12.0	9.7
800 F	15.2	-	15.9	-	15.0	14.4	10.8 (800 F Limit)	12.8	12.8	11.1
700 F	15.9	-	16.3	-	15.0	15.0	14.4	13.4	13.4	12.1

A. Calculated from Battelle-Columbus data.

B. From "Handbook of Stainless Steels", Becker and Bernstein, eds., ASM unfixed vessel boiler code data.

Because specific creep rate and 100,000-hour rupture data are scarce for many o the alloys under consideration, some conservative extrapolation of published data was attempted to provide a basis for comparison and the resulting maximum allowable stress values are listed in Tables 4-36 and 4-37.

Calculating the stress generated by the working fluid from ASME Section 1.0, Paragraph PG27.1, where:

$$\text{stress} = P\left[\frac{D-(t-0.005\ D-e)}{2t-0.01D-2e}\right]$$

where P is the pipe internal pressure, D is the pipe OD, 2 in., t is the pipe wall thickness, 0.25 in., and e = 0.0105, then for 50 psi internal Pressure, the stress is 1.93 ksi. For pressures of 300 and 150 psi, the stresses are 1.16 and 0.58 ksi, respectively.

The leading alloy candidates with strength capabilities for use at ~1600 F are as follows:

- Haynes 188--A carbide- and solid-solution-strengthened cobalt-base alloy, arguably the strongest available alloy that can be fabricated to tube, although creep data are available only for up to 10,000 hours. Alloy is weldable (with some difficulty) and possesses excellent high-temperature oxidation resistance. However, this alloy is expensive and was not evaluated in these tests.
- Inconel 617--A wrought, solid-solution-strengthened Ni-base alloy that has excellent creep and rupture strength to 1800 F, good tensile elongation after extended elevated temperature service, and is weldable. Corrosion experience in a fluidized bed combustor indicates that at the contemplated temperatures of application this alloy will need a protective cladding. A major problem with this alloy, which is in the semiproduction scale stage, is that its cobalt content prevents the recycling of scrap through the Huntington alloys system for fear of contaminating other alloys qualified for nuclear applications. With scaled-up production, this problem could disappear. In addition, 617 i difficult to process which, with its content of cobalt, probably ensures

that it will always be expensive. However, in the meantime, Huntington have developed a derivative of 617 strengthened by W + Fe rather than Mo + Co, designated Inconel 618 E. The objective of this exercise was apparently to remove Co for economic/availability reasons as much as to reduce process recycle problems. Inconel 617 remains a major candidate alloy in this program.

- Inconel 618 E,--A development of Inconel 617, with almost comparable mechanical properties, has been included in the program since it represents possibly a better commercial prospect than 617. There are no AFB corrosion data for this alloy.
- Hastelloy X--A wrought, solid-solution-strengthened nickel-base alloy, with excellent oxidation resistance to 2200 F and moderately high srength above 1450 F. However, its corrosion behavior in an AFB environment has been variable. It age-hardens somewhat after long exposure at 1200 to 1800 F, after which it loses some formability. It can be welded by most fusion welding procedures. This alloy is considered as a backup choice to the higher-strength Inconel 617/618 E, and it was intended that it be carried through the whole program of testing. However, the inability to obtain material from which specimens could be fabricated precluded its use on corrosion probes.
- Nimonic 86--A new solid-solution-strenghtened nickel-base alloy in the same class as Hastelloy X, with slightly lower strength but probably increased high-temperature corrosion resistance because of its higher Cr content, and its addition of Ce. No AFB corrosion data have been reported for Nominic 86, but the alloy has been included in the program because of its good potential and its compatibility with current processing practice.
- Alloys Hastelloy C, Inconels 625 and 600, and RA 333---Also belong to the same class as Hastelloy X, but were not selected for inclusion in the test program for various reasons. Hastelloy C is expensive, its high-temperature rupture behavior is not documented, and it may have insufficient high-temperature corrosion resistance since it contains only 16% Cr, with 16 Mo; Inconels 625 and 600 have been shown to be highly susceptible to sulfidation in a fluidized bed combustor. RA 333 offers no advantages in AFB corrosion resistance nor strength over Hastelloy X.

- Alloy 556 (N-155/Multimet)--This is probably the strongest of the iron-base austenitic alloys considered and appears to be intermediate betweer. Hastelloy X and Inconel 618 E at 1500 and 1600 F (Table 4-38). However, this alloy contains 20% Co with the attendant cost penalties and so was not included in the program.
- Incoloy 800 H--A very widely used, nonheat-treatable austenitic iron-chromium-nickel-base alloy with good high-temperature strength to at least 1500 F, and good high-temperature oxidation resistance. The H designation indicates a carbon content at the top end of the specification and a coarse grain size, both of which contribute to the high-temperature creep strength. The extensive experience with this alloy, and its good availability in tube and pipes, make it an obvious choice for investigation, but its creep-rupture limit makes it suitable for only the lower working fluid pressure or temperature applications.
- HK-40--A high carbon Fe-Cr-Ni-base alloy with useful high-temperature strength to 1500 F. Its great virtue is its low cost, made possible by production via centrifugal casting. Unfortunately, this imposes a lower tube diameter limit of about 3 inches, too large for the CCGT but acceptable for the OCGT Heat Exchanger designs.

For lower temperature service requirements for in-bed tubes, up to ~1300 F metal temperature, it is expected standard steam boiler materials practice will be followed, with due modification to allow for established corrosion rate differences. Boiler practice is to use carbon steel for the bulk of the tubes below about 785 F, with T-22 (2 1/4 Cr-1 Mo) up to about 1050 F, a corrosion-limited temperature, and austenitic alloys such as AISI 304 or 347 at higher temperatures. Where fireside corrosion is a problem, Incoloy 800 or Incoclad 671/800H or AISI 310-based claddings are used as a last resort. Mechanical shielding devices also are used sometimes. In some cases, notably in the United Kingdom, the 5 Cr-1 Mo (or 9 or 12 Cr-1 Mo) ferritic alloys sometimes are used where corrosion problems are encountered with 2 1/4 Cr-1 Mo. Typical maximum allowable stress values for this range of alloys are given in Table 4-37.

Limited available corrosion data in the AFB bed environment indicate that T-22 (2 1/4 Cr-1 Mo) should be limited to a maximum metal temperature of 950 F, so tha it is envisaged that the 300-series stainless steels, most likely 304 H, will bu

ed from 950 F upwards, until and unless more reliable in-bed corrosion data are forthcoming. Nominally, therefore, there will be no low-alloy steel tubes in the bed itself.

For freeboard tubes, in the absence of corrosion test data for tube alloys at the temperatures of interest, the best alternative is again to follow conventional boiler practice. In the current AFB heater design, the nominal metal temperature expected in the freeboard tube bank is approximately 1000 F, with some fluctuation depending on load. This suggests that the freeboard tube bank may comprise exclusively C-steel and 2 1/4 Cr-1 Mo.

The question of whether any significant cost penalty is involved in making a transition from 2 1/4 Cr-1 Mo directly to 304 H to combat corrosion, rather than using the low-chromium ferritic steels up to their strength limit (possibly up to 1000 F in this application) has not been addressed. The 9 Cr-1 Mo alloy in particular appears, from the few corrosion data available, to be more resistant to corrosion in the bed than 2 1/4 Cr-1 Mo. However, these low-chromium ferritic steels are not widely used in conventional steam boilers in this country because of fabrication and welding peculiarities, so that the cost margin versus 304 H (20%) is often insufficient to warrant the inventory costs for an extra material.

Current boiler practice in this country favors the use of AISI 304H over any other of the 300-series stainless steels. From a corrosion resistance viewpoint, AISI 310 (25% Cr-20% Ni) has intrinsically higher temperature capabilities than 304H, but suffers from precipitation of sigma phase (an embrittling phase) at grain boundaries after extended high-temperature exposure, is more difficult to weld and is more susceptible to hot tearing than 304H. The addition of niobium (as in AISI 347) to control carbide precipitation and produce a "stabilized" alloy increases the welding and hot tearing problems. However, use of these more corrosion-resistant grades as claddings for stronger, but less corrosion-resistant alloys should be considered.

Alloys chosen for further study in this program in load-bearing or in protective cladding roles are listed in Table 4-38. It is anticipated that the nickel-base alloys may require some form of cladding for protection from fireside corrosion in the AFB environment.

TABLE 4-38. ALLOYS SELECTED FOR ADVANCED CCGT HEAT EXCHANGER DUTY WITH USE TEMPERATURE LIMITS

Alloy	Temperature Limit, °F for Given Internal Pressure, psig			Limiting Factor
	150	300	500	
(1) Load-Bearing Alloys				
Inconel 617	1800	1780	1685	Strength (See Note A)
Inconel 618E	1800	1725	1605	Strength (See Note A)
Hastelloy X	1700	1690	1635	Strength (See Note A)
Nimonic 86	1800	1680	1590	Strength (See Note A)
Incoloy 800H	1700	1660	1560	Strength (See Note B)
AISI 304H/347H	1525	1525	1440	Strength (See Note C)
2 1/4 Cr-1 Mo	785-950	785-950	785-950	Corrosion
Carbon Steel	785	785	785	Corrosion
(2) Cladding Alloys				
FeCrAlY				Protective to 2200F
310				Corrosion Limits to Be Determined
347				

A: Nickel-base alloy; probably susceptible to sulfidation attack; corrosion may further limit use temperature unless used with a protective cladding.

B: Based on AFB corrosion tests, EPRI personnel have suggested this alloy is sometimes susceptible to sulfidation; need to consider using with a cladding unless corrosion behavior can be better defined.

C: Available corrosion data suggest that these temperatures may not be appropriate; may be corrosion-limited to 1400 F.

D: OD is 2 inches, wall thickness 0.25 inches.

lloy Procurement. The compositions of the actual alloys obtained are listed in Table 4-39. Alloys Inconel 617, 618E, and the FeCrAlY- or 347-clad versions of these alloys, respectively, together with Incoloy 800H, were obtained from Huntington Alloys.

Inconel 617 was in the form of cold drawn pipe of nominally 1.5 inch-OD (actually 1.9 inch-OD) schedule 80 and was supplied in the pickled and solution-annealed condition. Cross sections of the alloy indicate that it possesses a large (230 m) equiaxed grain structure, with precipitates of presumably TiN within the grain bodies and occasionally at grain boundaries (Fig. 4-104). Some grain boundaries exhibited other fine precipitates (Fig. 4-104d) which were identified.

Inconel 618E, 347 clad 618E, and FeCrAlY-clad 617 were specially made for this program by Huntington Alloys. 618E was extruded and finally cold drawn to 2 inches OD x 0.25 inch average wall thickness, it was delivered in the pickled and annealed condition. Figures 4-105 and 4-106 show this alloy to have a smaller equiaxed grain size than 617, and to have more numerous grain boundary precipitates, which are probably titanium nitrides and chromium carbides. A few areas of inhomogeneity also were evident, as shown in the figures.

Nimonic 86 was obtained from Wiggin Alloys, Ltd., in the United Kingdom. This alloy was air melted, vacuum refined and produced as cold-drawn, pickled, and annealed tube of 2 inch OD x 0.25 inch wall. Metallography showed this alloy to have equiaxed grains some 67 m average size (Fig. 4-107 and 4-108). Twinning was evident, along with some less-than-uniform precipitation in grains and grain boundaries.

Incoloy 800H was obtained from Huntington Alloys in the form of schedule 80 cold-drawn pipe, in the pickled and annealed condition. Figure 4-109 shows the typical annealed microstructure of this alloy, with twinned grains from 82 μm average size and carbide/TiN precipitates.

AISI 310 in the form of schedule 80 hot-forged seamless pipe was obtained from Rolled Alloys. Figure 4-110 shows the microstructure of this alloy, with an average grain size of 120 μm, and strings of tramp carbides and sulfides extending in the direction of forging.

TABLE 4-39. COMPOSITIONS OF ALLOYS USED IN FBC CORROSION TESTS

Alloy	Heat No.	Composition, Weight Percent										
		Fe	Ni	Co	Cr	Mo	W	Mn	Si	Aℓ	C	Other
Inconel 617	XX35A5UK	.34	55.44	12.12	21.53	9.03	--	0.1	.10	1.11	.06	--
Inconel 617*	XX40A5UK	.57	54.73	12.32	21.74	9.11	--	.01	.11	1.05	.08	--
Inconel 618E	Y75B1	14.97	55.50	--	22.78	--	6.24	.04	.08	--	.05	.32Ti
Inconel 618E**	Y71B9U	15.09	54.80	--	23.39	--	6.26	.06	.07	--	.05	.26Ti
Nimonic 86	2NJ9737	1.76	BAL	.53	25.4	10.4	--	.48	.35	.02	.06	.03Ce
Incoloy 800H	HH0307A	43.55	32.57	--	21.36	--	--	.88	.38	.31	.08	.37Ti
AISI 310	96735	BAL	19.62	--	24.76	.24	--	1.46	.56	--	.061	--
AISI 304H	97112	BAL	8.25	--	18.12	.27	--	1.91	.39	--	.080	--
Claddings												
FeCrAℓY	508/2A	Bal	.007	--	15.78	--	--	--	.042	4.86	.014	.488Y
FeCrAℓY	510/2B	Bal	.007	--	15.4	--	--	--	.402	4.81	.011	.456Y
AISI 347												

*Alloy clad with FeCrAℓY

**Alloy clad with 347

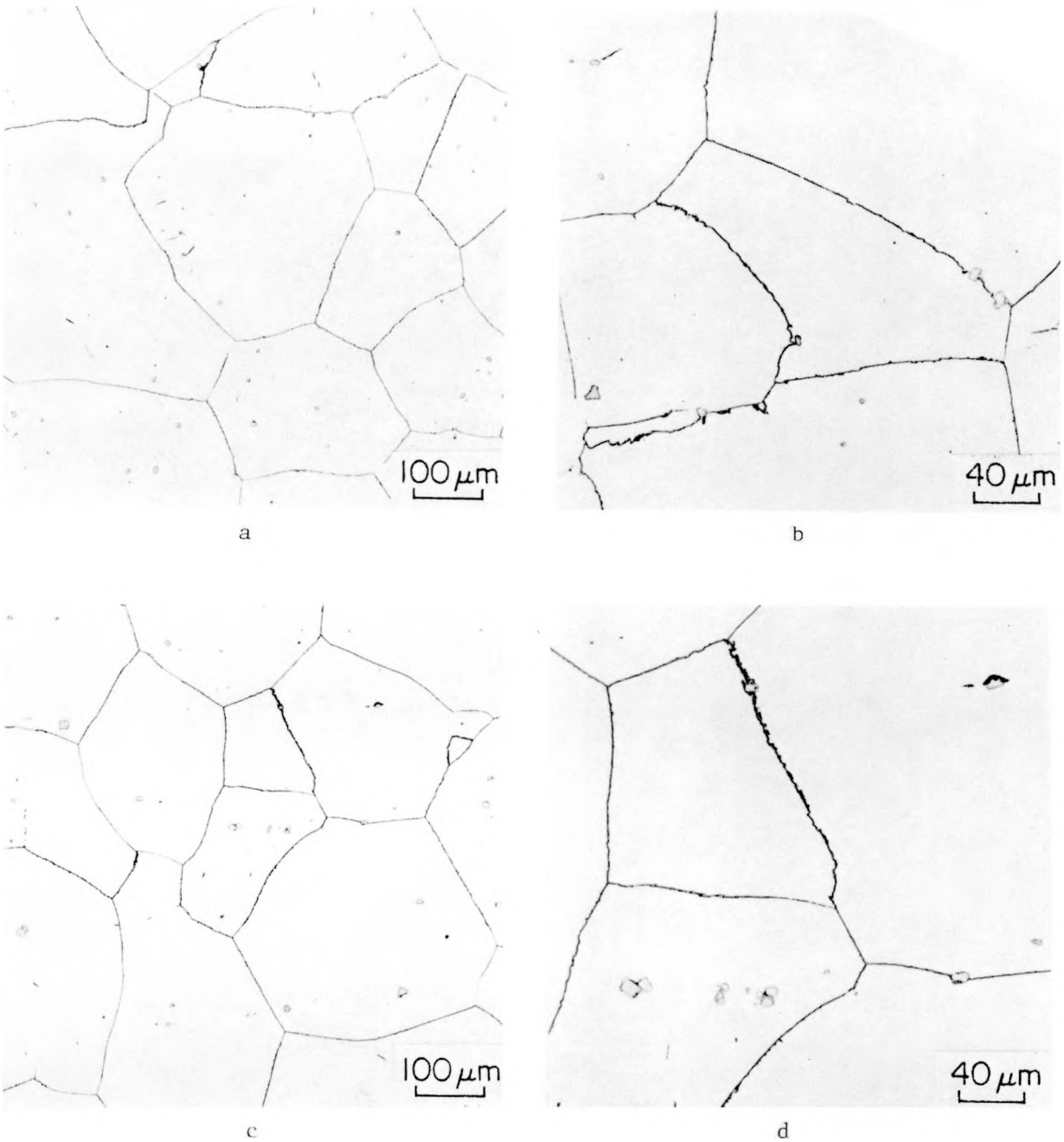


Figure 4-104. INCONEL 617 Etched in 10% Oxalic Acid
a, b: Transverse Sections
c, d: Longitudinal Sections

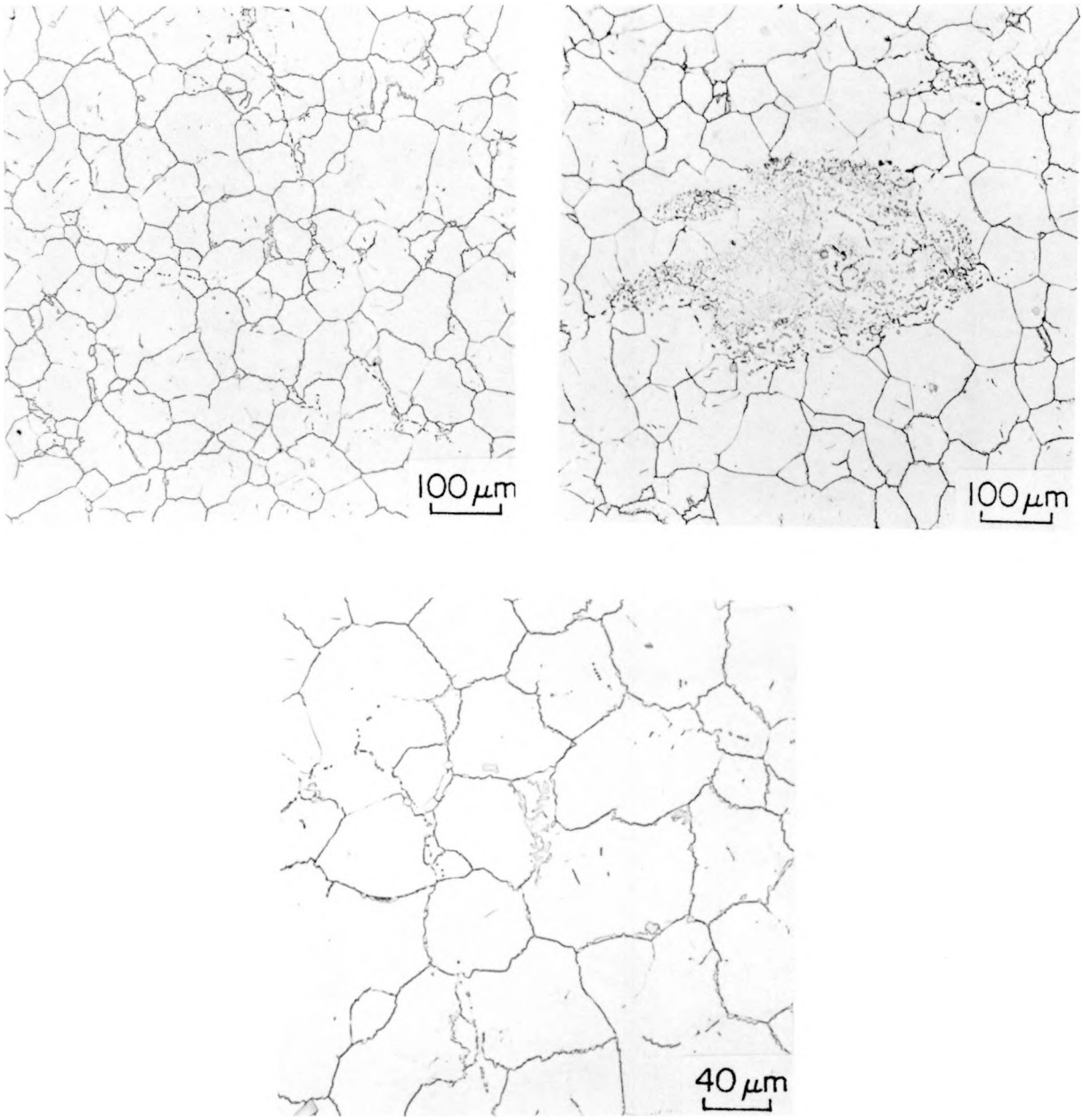


Figure 4-105. INCONEL 618E, Transverse Sections Etched in 10% Oxalic Acid

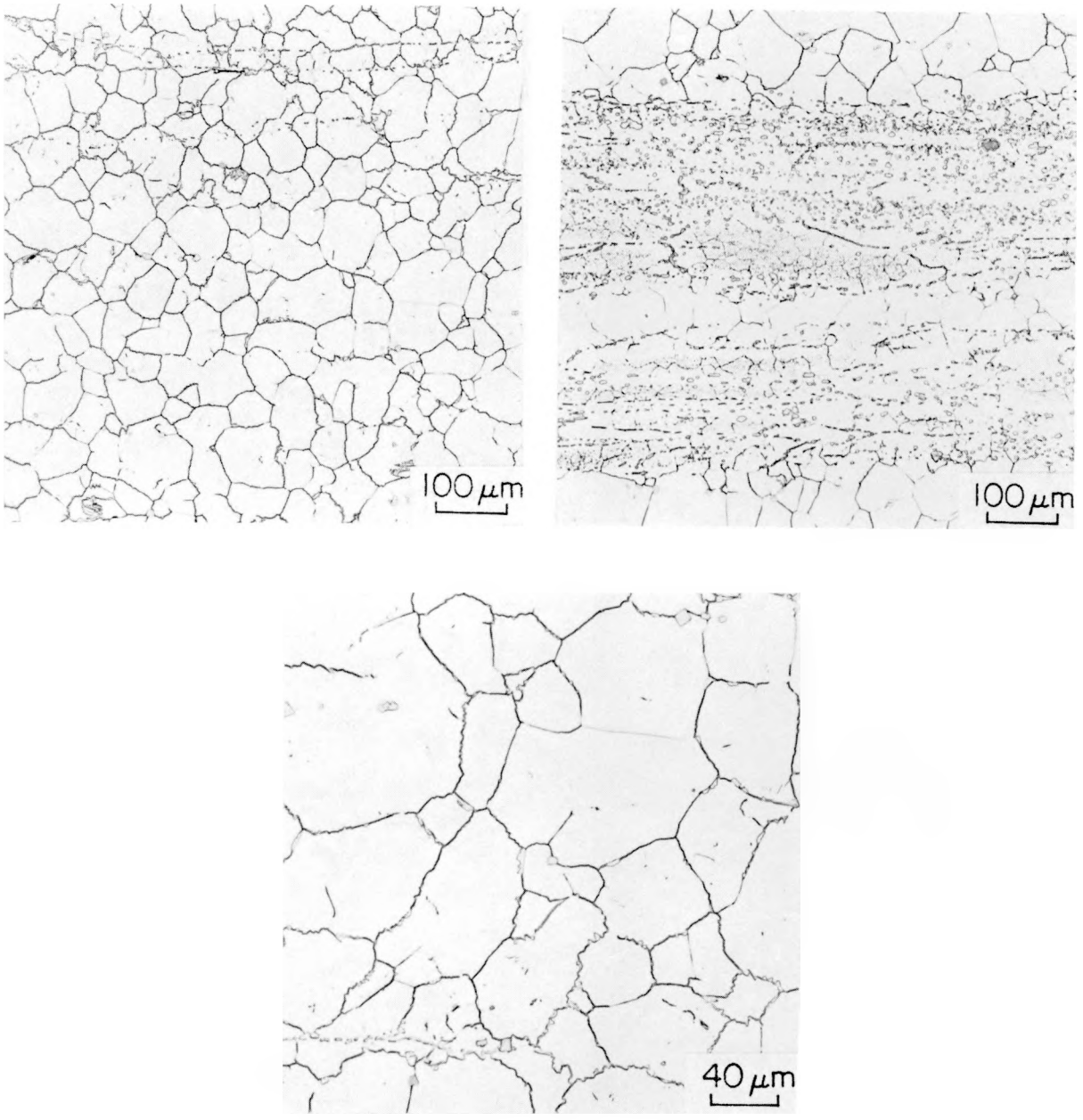


Figure 4-106. INCONEL 618E, Longitudinal Sections Etched in 10% Oxalic Acid

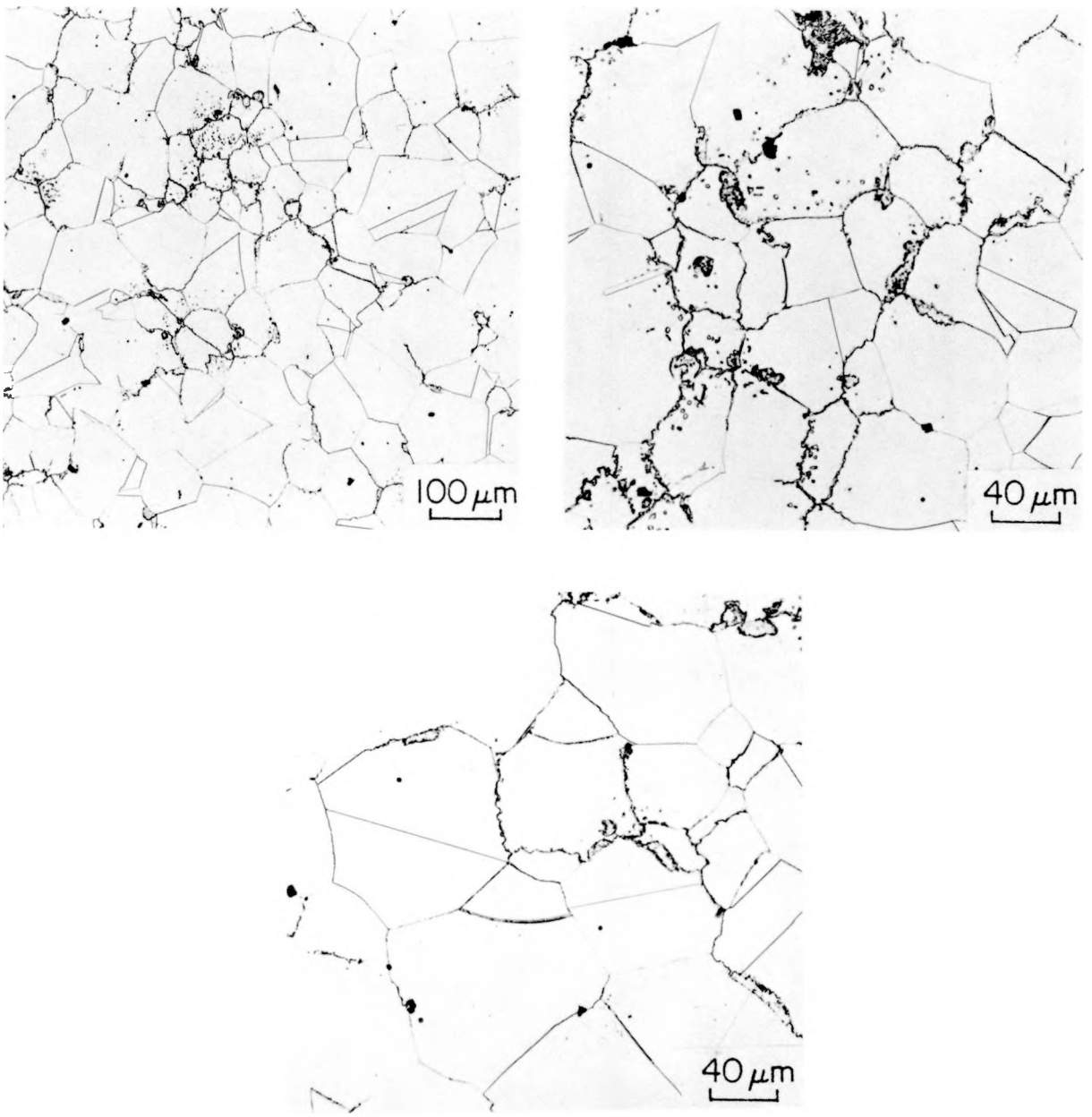


Figure 4-107. NIMONIC 86, Transverse Sections Etched in 98 HCL, 2 HNO_3 0.5g $CuCl_2$

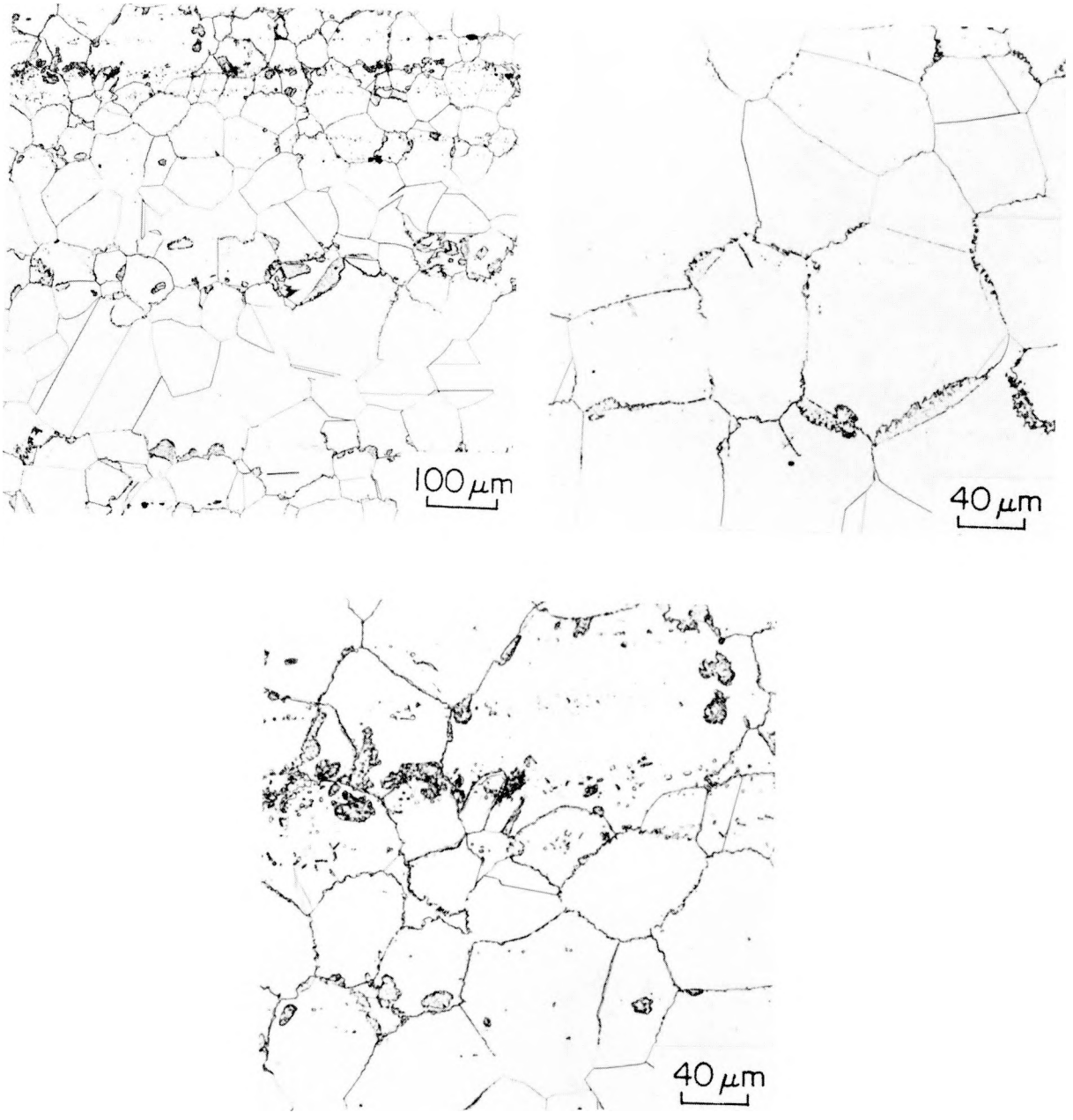


Figure 4-108. NIMONIC 86, Transverse Sections Etched in 98 HCL, 2 HNO_3 0.5g $CuCl_2$

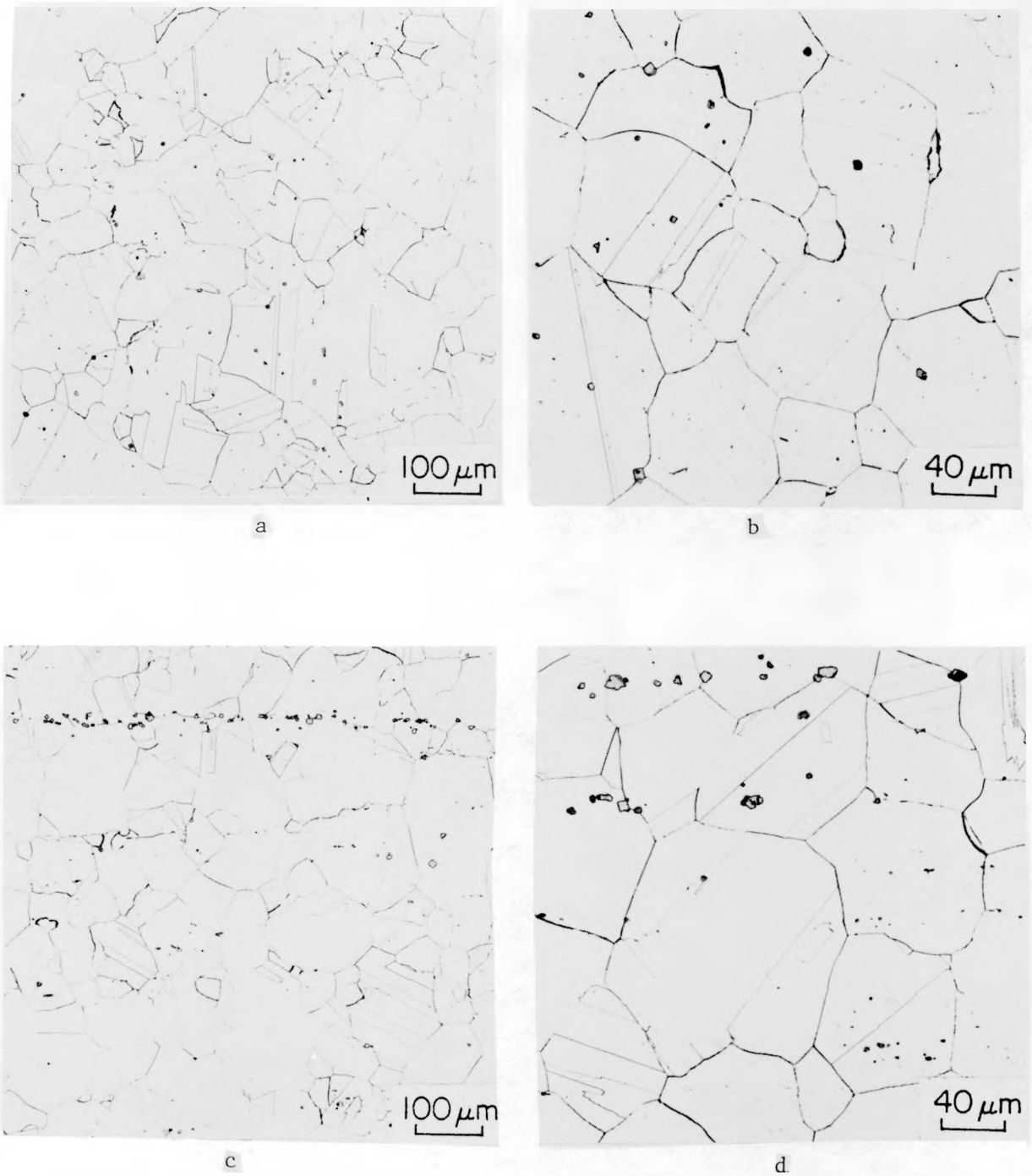


Figure 4-109. INCONEL 800H Etched in 10% Oxalic Acid
a, b: Transverse Sections
c, d: Longitudinal Sections

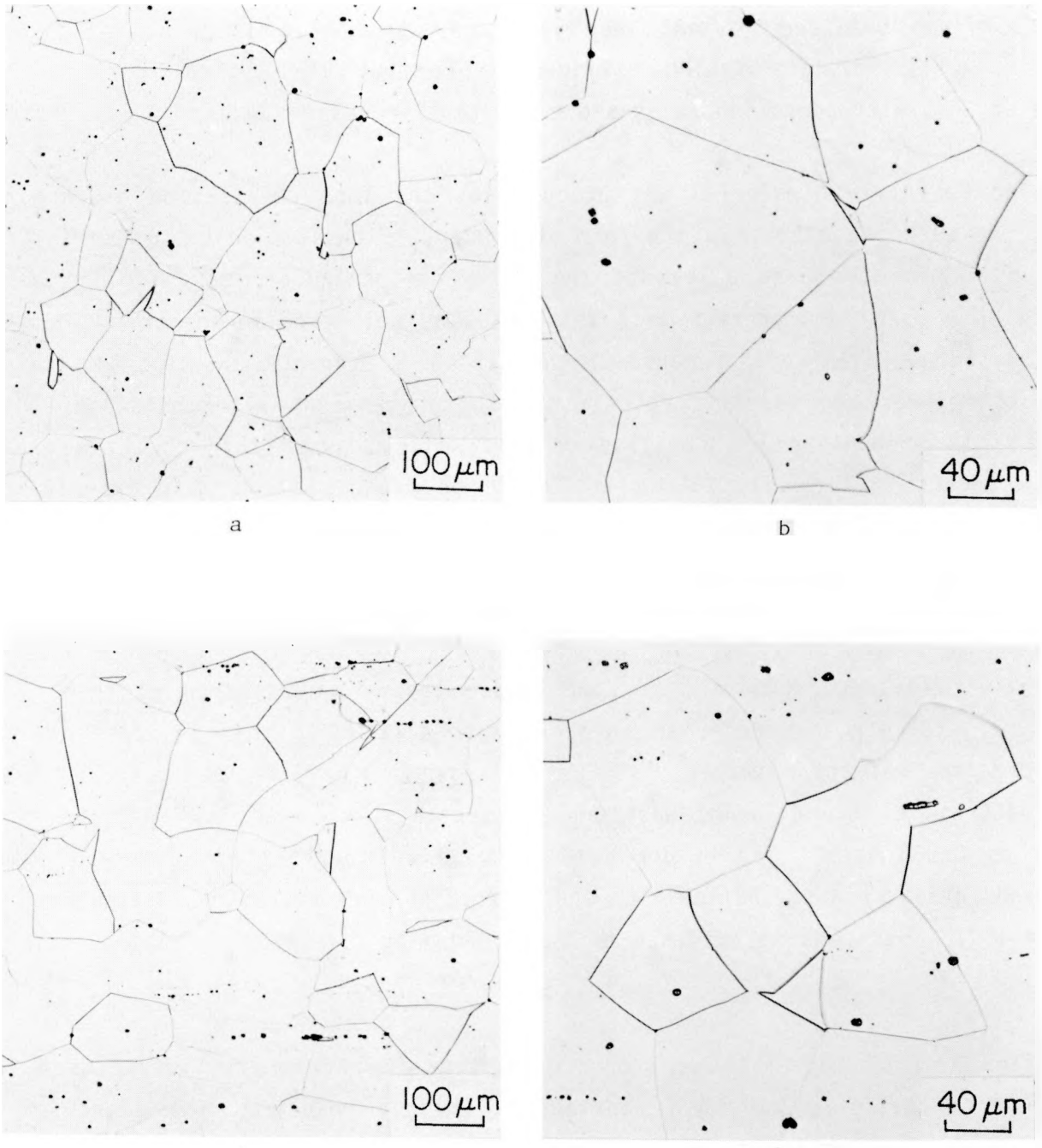


Figure 4-110. AISI 310, Etched in 98 HCL, 2 HNO_3, 0.5g $CuCl_2$
a, b: transverse Sections
c, d: Longitudinal Sections

AISI 304H was obtained from Al Tech via Tubesales, in the form of 2-inch-OD x 0.25-inch-wall seamless tubing. Figure 4-111 shows the typical structure of annealed 304, with annealing twins and a few fine inclusions.

Incoclad FeCrAlY/617 material was produced by the Inco coextrusion process, in which the cladding alloy, in the form of powder, is positioned by means of a can on a billet of the base alloy and the whole is coextruded. The final tube of 2 inch OD x 0.25 inch average wall thickness was delivered in the cold-finished, pickled and annealed form. Because of the extreme differences in high-temperature strength between the ferritic FeCrAlY and the austenitic 617, considerable difficulty was encountered in coextruding these allows, with the result that only short lengths (5.25 to 62.25 inches) could be produced from this experimental batch. Figure 4-112 shows the interface region of the coextrusion, with the FeCrAlY etched. A 70 to 110 μm wide interdiffusion zone is evident, which constitutes a brittle intermetallic compound, which may lead to some degradation of the bonding during service. The bonding of the cladding to the base alloy was generally excellent. However, in some cases, separation occurred at the intermetallic layer-617 interface, as shown in Fig. 4-113. In this case, the extent of separation was approximately 13% of the length of the interface. In addition, the thickness of the cladding was somewhat variable, ranging, for instance, from 0.028 to 0.063 inch. The powder metallurgy FeCrAlY exhibited a small (18 μm) equiaxed grain cross section in the direction of extrusion, as shown in Fig. 4-112. There was no evidence of such debonding affecting corrosion in these tests.

Incoclad 347/618E material was produced by the same coextrusion route used for Incoclad FeCrAlY/617, but with considerably better results. The 2-inch OD x 0.25-inch-average wall tube was delivered in two 6-foot lengths, in the cold finished, pickled and annealed condition. Figure 4-114 the 347-618E interface region, with the 347 etched. Bonding was found to be excellent around the complete circumference of the tube, with no separate intermetallic layer. The structure of powder metallurgy 347 was typical of the annealed alloy, with annealing twins and an equiaxed grain larger (35 μm vs 26 μm) than that of a typical 347 seamless tube product (Fig. 4-115) but of a similar size to that of the AISI 340H used in this program. For alloys of this type (18Cr-8Ni), decreased grain

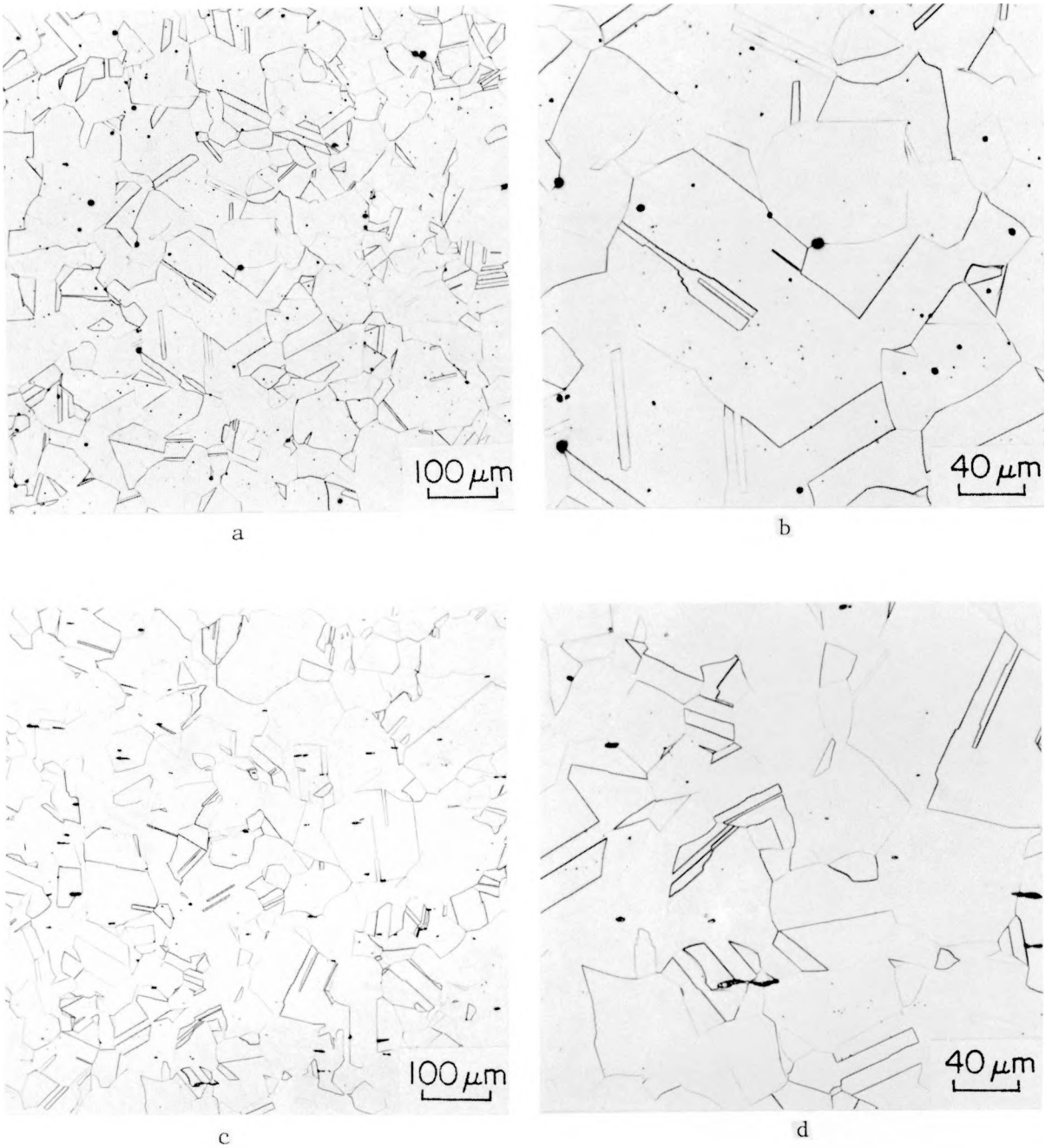


Figure 4-111. AISI 304 Etched in 98 HCL, 2 HNO_3, 0.5g $CuCl_2$
a, b: Transverse Sections
c, d: Longitudinal Sections

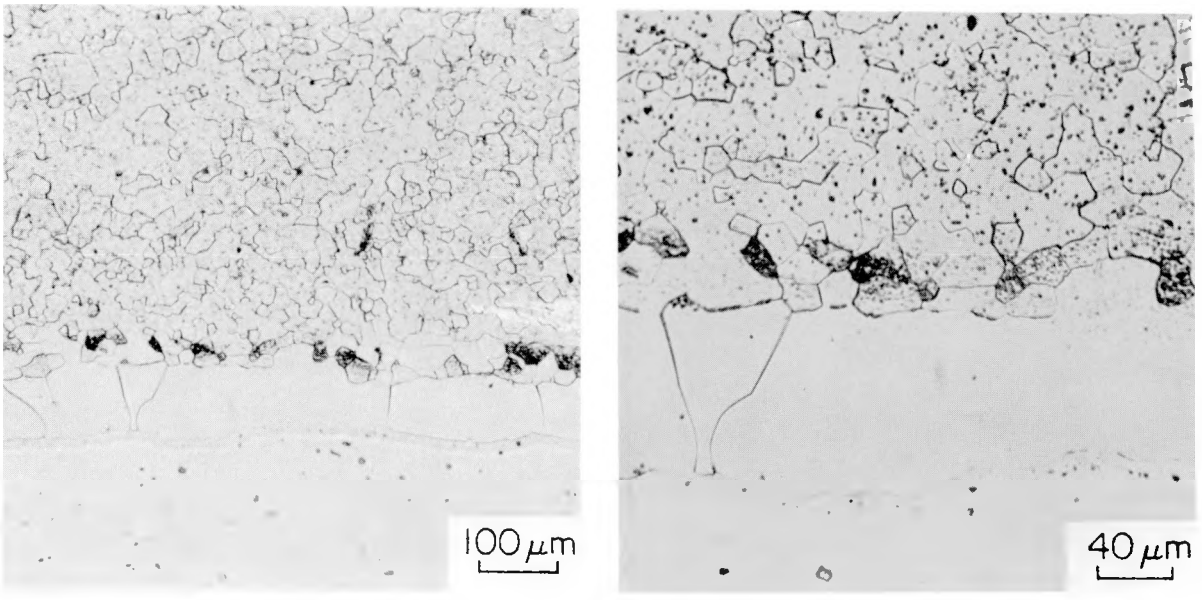


Figure 4-112. INCOCLAD FeCrAlY/617, Transverse Sections Showing Cladding Interface

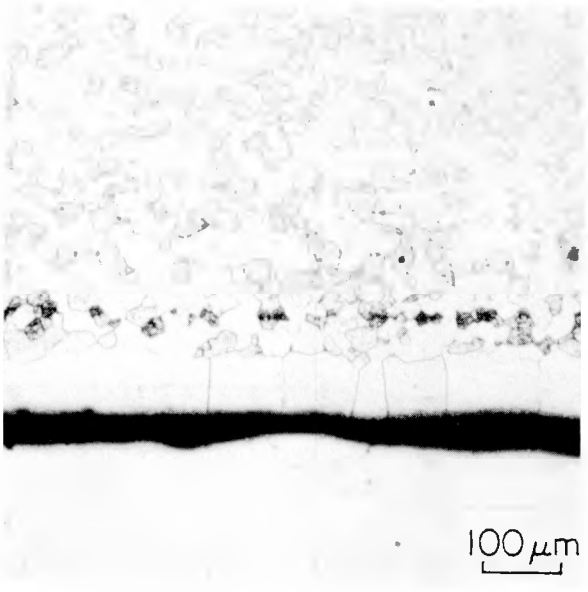


Figure 4-113. INCOCLAD FeCrAlY/617, Transverse Section Showing Lack of Bonding

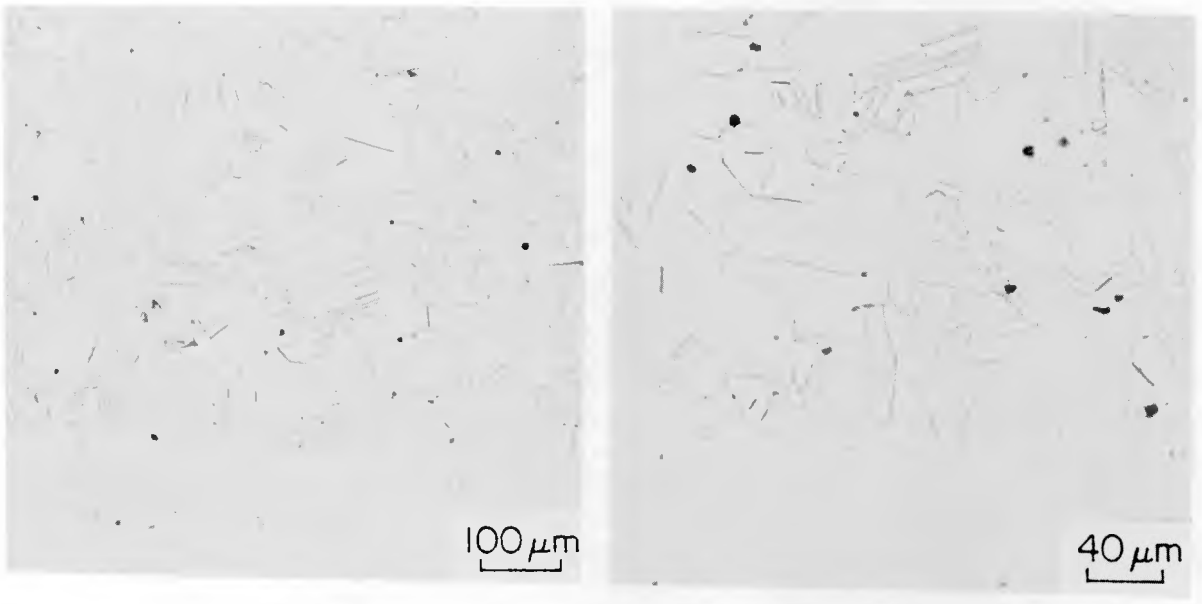


Figure 4-114. INCOCLAD 347/618E, Transverse Section Showing Cladding Interface

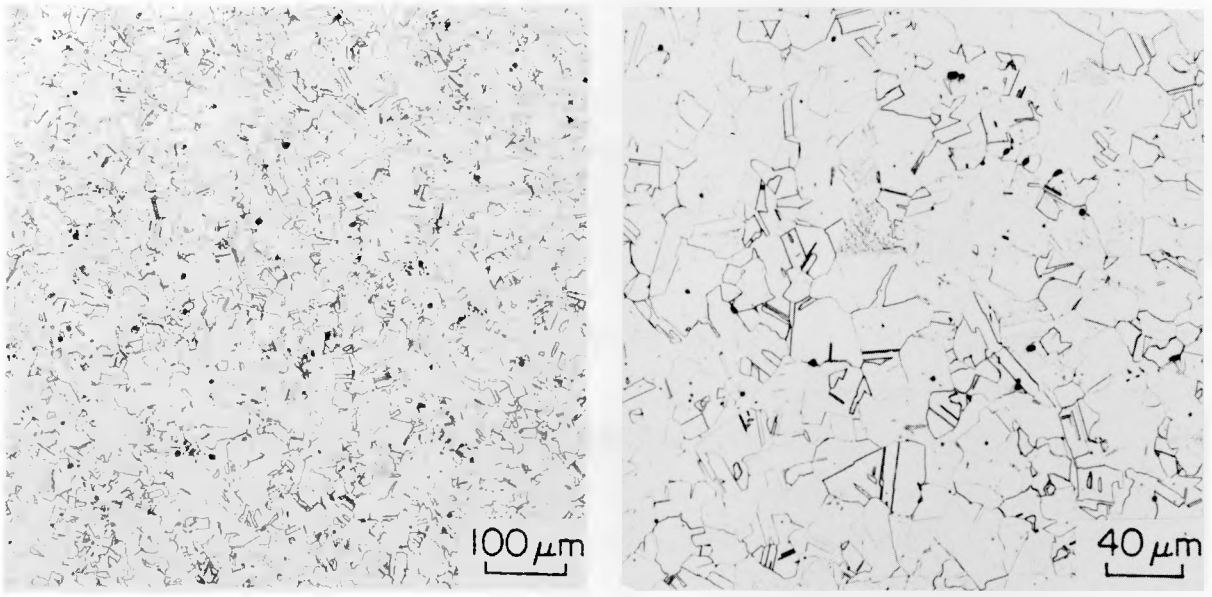


Figure 4-115. Typical Transverse Section of Seamless AISI 347 Tubing Etched in 98 HCL, 2 HNO_3, 0.5g $CuCl_2$

size can often confer a degree of increased corrosion resistance because of an increase in chromium diffusion rate resulting from the more numerous grain and twin boundary paths.

Corrosion Probes. The corrosion exposures were carried out in BCL's 24-inch-diameter AFB using a corrosion probe design shown schematically in Fig. 4-116. Six probe bodies in all were constructed; four such probes were installed at a given time in the AFB. They consisted of a support section made of three concentric tubes (1) a water-cooled jacket; (2) a cooling air passage; and (3) a tube for thermocouple feedthrough. The central tube extended through the 24 lap-joint test specimens. This was welded to a spider web plate lap-fitted into the end specimen. A compression spring provided a load to hold specimens tightly against each other and to the water-cooled support structure. A tapered cone fitted over the central tube through the test section produced a varying cooling air velocity that decreased along the probe, providing a nearly linear temperature gradient from the first to the last specimen. The cooling air flow was regulated by a motorized valve activated by a temperature controller. The thermocouple for control was inserted in a specimen for which the desired test temperature was near the hot end of the temperature range, since, in these tests, this was essentially bed temperature. Type K thermocouples were inserted in recesses drilled lengthwise into one end of appropriate specimens for control and recording purposes.

Specimens. The test specimens were machined from tube stock to the specifications shown in Fig. 4-117. Those materials produced to schedule 80 tube specification were not subjected to machining of the outer surface to minimize the outside diameter difference between them and the 2-inch-OD tubes. Hence, the schedule 80 tube materials were exposed with an as-received outer surface finish. A fiducial mark (dimple) was made on each specimen to aid radial positioning of the specimen on the probe, and the specimen indentity was engraved on the inside surface.

Before exposure, each specimen was degreased and from then on handled with cotton gloves. Measurements were made of outside diameter and wall thickness at a diameter through the fiducial mark, and at 90 degrees to this. Finally, each specimen was weighed and then stored in a desiccator until used.

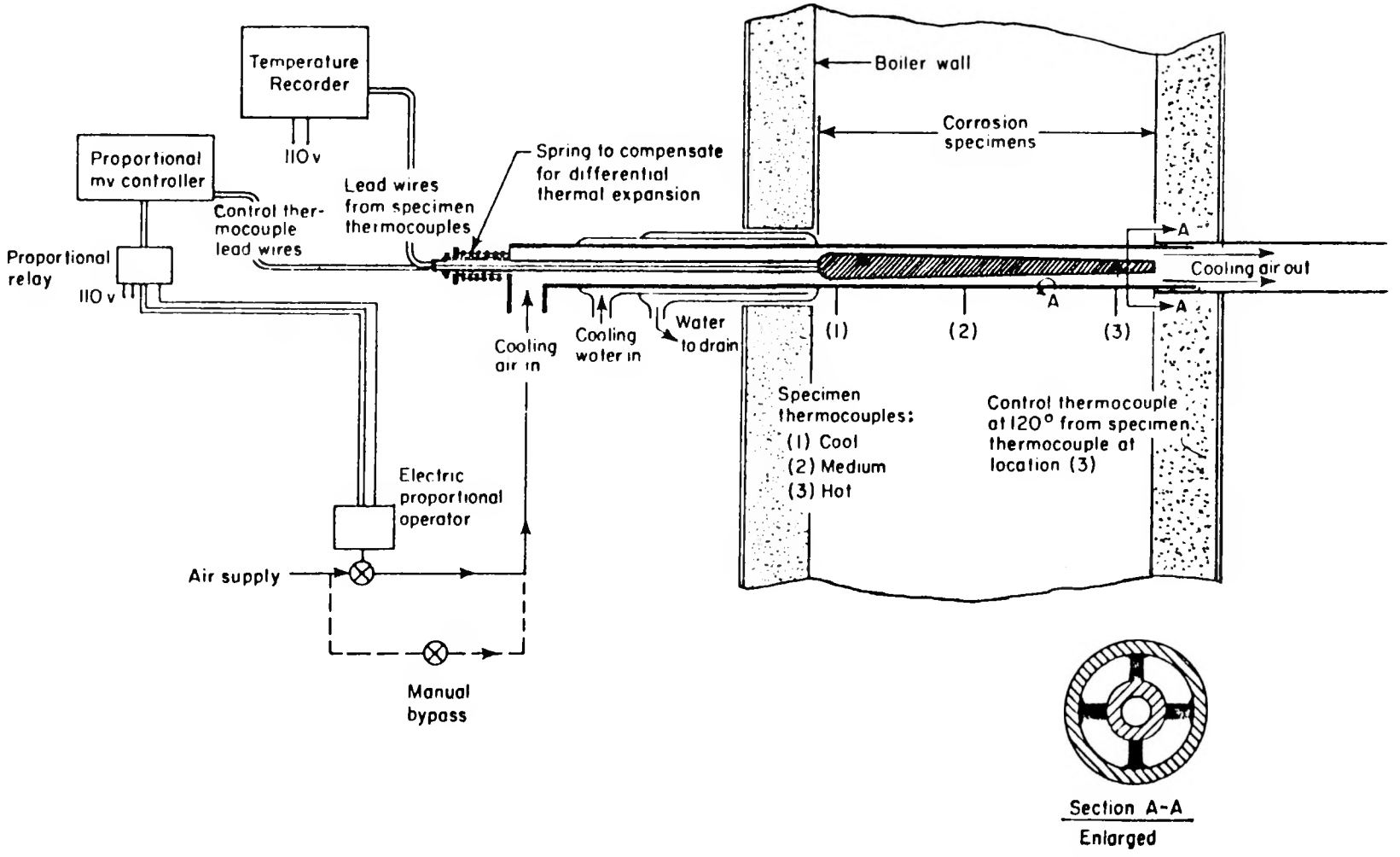


Figure 4-116. Schematic Diagram of BCL Corrosion Probe Installed in FBC

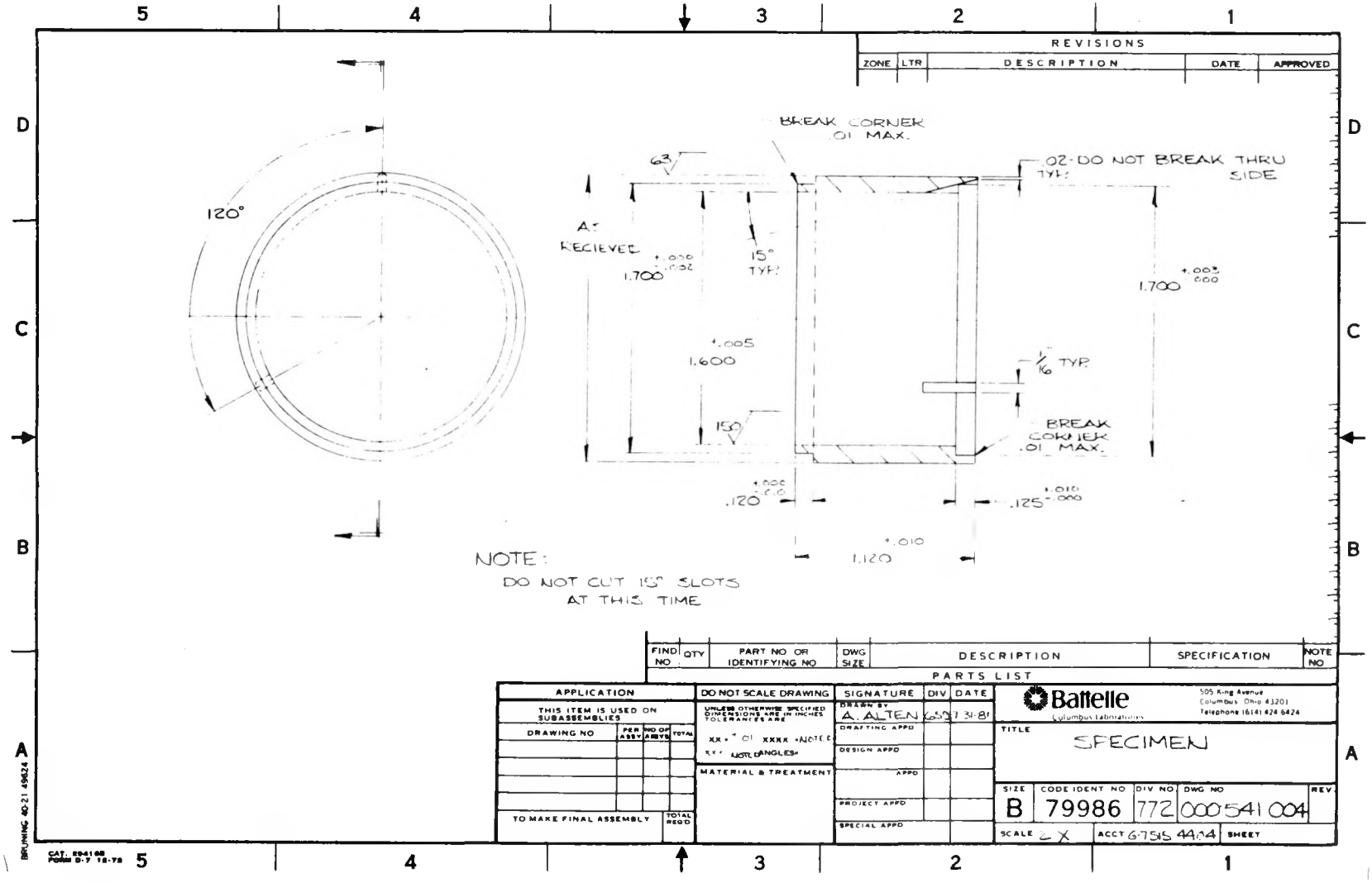


Figure 4-117. Details of Corrosion Probe Specimen

.he specimens were assembled into two types of probes: one type contained three iterations of each of the eight alloys and was referred to as a "multialloy" probe; the other type contained alternating specimens of Incoloy 800H and 304H, and was referred to as a "binary" probe. The intent of the binary probes was to provide a correlation with measured local oxygen partial pressure across the bed. On the former probes the alloy specimens were assembled in a sequence, from hotter to cooler end, of Nimonic 86; Inconel 618E/347; Inconel 617/FeCrAlY; Inconel 617; AISI 310; Incoloy 800H; and AISI 340H.

After exposure, specimens were disassembled carefully from each probe so as to retain as much deposit and corrosion product as possible, and stored in separate dessicated containers. After visual examination, most of the specimens were descaled cathodically in an inhibited solution of sulfuric acid, according to ASTM G1-72 (Section 4.0) and the weight loss resulting from corrosion was computed.

Specimens from two complete probes, one of each type, were mounted in epoxy to preserve all adherent corrosion products and deposit, and were sectioned, polished, and subjected to metallographic analysis.

Oxygen Probe. A stabilized-zirconia oxygen sensor manufactured by the automobile industry (Ref. 4-50) was modified for diagnostic use in the AFB. The electrochemical principles governing the use of these oxygen sensors and their application to the AFB environment were discussed in a previous paper (Ref. 4-51) and the detailed discussion of the AFB probe presented in Section 4.2.3. Figure 4-118 shows a schematic representation of the oxygen probe. Figure 4-119 shows a side view of the AFB, illustrating the locations where the corrosion and oxygen probes were positioned relative to the heat exchanger tube bundle. During the corrosion experiments, PO_2 measurements were taken at 5 different vertical locations corresponding to the ports 12, 32, 52, 82, and 103 in Fig. 4-119. The output (in mV) from the oxygen probe was recorded on a digital oscilloscope and converted directly to PO_2 data by utilizing the computing features of this data-acquisition device. The oxygen probe has a minimum response time of less than ^.1 second. Therefore, rapid changes or fluctuations in the oxygen partial pressure could be monitored accurately.

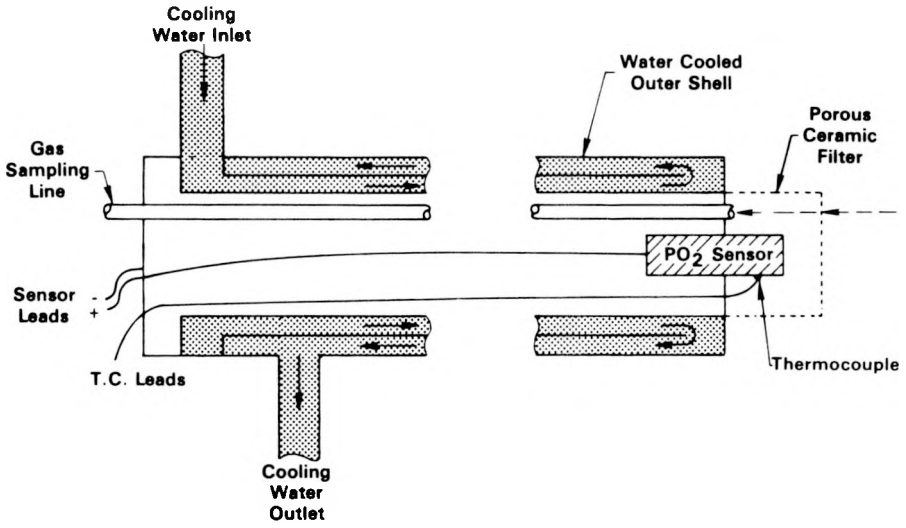


Figure 4-118. Schematic Diagram of Combined Oxygen Activity (PO_2) and Gas-Sampling Probe

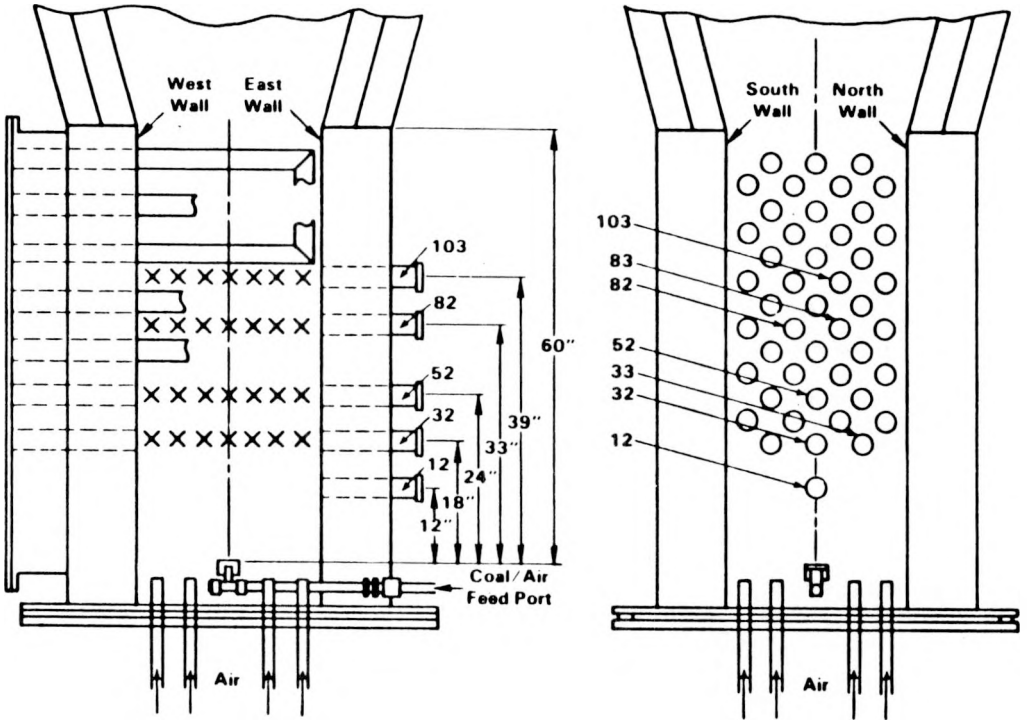


Figure 4-119. Schematic Diagram of 24-Inch-Diameter AFBC

luidized Bed Operations. The corrosion exposures were conducted in the BCL 24-inch diameter Research AFB, which had been modified to correspond to some of the internal features of the Rocketdyne 6' x 6' bed. The installed heat exchanger bank (made of AISI 304) consisted of 2-inch-OD heat exchanger tubes that entered and exited the combustor through the west wall, and which were formed into U-bends at the east wall. Entrance ports were provided for corrosion and sampling probes in the east wall of the combustor, along vacant heat exchanger tube locations, as shown in Fig. 4-119. Since the corrosion probes, diagnostic probes, and dummy probes were all 2 inch OD, the tube handle design was completed when all were positioned in the bed, with full symmetry and no gaps.

The numbered positions in the tube bundle in Fig. 4-119 indicate locations where metallic corrosion probes were installed (32, 33, 82, and 83), and where the oxygen probe was used (12, 52, and 103). Dummy tubes were reinstalled in locations 52 and 103 when the oxygen probe was withdrawn. Oxygen measurements also were made in the corrosion probe locations immediately prior to installation and immediately after removal at the end of the allotted exposure period.

A corrosion run was started by installing four corrosion probes in the cold bed, bringing the bed up to operating conditions, and making oxygen probe measurements at ports 12, 52, and 103. At nominally 100 hours into the run, one corrosion probe was removed from each location (32/33 and 82/83), oxygen probe measurements were made in the vacated locations, and new corrosion probes were installed. During this transition period, efforts were made to keep the bed operating condition constant. At the end of the 250-hour period, the corrosion probes were removed from each location in turn, oxygen probe measurements were made in these locations, and then the bed was shut down.

Upon removal from the bed, the corrosion probes were visually examined and photographed while hot and then wrapped in aluminum foil to retain the deposits and corrosion products. When cold, the probes were rephotographed and reexamined to determine any obvious differences along the probes or circumferentially. Finally, the probes were disassembled and the bodies refurbished with new specimens. The exposure locations, duration, and types of corrosion probes are summarized in able 4-40.

TABLE 4-40. SUMMARY OF CORROSION PROBES

PROBE NO.	TYPE	LOCATION	XS-AIR	TIME, HOURS
1	MULTI	83	20%	141
2	MULTI	82	20%	244
3	BINARY	32	20%	244
4	BINARY	33	20%	140
5	MULTI	83	20%	91
6	BINARY	33	20%	100
7	MULTI	82	0%	240
8	MULTI	32	0%	240
9	BINARY	33	0%	163
10	MULTI	83	0%	161
11*	MULTI	83	0%	70
12	BINARY	33	0%	70
13	BINARY	82	50%	146
14	BINARY	82	50%	93
15	MULTI	83	50%	245
16	MULTI	32	50%	264
17*	BINARY	33	50%	115
18	BINARY	33	50%	147

*PROBES NO. 11 AND 17 WERE NOT DESCALED

For the corrosion runs, the Battelle 24-inch-diameter AFB was operated for three 250-hour periods under conditions summarized in Table 4-41. A 4% S, Illinois No. 6 coal, screened to -8 mesh (2400 μm), was burned with Grove limestone (39% Ca, 59% CO_3) of size -8 + 60 mesh (850-2400 μm) at a Ca/S ratio based on the feed of 3.1 to 1. The sulfur emission was controlled to about 1.0 lb/MM Btu (500 ppm SO_2). The three runs were intended to produce excess air conditions of 20%, 0%, and 50%, respectively. During the 0% excess (XS) air run, a gradual reduction of the combustion air occurred over the first 120 hours as a result of operating problems. However, oxygen probe data indicate that essentially sub-stoichiometric conditions prevailed at the corrosion probe locations, so that the affect of the combustion condition changes on the corrosive environment is considered to have been small.

TABLE 4-41. SUMMARY OF COMBUSTION CONDITIONS USED IN CORROSION RUNS

	Run 1	Run 2	Run 3
Pressure	Atmospheric	Atmospheric	Atmospheric
Bed Temp (°F)	1645 ± 7	1650 ± 7	1645 ± 7
Fluidizing Velocity (ft/sec)	6.3	5.2	6.3
Excess Air Level (%)	17	0	50
Coal	Illinois #6	Illinois #6	Illinois #6
Limestone	Grove	Grove	Grove
Ca/S Mole Ratio	3.14	3.19	3.24
SO_2 Emission (ppm)	550 ± 200	--	470 ± 50
Duration (hr)	250	250	250

Results and Discussion

Bed Characterization: Oxygen Probe Data. Before discussing in detail the oxygen probe data, it is necessary to examine an important characteristic of the combustion process. When a fuel is burned with air, a wide range of oxygen partial pressures (PO_2) are possible in the flue gas, depending on the initial air/fuel ratio. This is illustrated in Fig. 4-120, which shows the calculated equilibrium partial pressures in the flue gas as a function of the air/fuel ratio for the combustion of coal (Illinois No. 6) with air. Of particular importance is the large drop in PO_2 when going from a lean combustion process with excess air (air/fuel 1.0) to a rich combustion process depleted in air (air/fuel 1.0). An oxygen partial pressure of approximately 10^{-1} atm is expected in the flue gas for any combustion process with excess air. If, however, excess air is not available, an oxygen partial pressure 10 to 15 orders of magnitude lower will result. Therefore, a combustion process with an air/fuel ratio equal to 1.0 (exact stoichiometric combustion) can have an oxygen partial pressure in the flue gas anywhere between 10^{-3} and 10^{-12} atm. With these considerations in mind, it is apparent that in situ oxygen probe data can provide extremely useful information concerning the nature of the combustion process.

Figure 4-121 shows the type of oxygen probe data generated in the fluidized bed when the coal was burned with 50% excess air (run 3). While one would expect an oxygen partial pressure of 10^{-1} atm to prevail, this was not always the case. In areas of the bed, particularly above the coal feed port and along the walls, large fluctuations in the oxygen partial pressure at frequencies near 1 Hz were observed. The oxygen partial pressure fluctuated from a somewhat baseline value of 10^{-1} atm down to low values between 10^{-12} and 10^{-16} atm. These fluctuating PO_2 measurements indicate areas in the fluidized bed that at one instant experienced excess air conditions, while at another instant experienced substoichiometric conditions. It seems probable that the mixing properties of particular areas of the fluidized bed were such that a continuous condition of excess air did not always exist, although the coal and air were fed at an air/fuel ratio of 1.5 (50% excess air). These areas of low PO_2 may be the consequence of two factors, i.e., insufficient mixing of coal and air (areas in the bottom of the bed and near the coal feed port) and/or nonuniform flow patterns (along walls or

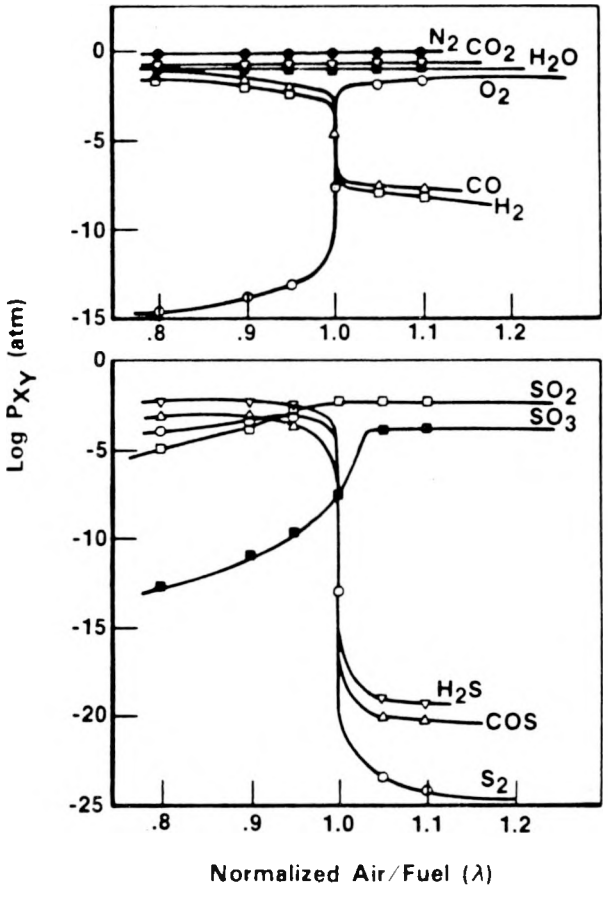


Figure 4-120. Equilibrium Partial Pressures in Flue Gas as a Function of Air/Fuel Ratio. (Illinois No. 6 Coal; Temperature = 1650 F)

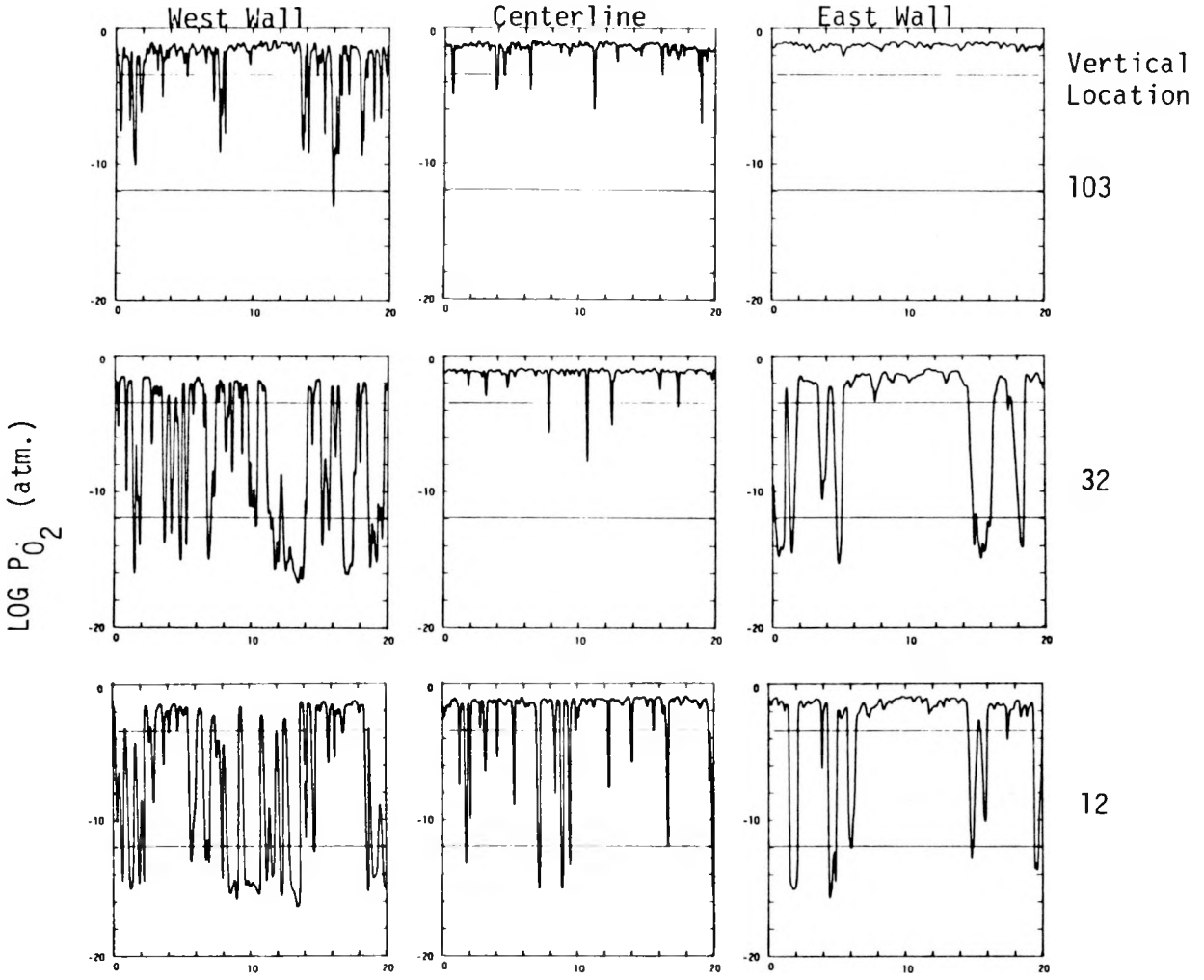


Figure 4-121. Oxygen Probe Output vs Time for Various Bed Locations During Third 250-Hour Run (50% Excess Air)

near corners and joints). Indeed, Fig. 4-121 illustrates that as the flue gas progressed upward through the fluidized bed (longer mixing time, increased uniformity of mixing) the fluctuations to low-oxygen pressures occurred at slower frequencies. Also, the magnitude of the PO_2 fluctuations was less severe (only a few orders of magnitude). Note that the data from the centerline of the bed closely correspond to those values expected, based on the initial air/fuel ratio, especially once the flue gas reached the middle of the heat exchanger tube bundle. The data in Fig. 4-121 also indicate that the mixing properties near the east wall (return ends of the heat exchanger tubes) were better than those near the west wall (penetrated by the heat-exchanger tubes).

In comparision with Fig. 4-121, Fig. 4-122 shows the oxygen probe data for a combustion process with nominally 20% excess air (run 1). While the same type of PO_2 fluctuations are observed, a few differences are immediately obvious. The magnitude of the PO_2 fluctuations was similar to those in Fig. 4-121, however, the frequency of the fluctuations was greater. Also, as the flue gas advances upwards in the bed, apparently more time was necessary before excess air conditions were indicated. Fluctuations to PO_2 values of 10^{-12} to 10^{-14} atm were still present in the middle of heat exchanger tube bundle. Apparently, a decrease in the amount of excess air (50% down to 20%) required more mixing time before PO_2 values corresponding to excess air conditions became dominant. However, the PO_2 fluctuations still decreased in magnitude and frequency as the flue gas progressed upward through the bed. (Once again, the east wall seemed to have better mixing properties than the west wall.)

Figure 4 123 shows the oxygen probe data when the AFB was operated at 0% excess air. In almost every area of the bed (only one exception), a baseline PO_2 value of 10^{-16} atm was measured, with frequent fluctuations to higher oxygen pressures. The PO_2 data from the bottom of the heat exchanger tube bundle at the centerline show very rapid fluctuations from 10^{-1} to 10^{-15} atm, indicating a combustion process that "hovered" around the air/fuel ratio of 1, i.e., stoichiometric combustion. However, the PO_2 data from most areas of the bed indicate purely substoichiometric conditions existed. An air leak in one of the corrosion probes resulted in the high PO_2 values in the upper region of the east wall.

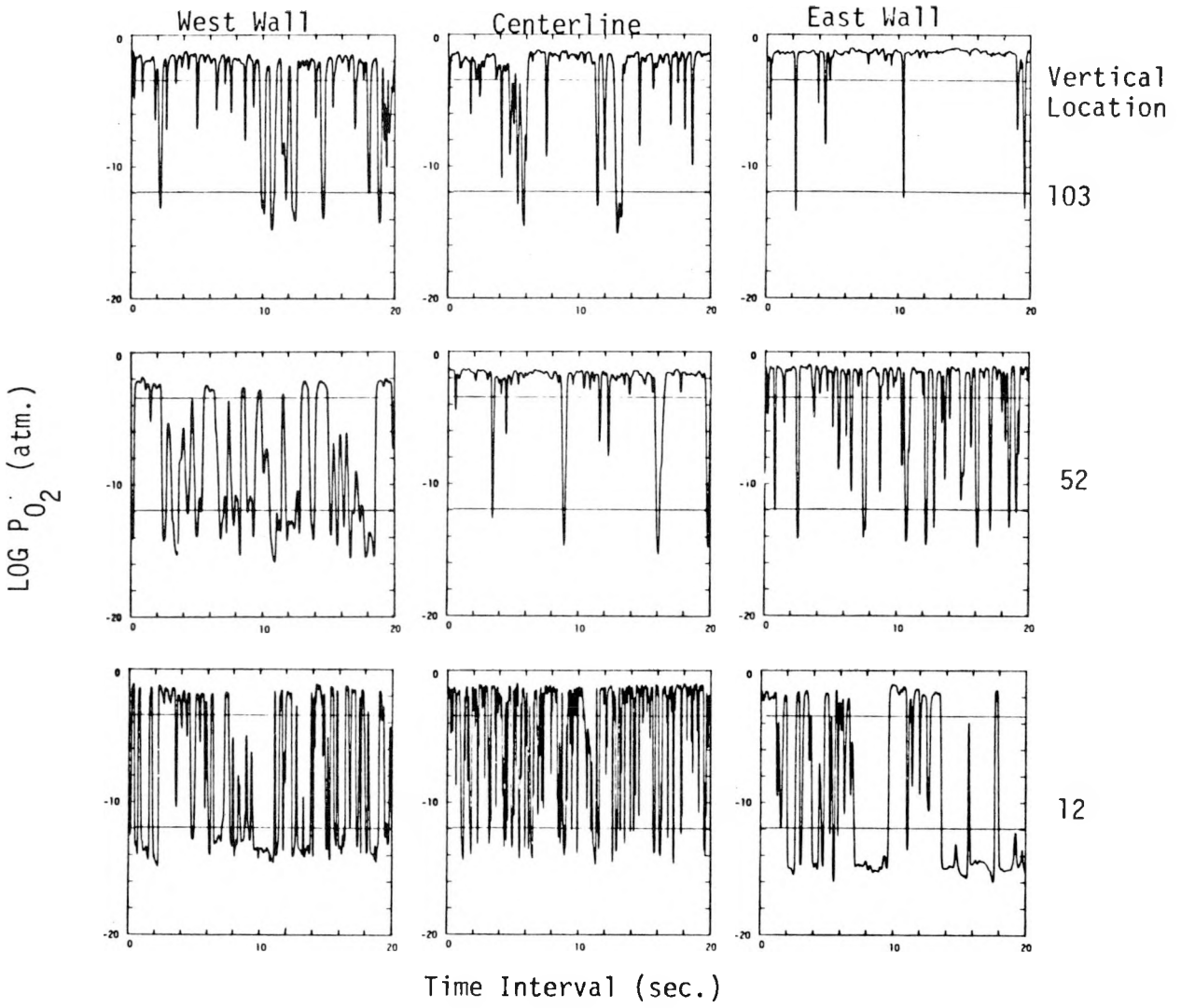


Figure 4-122. Oxygen Probe Output vs Time for Various Bed Locations During First 250-Hour Run (20% Excess Air)

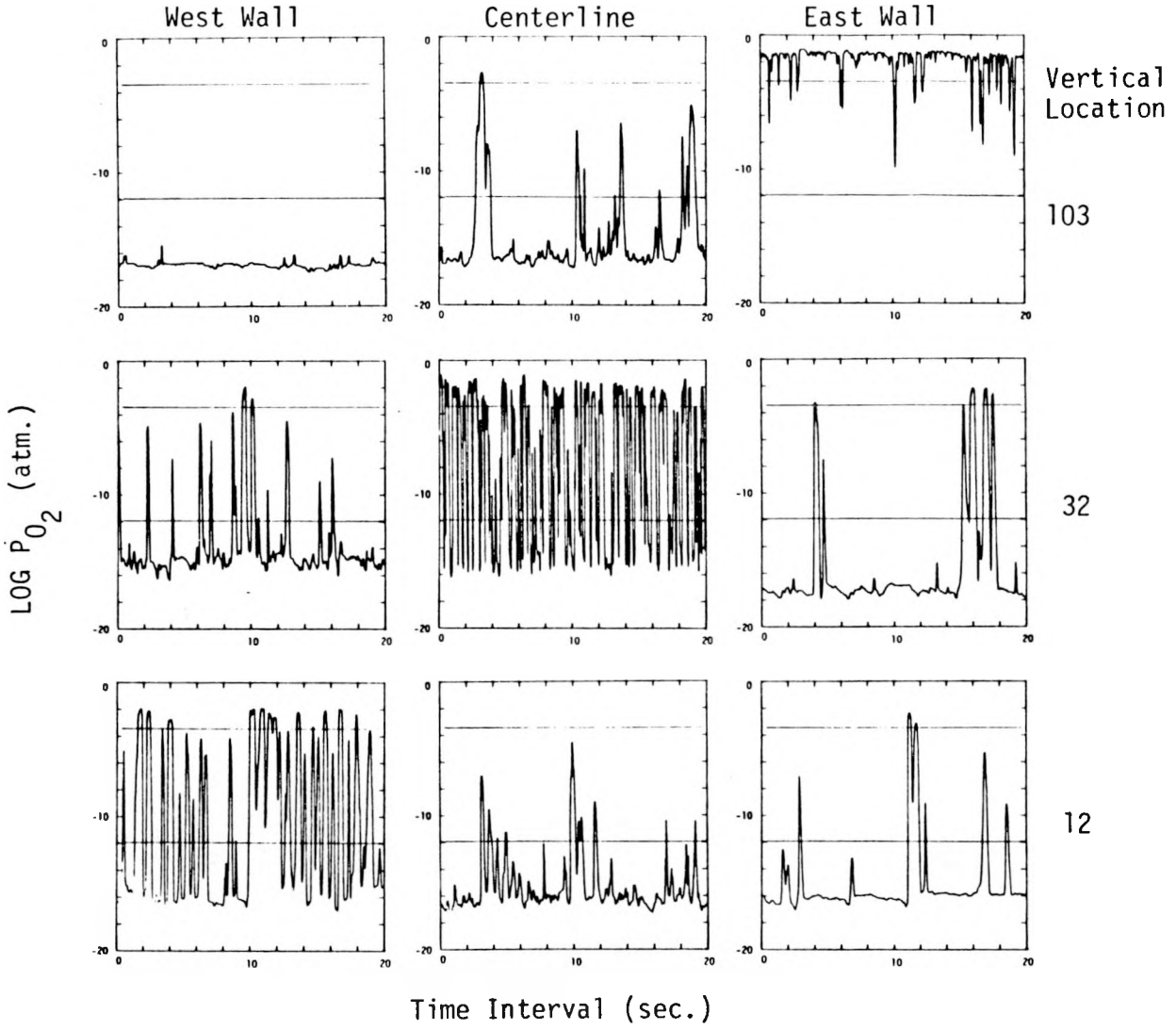


Figure 4-123. Oxygen Probe Output vs Time for Various Bed Locations During Second 250-Hour Run (0% Excess Air)

To provide better insight into how the fluidized bed environment varied w location, the data from the oxygen probe were manipulated into graphical representations illustrating the amount of time a particular location in the fluidized bed experienced excess air and/or substoichiometric conditions. The fraction of time spent above an oxygen partial pressure of 10^{-3} atm (i.e., flue gas from an excess air combustion process) was labeled XS Air and plotted as a function of the radial distance across the bed (for the various vertical probe locations). Likewise, the fraction of time spent below an oxygen partial pressure of 10^{-12} atm (i.e., flue gas from a substoichiometric combustion process) was labeled substoichiometric and plotted in a similar manner. These graphical representations of the oxygen probe data are illustrated in Fig. 4-124 for the three 250-hour runs. The fraction-of-time values and substoichiometric conditions i.e., a probability of encountering XS Air conditions equal to 0.75, means that particular location of the bed had an oxygen partial pressure greater than 10^{-3} atm for 75% of the time.

The following points summarize the data presented in Fig. 4-124 and help characterize the gaseous environment in the AFB:

- In general, as the amount of excess air (initially introduced with coal) decreased, the amount of time a particular location experienced excess air combustion conditions also decreased.
- The 50% excess air experiment (run 3) resulted in a flue gas with oxygen partial pressures that indicated excess air combustion conditions existed most of the time in every location of the fluidized bed. The main exceptions were those locations near the west wall, which experienced both excess air and substoichiometric combustion conditions.
- The 20% excess air experiment (run 1) resulted in a flue gas with oxygen partial pressures that also indicated excess air combustion conditions existed most of the time in every location of the fluidized bed. However, the amount of time substoichiometric combustion conditions existed increased (compared to the 50% excess air experiment), particularly in locations near the walls.

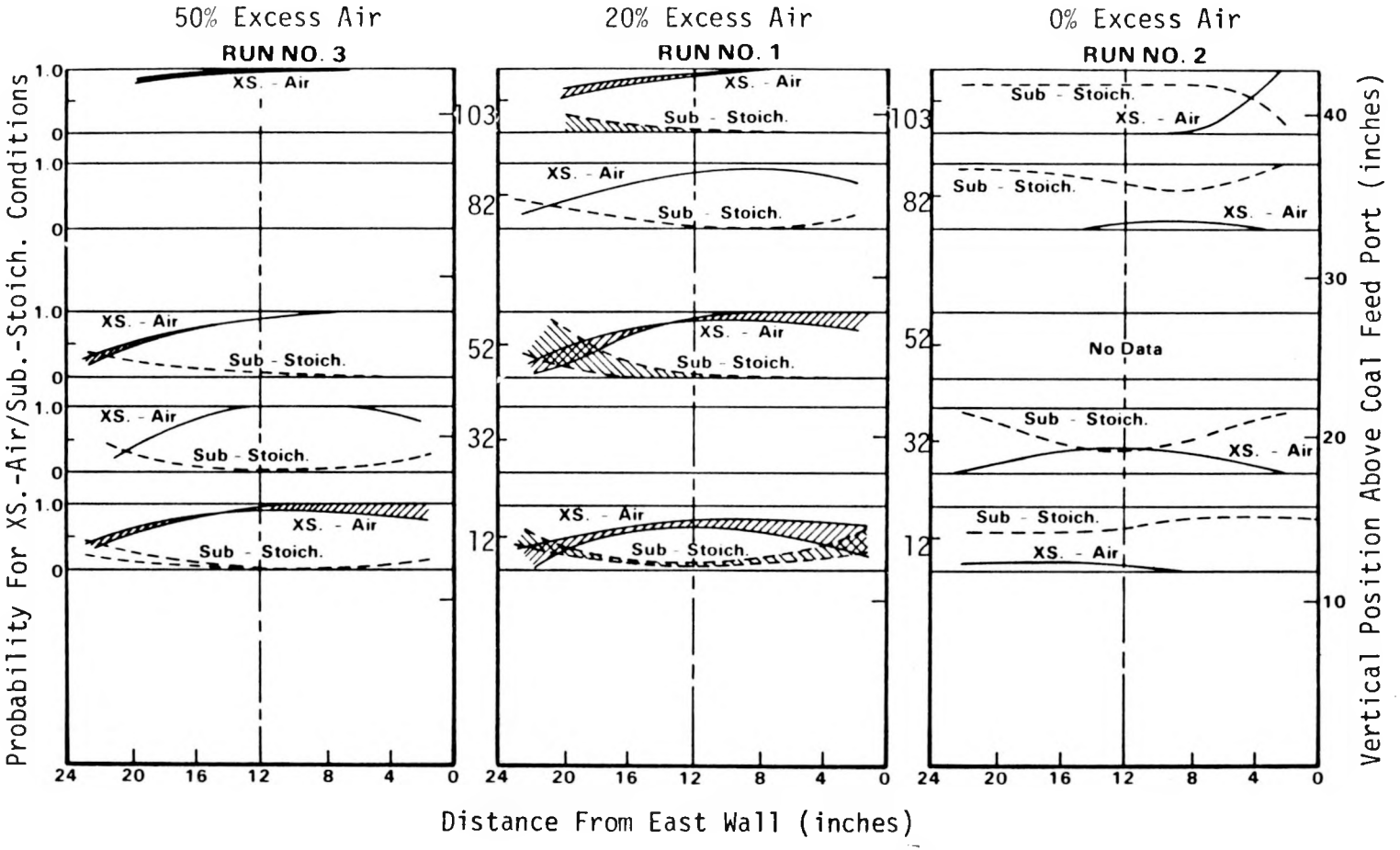


Figure 4-124. Summary of XS Air/Substoichiometric for the Various 250-Hour Runs as a Function of Bed Location

- The 0% excess air experiment (run 2) resulted in a flue gas with oxyg partial pressures that indicated substoichiometric combustion conditions existed most of the time in every location of the fluidized bed. The only exception was the centerline location at the bottom of the heat exchanger tube bundle (port 32), where the oxygen partial pressures indicate the combustion process hovered around exact stoichiometry, i.e., 50% of the time - excess air, 50% of the time - substoichiometric.

In summary, data from the oxygen probe provided important information concerning the characteristics of this particular fluidized bed. The data accurately characterized the chemical condition of the gaseous environment in terms of the oxygen partial pressure. This information is extremely important when evaluating the corrosion behavior of candidate alloys for the heat exchanger tubes. Variations in the oxygen partial pressure with location in the AFB indicated the gaseous environment in the fluidized bed was not as uniform as expected. Apparently, the mixing of coal and air was better at locations near the centerline of the fluidized bed, and often near the east wall. Alternatively, the mixing properties at locations near the west wall were not as good. Also, as the mixing time increased, i.e., as the coal, air, and flue gas progressed upward through the fluidized bed, the oxygen partial pressures corresponded more closely to those values expected, based on the initial air/fuel ratio.

In conclusion, the type of chemical condition (oxygen partial pressure) in a particular location in the fluidized bed was influenced strongly by the physical conditions characteristic of that location.

Implications for Corrosion of Heat Exchanger Materials. The average oxygen content of the in-bed environment when operating under excess-air operating conditions would be expected to be approximately 3 vol % or greater, which implies a relatively oxidizing environment, which might be expected to pose no exceptional corrosion threat to in-bed heat exchanger materials. The oxygen probe results, however, indicate that the in-situ oxygen partial pressure in the bed under these same "oxidizing" conditions could be as low as 10^{-14} atm. Previous corrosion experiments (Ref. 4-2, 4-12, 4-41, 4-42, 4-46, 4-52, and 4-58) in various fluidized bed coal combustors have indicated that some of the commercially availab

-at exchanger alloys can undergo very severe sulfidation attack within the -bed environment. Observations of such corrosion, however, have not been well correlated to bed operating or design variables. An issue of considerable interest in this program, therefore, is whether the regions where low oxygen partial pressures occur within the bed correspond to the locations where sulfidation attack has been observed.

The corrosive potential toward alloy systems of high-temperature gaseous environments containing oxidizing and sulfidizing species can be represented conveniently through the use of thermodynamic phase stability diagrams, (Ref. 4-54) although it should be realized that these apply strictly for equilibrium conditions, while high temperature corrosion processes are strongly influenced by competing kinetic processes. Nevertheless, corroding metal surfaces have good catalytic activity so that the assumption that local equilibrium conditions are attained is considered reasonable. Figure 4-125 presents the ranges of oxygen and sulfur partial pressures over which various phases in the Cr-O-S, Fe-O-S, and Ni-O-S systems are stable at 1650 F, the temperature of operation of the fluidized bed combustor. The lines drawn in these simplified diagrams corresponding to oxygen partial pressures of 10^{-12}, 10^{-13} and 10^{-14} atmospheres, typical of the lowest values measured by the in-situ oxygen probe, indicate that Cr_2O_3 is stable at all values of sulfur partial pressure, while iron sulfide is stable at sulfur partial pressures of 10^{-3}, 10^{-4}, and 10^{-5} atm, respectively, and nickel sulfide is stable above $10^{-7.8}$ atmospheres of sulfur.

All of the alloys tested in this research (except the FeCrAlY cladding) rely upon the formation of a chromium oxide (Cr_2O_3) scale for protection against accelerated oxidation and/or sulfidation. It should be emphasized that Cr_2O_3 is thermodynamically stable in all the fluidized bed environments characterized by the oxygen probe data. Therefore, all of the alloys tested would be expected to exhibit protective behavior when exposed to the flue gas from an excess air and/or substoichiometric combustion process. However, sulfides of many of the major alloying elements, particularly chromium sulfide, are thermodynamically stable beneath the Cr_2O_3 surface scale, provided sufficient sulfur (high PS_2) is transported to the alloy/oxide interface. The presence of discrete '-ernal chromium sulfides beneath Cr_2O_3 surface scales is expected and com-
when high-temperature alloys are exposed to oxidizing gaseous environments

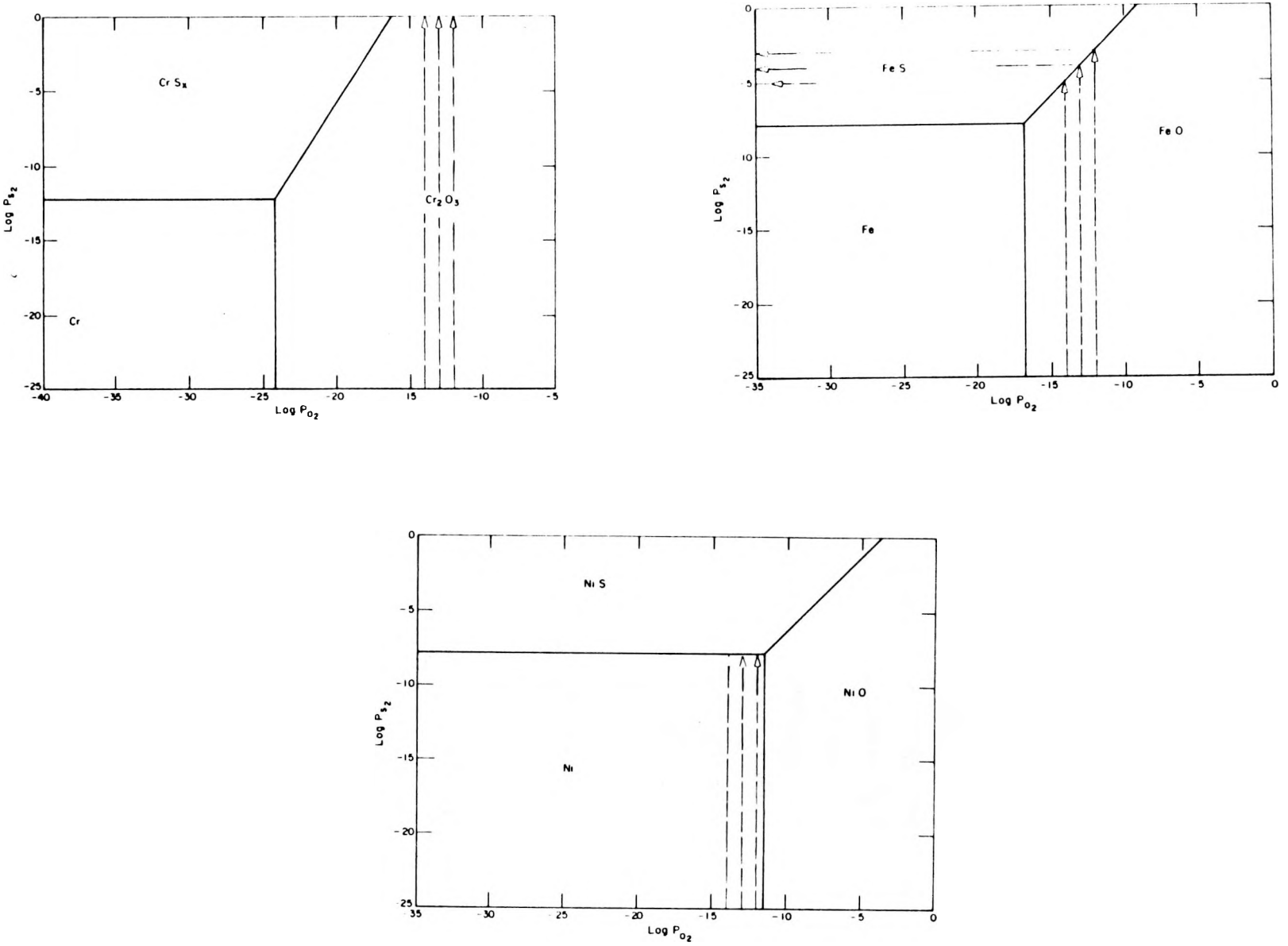


Figure 4-125. Phase Stability Diagrams for the Systems Fe-O-S, Ni-O-S, and Cr-O-S, at 1172 K, 1 ATM

ith high sulfur pressures. However, the continued formation and internal growth chromium sulfides (usually at the alloy grain boundaries) can deplete the alloy of chromium, the element necessary for protective scale formation. Sulfides precipitated along the alloy grain boundaries can also provide rapid diffusion paths for sulfur penetration further into the alloy.

Although oxides of all the major alloying elements are thermodynamically stable in the excess air environments, the sulfides of iron and nickel may be thermodynamically stable in the substoichiometric environments. Hence, their formation as external, solid, corrosion products on alloys exposed in these environments may be expected. These solid sulfides have highly defective structures and promote accelerated corrosion. In addition, these sulfides form low melting eutectics (especially nickel sulfide), and their presence as liquid corrosion products could result in catastrophic sulfidation attack.

CORROSION RESULTS

Descaling Data. The results from the descaling operations are presented (as weight-loss in mg/cm^2 vs distance into the AFB) in Fig. 4-126 through 4-137, in order of 50%, 20%, and 0% excess air and in order of increasing exposure time. Problems. of descaling-related pitting were encountered with specimens from probe No. 1, 2, 3, 5, 7, and 8, where uncertainties about the true weight changes could not be resolved satisfactorily, the data were rejected. The number and location of the corrosion probe, the amount of excess air, and the total exposure time also are given in each figure. Excess Air and Substoichiometric curves, generated from oxygen probe data taken from the same location as the corrosion probe, are presented below the weight-loss data. Beneath the oxygen probe data is the temperature profile of the air-cooled corrosion probe.

The weight-loss data represent the metal lost due to the descaling of the corrosion products (oxides, sulfides, and/or sulfates) formed on the exterior surface of the corrosion specimen during exposure in the AFB. The presence of internal corrosion products not connected directly to the exterior surface, i.e., as discrete precipitates in the alloy matrix, cannot be detected by the descaling operation. Therefore, their formation during exposure in the AFB is not reflected in the weight-loss data.

The following points summarize the data presented in Fig. 4-126 through 4-137:

- The weight-loss data from all three runs are within one order of magnitude. There appears to be no simple or direct correlation between the weight-loss data and the amount of excess air, although weight losses in substoichiometric conditions are among the largest measured. Apparently, the amount of external corrosion products formed during exposure in the 0% excess air experiment (run 2) was approximately equal (by weight) to the amount of external corrosion products formed during exposure in both the 20% and 50% excess air experiments.

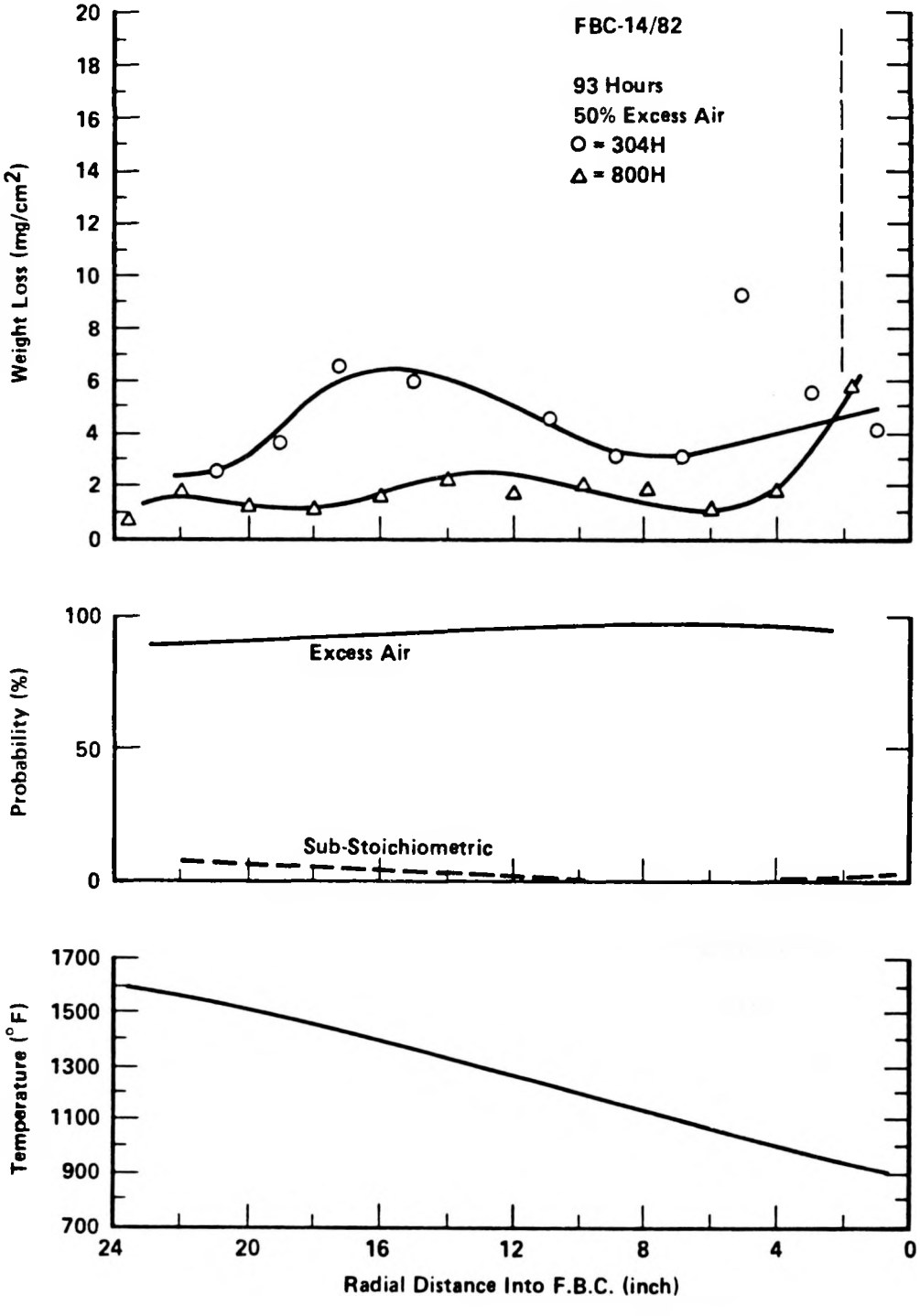


Figure 4-126. Plots of Weight-Loss Data, Probabilities for XS Air/Substoichiometric Conditions and Corrosion Probe Temperature vs Radial Distance into Fluidized Bed Combustor 50% Excess Air

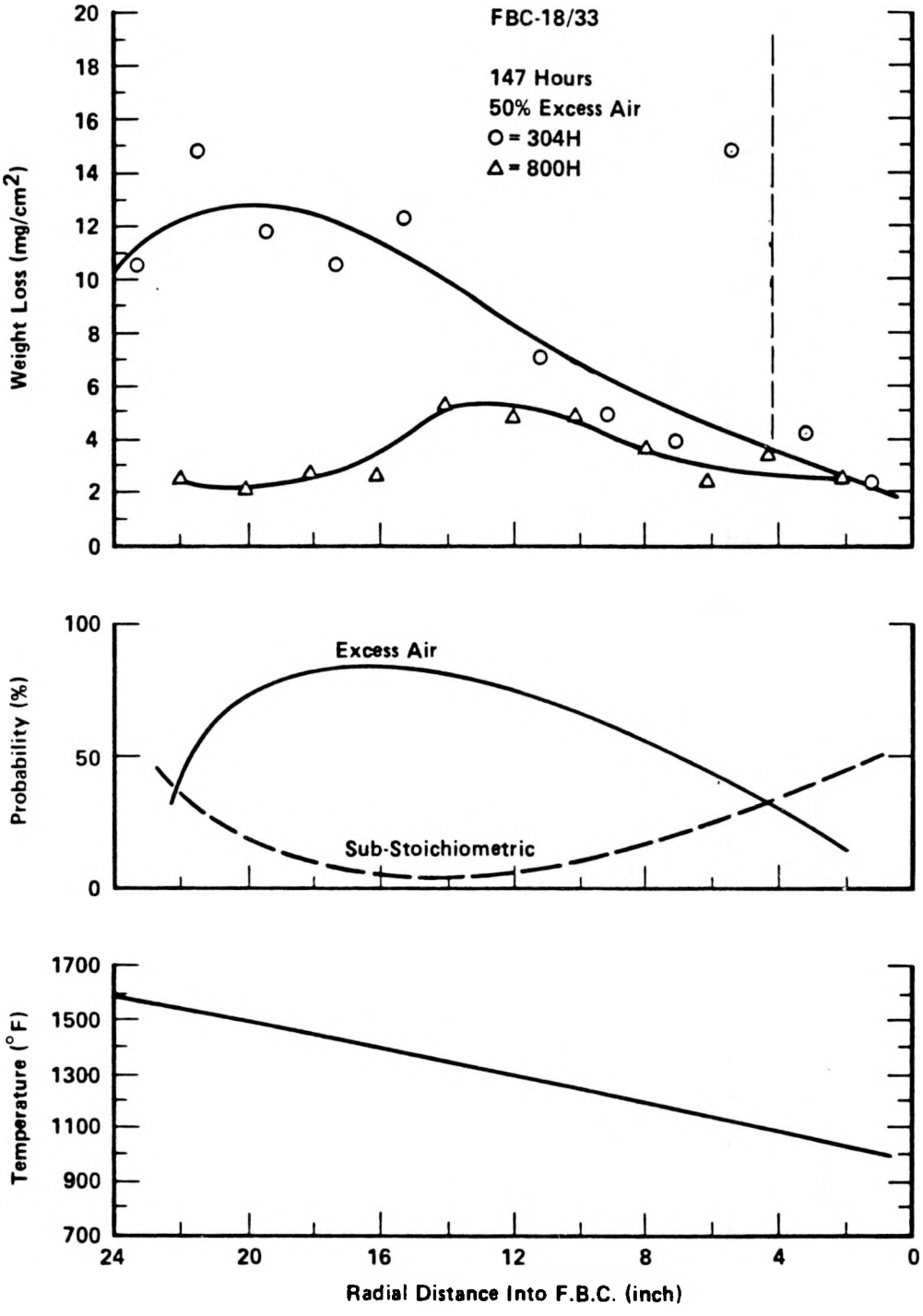


Figure 4-127. Plots of Weight-Loss Data, Probabilities for XS Air/Substoichiometric Conditions and Corrosion Probe Temperature vs Radial Distance into Fluidized Bed Combustor 50% Excess Air

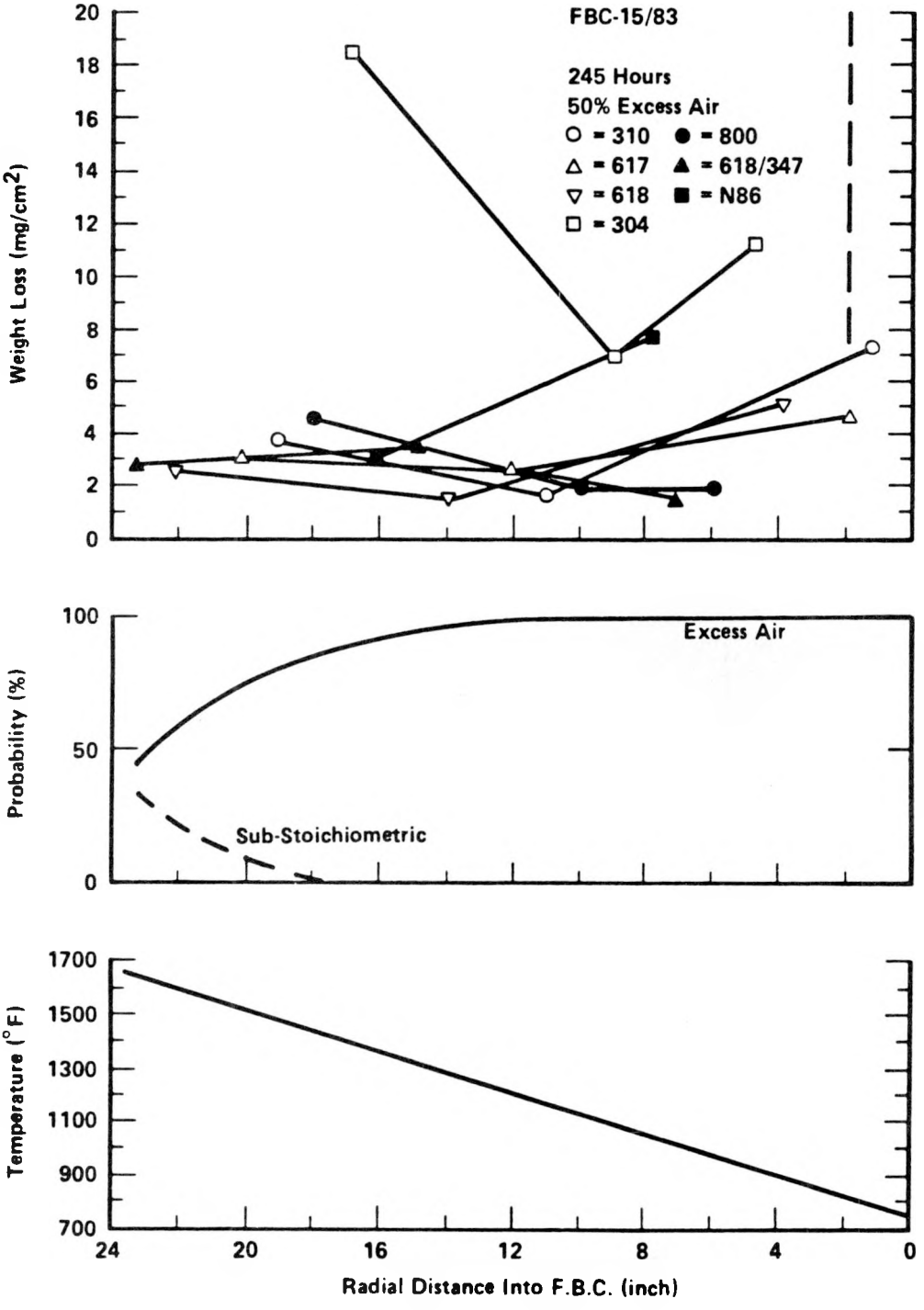


Figure 4-128. Plots of Weight-Loss Data, Probabilities for XS Air/Substoichiometric Conditions and Corrosion Probe Temperature vs Radial Distance into Fluidized Bed Combustor 50% Excess Air

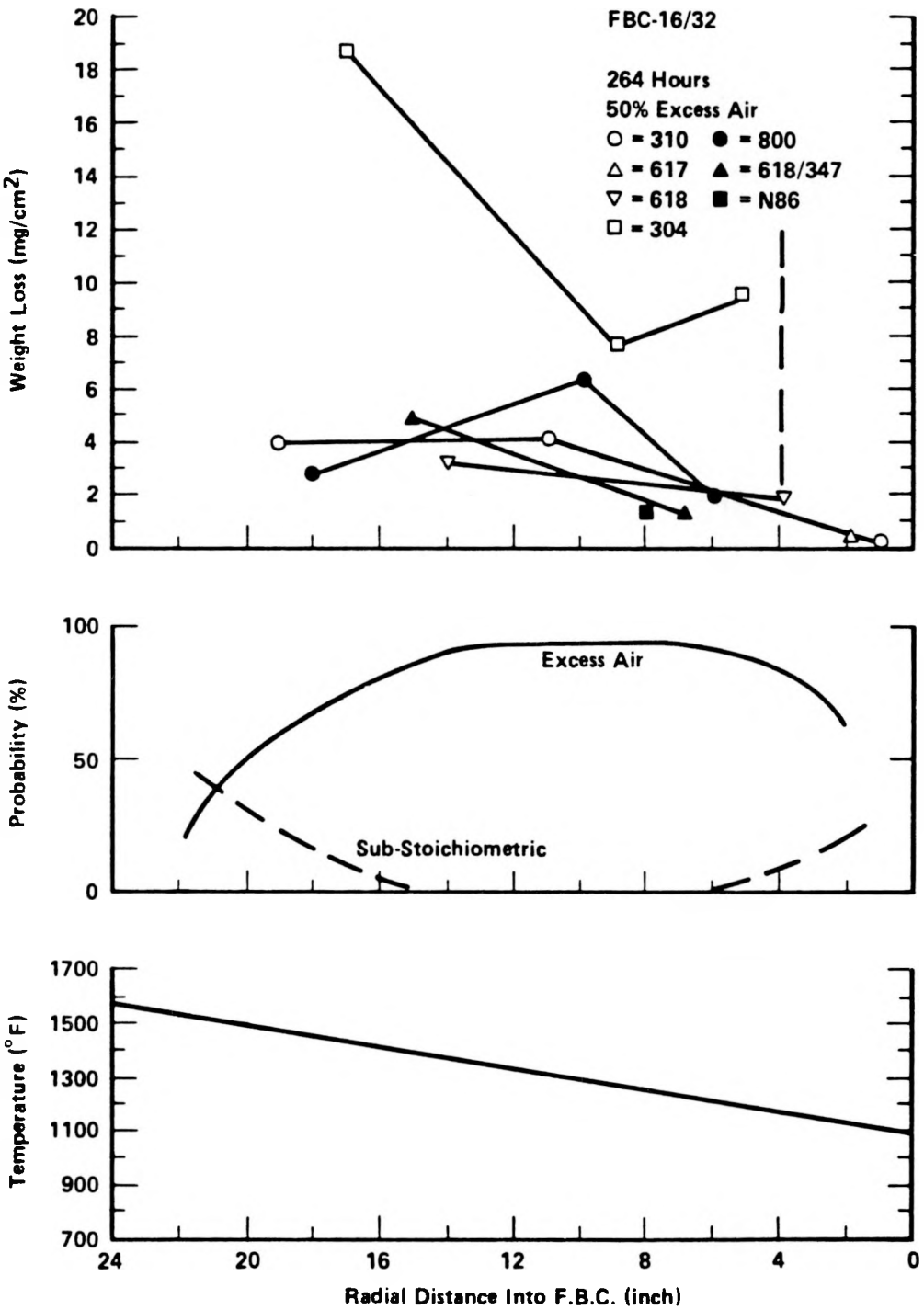


Figure 4-129. Plots of Weight-Loss Data, Probabilities for XS Air/Substoichiometric Conditions and Corrosion Probe Temperature vs Radial Distance into Fluidized Bed Combustor 50% Excess Air

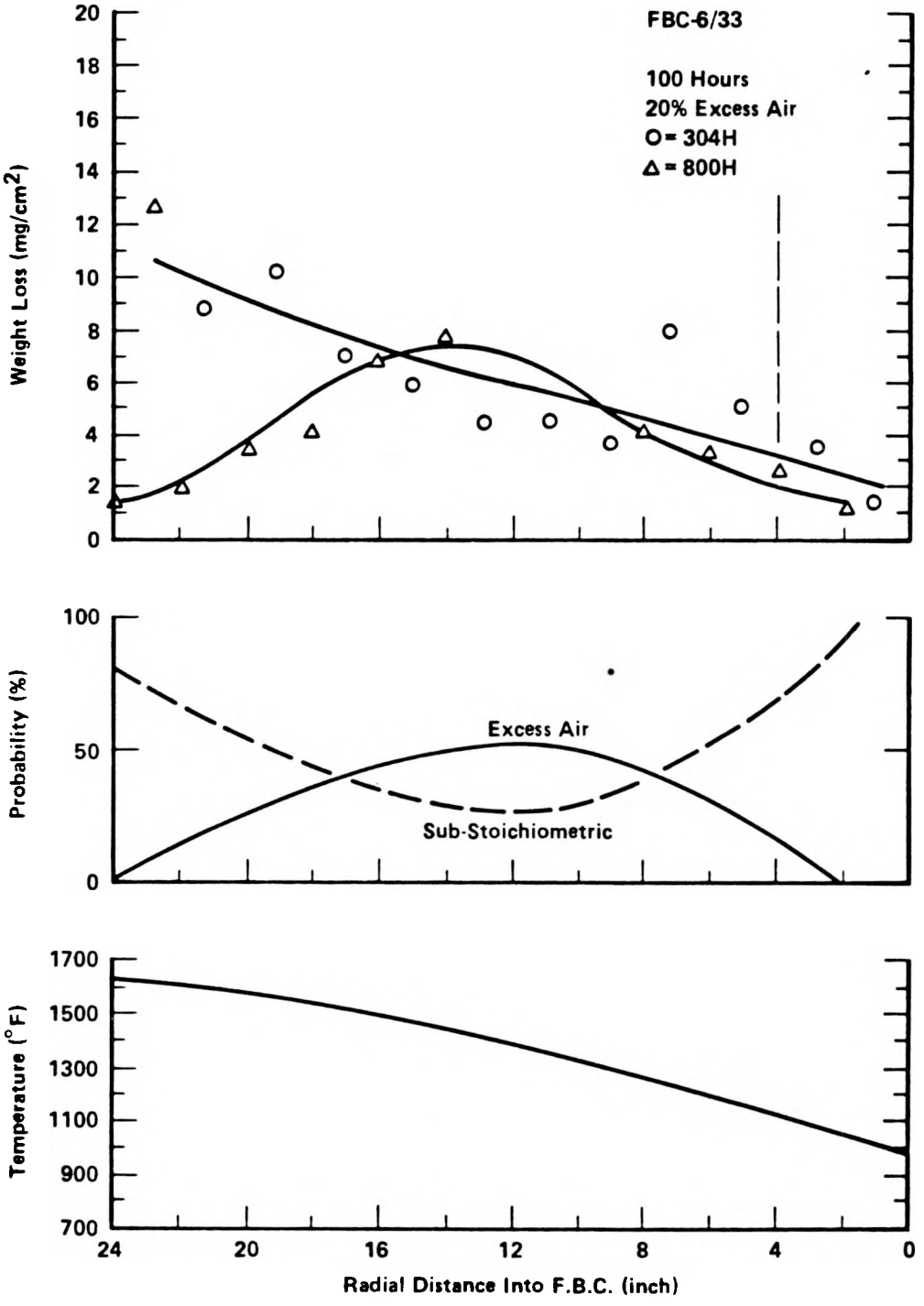


Figure 4-130. Plots of Weight-Loss Data, Probabilities for XS Air/Substoichiometric Conditions and Corrosion Probe Temperature vs Radial Distance into Fluidized Bed Combustor 20% Excess Air

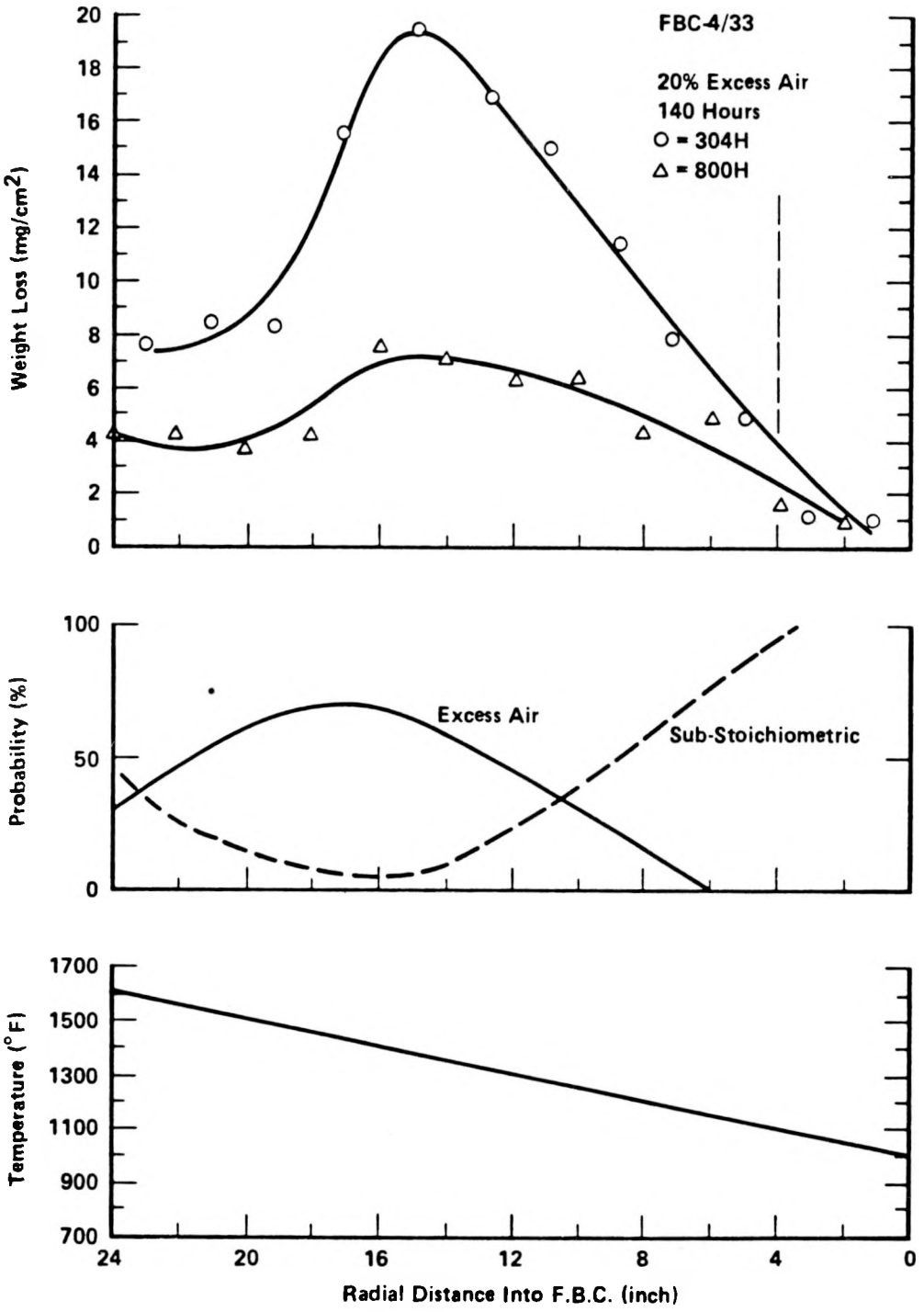


Figure 4-131. Plots of Weight-Loss Data, Probabilities for XS Air/Substoichiometric Conditions and Corrosion Probe Temperature vs Radial Distance into Fluidized Bed Combustor 20% Excess Air

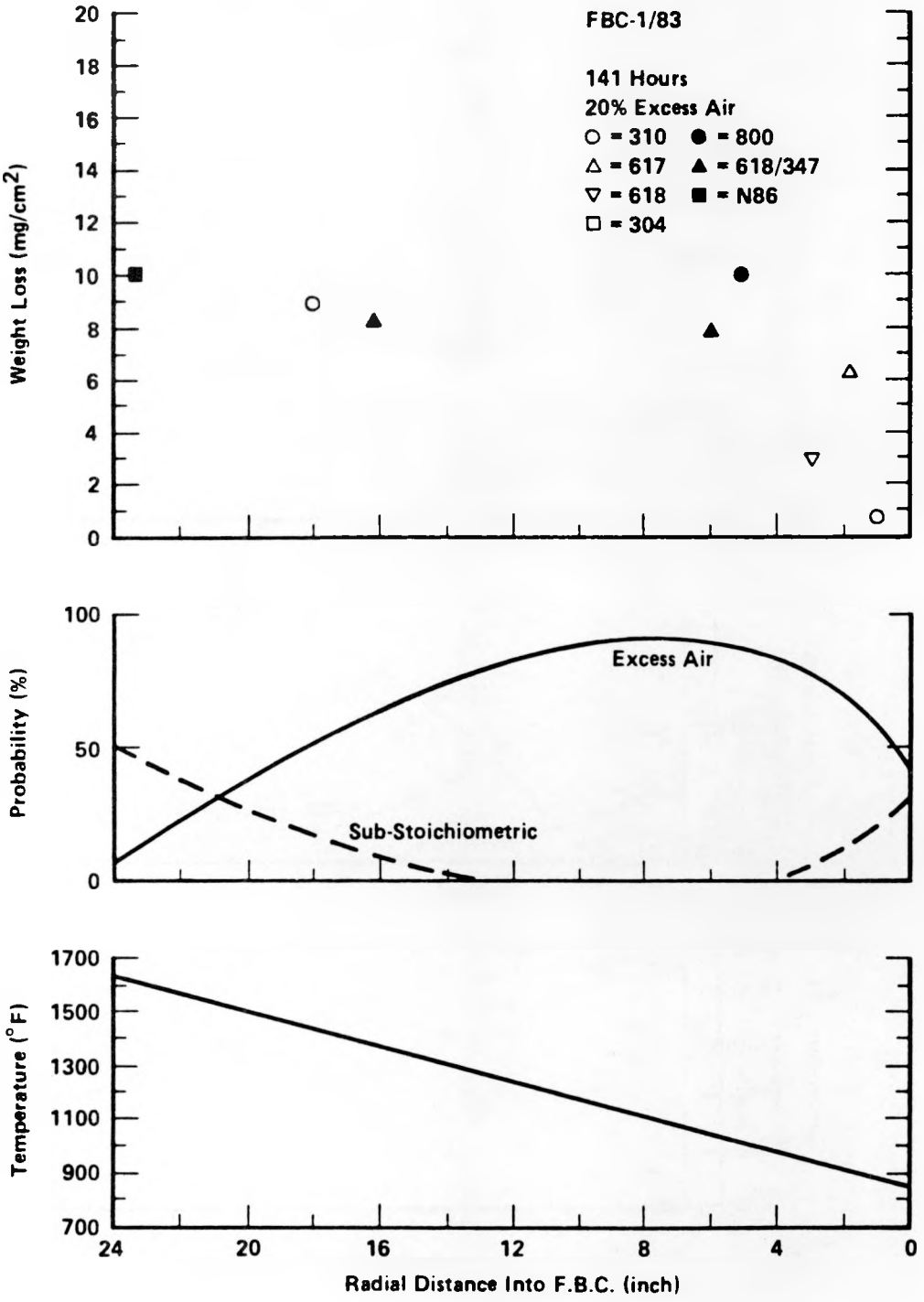


Figure 4-132. Plots of Weight-Loss Data, Probabilities for XS Air/Substoichiometric Conditions and Corrosion Probe Temperature vs Radial Distance into Fluidized Bed Combustor 20% Excess Air

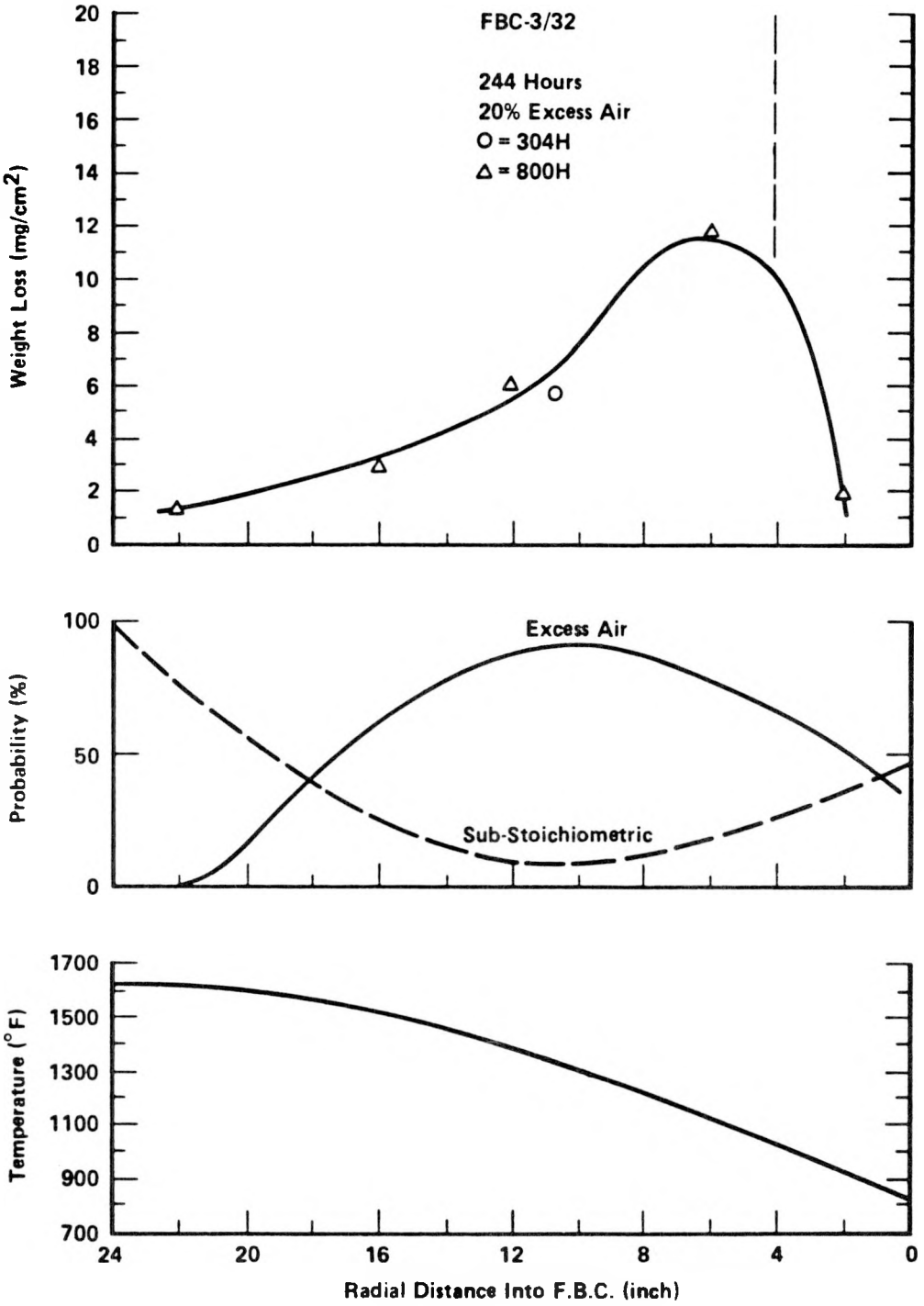


Figure 4-133. Plots of Weight-Loss Data, Probabilities for XS Air/Substoichiometric Conditions and Corrosion Probe Temperature vs Radial Distance into Fluidized Bed Combustor 20% Excess Air

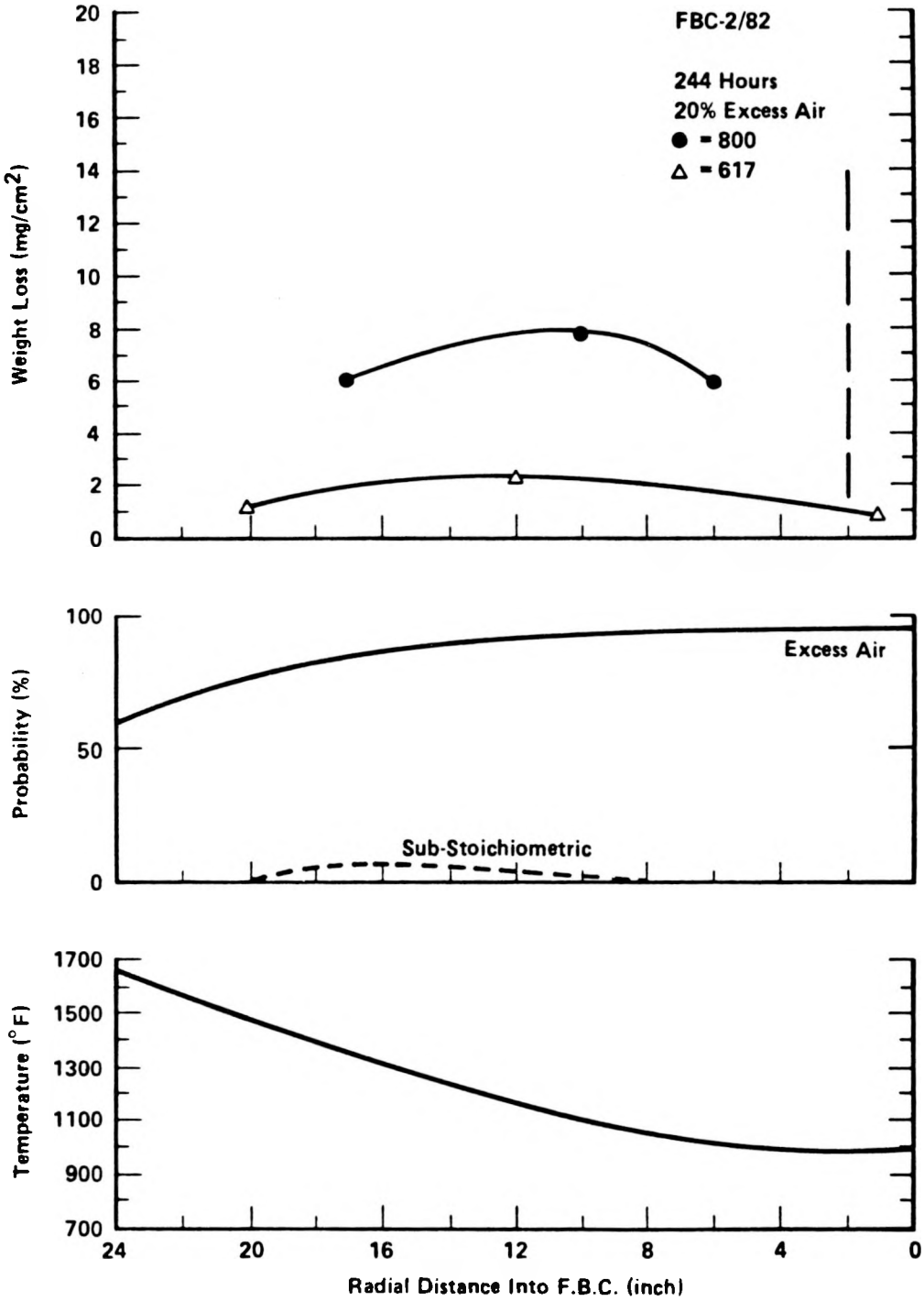


Figure 4-134. Plots of Weight-Loss Data, Probabilities for XS Air/Substoichiometric Conditions and Corrosion Probe Temperature vs Radial Distance into Fluidized Bed Combustor 20% Excess Air

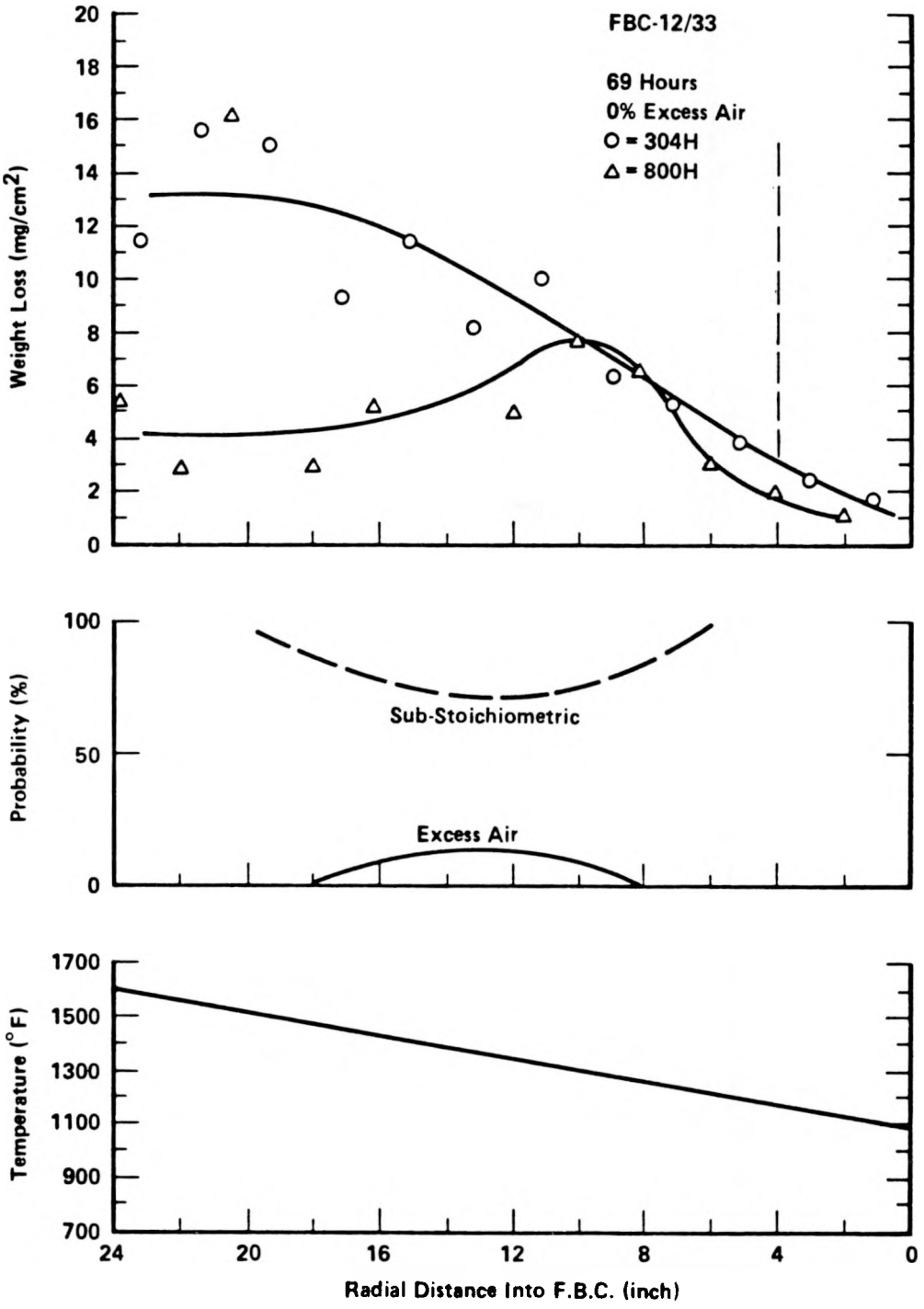


Figure 4-135. Plots of Weight-Loss Data, Probabilities for XS Air/Substoichiometric Conditions and Corrosion Probe Temperature vs Radial Distance into Fluidized Bed Combustor 0% Excess Air

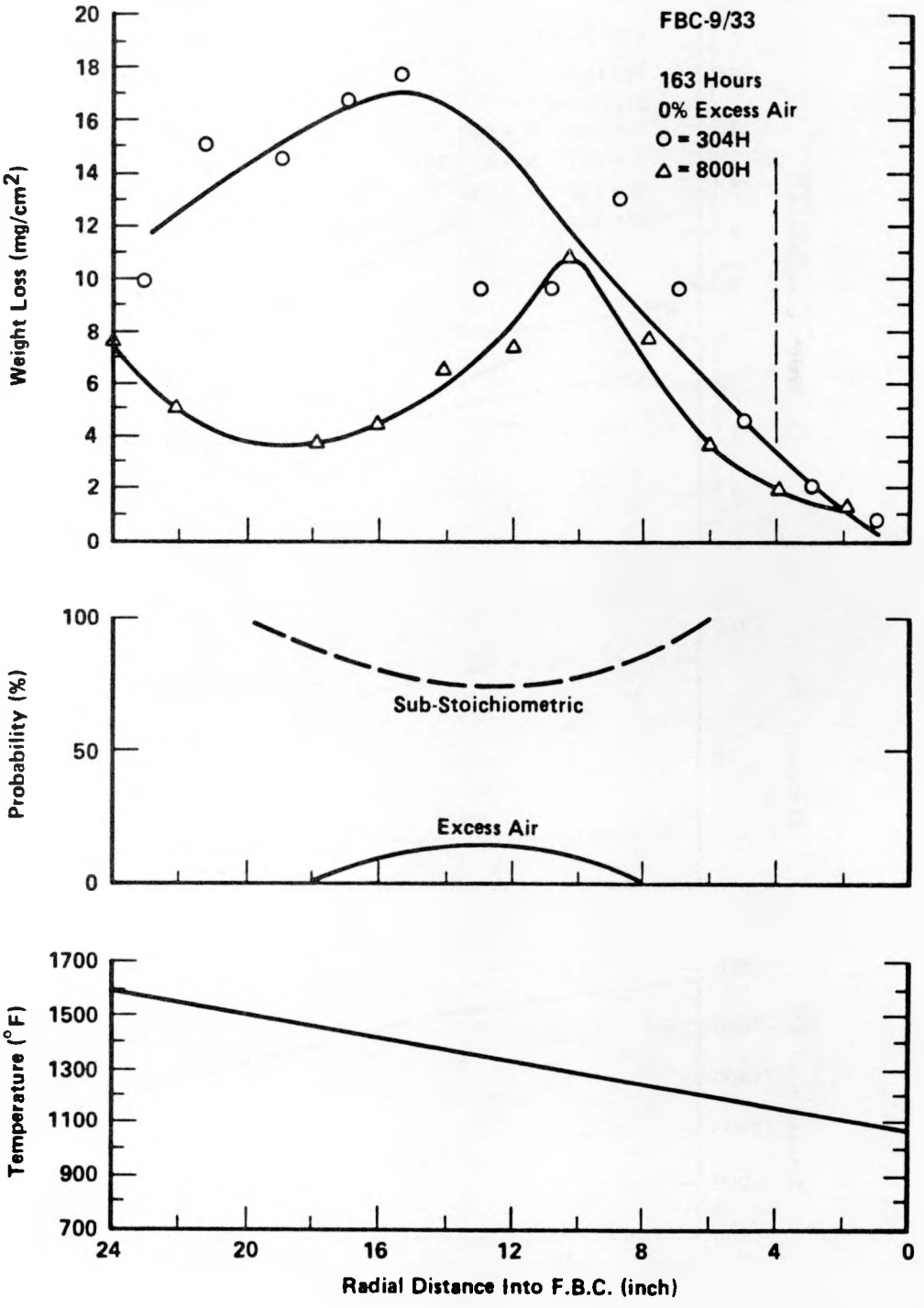


Figure 4-136. Plots of Weight-Loss Data, Probabilities for XS Air/Substoichiometric Conditions and Corrosion Probe Temperature vs Radial Distance into Fluidized Bed Combustor 0% Excess Air

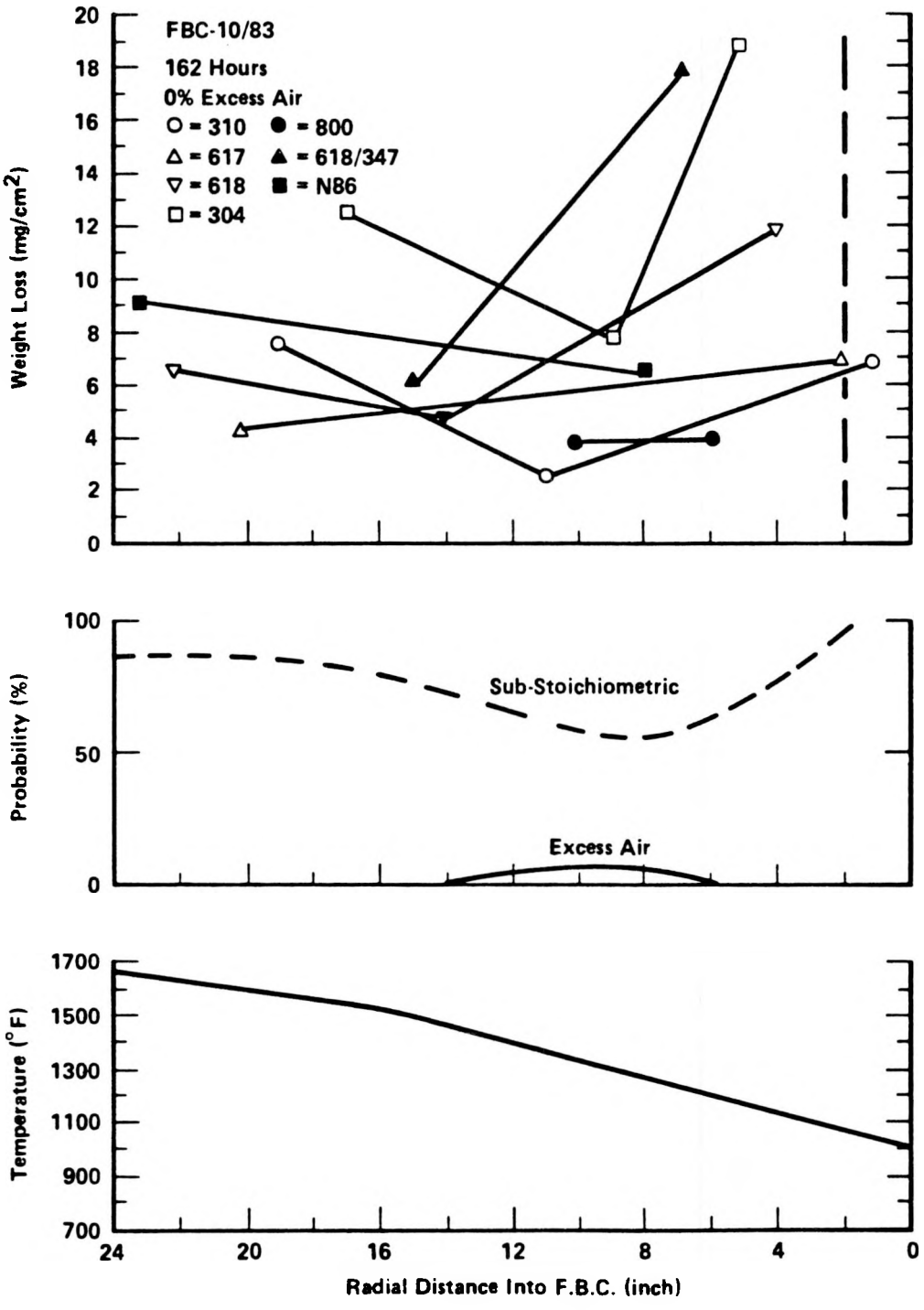


Figure 4-137. Plots of Weight-Loss Data, Probabilities for XS Air/Substoichiometric Conditions and Corrosion Probe Temperature vs Radial Distance into Fluidized Bed Combustor 0% Excess Air

- As the total exposure time increased, the weight-loss value for a particular alloy at a given location also increased. However, even after the 250 hour total exposure time, the magnitude of the weight-loss values was still relatively small, indicating that none of the alloys experienced catastrophic attack under these experimental conditions. (As will be discussed later, metallographic examination showed that some of the alloys had experienced the early stages of sulfidation which, while not contributing significantly to the weight-loss data at this stage, would be expected to develop into significant corrosion problems during prolonged exposures under the same conditions.)

- The weight-loss curves for the corrosion probes using only alloys Incoloy 800 and AISI 304 (binary probes) exhibited a bell-shaped trend with distance across the bed. These alloys usually suffered the highest weight-loss values at locations near the centerline of the bed, and the lowest weight-loss values at locations near the walls. (Similar trends toward increased metal loss along the centerline have been observed during other experiments in small fluidized bed combustors [Ref. 4-55]).

It was concluded earlier that the oxygen probe data from the AFB provided information that revealed the extent of mixing between the coal and air. The good mixing properties characteristic of locations near the centerline suggest the motion of all the bed materials (coal, limestone, gas) was very turbulent in these areas. Similarly, the poor mixing properties characteristic of locations near the walls suggest the motion of the bed materials was less turbulent than in the center. Visual observation of the exposed corrosion probes suggested that the vigorous motion of the bed materials mechanically influenced the corrosion behavior of the alloy specimens. This is illustrated in Fig. 4-138. These photographs show grooves and pits on the surface of many of the ring specimens, which indicate cutting or chipping of the deposit and corrosion products occurred during exposure. These grooves and pits appear only on the bottom half of the ring specimens, where the heat exchanger tubes (corrosion probes) impede the upward motion of the bed materials. Ring specimens exposed at locations near the centerline of the bed (presumably areas of good mixing or turbulence) experienced more mechanical attack than the ring specimens exposed at locations near the walls (less turbulence). This mechanism of mechanical attack resulted in

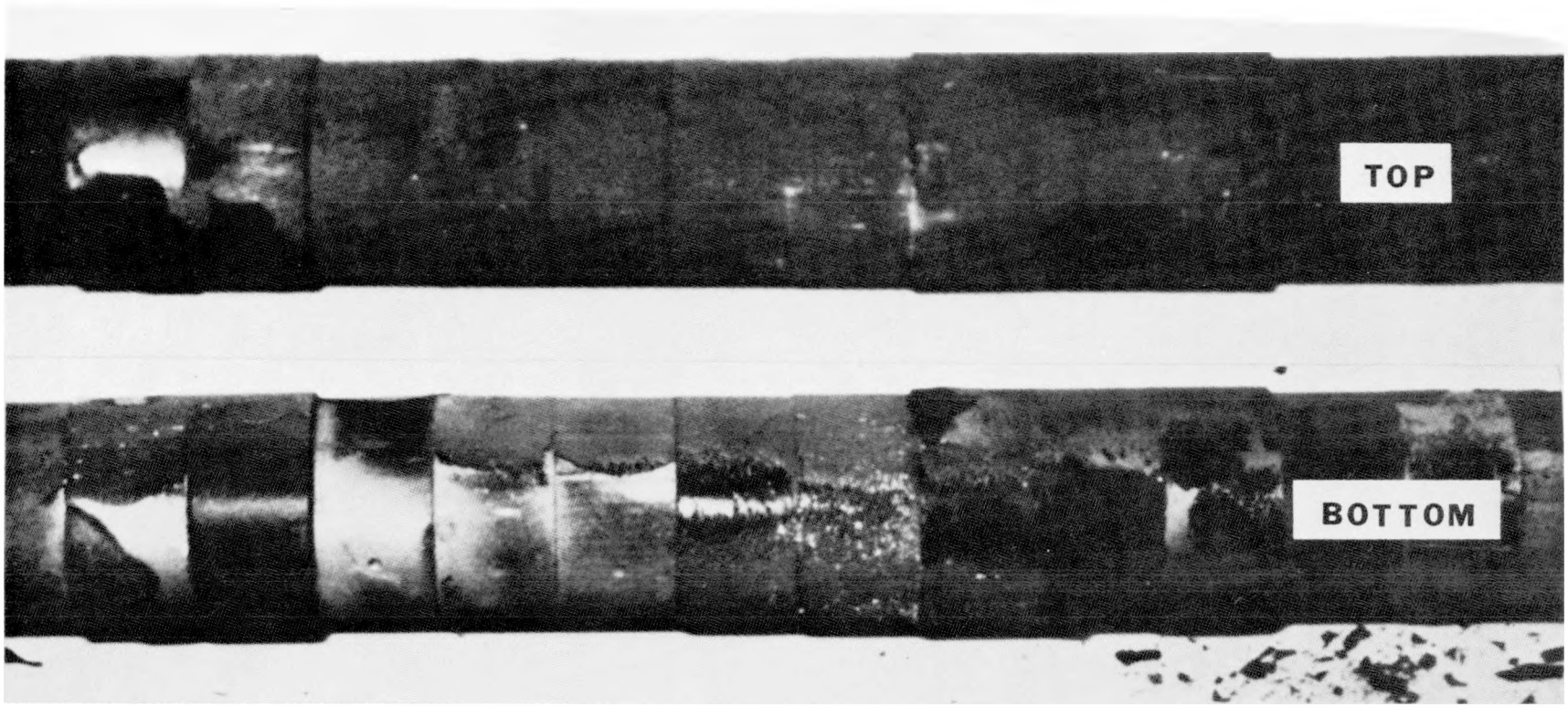


Figure 4-138. Surface Appearance of Exposed Corrosion Probe

significantly higher weight-loss values, compared to specimens that experienced corrosion only, and can explain the bell-shaped weight-loss curves. This corrosion/erosion mechanism, and its influence on alloy behavior, is discussed in more detail in the metallographic analysis section of this report.

It is difficult to develop a straightforward interpretation of the weight-loss data in terms of the corrosion behavior of the alloys for specimens exposed at different temperatures. The diffusion of alloying elements, the stability of various compounds, and the actual reaction rates are influenced significantly by the metal temperature. Therefore, comparision of weight-loss data without corresponding metallographic data from two alloy specimens that had significant temperature differences could be very misleading. Also, the descaling procedure does not qualitatively evaluate the corrosion behavior of a particular alloy. First, it does not characterize the corrosion product morphology, i.e., what was descaled (oxides? sulfides? etc.) was not determined. Secondly, the formation of internal corrosion products, which may be more deleterious than external corrosion products, was not detected during the descaling procedure. Because of these uncertainties in the weight-loss data, a detailed metallographic examination of selected alloy specimens was conducted. The results from the metallographic analysis, which support the oxygen probe and weight-loss data, are summarized later in this section.

Comparison With Published Data. In an attempt to evaluate the relevance of the descaled corrosion data, all the data points for two alloys, AISI 340H and Incoloy 800H, were plotted out for comparison with data from the literature. All the corrosion data were converted to common units of 10^{-3} μm/hr. In the case of the BCL data, which were weight losses after descaling, average thickness of metal loss was calculated by:

$$\text{Average metal loss} = \frac{10\Delta W}{p.t} \ (10^{-3}\mu m/hr)$$

where

W is the weight change (mg/cm^2)
p is the alloy density (g/cm^3)
t is the run duration (hour)

This assumes the metal loss to be uniformly distributed around the specimen circumference and, hence, could underestimate the loss by as much as a factor of 3 in cases where localized attack, such as erosion, occurs. No attempt has been made to adjust these data for specimens where erosion was thought to have played a role.

The corrosion data from the literature were selected from work in which measurements of corrosion penetration had been made. As far as could be determined, these measurements describe the depth of penetration of visible corrosion products beneath the metal surface after the corrosion exposures. Since such measurements apparently do not include the thickness of metal actually removed (penetration should be measured from the original metal surface), then there is probably an underestimation of total attack here also. These data are represented as maximum depth of affected metal, in 10^{-3} m/hr.

The various results for AISI 304H are plotted in Fig. 4-139 and 4-140, and for Incoloy 800H in Fig. 4-141 and 4-142. Included in the 304 plots are data for alloys 347 and 310. The majority of the data points are for cooled tube/ring specimens; where uncooled coupons were used, these are indicated. All the corrosion data were collected in atmospheric pressure fluidized bed combustors. A yardstick by which these data might be judged is that attributed to the Central Electricity Generating Board in the United Kingdom, which sets a tube wastage limit of $30\mu g/cm^2$ hr, or $0.038\mu m$/hr, or 38 on the ordinate used here. A note of caution, however, is that this criterion assumes that the material degradation is a linear function with time, whereas many high-temperature corrosion reactions exhibit rates that decrease with time. In this context, the points marked A (1000-hour results) and C (2000-hour results) might be more pertinent. Details of the bed operating conditions for the data listed in Fig. 4-141 and 4-142 are listed in Table 4-42. Table 4-24 shows the bed location and type of corrosion probe referred to in Fig. 4-140 and 4-142.

The literature data for AISI 304 (and 347 and 310) show an overall trend to steeply rising corrosion loss with increasing temperature (Fig. 4-139). Substoichiometric conditions do not appear to be obviously more aggressive than excess air, while there is some indication that limestone-free beds promote reduced corrosion, at least to 1300 F. Most of the data are for 250-hour tests,

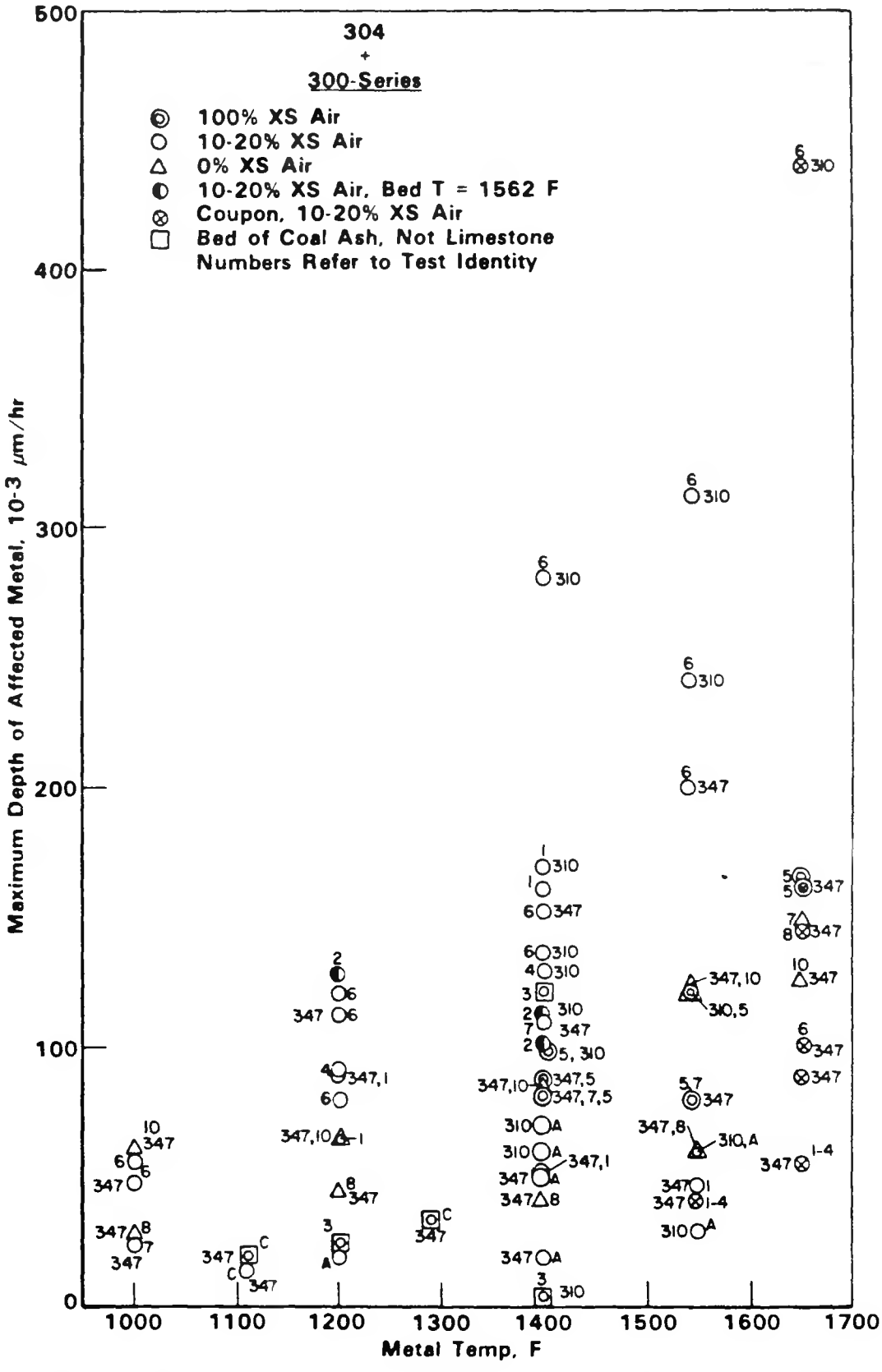


Figure 4-139. Fluidized Bed Combustor Data from the Literature for 300-Series Stainless Steels

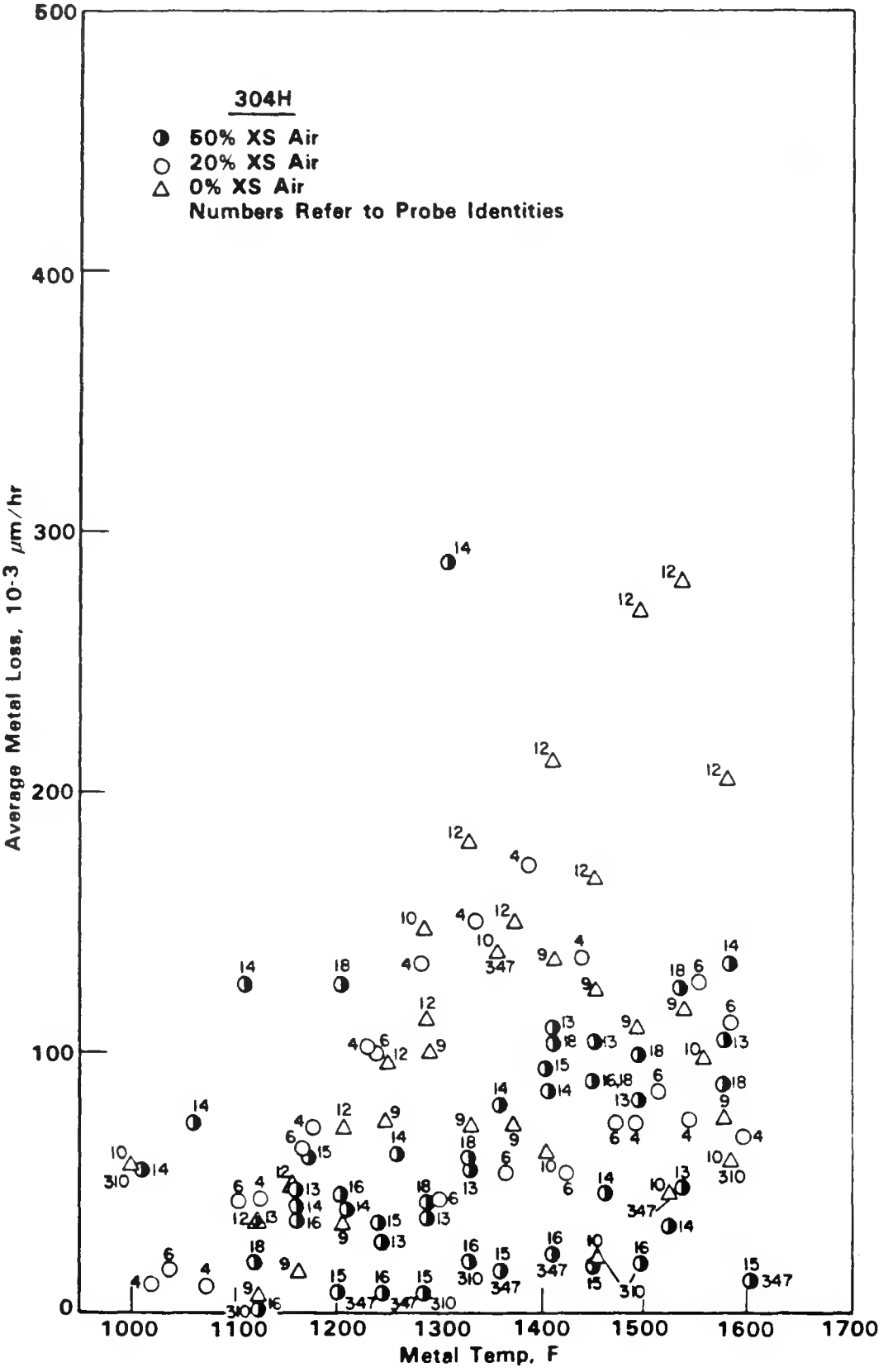


Figure 4-140. BCL 24-Inch Bed Corrosion Data for 304H

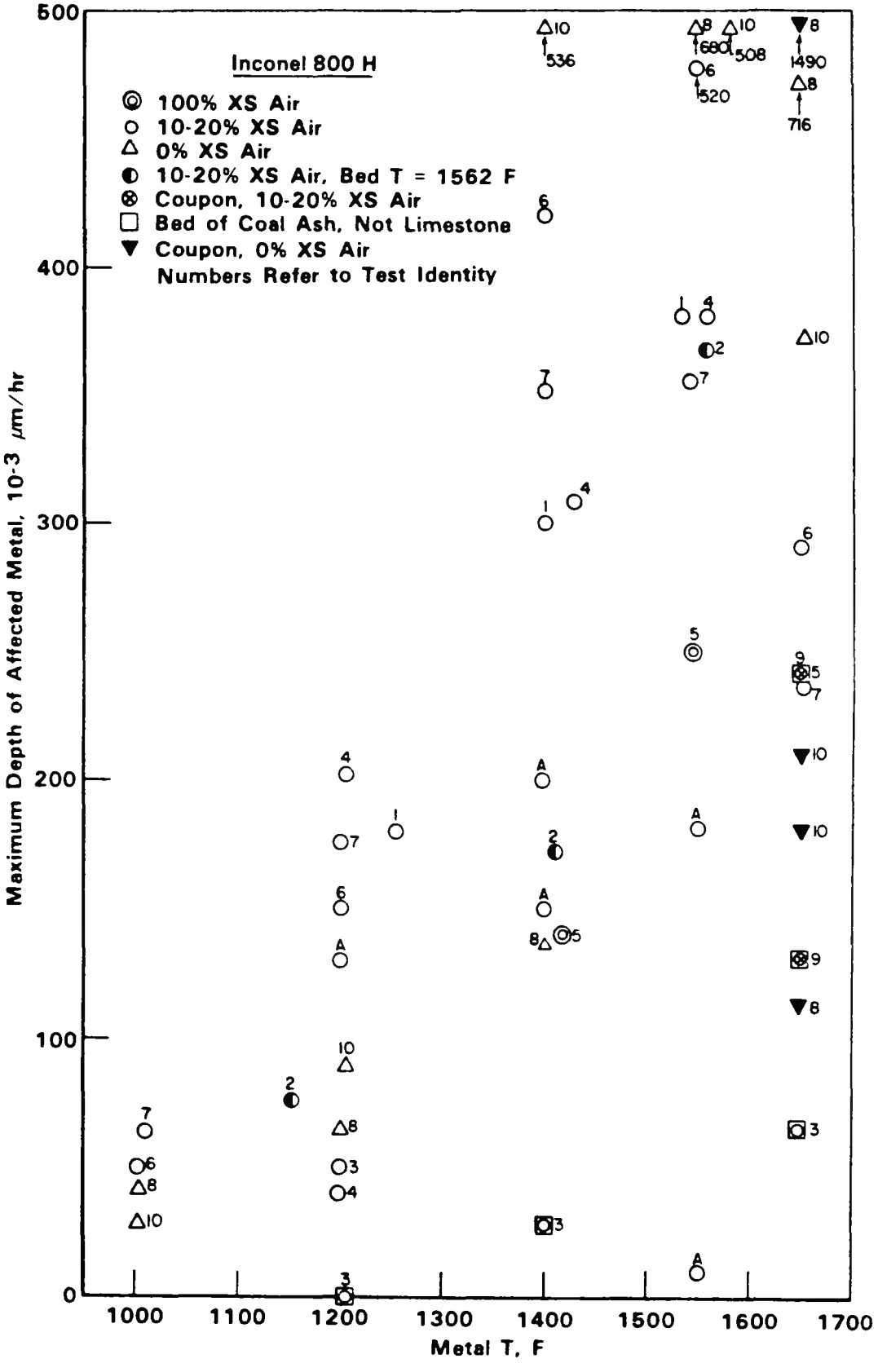


Figure 4-141. Fluidized Bed Combustor Corrosion Data from the Literature for Incoloy 800

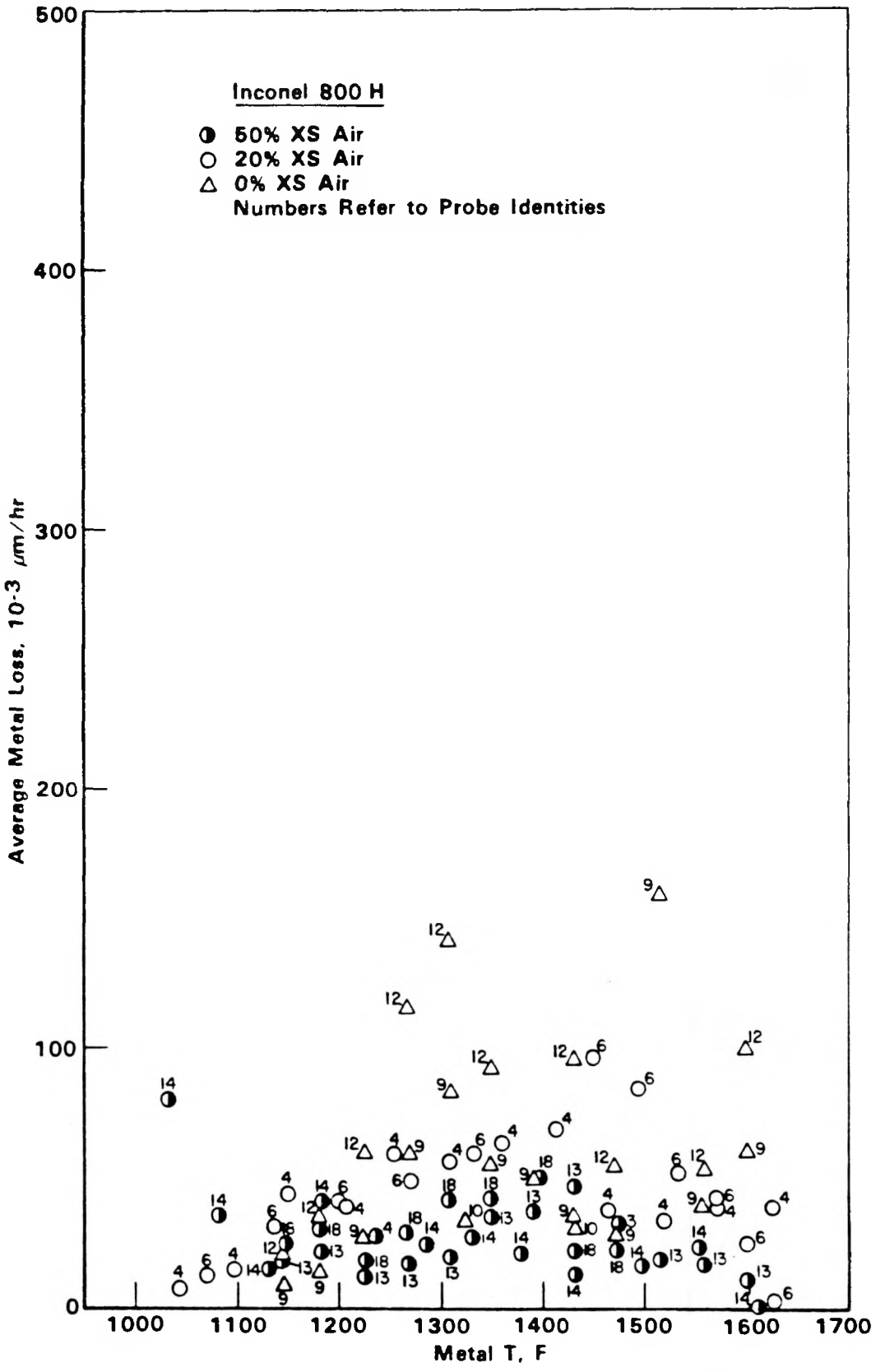


Figure 4-142. BCL 24-Inch Bed Corrosion Data for Incoloy 800H

TABLE 4-42. INDEX TO COMBUSTION CONDITIONS USED ON CORROSION RUNS

	Test 1	Test 2	Test 3	Test 4	Test 5	Test 6	Test 7	Test 8	Test 9	Test 10	A	B	C	D	E
Pressure	Atmospheric	Atmospheric	Atmospheric	Atmospheric	Atmospheric	Atmospheric	Atmospheric	Atmospheric	Atmospheric	Atmospheric	Atmospheric	Atmospheric	Atmospheric	Atmospheric	Atmospheric
Bed temp. (°F)	1652	1562	1652	1652	1652	1652	1652	1652	1652	1652	1652	1652	--	--	--
Fluidising velocity (Fe/sec)	3	3	3	3	3	3	3	3	3	3	3	3	--	--	--
Excess air level (%)	10-20	10-20	10-20	10-20	100	10-20	10-20	0	10-20	10-20	10-20	10-20	--	--	--
Coal	Illinois No. 6	Illinois No. 6	Illinois No. 6	Illinois No. 6	Illinois No. 6	Eccles (UK)	Illinois No. 6	Illinois No. 6	Wellbeck (UK)	char (from Illinois No. 5)	Illinois No. 6	Illinois No. 6	Humphrey No. 7	Humphrey No. 7	Humphrey No. 7
Limestone	Penrith (UK)	Penrith (UK)	None	Wenlock (UK)	Penrith (UK)	Penrith (UK)	Plum Run Dolomite	Penrith (UK)	None	Penrith (UK)	Penrith (UK)	Penrith (UK)	None	Limestone	Limestone
Ca/S Mole ratio	3	3	--	3	3	3	3	--	--	3	3	3	--	--	--
SO_2 emission (ppm)	--	--	--	--	354	378	319	357	1170	460	369	340	--	--	--
Duration (hr)	250	250	250	250	250	250	250	250	250	250	1000	1000	500	500	1000
Reference	27	27	27	27	22	22	22	28	28	28	13	13	22	22	22

and do little to discriminate between 304, 347, and 310. The longer-term data (1000-hour marked A, 2000-hour marked C) are in general at the lower corrosion rate end of the scatter plot and suggest that the corrosion performance of these alloys, in nominally oxidizing conditions may be satisfactory up to 1544 F.

The corrosion data for 304H from the BCL 24-inch bed, shown in Fig. 4-140, also exhibit a sharp increase in metal loss with increasing temperature. With the exception of a few points, an overall trend for the specimens exposed in the sub-stoichiometric run to exhibit the greatest metal loss is apparent; the behaviors of the 20 and 50% XS air specimens are less easy to discriminate. The data for the few specimens of 347 (powder metallurgy cladding) and 310 are at the low end of the scatter band for excess air conditions and also show some tendency to increased metal loss in the substoichiometric run.

The Incoloy 800 data from the literature show an overall trend to greatly increased corrosion with increasing metal temperature (Fig. 4-141). Ring specimens in a bed run without limestone showed excellent corrosion behavior, whereas coupons in a similar run, but located near the combustor wall, were heavily attacked (Ref. 4-2). The few data for 100% XS air runs did not suggest any obvious beneficial effect. Specimens in substoichiometric conditions did not necessarily corrode to any greater extent than those in nominally oxidizing conditions.

In contrast, the BCL data (Fig. 4-142) show a marked trend to increased corrosion under substoichiometric conditions, while the lowest, corrosion rates generally corresponded to the highest excess air conditions (50%) used in the test series. The trend with temperature of these data is somewhat obscured by an observed mechanical/erosion effect in the center of the bed, which corresponds to the location of specimens with temperatures in the range of 1250 to 1450 F.

Metallographic Analysis. Two of the corrosion probes exposed in the AFB were not descaled so that qualitative information about the corrosion product morphologies could be obtained through metallographic examination.

Binary Alloy Probe. The binary alloy corrosion probe used for this purpose was exposed for 115 hours during the 50% excess air experiment at location No. 33. Visual examination of the exposed corrosion probe suggested that the bottom half of the ring specimens located near the center of the probe had been attacked mechanically (Fig. 4-138). Metallographic examination of selected ring specimens provided more evidence of the nature of this erosion mechanism. Figures 4-143 and 4-144 show the corrosion morphologies of specimens of 304H and 800H, respectively, at different locations along the probe. Note that there is a significant difference between the top (downstream) side and the bottom (upstream) side of the specimens. The external scales and attached deposit are still in place on the top of the tubes, but are missing from the upstream side, except on the lower temperature specimens (6 and 7 inches). Note also that the precipitation of internal sulfides is more advanced in the upstream side for both alloys.

These features are elaborated in Fig. 4-145, which shows the typical corrosion product morphologies of the Incoloy 800 specimens taken from the center of this probe. Figure 4-145a is the cross section from an area on the top half of the ring specimen, which shows a deposit of the bed material that formed on the ring specimen and adhered during exposure. A thin, continuous, protective Cr_2O_3 scale formed at the alloy/deposit interface. In contrast, Fig. 4-145b shows the cross section from an area on the bottom half of the same ring specimen.

The deposit of the bed material is absent, as is the protective Cr_2O_3 scale. Only internal oxides and sulfides, precipitated at grain boundaries, remain on the specimen. (Cross sections of the spalled deposits showed a thin layer of corrosion products adhered to the deposit at what once was the deposit/alloy interface, to be discussed below.)

Apparently two different mechanisms of attack influenced the corrosion behavior of these two alloys during exposure. Both the location on the ring specimen and the location on the corrosion probe determined which mechanism was more significant. Initially, a porous deposit of bed material formed around the entire ircumference of all the ring specimens. This deposit adheres strongly to the orrosion products formed during the early stages of the combustion experiment,

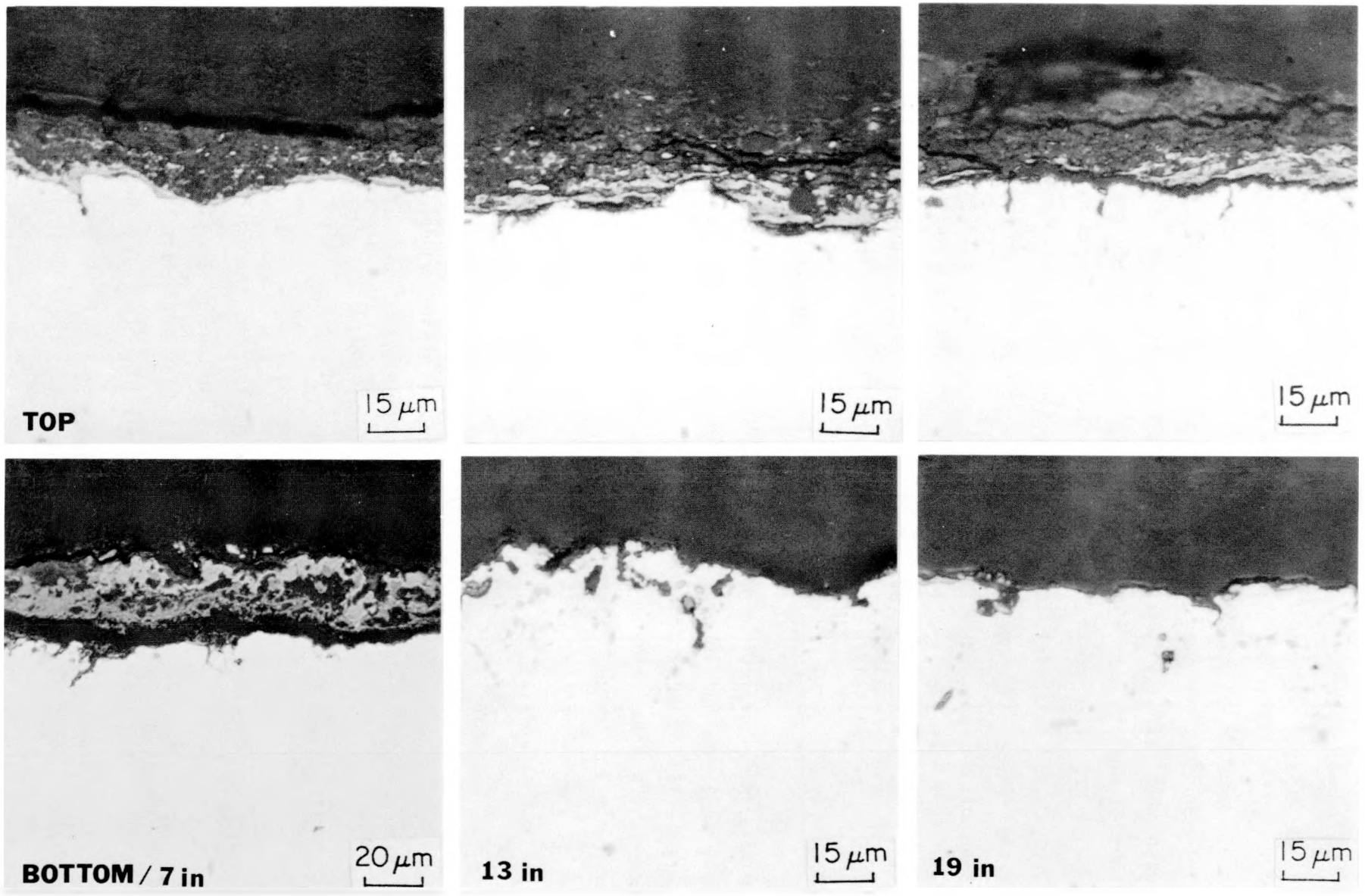


Figure 4-143. Cross Sections of AISI 304H after 115 Hours in 50% XS Air Run. Pairs Represent Morphologies from Top and Bottom Locations of Specimens, Exposed at the Indicated Distances along the Probe. The Specimen Temperature Increases with Increasing Distance along the Probe.

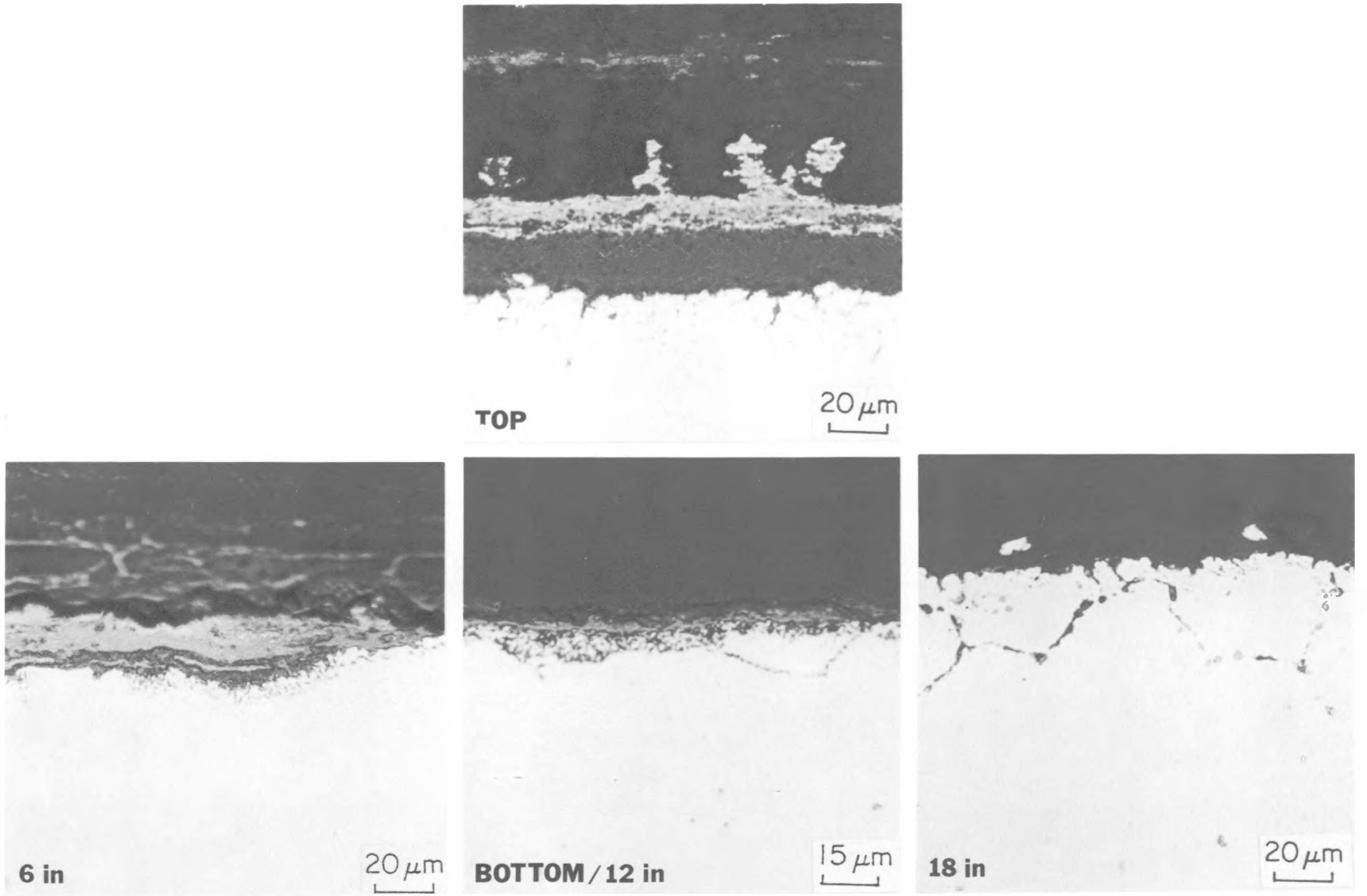


Figure 4-144. Cross Sections of Incoloy 800H after 115 Hours in 50% XS Air Run (Locations at which specimens were exposed on probe are indicated)

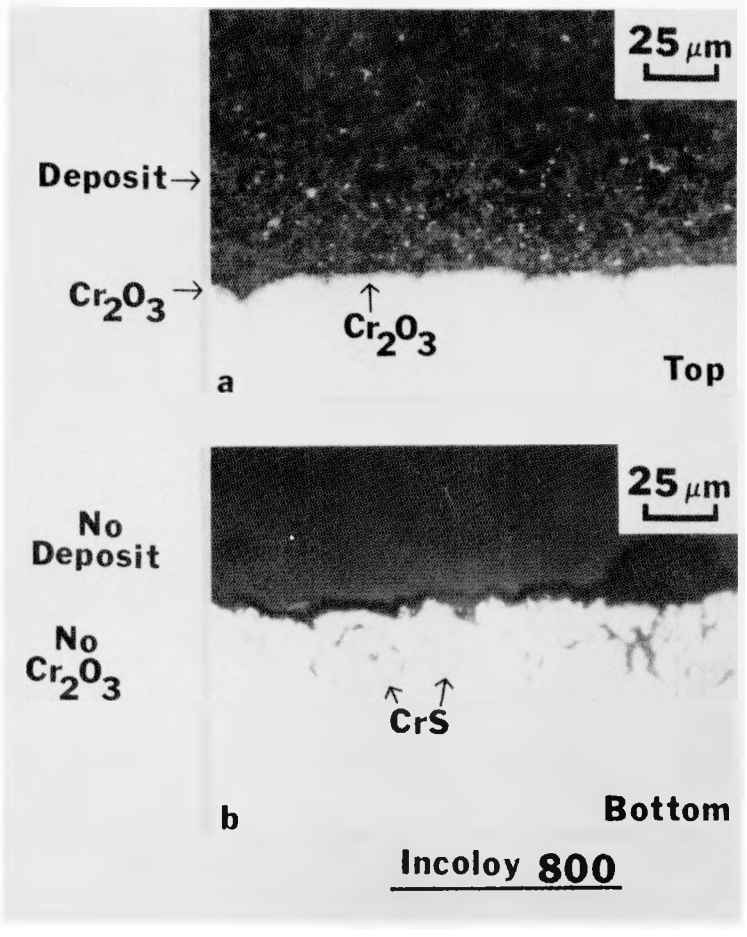


Figure 4-145. Typical Cross Sections of Incoloy 800H; 115 Hours, 50% XS Air, Port 33, Middle of Probe

i., transient oxides of iron and/or nickel, mixed oxides, and Cr_2O_3 protective scale. The top half of all the ring specimens and the bottom half of the specimens located near the walls were relatively unaffected by the flow of bed material, and the deposit and corrosion products remained intact during exposure.

However, the bottom half of the ring specimens located near the center of the probe were affected significantly by the motion of the bed material. The deposit and corrosion products at these locations on the corrosion probe directly impeded the upward motion of bed materials and flue gas, and were removed mechanically from the specimen surface. This corrosion/erosion mechanism is illustrated in Fig. 4-146. The repeated process of alloy corrosion/deposit formation followed by mechanical removal of the deposit and corrosion products resulted in specimens with weight-loss values much larger than the weight-loss values from specimens that experienced corrosion only. This corrosion/erosion mechanism was the most significant in areas of the bed with good mixing properties (i.e., near the centerline) and explains the bell-shaped weight-loss curves generated from the descaled corrosion probes.

Multialloy Probe. The multialloy probe was exposed for 70 hours during the 0% excess air experiment at location No. 83. The same type of mechanical attack was observed on this corrosion probe and the corrosion product morphologies on the bottom half of the ring specimens of all the alloys were very similar to the morphology illustrated in Fig. 4-145b for Incoloy 800. However, the bottom half of the specimens located near the walls and the top half of all the specimens exhibited corrosion product morphologies much different than those formed during exposure in the 50% excess air experiment. Figures 4-147 and 4-148 illustrate the upstream and downstream corrosion morphologies, at various locations along the probe, for alloys 304H and 800H, respectively. In these, the upstream locations were chosen to show intact oxide scales and are representative of locations adjacent to the areas where the scale and deposit were removed. There is, again, a marked difference between the corrosion behavior on the upstream and downstream surfaces. In particular, the external scales on the upstream surfaces are generally considerably thicker and internal sulfide penetration is more ensive than on the downstream (top) surfaces.

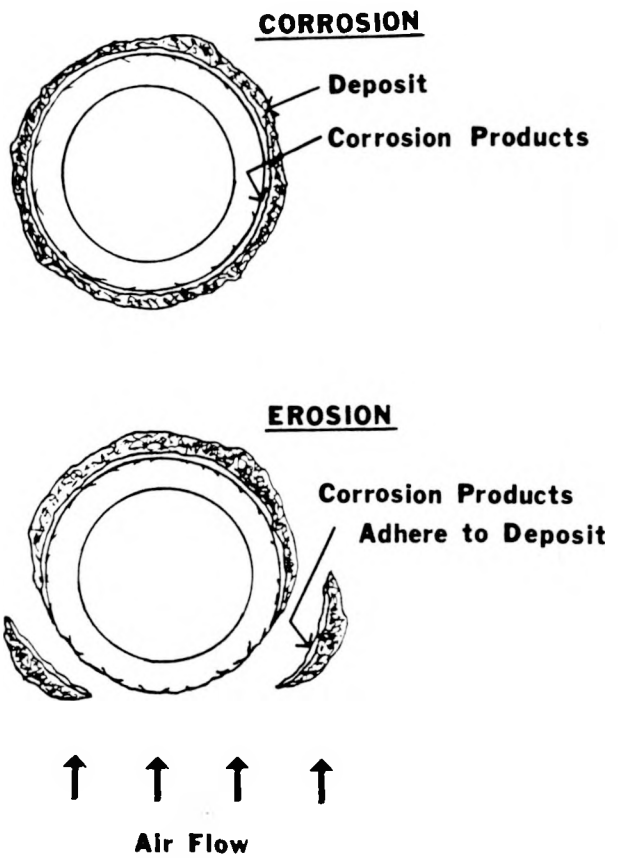


Figure 4-146. Schematic of Corrosion/Erosion Mechanism

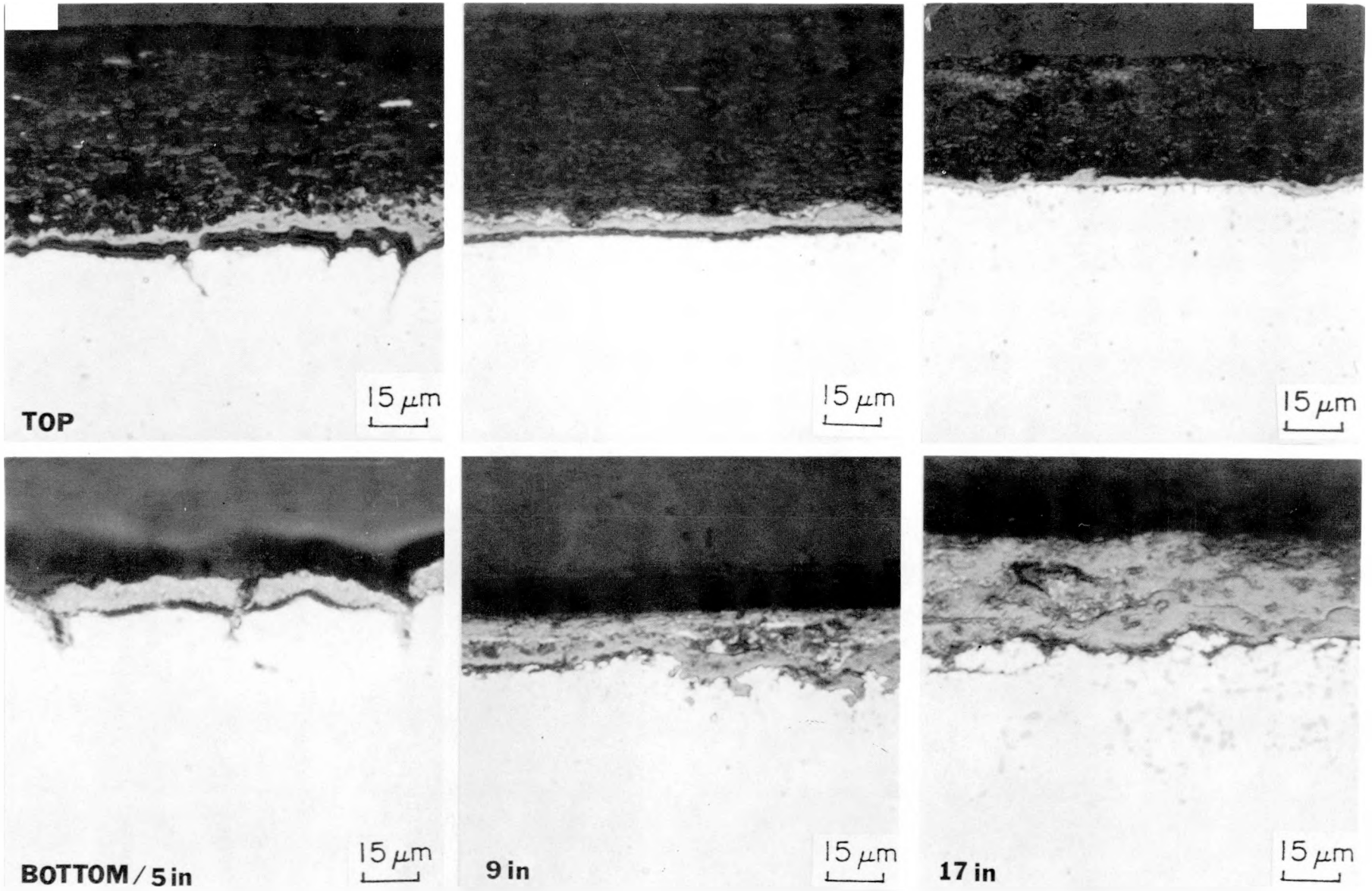


Figure 4-147. Corrosion Morphologies on Top and Bottom Surfaces of AISI 304H, as a Function of Location on Probe, after 70-Hours Exposure in 0% XS Air

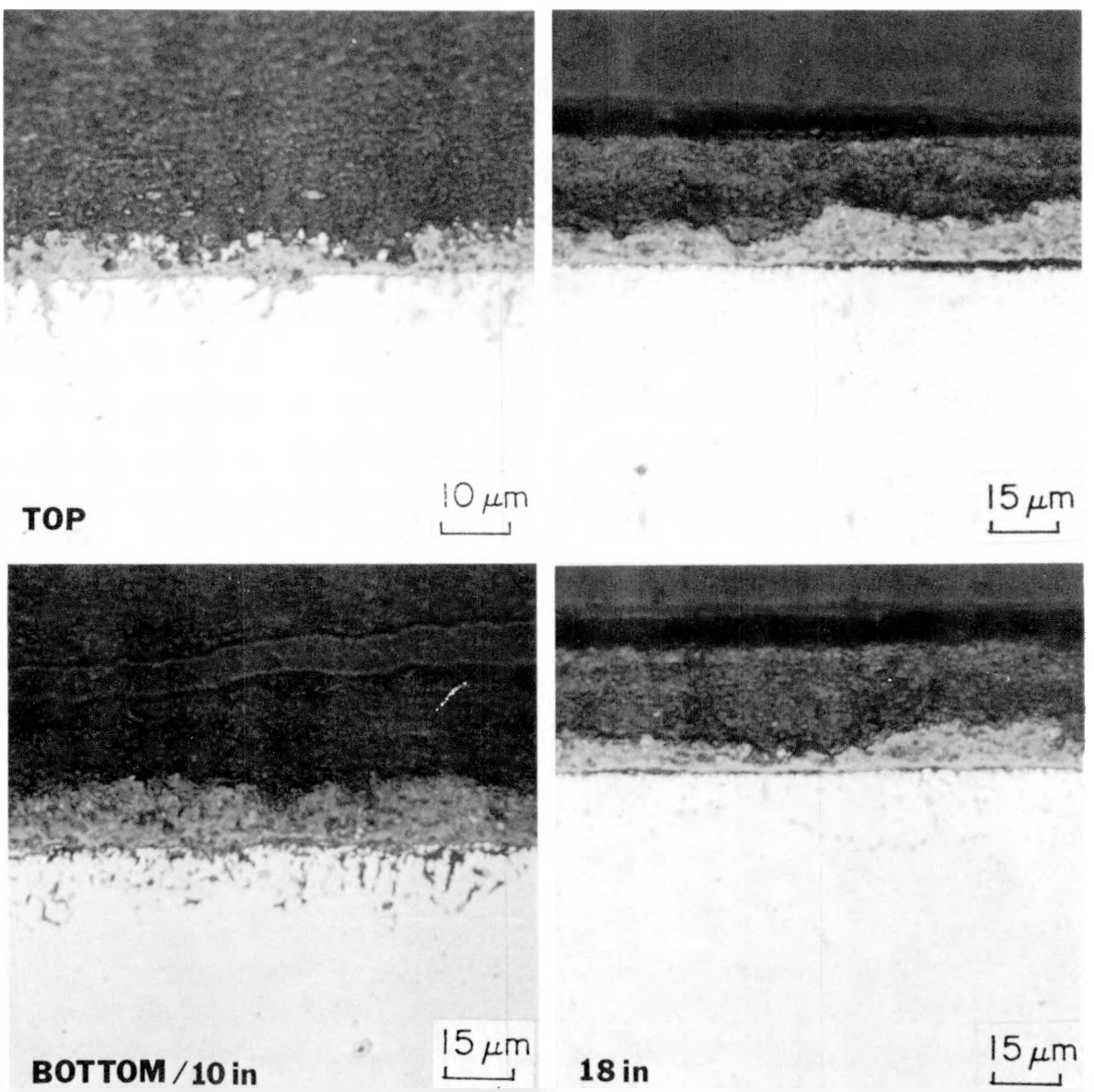


Figure 4-148. Corrosion Morphologies on Top and Bottom Surfaces of Incoloy 800H at 10-Inch and 18-Inch Locations on Probe, after 70-Hour Exposure in 0% XS Air

Figures 4-149 through 4-151 show typical morphologies observed on the top of the ring specimens from Inconel 800H, Inconel 617, Nimonic 86, Inconel 618E, 310, and Incoclad 347-618E. In summary, the corrosion product morphologies observed on alloys exposed to substroichiometric environments are characterized by the following points:

1. The presence of a black, adherent, deposit of bed material
2. The formation of iron and/or nickel sulfides, usually at the corrosion product/deposit interface
3. The formation of thick mixed oxide layers between the deposit and protective Cr_2O_3 scale
4. Local areas without a protective Cr_2O_3 scale
5. Voids at the corrosion product/alloy interface
6. Internal oxidation and sulfidation along the alloy grain boundaries

EDAX and microprobe analyses indicated that the corrosion products formed during excess-air conditions consisted solely of oxides, i.e., an (Fe, Ni)Cr_2O_4 mixed oxide with an underlying Cr_2O_3 protective layer. However, when exposed to substoichiometric conditions, nickel-rich sulfides formed at the corrosion product/deposit interface. Typical corrosion morphologies developed on the downstream tube surfaces in the 50% XS air, and 0% XS air runs, are compared in Fig. 4-152. As mentioned earlier, the presence of molten sulfides and the absence of a Cr_2O_3 scale usually leads to accelerated oxidation and sulfidation of the alloy. The corrosion product morphology illustrated in Fig. 4-152b resulted from only 70 hours total exposure time and would be expected to develop into serious corrosion problems during prolonged exposures under similar conditions. The relationship between the corrosion product morphologies and the oxygen partial pressure data is illustrated again in Fig. 4-153. Figure 4-153a shows the corrosion products formed on the FeCrAlY cladding exposed during the 50% excess air experiment, and Fig. 4-153b shows the corrosion products formed on the FeCrAlY cladding during the 0% excess-air experiment. Once again, only oxides formed when excess air conditions were dominant, whereas both oxides and sulfides (Fe rich) formed when substoichiometric conditions were dominant.

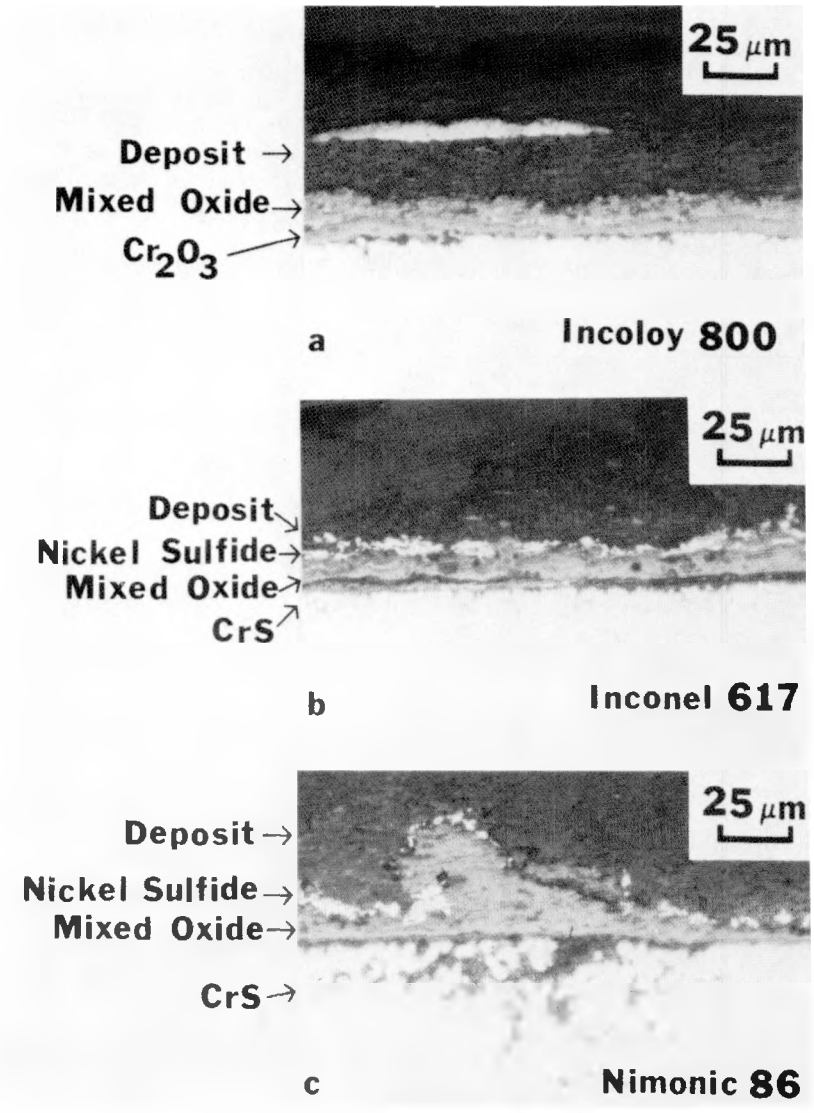


Figure 4-149. Cross Sections of Incoloy 800, Inconel 617, and Nimonic 86. 70 Hours, 0% XS Air, Port Number 83, Middle of Probe

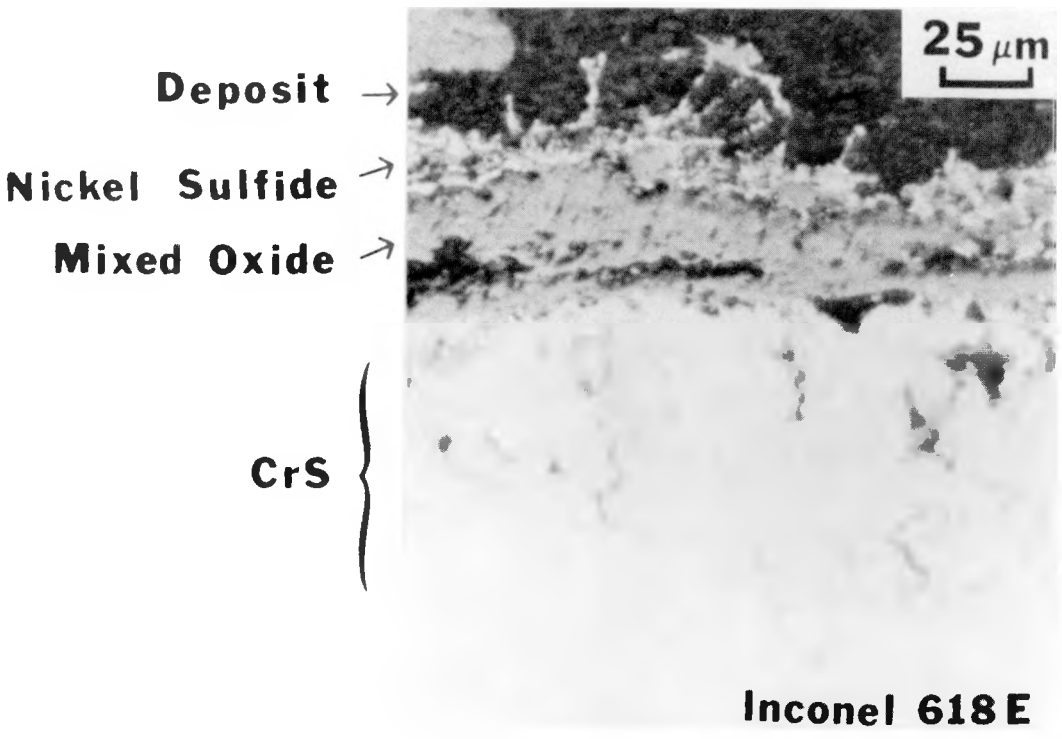
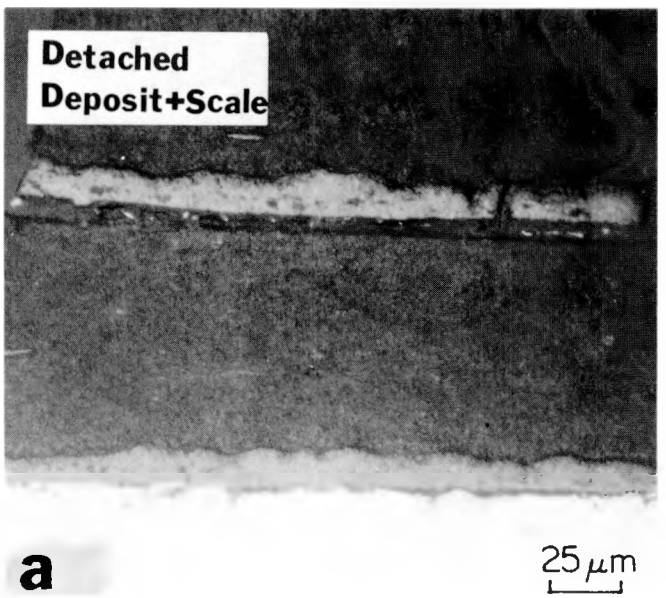
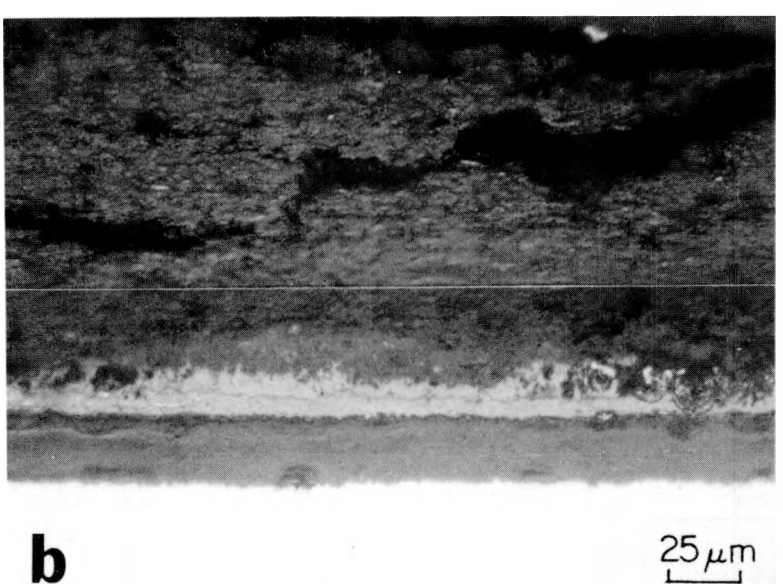


Figure 4-150. Downstream Surface Corrosion Morphology on Inconel 618E after 70 Hours in 0% XS Air Run



AISI 310



Incoclad 347/618E

Figure 4-151. Cross Sections after 70-Hours-Inch, 0% XS Air, Both from Middle of Probe

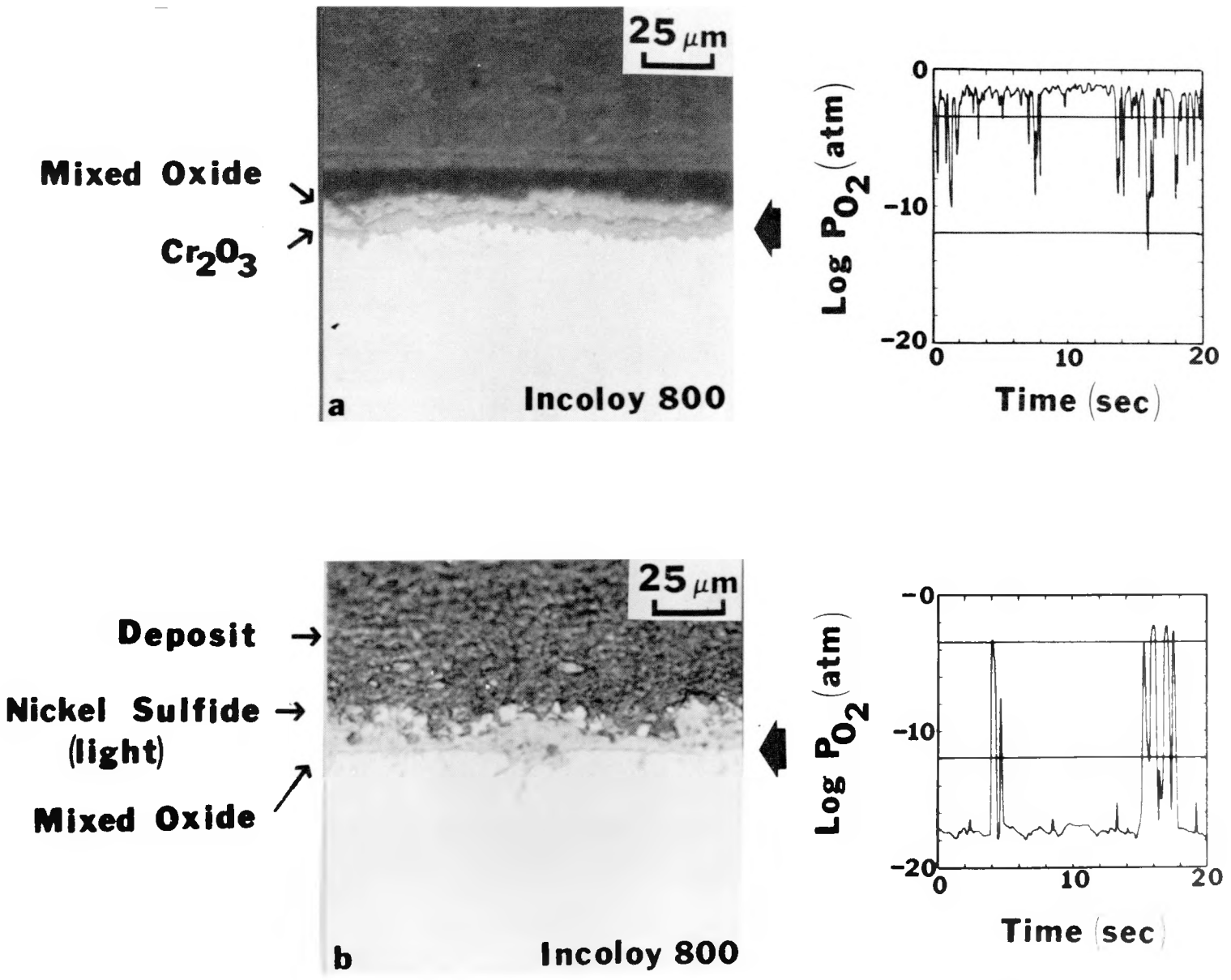


Figure 4-152. Corrosion Products Formed on Incoloy 800H
(a) 50% XS Air, 115 Hours
(b) 0% XS Air, 70 Hours

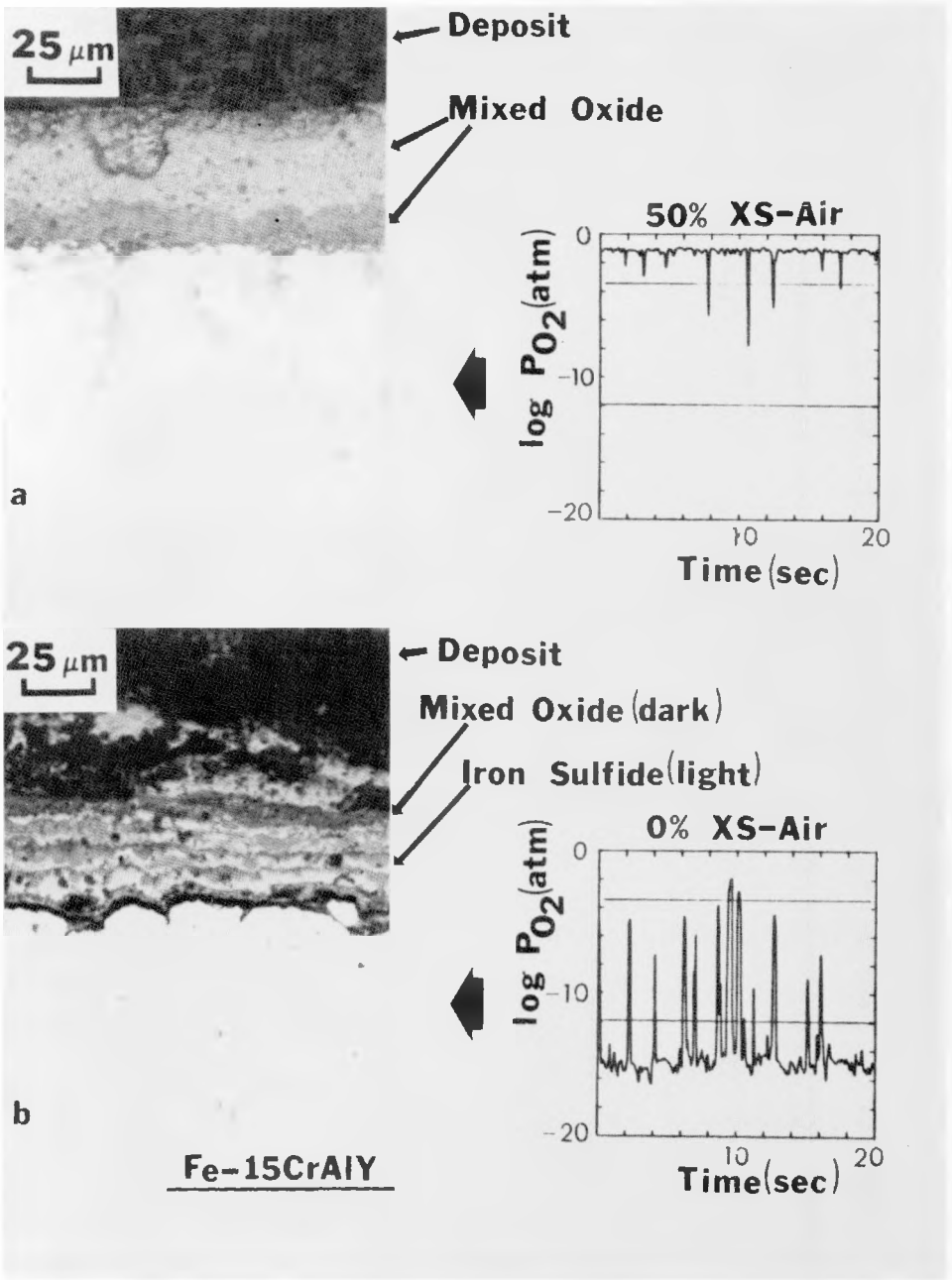


Figure 4-153. Cross Section of FeCrAlY Cladding and Corresponding PO_2 Data

The formation of iron and nickel sulfides on specimens exposed to areas of the bed where the oxygen probe indicated the existence of substoichiometric conditions suggests the external corrosion product morphologies are determined by the oxygen partial pressure in the gas phase. Apparently the deposits formed in the AFB were either thin enough and/or porous enough so that intimate gas-metal contact was possible. Alternatively, the change in gas composition, resulting from the shift in combustion conditions, may have altered the chemical composition of the deposit, which determined the corrosion product morphology. Whether the gas phase or the deposit (or both) had the most significant role in determining the external corrosion product morphology cannot be determined at this time. However, it is now obvious that substoichiometric combustion conditions, as indicated by the oxygen probe, promote accelerated oxidation and sulfidation of these alloys. In contrast, external sulfides or iron and/or nickel were never observed on alloys exposed to excess air environments.

In-Bed Tube Deposits. Observations of the corrosion probes after exposure indicated that all were covered with a deposit of bed material, which generally ranged in color from orange-red in the 50 and 20% XS runs, to black or pale orange/yellow in the 0% XS run. Extensive spallation of large pieces of deposit occurred as the probes cooled from exposure temperature.

As discussed earlier, some of the deposit-covered tubes had a smooth, even, polished appearance and there was evidence that the deposit was thinner or missing on the leading edge of specimens that had been located in the center of the bed, with signs of chamfering of the thicker deposits at positions on the specimens corresponding to approximately 4 and 8 o'clock. The surface of the deposit immediately next to the chamfered edge was often grooved, indicating a cutting or plowing action of the bed particles as they moved past the tube.

Pieces of spalled deposit were collected and mounted for metallographic analysis. Figures 4-154 and 4-155 are cross sections of deposit spalled from 244-hour probes from the 20% XS air run. Both were samples of the complete thickness of the deposit layer and were brick-red on the outer surface, shown at the top of each micrograph, and black on the inner surface. These deposits exhibit an obvious layered structure, with incorporated bright-appearing particles. In addition, the outer 25 to 50% of the deposit thickness appears to be quite dense,

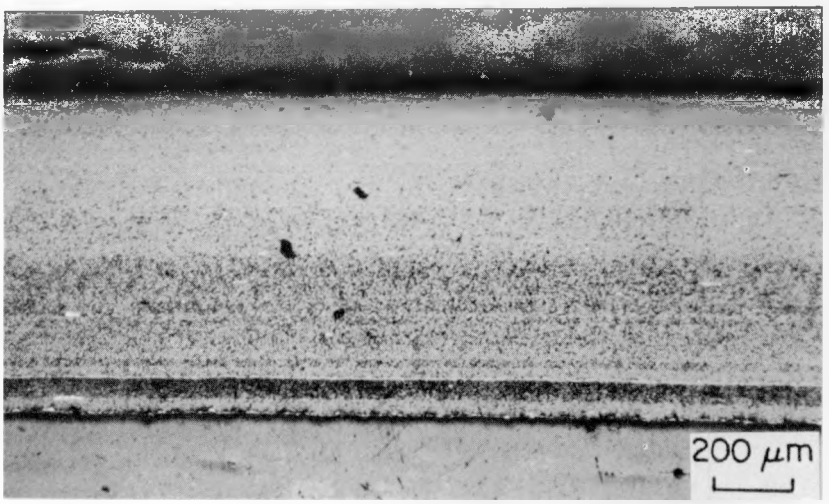


Figure 4-154. Deposit from Probe No. 2
(Run 1, 20% XS Air,
244 Hours, Location 82)

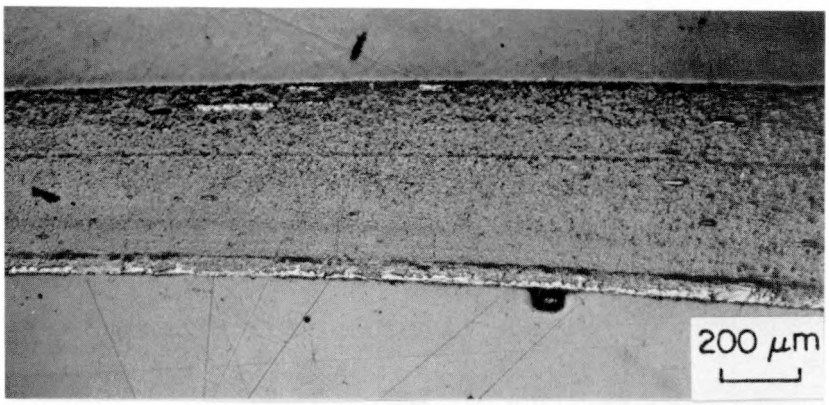


Figure 4-155. Deposit from Probe No. 3
(Run 1, 20% XS Air,
244 Hours, Location 32)

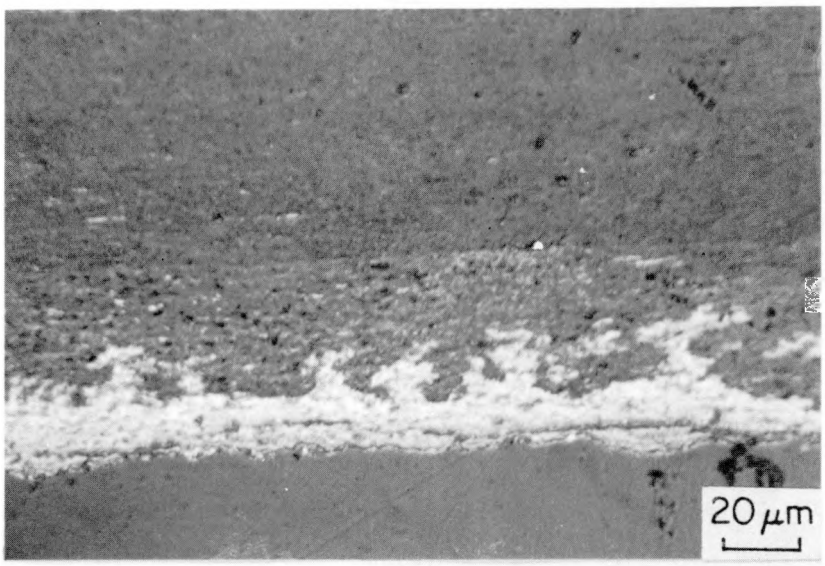
hereas the inner portion appears to contain significant porosity. Some of the cracking of the outer, dense layer of the deposit from probe No. 3, Fig. 4-155, may have occurred during cooling. However, the damage to the deposit at the right-hand side of this figure probably occurred during the corrosion exposure, since the layered structure is disturbed in this region. Unfortunately, the location on the probes from which these deposits came is not known.

Figures 4-156 through 4-160 show typical deposits from the 240-hour probes exposed in the 0% excess air run. The sample from the middle of the bed, shown in Fig. 4-156, was quite similar to those from the 20% excess air run, though somewhat thinner. Its outer surface was brick-red in color, while the inner surface was black, but in cross section appears bright. Figure 4-157 is a scanning electron micrograph of the outer surface of this deposit, and shows dimpling or grooving, and a hole where some deposit has been lost. The detailed structure of the surface is shown in Fig. 4-157. Figure 4-158 shows the features of the inner surface of this deposit, and very clearly indicates that the features shown were in intimate contact with the alloy surface. Figure 4-159 gives details of the inner part of this deposit, and shows that the bright-appearing layer is rich in chromium, with particles rich in iron at the interface with the darker-appearing deposit. Since the bulk of the dark-appearing deposit comprised calcium and sulfur, it is difficult to assess the extent of association of sulfur with the bright-appearing layer. Nevertheless, this inner layer appears to correspond to the type of corrosion scale expected to form on the alloys under test. The concentration of chromium suggests that the scale would probably have been considered to be protective.

A section of a deposit from a probe in the bottom of the bed in the 0% XS air run (shown in Fig. 4-160) was damaged extensively, with localized areas of crazing. The structure of the deposit was, however, quite similar to those shown earlier with layering, incorporating stringers of bright-appearing material and an apparent decrease in porosity from the outer to the inner edge. The sample shown in Fig. 4-160 probably does not represent the full thickness of the deposit; its outer surface was black, while the inner edge was rust red.

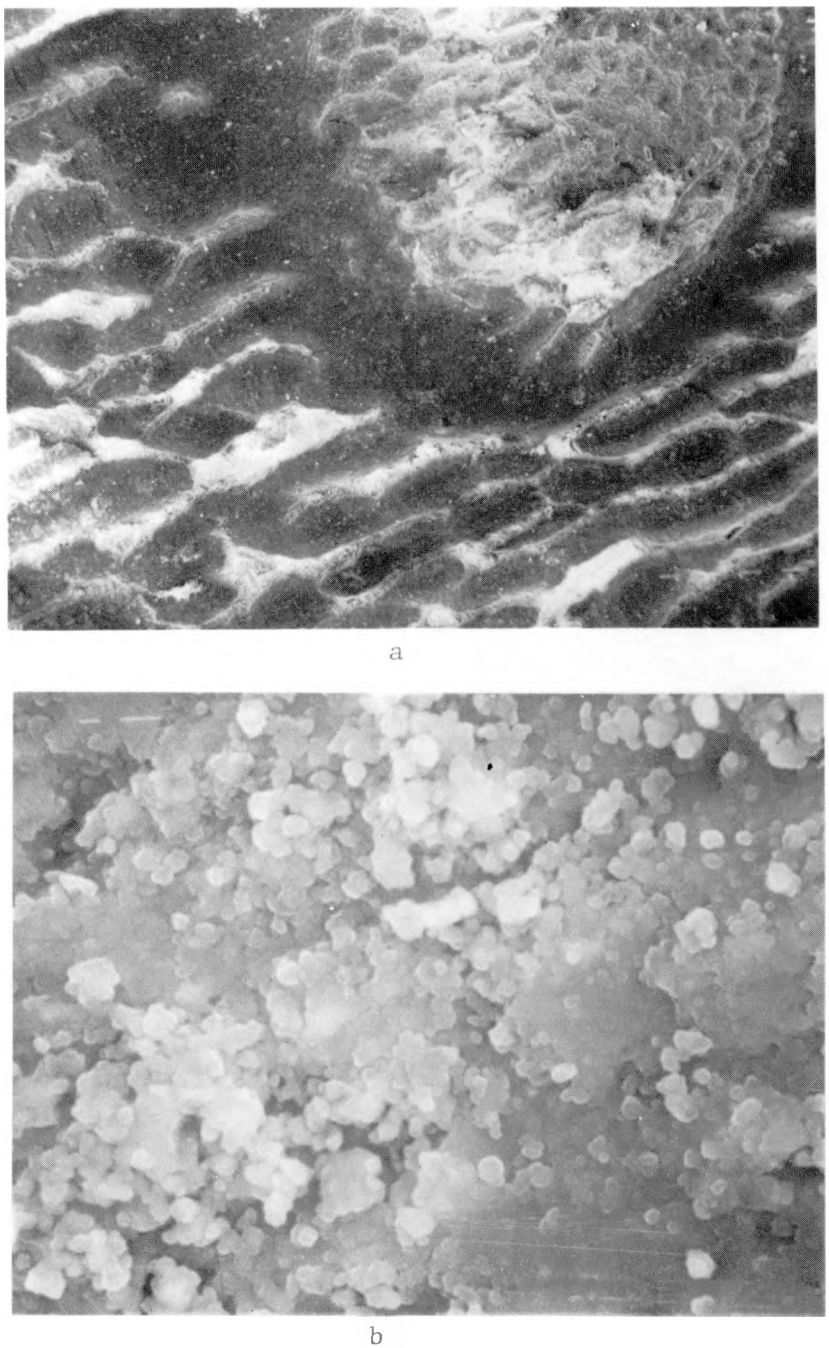


a



b

Figure 156. Deposit from Probe No. 7 (Run 2, 0% XS Air, 240 Hours, Location 82)



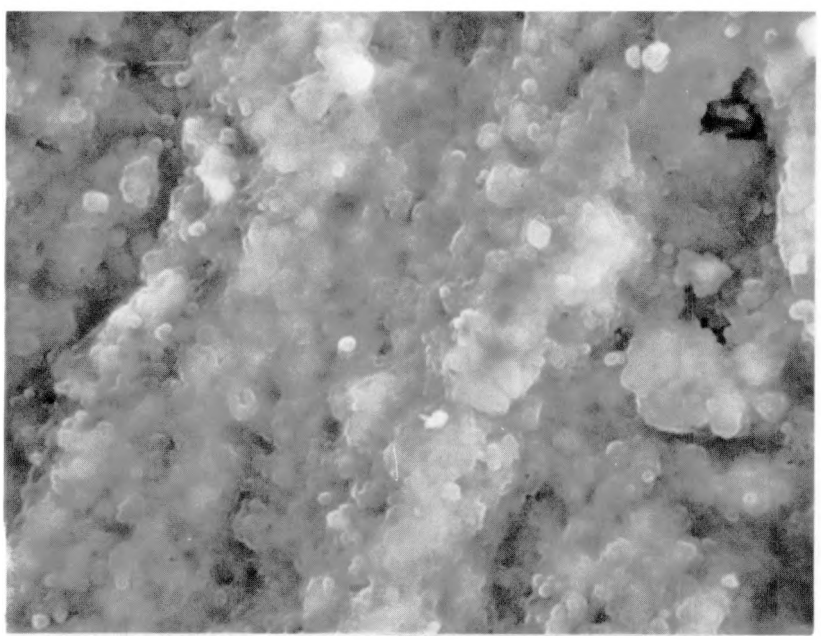
a

b

Figure 4-157. Outer Surface of Deposit from Probe No. 7 (Run 2, 0% XS Air, 240 Hours, Location 82)



a



b

Figure 4-158. Inner Surface of Deposit from Probe No. 7 Showing Machining Marks from Alloy Surface, and Apparently a Joint Between Specimens

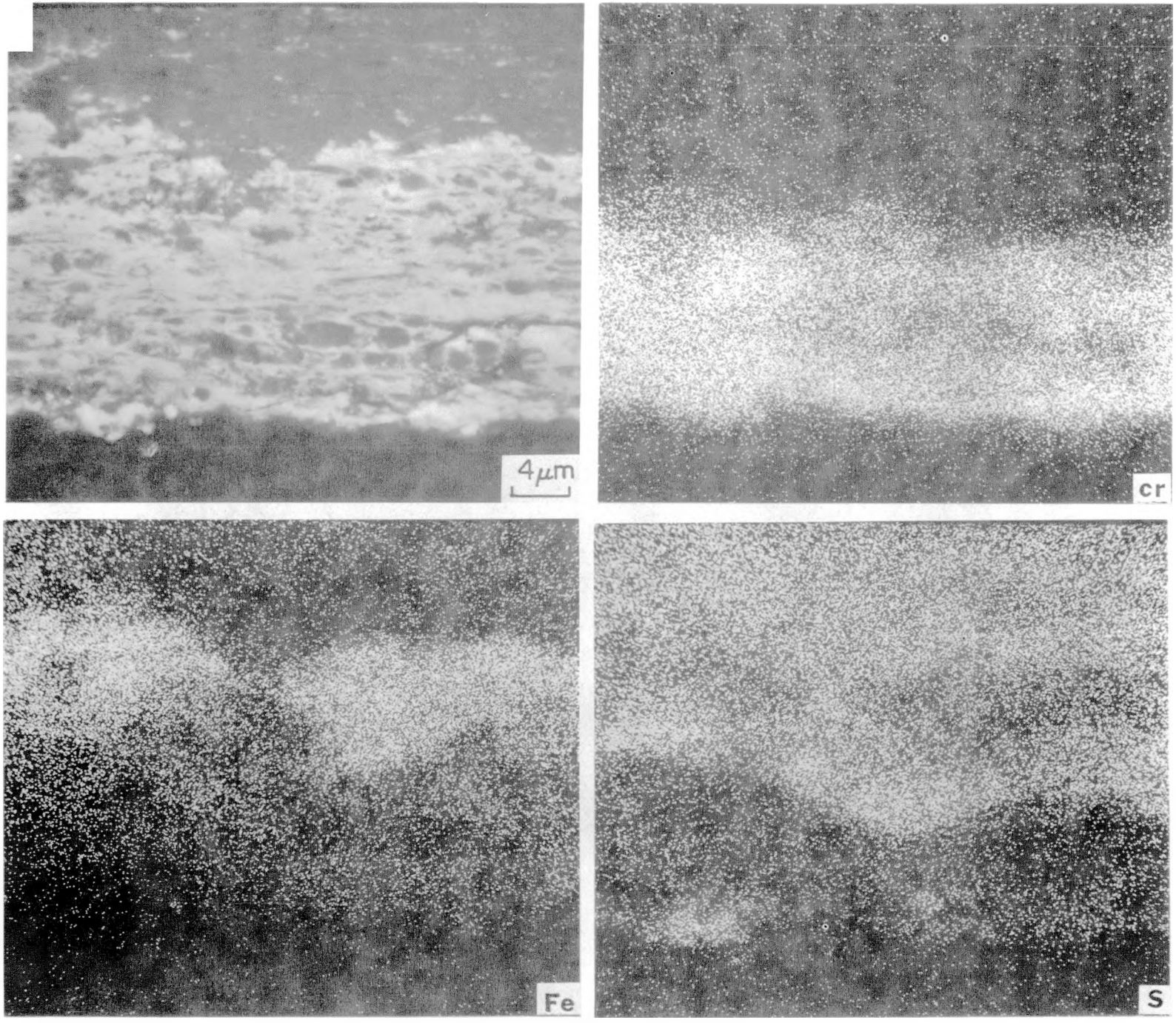


Figure 4-159. Detail of Inner Edge of Deposit from Probe No. 7, Showing Optical Image and Corresponding X-Ray Images for Cr, Fe, and S

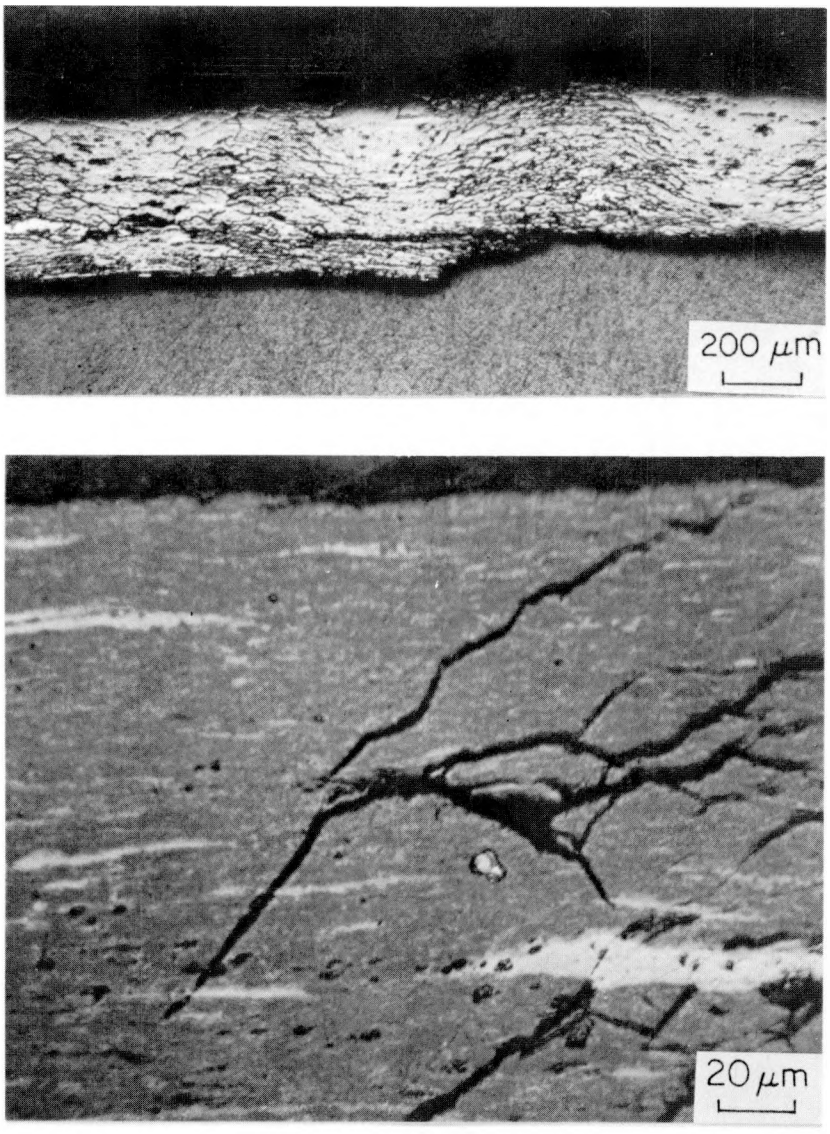


Figure 4-160. Deposit from Probe No. 8 (Run 2, 0% XS Air, 240 Hours, Location 32)

orrected X-ray intensities from counting over a large area of the surfaces of each of the deposits discussed are listed in Table 4-43 for both the inner and outer surfaces. An attempt to sort out these data into the possible or probable compounds present by mass balance led to the tentative compositions listed in Table 4-44. From this it appears that the deposits from the 20% XS air run are mainly mixtures of calcium sulfate and calcium oxide, with the sulfate in predominance. The inner surface of the deposit from probes No. 2 and 7 apparently consisted of the protective chromia scale from the alloy to which the deposit had been attached, together with some iron sulfide and bed material. The outer surfaces of all the deposits comprised calcium sulfate and calcium oxide, with the former in predominance except in the sample from probe No. 8. Curiously, this apparently calcium oxide-rich deposit was the one which was crazed.

GENERAL DISCUSSION

The in-situ oxygen probe has provided extremely useful information concerning the nature of the combustion process in particular areas of the AFB. Variations in the oxygen partial pressure with location indicated that the gaseous environment in the fluidized bed was not as uniform as expected. This suggests that the flow patterns of the air and coal were not uniform and local variations in the combustion process (% excess air) resulted. This less-than-ideal mixing of coal and air was most significant at locations near the bottom of the bed and along the west wall. However, as the coal, air, and fluid gas progressed upward through the bed, the oxygen partial pressures more closely corresponded to those values expected based on the initial air/fuel ratio.

Descaling and metallographic operations conducted on the exposed alloy specimens indicated two mechanisms of material degradation occurred in the AFB. The first mechanism was alloy corrosion beneath an adherent deposit of bed material. All the alloys tested developed protective Cr_2O_3 scales as expected when exposed in areas of the bed where the probe indicated high-oxygen partial pressures existed. However, some of the alloys, particularly the nickel-base alloys, experienced the early stages of sulfidation when exposed to low-oxygen partial pressures. This behavior would be expected to develop into serious corrosion problems during prolonged exposures under the same conditions.

TABLE 4-43. CORRECTED X-RAY FLUORESCENCE ANALYSIS OF DEPOSITS

	Element	Probe Number 2	3	7	8
Inner Surface	Fe	9.8	19.5	3.7	17.8
	Cr	76.7	--	71.7	--
	S	5.6	18.5	5.5	7.7
	Ca	--	37.2	5.9	56.5
	Aℓ	--	8.0	2.6	5.1
				(0.2K)	(1.2Cℓ)
Outer Surface	Fe	8.7	8.6	8.6	13.8
	Cr	--	--	--	--
	S	27.9	21.2	27.6	3.0
	Ca	48.2	60.7	46.2	59.3
	Si	9.6	5.9	9.6	15.2
	Aℓ	5.0	3.1	4.9	6.7
			(0.4K)	(1.4K, 1.2Na)	(0.8Cℓ)

TABLE 4-44. POSSIBLE COMPOSITIONS OF DEPOSITS

	Probe Number			
	2	3	7	8
Inner Surface	Cr_2O_3, FeS SiO_2	$CaSO_4$:CaO 4:1 (FeAℓSi)Oxide	Cr_2O_3, $CaSO_4$, FeS, (AℓSiCa)Oxide	$CaSO_4$:CaO 1:2 (FeSiAℓ) Oxide
Outer Surface	$CaSO_4$:CaO 7:1 (FeAℓSi)Oxide	$CaSO_4$:CaO 2:1 (FeAℓSiK)Oxide	$CaSO_4$:CaO 7:1 (NaK)Oxide	$CaSO_4$:CaO 1:6 (Cℓ)

The second mechanism, alloy corrosion/deposit formation followed by the mechanical removal of the deposit and corrosion products, was the most significant form of material degradation observed in these tests. This coupled corrosion/erosion mode of attack was attributed to the vigorous motion of the bed constituents and the maximum weight-loss values occurred on specimens located near the centerline of the bed.

The corrosion and combustion diagnostic data obtained during this research suggest that nonuniform flow patterns can significantly influence the corrosion behavior of the heat exchanger tubes. Because flow patterns appear to be controlled by combustor size and shape, as well as heat exchanger and feed port geometries, considerable attention should be given to design approaches which minimize the occurrence of local, substoichiometric combustion conditions. Optimum AFB design, in conjunction with the systematic use of an in situ oxygen probe, could virtually eliminate the catastrophic alloy sulfidation caused by low PO2 environments, assuming, of course, that these are the source of the sulfur species. However, locations on the heat exchanger tubes subjected to a prolonged corrosion/erosion process could become depleted in chromium, leaving them very susceptible to sulfidation and/or accelerated oxidation. The data from this research suggest these locations would be the first to experience heat exchanger tube failures. While the apparent vigorous centerline motion may be peculiar to this particular AFB, or to small AFBs in general, some form of this corrosion/erosion process may be associated with all fluidized bed combustors. Determining the magnitude of its effects on materials degradation would be necessary for optimum heat exchanger design and proper materials selection.

It should be pointed out that the above reasoning is based on the assumption, without direct evidence, that the most likely source of the locally high sulfur partial pressures is the combusting coal. Stringer and Whittle (Ref. 4-16) have suggested that another source could possibly be the $CaSO_4$ component of the limestone bed. If the deposit proves to be the major supplier of sulfur to the alloys, then the remedial measures discussed above would require serious reconsideration. This argument involves the equilibria between CaO and $CaSO_4$ and CaS. These can be represented conveniently on a thermodynamic phase stability diagram, (shown in Figure 4-161). At oxygen partial pressures of 10^{-12} to

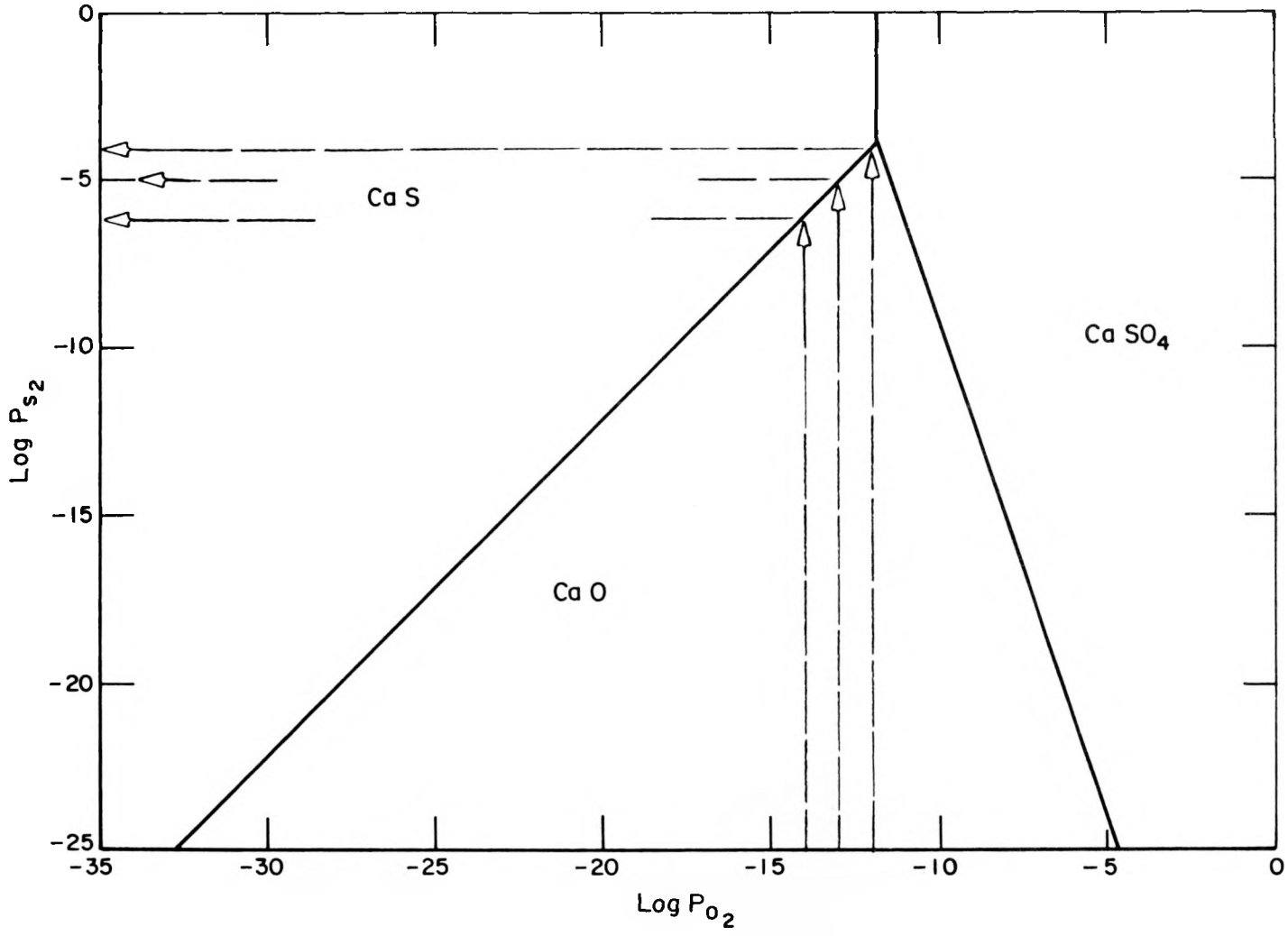


Figure 4-161. Phase Stability Diagram for Ca-O-S System at 1650 F, 1 Atm

10^{-14} atm in the presence of the sulfur partial pressures generated by the combustion of 4% sulfur coal, the formation of CaS is favored. If CaO and CaS are deposited on in-bed metallic surfaces to form an impervious layer, the CaO-CaS equilibrium could maintain a persisting low-PO_2, high-PS_2 condition, which, in turn, could pose a sulfidation threat at points of contact with the alloy surface. The presence of CaS in the fluidized bed combustor is, however, considered likely to be only a transient phenomenon, possibly occurring only in areas where substoichiometric conditions persist. Sampled bed material is more usually a mixture of CaO and $CaSO_4$ and, as previously shown, these usually comprise the bulk of the deposits formed on in-bed surfaces. A sufficiently high-sulfur partial pressure to cause sulfidation of nickel and nickel oxide, but not of iron, could be generated beneath a mixed CaO-$CaSO_4$ deposit, again provided that the deposit was sufficiently impervious to prevent ambient excess air conditions from gaining access to the alloy surface. Some support for sulfur generation by the sulfur sorbent was provided by corrosion experiments in FBC runs with, and then without, limestone as the bed material (Ref. 4-56). Whereas the initiation of sulfidation was observed with Illinois No. 6 coal and limestone, none was observed in a repeat run without limestone. In a further run with a coal ash bed, burning a Wellbeck (0.5% Cl, 1.6% S) coal, sulfidation was observed in alloy coupons located near the combustor wall where deposits of bed ash had accumulated (Ref. 4-2). Laboratory experiments to further explore this point were carried out in this program, and are reported in Section 4.1.4.

The observations in this study that surface sulfides were formed on alloys exposed under substoichiometric conditions, but were not present in excess air exposures, have been interpreted as evidence that the ambient gaseous environment was controlling the corrosion behavior, that is, the deposit layers were sufficiently porous to allow direct contact of the ambient gas with the alloy surfaces. An alternative explanation, which cannot be dismissed at this time, is that the corrosion was controlled by the deposits and the composition of the deposits was related directly to the prevailing gaseous environment. In substoichiometric areas, the deposits may have contained CaS, which can create an aggressive sulfidizing environment to the alloys. This alternative case implies that less direct control of the corrosion behavior of heat exchanger tubes would be possible through manipulation of the combustion conditions.

onclusions

The following conclusions can be drawn from the results of this program:

- Persistent substoichiometric conditions promoted accelerated oxidation and sulfidation attack of all the alloys studied

- The nickel-base alloys were the most prone to attack, as was expected. In these limited time tests, only one case of catastrophic attack was observed on Inconel 618E. In general, corrosion morphologies recognized as precursers to rapid sulfidation-related degradation were developed

- The FeCrAlY cladding alloy also suffered accelerated oxidation and oxidation-sulfidation in some cases, although the attack was quite uniform. The extent of attack was greater than anticipated, and suggests that the 25% Cr version of this alloy should be considered, instead of the 15% version used here

- Of the iron-base alloys, AISI 304 exhibited accelerated oxidation attack, particularly in substoichiometric conditions. Its behavior in oxidizing conditions was as expected, and the rapid oxidation rates observed suggest a temperature limit in the 1400 F range

- AISI 347 and 310 exhibited quite acceptable behavior in general, with lower apparent rates than 304

- Incoloy 800H showed essentially good behavior in oxidizing (excess air) conditions, with a marked increase in corrosion in substoichiometric conditions. However, no indications were found in these tests that this alloy was susceptible to catastrophic attack; the corrosion morphologies were consistent with this alloy being intermediate in nickel content between the stainless steels and the nickel-base alloys

- A mechanical acceleration of the degradation process was observed to ope ate in the center region of the fluidized bed. Bed deposit formed on the specimens apparently was removed periodically, stripping protective oxide from the alloy surfaces and exposing them to the ambient gas. This was the most serious form of degradation experienced in this program, and suggests that motion in the bed, and the deposit formation/removal phenomenon, are important factors that require further investigation

- In the absence of this mechanical interaction, excess air combustion conditions promoted the formation of apparently normal protective chromium oxide scales on all the alloys (except FeCrAlY)

- The in situ oxygen probe provided a reliable means of identifying local variations in the nature of the combustion process, and identified regions of the bed with high corrosive potentials. Characteristic signals from such regions showed a prevailing low-oxygen partial pressure ($\leq 10^{-12}$ atm)

- Oxygen probe signals characteristic of excess air conditions (a prevailing oxygen partial pressure of $\leq 10^{-2}$ with excursions to lower values) are considered to indicate an environment in which the alloys tested will exhibit protective corrosive behavior. The boundary of these "safe" conditions appears to be where the oxygen probe indicates an exactly stoichiometric combustion condition, i.e., a signal continuously oscillating between limits of $\sim 10^{-2}$ and $\sim 10^{-12}$ atm

4.4 ROCKETDYNE 6' x 6' AFB RESEARCH TEST BED COMBUSTOR SYSTEM

The Phase II program major experimental effort consisted of designing, fabricating, and operating a 6' x 6' AFB with a 1650 F bed and a 1550 F working fluid heat exchanger, and using this AFB as a test bed for metal heat exchanger material specimens. As previously discussed, the research was supported by information obtained by operating at BCL a smaller cylindrical 24-inch-diameter AFB research test combustor, performing at BCL Accelerated Corrosion laboratory metal specimens testing, and operating a Rocketdyne funded 18" x 18" AFB test unit combustor (IR&D).

The 6' x 6' Atmospheric Fluidized Bed (AFB) is an experimental facility (Fig. 4-162) for advancing the technology of metal heat exchangers operating in an AFB for the Closed Cycle Gas Turbine (CCGT) process. While much work is being done on AFB combustors for boiler applications, the 6' x 6' AFB program prepresents the major effort oriented toward the CCGT heat exchanger development on a suitable scale with the significantly higher metal temperatures as compared to boiler type heat exchangers.

This is the major experimental effort of the Phase II program effort. The system was assembled and tested at the Rockwell NAAD Aerothermal Laboratory in El Segundo, Ca. The system is sized to allow research data from the other supporting Phase II test activities to be utilized in R&D hardware of a size approaching minimum demonstration dimensions. The 6' x 6' AFB system was used for AFB operational data and for heat exchanger materials exposure data testing. It represents the CCGT operating at a 1550 F working fluid discharge temperature. But, the turbine and generator are not included in this system at this time in Phase II . Compressed air from NAAD facility compressors provided the working fluid air for the heat exchangers. The heated air was dumped into the atmosphere at the heat exchanger exit. However, the potential exists for in the future adding turbomachinery to this 6' x 6' AFB system, should present plans for that be approved.

This experimental unit was designed to address the technical issues related to long-life heater design for the CCGT application, particularly erosion and corrosion of he heater tube materials. This test unit provides versatile hardware for exploring CCGT technical issues for the system consisting of the combustor/heater assembly plus a large amount of equipment for the ancillary systems.



Figure 4-162. 6" x 6" AFB Experimental Facility

The planned and performed program consisted of a bed characterization test series and an erosion/corrosion test series with a planned accumulated duration of approximately 500 hours of operations split between the two test series. This was successfully accomplished along with an additional 100 hours of erosion/corrosion testing. The experimental facility and hardware were designed with a great degree of flexibility and range, and the unit is capable of, and is being used to extended operation well beyond the initial test objectives (Table 4-45).

TABLE 4-45. 6" X 6" AFB TEST PROGRAM OBJECTIVE

- LARGER-SCALE EXPERIMENTAL UNIT
- PROVIDES AFB COMBUSTION ENVIRONMENT
  - BASIC COMBUSTION DATA
  - EROSION/CORROSION TESTING (PROBES)
  - OPERATING DATA WITH WIDE RANGE OF CONDITIONS
- DESIGN CRITERIA FOR CONCEPTUAL COMMERCIAL DESIGN
- OPERATING EXPERIENCE ON CCGT COMPONENTS
- BASIS FOR FUTURE EXPANDED TESTING

The experimental facility with several supporting systems and their auxiliary equipment represents a complex research test system. Being a research tool, the system has extensive instrumentation and diagnostic measurements. The feed systems, particularly the coal and combustion air, were designed to be versatile to allow control as well as measure most of the combustion environment.

Throughout the course of the planning and design effort, details and information were documented in the form of topical as well as quarterly reports (Ref. 1-5 through 1-19).

In this section, a description is presented of the 6' x 6' AFB hardware that makes up the main experimental unit, as well as the supporting hardware equipment, including an overall description of the system and its operating conditions and capabilities. Appendix A presents the fabrication drawings.

This section consists of:

Section 4.4.1 System Description
Section 4.4.2 Combustor/Heater Description
Section 4.4.3 Combustor/Heater Components
Section 4.4.4 Auxiliary Equipment

4.4.1 System Description

The objectives are summarized in Table 4-45, where the major objective is to investigate the combustion environment that influences the corrosion and erosion of the heater materials. The technical approach is to find materials that are resistant to the combustion environment, and to create a "healthy" environment that minimizes the conditions that promote corrosion and erosion of the heater materials.

Another objective is to investigate auxiliary systems and equipment unique to the CCGT, especially in the area of heater response and control. Much of the supporting systems equipment is established state of the art, and development is well underway for fluidized bed combustion for boiler applications. However, there are some special AFB aspects of these systems that relate to the CCGT, such as control of the combustion air and coal to maintain a healthy heater tube environment under all operating conditions, including startup, load following and upset conditions. Thus, design criteria will be development for the design of commercial systems from the Phase II data derived from this 6' x 6' AFB system hardware.

The experimental unit was designed to provide operating data over a wide range of conditions, as summarized in Table 4-46. This includes superficial bed velocities from 2 to 8 fps and ash recycle rates up to three times the coal feed rate.

TABLE 4-46. RANGE OF TEST CAPABILITY

SUPERFICIAL VELOCITY, FT/SEC	2 TO 8
WORKING FLUID OUTLET TEMPERATURE, F	1450 TO 1550
EXCESS AIR, %	20 TO 50
C_A/S MOLAR RATIO	2 TO 4
ASH RECYCLE	0 TO 3 X COAL FLOWRATE

A simplified schematic is presented in Fig. 4-163, which depicts the major items that make up the experimental equipment. A layout is presented in Fig. 4-164 which shows the plan arrangement at the test site while Fig. 4-162 presents a view of the facility. The working fluid air is supplied to the combustor portion of the closed cycle working fluid system where air is provided by the facility air system at a specified flowrate (up to 17 lb/sec) and inlet temperature (up to 425 F). The working fluid air then is heated by first the convection bank and then the in-bed bank, and upon leaving the combustor is, for the time being simply discharged to the atmosphere. Combustion air is provided by a forced draft blower and passes through a preheater to exchange heat between the flue gas and combustion air. Flue gas leaving the combustor passes through a cyclone separator, the preheater, baghouse, and induced draft fan. The cyclone removes most of the solid particulate, which then can be either disposed of, or recycled back into the combustor. The baghouse provides a final cleanup of the flue gases so the gases discharged are cleaner than the new-source air pollution standards. The induced draft fan is used to maintain a balanced draft in the freeboard section of the combustor. The solids feed systems are coal, limestone, and flyash reinjection.

The nominal design point is a superficial velocity of 6 ft/sec, 25% XS air, bed temperature of 1650 F, and working fluid outlet temperature of 1550 F. The nominal design parameters are presented in Table 4-47 while an analytical pressure/ temperature profile of the combustion side is presented in Table 4-48.

4.4.2 Combustor/Heater Description

Coal fired heaters for CCGT/cogeneration service have many requirements in common with conventional steam boilers. These typically include high combustion efficiency, reliability, safety, operability and an affordable cost. It is the differences between steam boiler service and CCGT heater service which establish the technology needs of the CCGT heaters and thus form the basis for the current R&D program. These differences, and the related technology needs are summarized in Table 4-49. Perhaps the most powerful difference is that the CCGT application requires significantly higher heating surface operating temperatures than the boiler plication, with the attendant possibility of excessive heat exchanger corrosion rates. Additionally, the CCGT heater has much more stringent limitations on the

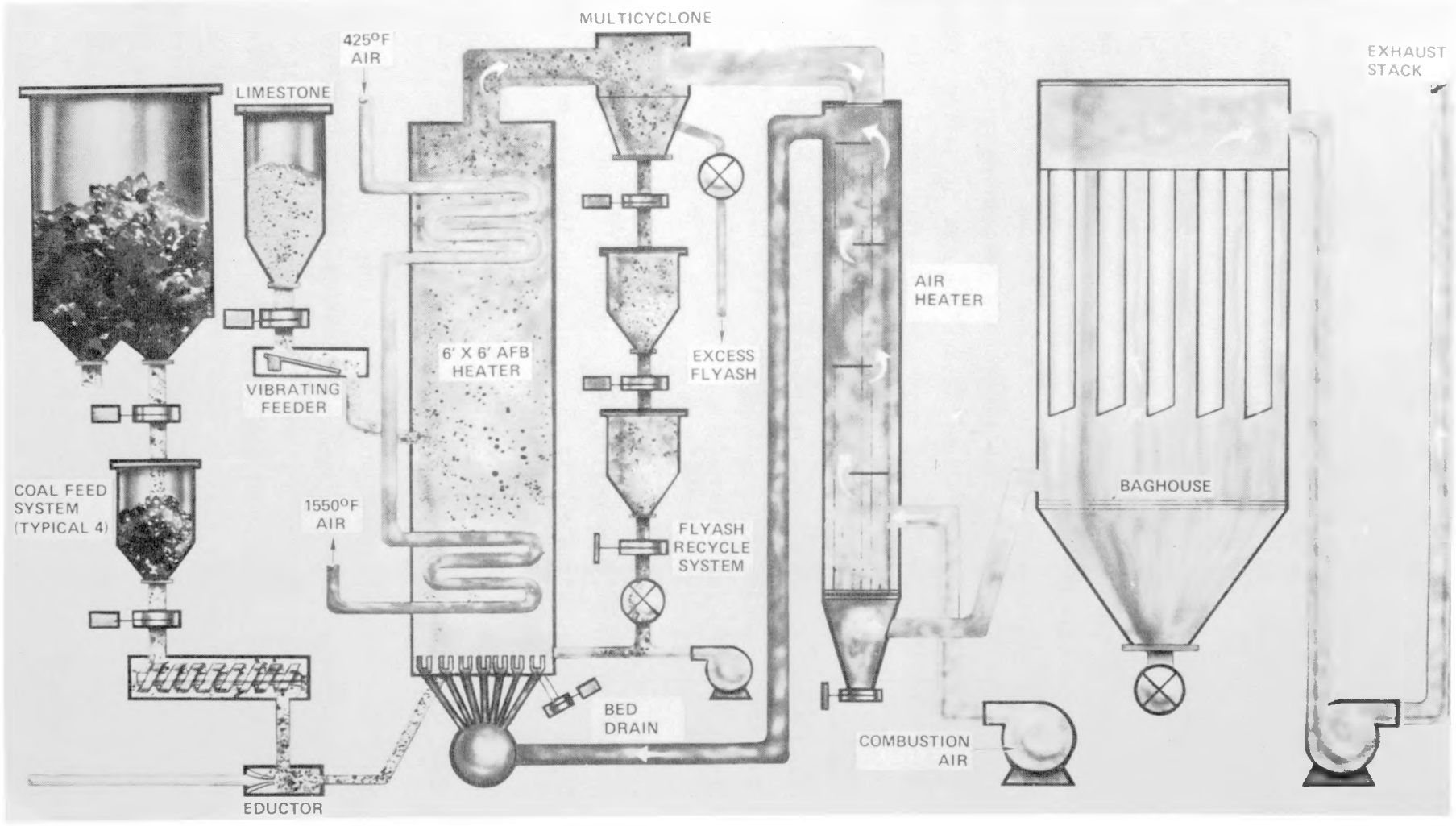


Figure 4-163. Overall Schematic

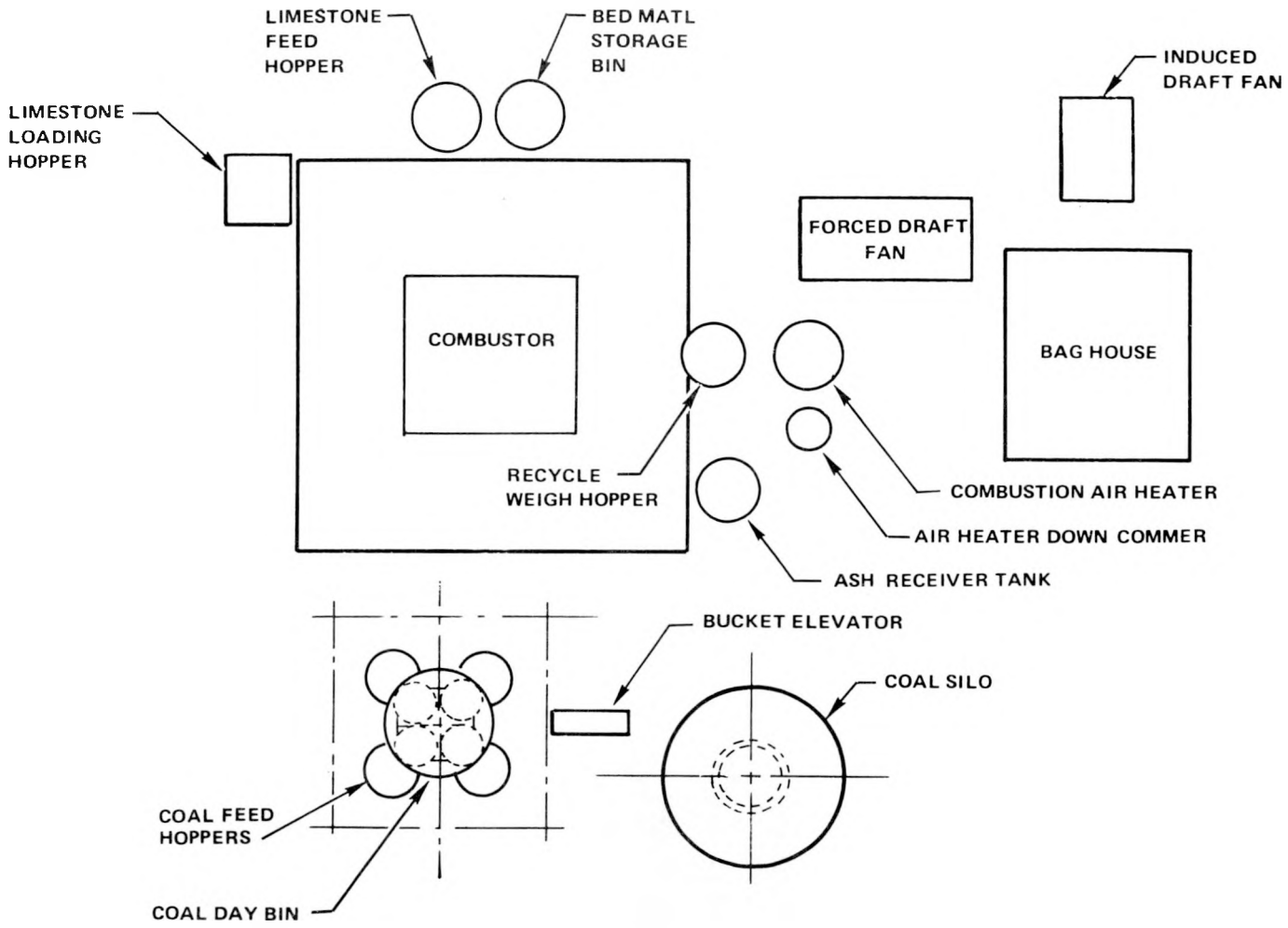


Figure 4-164. 6' x 6' CCGT/AFB Facility Plan

TABLE 4-47. 6" X 6" AFB NOMINAL DESIGN PARAMETERS

SUPERFICIAL VELOCITY, FT/SEC	6
COMBUSTION	
COAL FLOWRATE, LB/HR	1300
AIR FLOWRATE, LB/HR	13,900
EXCESS AIR, %	25
BED TEMPERATURE, F	1650 F
WORKING FLUID (AIR)	
EXIT TEMPERATURE, F	1550 F
FLOWRATE, LB/HR	40,600
HEAT RELEASE, BTU/HR	12.0×10^6 ($3.5\ MW_T$)

TABLE 4-48. 6" X 6" AFB FLOW PROFILE AT 8 FT/SEC

LOCATION	PRESSURE (IN. W.G.)	TEMPERATURE (F)	FLOWRATE (LB/HR)	COMMENTS
INLET	0	70	16,300	Sea Level Air
F.D. BLOWER/DAMPER	112	125	16,300	
AIR PREHEATER	110	640	16,300	
DISTRIBUTOR MANIFOLD	107	640	16,300	INCLUDES FLOWMETER LOSS
BED BOTTOM	64	640	17,900	INCLUDES 10% CONVEYING AIR
FREEBOARD	0	1650	20,600	COMBUSTION GAS
CONVECTION BANK EXIT	-1	802	20,600	
CYCLONES	-4	802	20,600	
AIR PREHEATER	-8	398	20,600	
BAGHOUSE	-13	398	20,600	
I.D. FAN/DAMPER	0	398	20,600	

TABLE 4-49. CCGT HEATER TECHNOLOGY NEEDS

CCGT HEATER CHARACTERISTIC	EFFECTS	COMPARISON VERSUS "STATE-OF-ART" STEAM CYCLES
Non-condensing working fluid (W.F.)	a) High power compressor to repressurize working fluid.	a) Condensible working fluid - steam/water.
	b) W.F. aide heater P must be minimized, $(\frac{\Delta P}{P} \simeq 0.03)$, relatively low W.F. side heat transfer coefficient.	b) W.F. side ΔP less important. High W.F. mass flux, plus much boiling heat transfer, provides higher heat transfer coefficient.
	c) Different working fluids = different corrosive conditions.	
~1450°F minimum W.F. temperature required for competitive cycle efficiency	a) Tends to accelerate corrosion.	a) 1000°F to 1050°F maximum.
	b) Reduced materials working stresses.	b) Alloys more exotic than austenitic SS seldom required.
	c) Stirs interest in advanced corrosion resistant high strength alloys.	
Thermodynamic performance a function of pressure ratio, not pressure	a) W. F. pressures of 250 to 600 psia expected.	a) W. F. pressure of 600 to 2400 psi.
	b) Low pressures tend to offset reduced available working stresses.	
Cycle thermodynamics favor a higher working fluid temperature at the fired heater inlet	a) Working Fluid inlet temperature of 700°F or higher frequently desired.	a) Boiler feedwater temperatures to fired heater typically 300°F to 450°F. Easy to provide 250° - 300°F stack.
	b) Difficult to attain acceptable stack temperatures.	
All working fluid in heater is in gaseous form	a) Energy stored in the working fluid content of the heater is relatively small versus steam boilers, but large versus direct fired gas turbines.	a) Large content of saturated water provides a "flywheel" effect, mismatch between heat in and out is accommodated by pressure changes.
	b) Control of transients, and heater; turbine interactions needs development.	b) Turbine trips, overspeed protection load regulation via throttleshutoff valve at turbine inlet.

oolant side mass flux (arising from pressure drop limitations on the cycle), different requirements with respect to response to transient load changes and different heat distribution requirements. The current R&D program was directed toward resolving the technical issues relating to these differences while at the same time utilizing as much as possible of the fluidized bed combustion and heat transfer technology and significant design details in a test combustor sufficiently large to provide criteria for a commercial design. The 6' x 6' plan area combustor was designed for this purpose.

The 6' x 6' AFB is modeled after the conceptual commercial AFB concept illustrated in Fig. 4-165. The features of the conceptual commercial concept are summarized in Table 4-50. As can be seen from Table 4-50, many of the design features of the conceptual commercial concept derive from the high operating temperatures of the metal heating surface buried in the fluidized bed, and the desirability of maintaining a uniformly oxidizing atmosphere in the bed by exercising close control of the admission of coal and combustion air. Other design features, such as refractory walls, related to the pressure drop and temperature considerations of the working fluid.

Objectives. The objectives of the 6' x 6' AFB design are summarized in Table 4-51. They require a balance between a strict modeling of the conceptual commercial design versus providing for taking the many measurements typical of an R&D program, as well as making provision for modification during testing.

Design Criteria. Based on the design objectives presented above, design criteria were established for the 6' x 6' test combustor. These are divided into three categories: size and performance criteria are presented in Table 4-52, structural criteria are presented in Table 4-53, and test provisions are presented in Table 4-54. The performance criteria come directly from the conceptual commercial design, which in turn was derived from existing AFB boiler technology. The combustor is designed for a range of superficial velocities in order to investigate the load following. Both excess air and ash recycle were varied to establish the optimum operating point for efficiency and uniformity of corrosion conditions. The 200 psig maximum operating pressure represents the lower end of expected commercial practice and the upper limit of the facility air supply and the in-bed tube bundle.

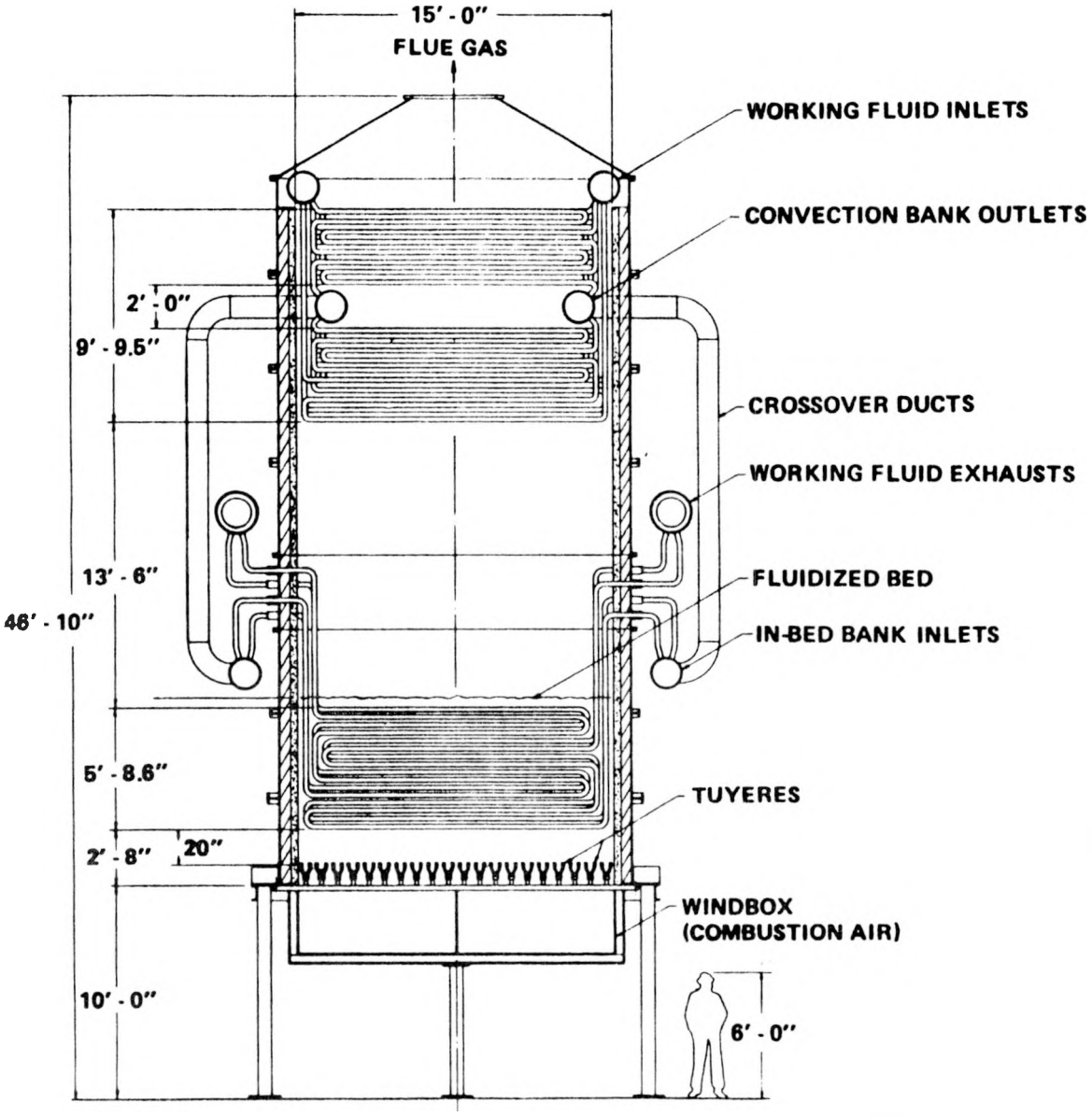


Figure 4-165. Conceptual Commercial CCGT Heater

TABLE 4-50. APPROACH TO 1450 TO 1550 F AFB FIRED HEATERS

Fluidized Bed operating temperature about 1600-1650F, good sulfur capture, ceiling on metal temperatures, no ash melting.

Superficial bed velocity 6 to 8 fps @ design capacity - minimizes erosion while limiting plan area.

Unit sizes to 12' x 50' plan area - provide up to 35 MWe per unit in cogeneration applications at 1.0 power to heat ratio.

Fly ash recycle to provide adequate carbon burn up efficiency & limestone utilization efficiency.

Refractory setting, welded steel casing.

a. Provides for maximum heat input to high temperature working fluid, maximizes LMTD*

b. Cool outer steel casing minimizes differential thermal expansion problems.

Heat exchanger banks suspended from top of setting.

a. In-bed bank has no restricted bed circulation zones to cause corrosion.

b. Heat exchanger tubes are supported off downcomers, reliable support, adequate expansion provisions.

Provisions for monitoring combustion air flow distribution.

---

* Log Mean Temperature Difference

TABLE 4-51. OBJECTIVES OF 6' X 6' EXPERIMENTAL COMBUSTOR DESIGN

Model important design details of conceptual commercial design.

Permit materials evaluation via corrosion & diagnostic probes in representative locations.

Provide combustion conditions consistent with: Adequate combustion efficiency; Ca/S ratio; SOx, NOx & other emissions.
(for a realistic corrosion environment)

Permit detailed measurement of operational parameters.

Permit easy modification.

TABLE 4-52. 6' X 6' AFB SIZE AND PERFORMANCE CRITERIA

Inside plan dimensions	6' x 6'
Distributor to first tube row	18"
Freeboard height	13 ft
Superficial velocity	2-8 ft/sec
	6 ft/sec nominal
Nominal bed temperature	1500-1650F
Nominal coal flow/size	1,370 lb/hr, under 4 mesh
Excess air	20%-50%
Combustion air temperature	620F nominal
Calcium/sulfur mol ratio	2 to 4
Limestone size	-8 + 20 mesh
Working fluid (tube coolant)	air
Outlet temperature	1450 - 1550F
Outlet pressure	Up to 200 psig
Ash recycle rate	0 to 3 times coal flow rate

TABLE 4-53. STRUCTURAL DESIGN CRITERIA

- LIFE - DESIGN GOAL — 8000 HOURS, 500 CYCLES
  CONTRACT — 500 HOURS, 50 CYCLES
- WORKING FLUID PRESSURE PARTS DESIGN TO INTENT OF ASME BOILER & PRESSURE VESSEL CODE
- UNIT MUST BE SAFE TO WORK AROUND DURING OPERATION
- IN-BED TUBE LOADING CRITERIA
  - OREGON STATE UNIVERSITY COLD FLOW TEST DATA
- COMPATIBLE WITH FACILITY SUPPORT STRUCTURE
  - WEIGHT
  - LATERAL LOADING "EARTHQUAKE" 0.4G
- HANDLING & TRANSPORTATION CONSIDERATIONS

TABLE 4-54. TESTING PROVISIONS

- CORROSION/DIAGNOSTIC PROBE PORTS
- TEMPERATURE/PRESSURE INSTRUMENTATION
- MANWAYS
- INSPECTION PORTS
- EASE OF DISASSEMBLY AND MODIFICATION
- READILY ACCESSIBLE FROM WORK PLATFORMS
- MONITOR COAL AND COMBUSTION AIR DISTRIBUTION

The structural design criteria were established to satisfy the requirement of the Phase II contract and also an extended test program. A life of 500 hours and 50 start-stop cycles is adequate to satisfy the existing Phase II contract. An 8000-hour life would be sufficient for an extended test program.

The area of loads on the in-bed tubes due to bed pulsation was the least well-defined part of the structural design. Cold-flow data developed at Oregon State University (Ref. 4-33) was the only data available and were used in the design of the 6' x 6'. More comprehensive data from operating beds is necessary for the commercial unit design.

4.4.3 Combustor/Heater Components

Overall Assembly. The overall assembly for the 6' x 6' heater is shown in Fig. 4-166, and the design features are summarized in Table 4-55. The test combustor is designed to demonstrate the essential features of the commercial design, but also has additional provisions for instrumentation, inspection, and modification during development. The setting is divided into eight vertically stacked assemblies bolted together. The in-bed convection tube banks are supported off of small sections of the setting so that the entire tube bank can be removed for inspection or repair, or even replacement by another configuration, without cutting or welding. Construction of the refractory lined steel casing is the same as for a commercial unit. The distributor/windbox assembly is removable from the bottom of the setting.

Provisions have been made to extend the distance between the distributor and first row of in-bed tubes by 18 inches, if necessary for acceptable coal mixing and/or control of reducing zones in the tubes bundle region.

Building the unit in several sections eases the handling and fabrication problems, since the completed unit weighs about 60 tons and stands 42 feet high. The heaviest section, which is the lower section of the setting, weighs 13 tons.

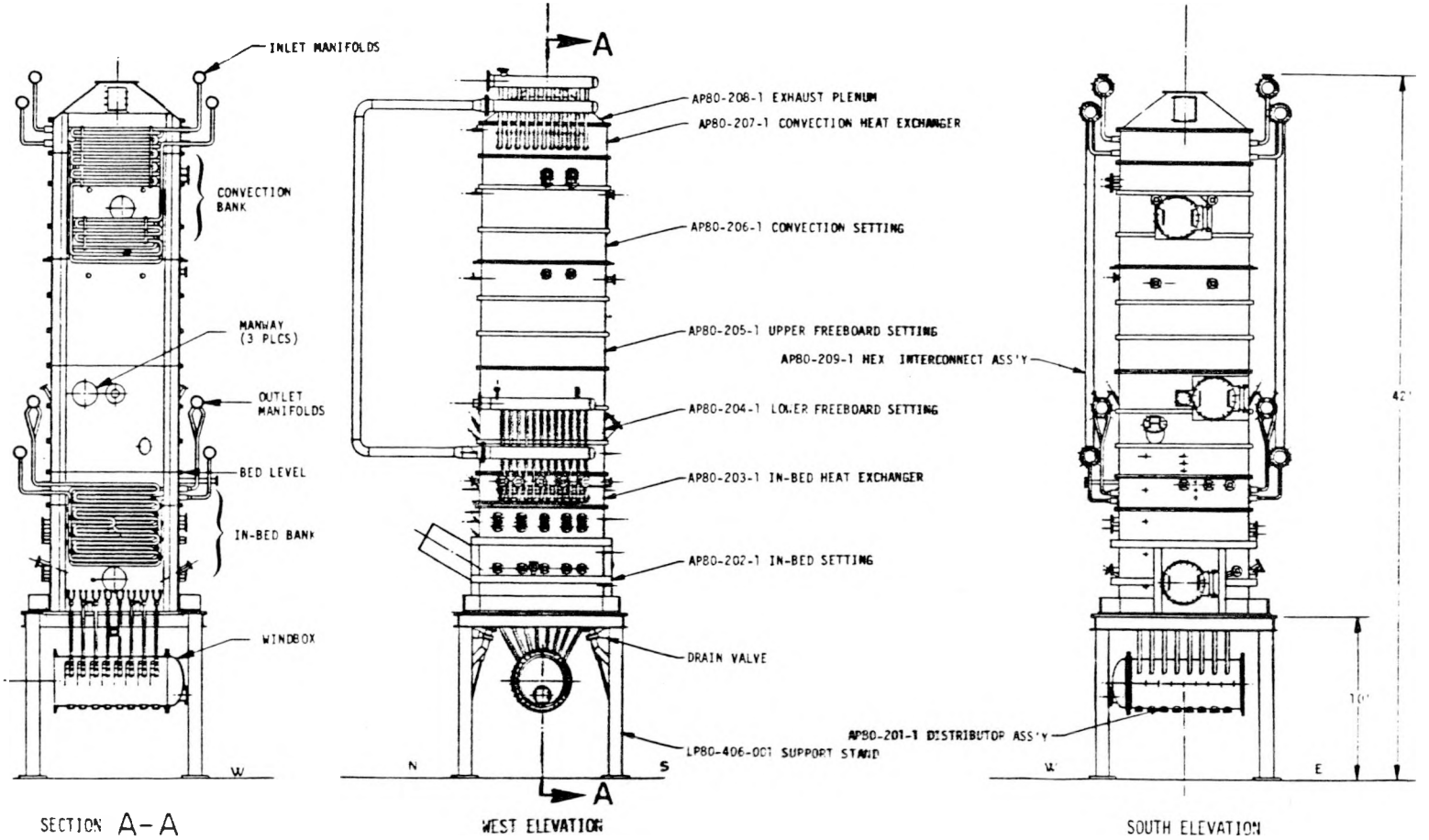


Figure 4-166. 6' X 6' Overall Assembly

TABLE 4-55. 6' X 6' AFB OVERALL ASSEMBLY DESIGN FEATURES

- Refractory lined steel setting
- 8 major vertically stacked sections
- Bottom supported
- Manways and inspection openings
  - Between in-bed bank and tuyeres
  - In freeboard
  - In convection bank soot blower cavity
  - Above convection bank
- Heat exchanger banks suspended from short sections of setting, removable for inspection and repair
- Distributor removable from bottom for ease of service and modification
- Under-bed coal feed
- Ash recycle provisions below in-bed bank
- Comprehensive probe, pressure, and temperature instrumentation provisions
- Provision for adding 18 inches between distributor and first row of tubes

The 6' x 6' plan area was chosen based on the coal feed configuration criter Four coal feed ports were considered the minimum number to get a realistic simulation of the conditions in a commercial unit. The accepted area per coal feed port was 9 sq ft, thus the 6' x 6' size. Bed depth of 7' - 4" is the result of the required amount of heat exchanger surface and the distributor to tube distance. CCGT heaters with their higher working fluid outlet temperature and resultant lower log mean temperature difference (LMTD) require more in-bed surface than a comparable boiler unit. This, plus the lack of water-cooled walls, results in a deeper bed. The use of the refractory lined setting provides the maximum amount of heat to the high temperature fluid. The bed operating conditions of 6 ft/sec and 20% excess air are typical of boiler type units. The bed temperature is slightly higher, however, to provide sufficient temperature differential to achieve the 1550 F outlet temperature with a reasonable bed height. The 200 psig working fluid exit operating pressure represents the upper limit that can be achieved using the existing facility compressor system and is also the upper limit of the 304H CRES in-bed heat exchanger. This pressure represents the lower end of the commercial spectrum.

Since ash recycle is believed to be an essential part of any commercial unit to achieve high-combustion efficiency and minimize limestone utilization, it has been included in the 6' x 6' unit.

The combustor has been equipped with over 50 ports that will accept corrosion or diagnostic probes. The diagnostic probes were used to characterize the bed operating conditions and the corrosion probes were used to expose a variety of metal samples at different locations in the bed and convection bank. Numerous other ports are provided for pressure and temperature instrumentation to monitor operations, as well as inspection ports and manways. A view port for looking down on top of the bed during operation has also been included.

Combustion System. The combustion system consists of coal, air, limestone and ash injection provisions, as well as start-up burners. Design characteristics are shown in Table 4-56, and the system features are shown in Table 4-57. Since the uniformity of coal and air mixing before it encounters the tube bundle is considered important to acceptable tube corrosion performance, the details of the coal injectors

TABLE 4-56. COMBUSTION SYSTEM CHARACTERISTICS

COMBUSTION AIR

AIR FLOW RATE 4,700 TO 18,400 LBS/HR

AIR TEMPERATURE 490 TO 650F, 900F FOR START

DISTRIBUTOR TYPE - BUBBLE CAP

PATTERN - 16 x 16 = 256 BUBBLE CAPS ON 4.5" SQ. PATTERN

ORIFICE DELTA P	SUPERFICIAL "V"	SET 1	SET 2
	2 FT/SEC	10" H20	
	4 FT/SEC	40" H20	10" H20
	8 FT/SEC		40" H20

ORIFICE SIZE		
.169 DIA.	SET 1	4/CAP
.169 DIA.	SET 2	8/CAP

WINDBOX STRUCTURAL DESIGN CONDITIONS

	MAX OPERATING	F.D. FAN STALL DESIGN	
PRESSURE	3.9 PSIG	8.5 PSIG	14 PSIG
TEMPERATURE	650 - RUN	900F	
	900 - START UP		

DISTRIBUTOR PLATE STRUCTURAL DESIGN CONDITIONS

	MAX. OPERATING	DESIGN
BED PRESURE	2.5 PSIG	7 PSIG
CASING TEMPERATURE	200F	650F

TABLE 4-56. (Continued)

COAL FEED

FLOW RATE 470 TO 1,850 LBS/HR

4 UNDERBED PORTS, 9 FT^2 BED AREA EACH, PROVISION FOR 16 PORTS

MAXIMUM FEED PORT SIZE - 2-1/2" PIPE

18 INCHES BETWEEN COAL INLETS AND BOTTOM TUBES, CAN BE INCREASED TO 36 INCHES

LIMESTONE FEED

FLOW RATE 144 TO 576 LBS/HR NOMINAL

ONE ABOVE-BED 2" PORT

18" ABOVE TOP OF PROBES

ASH REINJECTION

FLOW RATE 0 - 5,550 LBS/HR

4 PORTS BETWEEN TUYERES & IN-BED TUBES

INJECTION NEEDLES DISTRIBUTE BETWEEN COAL PORTS

BED DRAIN

DRAIN MATERIAL APPROX. 400 LBS/HR

TEMPERATURE -1650F

TWO 3" PORTS -ONE FOR NORMAL OPERATION
- ONE SPARE IN CASE OF MALFUNCTION OF PRIMARY DRAIN

DESURIK KNIFE GATE VALVE WITH PNEUMATIC ACTUATOR

MANUAL RAMROD FOR UNPLUGGING PORT

PNEUMATIC PURGE PORT ABOVE VALVE

STANDPIPE THROUGH STATIC BED ZONE

TABLE 4-56. (Concluded)

MATERIALS

PARTS EXPOSED TO ACTIVE BED & THERMAL SLEEVES - 304 CRES

REMAINDER OF COMPONENTS - LOW CARBON STEEL

TABLE 4-57. COMBUSTION SYSTEM DESIGN FEATURES

COMMON WINDBOX WITH INDIVIDUAL FEED PIPES TO EACH TUYERE

- PERMITS VENTURI IN EACH FEED PIPE TO DETECT TUYERE PLUGGING
- ALLOWS FREE CONVECTION COOLING OF DISTRIBUTOR PLATE (FROM BELOW)
- ACCOMODATES RELATIVE THERMAL EXPANSION BETWEEN DISTRIBUTOR AND WINDBOX
- NEARLY VERTICAL PIPES AND LOW AIR VELOCITY ALLOW SIFTED BED MATERIAL TO FALL TO BOTTOM OF OVERSIZED WINDBOX

DISTRIBUTOR PLATE INSULATED FROM BED BY STATIC LAYER OF BED MATERIAL

ENTIRE DISTRIBUTOR REMOVABLE

REPLACEABLE TUYERES AND BUBBLE CAPS

REPLACEABLE UNDER-BED COAL INJECTORS

4 ASH RECYCLE PORTS WITH INJECTION NEEDLES TO INJECT RECYCLED ASH BETWEEN COAL PORTS, JUST ABOVE TUYERES

BED DRAIN PORTS IN DISTRIBUTOR PLATE

THERMAL SLEEVES PROVIDE ISOLATION BETWEEN HOT COMBUSTION AIR FEED PIPES AND COOL DISTRIBUTOR PLATE

INSPECTION ACCESS THROUGH MAN-WAY

were previously developed separately in the BCL 24-inch and the Rocketdyne 18" x 18" combustors and further refined by testing with 6' x 6' AFB. The distributor (Fig. 4-167) contains two under-bed coal port design layout patterns. The primary pattern consists of four ports, one in the center of each quadrant. A back-up pattern capability of 16 ports on a 4' x 4' square pattern also was provided and later used in one quadrant.

Combustion air is fed from a single windbox up through individual pipes to each tuyere. Each tuyere contains four bubble caps in all on a 4.50-inch square pattern to provide uniform air distribution. A venturi is provided at the inlet to each of the 64 air pipes for monitoring of the flow to each tuyere during testing. Since reducing conditions caused by a plugged tuyere would adversely affect corrosion results on test specimens. The distributor plate itself was designed to run cool to be compatible with the adjacent steel casing. It is insulated from the bed by a 13-inch layer of static bed material below the air injection orifices. Two bed drains for controlling bed level are provided through the distributor plate.

Ash recycle port locations are show in Fig. 4-168. Four potential ports are provided, and if equipped with injection needles, provide four injection locations between the coal feed port and just above the tuyeres. Only one port was used for ash recycle.

Bed Band. The in-bed heat exchanger is shown in Fig. 4-169. The design characteristics are shown in Table 4-58, and design features are shown in Table 4-59. The in-bed bank is made up of 2-inch-OD 304H stainless-steel tubing. The bank is 20 rows high and 12 tubes wide in a staggered pattern. There are 24 parallel circuits, 12 fed from the east and 12 fed from the west side of the combustor. Coolant air for the bed bank is supplied at about 800 F from the convection bank. The inlet air flows to the bottom of the circuit through 12 downcomer tubes on each side of the bed. These relatively cool vertical tubes on each wall form the basic structure from which the horizontal tube runs are supported. Inlet manifolds are necessary on both sides of the combustor to feed the downcomer support tubes. The downcomers also provide the coolest air working fluid to the bottom of the heat exchanger bank. where the worst fire side maldistribution conditions are expected to exist. This the same type of support and circuit arrangement used on the conceptual commercial

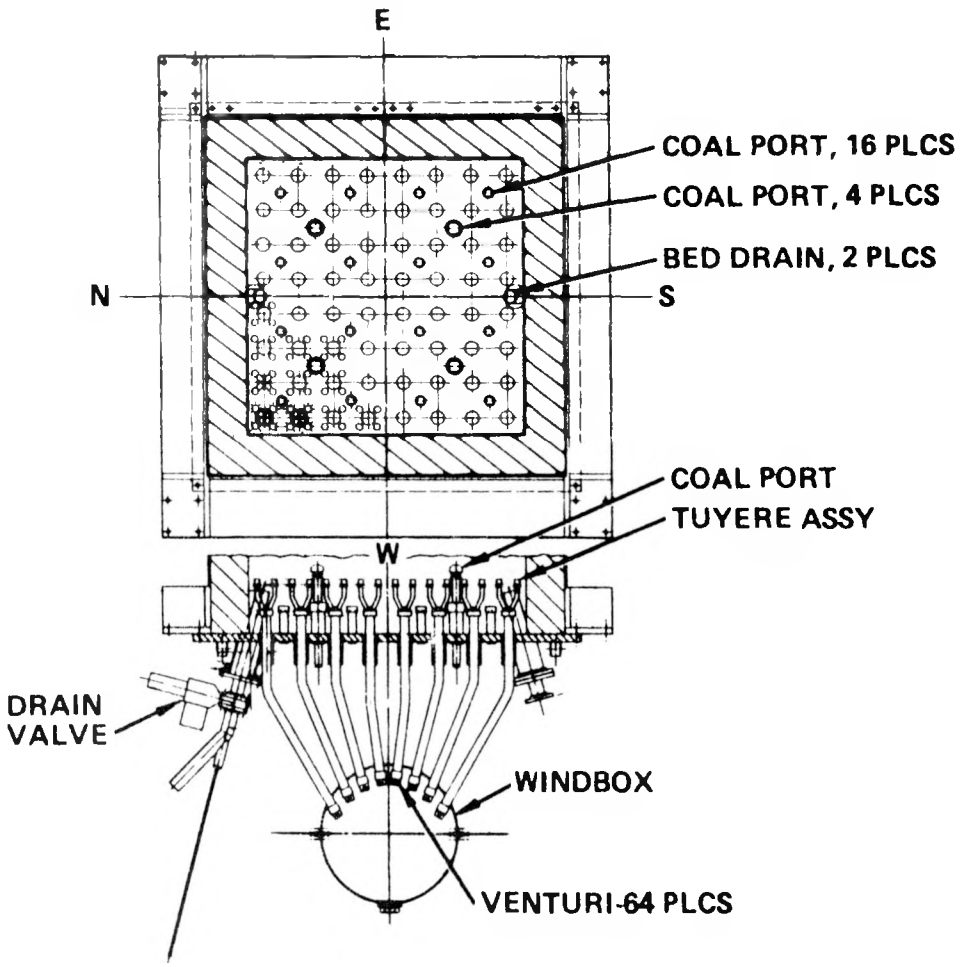


Figure 4-167. Distributor Assembly

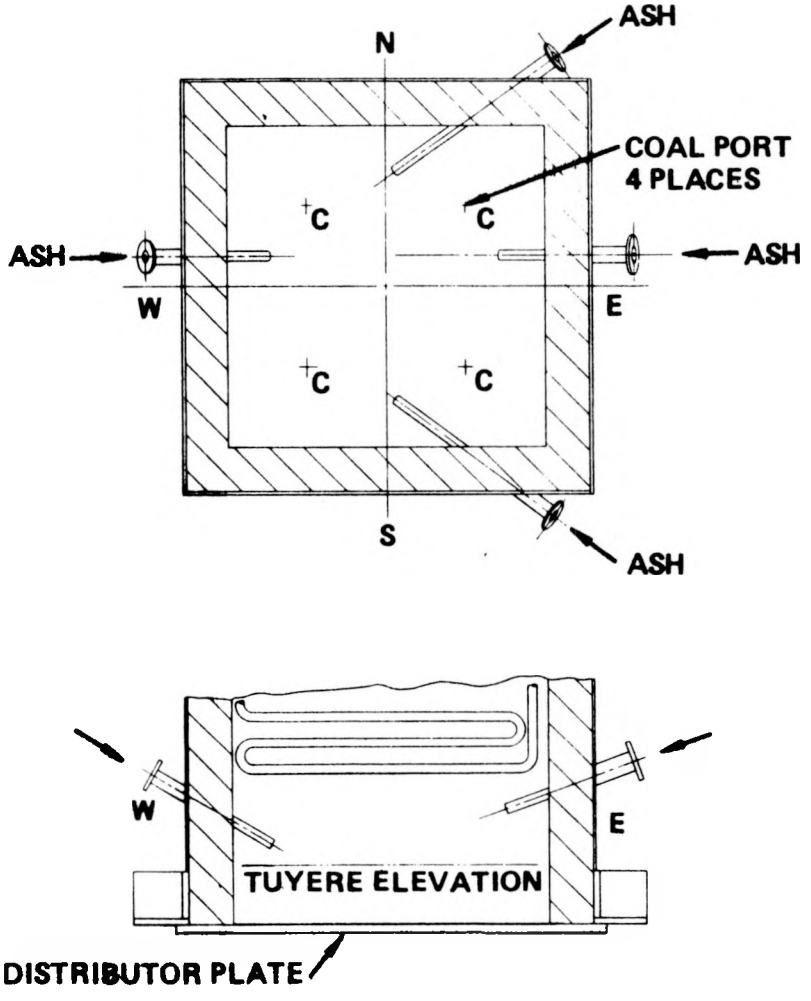


Figure 4-168. Ash Recycles Ports

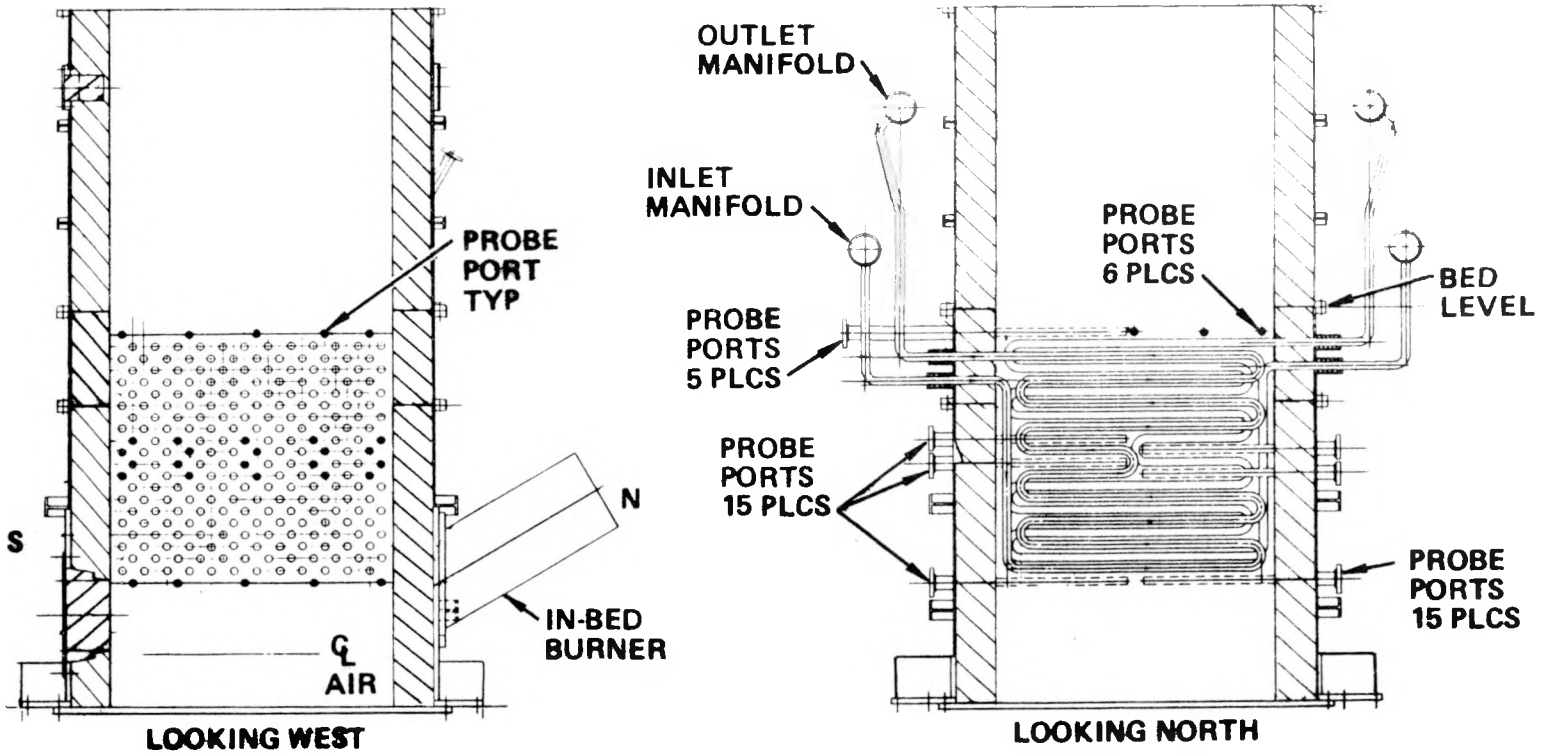


Figure 4-169. In-Bed Heat Exchanger 6' x 6' AFB

TABLE 4-58. BED BANK CHARACTERISTICS

WORKING FLUID SIDE (COOLANT AIR)

- FLOW RATE	14,780 TO 61,630 LBS/HR	
	IN	OUT
- TEMPERATURE, NOMINAL	769 to 854F	1450 to 1550F
- PRESSURE	210 psig MAX	200 psig MAX

HEAT EXCHANGER BANK

- 2.00 O.D. x 0.180 W TUBES, BOTTOM 8 TUBES
- 2.00 O.D. x 0.260 W TUBES, TOP 12 TUBES
- 20 ROWS HIGH, 12 TUBES WIDE, STAGGERED
- 3.00" BACK SPACING, 5.75" SIDE SPACING
- 24 TUBES IN PARALLEL
- LENGTH/TUBE 58 FT, 4 IN.
- TOTAL IN-BED TUBE LENGTH, 1400 FT
- SURFACE AREA 732 FT^2
- CORROSION ALLOWANCE 0.020"
- TUBING MATERIAL ASME SA-213TP304H

TUBE SUPPORTS

- BED LOAD 0.9 PSI VERTICAL, 0.3 PSI HORIZONTAL
- OPERATING TEMPERATURE 1690F MAX
- MATERIAL 304H CRES

TABLE 4-58. (Concluded)

MANIFOLDING

- INLET MANIFOLD SIZE 8" - SCH 40 PIPE
- OUTLET MANIFOLD SIZE 8" - SCH 160 PIPE
- INLET MANIFOLD STRUCTURAL DESIGN CONDITIONS
  - TEMPERATURE, WITH UNBALANCES 912F
  - PRESSURE 210 psig
- INLET MANIFOLD MATERIAL LOW CARBON STEEL
- OUTLET MANIFOLD STRUCTURAL DESIGN CONDITIONS
  - TEMPERATURE, WITH UNBALANCES 1500F
  - PRESSURE 200 psig
- OUTLET MANIFOLD MATERIAL 304H CRES

TABLE 4-59. BED BANK DESIGN FEATURES

DUAL INLET AND OUTLET MANIFOLDS

- COOL DOWNCOMERS FOR SUPPORT ON BOTH SIDES
- LOWEST TEMPERATURE TUBES AT BOTTOM OF BANK

WALL PENETRATIONS

- EXPANSION GAP BETWEEN TUBE AND REFRACTORY
- ADDITIONAL CORROSION ALLOWANCE
- THERMAL SLEEVE REDUCES THERMAL STRESS AND HEAT CONDUCTED TO SETTING

ENTIRE BANK REMOVABLE FROM SETTING

TUBE SIZE AND SPACING

- SIMULATES COMMERCIAL DESIGN CONCEPTS
- SIMILAR TO EXISTING BOILER TYPE TEST AFBs

HANGERS

- TAKE VERTICAL AND HORIZONTAL LOADS
- MINIMUM RESTRICTION OF BED MATERIAL
- ALLOW THERMAL MOVEMENT
- PROVIDE HORIZONTAL & VERTICAL SPACING
- WORK IN BED MATERIAL WITHOUT BINDING

PROVISION FOR DIAGNOSTIC AND CORROSION PROBES

design. Loads in the vertical support tubes are carried out through the refractory wall through a heavy cantilevered portion of tubing (Fig. 4-170) and, finally, through thermal sleeves back to the combustor casing. The thermal sleeves minimize the heat transfer from the hot tubes to the cool casing, and also minimize the thermal stress in this area. Water coolant tubes (25 gal/hr) also are provided next to the hot-wall penetrations to minimize casing distortion and maintain the casing bolted joint integrity.

The tube supports used to attach the horizontal tubes to the vertical support tubes are shown in Fig. 4-171 and their locations are shown in Fig. 4-172. The purpose of the tube supports is to resist the loads imposed on the tubes by the bed and gravity, provide uniform tube spacing and allow free thermal expansion. A pin arrangement, types 2 and 3, is used for tubes in the same plane as the support tubes. and a sliding bar type 1 support is used for the tubes along side of the support tubes. Care was taken in the design of the supports to minimize crevices next to the tubes and to eliminate binding due to entrapped bed material or thermal warpage.

The locations for diagnostic and corrosion probes in the bed are shown in Fig. 4-169. The black dots are corrosion and diagnostic probe locations. Probe locations can be used for either diagnostic or corrosion probes. The locations are arranged to permit evaluation of conditions at the bottom, middle, and top of the tube bank. In addition, the probes can be located near walls, near the center, over coal feed ports, and between coal feed ports.

All probes are bayonet style and extend about 3 feet into the bed. To locate probes within the tube bank it was necessary to shorten some of the tube loops. This was what was done with the 20 locations in the middle of the tube bank, thus providing vertical pairs of locations. Probes above and below the tube bank are installed outside of the tube bank in order to minimize the disruption of the basic circuit.

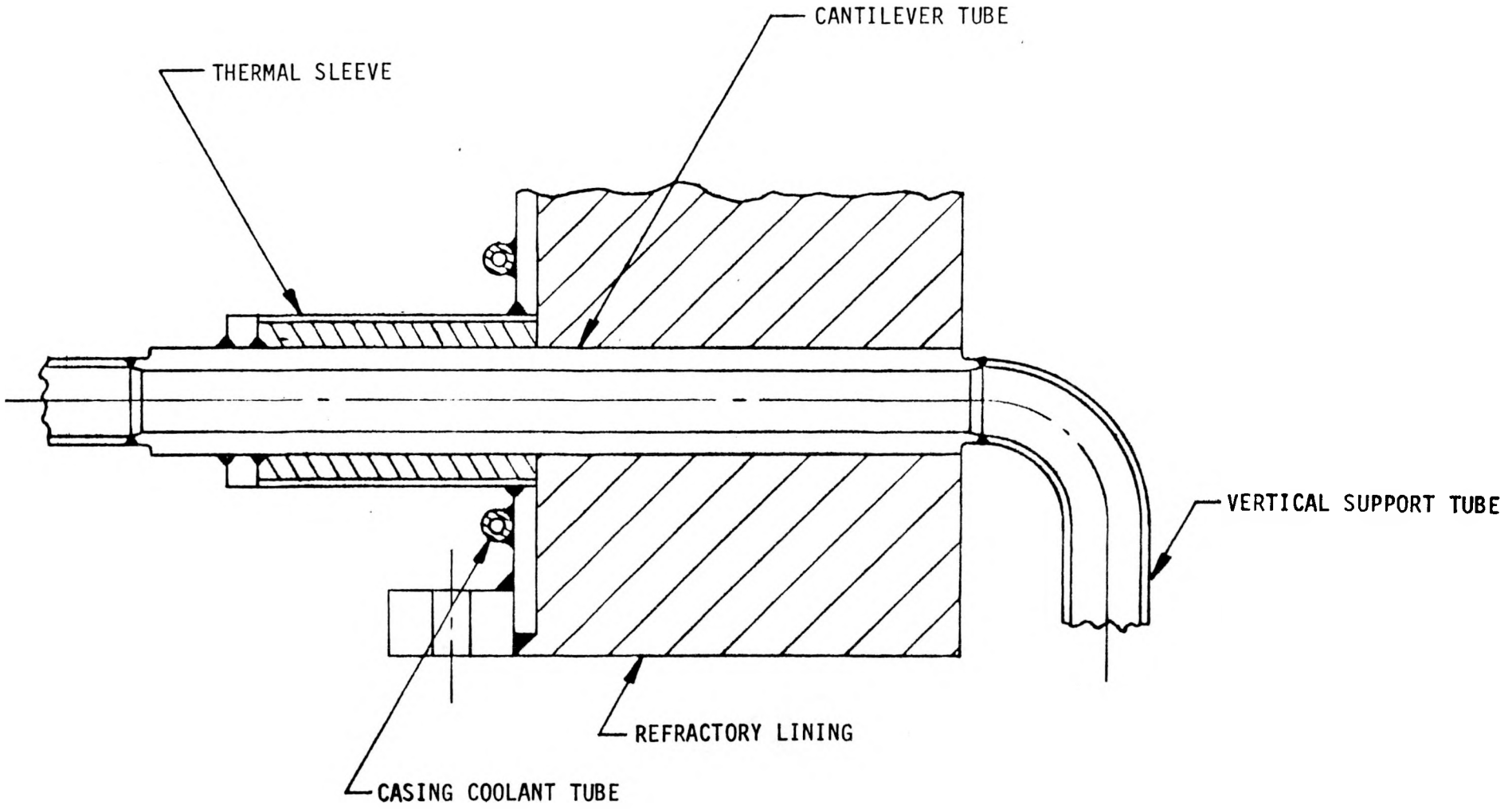


Figure 4-170. In-Bed Wall Penetration Detail, 6' x 6' AFB

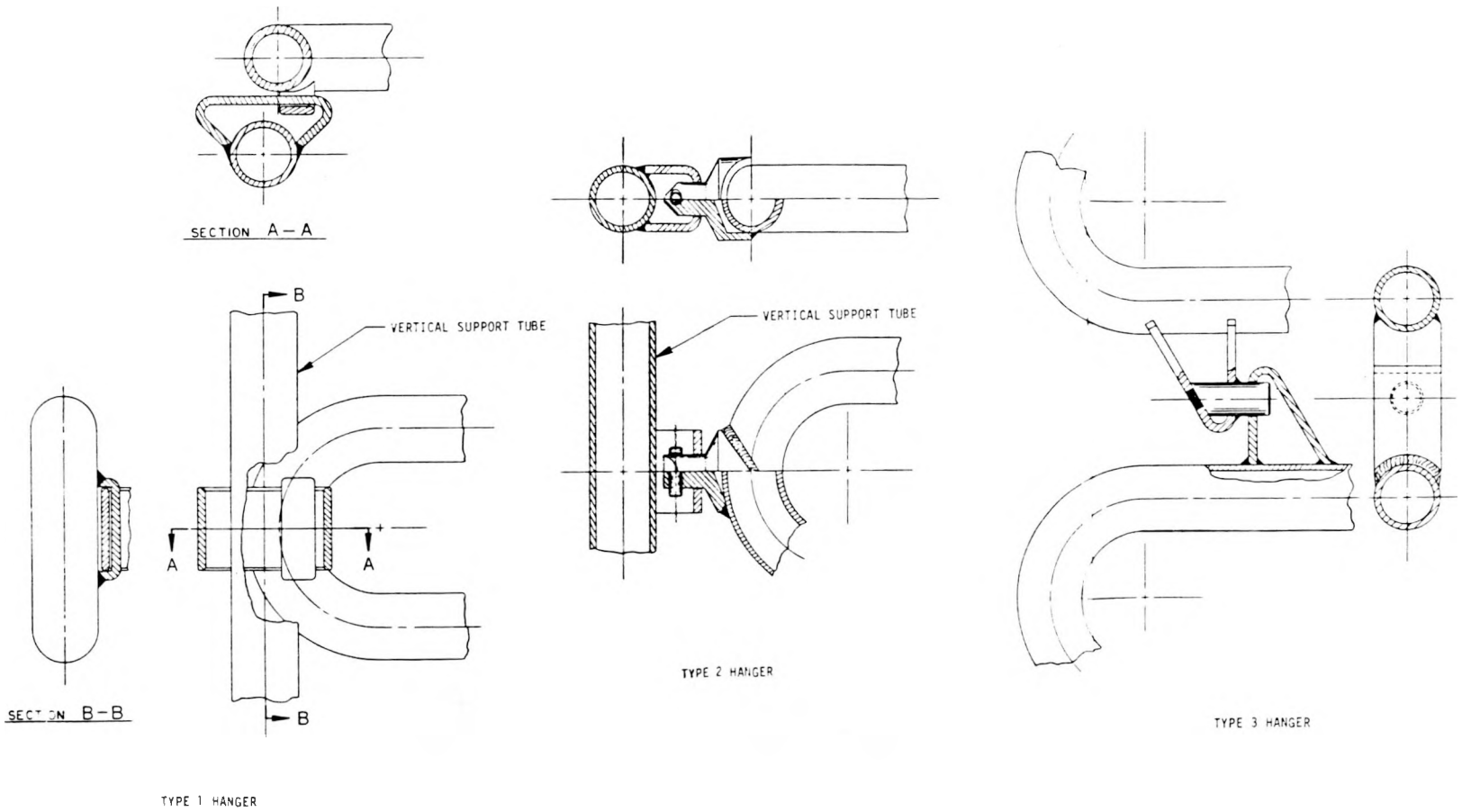


Figure 4-171. Hanger Types

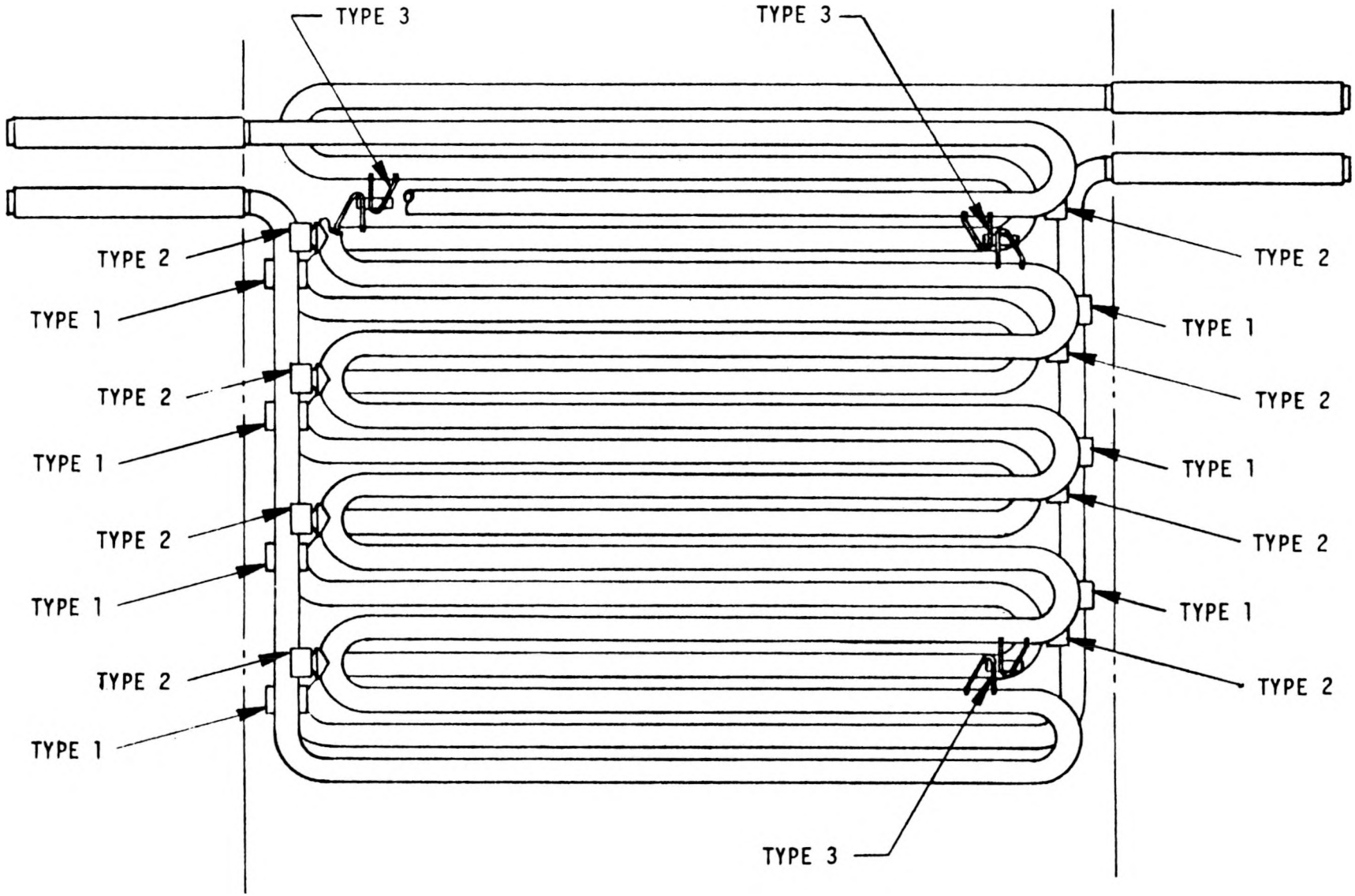


Figure 4-172. In-Bed Tube Support Locations

Convection Bank. The convection bank is shown in Fig. 4-173. The design characteristics are shown in Table 4-60, and design features are shown in Table 4-61. The upper section is made of low carbon steel and the lower section below the soot blower cavity, which is exposed to radiation from the bed, is made from 304H stainless steel.

The bank is 16 rows high by 22 tubes wide. The bottom four rows are staggered, rather than in line, to reduce convection heat input in the tubes that are exposed to the bed radiation. The top portion of the circuit is counter-cross flow to efficiently reduce the flue gas leaving temperature. The lower portion of the circuit, however, is a parallel cross-flow arrangement so that the highest fluid temperature tubes are not exposed to radiation from the bed. This reduces the maximum tube wall temperature. This type of circuit is expected to be important for the commercial designs where working fluid temperatures leaving the convection bank are expected to be above 900 F and metal temperatures may approach levels where corrosion has been encountered in convection passes of PC boilers.

Support of the top portion of the convection bank is off of the inlet tubes which come in from both sides at the top. Support of the lower portion of the convection bank is from the exit tubes that run up past the soot blower cavity to the area just below the inlet tubes. Corrosion/diagnostic probe ports are provided below the convection bank, in the soot blower cavity, and in the top section of the bank.

Setting Design. The combustor setting is based on typical refractory-lined furnace practice, as shown in Fig. 4-174. Design characteristics are shown in Table 4-62 and design features are shown in Table 4-63. It consists of a two-part cast refractory lining in a carbon steel structural shell. The shell is designed to operate at a uniform low temperature of about 200 F to minimize heat loss and thermal stresses. High-temperature penetrations of the casing, such as the heat exchanger tubes, are provided with thermal sleeves and insulation to prevent local heating of the casing and minimize heat loss from the working fluid. The two-part cast lining consists of a 4-inch, erosion-resistant hot face and a 6-inch, lightweight insulating backup. Cast material was chosen to eliminate the joints and potential flue gas channeling problems associated with brick work and to more easily

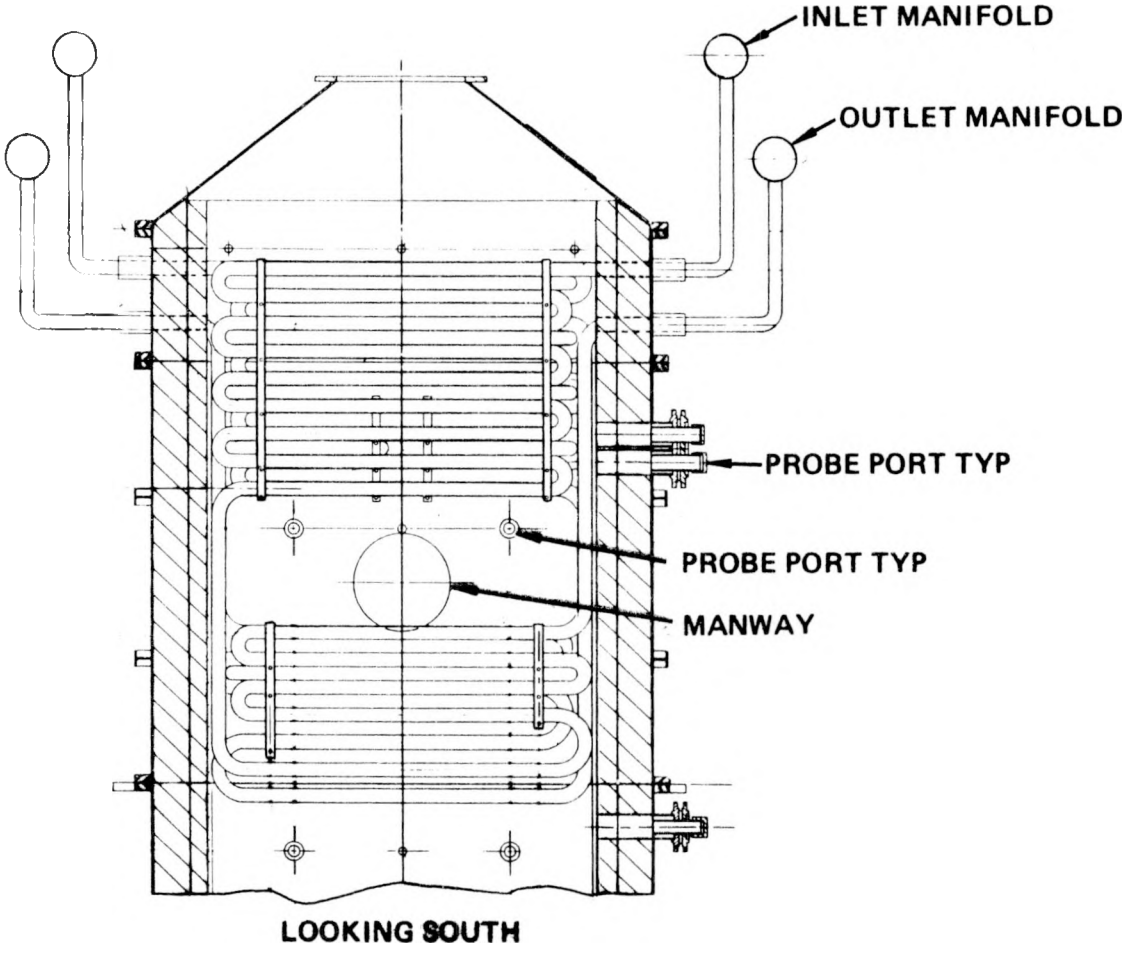


Figure 4-173. Convection Heat Exchanger

TABLE 4-60. CONVECTION BANK CHARACTERISTICS

WORKING FLUID SIDE (COOLANT AIR)

- FLOW RATE 14,780 TO 61,630 LBS/HR

	IN	OUT
- TEMPERATURE, NOMINAL	425F	769 to 854F
- PRESSURE	215 psig MAX	213 psig MAX

HEAT EXCHANGER BANK

- 2.50 O.D. x .200 W TUBES
- 16 ROWS HIGH, 12 IN LINE - 4 STAGGERED
- 22 TUBES WIDE
- 5.00" BACK SPACING, 3.25" SIDE SPACING
- 22 TUBES IN PARALLEL
- LENGTH/TUBE 86 FT - 4 IN.
- TOTAL EXPOSED TUBE LENGTH 1900 FT
- SURFACE AREA 1,243 FT^2
- MATERIAL UPPER SECTION ASME SA-192 CARBON STEEL
  LOWER SECTION ASME SA-213 TP304 H

TABLE 4-60. (Concluded)

MANIFOLDING		
- MANIFOLD SIZE	8" - SCH 40 PIPE	
- INLET MANIFOLD STRUCTURAL DESIGN CONDITIONS		
TEMPERATURE, WITH UNBALANCES		425F
PRESSURE		215 psig
- INLET MANIFOLD MATERIAL	LOW CARBON STEEL	
- OUTLET MANIFOLD STRUCTURAL DESIGN CONDITIONS		
TEMPERATURE, WITH UNBALANCES		912F
PRESSURE		213 psig
- OUTLET MANIFOLD MATERIAL	304H CRES	

TABLE 4-61. CONVECTION BANK DESIGN FEATURES

DUAL INLET AND OUTLET MANIFOLDS

- PROVIDE SUPPORT TUBES ON BOTH SIDES

ENTIRE BANK REMOVABLE FROM SETTING

TUBE SIZE & SPACING

- REPRESENTATIVE OF COMMERCIAL DESIGN

CIRCUIT ARRANGEMENT

- COUNTER/CROSS-FLOW TOP SECTION FOR LOW FLUE GAS LEAVING TEMPERATURE
- PARALLEL/CROSS-FLOW BOTTOM SECTION TO KEEP MAXIMUM METAL TEMPERATURES DOWN

LADDER TYPE TUBE SUPPORT SYSTEM

- STRAPS HUNG OVER TUBES
- CROSS RODS FOR TUBES TO REST ON
- TOP SECTION SUPPORTED FROM OUTLET TUBES

PROBES FOR CORROSION AND DIAGNOSTIC PROBES

SOOT BLOWER CAVITY

- PROVIDES FOR CLEANING AND INSPECTION

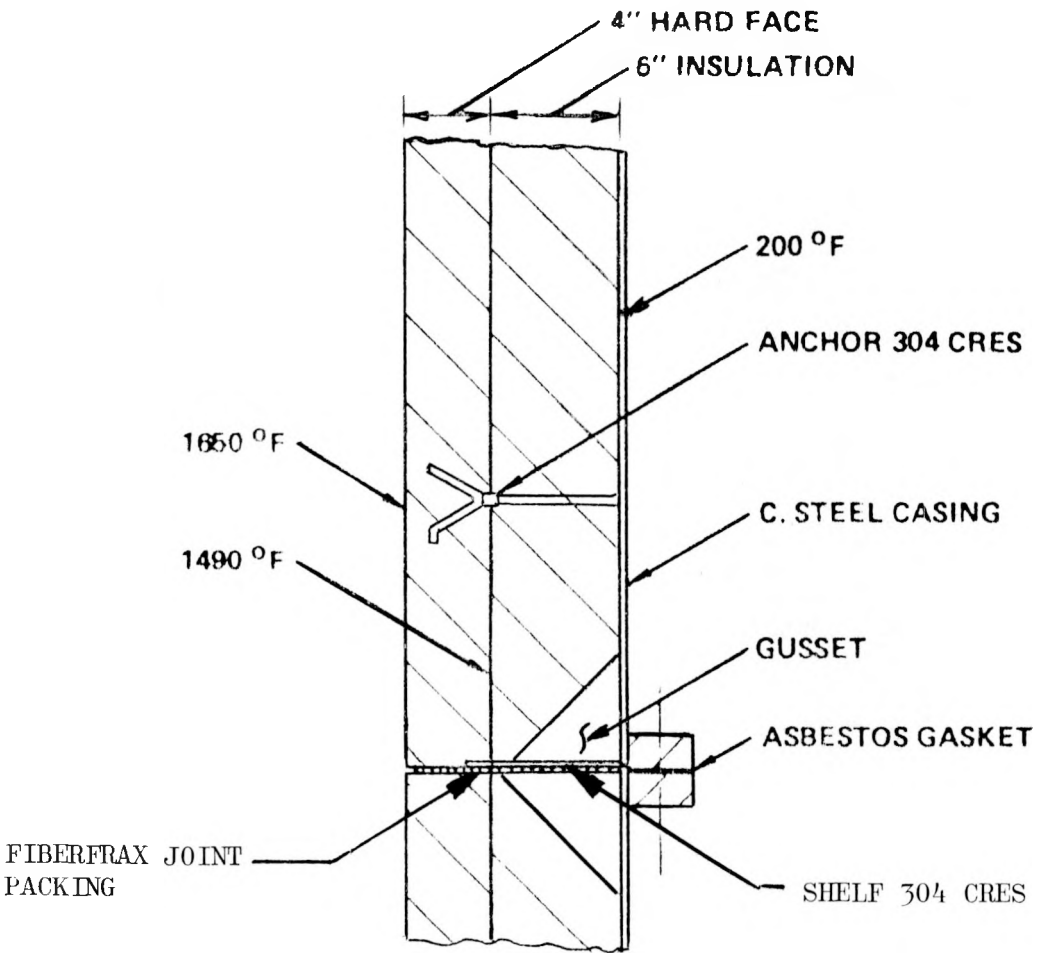


Figure 4-174. Typical Setting Construction

TABLE 4-62. COMBUSTOR SETTING CHARACTERISTICS

CASING MATERIAL - LOW CARBON STEEL

IN-BED STRUCTURAL DESIGN CONDITIONS

	OPERATING	DESIGN
BED PRESSURE	2.5 psig	7 psig
CASING TEMPERATURE	200F	650F

ABOVE BED STRUCTURAL DESIGN CONDITIONS

	OPERATING	DESIGN
FLUE GAS PRESSURE	0.8 H20	1 psig
CASING TEMPERATURE	200F	650F

EXHAUST PLENUM STRUCTURAL DESIGN CONDITIONS

	OPERATING	DESIGN
FLUE GAS PRESSURE	0.8 in H20	0.5 psig*
CASING TEMPERATURE	814F	850F

COMBUSTOR SUPPORT

WEIGHT, 60 TONS, TAKEN OUT THROUGH BASE OF UNIT

SIDE LOADS, 0.4g, TAKEN OUT THROUGH BASE AND AT FLANGE NEAR BOTTOM OF CONVECTION BANK

HEAT LOSS 4% AT 2 FT/SEC

1% at 8 FT/SEC

HOT FACE LINING

MAXIMUM TEMPERATURE 1790F

MATERIAL HARCAST ER ** with 3% BY WT. 304 STAINLESS FIBERS

DENSITY 145 LBS/FT^3

THICKNESS 4 INCHES

INSULATION LAYER

MAXIMUM TEMPERATURE 1630F

MATERIAL, LIGHT WEIGHT 20**

DENSITY 36 LBS/FT^3

THICKNESS 6 INCHES

* FLUE GAS RELIEF VALVE SET PRESSURE

** HARBISON-WALKER REFRACTORY CO.

TABLE 4-63. SETTING DESIGN FEATURES

REFRACTORY LINED, MILD STEEL CASING

SIMULATES COMMERCIAL DESIGN

- MAXIMIZES HEAT AVAILABLE TO HOTTEST WORKING FLUID

COOL OUTSIDE SHELL TEMPERATURE

- CONTROLS HEAT LOSS
- UNIFORM LOW METAL TEMPERATURES MINIMIZE THERMAL STRAINS
- REASONABLE TO WORK AROUND

LARGE SAFETY MARGIN ON STEEL CASING TEMPERATURE

- TEMPERATURES TO 650F DO NOT DEGRADE STRENGTH
- HOT SPOTS ALLOW DETECTION OF REFRACTORY DEGRADATION BEFORE SAFETY HAZARDS EXIST

TWO-PART CAST LINING

- 4 INCH HARD FACE
- 6 INCH INSULATING BACK-UP

STEEL FIBERS IN HARD FACE INCREASE SPALLING & THERMAL SHOCK RESISTANCE

STEEL ANCHORS AND SHELF SUPPORT REFRACTORY

MANWAYS AND INSPECTION PORTS

- INSPECTION ACCESS
- REPAIR AND MODIFICATION ACCESS
- CLEANING ACCESS

commodate the large number of wall penetrations. Steel anchors and shelves are used to hold the liner in place and steel fibers are used in the hot face material to increase resistance to thermal cycling and reduce spalling.

The design pressures for the structural steel casing were selected with a large margin of safety to allow for off-design conditions such as failure of the induced draft fan or starting transients during initial bed fluidization. The exhaust plenum is the weakest part in the system and will be protected from overpressure by a relief system in the flue gas ducting.

In addition to resisting internal pressure, the casing must support the weight of the entire combustor, and be rugged enough to withstand handling during fabrication, transportation, and erection. The higher pressure in-bed sections are fabricated from 1/2 inch steel plate with buckstays for reinforcement. Local, highly loaded areas such as the mounting flange and areas around the manway and burner port are made from 1-1/2-inch steel plate. The upper casting sections are made from 1/4-inch steel plate with smaller buckstays.

Bolted flange joints are used between casing sections to facilitate erection and later disassembly for modification or repair. Soft, 1/4-inch-thick asbestos gaskets are used to ensure a reliable joint at the large rectangular flanges. A fiberfrax ceramic blanket material (Fig. 4-174) is used between mating refractory sections at each joint to prevent flue gases from overheating the steel casing.

Diagnostic and Access Ports. Both diagnostic and corrosion probes were used in the 6' x 6' combustor. Diagnostic probes were used to characterize the bed atmosphere, determine desirable operating conditions and monitor the operation. Oxygen partial pressure and flue gas sampling analysis were performed. Corrosion probes were used to expose a variety of materials to the combustor atmosphere under measured and controlled flue gas and specimen temperature conditions. In addition, comprehensive instrumentation was used to monitor the performance of the combustor. A summary of the ports, probes and instrumentation is given in Table 4-64.

Instrumentation provisions are summarized in Table 4-64. Comprehensive pressure and temperature instrumentation is provided on both combustion and working fluid sides. Instrumentation of particular interest on the 6' x 6' combustor is that used to characterize and control the operation of the bed. Bed temperatures are measured at 2-foot height intervals along two sides of the combustor. Two systems are included to measure bed height. The ports used are 3/8 Schedule 80 CRES pipe extending downward at 45 degrees through the refractory lining. The downward angle, plus a small purge, is used to keep the ports clear of the bed material. A plot of pressure versus height locates the bed height where the plot reads freeboard pressure.

Additionally, there are manhole ports that allow posttest inspection of the various sections of the interior of the combustor. A view port is located in the lower freeboard section which allows viewing the bed during the operation since there will be a slight negative pressure in the location of the viewport. Manhole access covers are located in the area below the in-bed tube bank, freeboard section, and soot blower cavity section of the connection tube bank, and these ports are sufficient to allow complete access to these areas.

A typical probe port is shown in Fig. 4-175. The port configuration shown is for a diagnostic probe that would be removed during combustor operation. The port consists of a pipe and flange welded to the steel combustor casing. A sleeve is clamped in a counterbore in the flange and is used to center and support the probe. The purpose of the ball valve is to allow removal and insertion of the probe during operation. To install a probe, it is inserted through the packin

TABLE 4-64. PORTS, PROBES, INSTRUMENTATION

IN-BED CORROSION/DIAGNOSTIC PROBE PORTS

- BELOW TUBE TANK -10 each
- IN TUBE BANK -20 each
- ABOVE TUBE BANK -11 each

FREEBOARD DIAGNOSTIC PROBE PORTS

- ABOVE BED -3 each

CONVECTION BANK CORROSION/DIAGNOSTIC PROBE PORTS

- BELOW TUBE BANK -4 each
- IN SOOT BLOWER CAVITY -2 each
- IN UPPER BANK -4 each

TYPES OF PROBES

- CORROSION - TUBE MATERIALS
- CORROSION - HANGER MATERIALS
- DIAGNOSTIC - OXYGEN MATERIAL PRESSURE/GAS SAMPLING

INSTRUMENTATION

- BED PRESSURE/HEIGHT, EVERY 12 INCHES
- BED TEMPERATURE, EVERY 24 INCHES
- HEAT TRANSFER PROBES TO DETECT BED SURFACE
- NUMEROUS PRESSURE AND TEMPERATURE MEASUREMENTS

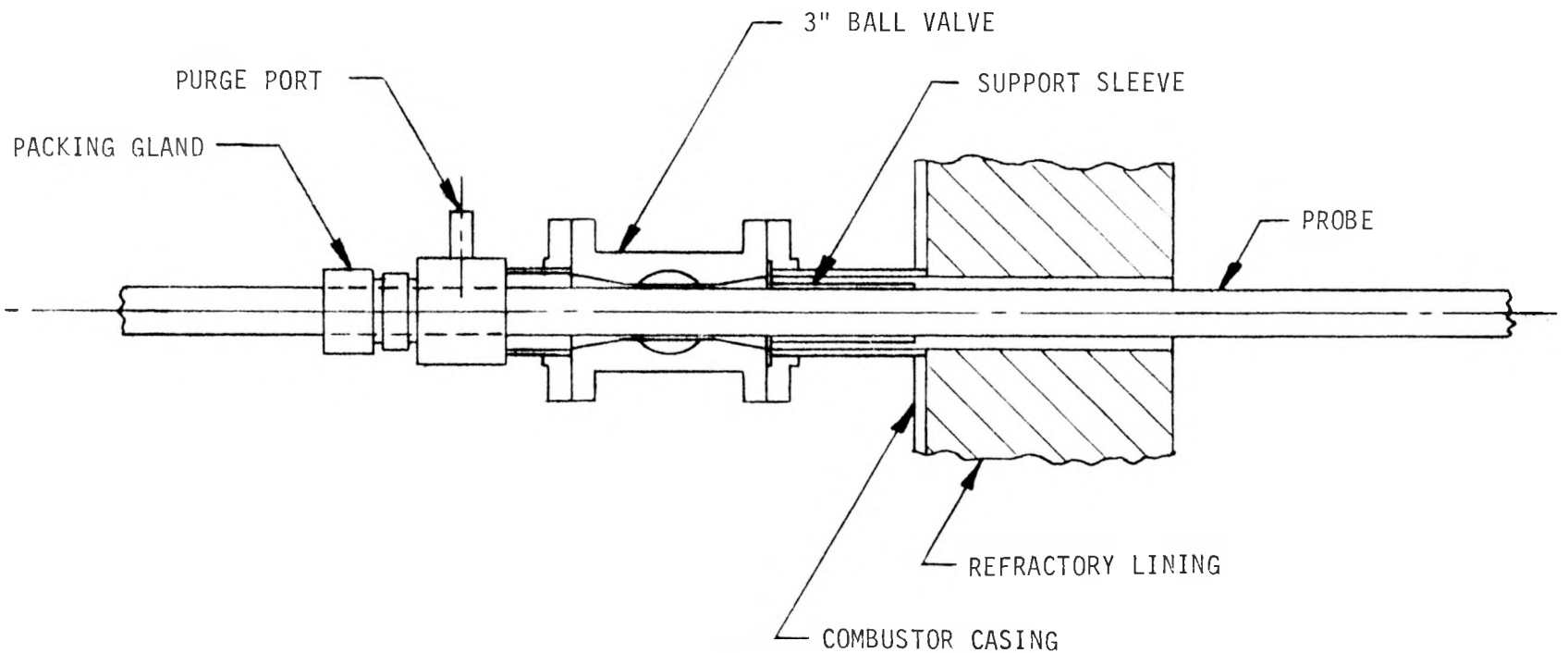


Figure 4-175. Diagnostic Probe Port

land with the valve closed. The valve is then opened and purge gas is introduced to blow bed material out of the port. The probe is then inserted to the desired depth. Ports used with corrosion probes do not require valves, since the probes are not inserted or removed during operation.

Materials Corrosion/Erosion Probe. The design of the in-bed materials corrosion probe is shown in Fig. 4-176. The probe characteristics are shown in Table 4-65, and features are shown in Table 4-66. The probe outside diameter is 2.00 inches to match the size of the 6' x 6' in-bed tubes.

The in-bed corrosion probe is designed to expose 31 material specimens to the AFB environment, while maintaining a desired temperature profile along the specimens. A plot of temperature profile versus coolant flow is shown in Fig. 4-177. The specimens are rings mounted coaxially on a tube of slightly smaller outer diameter than the inside diameter of the specimen rings, and held concentrically to the inner tube by four spacer wires between specimens and tube. Air flows through the annulus, created by the difference in diameters, at a predetermined rate, to maintain the temperature profile. The specimens are located axially along the probe by a spring-loaded outer tube of the same diameter as the specimens. Four thermocouples are embedded in specimens along the "stack" which are monitored during AFB operation to verify that the correct temperature profile is being maintained. A thermocouple also is located at the air coolant discharge to monitor the coolant temperature rise.

The inner (core) tube is made of 304 stainless steel and acts as the structural member of the probe. Four stainless-steel wires are welded along the outside of the tube to locate the specimens and outer tube concentrically with the inner tube. Coolant flows through the annular gap, which is 0.74-inch wide between specimens and inner tube, cooling the inner tube, while maintaining the prescribed temperature profile along the specimens. Holes are drilled through the inner tube at the hot end for the coolant to pass into the inside of the tube. Sufficient clearance exists between the spacer wires and the specimens and outer tube to allow relative axial motion of the parts caused by differing thermal expansions. Bed forces acting on the specimens are transferred through the spacer wires to the inner tube, which is cantilevered into the AFB combustor.

CORROSION TEST PROBE

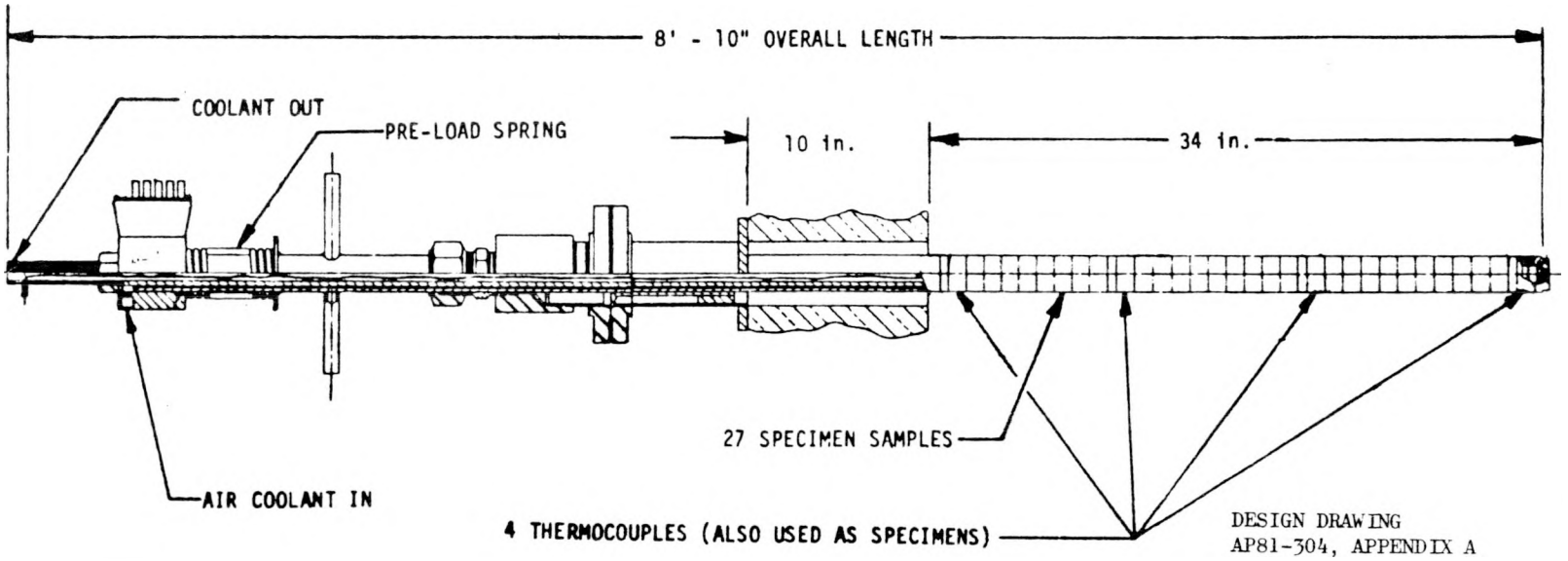


Figure 4-176. Materials Corrosion Probe, 6' x 6' AFB

TABLE 4-65. IN-BED CORROSION PROBE CHARACTERISTICS

SIZE	
EXTERNAL: 2 INCHES OD x 106 INCHES (8 FEET 10 INCHES) LONG	
WEIGHT	
TOTAL: 60 POUNDS	
SPECIMENS	
NUMBER PER PROBE:	31
MATERIALS:	304H STAINLESS STEEL
	310 STAINLESS STEEL
	INCOLOY 800H
	INCONEL 617
	INCOCLAD 347/618 E
	INCONEL 618E
	INCOCLAD FeCrAl Y/617
	NIMONIC 86
	HASTELLOY X
	HAYNES 188
	HK 40 (CENTRIFUGALLY CAST)
THERMOCOUPLES	
NUMBER PER PROBE:	5
TYPE:	CHROMEL-ALUMEL WITH 304 STAINLESS STEEL SHEATH
SIZE:	0.062 INCH DIAMETER
COOLANT	
TYPE:	AIR
FLOWRATE:	0.015 LBM/SEC NOMINAL
INLET TEMPERATURE:	80 F
OUTLET TEMPERATURE:	760 F NOMINAL
PRESSURE DROP:	2 PSI NOMINAL
MAJOR COMPONENTS	
MATERIAL:	304 STAINLESS STEEL

TABLE 4-66. IN-BED CORROSION PROBE FEATURES

SPECIMENS

- 31 PER PROBE
- SHIP LAP JOINT BETWEEN SPECIMENS
- SPRING LOADED TO MAINTAIN SEAL
- FOUR THERMOCOUPLED SPECIMENS FOR TEMPERATURE MONITORING AND CONTROL

COOLANT

- AIR
- FLOW ADJUSTABLE TO OBTAIN DESIRED SPECIMEN TEMPERATURES
- LOW PRESSURE DROP
- READILY AVAILABLE AND INEXPENSIVE

STRUCTURAL DESIGN

- CANTILEVERED FROM PROBE PORT
- COOL INNER TUBE PROVIDES SUPPORT FOR SPECIMENS
- DESIGNED TO TAKE CYCLIC BED LOADING
- PRELOAD SPRING AND SLIP JOINT IN OUTER TUBE ACCOMMODATE THERMAL EXPANSION

COOLANT FLOW CIRCUIT

- INLET FLOW INTO ANNULUS COOLS EXPANSION JOINT, SPRING, SPECIMENS
- WIRE SPACERS MAINTAIN COOLANT ANNULUS
- CONCENTRIC CIRCUIT RETURNS COOLANT TO OUTSIDE THROUGH CENTER TUBE

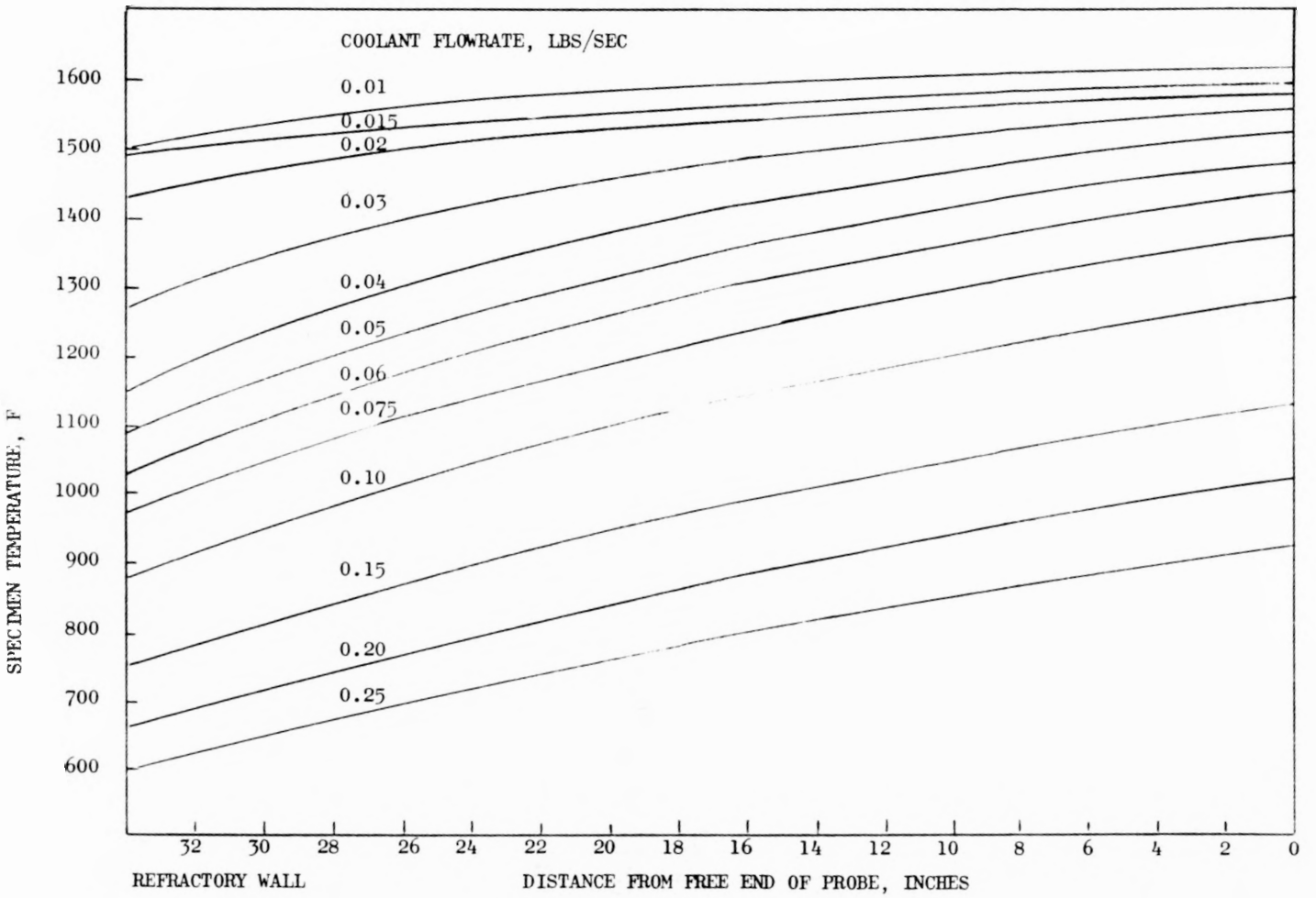


Figure 4-177. Specimen Temperature vs Coolant Flow

The specimens are rings 1-inch long with 1.580 inch nominal ID, and are cut from either 2-inch tube, 1-1/2-inch Schedule 80 pipe, or round bar stock, depending on availability of the material. Mating grooves are machined into each end of the specimen, and the specimens are held together in a loose running fit. Some coolant is expected to leak from each probe into the bed, but this small amount should not affect combustor operation nor compromise results of the corrosion tested in any way. Specimen materials are listed in Table 4-65. Each probe will not expose all alloy materials; rather, the specimen materials for each probe will be individually selected and several iterations of those materials will be placed along the probe to test against differing environments across the fluidized bed.

A thermocouple is brazed into each of four 304 CRES specimens installed along the length of the probe. Alignment marks are provided on the thermocouple specimens to ensure that the thermocouples all monitor temperature at the same circumferential position. Wires from the thermocouples pass through holes in the inner tube and exit the probe through the inside of the inner tube. The holes in the inner tube are larger than the thermocouple wires and slanted to allow the wire to slide in and out during differential thermal expansion of the materials. One thermocouple also monitors the coolant exhaust temperature. After exiting the probe, the wires are connected to junctions which may be plugged into the facility instrumentation.

The outer tube of the probe locates the specimens axially and acts as the probe support at the combustor wall. It is made from 2-inch by 0.188-inch wall 304 stainless-steel tubing. Alignment marks are provided on the outer tube to visually determine the circumferential position of the thermocouples. Two handles are welded onto the outer tube to aid in insertion and extraction of the probe.

A gland of 304 stainless-steel is located near the external end of the probe. A boss is machined into the gland, into which an orifice is installed. The orifice is connected to the coolant inlet line and controls the coolant flowrate through the probe. An O-ring in the gland provides for axial expansion. The gland also serves as the spring stop and thermocouple wire junction mount.

A hardened steel spring is provided to keep the specimens in contact and account for thermal expansion of the parts. The spring preload is set at 375 pounds to provide axial load on the specimen joints without overstressing any of the hot components.

The design of probes for in-bed hanger materials was the same as the probes just described, except hanger material specimens were welded to the outside of the specimen rings. The specimens protruded into the bed, simulating the conditions on an actual hanger. The weld to the specimen provides joint data as well.

Convection bank corrosion probes were similar to the in-bed probes except they were 2-1/2 inches in diameter to interface properly with the convection bank tubes and used different specimen materials, as listed in Table 4-67.

TABLE 4-67. CONVECTION BANK PROBE MATERIALS

304H	STAINLESS STEEL
AISI 1010	(CARBON STEEL)
ASTM A 213 T2	(1/2 Cr-1/2 Mo STEEL)
ASTM A 213 T22	(2-1/4 Cr-1 Mo STEEL)
ASTM A 213 T9	(9 Cr-1 Mo STEEL)

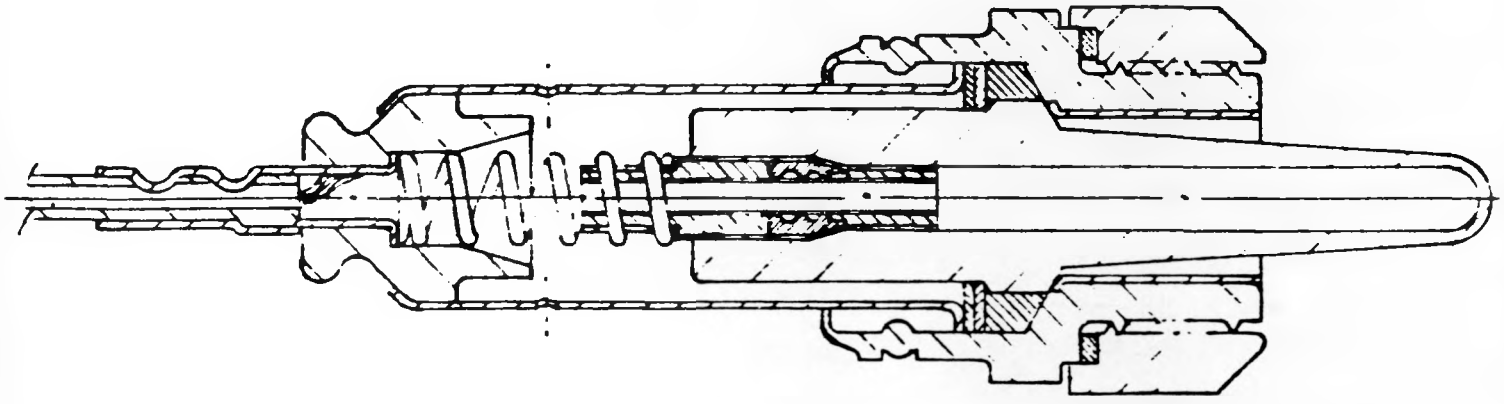
Oxygen Partial Pressure Probe. The oxygen partial pressure (PO_2) probe measurements in the AFB combustor provide a direct evaluation of the sulfidation potential environment that the heat exchanger tubes materials are exposed to on a location and time basis. The sulfidation potential is inversely proportional to the oxidation potential, and the oxidation potential is measured with a special high-response probe.

Battelle - Developed PO_2 Probe. A combined oxygen partial pressure and gas-sampling probe was developed by Battelle Columbus Laboratories to monitor real-time oxygen levels in the fluidized bed and to extract gas samples during bed operation. The Battelle probe is 7 feet long and will penetrate 33 inches into the Rocketdyne 6' x 6' AFB combustor when inserted into the short probing ports.

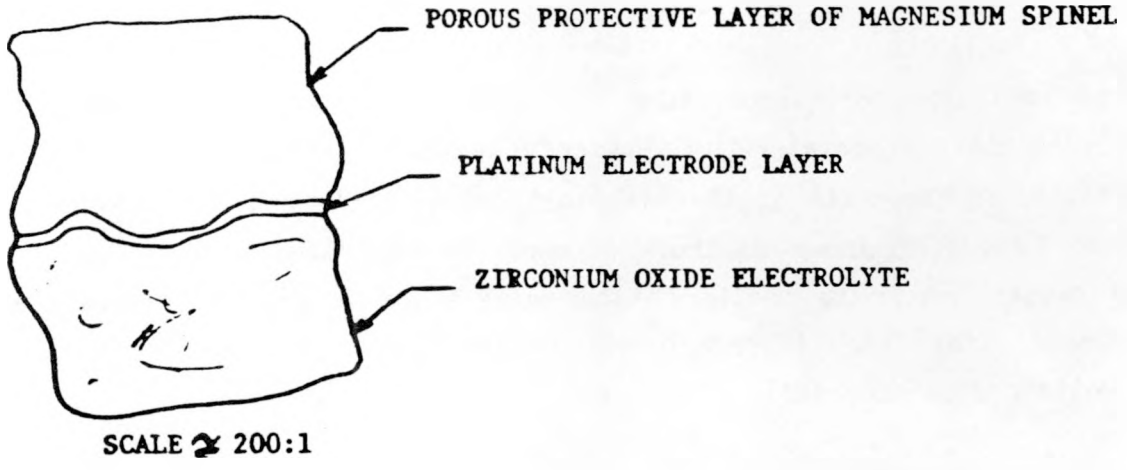
The probe body consists of three tubes, forming two annular coolant passages. The outer tube is a 2-inch OD stainless-steel tube; the middle tube is a thick aluminum tube with a spiral channel machined into the OD, and the inner tube is a 1-1/8-inch, stainless-steel, thin-walled tube. Cooling water flows into the probe, through the inner annulus, returns through the spiral outer annulus, and exits from the probe. The coolant flowrate is such that boiling does not occur, and the aluminum tube remains cool for structural integrity.

A Bosch automobile exhaust oxygen sensor is threaded into a plate at one end of the probe body. The slotted protective shield over the original factory sensor element was removed before installation on the probe body to allow combustion gases to circulate freely around the sensor element, giving better response to rapidly changing oxygen levels in the bed. Wrench flats were machined off to allow clearance between the sensor and other parts of the probe. A positive electrical lead exits from the sensor body, and is connected to a high temperature insulated wire, which runs through the center of the probe, and connects to instrumentation lines at the end of the probe opposite the sensor. The sensor is grounded to the probe body when threaded into it, and the negative instrumentation lead is connected to the probe body.

The sensor unit is a platinum-zirconia type oxygen sensor used in automotive emission control systems, and its cross section is shown in Fig. 4-178. The sensor itself is a platinum/zirconia (Y_2O_3 stabilized)/platinum, high-temperature galvanic cell, the zirconia being the solid-state electrolyte, with platinum electrodes. The electrolyte operates between 950 F and 2500 F, and oxygen pressures of 10^{-20} to 1 atm. As shown in Fig. 4-178, the outer platinum electrode is overlaid with a thin magnesia spinel ceramic coating to protect the sensor from corrosive environments. The contact spring, contact bushing, and housing are made of carbon steel, and must be maintained below 1000 F; other components of the sensor unit can operate at temperatures found in AFB combustors. At high temperatures (above 1200 F), oxygen ions in the inner lattices of the zirconia-based electrolyte become active, and oxygen molecules in the gases on both sides of the electrolyte tend to pull electrons off of the electrolyte to fill outer shells. When the sensor is used for monitoring combustion gases, the reference air has a constant, but higher concentration of oxygen molecules than



Cross-Section of Bosch Oxygen Sensor



Detail of Ceramic-Platinum and Protective Coating of Oxygen Sensor

Figure 4-178. Bosch Oxygen Sensor

does the combustion gas, making the platinum electrode at the reference air junction the cathode. The platinum electrode exposed to the combustion gases then becomes the anode of the cell, and the voltage across the cell varies with the ratio of the oxygen concentration in the reference air to that in the combustion gas.

The output of a platinum-zirconia sensor operating in the voltage mode is given by the Nernst equation:

$$V = kT \ln \frac{PO_2^r}{PO_2^x}$$

where

V = cell voltage, mV
K = 0.0215 mV/K
T = cell temperature, K
PO_2^r = Oxygen partial pressure of reference air, 0.219 atm
PO_x^r = Oxygen partial pressure of gas sample, atm

As can be seen, the cell temperature is required when using the Nernst equation. To determine cell temperature, a 304 CRES sheathed chromel-alumel thermocouple was installed in the probe so that it protrudes into the bed the same distance as the sensor cell protrudes. Another thermocouple was embedded in the plate holding the oxygen sensor to monitor plate temperature to ensure temperatures that could damage either the silicone O-ring or the carbon steel parts in the oxygen sensor would not be exceeded.

Rocketdyne-Designed PO_2 Probe. An oxygen partial pressure probe built by Rocketdyne (Fig. 4-179) is very similar to the Battelle probe, with the following differences. The Rocketdyne Probe has a working length of 8 feet, or approximately 18 inches more than the Battelle probe, enabling bed penetrations 33 inches deep in the long upper combustor ports. The Rocketdyne probe utilizes a stainless-steel tube with a thick wire welded spirally on the outer diameter for a coolant channel, instead of the machined aluminum tube used by Battelle.

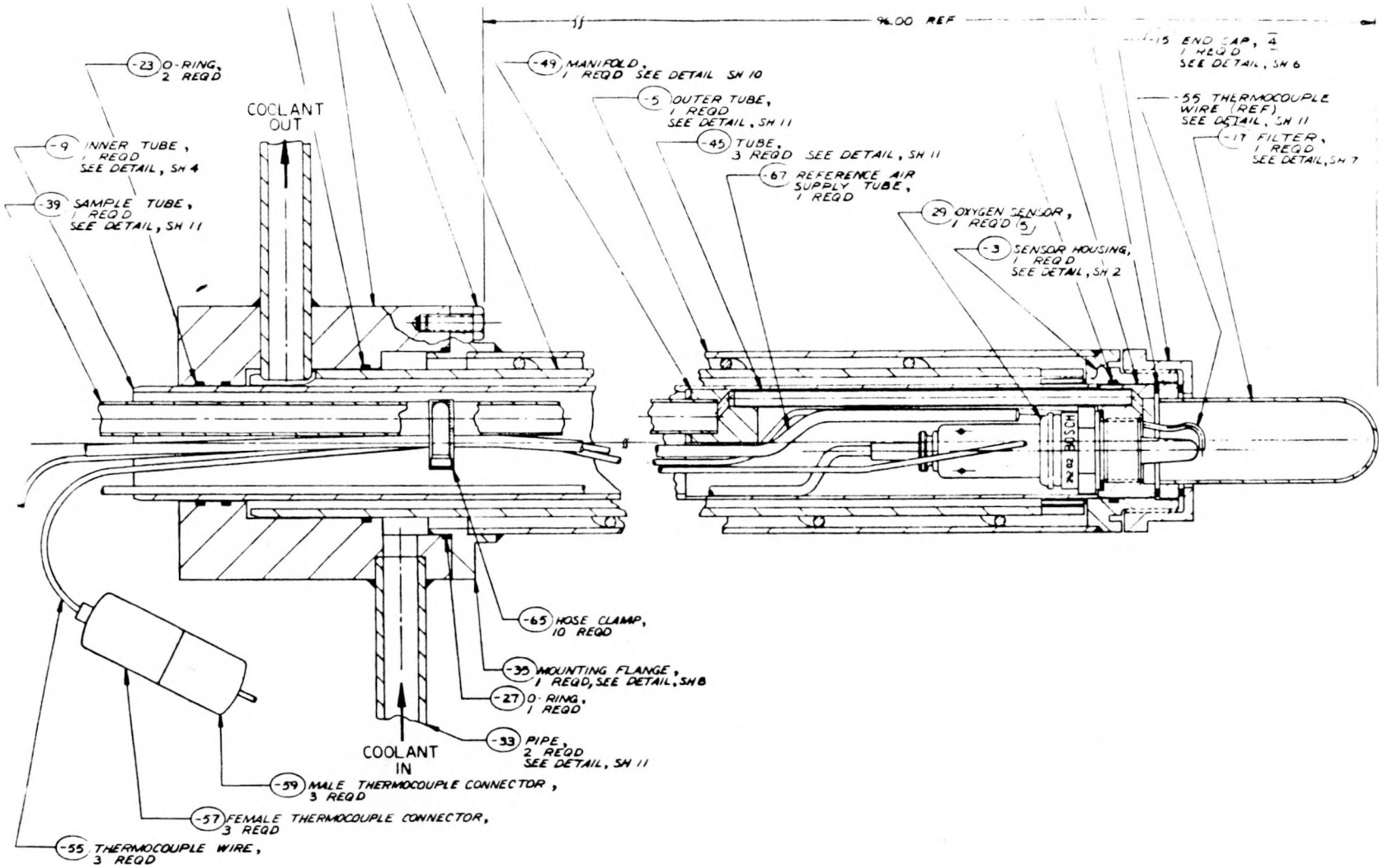


Figure 4-179. Oxygen Partial Pressure Probe

The Rocketdyne probe has two thermocouples to measure combustion gas temperature, but only one is used during operation, the second being a backup. The only other differences in the two probes are minor dimensional changes to allow use of different O-rings and clearances for various parts.

Data Collection and Reduction. Sensor output voltage and temperature are recorded at a rate of 100 times per second on a digital data acquisition system. The data are subsequently reduced, by computer, utilizing the Nernst Equation, rearranged as:

$$PO_2 = 0.209\ e^{[-8.361 \times 10^4\ (\frac{V}{T})]}$$

where

V = oxygen sensor output, volts
T = oxygen sensor temperature, R
PO_2 = oxygen partial pressure, atm

Each file is divided into records, each record containing 1.2 seconds of sensor voltage and temperature data. The sensor voltage and temperature at each data sampling point (125 points per record) are inserted into the above Nernst equation, and the percent of samples in each record that correspond to:

1. PO_2, $>10^{-3.4}$ atm (oxidizing environment)
2. $10^{-12} < PO_2 < 10^{-3.4}$ (of no interest)
3. $PO_2 < 10^{-12}$ atm (reducing environment)

are tabulated for each probe location. The percentage of oxidizing and reducing potential are then used to assess the local bed environment for the particular operating conditions.

Fabrication. Fabrication of the 6' x 6' combustor was to the detail drawings and specifications produced by Rocketdyne and included in this section. Actual construction was performed by a fabricator located in the Los Angeles area. The areas of expertise required were:

- Section I code authorization
- Steel fabrication experience
- Refractory-lined vessel experience

For both safety and quality control reasons, the pressure parts were fabricated to the requirement of Section I, Power Boilers, of the A.S.M.E. Boiler and Pressure Code. This included the use of code-approved materials, certified weld procedures, pressure checks, inspection by an authorized Code inspector, and submittal of appropriate Code paperwork. Fabrication of structural steel components, such as the casing sections, was done by certified welders. Casting of the refractory lining was performed by an experienced commercial installer using Rocketdyne specified materials, and initial curing, bake-out of the refractory, was performed at the fabricator's facility. Final curing was performed as part of the initial hot-firing run of the combustor.

Final cleaning of the pressure parts was performed at the fabricator's facility using commercial methods specified by Rocketdyne. The primary purpose of the cleaning procedures is to remove any contaminants, expecially chlorides, that would cause stress corrosion during operation. Additionally, oil or grease or other organic material present on the interior surfaces would carbonize, and might possibly interfere with obtaining valid measurements of heat transfer effects, which is one of the important program objectives.

The eight major sections that make up the combustor are shown in Fig. 4-180, along with their weights. Each section was assembled at the fabricator, including painting, installing all port and manway covers, and sealing all openings. The eight sections were assembled, as shown in Fig. 4-181, for transportation by truck to the test facility.

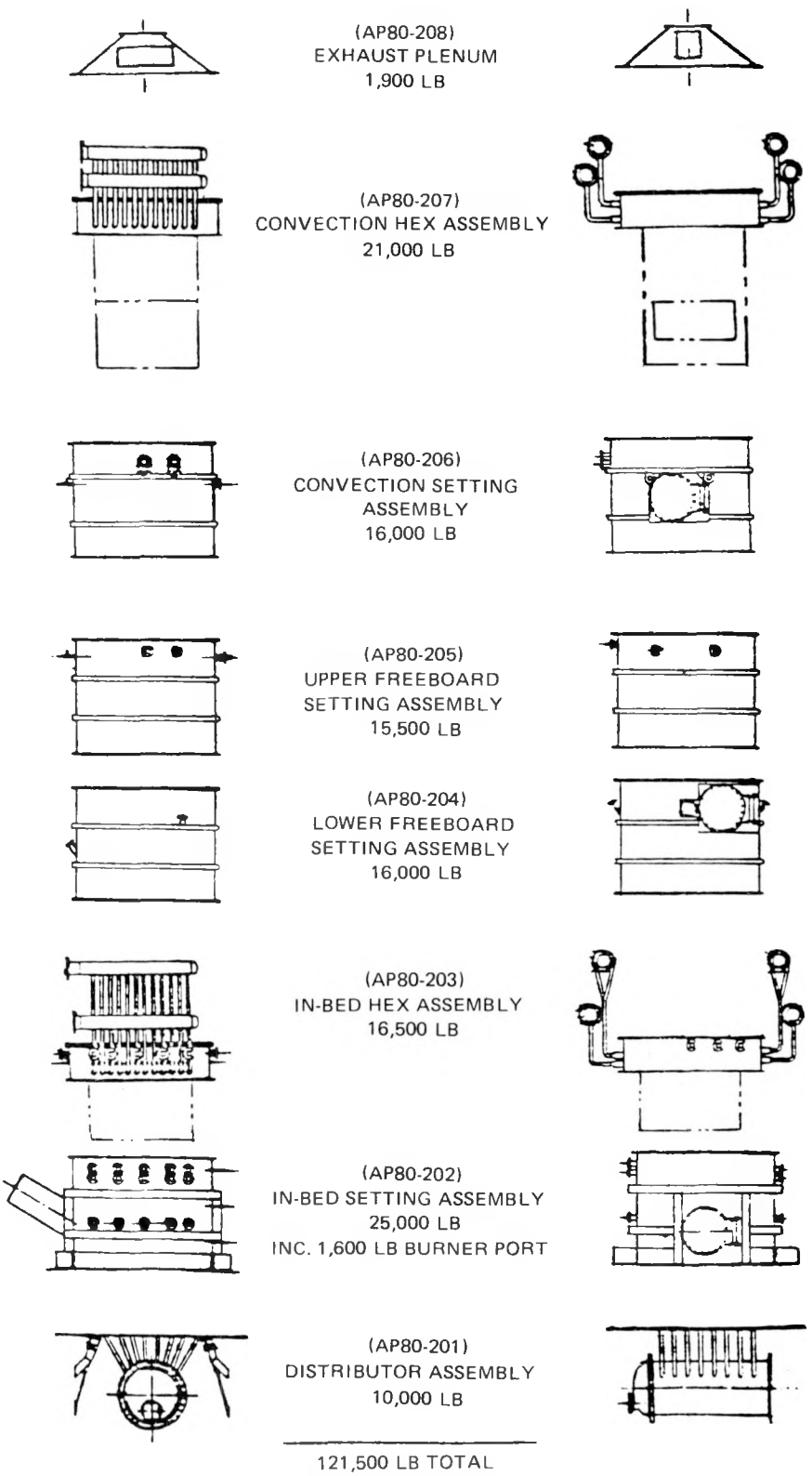


Figure 4-180. 6' x 6' AFB Nominal Weights

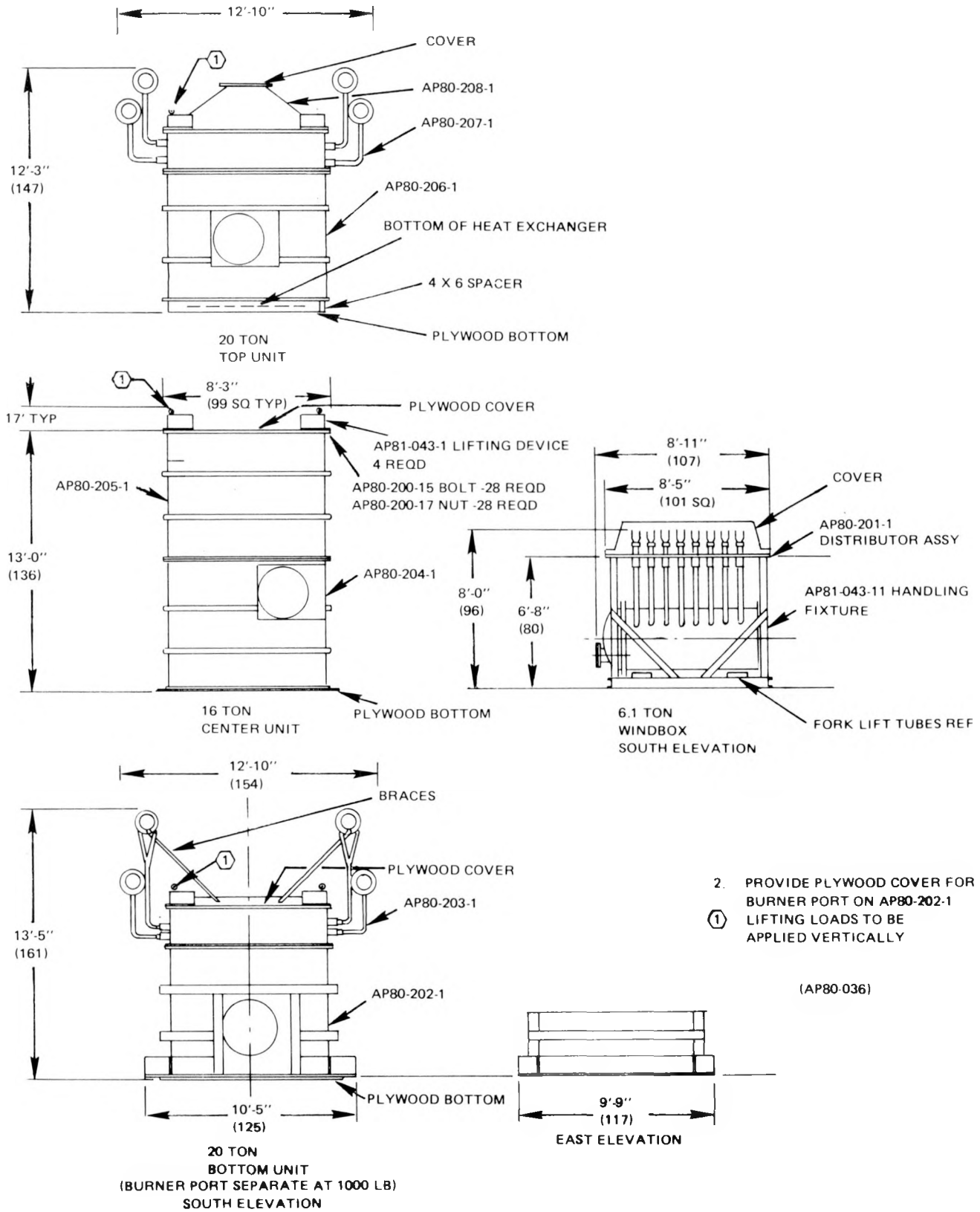


Figure 4-181. 6' x6' AFB Preparation for Transportation

4.4.4 Auxiliary Equipment

The auxiliary equipment is made up of a number of items, and most of these components were commercially available items procured in accordance with specifications based on the system requirements. Some of the components were functionally designed by Rocketdyne and fabricated by outside vendors. These components are described along with their performance and capabilities.

Forced Draft Blower. This unit provides combustion air to the distributor and fluidized bed, and the unit has to operate over a wide range of flow and back pressure conditions. The pressure drop is from the inlet to the freeboard section the combustor where a balanced draft is maintained by the induced draft fan. This pressure drop is determined by the ducting, air heater, distributor, and fluidized bed, where the latter is the major contributor to the pressure drop. The bed pressure drop has the greatest fluctuations since the effective bed density varies with time and bed composition. The flow requirements for the blower are shown in Fig. 4-182 for empty and full bed conditions. The distributor is the second major pressure drop where the tuyere orifices are sized to provide a minimum of 10 inches water gauge (W.G.). Two sets of tuyere orifices were considered to cover the operating range, and this is reflected in Fig. 4-182, where only one set of orifices was used at superficial velocities from 4 to 8 ft/sec.

The blower is a Hoffman Model 75105A skid-mounted package (Fig. 4-183) complete with air inlet filter/silencer, flow control damper, and automatic blowoff surge control system. The expected performance of this unit are presented in Fig. 4-184 and Table 4-68 presents the details. The blowoff system automatically measures the flow using the motor current, and at low flowrates, the blowoff system will automatically blow off sufficient flow to prevent operating in the surge region.

Air Preheater. The air preheater is used to exchange heat between the exhaust flue gas and the combustion air. The flue gas is cooled to less than 400 F so it can be safely handled by the baghouse, and the combustion air is heated to about 700 F. The preheater was designed to have flow characteristics and pressure drop that correspond to typical boiler practice, and the design performance is reflected in the operating temperature and flow profiles previously presented.

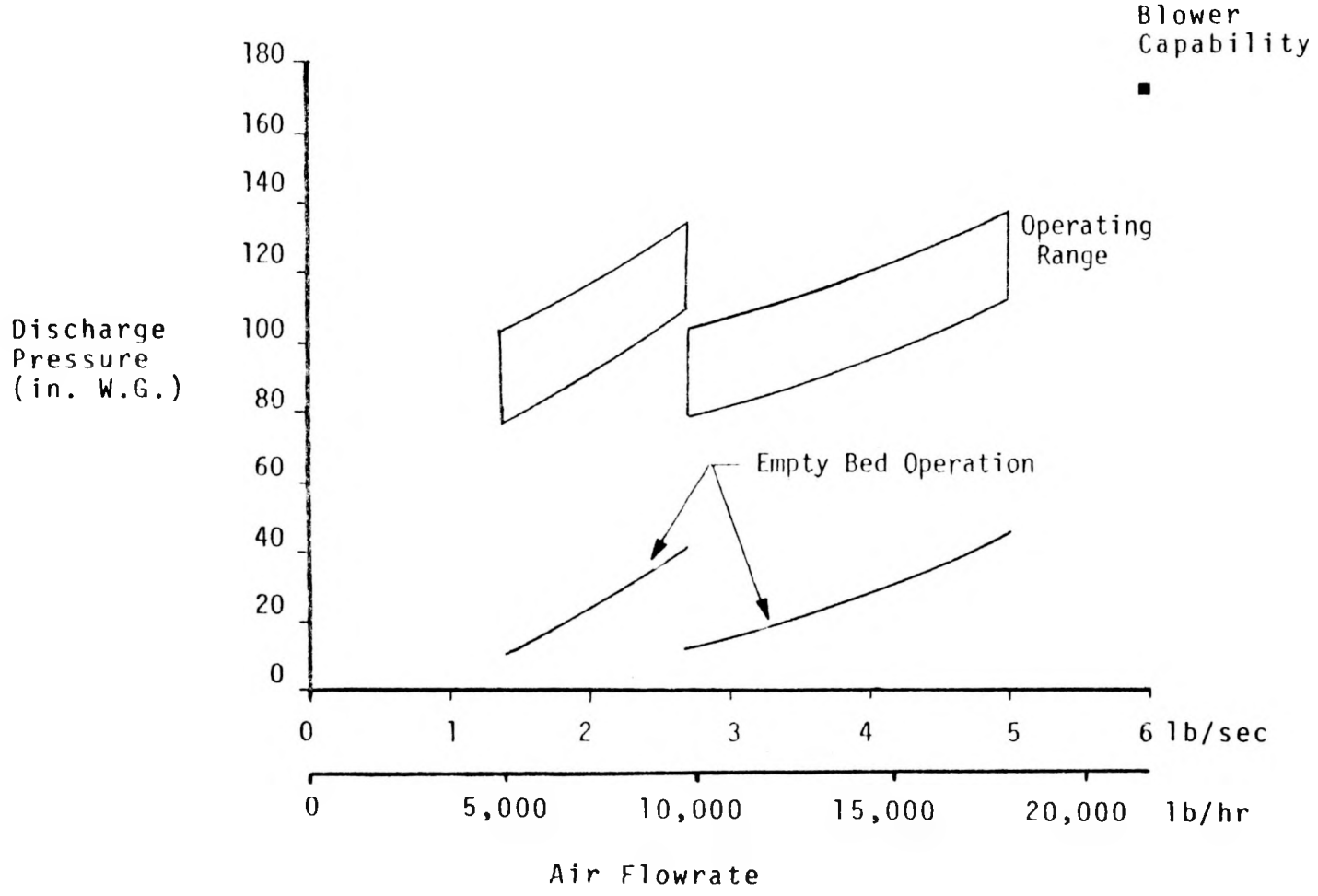


Figure 4-182. Forced Draft Blower Operating Range

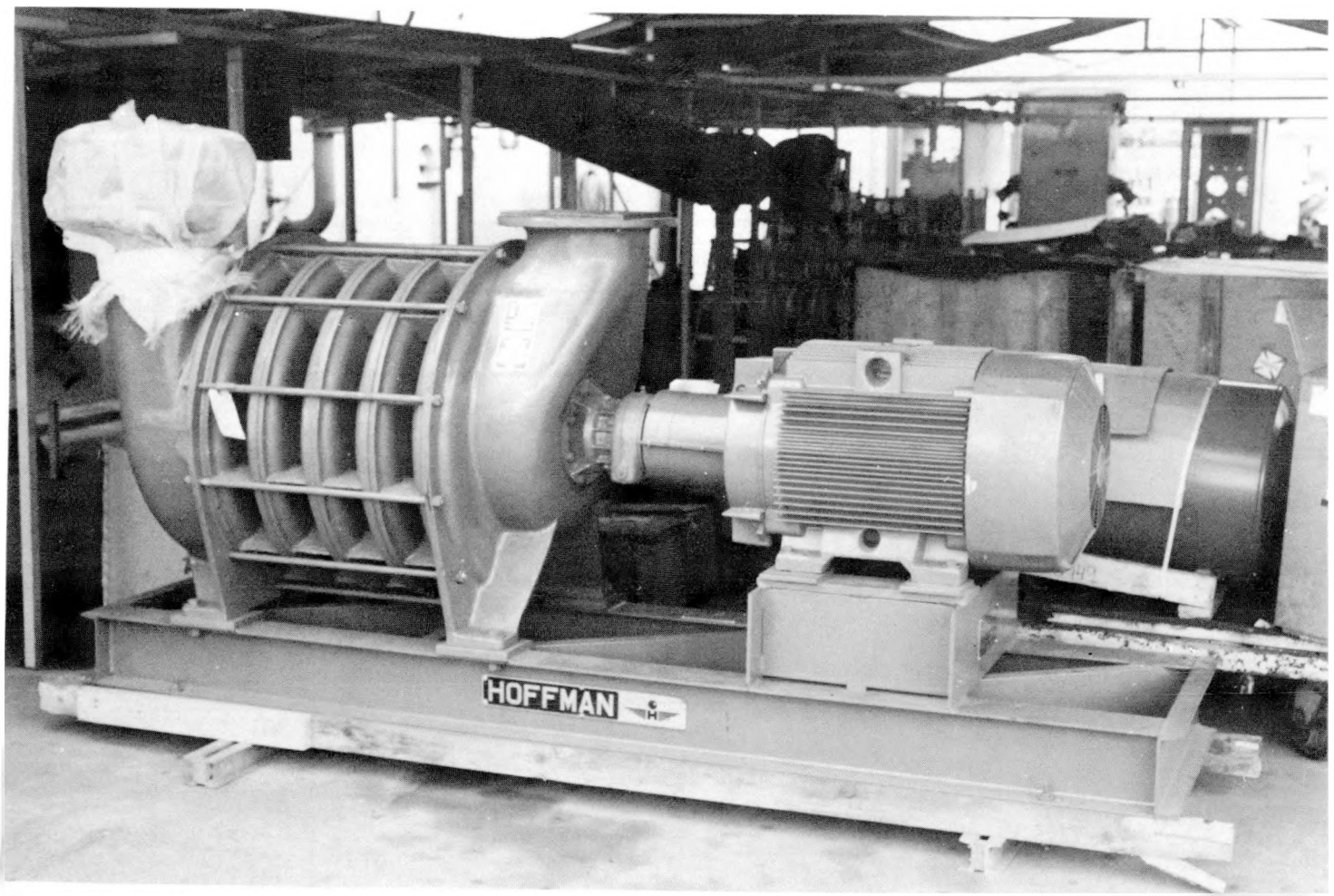


Figure 4-183. Hoffman Blower

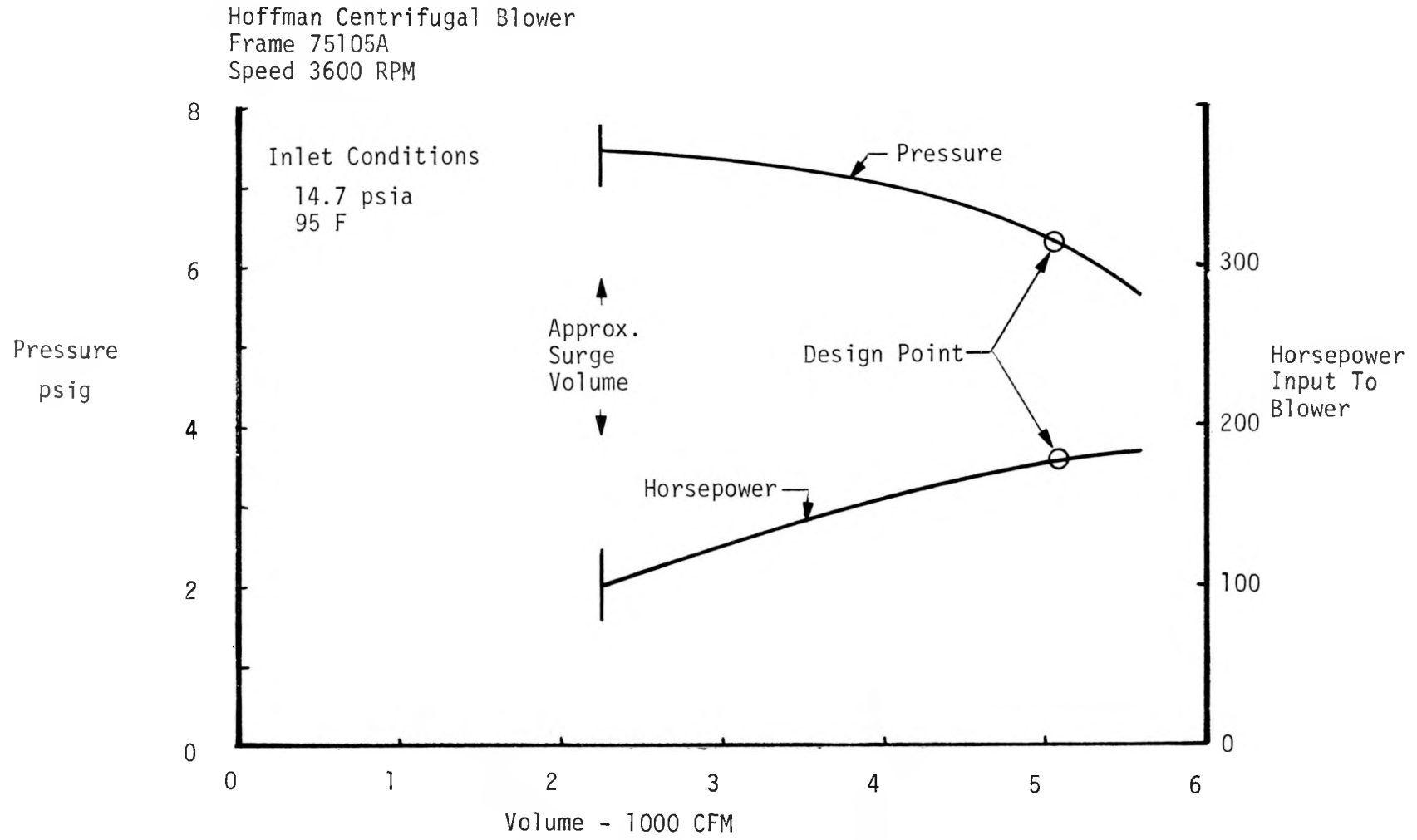


Figure 4-184. Forced Draft Blower Estimated Performance Curve

TABLE 4-68. FORCED DRAFT BLOWER

HOFFMAN AIR AND FILTRATIONS (DIVISION OF CLARK INDUSTRIES) MODEL 75105A
MOTOR; 200 HP, TEFC, 3600 RPM, 460 VAC, 3-PHASE FULL VOLTAGE STATING
12-INCH INLET THROTTLING VALVE
KEYSTONE MODEL 100
KEYSTONE EPICYCLIC ELECTRIC ACTUATOR F-777, EPI-50, 125 VAC
OPERATING SIGNAL
BLOWOFF SYSTEM - MODEL HB-5
ACCESSORIES
INLET FILTER/SILENCER
COUPLING GUARD
CALIBRATED AMMETER

A tube and shell design was used where the flue gas passes inside the tubes and the combustion air made five passes across the outside of the tube bundle. A circular shell is used as shown in Fig. 4-185, and internal baffles are used to control the passes. Any solid particulate that may settle out will collect in a hopper located at the bottom of the unit. The unit characteristics are presented in Table 4-69, and Fig. 4-186 shows the completed unit.

A specification control drawing was prepared by Rocketdyne, and then a boiler fabricator prepared the shop drawings and fabricated the unit.

Cyclone. The cyclone removes most of the solid particulate from the flue gas and is located between the combustor and the air heater. The solid particulates that are collected are then drained for disposal and/or recycle. For this application, it is desirable to have as high an efficiency cyclone as practical for two reasons: (1) to minimize the dust loading to the downstream air heater, ducts, and baghouse; and (2) to collect as much flyash as possible for maximum ash recycle, since one of the objectives of this experiment is to vary the recycle rate.

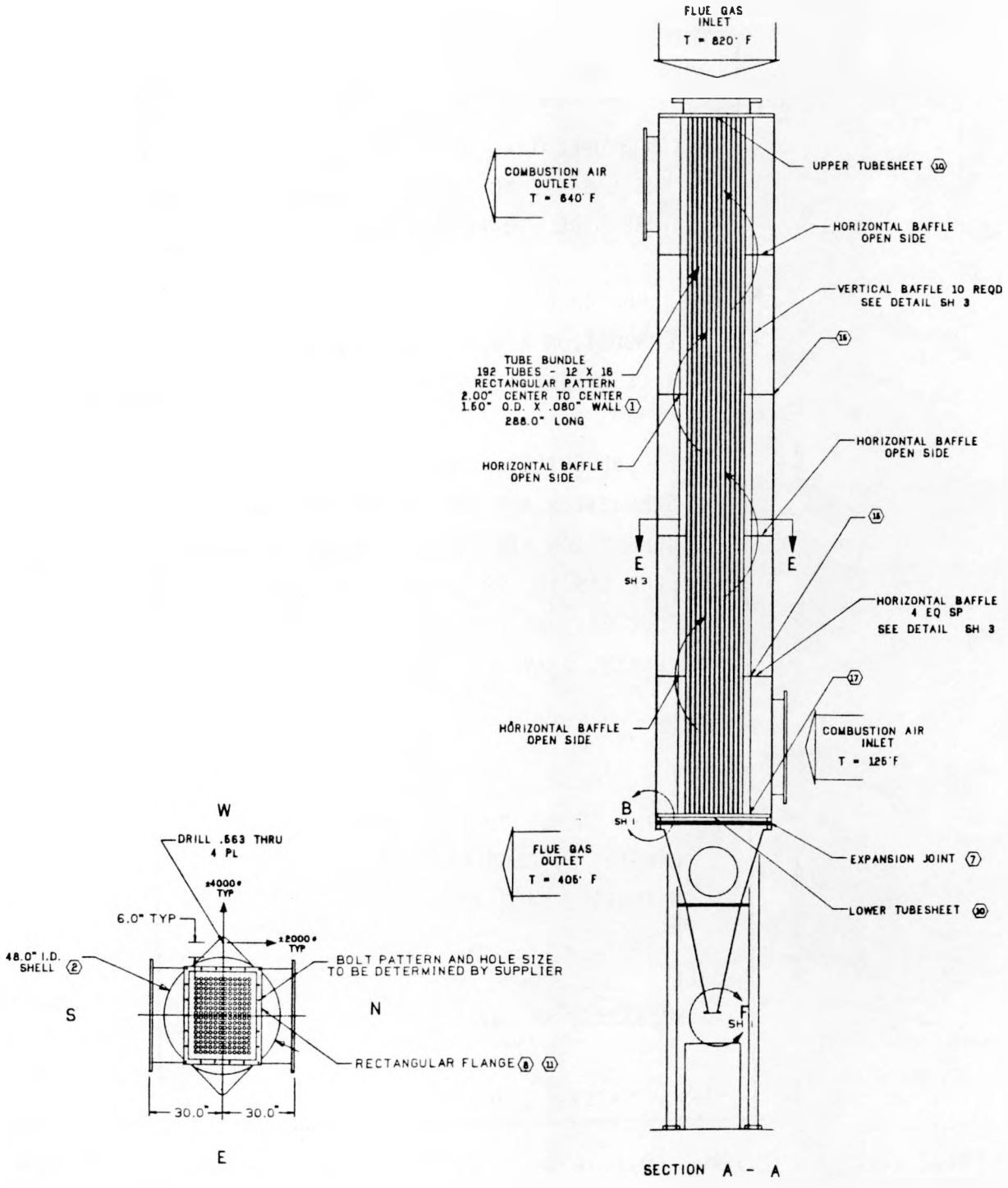


Figure 4-185. Air Preheater Layout

TABLE 4-69. AIR PREHEATER

FABRICATOR - REPCO ENGINEERING INC.

MAXIMUM OPERATING PRESSURE
- SHELL SIDE, 10 PSI
- TUBE SIDE, 10-INCHES W.G.

PRESSURE DROP (SV = 8 FPS)
- COMBUSTION AIR, 2-INCHES W.G.
- FLUE GAS, 4-INCHES W.G.

INLET AND OUTLET FLANGES
- COMBUSTION AIR IN, 36-INCHES DIAMETER
- COMBUSTION AIR OUT, 36-INCHES DIAMETER
- FLUE GAS IN, 28-INCHES x 36-INCHES
- FLUE GAS OUT, 20-INCHES DIAMETER

ASH DRAIN, 6-INCHES -150 POUNDS

TUBE BUNDLE
- 192 TUBES
- 1-1/2-INCHES OD WITH 0.083-INCH WALL
- LENGTH, 24 DEGREES
- MATERIAL, SA 214 CS

SHELL
- MATERIAL, 515-70 CS, t = 3/16 INCH

SURFACE AREA, 1800 FT^2

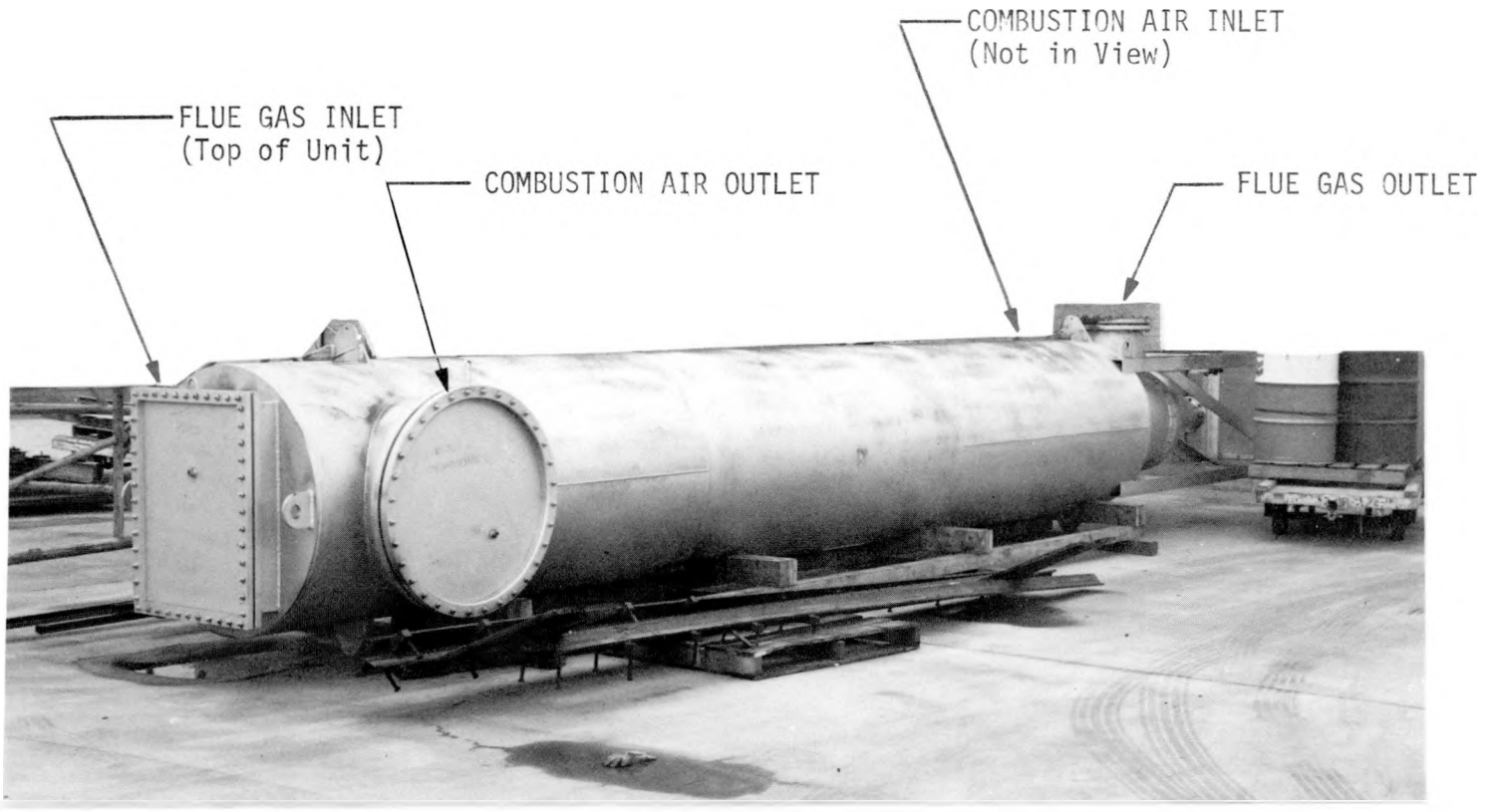


Figure 4-186. Air Heater

The collection efficiency of a cyclone design is related to pressure drop (inlet velocity) and the size of the cyclone unit. The higher the pressure drop (within limits up to about 4 inches W.G.), the higher the efficiency; and the smaller the unit, the higher the efficiency. Also, plugs were procured so that a selected number of individual units could be plugged off to maintain a high pressure drop of 3 to 4 inches W.G. for high efficiency in the units left operating. This is important since the experimental unit is capable of operating over a wide range of flue gas flowrates. Thus, the cyclone pressure drop could be optimized for a given experiment by plugging the appropriate number of individual units.

The selected unit is a multicyclone (Fig. 4-187) from the Air Correction Division of UOP Incorporated, Model 6UPOWHS No. 6-36. The individual cyclone is depicted in Fig. 4-188, and the, operating characteristics and expected performance are presented in Table 4-70. With a pressure drop of 3 inches W.G. and an estimate dust distribution as shown in Table 4-71, the collection efficiency of 94% is obtainable. This unit is equipped with a 20 inch cleanout door and an 8 inch Meyer rotary valve for bottom dust removal. Also, wear shields are provided on the first two rows of cyclone units.

Baghouse. A fabric filter baghouse is used for final cleanup of the flue gas particulate. This unit allows the experimental installation to meet all federal standards (0.1 lb per 10^6 Btu). The selected unit shown in Fig. 4-189 is a Johnson-March fabric filter baghouse design with a high cloth area for high collection efficiency. The characteristics are shown in Table 4-72, and the unit is designed for on-line pulse-jet cleaning where the jet cleaning is sequenced by timer. The unit is compartmentalized into three sections so that it can be easily converted to off-line cleaning in the future if this is necessary for more complete cleaning of the bags. Each section has a separate outlet so that a control damper could be added, although the existing installation will simply manifold together the three outlets.

Induced Draft Fan. This fan draws the flue gas and maintains the freeboard section of the combustor at a slightly negative pressure of about -2 inches W.G. The selected fan is a Zurn/Clarage unit with a discharge control damper. The unit is shown in Fig. 4-190, and the characteristics of this unit are tabulated in Table 4-73.

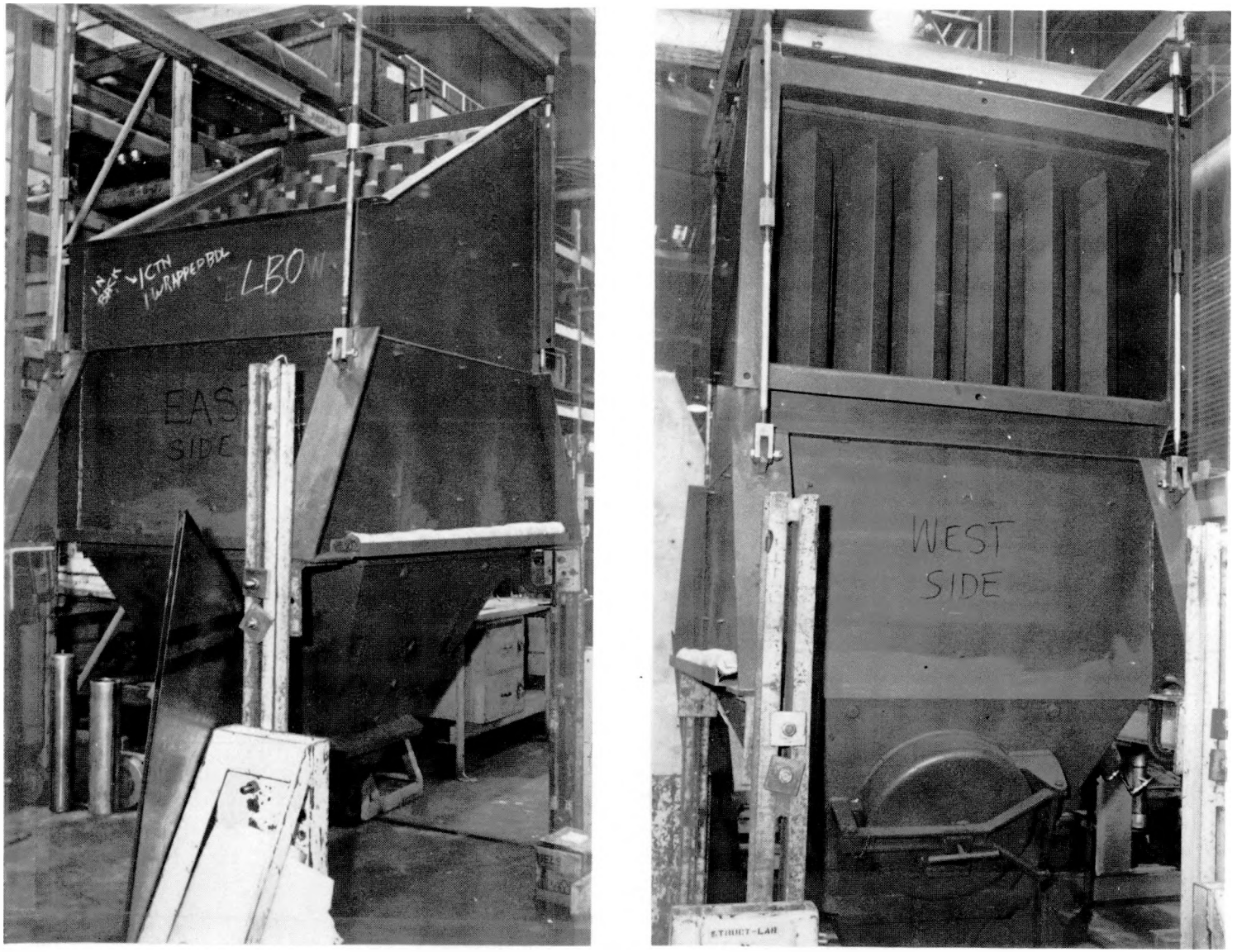


Figure 4-187. Multiclone Dust Collector

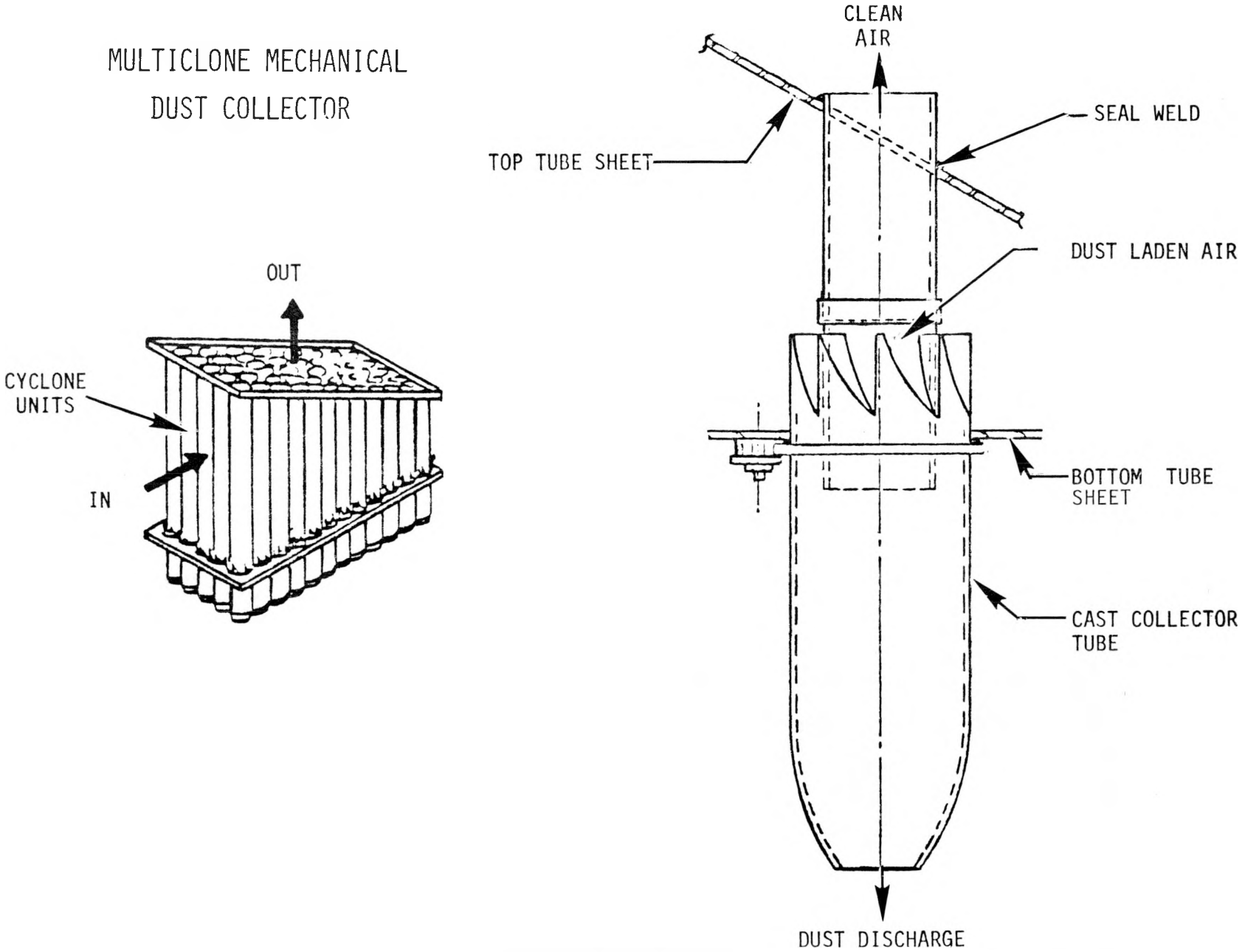


Figure 4-188. Cyclone

TABLE 4-70. CYCLINE

MANUFACTURER: AIR CORRECTION DIVISION, UOP INC.
MODEL: NO. 6 UPOWHS NO. 6-36
CASING PRESSURE: ±20 INCH W.G.
CASING TEMPERATURE: 830 F
ROTARY FEEDER: 8-INCH MEYER
GAS VOLUME: 10,300 ACFM
EMPTY WEIGHT: 4,300 POUNDS
DUST LOAD: 1,100 POUNDS (20 FT^3)

TABLE 4-71. CYCLONE EXPECTED PERFORMANCE

PARTICLE SIZE, MICRONS		AVERAGE SIZE, MICRONS	% IN GAS STREAM	EFFICIENCY, %	
				4-INCH W.G.	1-INCH W.G.
	+60	60	17	100	100
-60	+40	50	10	100	100
-40	+30	35	8	100	100
-30	+20	25	13	100	99.8
-20	+15	17.5	9	99.8	98.5
-15	+10	12.5	13	99.0	95.5
-10	+7.5	8.75	7	96.5	89.0
-7.5		3.75	23	77.5	61.0
				94.4 (AVERAGE)	89.5 (AVERAGE)



Figure 4-189. Baghouse

TABLE 4-72. BAGHOUSE

MANUFACTURER: JOHNSON-MARCH CORP.

MODEL: PT 10-13-12 MODIFIED

BAGS: 14 OZ. NOMEX FELT, 6-INCH DIAMETER, 10 FEET LONG, GROUNDED

FILTERING AREA: 2,445 FT^2 (GROSS)

CAPACITY: 9,500 ACFM AT 400 F

AIR TO CLOTH: 3.88:1

CLEANING: PULSE JET ON-LINE CLEANING (SEQUENCED BY TIMER OR PRESSURE DROP)

HANDRAILS AND ACCESS LADDERS

HOPPER CLEANOUT VALVE: 8-INCH MEYER ROTARY, 1/2 HP

EMPTY WEIGHT: 12,500 POUNDS

COLLECTION EFFICIENCY: +99%

COMPARTMENTS: 3 SECTIONS FOR FUTURE CONVERSION TO OFF-LINE CLEANING

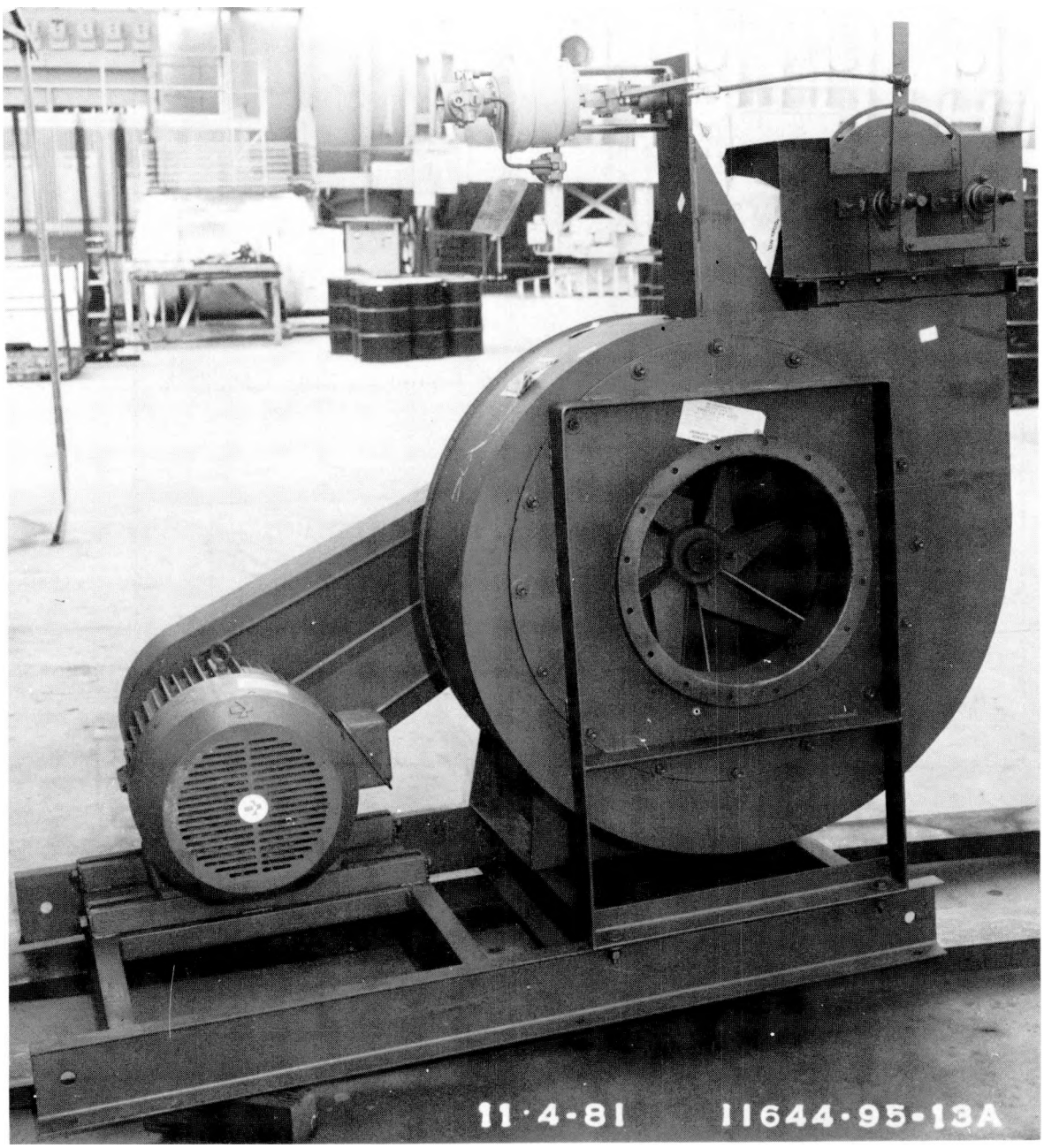


Figure 4-190. Induced Draft Fan

TABLE 4-73. INDUCED DRAFT FAN

MANUFACTURER: ZURN/CLARAGE
MODEL: TYPE 217 XL, DESIGN 22, ARRANGEMENT NO. 1, FLAT BLADE
FRAME MOUNTED
FLOW CONDITIONS:
DESIGN: 10,022 ACFM AT -17 INCHES W.G., 425 F
MINIMUM: 2,151 ACFM AT - 2 INCHES W.G., 290 F
MOTOR: TEFC, 50 HP, 1750 RPM
OUTLET DAMPER WITH PNEUMATIC OPERATOR

Ignition System. The ignition technique consists of first preheating the distributor combustion air to 700 F to preheat a partially loaded bed. Additional heat is added to raise the bed temperature to 1000 F, at which point coal is introduced and will ignite smoothly. Two natural gas and air burners are used for the duct burners to preheat the distributor air, and an in-bed burner is used for the additional heat input to the bed. (The duct burner cannot be used to preheat the bed to 1000 F since the ducting is limited to a maximum temperature of 900 F). After coal ignition, the burners are shut down and the in-bed burner is cooled by a small purge flow of air.

The burners were manufactured by Sur-Lit Corporation per Rocketdyne specifications, and the operating characteristics are presented in Table 4-74, while the burners are shown in Fig. 4-191 and 4-192. The duct "flame bath" type installed into the side of the 30-inch-diameter air duct on the long vertical section from the air preheater to the combustor windbox. Fuel is burned with the air in the duct and mixes so as to automatically maintain a selected gas temperature as measured in the horizontal duct near the windbox. The in-bed burner uses fuel and air and fires in a refractory-lined burner port located at the side of the combustor. The burner port is angled downward to direct the hot gases into the bottom of the bed in the region between the tuyeres and the bottom of the bed bank. This in-bed burner is controlled to maintain a selected heat input (fuel flowrate) and flame temperature. This technique was developed and used successfully the Rocketdyne 18" x 18" AFB unit.

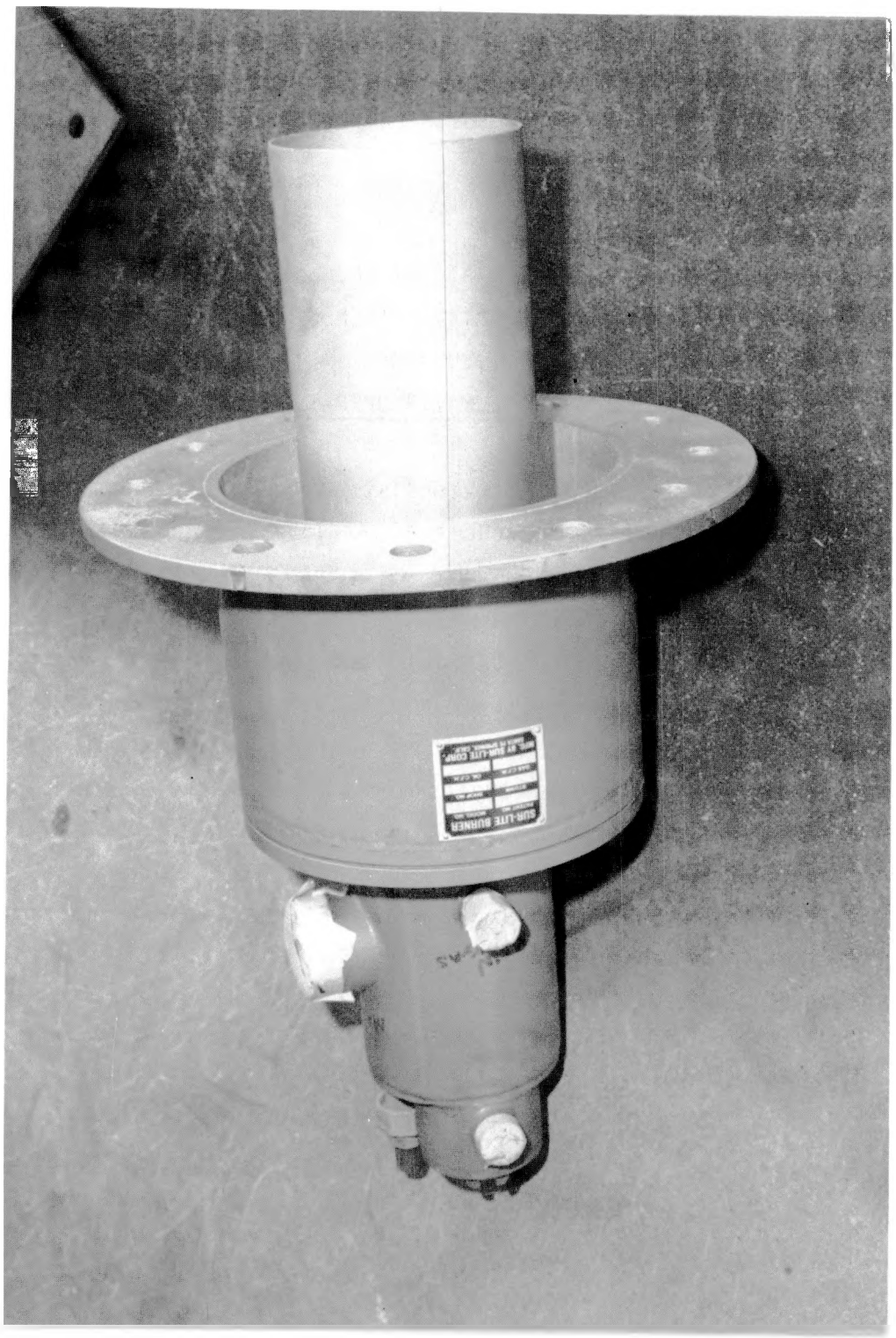


Figure 4-191. In-Bed Ignition Burner

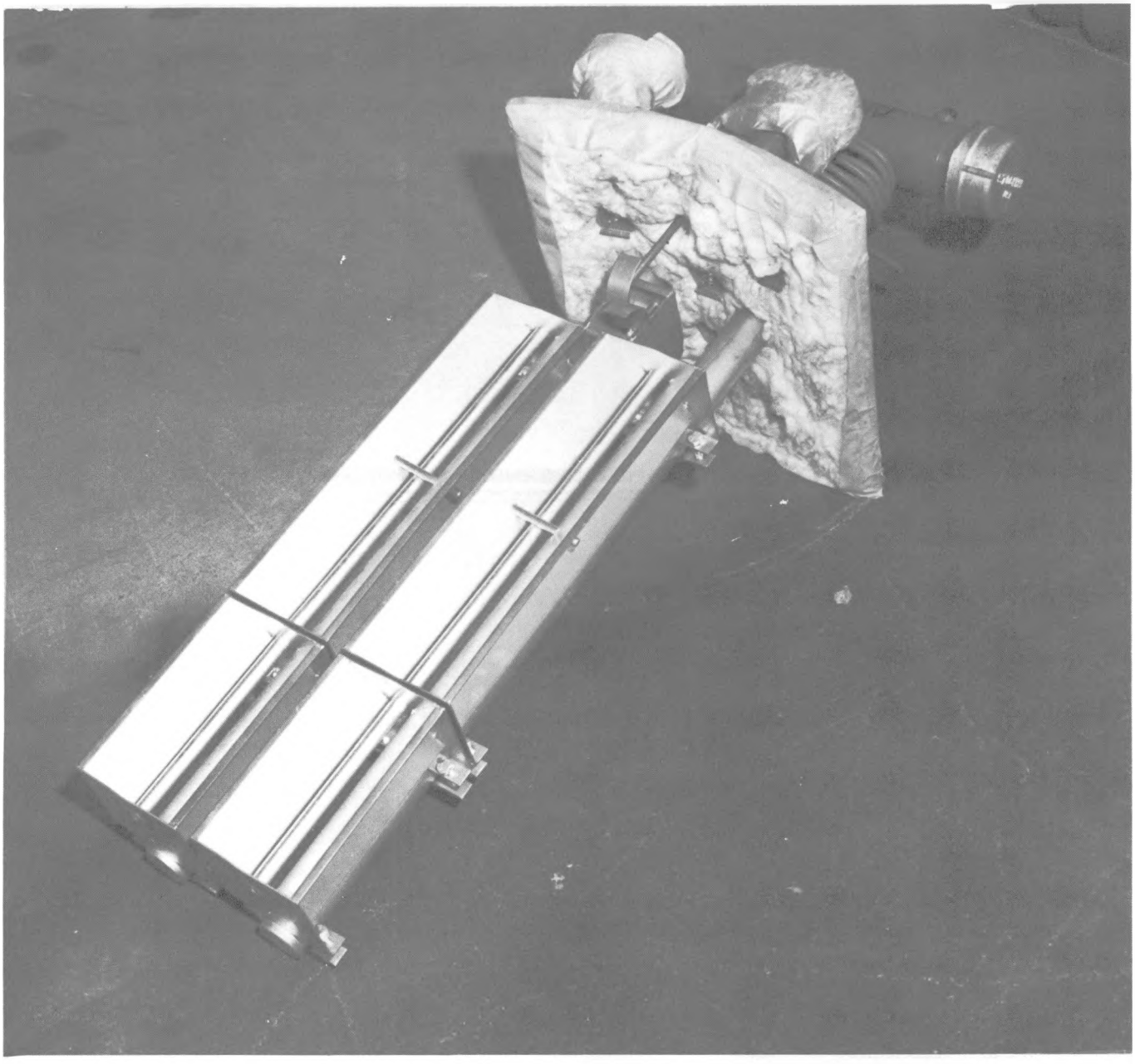


Figure 4-192. Combustion Air Duct Ignition Burner

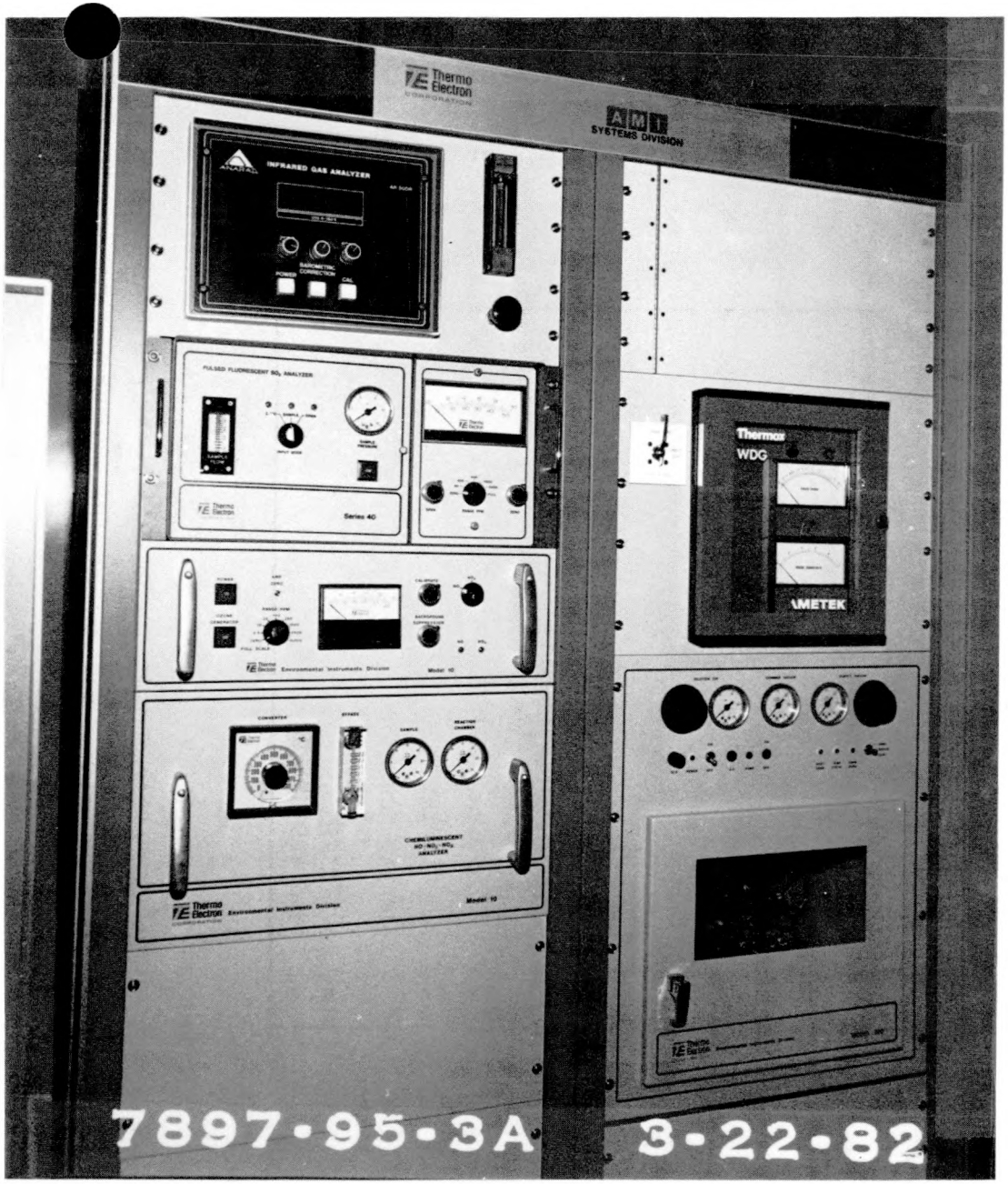
TABLE 4-74. IGNITION BURNERS

MANUFACTURER: SUR-LITE CORP.
FUEL: NATURAL GAS, 5 PSIG SUPPLY
DUCT BURNER:
RATING: 5×10^6 BTU/HR
AIR SUPPLY: DUCT AIR
TURN DOWN: 10:1
MIXED TEMPERATURE: UP TO 700 F NOMINAL, 1200 F MAXIMUM
FUEL INLET: 2 INCHES NPT
IN-BED BURNER:
RATING: 2.5×10^6 BTU/HR
AIR SUPPLY: 60 PSIG
TURN DOWN: 10:1
FLAME TEMPERATURE: 2000 TO 2800 F
FUEL INLET: 1/2 AND 1 INCH NPT
AIR INLET: 2 AND 3 INCHES NPT

Flue Gas Monitoring System. A series of gas analysis equipment was used to monitor and control the operation of the combustor and the gas constituents which were continuously monitored are:

1. Excess Oxygen: This was used to control the fuel and combustion air to maintain a given overall oxygen-rich operating condition
2. Sulfur Dioxide: This was used to adjust limestone feedrate for minimum output of SO_2
3. Oxides of Nitrogen: This monitored the output of NO_x
4. Carbon Dioxide: This measurement was used in determination of combustion performance
5. Combustibles (CO & H_2): This ensured safe operation during startup and shutdown.

A complete packaged system (Fig. 4-193) was used to monitor these gas constituents, and the system characteristics are summarized in Table 4-75. The gas measurements were displayed on meters in the control center as well as recorded on the data acquisition system.



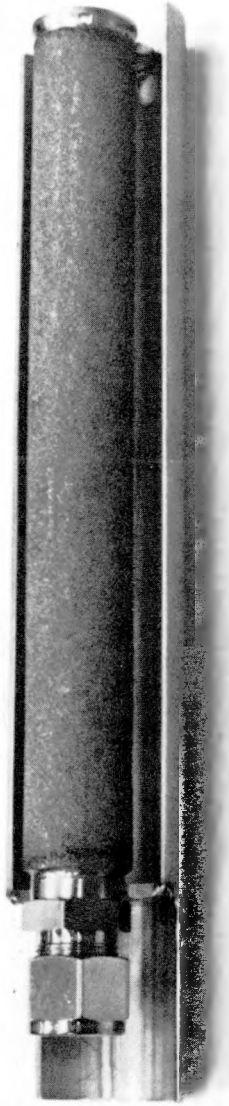


Figure 4-193. Flue Gas Monitoring Console and Stack Probe

TABLE 4-75. FLUE GAS MONITORING SYSTEM

MANUFACTURER: ENVIRONMENTAL SYSTEM DIVISION, THERMO ELECTRON CORPORATION

SYSTEM:

- ANALYZERS
- SAMPLE CONDITIONING SYSTEM
- EQUIPMENT ENCLOSURE
- STACK SAMPLE PROBE
- HEATED SAMPLE LINE (BY OTHERS)

ANALYZERS:

- OXIDES OF NITROGEN (NO/NO_x)
  - THERMO ELECTRON MODEL 10 A/R
  - 8 RANGES; 2.5 TO 10,000 PPM
  - 0-5 V OUTPUT
- SULFUR DIOXIDE
  - THERMO ELECTRON MODEL 40
  - 5 RANGES: 50 TO 5,000 PPM
  - 0-10 V OUTPUT

OXYGEN/COMBUSTIBLES (O_2/CO AND H_2)

- AMETEK/THERMOX MODEL WDG-IIIC
- O_2 RANGE: 0-20%
- COMBUSTIBLES RANGE: 0-1%
- 0-100 mVDC OUTPUT

CARBON DIOXIDE

- ANARAD MODEL 500
- RANGE: 0-20%
- 0-5 VDC OUTPUT

since the excess oxygen is a critical parameter, a separate redundant meter was used in addition to the above system. This meter is a Teledyne Model 9400, in situ stack-mounted analyzer with remote readout in the control center.

Coal Feed System. This system accurately fed coal to each of the four feed points on the underside of the combustor. The overall system consists of the receiving and storage system and the coal feed system.

Coal (Illinois No. 6) was prepared by crushing and drying at an existing facility located at the Rockwell Energy Systems Group. The prepared coal was then received and stored in a silo. This system was designed and installed by the NAAD test facility organization. The system consisted of a truck dump station, conveyer, elevator and silo. The coal was stored in the silo with a nitrogen atmosphere to prevent oxidation during prolonged periods of storage.

The coal feed system is the more complex and critical for the combustor operation, and this system was designed by Burns & Roe. Coal is fed pneumatically to the combustor and to the inlet feed points on the underside of the distributor and Fig. 4-194 presents a schematic of the system. This system measured and controlled the coal delivery rate to each of the four individual feed lines.

Size coal (1/4-inch top size, as received) was moved horizontally from the coal silo bottom outlet by screw conveyor to bucket elevator. The coal drops from the bucket elevator outlet chute onto a vibrating screen which scalps off material larger than 1/4 inch that may have been received. The screen has provision for future undersized material removal. Oversized particles, scalped off the upper deck, are dropped for disposal. The sized coal is deposited directly into the coal day bin which has a 16,000-pound capacity. This system, with its associated equipment, is designed to fill the coal day bin in less than 2 hours.

The coal day bin feeds coal through four bottom outlet cones, into the coal feed hoppers. Each hopper holds 2000 pounds of coal, sufficient for 5 hours of operation at the design coal-firing rate. The coal feed rate through each individual line is determined from measurements by the feed hopper weigh cell system. The day bin, feed hoppers, and bucket elevator are vented through the fabric filter for dust control.

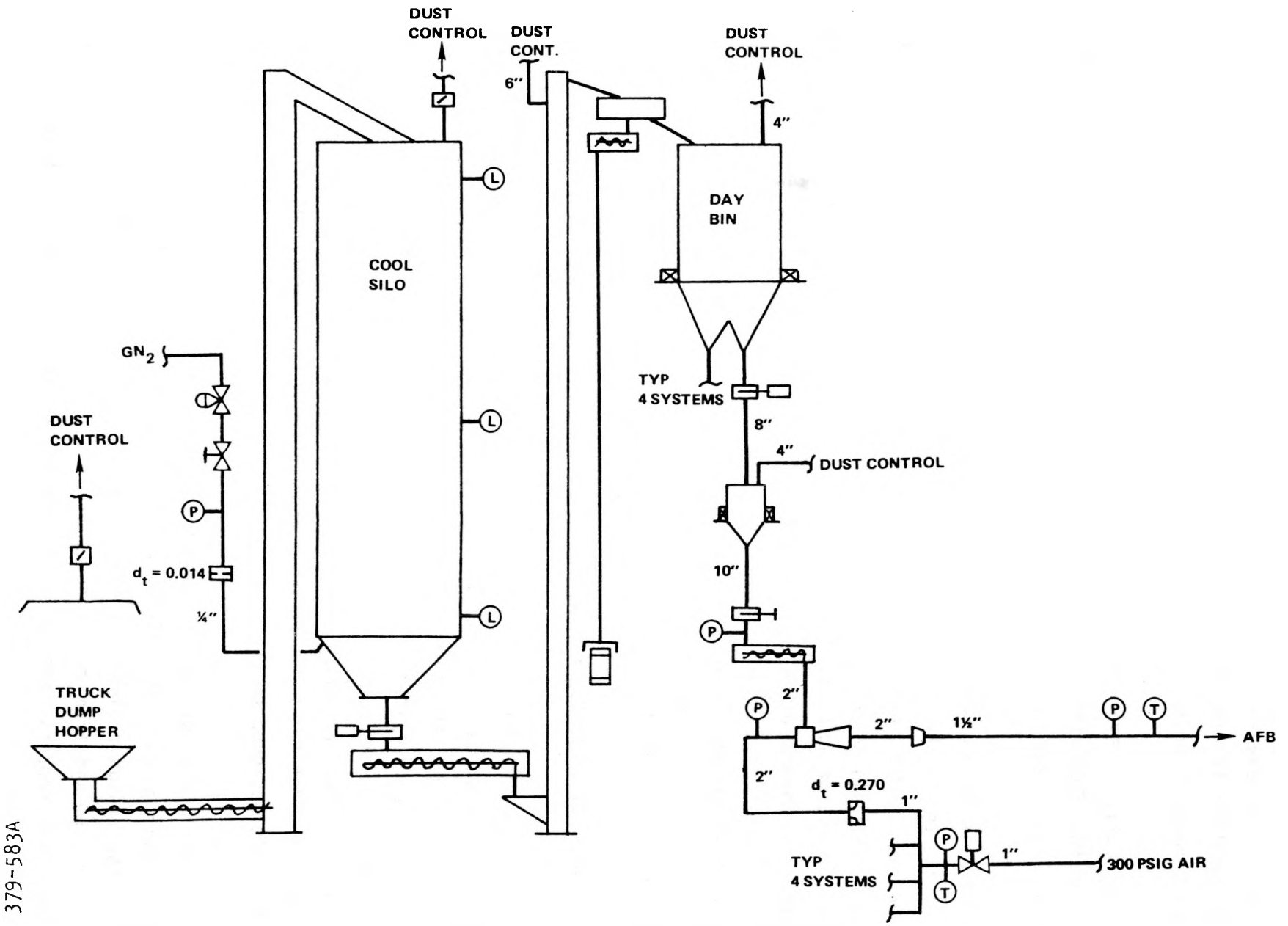


Figure 4-194. Coal Feed Schematic

379-583A

Screw feeders located below the feed hoppers control the rate of coal feed. Eductors at the screw feeder discharge provide the means of injecting coal feed into the transport lines. Provisions were made for insertion of rotary air lock feeders between the coal screw feeder and the eductor, which was done in January 1983 for use in run 003.

The air supply for coal feeding is provided by the facility air system, and the air flow is split into the four systems prior to the coal eductors. The 1- to 1-1/2-inch line sizes are at least four times larger than the largest size of the coal particles since the coal will be screened twice, once during preparation and once prior to loading the daybin.

To maintain a constant air velocity in each of the four transport lines, sonic venturi's are installed in the lines prior to the coal pickup points. These ensure constant flow by responding to the common upstream pressure regardless of downstream conditions.

The coal system consists of many components of which most are standard manufactured items, and Table 4-76 lists those components along with some of the pertinent characteristics. The responsibility for the receiving and storage system was assigned to the NAAD test laboratory. The responsibility for the coal feed system was that: (1) Rocketdyne provided the overall requirements and procured all of the major components, (2) Burns & Roe designed the feed system, provided the critical specifications for the components and provided the detailed design of the system support structure, and (3) NAAD test laboratory provided the additional miscellaneous items and installed and assembled the system.

Limestone Feed System. This system feeds limestone to the combustor at a specified flowrate, where the flowrate is determined by the rate required to maintain sulfur removal or to adjust the bed height. A schematic of the system is presented in Fig. 4-195 and a list of the components is presented in Table 4-77.

The limestone is received at the test facility in 55-gallon drums. As required, he limestone is deposited in the limestone loading hopper and fed into the limestone transport line via a rotary feeder.

TABLE 4-76. COAL FEED SYSTEM COMPONENTS

RECEIVING AND STORAGE SYSTEM
  TRUCK DUMP STATION, SCREW CONVEYOR, BUCKET ELEVATOR, SILO
  LOAD CAPACITY, 25 TON/HR
  SILO CAPACITY, 48 TONS

SILO SCREW CONVEYOR
  CEN-CAL CO.
  5 TON/HR

COAL SYSTEM ELEVATOR
  KING BEARING CO.
  5 TON/HR
  42 DEGREE LIFT

COAL SCREEN
  KINERGY CORPORATION
  SIFTER STROKE TYPE
  AREA, 12.5 FT^2
  MODEL KDSSN-30-SD
  MOTOR, 1/2 HP

SCREEN SCREW CONVEYOR
  CEN-CAL CO.
  2 TON/HR

DAY BIN
  MANUFACTURER: CEN-CAL Co.
  EMPTY WEIGHT: 3,800 POUNDS
  CAPACITY: 16,800 POUNDS (345 FT^3)

FEED HOPPERS
  MANUFACTURER: CEN-CAL CO.
  EMPTY WEIGHT: 800 POUNDS
  CAPACITY: 2,000 POUNDS (40 FT^3)

SCREW FEEDERS
  VIBRA SCREW INCORP.
  MODEL HD-2, 2 INCHES WITH 1-1/2-INCHES DIAMETER SCREW
  MOTOR: 1 HP, SCR DRIVE

EDUCTORS
  FOX VENTURI CO.

LOAD CELLS (3 PER TANK)
  LEBOW MODEL 1211-AE (COMPRESSION ONLY)
  CAPACITY:
    DAY BIN, 10,000 POUNDS
    FEED HOPPER, 5,000 POUNDS

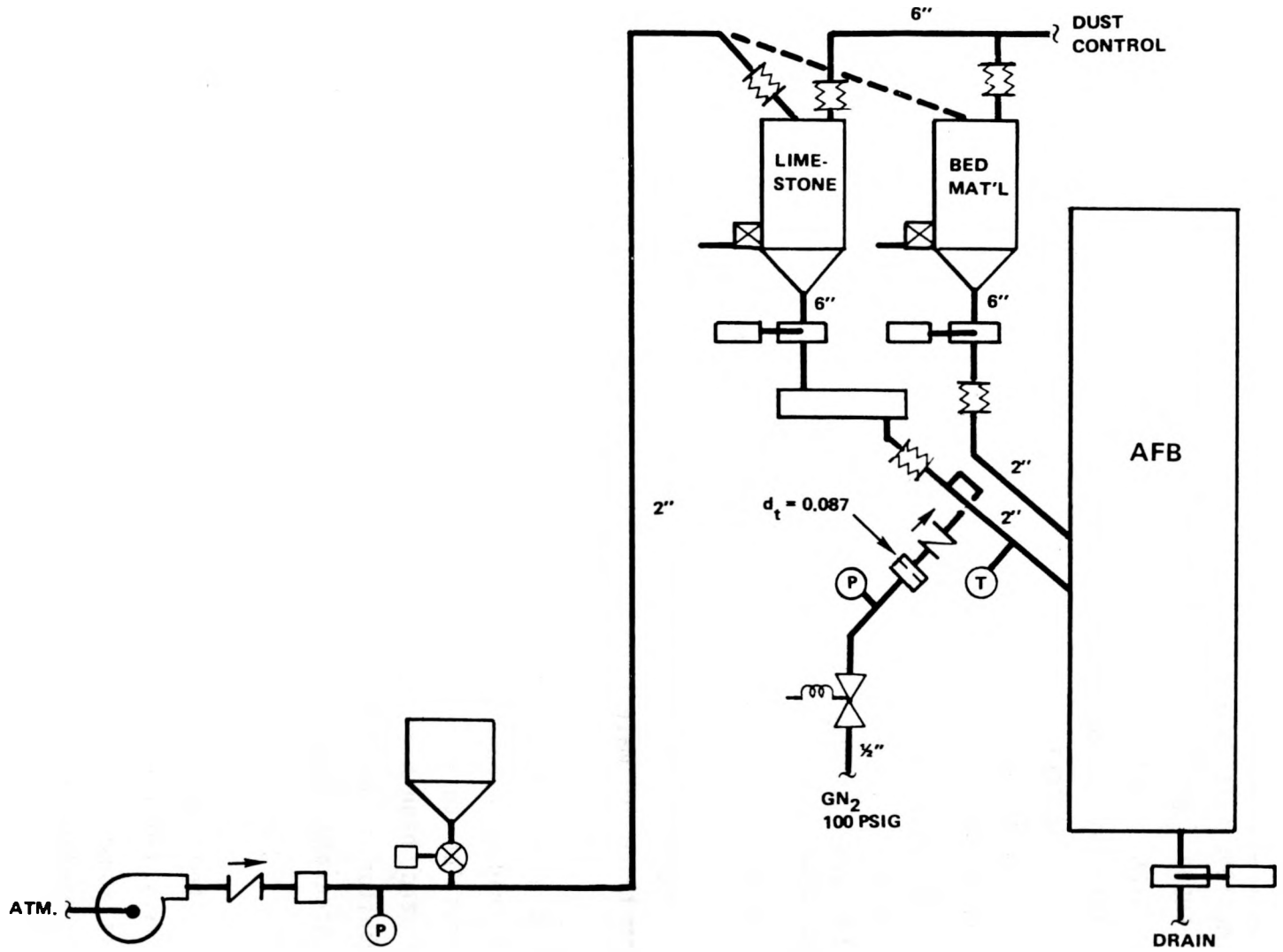


Figure 4-195. Limestone and Bed Material Schematic

379-586 A

TABLE 4-77. LIMESTONE FEED SYSTEM

LIMESTONE FILL SYSTEM
VENDOR: DUCON
SYSTEM: ROTARY BLOWER, FILL BIN, ROTARY VALVE, INTAKE TEE
CAPACITY: 1 TON/HR
LIFT: 40 FEET
VIBRATING FEEDER
ERIENZ MAGNETICS MODEL 40A, 3 UNITS, CONTROL MODEL NO. G-115
4 INCHES WIDE BY 93 INCHES LONG
DAY BIN
CAPACITY: 5 TONS (110 FT^3)

The material is then elevated and transported pneumatically to the limestone feed hopper where it is stored until required for injection into the combustor. A weigh cell arrangement is provided to indicate the inventory of the limestone in the hopper and to record material fed into the combustor.

Plant operation personnel determine the refill schedule. The rotary feeder for the limestone loading hopper is started manually after the air blower is in operation. In addition to weight indication, the feed hopper weigh cell can trip low-low-level and high-high-level alarms when required. Control of limestone into the combustor is provided by a variable capacity vibrating feeder which is sufficiently accurate since high accuracy is not required for the limeston delivery rate.

Ash Recycle System. Much of the solid particulate is removed by the cyclone where it is recycled back into the combustor and/or disposed of. The recycle feed system is shown in Fig. 4-196 and this system is designed to pneumatically transport and reinject all material collected in the dust collector up to a rate of 6000 lb/hr. The material is fed into the combustor through a series of hoppers, a variable-speed rotary feeder which controls the rate of feed, and an air supply.

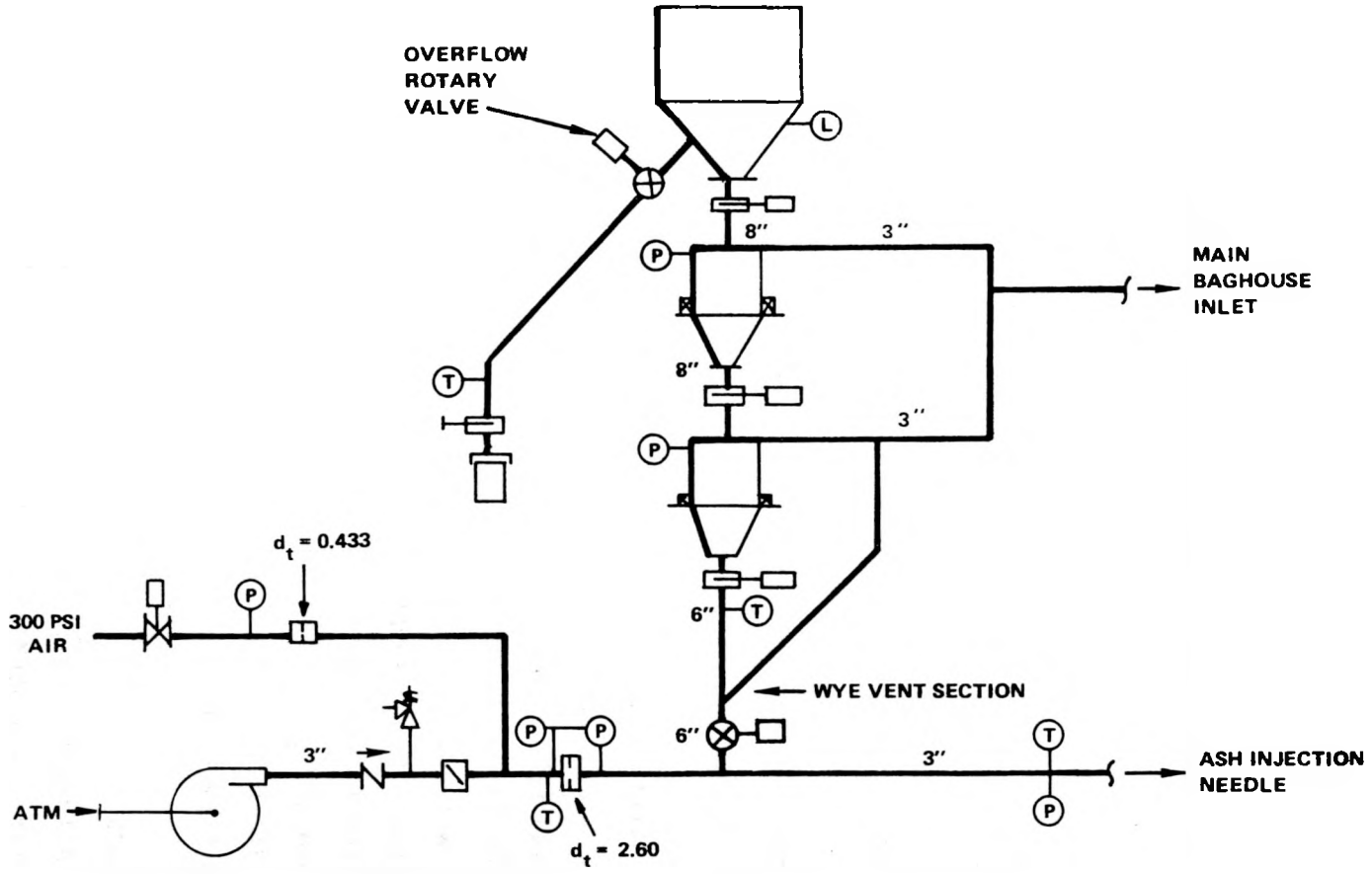


Figure 4-196. Ash Recycle Schematic

379-584A

Material is fed into the combustor from the lower hopper while cyclone drain material is accumulated in the upper hopper. Periodically, the lower hopper is batch filled from the hopper. Both hoppers are on a load cell weight system, and the weight change with time is used to determine the recycle feed rates.

Pneumatic transport air is supplied by either a positive displacement blower, or a facility air supply.

During the characterization test program, this system underwent several modifications, and a more complete description can be found in Section 4.5. In the final configuration, the facility air supply was used for transport air. A series of valves was used to equalize pressures and batch fill the lower hopper; thus, the lower hopper was essentially a lock hopper system.

The equipment used in this system is listed in Table 4-78 along with some of their pertinent characteristics.

TABLE 4-78. ASH RECYCLE SYSTEM

WEIGHT AND FEED HOPPER
FABRICATOR: CEN-CAL CO.
EMPTY WEIGHT: 850 POUNDS
CAPACITY: 3,500 POUNDS (57 FT^3)
LOAD CELLS (3 PER HOPPER)
ELBOW MODEL 3674 - 5K (COMPRESSION ONLY)
ROTARY VALVE
DUCON 6-INCH TYPE B
MOTOR: 1 HP SCR DRIVE
COMPRESSOR
MANUFACTURER: ROOTS
CAPACITY: 420 SCFM AT 8 PSIG
MOTOR: 20 HP

Bed Material System. This system permits initially loading the bed with used bed material. If the bed is charged with new limestone, several hours of operation are required to stabilize the bed. The sulfur capture rate of a new bed is very high for several hours without any addition of limestone. To eliminate this "break-in" period, most tests will be started with used bed material so that the stabilized condition can be reached quickly.

A bed material hopper is located side-by-side with the limestone hopper, and both hoppers are identical in capacity and load cell arrangement. Each tank has a capacity of 115 cu ft, or approximately 5 tons of material. Prior to a test, used bed material will be loaded using the limestone bin transfer system.

The bed will be charged using a gravity fill system with a position controlled slide gate valve until the desired bed height is obtained.

Control System. The overall operation required a number of control functions and, as this was an experimental unit subject to modifications during the development testing, most of the control functions were manual, as shown in Table 4-79. This method of operation was satisfactory for the experimental unit since the unit and supporting systems operated very stably and only occasional adjustments were required. The combustion air blower and the draft control were automatically controlled by a Micon microprocessor shown in Fig. 4-197.

Coal and Limestone. The coal will be Illinois No. 6, and this was purchased in a sufficient quantity for the current planned program. The coal is shipped by railcar to a receiving yard in the Los Angeles area, where it is placed in interim storage. As required, the coal is trucked to the existing Energy Systems Group coal preparation facility at SSFL. The coal is crushed to a -4 by 0 mesh size and dried to approximately 4% moisture. The prepared coal is then trucked to the test site for storage in a protected environment in the coal silo.

The limestone is Grove (ANL-9501). An initial shipment of 125 tons of this limestone was purchased as dry (0.1 to 0.3% moisture), double-screened (-8 x +20 mesh) limestone packaged in sealed drums. The drums were then shipped directly to the test site for storage.

TABLE 4-79. CONTROL FUNCTIONS

SYSTEM	MANUAL	AUTO.	CONTROL PARAMETER	CONTROL DEVICE
COAL RECEIVING	X	-	-	CONVEYER, ELEVATOR, BAGHOUSE
COAL TRANSFER (DAYBIN)	X	-	DAY BIN WEIGHT	CONVEYERS, ELEVATOR, SCREEN
COAL FEED HOPPER TRANSFER*	X	-	HOPPER WEIGHT	VALVE
COAL FEED RATE*	X	-	SELECTED RATE	SCREW FEEDER
LIMESTONE TRANSFER	X	-	HOPPER WEIGHT	BLOWER, ROTARY VALVE, BAGHOUSE
LIMESTONE FEED RATE	X	-	SELECTED RATE	VIBRATING FEEDER
ASH HOPPER TRANSFER	X	-	FEED HOPPER WEIGHT	VALVES
ASH OVERFLOW	X	-	CYCLONE HOPPER LEVEL	ROTARY VALVE
ASH FEED RATE	X	-	SELECTED RATE	ROTARY VALVE
COMBUSTION AIR	X	X	SELECTED RATE	DAMPER
FREEBOARD PRESSURE (DRAFT)	X	X	SELECTED DRAFT	DAMPER
WORKING FLUID	X	-	SELECTED RATE & TEMP.	FACILITY SYSTEM
COAL TRANSPORT AIR	X	-	SELECTED RATE	VALVE
BED DRAIN	X	-	BED HEIGHT	VALVE

* FOUR INDEPENDENT FEED SYSTEMS

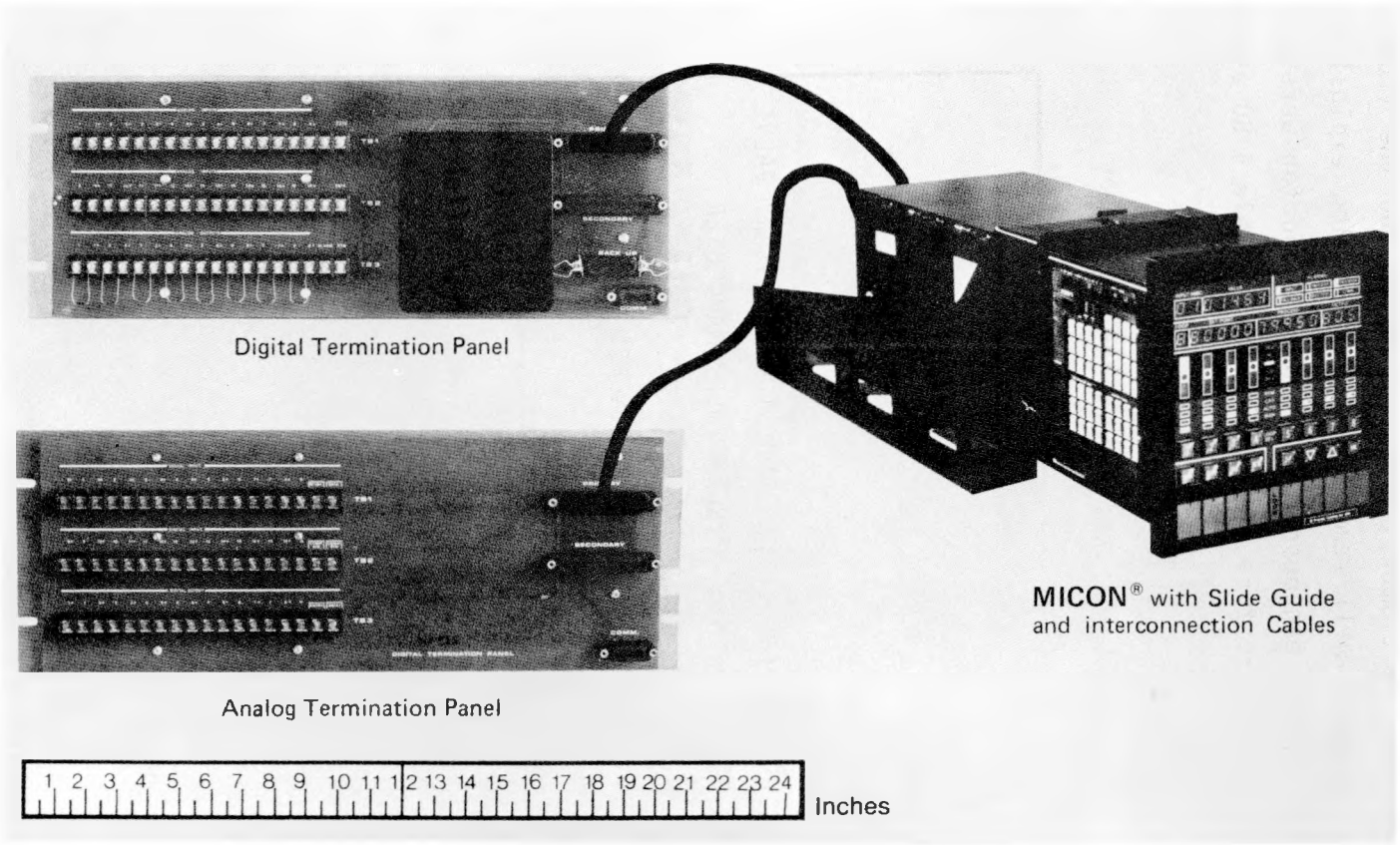


Figure 4-197. Combustion Control Unit

Dust Control. A dust control system is connected to many of the systems and bin and, in the case of the bucket elevators, the dust control system will prevent the accumulation of coal dust and prevent potential dust-air explosive mixtures. The main component of the system is the fabric filter baghouse and fan. Air is drawn from the various bins, elevators, the coal silo, and the truck dump station. This free air movement will remove dust, preventing explosive mixtures, and the dust is removed at the baghouse. The baghouse and fan were purchased as an integral unit. The characteristics are presented in Table 4-80 and a photo is shown in Fig. 4-198.

TABLE 4-80. DUST CONTROL UNIT

MANUFACTURER: MIKROPUL CORP.
MODEL: 363-10-30
FILTER: 36 AT POLYESTER FELT BAGS
FILTER AREA: 425 FT^2
AIR-TO-CLOTH RATIO: 5.88:1
FLANGED CLEANOUT FOR FUTURE ADDITION OF ROTARY VALVE
REVERSED JET CLEANING: CYCLE TIMER, MANOMETER
BLOWER: N.Y. SIZE 224, SERIES 15 GI, 10 HP
MAXIMUM CONDITIONS: 200 F, $\pm$30 INCHES W.G.
AIR FLOW: 2500 ACFM

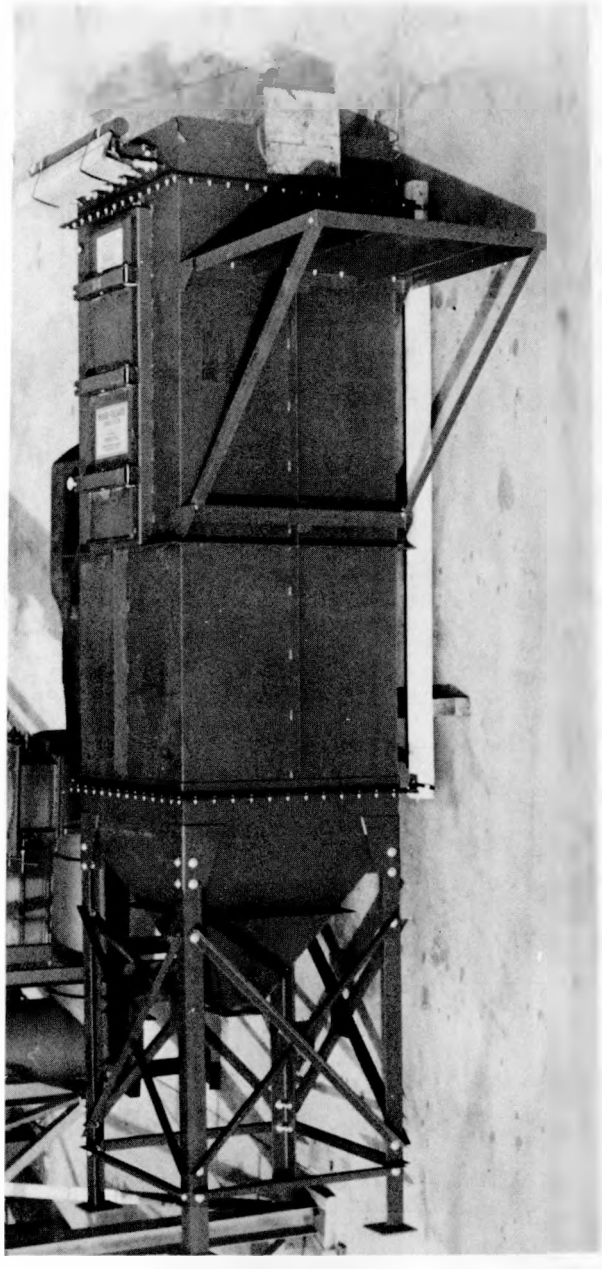


Figure 4-198. Dust Control Fabric Filter Baghouse

4.5 6' x 6' AFB ADVANCED HEAT EXCHANGER METAL ALLOY CORROSION/EROSION RESEARCH TESTING

The 6' x 6' atmospheric fluidized bed, coal-fired system is located at the Rockwell Thermodynamics Laboratory in El Segundo, California. This experimental unit was designed, constructed, and placed into operation to provide a research test bed. Its purpose is to produce advanced technology research CCGT/AFB cogeneration test data for metal alloy heat exchanger tube materials operating in the unique AFB air heater environment. A major factor for heat material life is the higher material temperatures for air heater service, as compared to more conventional steam service. This unit is nominally rated at 4 MW of overall thermal power. It operates on 1/4-inch maximum size crushed coal and used Illinois No. 6 coal for the tests reported in this section.

The test program consisted of two phases, the characterization and material specimen exposure test series. The characterization test series consisted of 6 runs with an accumulated duration of 238 hours at design bed temperatures. During this series, the system operation was refined, the operating parameters established to create a combustion environment as benign as possible for long material life, and the bed environment was characterized. Achieving these objectives led to the next material specimen exposure test series where a variety of heat exchanger metal specimens were exposed for over 350 hours in a series of two runs. (A 1-year extension to this Phase II research program effort, now in progress, extends the analytical work and the research material exposures for an additional 650 hours, for an overall total of 1000 hours.)

The experimental facility was erected following the requirements outlined in the detailed test plan (Ref. 1-22). During the final erection and development testing, several modifications were made to the system and operations. These modifications and the test results were documented in a series of three test reports, and these reports were included in the program quarterly reports. Runs 001 through 004 can be found in Ref. 1-17, runs 005 and 006 can be found in

ef. 1-18, and runs 007 and 008 can be found in Ref. 1-19. The results of the 6' x 6' AFB test program, as detailed in the three references, have been merged to form this section.

This section summarizes the 6' x 6' AFB test program including descriptions of the actual tests and conditions, results, and conclusions. The results were obtained in many areas of both the experimental system and performance. To facilitate the presentation of these results, the discussion is divided into several sections as follows:

SECTION 4.5.1 SUMMARY OF TEST PROGRAM - This section presents a general overall description of the test program.

SECTION 4.5.2 DESCRIPTION OF INDIVIDUAL RUNS - This section presents a description of the individual runs including the events and configuration.

SECTION 4.5.3 GENERAL TEST PROCEDURES - This section describes the general procedures for operating and controlling the facility to achieve the run objectives.

SECTION 4.5.4 SUMMARY OF DATA - Tabulations of the averaged pertinent data are presented without comment.

SECTION 4.5.5 COMBUSTOR/HEATER MODIFICATIONS - A number of modifications were made to the coal and air distributors to investigate the influence of these parameters on the fluidized bed environment, and these modifications are described in this section.

SECTION 4.5.6 SYSTEM OPERATIONS - The many areas of results have been divided into several sections to facilitate the presentation. This area of operations pertains to modification and operation of the experimental unit systems.

SECTION 4.5.7 PERFORMANCE RESULTS - This section presents the measured performance of the combustor/heater as well as some major system components.

SECTION 4.5.8 SOLIDS ANALYSIS - This section presents a tabulation of the solids chemical analysis which were used in obtaining the results presented in other sections.

SECTION 4.5.9 OXYGEN PARTIAL PRESSURE CHARACTERIZATION - Extensive PO_2 characterization of the fluidized bed was conducted for a variety of configurations and operating conditions, and this section summarized these results.

SECTION 4.5.10 HARDWARE INSPECTION - Comments are presented on the condition of the combustor/heater and system components.

SECTION 4.5.11 CONCLUSIONS - This section presents the overall conclusions from the test results.

4.5.1 Summary of Test Program

The 6' x 6' AFB test program consisted of two test series: the characterization and material specimen exposure test series. The characterization test series was a development program to bring the experimental unit on-line and measure the resultant conditions. The material exposure test series was steady-state operation at the nominal conditions to expose the many specimens of heat exchanger materials.

The characterization test series consisted of 6 runs with an accumulated operation of 238 hours at the design bed temperatures, and Tables 4-81 and 4-82 summarize the entire series. Throughout this series, the facility systems were continuously checked out and modified to improve the operation and, by the end of this test series, all systems were performing very well as evidenced by the smooth operation experienced on run 006. The bed operating characteristics were well established including mapping of the oxygen partial pressure for a variety of physical and operating conditions. Data were generated on the conditions required to create a "healthy" combustion environment throughout the heat exchanger to achieve long life of the heat exchanger materials. Some of the configurations used on runs 005 and 006 achieved this criterion of "healthiness" which is to have a predominantly oxidizing environment throughout the bed heat exchanger.

The material specimen exposure (erosion/corrosion) test series consisted of two runs with an accumulated duration of over 350 hours at operating conditions. Rur

TABLE 4-81. SUMMARY OF THE 6' x 6' AFBC CHARACTERIZATION TEST PROGRAM

TEST NO.	DATE	OBJECTIVES	DURATION (HOURS)	OPERATING CONDITIONS
001	10/19/82	(1) Refractory Curing (2) Equipment Checkout (3) Initial Checkout	14	4 fps 50% Excess Air
002	12/13/82	(1) Initial Steady-State (2) Preheated Working Fluid	18	6 fps 30 to 50% Excess Air
003	1/17/83	(1) Modified Coal Feed (2) Flyash Recycle (Attempt) (3) Modified Start Sequence (4) Initial PO2 Probing	50	4 to 6 fps 20 to 50% Excess Air
004	2/9/83	(1) PO2 Characterization (2) Flyash Recycle (Attempt)	52	6 fps 25 to 30% Excess Air
005	4/18/83	(1) PO2 Characterization (2) Feed System Variations (3) Flyash Recycle (4) Material Probe Characterization	52	6 fps 25 to 30% Excess Air
006	5/16/83	(1) PO2 Characterization (6 fps) (2) Feed System Variations (3) Flyash Recycle	52	6 to 8 fps 25% Excess Air
			238	

TABLE 4-82. SUMMARY OF TEST CONDITIONS

RUN NUMBER	001	002		003				004		005		006	
		A	B	A	B	C	D	A	B	A	B	A	B
SUPERFICIAL VELOCITY-fps	4.0	6.3	5.9	6.3	6.3	6.0	4.2	6.2	6.4	5.7	5.9	7.8	6.2
BED TEMPERATURE-F	1561	1607	1494	1611	1590	1587	1594	1573	1585	1606	1608	1587	1655
WORKING FLUID INLET TEMPERATURE-F	84	74	442	450	441	436	438	467	426	399	407	80	375
WORKING FLUID OUTLET TEMPERATURE-F	1416	1452	1441	1516	1491	1477	1520	1470	1488	1475	1499	1460	1540
COMBUSTION AIR/COAL RATIO	12.3	12.0	12.8	11.6	11.1	9.3	10.9	10.2	10.4	10.0	11.9	10.4	9.3
EXCESS OXYGEN - %	6.0*	5.5	6.4	6.8	6.3	3.8	4.5	3.7	4.5*	3.2*	6.3	5.0	4.2
BED HEIGHT - In.	55	57	77	72	69	75	69	92	86	71	80	72	92

* ESTIMATED VALUE

07 was initiated on August 8, 1983 and consisted of 176.5 hours of operation, and run 008 was initiated on September 19, 1983, and consisted of 194.5 hours of operation. This results in a total of 371 hours of material specimen exposure time. Almost all of the operation was at the nominal conditions of 6 ft/sec superficial velocity, 1650 F bed temperature, 25% excess air, and 90% sulfur capture. Approximately 29 probes containing a large number of candidate tube and hanger material specimens were exposed in both the fluidized bed and convection region. Ash recycle was used throughout the operation with a recycle rate of about two times the coal feedrate. A limited amount of probing was conducted with the oxygen partial pressure probe to verify the condition of the bed environment.

These tests, with an accumulated duration of 609 hours, were successfully conducted as planned with the combustor/heater and all supporting systems operating satisfactory. One of the cooled material specimen probes was removed for subsequent analysis, while all of the other probes remain in the unit for the next planned test series of 650 hours of continued exposure or a total of 1000 hours of exposure. The unit was inspected and found to be in excellent condition except for some erosion of the augmented air lines and ash injection needle. All of these areas of erosion are of secondary importance to the experiment and can be easily remedied for the next test series.

4.5.2 Description of Individual Runs

A description of each run is presented which includes the run objectives, actual content of the run and significant events, and modifications to the combustor/heater and system. The first six runs (001 through 006) were part of the characterization series while the latter two runs (007 and 008) were part of the material specimen exposure series.

Characterization Run 001. The test run consisted of 116 hours of operation, including 50 hours of coal burning and 14 hours at the bed operating conditions for a bed temperature of 1500 F at approximately 50% of the design power level.

The test conditions were 6 ft/sec superficial velocity, 50% excess air for 7 excess oxygen in the exhaust gases.

Description. This test was planned as the initial system heating test to allow slow heatup curing of the combustor refractory insulating liner. Two of the combustor liner sections were not individually bake-cured during fabrication; this heating was primarily to cure them and, at the same time, slowly drive off any existing moisture in the rest of the refractory. Using recommendations from the refractory vendor and refractory consultants, a minimum heatup rate and heat-soak schedule was planned, as indicated by the bed temperature profile in Fig. 4-199.

Heating was initiated by operating the air duct burner (combusting natural gas and air) for bed temperatures up to about 500 F. During this time, limestone was added to the bed to provide bed material in the combustor before burning the bed heater to bring the bed temperature up to 900 to 1000 F. At this temperature, the coal feed was started and coal burning in the fluidized bed commenced.

On the morning of Thursday, 14 October, 2 hours were spent checking the system, verifying procedures, and getting the bed and bed material feed system ready to add limestone for the first bed. The combustor was then heated using the duct heater to 250 F and held for 10 hours, and then at 30 F per hour ramped to 350 F and held for 5 hours. Further ramping to 450 F and a hold for 10 hours preceded the start of a planned ramp to 1000 F. But the bed burner at this time malfunctioned, and emergency repairs were made while more limestone bed material was being loaded. The temperature was maintained in the 440 to 600 F range for about an additional 9 hours. The bed was then heated up to over 900 F, using the 30 F/hour ramp rate, and held for 12 hours.

At this point, coal burning was initiated, but the temperature of the bed was held at 1000 F for an extra 23 hours to allow the installation of working fluid exhaust mufflers with a crane and a weld crew. The bed temperature was limited to this level because without any working fluid cooling in convection bank, its tubes might overheat. When muffler installation was complete, the coal feed rate

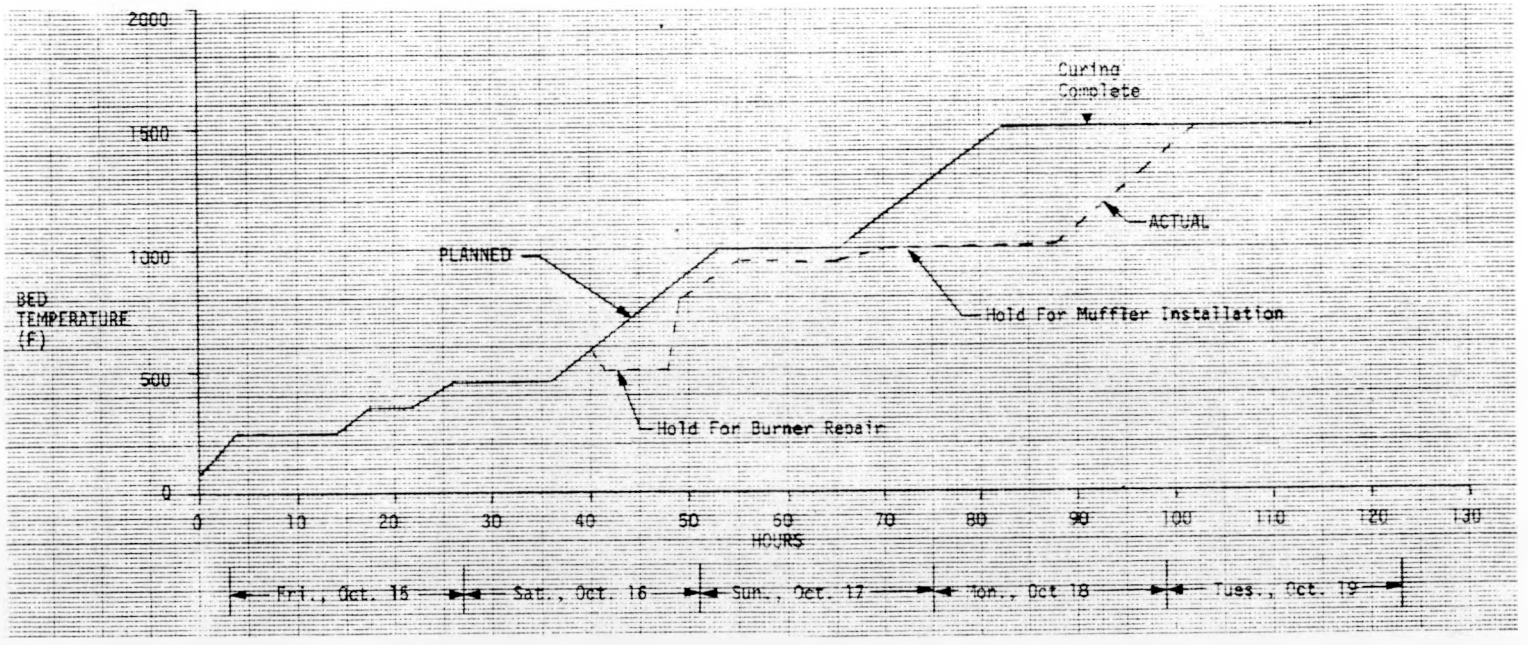


Figure 4-199. Run 001 Test Schedule

was increased, the working fluid flow established, the natural gas heaters turned off, and the combustor temperature slowly ramped up to 1500 F. This 1500 F temperature was planned for a minimum of 11 hours, and was actually held for 14 hours until 4 p.m. Tuesday, 19 October, when the coal supply was shut off, the bed was cooled and then slumped at 1350 F. After shutdown, the baghouses, cyclone, and ash overflow systems were emptied and inspected.

The post inspection of the combustor, heat exchangers, and equipment indicated all except the cyclone were in excellent condition. The cyclone system was plugged, and the chamber under it filled with ash. This cyclone inspection seemed to indicate a carbon fire had burned in this ash at some time during the run, causing minor surface damage to the bottom edges of the dump holes on a few of the cyclone units. The cyclone was emptied and was functionally ready for the next test. The ash overflow dump experienced some clumping of ash material dumped from it a few days after the test. Inspection of the baghouse showed it to be in excellent condition. The overall conclusion was that the refractory cure first test run had been a spectacular success and, in addition had operated as the highlight of the CCGT/AFB Conference Seminar. However, many systems remained to be activated, checked out, calibrated, and put into functional service.

Configuration. The combustor/heater and system configuration was the initial design and was essentially the system as outlined in Section 4.4.

Characterization Run 002. The second test run was successfully performed at two bed operating conditions. For both conditions, the superficial bed velocity was 6 ft/sec and the nominal bed temperature was 1550 F. The excess combustion air was maintained at 50% during the first period of the test, and at 30% for the remainder of the test duration. The working fluid inlet temperature was 70 F (ambient) except near the end of the second period, when the facility air heater was turned on to supply 425 F heated air to the heat exchangers. The AFB operated at an average power level of about 70%.

Description. The schedule of events is depicted in Fig. 4-200. The test generally went as planned. The bed burner and natural gas regulator system had been changed from its run 001 configuration, and the newly installed natural gas pressure regulator on the bed burner proved defective. A second new regulator was obtained and installed in the bed burner and, after a 3-hour hold at 400 F, the testing went on as scheduled. The combustor used spent bed material from run 001 that had been removed to allow posttest inspection inside the combustor. During the run 002 heatup cycle, this material was reloaded into the combustor.

The oxygen partial pressure (PO_2) probe insertion into, and removal from, the operating bed was practiced and proved satisfactory. The viewport window was cracked by thermal stress. At about midnight, Monday (13 December) during the first 12-hour operating point, the coal feed began to diminish and the bed temperatures dropped. The bed burner was reignited to keep the bed hot while this situation was evaluated. It was eventually established the baghouse was not being adequately cleaned to keep its delta pressure below 4 or 5 inches of water, and had raised the combustor pressure enough to pressure-oppose the coal feed eductors and degrade the coal flow rates. This was a procedural problem that was remedied, and the test went on as scheduled.

During run 002, there were 28 hours of operation, of which 19 were coal burning, and 18 were nominally at operating conditions. During the final hours of the test, the coal feed and combustion air supply were set and left unchanged, with minimum control variations on the working fluid air flowrate. The bed temperature rose and maintained itself in the region of 1600 to 1640 F, and the combustion fuel mixture ratio remained essentially constant (indicated by constant exhaust gas excess oxygen percentage) during that time. This demonstrated the combustor could be controlled as intended to run steadily at constant combustion conditions as required for planned testing of the metal alloy samples. During operations, a short duration bed draining was performed without problems.

The posttest inspections revealed the cyclone was plugged in some cyclone units, but the volume below was not filled as it had been in run 001. Run 002 had the

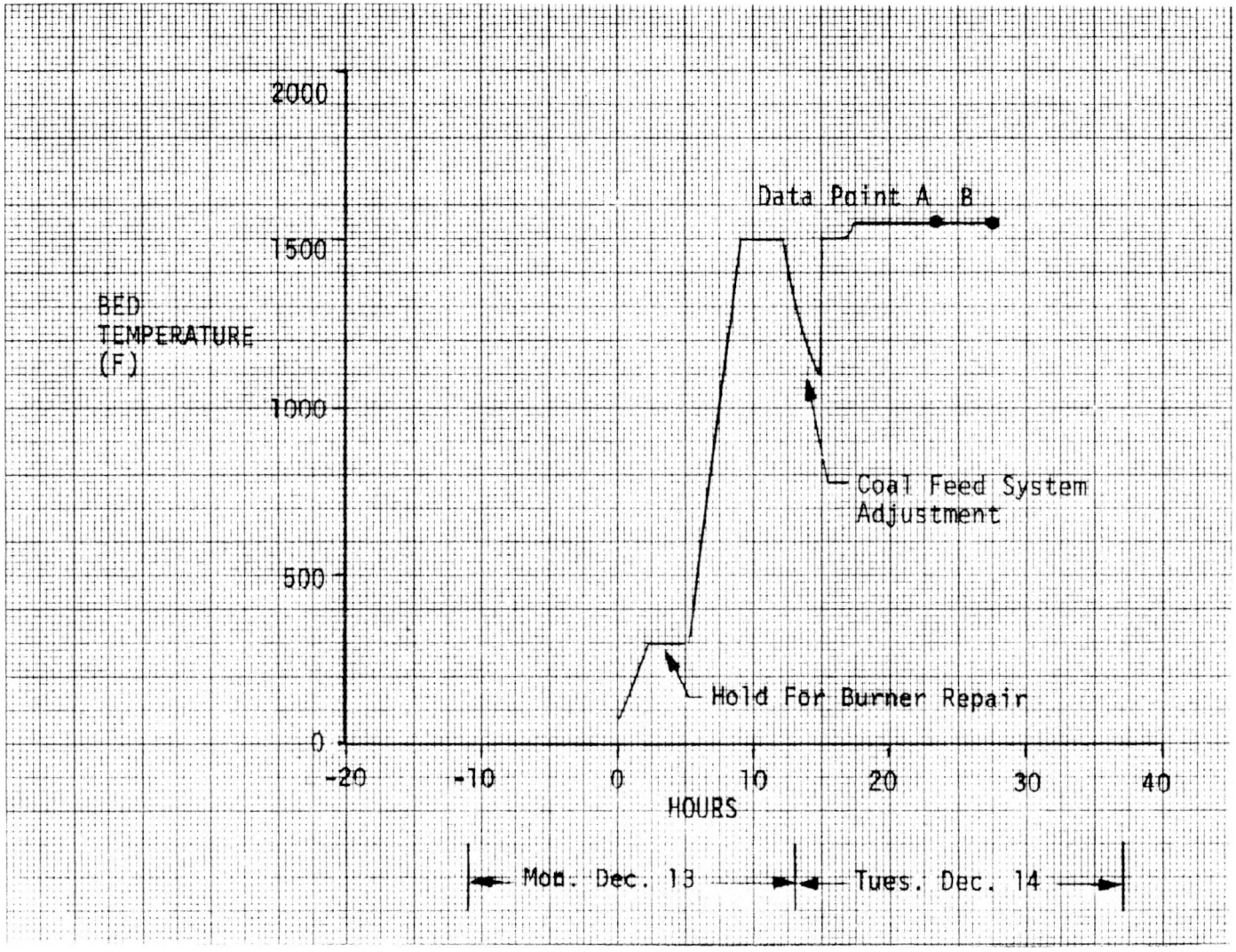


Figure 4-200. Run 002 Schedule of Events

ash overflow valve operating all the time, in contrast to operating it periodically on run 001. The cyclones were cleaned out. Inspection of the convection heat exchanger revealed collections of solid ash deposits. These deposits were broken up and removed.

Configuration. The configuration was the original design except that pressure balancing lines were installed on the four feed systems screw feeders. During run 001, it was found that the screw feeders were very sensitive to pressure unbalance and the pressure equalizing lines were partially successful.

Characterization Run 003. The run 003 plan was to operate the combustor at several bed operating conditions, activate the ash recycle system, verify the modified coal feed system operation, take measurements with the oxygen partial pressure (PO_2) probe, drain the bed material while operating, verify improved efficiency of the cyclone, use a modified start procedure, and perform a more extended duration test.

Description. Run 003 ran for 63 hours of which 54 hours were with coal burning, and 50 hours were at bed operating temperature. The superficial velocity was 6 ft/sec for the first three operating points and 4 ft/sec for the last point. The excess air was varied at levels of 50, 30, and 20%. Ash recycle was planned during some of these points, but this system failed to operate satisfactorily and no data were obtained with ash recycle. The bed temperature was 1600 F, working fluid inlet was 425 F, ash conveying air was 40 ft/sec, bed draft was -0.5 inch W.G., and bed height was 80 inches. Limestone was used to control the sulfur dioxide emissions. The actual events are depicted in Fig. 4-201.

Run 003 started Monday at about 8:00 a.m. when the prewarming was initiated. The data acquisition system was experiencing some severe problems, and further heating, using the duct burner, was delayed until noon. At 3:00 p.m., the data system was ready and the system was shut down for instrumentation zeroes. The operation resumed with both duct and bed burners. Prior to burning the bed burner, 2000 pounds of spent bed material were loaded into the unit. Bed loading continued, and the bed was heated to above 900 F by 5:45 p.m., when coal burning

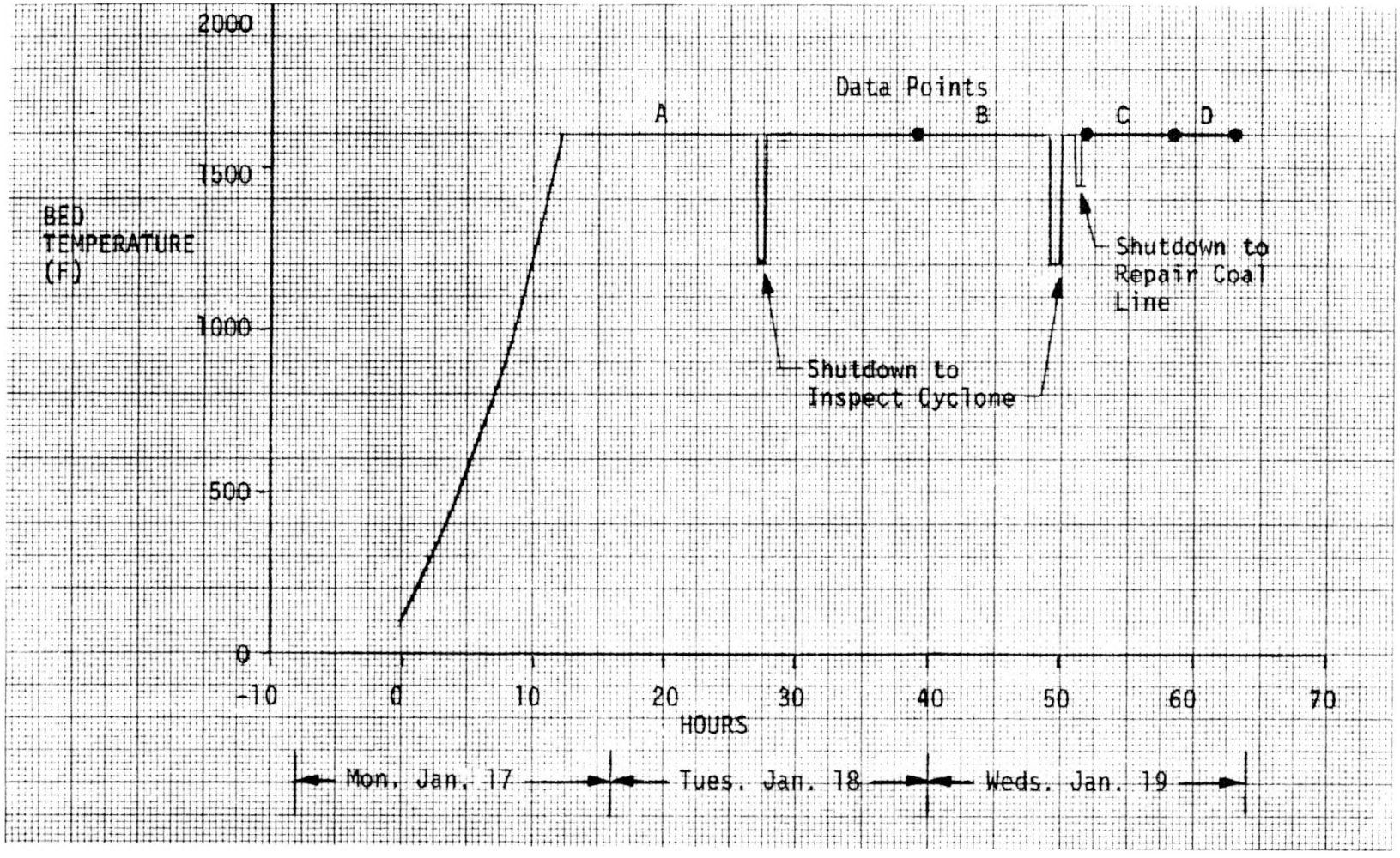


Figure 4-201. Run 003 Schedule of Events

as initiated. Bed material loading continued until the full bed was loaded (about 8500 pounds).

For the first time, cyclone ash was collected for recycle. Before attempting ash recycle, the bed was slumped (10:40 a.m. Tuesday) for 30 minutes and the cyclone inspected found to be clean. The slumping and restart operation went smoothly. The ash recycle was started and operated for about 2 hours when the rotary valve began to experience difficulty, apparently due to temperature expansion clearance problems causing erratic operation of the rotary valve. The recycle operation was terminated, and the rotary valve disassembled at that time.

The oxygen partial pressure probe was used during the first and last data point. The operation was successful, and quite interesting data traces were obtained on the brush (strip chart) recorder. However, the data acquisition system had signal problems and no PO_2 data were recorded on that system. The data on the strip charts closely resembled the type of traces obtained during the Battelle testing.

Monitoring the excess oxygen in the exhaust gases indicated that the coal/air ratio remained very constant under constant setting conditions. Generally, the working fluid flowrate was set with only minor adjustments during the operation while the bed temperature remained constant. With ash recycle, there was an initial reduction in bed temperature due to adding cold inert material, but then the temperature increased as ash containing unburned carbon was introduced. There was also a significant reduction in the sulfur dioxide emissions with ash recycle.

The bed was slumped a second time to inspect the cyclone (9:10 to 10:10 a.m. Wednesday) and the cyclone was observed to be unplugged. During this slump the bed temperature was maintained at 1300 F. A third unplanned bed slump was performed (10:24 to 10:45 a.m. Wednesday) when a coal feed line broke, and this time the bed temperature was kept at 1450 F.

Configuration. The coal feed systems were modified by installing a rotary airlock in each of the four systems, and this improved the control of coal feed-rate considerably. In the cyclone, 12 of the 36 units were mechanically plugged to increase the individual unit air velocity and presumably cyclone efficiency. The startup procedure was changed where the unit was started by preheating the combustor/heater, cyclone, and baghouse using working fluid air heated by the facility heater to approximately 425 F. The combustion air system was used to move heat throughout the system so that the temperatures were above 300 F. This prewarming was to preclude condensation of moisture on the heat exchanger when the natural gas burners were used to further heat up the system. This was an attempt to prevent dust from collecting on the tubes and forming the deposits observed on the previous run.

The coal feed system with the new rotary airlocks improved the feed rate control considerably. During some of the operation, the feed rate average for each of the feeders was within +5% of the average feed rate without changing any of the settings. Thus, on the average, over several hours of operation, the feed systems appear to produce consistent and equal feed rates of coal.

Characterization Run 004. The major objectives were oxygen partial pressure characterization of the fluidized bed and ash recycle. The subsidiary objectives were to evaluate the material specimen probe operation and design, and operate the unit at the maximum working fluid design point of 1550 F outlet temperature. This was the first major characterization of the bed using the PO_2 probe, and the Battelle engineer who conducted the PO_2 experiments at Battelle joined the operations during the PO_2 probing effort.

Description

The planned test conditions were a superficial velocity of 6 ft/sec and bed temperature of 1600 and 1650 F. The excess air was 25% without ash recycle and 30% when ash recycle was to be used. The working fluid inlet was 425 F, combustor draft was -0.5 inch W.G., and bed height of 80 to 85 inches. The actual schedule of events is shown in Fig. 4-202, where the first operation (the as

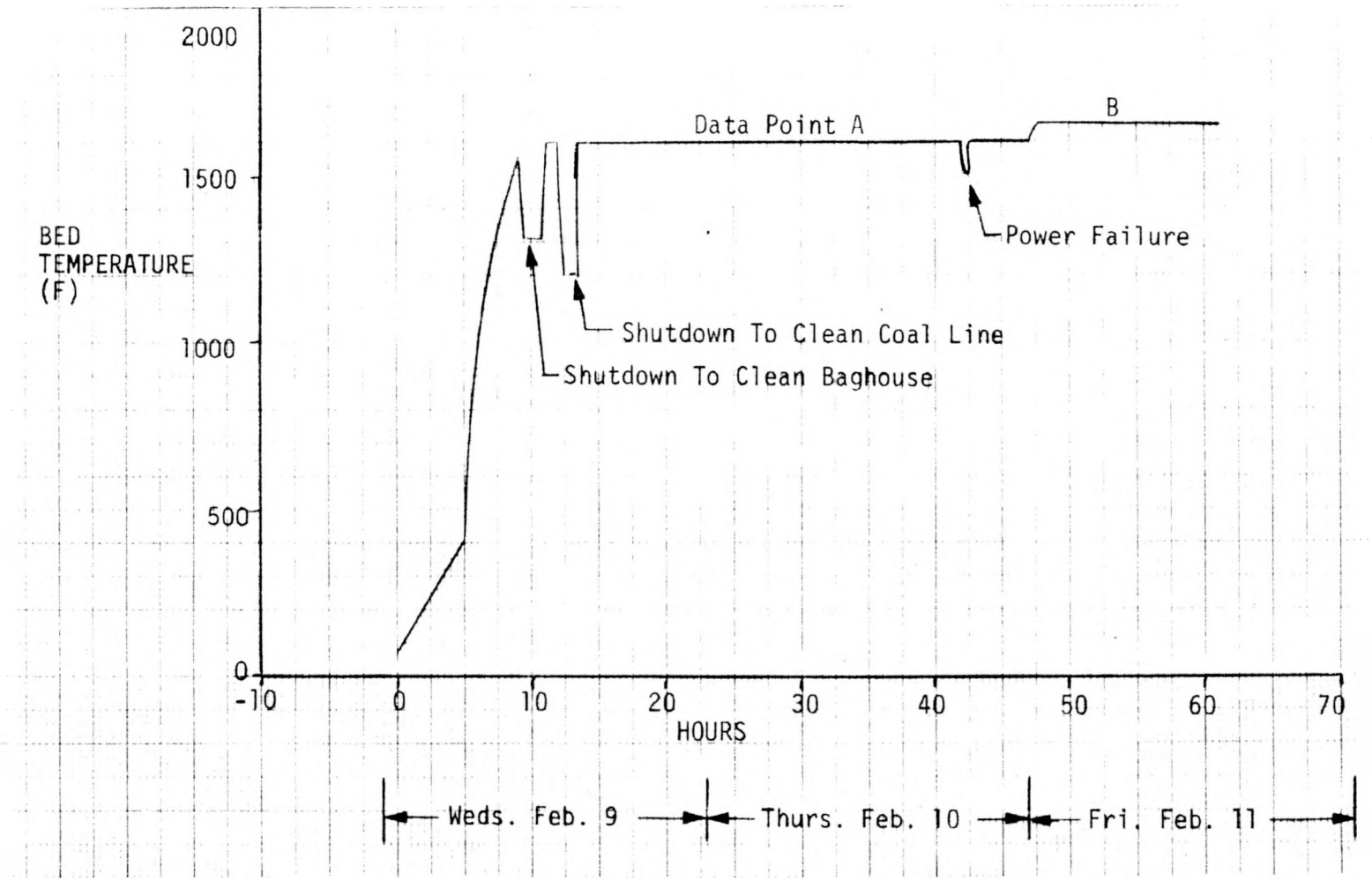


Figure 4-202. Run 004 Schedule of Events

recycle operation) was attempted, but this system did not operate satisfac torily. The last operation was at 1650 F bed temperature without ash recycle. Oxygen partial pressure characterization was conducted during the stabilized portions of each of the operations.

The startup operation began at midnight, Wednesday, using the preheated working fluid air. At 2:27 a.m. this operation was interrupted briefly to shut down the combustion air system and make a mechanical adjustment to the forced draft blower actuator. The startup operation resumed, using the same procedure used on the previous run. The unit was slumped briefly at 10:00 a.m. to inspect the baghouse hopper where a hard deposit was found plugging the hopper discharge. The unit was slumped again at 2:15 p.m. to inspect and clean one of the coal feed lines where some debris was found. The operation then resumed at the nominal conditions without ash recycle.

On Thursday at 2:00 a.m., the ash recycle operation was initiated. The ash air increased the excess air level from 25 to 30%. The ash recycle feed system worked well, and a considerable decrease in sulfur dioxide emissions occurred. However, the cyclone was not operating properly, and the ash bins were depleted in about 1 hour with most of this fly ash being passed through the system on to the baghouse. A modification was made to the ash system and, at 6:00 a.m., ash recycle was attempted again with the same results.

On Thursday at 6:00 p.m., all of the equipment on the AFB motor control center shut down as if the "master-cut" button had been pushed. The unit was quickly restarted.

The test operation was 62 hours, of which 52 were at bed temperature. The system operated at up to 98% of the design load. One major difficulty during the test was the malfunctioning of the gas analysis equipment, especially the oxygen meters. However, the basic test objective of characterizing the oxygen partial pressure was very successful. Long periods of stabilized operation were obtained during the PO_2 probing periods.

Configuration. The system configuration was the same as the previous run except modifications were continued to be made to the ash recycle system in an attempt to make this system operable.

Characterization Run 005. Run 005 consisted of 50 hours of operation at near nominal conditions (Table 4-83) both with and without ash recycle. This test had a number of objectives of which the most significant was investigation of the coal feed port configuration on the oxygen partial pressure characteristics. Each of the four quadrants has a somewhat different coal feed arrangement to investigate a number of variables. Ash recycle was used successfully for one of the data points. Other objectives included: (1) temperature profile about a material specimen probe, (2) material specimen probe coolant leakage, (3) a modified start sequence with an acoustic soot blower in the cycle to prevent fouling, and (4) visual inspection of a material specimen probe immediately upon shutdown. All of these objectives were completed, and the test operation was relatively smooth indicating that commissioning of the test equipment and operation was nearing completion.

TABLE 4-83. RUN 005 GENERAL RUN CONDITIONS

SUPERFICIAL VELOCITY, FT/SEC	6
BED TEMPERATURE, F	1600
WORKING FLUID INLET TEMPERATURE, F	425
SULFUR DIOXIDE EMISSIONS, % RETENTION	90
COAL AIR VELOCITY, FT/SEC (1 PORT/QUADRANT)	108
FT/SEC (4 PORTS/QUADRANT)	66
ASH AIR VELOCITY, FT/SEC	40
DRAFT, INCH	-0.5
BED HEIGHT, INCHES	80 TO 84

Description. Run 005 was conducted over the period of 18 to 21 April and was a 75-hour operation including 50 hours operating at bed temperature. A chronology of the major events is presented in Table 4-84 and Fig. 4-203 which indicate a number of planned and unplanned shutdowns.

TABLE 4-84. RUN 005 CHRONOLOGY

Event	Date	Time (Hours)	Activity
Startup	April 18	1200	Working fluid heating to 350 F.
↓		1530	Start burners to heat to 900 F.
↓		2000	Start coal to heat to 1600 F.
↓		2215	Slump bed briefly to clear system #3 coal lines.
Inspection	April 19	0200	Slump bed for planned inspection.
Test Point #1		0300	Start data point (no recycle).
↓		1150	Start PO2 probing
↓	April 20	0530	Complete PO2 probing and test point #1.
Inspection & Clean.		0545	Slump bed to inspect and clean air preheater and baghouse.
Test Point #2		1530	Restart to data point #2.
↓		1800	Start PO2 probing.
↓		2030	Slump to clear system #3 coal lines.
↓		2230	Resume operation
↓	April 21	1530	Complete PO2 probing and test point #2.

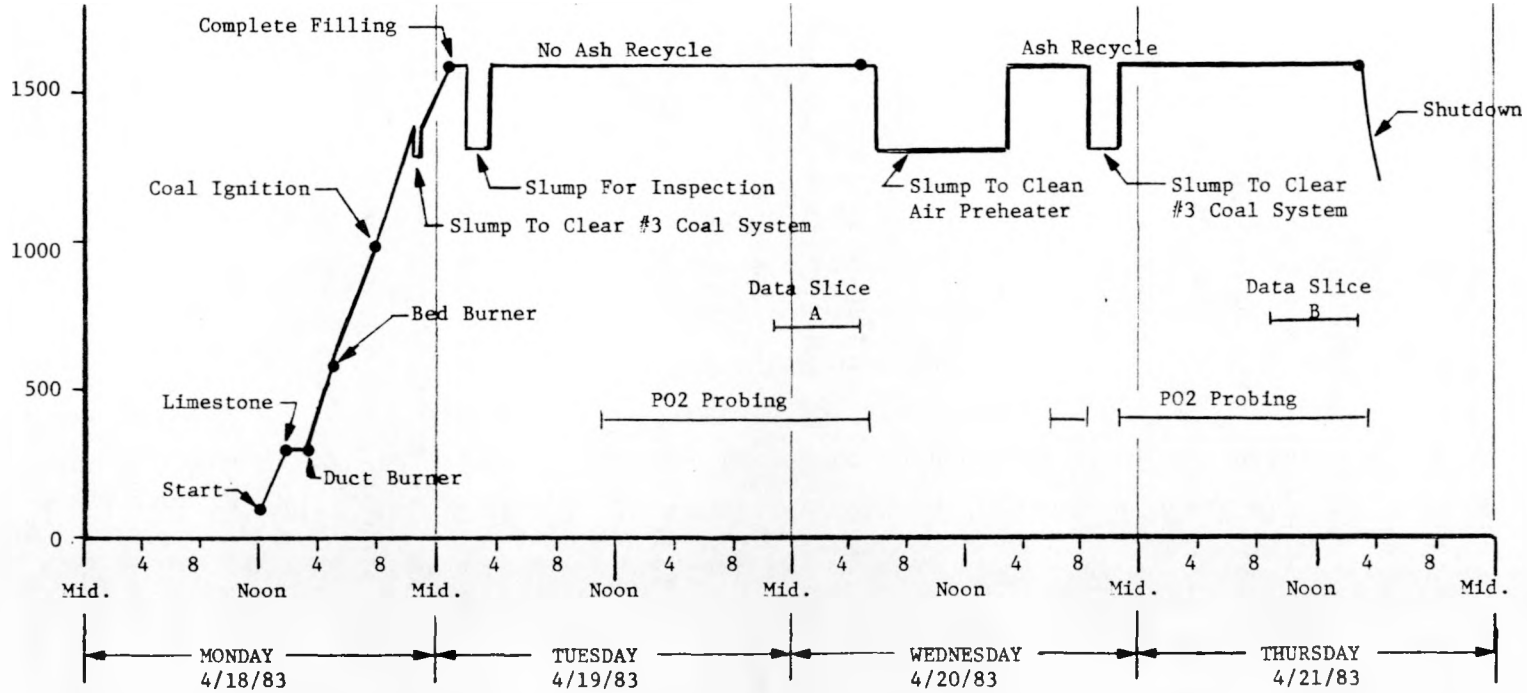


Figure 4-203. Run 005 Chronology of Events

The system was started by initially preheating the unit using heated workin fluid air and a shallow bed of fresh limestone. This modified start sequence wa› an attempt to prevent fouling of the convection bank and cyclone that had occurred on previous runs. A newly installed acoustic soot blower in the cyclone also was used throughout the run. After preheating, the normal sequence of burners and coal burning was used. The newly installed No. 3 coal system (4 ports per quadrant) showed indication of plugging in one line, and the unit was briefly shut down to inspect and clear the line. Debris was found near the coal port including a rag and wet coal. The startup resumed. The ash recycle system was operated to verify its operation, and this system performed satisfactorily except the hopper weight system experienced a failure. Therefore, the first test point was elected to be without ash recycle to allow time to repair the weight system.

After full temperature was achieved, the unit was shut down for a planned inspection which consisted of opening the manways to the cyclone hopper and convection heat exchanger soot blower cavity. The cyclone was found to be free of fouling, indicating that the modified start sequence and/or acoustic soot blower prevented fouling. Only limited inspection of the convection heat exchanger could be made due to the unit being at operating temperature; however, there was no visible evidence of fouling.

The unit was restarted, and the operating conditions brought to the nominal point without ash recycle. The oxygen partial pressure probing was started after a brief delay due to instrumentation problems, and the operation continued without difficulties until the planned PO_2 probe effort was completed.

During the latter portion of the first test point, the pressure drop in the flue gas system was noticed to have increased, and the effectiveness of the air preheater was noticed to have decreased. When the first series of PO_2 probing was complete, the unit was shut down for inspection of the air preheater and baghouse. Both of these units were subsequently cleaned. The air preheater pressure drop was found to have increased from a nominal 5 inches W.G. to 8 inches W.G. and the insides of the tubes were coated with an ash deposit. The

baghouse hopper drain was found to be plugged and the hopper filled with material. This inspection and cleaning operation lasted for 10 hours.

The unit was then restarted and brought to the second point which included ash recycle. The operation continued without problems while the planned probe activity was conducted. At one point, the No. 3 coal system indicated plugging in three of the four feed lines, and the unit was briefly slumped to clear the lines. Additional debris was found, and the unit was restarted. One of the feed ports remained plugged for the remainder of the run. The excess oxygen level was somewhat higher than planned due to failure of all of the oxygen meters at the start of point number 2. The fuel/air ratio was elected to be kept constant for the entire data point as it was more important to have consistent operating conditions for the PO_2 characterization than to maintain a given target condition.

At the completion of the planned data point 2 PO_2 probing, the unit was shut down. Immediately upon shutdown, a material specimen probe was removed in as high a temperature as possible for insepction by cognizant materials engineers. The scale condition was noted and photographically documented.

A summary of the expected and actual (numbers in parenthesis) averaged operating conditions is presented in Table 4-85.

Configuration. Initial oxygen partial pressure (PO_2) probing indicated that the baseline coal port configuration has an undesirable reducing zone above the coal port. Therefore, a number of changes were made to the coal and air distributors to evaluate several approaches to reduce or eliminate this reducing zone. A coal plume distributor was added to the first quadrant, the second quadrant remained unchanged, four coal ports with a coal feed splitter system were added to the third quadrant, and the fourth quadrant had provision for adding various amounts of augmented air above the coal port splash plate. (These modifications and the results are discussed in detail in Section 4.5.5 Combustion/Heater Modifications.) Also, an acoustic soot blower was added to the cyclone hopper to prevent buildup of the sticky ash deposits.

TABLE 4-85. RUN 005 EXPECTED (ACTUAL) OPERATION

DATA POINT	A	B
SUPERFICIAL VELOCITY - FPS	6.0 (5.7)	6.2 (5.9)
EXCESS AIR - PERCENT	25 (16)	30 (38)
WORKING FLUID TEMPERATURE - F		
INLET	425 (400)	425 (407)
BED HEAT EXCHANGER INLET	779 (746)	790 (840)
BED HEAT EXCHANGER OUTLET	1494 (1475)	1497 (1499)
COMBUSTION SIDE TEMPERATURES - F		
BLOWER	160 (161)	160 (167)
WINDBOX	581 (489)	587 (532)
BED	1600 (1581)	1600 (1583)
EXHAUST	696 (739)	705 (741)
AIR PREHEATER OUTLET	370 (466)	373 (442)
AIR FLOWRATES - LB/SEC		
WINDBOX	3.449 (3.419)	3.449 (3.403)
COAL CONVEYING AIR	0.460 (0.583)	0.460 (0.548)
ASH CONVEYING AIR	0.000 (0.0)	0.147 (0.158)
WORKING FLUID	12.30 (12.50)	12.17 (10.28)

Characterization Run 006. Run 006 consisted of 52 hours of operation which included 7 hours at a superficial velocity of 8 ft/sec while the remaining hours were at nominal conditions. The operating conditions and objectives were similar to the previous test where a primary objective was to characterize the bed environment (oxygen partial pressure) and the influence of the coal feed configuration on the environment. Based on the results of run 005, additional modifications were made to the coal feed port configurations, and extensive PO_2 probing was conducted at the nominal condition of 6 ft/sec superficial velocity. Other minor objectives were measurement of horizontal bed temperature profile. Run 006 was conducted as planned with all systems performing well.

Description. Run 006 was conducted over the period of 16 to 19 May 1983 and was a 74-hour operation including 52 hours at operating conditions. A chronology of the major events is presented in Table 4-86 showing the test was conducted essentially as planned, with only one major shutdown due to a malfunction of the facility compressor.

The system was started using the same procedure used on run 005 of prewarming the unit with heated working fluid air. An acoustic soot blower had been installed for run 005 on the cyclone unit, and another acoustic soot blower was installed for run 006 on the air preheater. In both cases, fouling of the units was not experienced after the soot blowers were installed and operated.

Just after startup, the unit was briefly shut down when the system equipment power panel shut down for an unexplained reason. The first data point was operated at 8 ft/sec superficial velocity for several hours to obtain basic operating data at this power level. (No oxygen partial pressure probing was conducted at this point.) The remainder of the operation was at the nominal superficial velocity of 6 ft/sec where extensive bed characterization was conducted using the PO_2 probe.

Just after adjusting the system to the second point, the facility compressor shut down and several hours were required to restart the compressor unit. During this second data point, the facility compressor performance was deteriorating and some

TABLE 4-86. RUN 006 CHRONOLOGY

Event	Date	Time(Hours)	Activity
Startup	May 16	0930	Prewarming with working fluid to 400 F.
"	"	1345	Start burner(s) to 900 F.
"	"	1800	Start coal.
"	"	2022	Slump briefly due to power panel failure.
8 fps Operation	May 17	0030	Start data point.
"	"	0730	Complete data point and change to 6 fps.
6 fps Operation	"	0730	Start data point
"	May 18	0925	Facility compressor down.
"	"	1630	Facility compressor back on line.
"	"	1700	Back on stabilized conditions. Ash recycle system off for repairs.
"	"	2000	Ash recycle back on.
"	May 19	1130	Complete data point. Shutdown.

NOTE: Unit at operating conditions for 52 hours.

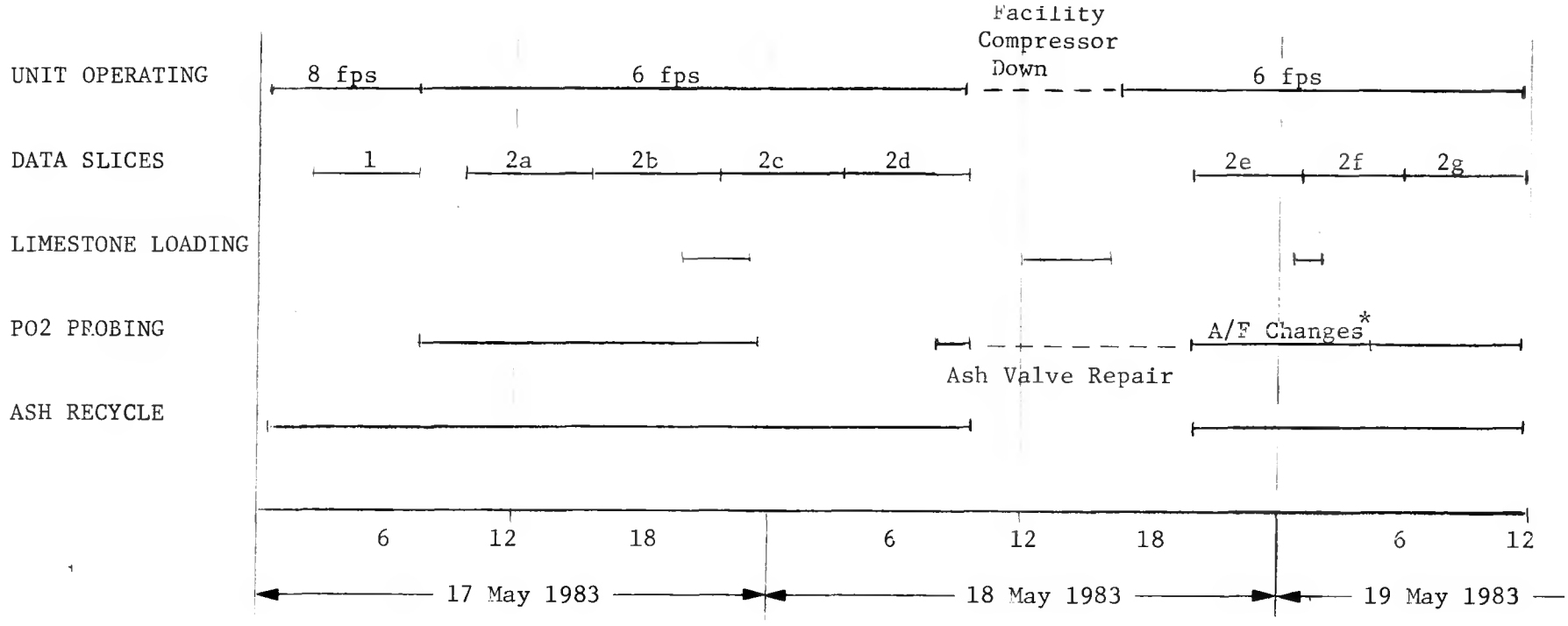
portions of the operation were conducted with reduced heater inlet temperature which reduces the amount of air required from the compressor.

The ash recycle system was used throughout the run, and this system performed well except for a seal leak on the rotary valve which created a dust problem in the area. This unit was repaired during the period that the facility compressor was shut down, and the ash recycle system was functional by the time that stabilized conditions were re-established.

The events of run 006 are depicted in Fig. 4-204 which indicates where PO_2 probing was conducted and the periods of the averaged data slices which are reported. During a period of the characterization, the excess oxygen was varied in a given quadrant to investigate the effects on the oxygen partial pressure characteristics. This was accomplished by simply varying the coal feedrate as appropriate in the quadrant of interest, and the coal feedrate in the opposite quadrant was varied to compensate for the change so that the overall excess air level remained at the target condition. A comparison of the target conditions with the actual averaged condition is presented in Table 4-87 where the actual conditions are the numbers in parentheses.

Configuration. Based on the results of the previous run, modifications continued to be made to the coal and air distributor. Augmented air was shown to be a promising approach to eliminate the reducing zone above the coal port, and the first quadrant was converted to augmented air with 13% of the combustion air for that quadrant. The second quadrant remained a reference configuration. The four coal ports remained unchanged as this approach had good PO_2 characteristics. The fourth quadrant was restored to the reference port configuration. Also, a second acoustic soot blower was added to the air preheater. These modifications and the results are discussed in more detail in Section 4.5.5.

Material Specimen Exposure Run 007. This was the first of two runs which was to operate at steady state at nominal conditions (Table 4-88) to expose a large number of heat exchanger material specimens.



* Air/Fuel ratio changes in selected quadrants to investigate excess air effects on oxygen partial pressure.

Figure 4-204. Summary of Run 006 Test Activities

TABLE 4-87. RUN 006 EXPECTED (ACTUAL) OPERATION

DATA POINT	1	2
SUPERFICIAL VELOCITY - FPS	8.0 (7.8)	6.0 (6.2)
EXCESS AIR - PERCENT	25 (29)	25 (23)
WORKING FLUID TEMPERATURE - F		
INLET	70 (80)	425 (375)
BED HEAT EXCHANGER INLET	625 (624)	800 (827)
BED HEAT EXCHANGER OULET	1492 (1459)	1528 (1540)
COMBUSTION SIDE TEMPERATURES - F		
BLOWER	160 (157)	160 (177)
WINDBOX	454 (497)	588 (562)
BED	1625 (1587)	1625 (1655)
EXHAUST	546 (623)	704 (726)
AIR PREHEATER OUTLET	316 (373)	373 (433)
AIR FLOWRATES - LB/SEC		
WINDBOX	4.262 (4.196)	3.065 (3.005)
COAL CONVEYING AIR	0.520 (0.540)	0.520 (0.592)
ASH CONVEYING AIR	0.147 (0.156)	0.147 (0.153)
AUGMENTED AIR	0.142 (0.142)	0.101 (0.101)
WORKING FLUID	12.62 (12.60)	11.75 (11.42)

TABLE 4-88. GENERAL RUN CONDITIONS
MATERIAL SPECIMEN EXPOSURE TEST SERIES

SUPERFICIAL VELOCITY, FT/SEC	6
BED TEMPERATURE, F	1650
EXCESS AIR, %	25
WORKING FLUID INLET TEMPERATURE, F	425
SULFUR DIOXIDE EMISSIONS, % CAPTURE	90
COAL AIR VELOCITY, FT/SEC	
1 PORT/QUADRANT	125
4 PORTS/QUADRANT	79
ASH AIR VELOCITY, FT/SEC	40
DRAFT, INCH	-1
BED HEIGHT, INCHES	90

Description. Run 007 was conducted over the period of 8 to 16 August 1983, and 176.5 hours of operating time was accumulated at the design temepratures. A chronology of the major events is presented in Table 4-89.

The system operation was the same as developed during the previous testing and was very similar to run 006 where the bed was extensively characterized with the oxygen partial pressure (PO_2) probe at nominal conditions. However, a greater emphasis was placed on maintaining even coal feed rates to all four quadrants.

As planned, the unit was started and brought to temperature with an excess air of 50%. The operation was stabilized for several hours while the coal feed rates were monitored. The coal feeders were adjusted and the feed rates were again monitored, and this process was repeated until all four systems were even. The feed rates were then adjusted in steps until the nominal condition of 25% excess air was achieved. This initial operation took about 24 hours to bring the unit to the nominal condition where the remainder of the test was run.

There were two shutdowns during the run. The first occurred during startup just after full bed temperature was achieved to inspect the cyclone hopper. A rag cloth was inadvertently left in the cyclone hopper, and this shutdown operation

TABLE 4-89. RUN 007 CHRONOLOGY

EVENT	DATE	TIME (HOURS)	ACTIVITY
Startup	Aug. 8	0800	Initiate startup.
Startup	Aug. 8	1715	Slump to remove rag from cyclone hopper.
Startup	Aug. 8	1845	Resume operation.
Point No. 1	Aug. 8	1900	Stabilized at 50% excess air. Slowly reduce excess air toward 25%.
Point No. 1	Aug. 9	1300	Initiate ash recycle.
Point No. 2	Aug. 9	1830	Stabilized at 25% excess air.
Point No. 2	Aug. 10	2345	Data system down. Except for brief operation on August 10, system down for remainder of test.
Point No. 2	Aug. 13	1645	Slump to service coal air regulator.
Point No. 2	Aug. 13	1715	Resume operation.
Point No. 2	Aug. 16	0446	Shutdown of facility compressor. End of Run 007.

to inspect and clear the cyclone was a 1.5-hour period. A second shutdown of 0.5-hour occurred during the run to service an air regulator in the coal feed system.

Finally, the facility compressor shut down due to a malfunction. Since this was a long-term repair, the run was terminated. The unit was subsequently drained, inspected, and found to be in good condition.

A number of material specimen probes (both cooled and uncooled) had been inst lled except for one cooled probe that was to be located over the coal feed

port that had been modified for augmented air prior to the run. This provided sufficient ports to PO_2 characterize this quadrant to verify that the modification had the expected, acceptable oxygen partial pressure environment. The test results showed that the modification was acceptable, and the final probe was then installed for the next test, run 008.

A problem occurred with the main data acquisition system during the early portion of the run. Most of the critical parameters related to the operating condition were recorded by manual logging of the indicators and/or data logger-type system with a printer. The loss of the main data system resulted in the loss of some of the many parameters. However, the two remaining systems provided sufficient information to operate the unit and assess the unit performance. System performance characteristics such as pressure drops had been well established during the previous test series, and loss of this type of data was not critical. A few parameters of interest to monitor system performance were added to the datalogger during the course of runs 007 and 008. Thus, the loss of the main data acquisition system did not compromise the objectives of the material exposure test series. The main effect was some small effect on the accuracy of some parameters and the posttest reduction effort was increased since the data were in a less convenient form.

Configuration. The system was essentially the final configuration developed during the previous characterization test series except for one change in the distributor area. An augmented air source was added to quadrant number 2 which was very similar to quadrant number 1 except that the air discharge over che coal feed plate was radially outward rather than upward as in quadrant number 1.

A large number of heat exchanger material probe specimens were installed to be exposed to the combustion environment. These included (1) 10 cooled bed probes containing 292 metal specimen sections of various materials, (2) 15 uncooled bed and convection probes containing hanger materials as well as simulated wall and bed surface probes, and (3) 2 cooled convection bank material probes. Essentially, all of these probes remain in the unit for an additional 650 hour of exposure as part of the Phase II extension program. These probes will then be

›ved for analysis. Therefore, the configuration and locations of these probes will be reported in the Addendum to the Final Report along with the results of the material analysis.

Material Specimen Exposure Run 008. This was the second run of the material specimen exposure series which culminated in over 350 hours of operation. The operating conditions were the nominal conditions as in run 007.

Description. Run 008 was conducted over the period of 19 to 28 September 1983, and 194.5 hours of operating time were accumulated at the design temperatures. A chronology of the major events is presented in Table 4-90.

TABLE 4-90. RUN 008 CHRONOLOGY

EVENT	DATE	TIME(Hours)	ACTIVITY
Startup	Sept. 19	1300	Initiate Startup.
Operation	Sept. 19	1800	Stabilize Operation at 25% excess air; 1650°F Bed.
Operation	Sept. 19	2000	Initiate Ash Recycle.
Operation	Sept. 22	0015	Burnout and Slump Bed on shutdown of Facility (CB) Compressor.
Operation	Sept. 22	1600	Resume operation after facility Compressor Repair.
Operation	Sept. 26	2000	Datalogger Output Loop Failure; Continue on Hand Data.
Operation	Sept. 27	0120	Datalogger back on using thermal Printer Tape.
Operation	Sept. 27	2050	Facility Heater (Todd) Bearing Failure; Continue without Working Fluid Preheat.
Operation	Sept. 28	0815	FD Fan Inlet Damper Control (MICON) Failure; Momentary Bed Slump; Continue on Local Damper Control.
ıutdown	Sept. 28	1230	Shutdown

The system configuration and operation was the same as the previous run, and t material specimen probes remained in these same configuration except for installation of one probe as previously discussed. The unit was started and brought to the nominal conditions of 6 ft/sec superficial velocity, 1650 F bed temperature, and 25% excess air. (The intermediate step of 50% excess air was not used.) Ash recycle was started when there was sufficient inventory in the recycle system.

There was one shutdown of 15 hours duration when the facility compressor malfunctioned. The compressor was repaired and the AFB unit was restarted without difficulty, and nominal operating conditions were achieved 1 hour later. The main data acquisition system was not functional, and data were accumulated and reduced in the same manner as run 007. The facility heater, used to preheat the working fluid air, failed toward the end of the run, and the test was finished with ambient temperature working fluid air. (The lower inlet temperature has a small effect on the heat exchanger material temperature and essentially no effect on the heat exchanger material specimen probes.)

A minor problem was failure of the datalogger printer toward the end of the run, and the auxiliary tape printer was used to record data. The Micron process controller signal to the combustion air control valve suddenly failed toward the end of the run causing the combustion air flow to stop, essentially slumping the bed. This was corrected within a few moments by transferring to manual control. The remainder of the test was made using manual control which resulted in a small variation in the combustion air flow during this period.

The run was continued until a total of 350 hours of material exposure time had been accumulated. The run then continued for an additional 21 hours until a convenient time when the coal and limestone systems were almost depleted. Posttest, the unit and all ash systems were drained.

Subsequently, the unit was inspected and one cooled bed material specimen probe was removed for dissassembly and analysis.

Configuration. The system configuration was the same as the previous run.

4.5.3 GENERAL TEST PROCEDURE

The procedures for establishing the test conditions and adjustments made are described and, during the characterization series, these procedures were refined. The refined procedures were then applied to material specimen exposure series where long durations were conducted under stabilized conditions.

Each given operating point is defined by operation at steady-state conditions at a specified superficial air velocity, excess air, and bed temperature. The working fluid inlet temperature also is specified. The other parameters, such as the working fluid flowrate, coal feed rate, and bed outlet temperature, are adjusted to maintain the specified conditions. This results in the following procedure:

1. The combustion air flowrates are set, including windowbox air, coal conveying air, and ash recycle air. These flowrates plus the bed temperature essentially set the superficial air velocity value. The purges used for the igniter and bed pressure measurements are small (less than 0.5%) and are ignored.
2. The coal feed rates are set to achieve the specified excess air as measured by the percent of excess oxygen in the exhaust gases.
3. The working fluid flowrates are adjusted to maintain the specified bed temperature.

Other operating conditions included adjusting the limestone feed rate to maintain the exhaust gas sulfur dioxide level, and setting fly ash recycle rate. Fly ash recycle is set simply as a constant speed on the metering ash recycle rotary valve.

The procedure developed during the characterization test series was used for both material exposure tests, and the operation was very smooth. The startup consisted of prewarming the unit and system to above 300 F using heated working fluid and the combustion side air system. During this period, the bed was empty. Then, 2000 to 3000 pounds of limestone was added while the duct burner s turned on. Final heating of the bed was made with the duct and bed burner

until a bed temperature of 900 F was obtained at which time coal is fed at a low rate. One minor change in procedure wasto not draw sample gas to the gas analysis console during the methane burner operation as some of the instruments in the gas analysis console were very sensitive to the high moisture in the methane combustion products. The unit was then brought to full temperature and height using 9000 pounds of spent bed material followed by additional limestone.

The sulfur dioxide emissions were essentially zero during this period due to the high limestone content of the bed. The sulfur dioxide level would start slowly increasing after about 12 hours of operation at which time limestone feeding would commence. When 2000 to 3000 pounds of ash inventory was accumulated in the ash recycle system, ash recycle was started. Completely stabilized operation of all systems and feed rates usually took about two days to occur.

A routine operation was followed as shown in Table 4-91. The coal run hoppers were recharged every two hours. The ash recycle run tank was recharged once an hour, and the recycle rate was adjusted so that the run tank inventory would be about depleted in 1 hour. Manual logging of some parameters was conducted each half hour, and the datalogger printed each quarter hour. The main data system took a single data point each 15 minutes.

After a few days of operation, the unit operated very smoothly with only occasional adjustments of the various systems. There were several instances of coal feed line plugging, particularily the four-port system, and plugging was cleared without shutting down the unit, usually in a short period of time. While clearing the coal lines, the coal in the problem system would be shut off while the remaining systems operated at their normal feed rate.

The nominal expected operation is presented in Table 4-92, and the working fluid air flowrate represents the condition without the cooled material probes in the bed. With the cooled probes, the actual working fluid flowrate was about 20% less as some of the heat was removed by the material probes.

TABLE 4-91. TANK FILLING PROCEDURES

COAL RUN HOPPERS

- Each Two Hours On the Even Hours
- Close Fill Valve At About 1200 lb.
- Fill Just After The Hour After Data Is Taken On All Systems. (Manual, Main and Autodata)

ASH RUN HOPPER

- Once An Hour On A Quarter Hour.
- Log Data On Manual Sheets.
- Adjust Feeder To Deplete Run Bin Inventory In About One Hour.

LIMESTONE BIN

- Minimize Number Of Filling Operations (Goal Of Once A Day).
- Fill In Long Continuous Operation.
- No Short Operations Or Topping Of Bin.
- Fill During Shutdown Periods If Long Shutdowns Occur.

BAGHOUSE DRAIN

- Check Each Half Hour.
- As Required.

BED DRAIN

- As Required.

COAL DAYBIN

- As Required.

TABLE 4-92. EXPECTED OPERATION

NOMINAL OPERATION	
SUPERFICIAL VELOCITY - fps	6
EXCESS AIR - percent	25
WORKING FLUID TEMPERATURE - °F	
INLET	425
BED HEAT EXCHANGER INLET	818
BED HEAT EXCHANGER OUTLET	1561
COMBUSTION SIDE TEMPERATURE - °F	
BLOWER	160
WINDBOX	595
BED	1650
EXHAUST	712
BAGHOUSE	373
AIR FLOWRATES - lb/sec.	
WINDBOX	2.901
COAL CONVEYING AIR	0.536
ASH CONVEYING AIR	0.147
AUGMENTED AIR	0.203
WORKING FLUID	11.250

4.5.4 Summary of Data

Analysis of the data was conducted by selecting reasonably steady-state operating periods and analyzing the various flow and performance parameters. These analyses indicated that the system performance was close to design, and the operating characteristics were repeatable.

Obtaining operating characteristics requires steady-state operation and measurement, which include the following factors:

1. Pressure, temperature, and gas flowrate measurements -- these measurements respond rapidly and steady-state values could be ascertained after a brief period of steady-state operation.
2. Thermal and bed chemistry equilibrium -- as the bed and some of the hardware has a large thermal inertia, obtaining thermal equilibrium of the bed takes hours of steady operation. Obtaining chemical equilibrium was not as important for most performance parameters, except limestone utilization and sulfur diozide emissions. Chemical equilibrium may take several hours to achieve.
3. Solids feedrate measurements -- with the bin weight system that was employed, hours of steady operation were required to obtain averaged feed rates. Also, the individual feed systems varied over a narrow band for a given set point, and reloading operations tended to interface with measurements of solids feed rates. The solids feed rates are of prime importance to combustion performance and limestone utilization calculations.
4. Proper operation of the instrumentation systems.

Thus, a good steady-state performance calculations require long periods of very smooth steady operation with all systems performing. A problem encountered was spending several hours at an operating point only to have a critical piece of instrumentation or a system fail. Thus, steady-state performance was often difficult to ascertain during the initial checkout tests.

The first four runs were primarily checkout and development in nature, and t... general operating conditions are presented in Table 4-81. Reasonably steady-- state operation was achieved during Run 003, and several data slices are presented in Table 4-93. By runs 005 and 006, the configurations and operations of the instrumentation and feed system had been developed, and the data from these runs are presented in Tables 4-94 and 4-95.

A summary of the pertinent data from the material specimen exposure is presented in Tables 4-96 and 4-97 for the two runs. Most of the critical parameters related to the operating condition were recorded by manual logging of the indicators and/or datalogger-type system with a printer. The loss of the main data system resulted in the loss of some of the many parameters; however, the two remaining systems provided sufficient data to operate the unit and assess the unit performance. Thus, the loss of the main data acquisition system did not compromise the objectives of the material exposure test series. The main effect was some small effect on the accuracy of the parameters and the posttest data reduction efforts were increased since the data were in a less convenient form.

TABLE 4-93. OPERATING DATA

RUN NUMBER	003A	003B	003C	003D
Date	1/18/83	1/19/83	1/19/83	1/19/83
Date Slice				
Start, hours	0800	0703	1502	2200
End, hours	0902	0800	1559	2259
Superficial Velocity - fps	6.3	6.3	6.0	4.2
Bed Temperature - F	1611	1590	1587	1594
Working Fluid Outlet Temperature - F	1516	1491	1477	1520
Windbox Air				
Air Heater Inlet Temperature - F	159	159	168	165
Air Heater Outlet Temperature - F	605	596	580	557
Windbox Temperature - F	579	570	554	524
Air Heater Inlet Pressure - In.	66.9	70.6	72.6	70.8
Air Heater Outlet Pressure - In.	66.4	70.3	72.0	71.3
Windbox Pressure - In.	66.0	69.6	70.7	70.8
Flowrate - lb/hr	12,270	12,210	12,200	8,100
Bed Pressures				
0" - In (Estimated)	51.0	58.0	58.0	67.0
5.7" - In	47.6	52.9	53.9	61.5
17.1" - In	39.7	43.4	41.7	50.3
29.7" - In	33.0	30.9	31.3	37.1
41.7" - In	21.2	21.7	26.1	29.7
53.7" - In	NG	NG	NG	NG
65.9" - In	NG	NG	NG	NG
77.9" - In	-0.1	0.0	0.3	0.0
90.1" - In	-0.1	0.0	0.3	0.0
102.1" - In	-0.1	0.0	0.2	0.0
230.1" - In	-0.5	-0.5	-0.3	-0.7
Bed Temperatures				
5.7" - F	1623	1603	1603	1607
27.7" - F	1629	1608	1607	1614
51.7" - F	1611	1590	1587	1597
75.4" - F	1616	1598	1598	1611
103.1" - F	1588	1603	1590	1581
229" - F	1454	1491	1477	1455
293" - F	987	1017	984	939
Bed Height - In	72	69	75	69

TABLE 4-93. (Continued)

OPERATING DATA

	003A	003B	003C	003D
Working Fluid - East				
Convection Bank Inlet Temperature - F	421	426	405	413
Convection Bank Outlet Temperature - F	844	835	766	818
Bed Bank Inlet Temperature - F	838	833	761	811
Bed Bank Outlet Temperature - F	1518	1490	1479	1519
Convection Bank Inlet Pressure - psig	40.9	50.2	52.2	30.6
Convection Bank Outlet Pressure - psig	38.5	47.4	49.5	29.6
Bed Bank Inlet Pressure - psig	37.8	45.5	47.9	27.6
Bed Bank Outlet Pressure - psig	10.3	14.3	17.2	5.2
Flowrate - lb/hr	15,850	19,180	19,860	12,910
Working Fluid - West				
Convection Bank Inlet Temperature - F	422	426	508	417
Convection Bank Outlet Temperature - F	830	822	745	805
Bed Bank Inlet Temperature - F	826	824	744	803
Bed Bank Outlet Temperature - F	1515	1492	1475	1521
Convection Bank Inlet Pressure - psig	42.6	51.1	57.1	31.0
Convection Bank Outlet Pressure - psig	39.4	47.1	53.1	28.9
Bed Bank Inlet Pressure - psig	37.0	45.8	47.8	28.4
Bed Bank Outlet Pressure - psig	10.1	14.7	15.8	5.8
Flowrate - lb/hr	16,992	19,735	21.890	13,486
Flue Gas				
Cyclone Inlet Temperature - F	748	767	742	691
Cyclone Outlet Temperature - F	747	725	717	657
Air Heater Outlet Temperature - F	406	409	397	376
Baghouse Temperature - F	351	356	349	328
Combustor Pressure (230") - In	-0.5	-0.5	-0.3	-0.7
Cyclone Inlet Pressure - In	NG	NG	NG	NG
Cyclone Outlet Pressure - In	-5.5	-5.5	-5.1	-2.7
Air Heater Outlet Pressure - In	NG	NG	NG	NG
Baghouse Outlet Pressure - In	-5.6	NG	NG	-3.2
Solids Feedrate				
Coal - lb/hr	1234	1329	1487	893
Limestone - lb/hr	NG	680	572	505
Flyash Recycle - lb/hr	0	0	0	0

TABLE 4-93. (Concluded)

OPERATING DATA

	003A	003B	003C	003D
Combustion Air				
Windbox - lb/hr	12,270	12,220	12,200	8,100
Coal Air - lb/hr	1,510	1,910	1,580	1,620
Ash Air - lb/hr	510	600	0	0
Total	14,290	14,730	13,780	9,720
Flue Gas Constituents				
SO_2 - ppm	NG	210	219	219
NO_x - ppm	NG	310	360	NG
O_2 - %	6.8	5.9	3.8	4.5
CO_2 - %	11.5	13.0	14.0	13.8

TABLE 4-94. RUN 005 SUMMARY OF DATA

RUN NUMBER	A	B
Date	4/19/83	4/21/83
Date Slice		
Start, hours	2300	0859
End, hours	0500	1500
Superficial Velocity - fps	5.7	5.9
Bed Temperature - F	1606	1608
Working Fluid Outlet Temperature - F	1475	1499
Windbox Air		
Air Heater Inlet Temperature - F	161	167
Air Heater Outlet Temperature - F	523	563
Windbox Temperature - F	489	532
Air Heater Inlet Pressure - In.	77.6	74.5
Air Heater Outlet Pressure - In.	78.0	74.7
Windbox Pressure - In.	76.4	73.4
Flowrate - lb/hr	12,355	12,250
Bed Pressures		
0" - In (Estimated)	66.0	60.0
5.7" - In	59.0	55.8
17.1" - In	51.7	45.1
29.7" - In	37.4	36.5
21.7" - In	29.4	26.7
53.7" - In	12.5	8.1
65.9" - In	0.6	0.1
77.9" - In	0.2	0.1
90.1" - In	0.2	0.3
102.1" - In	0.2	0.1
230.1" - In	-0.5	-0.6
Bed Temperatures		
5.7" - F	1602	1600
27.7" - F	1606	1608
51.7" - F	1581	1583
75.4" - F	1603	1600
103.1" - F	1599	1594
229" - F	1528	1630
293" - F	1052	1068
Bed Height - In	71	8

TABLE 4-94. (Continued)

Working Fluid - East		
Convection Bank Inlet Temperature - F	399	407
Convection Bank Outlet Temperature - F	754	852
Bed Bank Inlet Temperature - F	744	842
Bed Bank Outlet Temperature - F	1474	1498
Convection Bank Inlet Pressure - psig	62.9	49.6
Convection Bank Outlet Pressure - psig	59.4	46.8
Bed Bank Inlet Pressure - psig	56.0	45.2
Bed Bank Outlet Pressure - psig	21.7	15.7
Flowrate - lb/hr	22,475	18,803
Working Fluid - West		
Convection Bank Inlet Temperature - F	401	407
Convection Bank Outlet Temperature - F	752	845
Bed Bank Inlet Temperature - F	749	837
Bed Bank Outlet Temperature - F	1476	1499
Convection Bank Inlet Pressure - psig	62.5	50.7
Convection Bank Outlet Pressure - psig	57.8	46.8
Bed Bank Inlet Pressure - psig	57.7	45.2
Bed Bank Outlet Pressure - psig	22.8	16.1
Flowrate - lb/hr	22,511	18,210
Flue Gas		
Cyclone Inlet Temperature - F	734	741
Cyclone Outlet Temperature - F	724	730
Air Heater Outlet Temperature - F	466	442
Baghouse Temperature - F	392	364
Combustor Pressure (230") - In	-0.5	-0.6
Cyclone Inlet Pressure - In	-0.9	-1.4
Cyclone Outlet Pressure - In	-4.0	-4.5
Air Heater Outlet Pressure - In	-10.9	-9.8
Baghouse Outlet Pressure - In	-14.9	-13.6
Solids Feedrate		
Coal - lb/hr	1446	1243
Limestone - lb/hr	172	176
Flyash Recycle - lb/hr	0	1013

TABLE 4-94. (Concluded)

Combustion Air		
Windbox - lb/hr	12,355	12,250
Coal Air (System 1, 2, & 4) - lb/hr	1516	1300
Coal Air (System 3) - lb/hr	583	673
Ash Air - lb/hr	0	561
Total - lb/hr	14,454	14,784
Fue Gas Constituents		
SO_2 - ppm	NG	122
NO_x - ppm	NG	NG
O_2 - %	NG	6.2
CO_2 - %	11.1	9.2
Air Fuel Ratio		
System #1	9.2	10.7
System #2	10.8	10.7
System #3	9.5	12.1*
System #4	10.7	11.7
Overall	10.0	11.9

* Air/fuel ratio for system #3 is estimated over the three active coal ports assuming one port completely plugged.

TABLE 4-95. RUN 006 SUMMARY OF DATA

SLICE NUMBER	1	2a	2b	2c	2d	2e	2f	2g
Date	5/17/83	5/17/83	5/17/83	5/17/83	5/18/83	5/18/83	5/19/83	5/19/83
Slice Time - Hours								
Start	0230	0944	1544	2144	0345	1959	0101	0600
End	0729	1544	2144	0345	0917	0101	0600	1128
Superficial Velocity - fps	7.8	6.1	6.2	6.2	6.1	6.2	6.2	6.2
Bed Temperature - F	1587	1649	1671	1674	1632	1641	1640	1677
Working Fluid Outlet Temperature - F	1458	1548	1561	1557	1519	1532	1534	1566
WINDBOX AIR								
Air Heater Inlet Temperature - F	157	186	182	175	176	179	171	175
Air Heater Outlet Temperature - F	516	620	612	615	585	568	587	603
Windbox Temperature - F	497	592	584	589	559	542	559	575
Air Heater Inlet Pressure - in.	73.1	80.8	84.8	84.9	84.1	84.9	83.7	81.5
Air Heater Outlet Pressure - in.	72.8	80.5	84.8	85.2	84.2	85.1	84.0	82.0
Flowrate - lb/hr	15,106	10,868	10,843	10,822	10,829	10,872	10,832	10,678
BED PRESSURES								
0" - in. (Estimated)	51.0	69.0	73.0	71.0	73.0	73.0	71.0	70.0
5.7" - in.	47.5	65.2	69.1	66.2	69.2	68.8	67.1	65.8
17.1" - in.	37.4	53.6	59.2	57.8	57.6	57.1	56.9	55.4
29.7" - in.	27.5	43.1	48.2	47.2	45.8	45.6	45.9	43.4
41.7" - in.	21.2	36.6	41.3	39.4	39.8	38.3	38.5	35.6
53.7" - in.	12.5	27.7	31.2	29.7	29.5	29.7	26.1	26.4
65.9" - in.	4.0	16.9	21.0	20.5	19.9	19.9	17.5	17.0
77.9" - in.	1.4	8.9	11.9	12.0	10.3	10.9	10.0	6.8
90.1" - in.	1.4	1.8	2.5	2.8	1.1	1.6	1.2	1.2
102.1" - in.	0.0	-0.1	0.1	0.6	-0.4	0.0	-0.2	0.1
230.1" - in.	-0.4	-0.5	-0.5	-0.4	-0.6	-0.3	-0.6	-0.5
BED HEIGHT - in.	72	92	94	94	90	90	91	89

TABLE 4-95. (Continued)

SLICE NUMBER	1	2a	2b	2c	2d	2e	2f	2g
FLUE GAS SYSTEM								
Cyclone Inlet Temperature - F	623	755	756	757	724	670	715	737
Cyclone Outlet Temperature - F	624	755	741	748	706	640	699	726
Air Heat Outlet Temperature - F	373	440	451	458	436	416	425	442
Baghouse Temperature - F	356	386	375	377	359	344	358	358
Combustor Pressure (230") - in.	-0.4	-0.5	-0.5	-0.4	-0.6	-0.3	-0.6	-0.5
Cyclone Inlet Pressure - in.	-1.1	-1.1	-0.9	-1.1	-1.1	-0.9	-1.5	-1.7
Cyclone Outlet Pressure - in.	-4.1	-2.8	-2.8	-2.9	-2.9	-2.9	-3.0	-3.0
Air Heater Outlet Pressure - in.	-8.8	-6.5	-6.8	-7.0	-6.7	-6.6	-6.7	-6.9
Baghouse Outlet Pressure - in.	-16.5	-12.4	-12.8	-13.4	-13.7	-11.3	-12.4	-13.9
SOLIDS FEEDRATES								
Coal - lb/hr	1747	1394	1471	1491	1499	1476	1515	1533
Limestone - lb/hr	272	524	417	452	480	363	340	423
Flyash Recycle - lb/hr	1575	2426	2996	2492	2586	1985	2714	2708
Flyash/Coal Ratio	1.1	1.7	2.0	1.7	1.7	1.3	1.8	1.8
COMBUSTION AIR								
Windbox - lb/hr	15,105	10.870	10,845	10,820	10,830	10,870	10,830	10,780
Coal Air (System 1, 2, & 4) - lb/hr	1,305	1,410	1,440	1,430	1,460	1,445	1,435	1,445
Coal Air (System 3) - lb/hr	640	650	705	700	696	715	725	720
Ash Air - lb/hr	560	540	560	560	550	530	565	550
Augmented Air (System 3) - lb/hr	510	365	365	365	365	365	365	365
Total - lb/hr	18,120	13,835	13,915	13,875	13,900	13,925	13,920	13,865
FLUE GAS CONSTITUENTS								
SO_2 - ppm	NG	NG	NG	NG	NG	703	777	725
NOx - ppm	129	91	82	70	67	61	58	75
O_2 - %	4.9	4.9	NG	NG	4.0	3.9	4.2	3.9
CO_2 - %	13.4	14.7	14.6	14.7	15.2	17.3	17.2	17.7

TABLE 4-95. (Continued)

SLICE NUMBER	1	2a	2b	2c	2d	2e	2f	2g
BED TEMPERATURES								
5.7" - F	1596	1652	1673	1677	1636	1643	1640	1681
27.7" - F	1601	1659	1680	1684	1641	1649	1646	1686
51.7" - F	1564	1623	1648	1658	1610	1618	1615	1652
75.4" - F	1582	1648	1671	1671	1630	1642	1638	1679
103.1" - F	1593	1663	1683	1682	1641	1653	1651	1688
229" - F	1506	1575	1568	1580	1533	1560	1563	1574
293" - F	1008	1105	1094	1100	1036	1033	1069	1075
Ave. - F	1587	1649	1671	1674	1632	1641	1640	1677
WORKING FLUID - EAST								
Convection Bank Inlet Temperature - F	80	403	413	407	400	282	337	360
Convection Bank Outlet Temperature - F	634	885	878	876	818	789	833	850
Bed Bank Inlet Temperature - F	628	873	868	865	810	781	822	842
Bed Bank Outlet Temperature - F	1457	1547	1565	1563	1517	1530	1532	1566
Convection Bank Inlet Pressure - psig	61.0	53.5	57.0	59.6	60.4	59.6	58.1	59.4
Convection Bank Outlet Pressure - psig	58.8	50.4	53.8	56.1	57.1	54.2	54.9	56.4
Bed Bank Inlet Pressure - psig	57.0	49.0	51.0	52.6	53.7	51.5	52.9	54.7
Bed Bank Outlet Pressure - psig	22.1	16.5	18.7	19.7	20/1	19.0	19.8	20.5
Flowrate - lb/hr	22,396	19,159	20,142	20,760	21,287	20,291	20,319	20,790
WORKING FLUID - WEST								
Convection Bank Inlet Temperature - F	80	405	415	408	398	284	337	361
Convection Bank Outlet Temperature - F	631	871	867	867	809	774	817	833
Bed Bank Inlet Temperature - F	620	861	858	856	798	767	807	825
Bed BAnk Outlet Temperature - F	1460	1548	1557	1551	1521	1533	1536	1567
Convection Bank Inlet Pressure - psig	62.0	54.6	56.8	58.8	59.7	57.0	58.9	60.5
Convection Bank Outlet Pressure - psig	58.5	50.7	52.8	54.5	55.5	53.2	54.7	56.5
Bed Bank Inlet Pressure - psig	57.2	49.0	52.3	54.5	55.5	52.7	53.3	54.8
Bed Bank Outlet Pressure - psig	22.7	17.9	19.8	21.0	21.5	20.0	20.4	20.9
Flowrate - lb/hr	22,963	19,654	20,177	20,904	21,421	20,855	21,508	21,635

TABLE 4-95. (Concluded)

SLICE NUMBER	1	2a	2b	2c	2d	2e	2f	2g
AIR/FUEL RATIO								
System #1	8.9	8.9	8.8	8.5	8.0	8.0*	8.0*	8.0
System #2	12.8	11.3	10.6	10.4	10.9	10.5	8.8	9.6
System #3	10.0	9.1	9.3	8.4	9.2	9.2*	9.2*	9.2
System #4	10.5	9.3	9.4	10.4	9.5	9.1	8.3	9.5
Overall	10.4	9.9	9.5	9.3	9.3	9.4	9.2	9.0

* Mixture ratio excursions taking place for PO_2 experiments. Estimated nominal value presented.

TABLE 4-96. RUN 007 SUMMARY OF DATA

SLICE NUMBER	1	2	3	4	5	6	7	8
Date	8/9/83	8/10/83	8/11/83	8/12/83	8/13/83	8/14/83	8/15/83	8/16/83
Hours	24.0	24.0	24.0	24.0	23.5	24.0	24.0	4.5
Superficial Velocity - fps	6.1	6.0	6.0	6.0	6.0	6.0	6.0	6.0
Bed Temperature (28") - F	1654	1648	1652	1650	1650	1650	1649	1642
Working Fluid Outlet Temperature - F	1545	1539	1545	1539	1547	1545	1536	1538
WINDBOX AIR								
Flowrate - lb/hr	10,570	10,444	10,444	10,444	10,444	10,444	10,444	10,444
WORKING FLUID - EAST								
Convection Bank Inlet Temperature - F	391	348	350	352	370	376	382	380
Bed Bank Inlet Temperature - F	844	844	863	875	881	865	876	879
Bed Bank Outlet Temperature - F	1544	1538	1544	1538	1546	1545	1535	1537
Flowrate - lb/hr	17,682	18,072	17,136	16,416	16,740	17,352	17,280	17,064
WORKING FLUID - WEST								
Convection Bank Inlet Temperature - F	389	349	350	352	369	376	382	382
Bed Bank Inlet Temperature - F	837	832	846	860	868	851	861	864
Bed Bank Outlet Temperature - F	1546	1540	1545	1540	1548	1546	1537	1538
Flowrate - lb/hr	17,700	18,075	17,136	16,524	16,920	17,532	17,460	17,244
FLUE GAS SYSTEM								
Cyclone Inlet Temperature - F	729	715	715	715	723	727	739	733
Cyclone Outlet Temperature - F	722	710	-	-	-	-	-	-
Air Heater Outlet Temperature - F	439	439	432	432	436	437	431	441
Baghouse Inlet Temperature - F	371	363	362	362	366	367	361	373

TABLE 4-96. (Concluded)

SLICE NUMBER	1	2	3	4	5	6	7	8
SOLIDS FEEDRATE								
Coal - lb/hr	1253	1293	1244	1249	1262	1296	1263	1259
Limestone - lb/hr	302	517	474	592	776	536	574	450
Flyash Recycle - lb/hr	1229	2240	2333	2436	2016	2520	2594	2784
Flyash/Coal Ratio	1.0	1.7	1.9	2.0	1.6	1.9	2.1	2.2
COMBUSTION AIR								
Windbox - lb/hr	10,570	10,445	10,445	10,445	10,445	10,445	10,445	10,445
Coal Air (Systems 1, 2, & 4) - lb/hr	1,390	1,445	1,420	1,420	1,420	1,420	1,420	1,420
Coal Air (System 3) - lb/hr	660	500	500	525	525	500	500	510
Augmented Air (Systems 1 & 2) - lb/hr	720	715	715	720	715	705	705	740
Ash Air - lb/hr	550	570	535	555	530	535	580	585
Total - lb/hr	13,890	13,675	13,615	13,665	13,635	13,605	13,650	13,700
FLUE GAS CONSTITUENTS								
SO_2 - ppm	119	253	217	291	251	222	205	286
NOx - ppm	143	128	131	126	136	122	119	117
O_2 - %	5.0	3.6	4.1	4.6	4.7	4.1	4.5	4.3
AIR/FUEL RATIO								
System #1	11.0	10.5	10.7	11.2	10.8	10.6	10.8	11.2
System #2	11.0	10.9	11.3	11.1	10.8	10.4	10.9	11.0
System #3	11.7	10.5	11.1	10.9	11.0	10.7	11.0	10.8
System #4	11.0	10.7	11.0	11.0	10.9	10.7	11.0	10.7
Overall	11.1	10.6	11.0	11.0	10.9	10.6	10.9	10.9

TABLE 4-97. RUN 008 SUMMARY OF DATA

SLICE NUMBER	1	2	3	4	5	6	7	8	9
Date	9/20/83	9/21/83	9/22/83	9/23/83	9/24/83	9/25/83	9/26/83	9/27/83	9/28/83
Hours	24.0	24.0	8.0	24.0	24.0	24.0	24.0	24.0	12.0
Superficial Velocity - fps	5.9	6.0	6.0	6.0	6.0	6.0	6.0	6.0	6.1
Bed Temperature (28") - F	1655	1650	1643	1650	1547	1659	1653	1650	1647
Working Fluid Outlet Temperautre - F	1549	1550	1541	1544	1540	1546	1545	1548	1542
BED TEMPERATURE									
28" - F	1655	1650	1643	1650	1647	1659	1653	1650	1647
75" - F	1542	1643	1640	1645	1640	1654	1650	1646	1640
WORKING FLUID - EAST									
Convection Bank Inlet Temperature - F	391	392	394	389	402	407	392	346	79
Bed Bank Inlet Temperature - F	871	906	893	874	888	883	875	881	760
Bed Bank Outlet Temperature - F	1549	1550	1541	1543	1541	1546	1545	1547	1546
Flowrate - lb/hr	17,052	16,346	16,622	17,727	17,077	17,991	17,394	16,444	15,390
WORKING FLUID - WEST									
Convection Bank Inlet Temperature - F	391	393	397	389	403	407	392	346	80
Bed Bank Inlet Temperature - F	859	891	881	860	871	865	857	869	752
Bed Bank Outlet Temperature - F	1549	1549	1541	1544	1540	1547	1545	1548	1538
Flowrate - lb/hr	17,415	16,552	16,973	17,787	17,577	18,072	17,552	16,643	15,270
FLUE GAS SYSTEM									
Cyclone Inlet Temperature - F	744	766	754	752	761	750	757	758	642
Air Heater Outlet Temperature - F	440	447	433	444	450	453	451	449	399
Baghouse Inlet Temperature - F	360	365	360	364	370	372	364	372	350
Recycle Ash Temperature - F	582	608	614	610	645	631	633	630	554

TABLE 4-97. (Concluded)

SLICE NUMBER	1	2	3	4	5	6	7	8	9
SOLIDS FEEDRATE									
Coal - lb/hr	1270	1259	1300	1344	1324	1351	1348	1319	1320
Limestone - lb/hr	359	459	403	429	515	346	364	348	457
Flyash Recycle - lb/hr	2296	2804	2787	2695	2665	2583	2726	2822	2961
Flyash/Coal Ratio	1.8	2.2	2.1	2.0	2.0	1.9	2.0	2.1	2.2
COMBUSTION AIR									
Windbox - lb/hr	10,444	10,444	10,444	10,444	10,444	10,444	10,444	10,444	10,533
Coal Air (Systems 1, 2, & 4) - lb/hr	1,352	1,433	1,433	1,433	1,433	1,433	1,433	1,433	1,487
Coal Air (System 3) - lb/hr	470	501	501	506	506	520	520	556	570
Augmented Air (Systems 1 & 2) - lb/hr	721	715	721	727	721	721	721	721	721
Ash Air - lb/hr	540	553	532	537	553	550	550	550	546
Total - lb/hr	13,527	13,646	13,631	13,647	13,657	13,668	13,668	13,704	13,857
FLUE GAS CONSTITUENTS									
SO_2 - ppm	123	246	264	283	252	149	183	241	310
NOx - ppm	103	85	87	88	88	85	84	84	80
O_2 - %	4.6	4.8	5.0	4.3	4.3	4.0	4.0	4.6	4.1
AIR/FUEL RATIO									
System #1	10.5	10.9	10.4	10.3	10.4	10.0	10.1	10.4	11.1
System #2	10.7	10.9	10.7	10.2	10.4	10.1	9.8	10.3	9.3
System #3	10.6	10.7	10.5	10.1	10.3	10.1	10.1	10.5	10.8
System #4	10.8	11.0	10.5	10.1	10.3	10.4	10.7	10.4	10.9
Overall	10.6	10.8	10.5	10.2	10.3	10.1	10.1	10.4	10.5

4.5.5 Combustor/Heater Modifications

A number of modifications were made to the coal and air distributors to investigate the influence of these parameters on the fluidized bed environment as measured by the oxygen partial pressure probe. These changes were directed toward a practical configuration that would have a predominantly oxidizing environment throughout the bed heat exchanger region. The first four runs had the original coal port arrangement of one port per quadrant with even distribution of the windbox combustion air flow. On run 005, a number of modifications were made to investigate different configurations and operating conditions. This led to more changes for run 006. The results of these tests were used to select the coal/air arrangement used for the material specimen exposure series. This section discusses these configurations plus a brief discussion on the material specimen probe locations.

Distributor Area Modifications - Run 005. A number of changes were made to the distributor and coal port configurations to investigate the influence of these parameters on the combustion environment as measured by the oxygen partial pressure probe. It was presumed that a change in one quadrant did not have a significant effect on the neighboring quadrants. This allowed for all four quadrants to have a different configuration so that four configurations could be investigated during a single run.

A summary of the distributor area modifications is presented in Table 4-98 and identification of the quadrants is shown in Fig. 4-205. The configurations consisted of a reference quadrant, a coal plume distributor, four ports per quadrant, and augmented air above the coal port.

Coal Plume Distributor. Quadrant No. 1 was modified to include what was essentially a sacrificial heat exchanger tube bundle just above the coal port. This uncooled rake of tubes is shown installed in place in Fig. 4-206 and constituted of a crisscross arrangement of tubes. The purpose was to break up the volatiles plume before the gases reached the actual heat exchanger. Also, the coal port splash plate diameter was increased from 4 to 8 inches. To provide

TABLE 4-98. RUN 005 SUMMARY OF DISTRIBUTOR AREA MODIFICATIONS

- COAL FEED - QUADRANT NO. 1
  - Coal Plume Distributor
  - Increase Splash Plate Diameter From 4"to 8"
  - Increase Distributor Air Flow About Coal Port By 50 Percent
- COAL FEED - QUADRANT NO. 3
  - Four Coal Ports Per Quadrant (8" Diameter Splash Plate)
  - Coal Splitter System
  - Coal Plugging Monitoring System
    Line Pressures (4)
    Injection Temperatures (4)
- COAL FEED - QUADRANT NO. 4
  - Augmented Air Above Coal Port
- ASH INJECTION NEEDLE DEFLECTOR

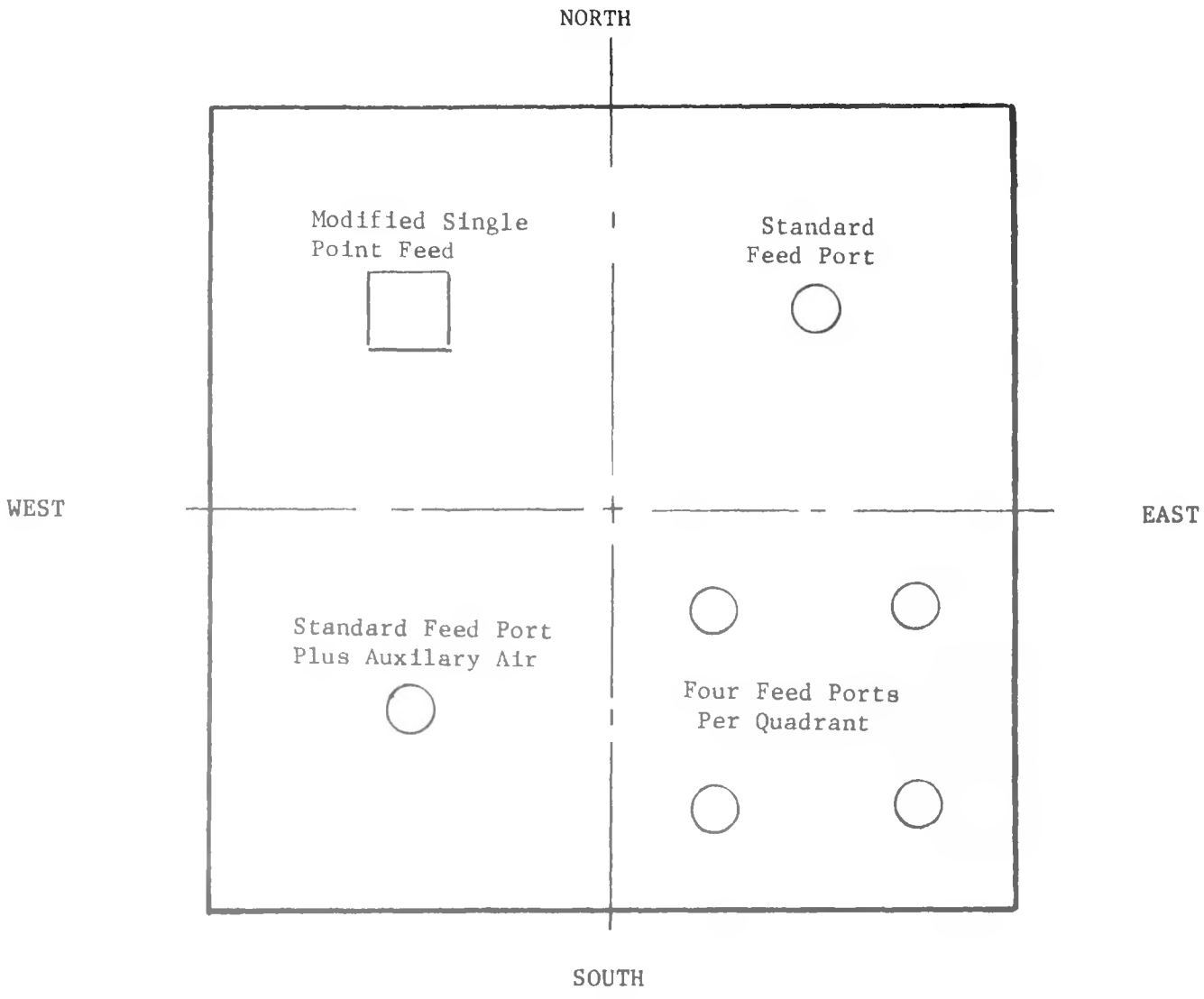


Figure 4-205. Run 005 Coal Feed Port Modifications

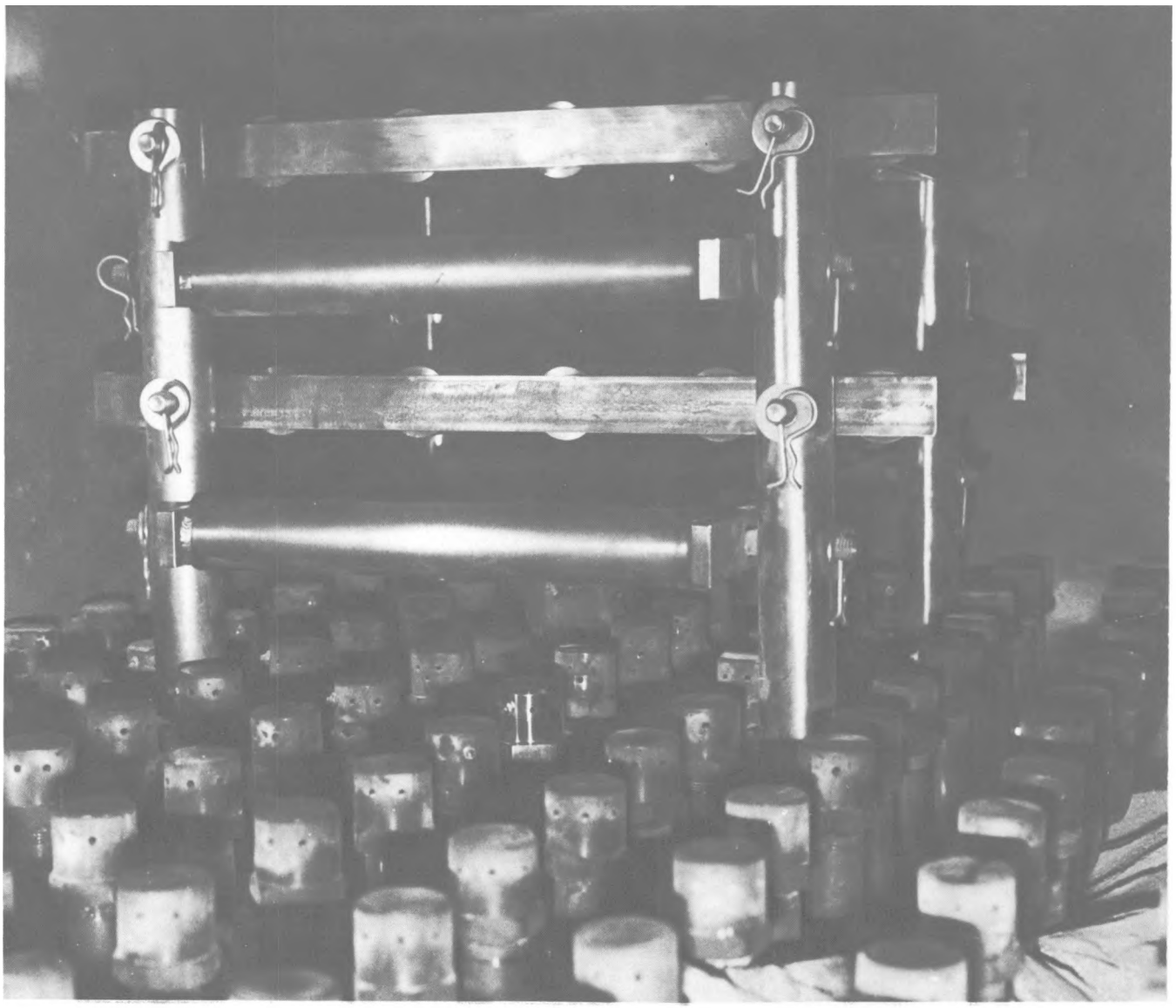


Figure 4-206. Coal Plume Distributor Installed in Quadrant No. 1 Prior to Run 005

more air in the region of the volatiles plume, the distributor tuyere caps were modified to increase the amount of air about the coal port by 50% with a corresponding decrease in the other regions so that the overall air flow remained unchanged. This modification is shown in Fig. 4-207 and consisted of simply adding or plugging holes in the caps.

Characterization of this quadrant showed that there was no significant improvement in the reducing zone above the coal feed port, and the distributor was removed for the next run.

Reference Quadrant. Quadrant No. 2 remained in the original configuration and served as a reference.

Four Coal Port Quadrant. Quadrant No. 3 was modified to contain four coal feed ports per quadrant. The normal coal feed system through the eductor was used; however, downstream of the eductor, a splitter system was installed as described in Section 4.5.6. The same eductor was used for this system as the other systems. Since the splitter system had a slightly higher pressure drop, a slightly higher conveying (motive) air flow was required to overcome the back pressure while maintaining a slightly negative coal inlet pressure.

During run 005, there was some initial plugging, and the unit was slumped to clear the lines. Debris such as wire and rags were removed along with wet coal. During the second test point on run 005, one of the coal ports could not be cleared and most of the run was conducted with only three of the ports functioning. Therefore, the coal feed rate was reduced to three-fourths to maintain the nominal air/fuel ratio above the functioning ports. Before run 006, the lines were thoroughly cleaned, and this splitter and feed system functioned perfectly with all line pressures indicating a well balanced air flow. There were no further problems of plugging even with 9% moisture in the coal.

Oxygen partial pressure characterization shows that this configuration provided a satisfactory oxidizing environment throughout the heat exchanger region with little or no indication of a volatiles plume above the coal port. Thus, the four

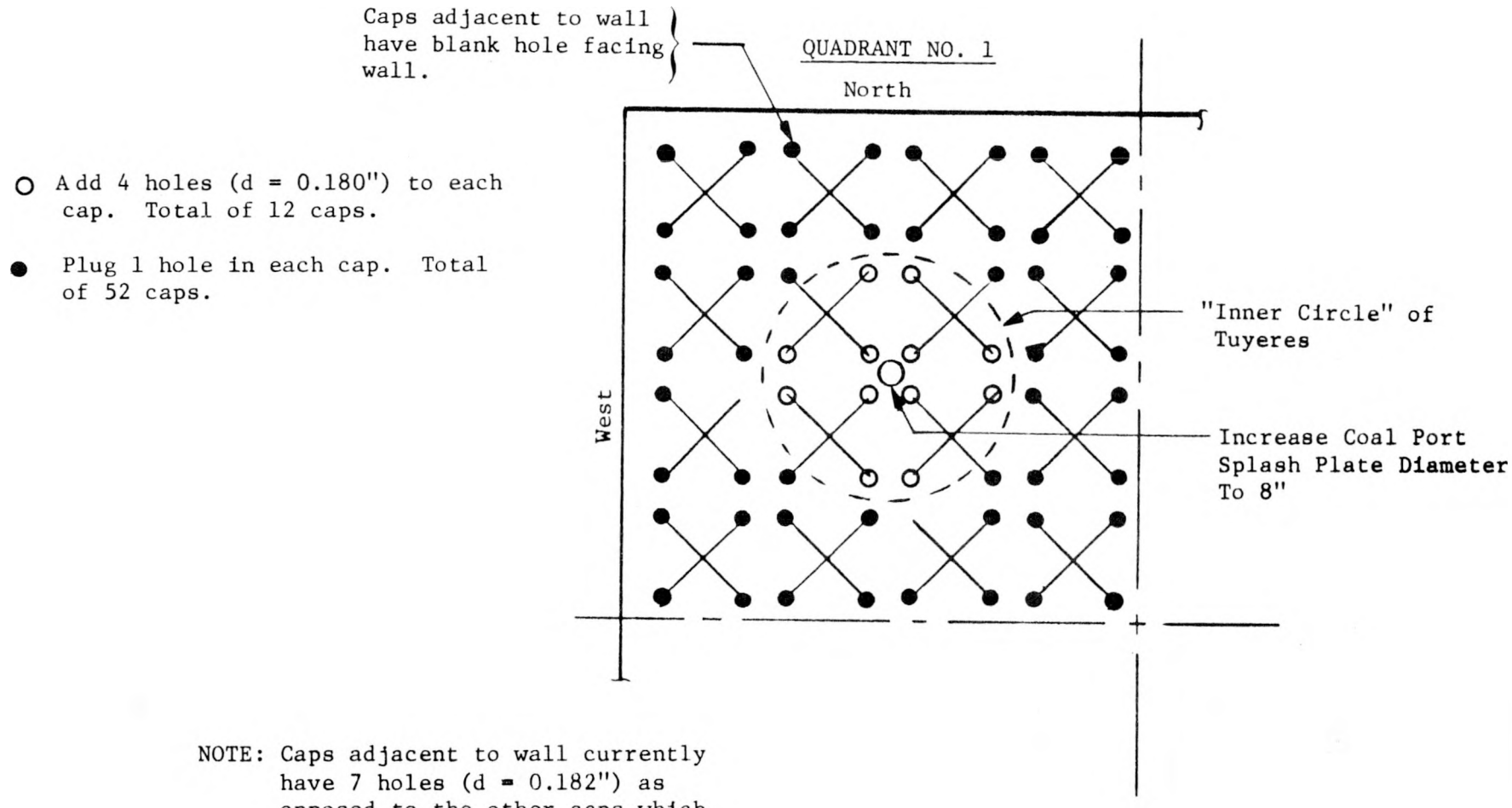


Figure 4-207. Run 005, Tuyere Cap Modification to Increase Air Flow Near Coal Port

›rts per quadrant gave the best oxygen partial pressure profile and met all criteria for "healthy" combustion environment.

Augmented Air. Quadrant No. 4 was basically a reference quadrant that had the original coal port configuration. However, an augmented air supply was added as shown in Fig. 4-208 which allowed additiohal air to be added just above the coal splash plate. The augmented air was discharged into a cup arrangement so that the augmented air tended to flow upward as shown in Fig. 4-209. The intention was to inject additional air directly into the volatiles plume to spread the plume as well as increase the combustion in this fuel-rich region. This quadrant was operated without the augmented air similar to the reference quadrant. Augmented air was added momentarily during probing activities so that oxygen partial pressure profiles were obtained at the referenced condition (no augmented air) and various quantities of augmented air.

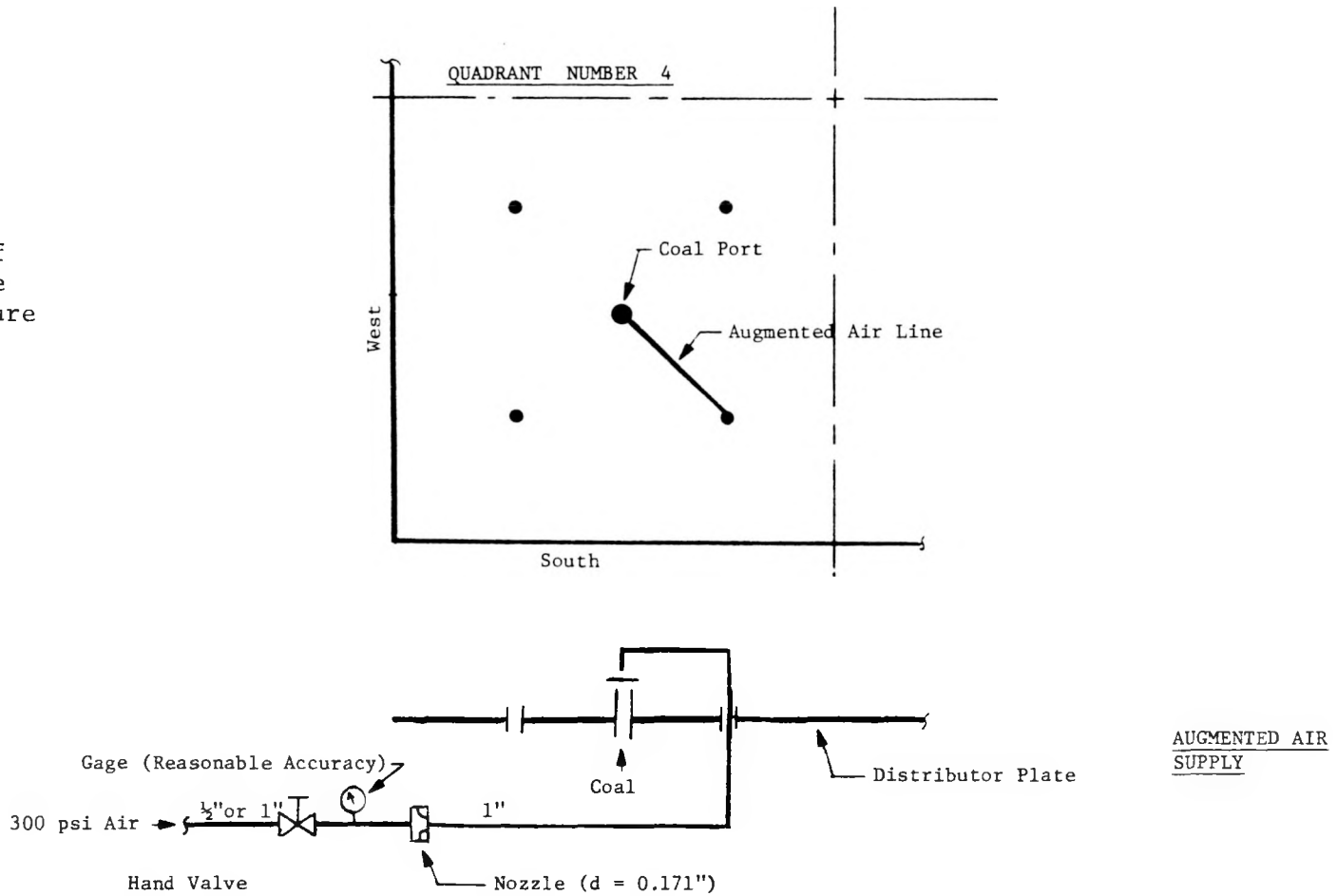
Oxygen partial pressure characterization indicated that the augmented air produced the predicted results of reducing the volatiles plume so that an acceptable oxidizing environment was achieved above the coal feed port with a modest quantity of air.

The augmented air/coal port installation is shown in the posttest condition in Fig. 4-210 where the coal plume distributor can be seen in the background.

Ash Injection Needle Deflector. The ash injection needle discharges the recycled ash and conveying air toward the center of the unit under the bed heat exchanger. The discharge had been a simple cutoff pipe; however, an extension was added prior to run 005 that contained some turning vanes which directed the air/ash downward toward the distributor plate. Figure 4-211 shows this modified ash needle installed in the unit.

The oxygen partial pressure results did not show any significant effect of the change in the ash needle discharge configuration.

- Augmented air supply to evaluate effects of various amounts of additional air on the oxygen partial pressure



NOTE: 300 psig is approximately 0.15 lb/sec of air.

Figure 4-208. Modifications to Quadrant No. 4

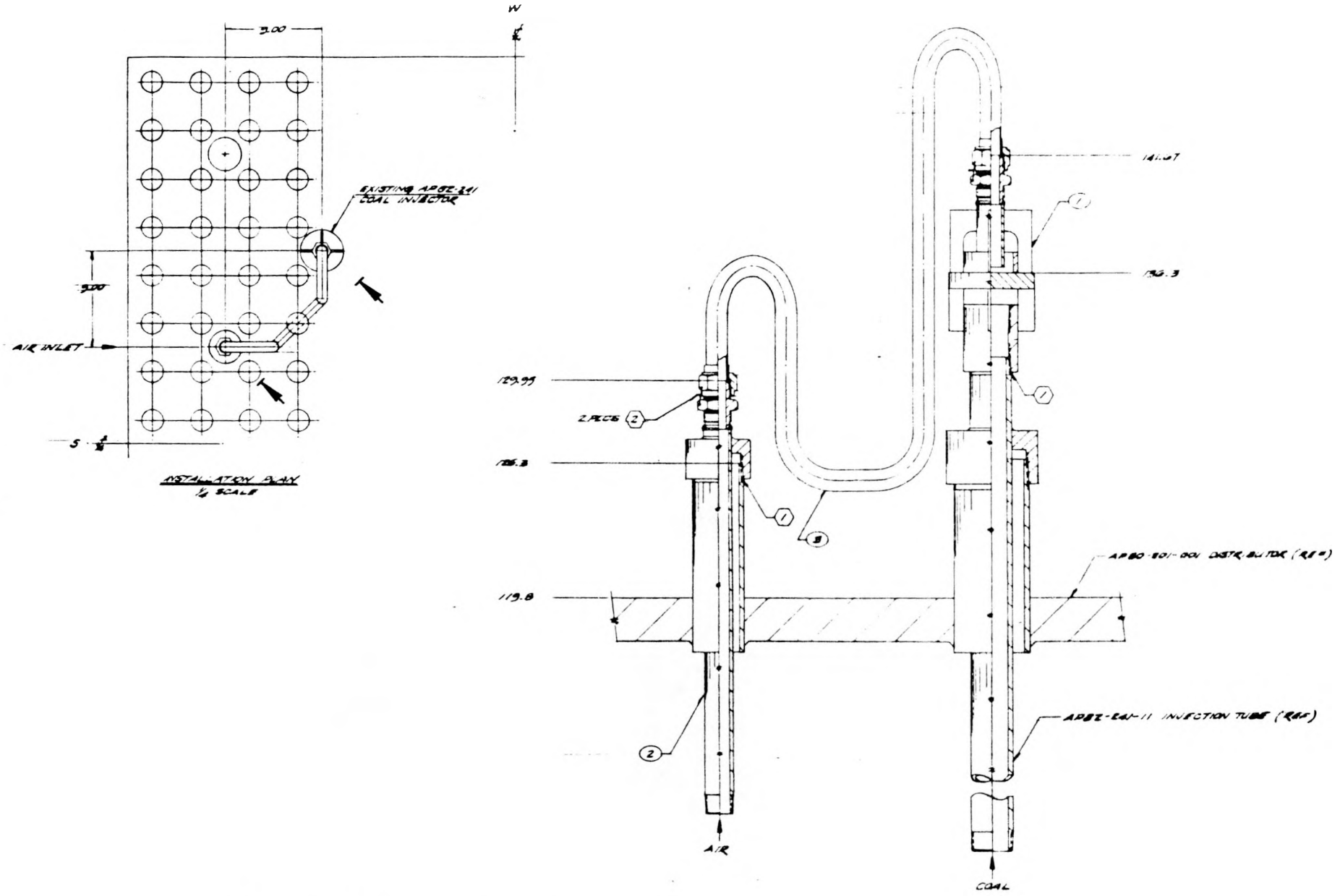


Figure 4-209. Augmented Air Supply Injected Over Coal Feed Port

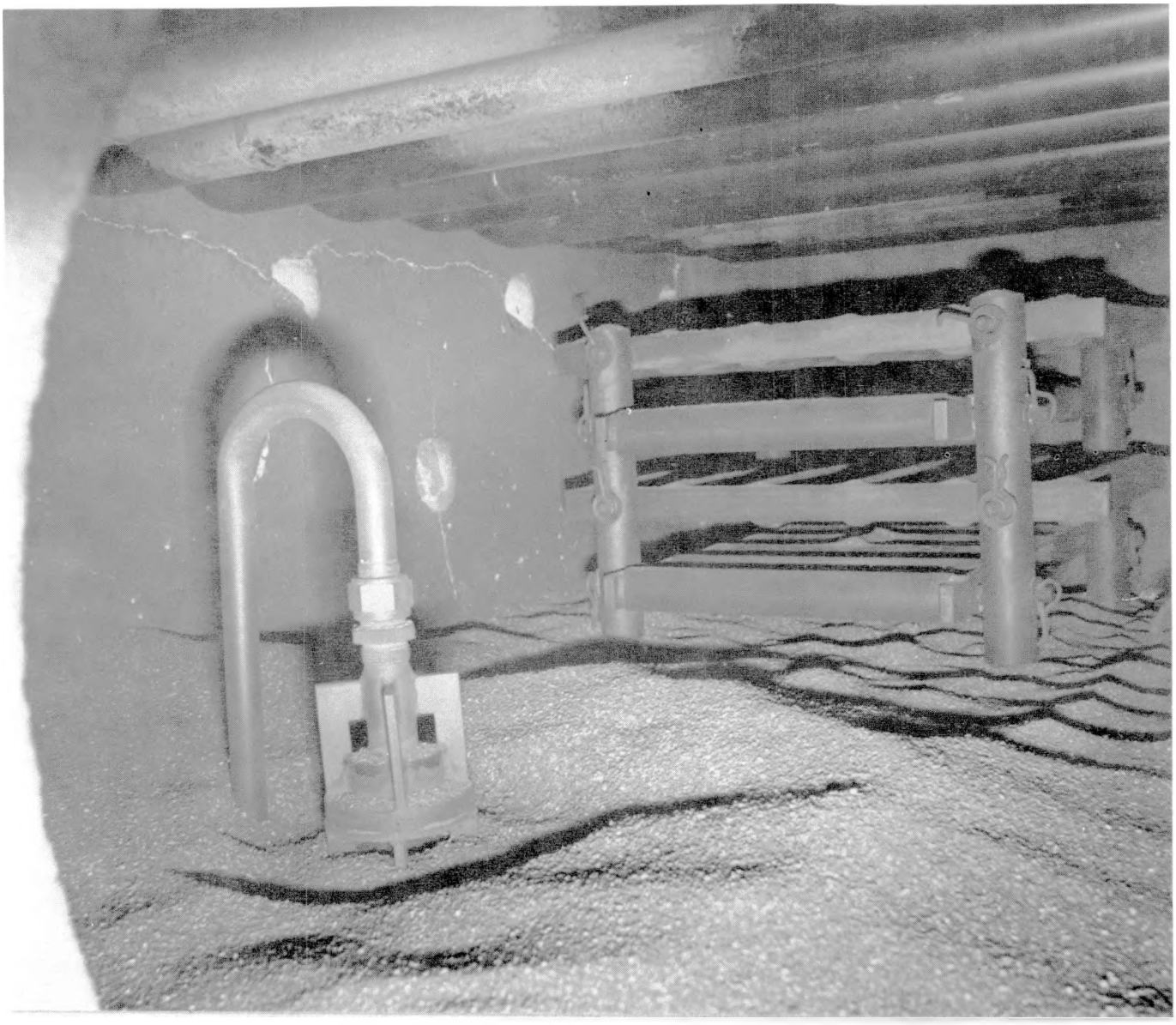


Figure 4-210. Posttest Installation of Augmented Air Port (Coal Plume Distributor in Background)



Figure 4-211. Ash Injection Needle with Extension and Turning Vanes (Four Ports per Quadrant; Splash Plates in Foreground)

Distributor Area Modifications - Run 006. Based on the run 005 results, the two coal feed configurations that gave acceptable oxidizing environments (especially over the coal ports) were selected for further evaluation. These configurations were the four ports per quadrant and the augmented port. Further oxygen partial pressure characterizations were obtained for a range of excess air conditions.

A summary of the distributor area configurations is presented in Table 4-99 and illustrated in Fig. 4-212. The configurations used were the augmented air, four ports per quadrant, and reference (original). The ash injection needle was the same as the previous run.

Augmented Air. This configuration was similar to the arrangement used on the previous test except the setup was relocated to quadrant No. 1. The system was designed to operate with 13% of the nominal distributor air flowrate being introduced as augmented air at all times. The tuyere flowrate was reduced in this quadrant by a corresponding amount by simply plugging one orifice hole per cap. The augmented air line and coal port are shown Figure 4-213. Characterization of this quadrant verified the results of the previous test and demonstrated that an oxidizing environment above the coal port could be achieved even at low overall excess air conditions.

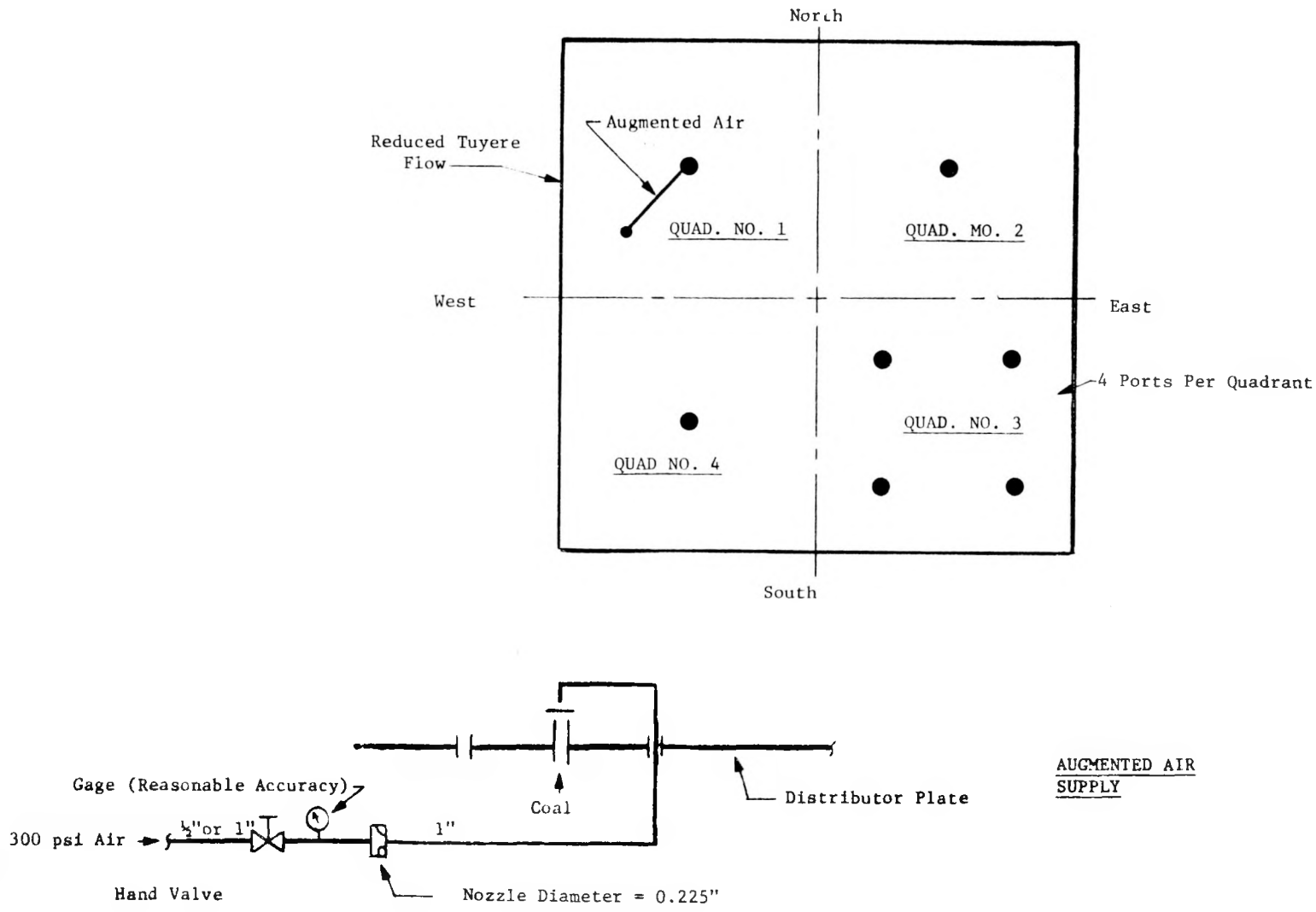
Reference Quadrants. Both quadrants No. 2 and 4 were in the original configuration, and characterization verified previous results which indicated an unacceptable reducing zone over the coal port.

Four-Coal-Port Quadrant. Quadrant No. 3 had four feed ports using a coal splitter system to divide the flow. This arrangement was the same as used on run 005. Characterization of this arrangement repeated the results from the previous run and showed good oxidizing environment over the coal feed ports over a range of low excess air conditions.

Distributor Area Modifications - Runs 007 and 008. The system configuration and operation for the material specimen exposure test series was essentially the same

TABLE 4-99. RUN 006 SUMMARY OF DISTRIBUTOR AREA MODIFICATIONS

- COAL FEED - QUADRANT NO. 1
  - Coal Port With Augmented Air (4" Diameter Splash Plate)
  - Reduced Tuyere Flow (Plug one Hole Per Cap Or Area Is 0.87 of Nominal)
- COAL FEED - QUADRANT NO. 2 & 4
  - Reference (Original) Configuration (4" Diameter Splash Plate)
- COAL FEED - QUADRANT NO. 3
  - Four Coal Ports Per Quadrant (8" Diameter Splash Plate)
  - Coal Splistter System
  - Coal Plugging Monitoring System
    - Line Pressures (4)
    - Injection Temperatures (4)
- ASH INJECTION NEEDLE DEFLECTOR (Same As Run 005)



NOTE: 100 psig is approximately 0.101 lb/sec of air.

9B

Figure 4-212. Distributor Area Configuration

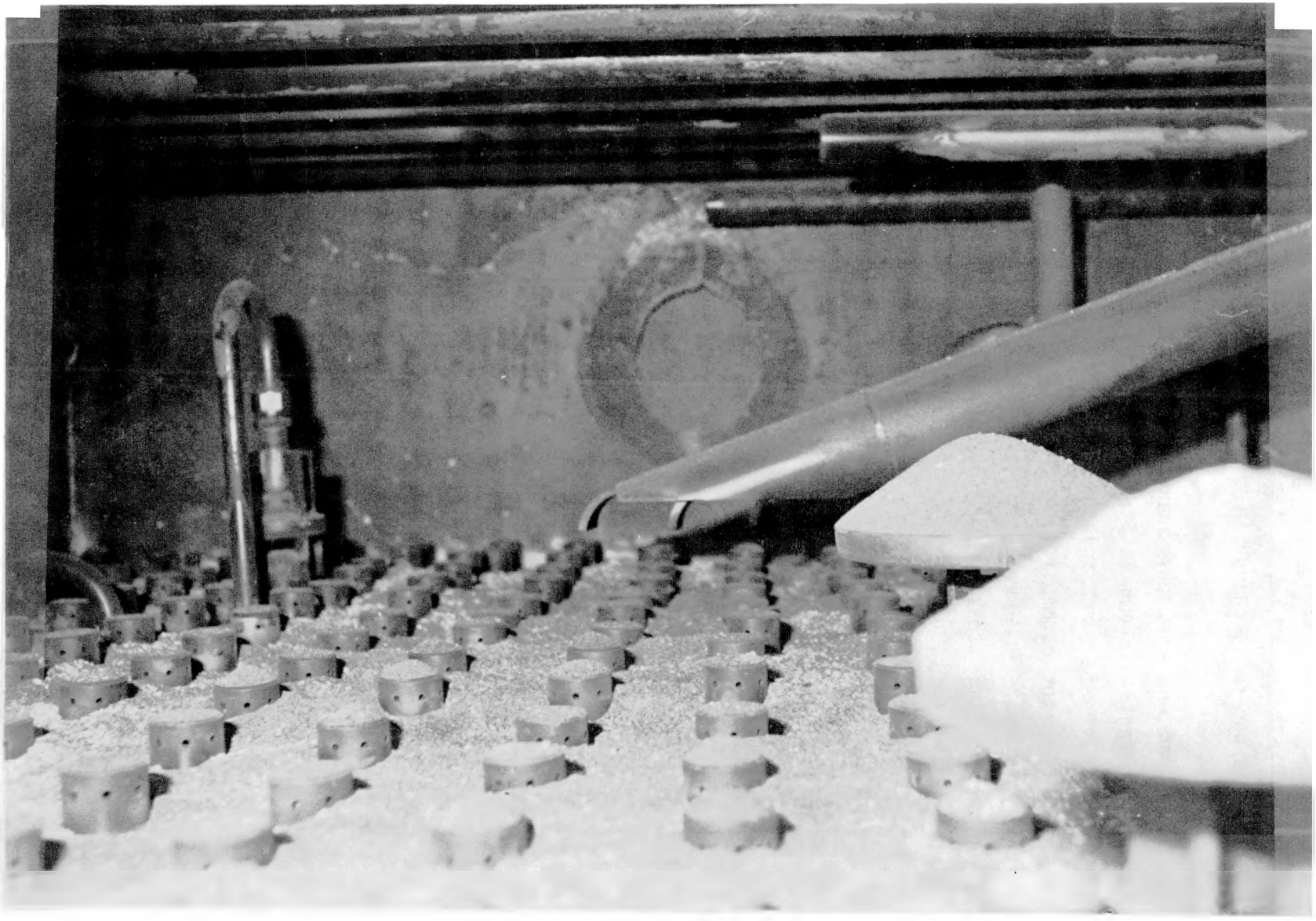


Figure 4-213. Post-Run 006 Distributor (Augmented Air Port at Left Rear, Ash Injection Needle in Center, and Coal Ports From Four per Quadrant in Right Foreground)

as developed during the characterization test series and used on the last run of that series. There was one small change in the distributor area.

The coal feed system had one port per quadrant for three of the quadrants, and four ports for one quadrant as shown in Fig. 4-214 and Table 4-100. Quadrant No. 1 had augmented air above the coal splash plate with some of the tuyere holes plugged to compensate for the augmented air flowrate such that all quadrants had equal combustion air flow. This was the same distributor area configuration developed during the previous test series. For the material exposure series, augmented air also was added to quadrant No. 2, and this system was identical to the other system except that the augmented air was discharged in a radial direction instead of upward. In summary, the four quadrants were: (1) augmented air with upward discharge, (2) augmented air with radial discharge, (3) four feed ports, and (4) reference configuration.

Material Probe Locations. A large number of both cooled and uncooled material probes were installed containing specimens of candidate tube and hanger materials for both the bed and convection heat exchanger. All of these probes were installed at the beginning of the exposure series except for one cooled bed probe. This probe was left out for run 007 to allow oxygen partial pressure characterization of the quadrant that had augmented air added to it. All probes remain in the unit for the planned additional 650 hours of exposure except for one probe which was removed for specimen analysis. This probe will be refurbished with new specimens and installed for the additional 650 hours of exposure.

After completion of the 1000 hours of operation, all of the probes will be removed, disassembled, and analyzed. The locations, probe configurations, and metallurgical analysis will be documented in the Phase II Extension Final Report.

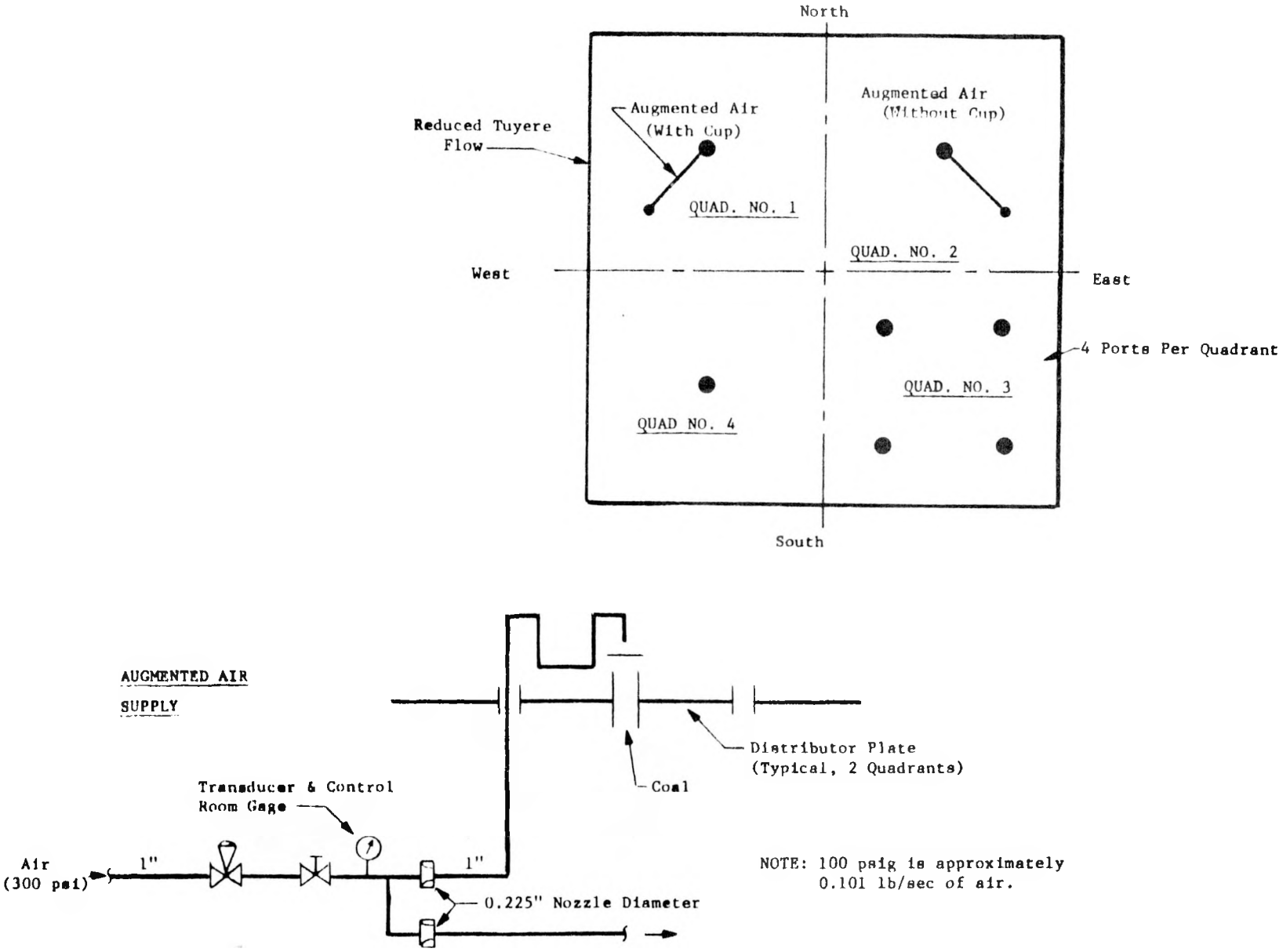


Figure 4-214. Distributor Area Configuration for Runs 007 and 008

TABLE 4-100. SUMMARY OF DISTRIBUTOR AREA MODIFICATIONS
(RUNS 007 AND 008)

- COAL FEED - QUADRANT NO. 1
  - Augmented Air With Cup
  - 4" Diameter Splash Plate
  - Reduced Tuyere Flow (Plug One Hole Per Cap or Area is 0.87 of Nominal)
- COAL FEED - QUADRANT NO. 2
  - Augmented Air Without Cup
  - 4" Diameter Splash Plate
  - Reduced Tuyere Flow (Plug One Hole Per Cap or Area is 0.87 of Nominal)
- COAL FEED - QUADRANT NO. 3
  - Four Coal Ports Per Quadrant (8" Diameter Splash Plate)
  - Coal Splitter System
  - Coal Plugging Monitoring System (Line Pressures and Injection Temperatures)
- ASH INJECTION NEEDLE DEFLECTOR (Same as Runs 005 & 006)

5.6 System Operations

Many of the systems and components were developed during the first four runs, and some of these systems required several modifications to achieve the intended results. These modifications as well as other pertinent areas of the system operation are presented in this section, while performance results are discussed in the following sections.

The results discussed in this section are:

- Startup Procedure
- Bed Slumping And Restart
- Bed Drain Operation
- Ash Recycle System
- Bed Height Measurement
- Coal Feed Systems
- Cyclone Operation
- Acoustic Sootblower
- Refractory Cure Operation

Startup Procedure. During the early tests, a somewhat hard ash deposit had sometimes formed on the top of the convection heat exchanger tubes and inside of the individual cyclone units. While this deposit did not create a problem with the convection heat exchanger, it was an area of concern.

These deposits had no significant effect on either flue gas pressure drop or heat exchanger heat transfer performance. However, the formation of the deposits was troublesome in that they may fall and plug the vertical spacing between operations. This would have an effect on the convection heat exchanger operation. In this test operation, the heat exchanger tubes were cleaned after runs 002, 003, and 004.

Analysis was performed on the deposits from the convection bank and the spent bed material used for startup. The purpose was to characterize these materials so that a mechanism could be proposed that would explain the formation of the deposits. Once the mechanism is understood, steps could be taken to eliminate their formation in the convection bank.

Preliminary results showed the following:

1. The spent bed material was composed of CaO with a minor amount of $CaSO_4$ and a very small amount of SiO_2
2. The deposits from the second and third runs, which were identical, were composed of $CaCO_3$, CaO, $CaSO_4$, and a small amount of SiO_2. The concentration of $CaSO_4$ was greater near the surface of the deposits.
3. No trace compositions that would be consistent with a liquid phase were found. Specifically, no significant levels of alkalies were found.
4. The level of iron was high, 0.4% in the deposit and 0.7% in the bed material.

A mechanism has been proposed that explains the formation of the deposit at low temperatures during heatup. The mechanism involves the formation of iron pentacarbonyl, $Fe(CO)_5$, that acts as an intermediate phase on the surface of the deposit. SO_2 could also play a part in the formation of the deposits.

On run 001, the initial heating was conducted using the windbox air duct burner and an empty bed until the air temperature in the heater was about 500 F. Enough limestone to fill the bed up to the bottom of the heat exchanger was added (2000 pounds), and the bed burner was then used to raise the temperature to 900 F. At that point, coal feeding and coal ignition was initiated. Post-run inspection showed no buildup of deposits on the heat exchanger tubes other than the expected accumulation of fly ash.

e run 002 startup procedure was the same except that spent bed material was used instead of fresh limestone. Also, the bed had been partially filled with about 2000 pounds of spent bed material prior to the startup. Post-run inspection showed deposits in the vertical spacing in the convection heat exchanger, while the bed heat exchanger was clean (except for normal fly ash). The deposits were sufficiently solid that they could be removed intact, but the deposits could be easily crumbled by hand.

A procedure was adopted for runs 003 and 004 that included a prewarming. The theory was that water from the combustion products of the natural gas fired duct burner may be condensing on the cold heat exchanger tubes. Dust from the spent bed material could then collect on the "wet" surfaces and form the observed deposits. The prewarming was accomplished by flowing heated air through the working fluid circuits with an empty bed with the combustion air systems working and all burners off. This heated the heater/combustor and the entire system, including the air heater, baghouse, and windbox to above 300 F. At that point, the normal startup procedure was used. Post-run inpsection still showed the buildup of deposits in the convection bank, although the amount of deposits was one-half and generally confined to the lower portion of the convection bank.

On runs 005 through 008, this same basic startup procedure was used except the initial filling of the bed was with 2000 to 3000 pounds of (fresh) limestone. By this time, the unit was heated to about 500 F with the duct burner. The bed burner was then turned on to complete the heating while the filling was completed with spent bed material. Also, an acoustic soot blower was installed in the cyclone hopper. Just after startup on run 005, the unit was slumped for a cursory inspection of the cyclone hopper and the convection bank soot blower cavity. There was no apparent evidence of ash buildup in either the convection bank or cyclone units. Posttest inspections confirmed that the buildup in the convection bank had been considerably reduced and the deposits were softer. Also, there were no deposits in the cyclone units indicating that the acoustic soot blower was an effective device for cleaning such units.

Bed Slumping and Restart. The bed was slumped on several occasions to allow fc inspection and/or repair of systems and then the unit was restarted with a hot bed. The operation was initiated by shutting down of the coal system and allowing the coal in the system and bed to burn out. This eliminated the possibility of a reducing condition in the slumped condition. The coal burnout period was five minutes or less. The combustion air system (forced draft and induced draft fan) were shut down, followed by the remaining air systems, such as the coal conveying air and air purges. The working fluid air (heat exchanger coolant) was then reduced to a trickle flow to keep the convection bank heat exchanger from overheating. Typically, the bed temperature was about 1400 F then the unit was slumped. This condition could be held for several hours as required.

The unit was then restarted by simply starting the air systems and turning on the coal feed systems. As long as the bed temperature was above 900 F, coal ignition would occur immediately. This procedure was used many times throughout the course of the test program. The unit could be slumped in about 10 minutes and brought back on line in 5 minutes, and a total down time of 1 hour was usually sufficient for most operations. Down times experienced during the program ranged from one-half hour to 15 hours, and the indications are that much longer down times could be tolerated where the unit could be brought back on-line without the use of the ignition burners. The restart times to bring the unit to the target conditions and bed temperatures were on the order of 15 minutes for short down times to 1 hour for the longer down periods.

Bed Drain Operations. The bed drain arrangmeent is a port located at the edge of the bed in the distributor plate. A variable position knife gate valve is used to control the draining operation where the material is drained through an uncooled line into a drum. Control of the knife valve is local, so that the operator can control the valve while observing the drum filling. This arrangement worked well for both hot draining of the bed during the run to maintain bed height, and post-run draining of the bed for purposes of inspection.

To control bed height, approximately one drum of material was drained each hour. A fork lift with a drum handling fixture could remove the drum immediately after filling and bring in an empty drum in preparation for the next draining operation. Even though the bed material was 1600 F, there was no overheating of the drain valve or line. Some paint on the drum would burn off, leaving cosmetic damage to the drum.

The bed material would drain without difficulty, except for the first drain operation where the bed drain "poker" would be required to initiate the flow of material. This would occur when used bed material had been left in the bed drain ports from the previous run. On some of the runs, the bed drain port had been filled with fresh limestone after the heater inspection. When this was done, the bed drain would start smoothly on the very first operation without having to use the poker.

After each of these runs, the bed was drained completely several days after the run was completed. This was done to allow complete inspection of the heater/combustor interior. The entire bed could be easily and completely drained by fluidizing the bed with cold air and using the normal drain procedure.

Ash Recycle System. After several modifications, the ash recycle system was successfully used starting with run 005. (A more detailed discussion of the various modifications can be found in Ref. 1-17 and 1-18.) A schematic of the final system is shown in Fig. 4-215. The flue gas passes through the multicyclone unit which consists of 36 each 6-inch cyclone units that can be mechanically plugged to tune the pressure drop to the given operating conditions. (The pressure drop for optimum collection efficiency is 3 to 4 inches.) Ash collected by the cyclone units drop into the fill hopper that functions as an accumulator. The lower run hopper is batch filled from the fill hopper, and the run hopper supplies the variable speed rotary feeder that meters the ash. When recycle is not being conducted, the fill hopper valve can be closed, and ash will overflow from the cyclone hopper into the overflow system for disposal.

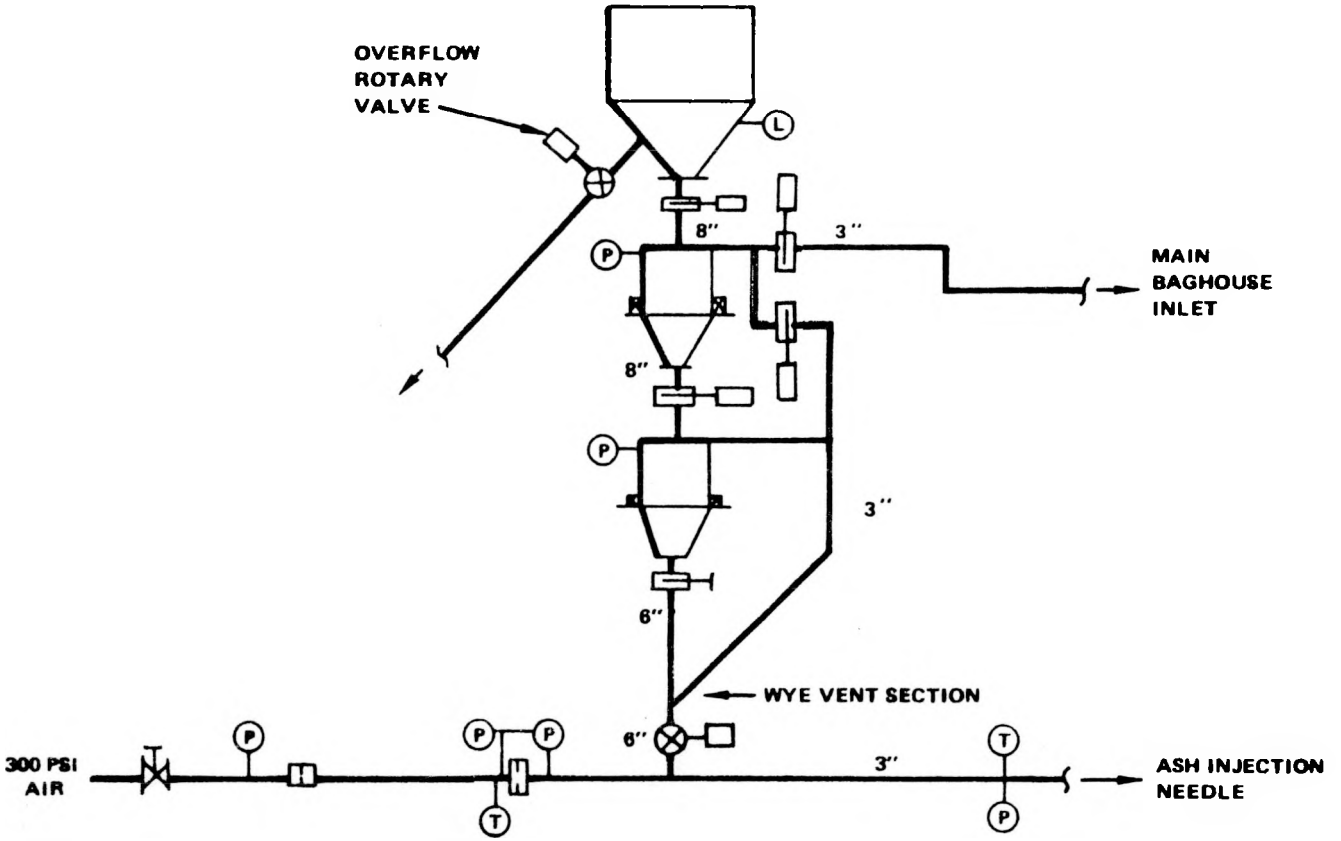


Figure 4-215. Ash Recycle Schematic

e fill hopper is normally open to the cyclone hopper and vented to the baghouse so that the pressure in these two hoppers is essentially equalized with some small gas flow bypassing from the cyclone hopper to the fill hopper to the baghouse. The run hopper is normally isolated from the fill hopper, and the run hopper pressure is essentially equalized with the rotary valve and ash injection line. This tends to be the same pressure 70 inches W.G., as the bottom of the bed that is the point of ash injection.

A variable-speed rotary valve is used to control the ash recycle rate into the ash injection line where the ash is pneumatically transported to the bottom of the bed. Conveying air is supplied from the facility air source where it is controlled by a sonic nozzle and measured by a sharp edge orifice. Typically, the ash conveying velocity was 40 ft/sec that is approximately 4% of the total combustion air at nominal conditions.

During most of the operation, the fill hopper is open to the cyclone and operates at negative pressure. The run hopper, as well as the rotary valve and ash injection line, operate at positive pressure of about 70 inches W.G. To refill the run hopper, the fill hopper is isolated from the cyclone and baghouse, the two hopper systems are then allowed to equalize through a vent line to the 70 inches W.G. pressure, and the ash is batch filled from the upper to lower hopper. Ash recycle can be continued uninterrupted during this brief filling operation.

It was originally intended that both the fill and run hoppers would operate at negative and equalized pressure with the rotary valve functioning as an air lock. The rotary valve will function as an air lock when a tight clearance is maintained between the rotor and the inlet shoe. However, when the system is started, the hot ash (500 to 700 F) heats the rotor while the housing remains near ambient temperature. The rotor expands against the shoe that is positioned by the housing, and the valve binds. To prevent binding, a large clearance is required to allow for thermal expansion, and the valve no longer functions as an air lock. This leakage through the shoe is so large that ash will be conveyed into the vent lines and plug the lines. With the plugged vent line, a pressure

unbalance then occurs with a positive pressure at the rotary valve and bottom o the hopper while the top of the hopper is negative. The ash will not freeflow into the valve under these conditions. Thus, it is necessary to pressure equalize the run hopper and rotary valve so that there is essentially little or no flow through the vent (equalizing) line.

The fill and run hoppers are on a load cell system that is used to monitor the filling operation and recycle rates.

Bed Height Measurement. The bed height from the level of the air holes in the tuyeres to the top of the tube bank is 79 inches, and an operating height of 90 inches was selected for most of the latter runs as this was sufficient to cover the material specimen probes located above the bed bank. Bed height was measured by a series of pressures at various bed levels. The bed pressure varies linearly with bed height so that a plot of pressure versus height can be used to determine the bed height as shown in Fig. 4-216. The pressure at the bottom of the bed could be determined by extrapolating the pressure profile to zero level.

Since the pressure levels are essentially evenly spaced, a series of pressure indicators could be used where lighted bars indicate the magnitude of the pressures. The operator could monitor the bed height by the slope of the series of bars versus a height scale. This was occasionally checked against a plot of the pressures as shown in Fig. 4-216. This technique provided a satisfactory means of controlling and monitoring the bed height.

Coal Feed Systems. The coal feed system consisted of four independent systems that feed each quadrant of the distributor. During the initial runs, modifications were made to the system, primarily to improve the control of the coal feed rate. The final configuration used on run 003 provided reasonable control and was used for the remainder of the test series. Starting with run 005, one of the feed systems was converted to a four-coal-port per quadrant arrangement with a coal line splitter system. This was to investigate the effect of more feed ports on the bed environment.

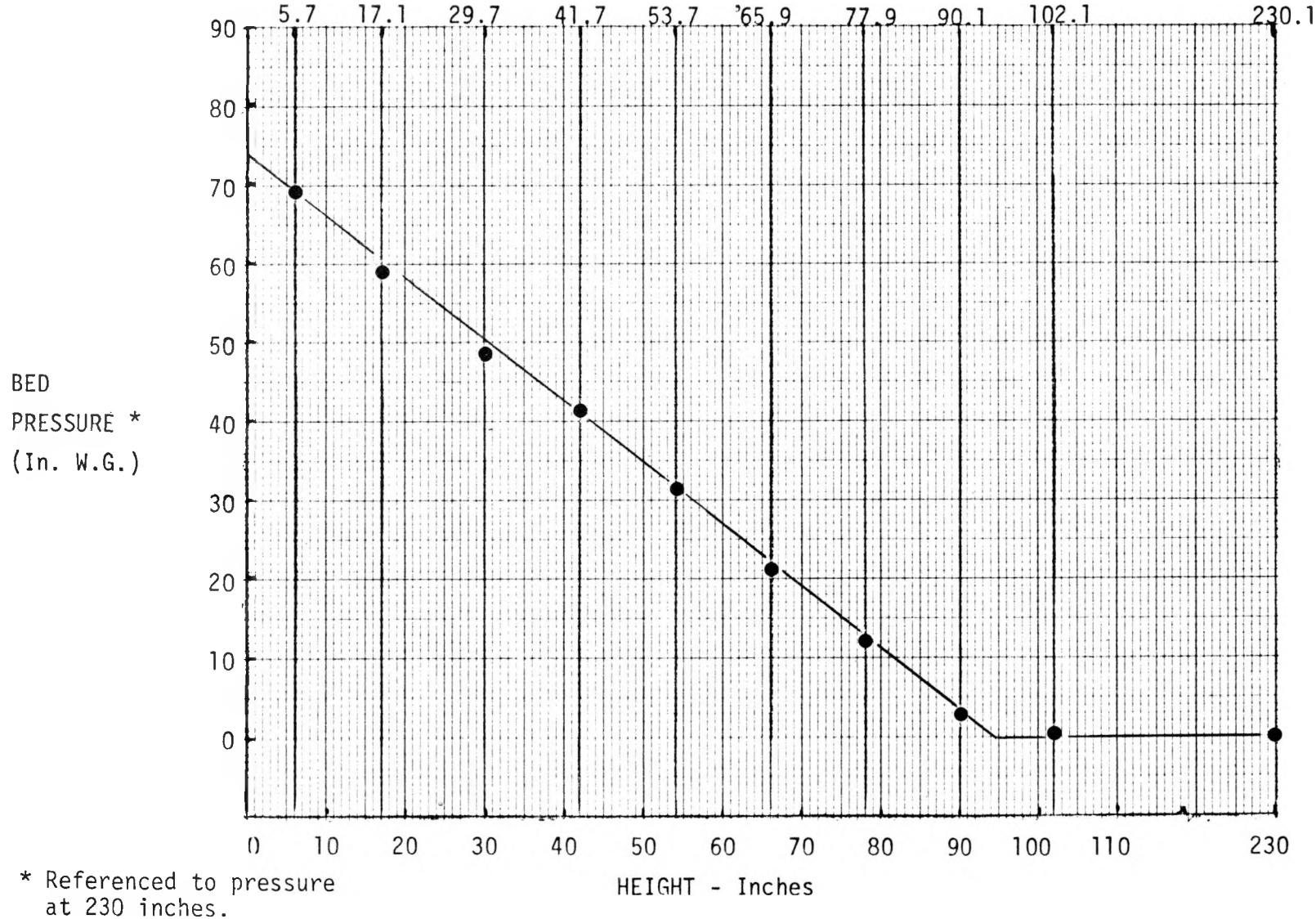


Figure 4-216. Typical Bed Pressure/Height Plot (Run 006, Data Slice 2b)

System Description. The initial feed system is shown in Fig. 4-217 wher each system consists of a run hopper on weight cells, a vibrascrew feeder to meter the coal, and an air/coal eductor. The intended design operation was that the eductor would create a near atmospheric pressure at the coal inlet, so that the pressure difference across the screwfeeder was nearly zero. It was believed that this screwfeeder would not be sensitive to small pressure differences across the screw. However, it was found that the screwfeeders were very sensitive to pressure unbalances, and the final modification was to add rotary airlocks to each system between the discharge of the screwfeeder and the coal inlet port. Also, the screwfeeder discharge was vented to atmosphere.

An important element of the system is the eductor, shown in Fig. 4-218, that was intended to provide a near atmospheric condition at the coal inlet while pneumatically feeding the coal/air mixture against the back pressure of the fluidized bed, plus the feedline pressure drop.

The eductor was calibrated, and the relationship between back pressure and coal inlet pressure is shown in Fig. 4-219. The coal inlet pressure is a function of the back pressure, motive air pressure and flowrate, and position of the motive air nozzle (Fig. 4-218).

Thus, the eductor is a point design device. The design can be optimized so that at a back pressure corresponding to the nominal bed condition and height, the coal inlet pressure can be made to be atmospheric for the design coal conveying air flowrate. At other values of back pressure, the coal inlet pressure will be somewhat positive or negative, and will leak or aspirate air at the coal inlet. Another mode of operation is to vary the motive air flowrate and pressure to maintain atmospheric coal inlet pressure for varying conditions of back pressure.

Run 001 Configuration. The configuration shown in Fig. 4-217 was used on run 001. Initially, coal was fed into a partial bed of fresh limestone. With the low bed, the eductor back pressure was low and the coal inlet pressure, therefore was low. Since the screwfeeder discharge to the eductor inlet was sealed, there was a negative pressure drop across the screwfeeder, and the screwfeeder tended to free-flow coal, even without the screw turning. When the screw was turned off completely and the vibrating feature stopped, the free flow tended to stop or be reduced.

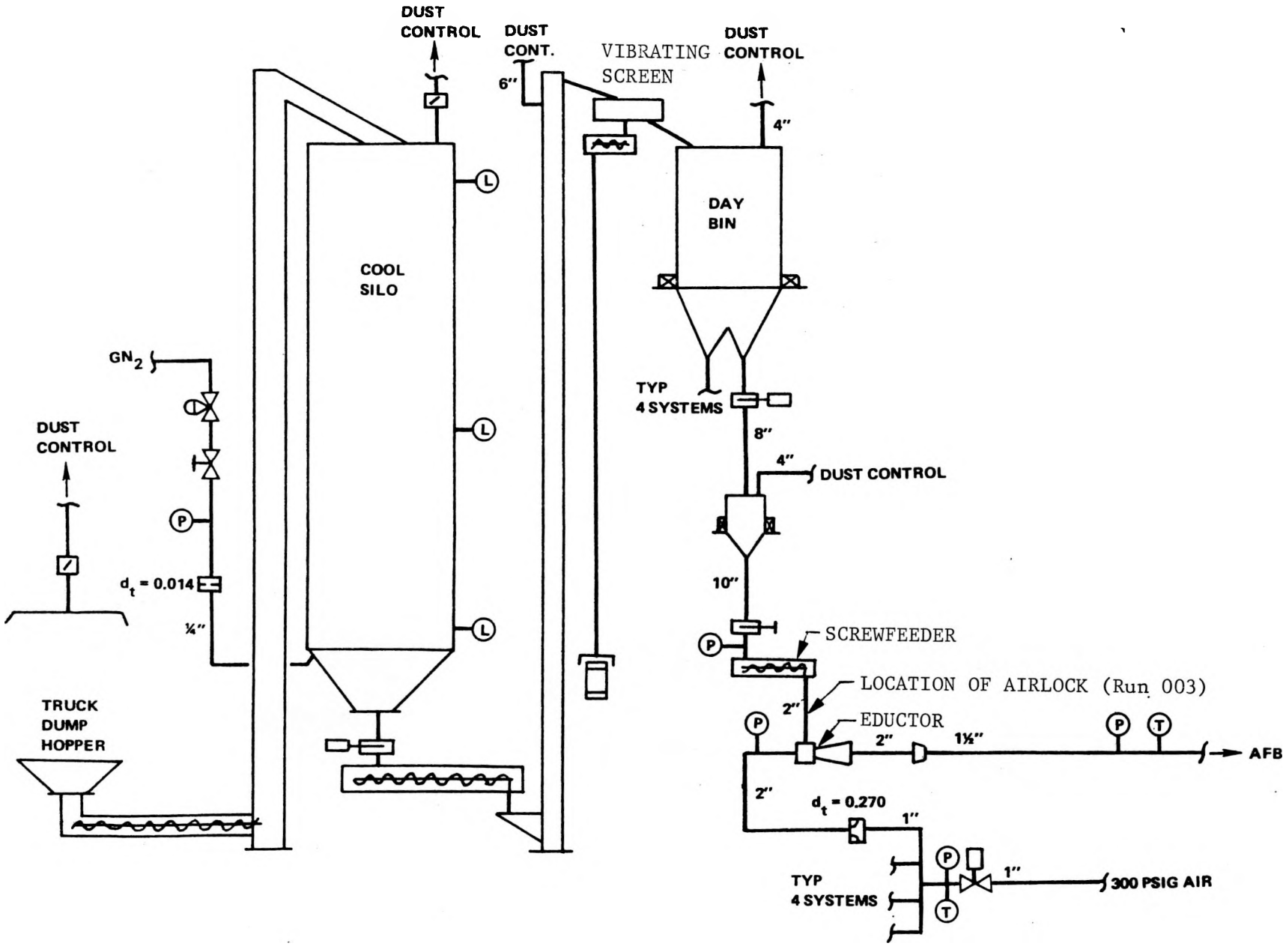
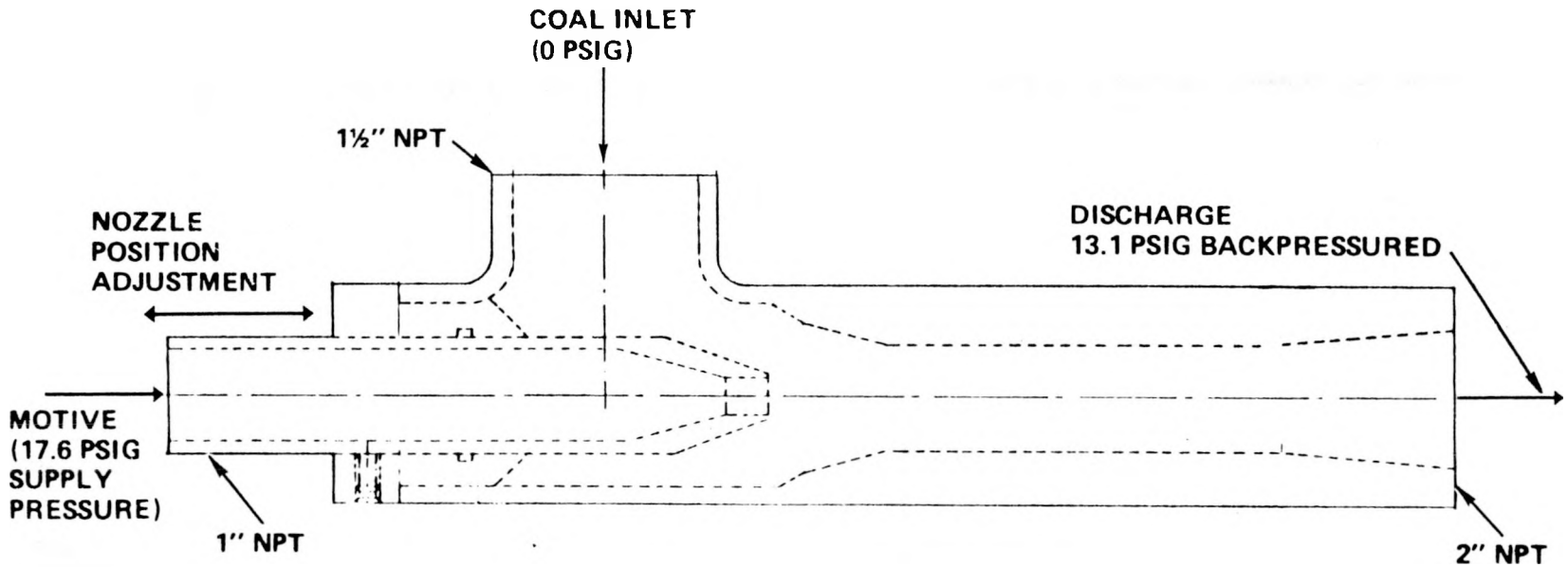


Figure 4-217. Coal Feed Schematic



NOTE: 1½" FEEDLINE, 80 FPS CONVEYING AIR VELOCITY

Figure 4-218. Coal Eductor Configuration

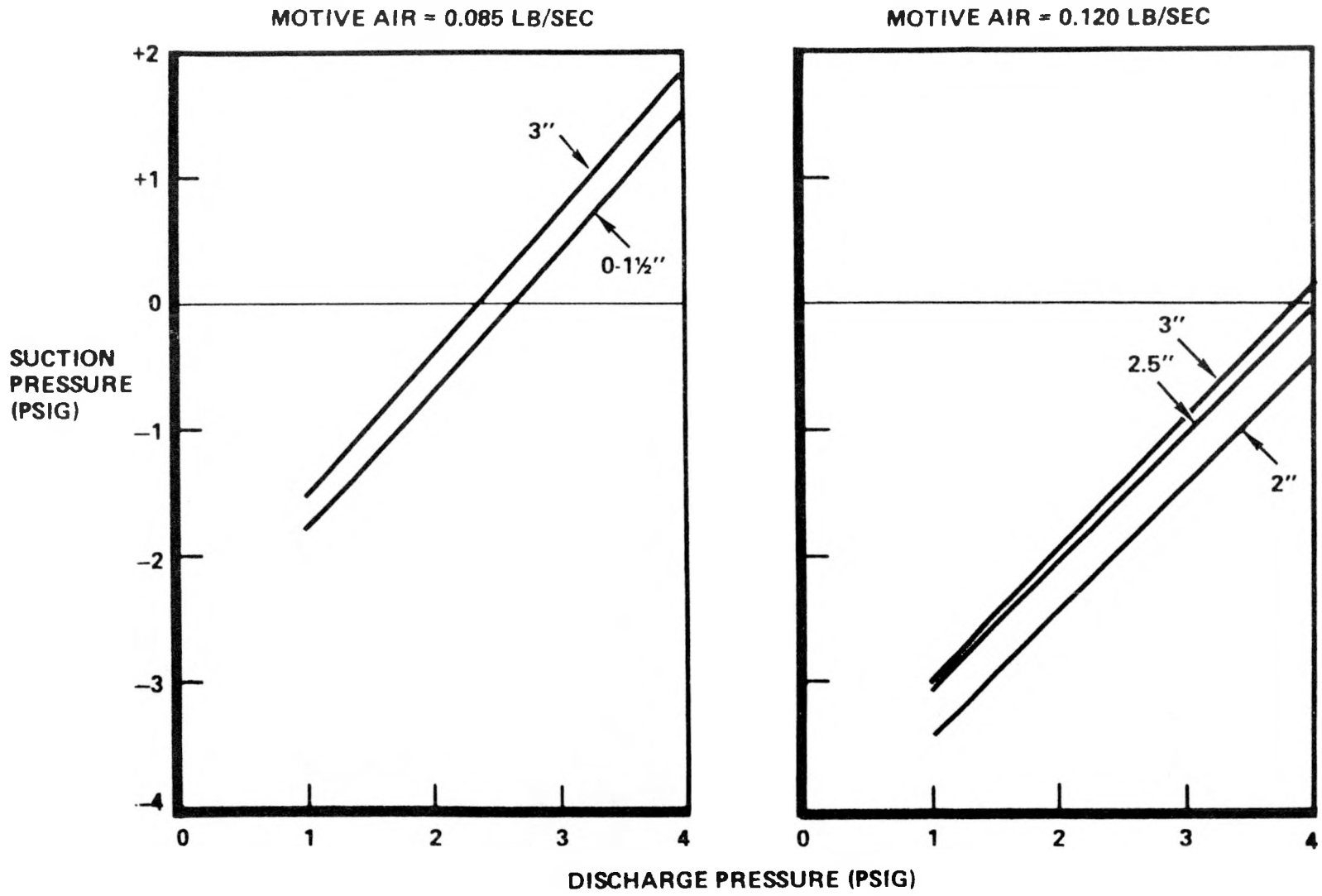


Figure 4-219. Eductor Coal Flow

As the bed level was built up to nominal level, the back pressure was increased, the coal pressure was less negative, and the free flow of coal was reduced. Correspondingly, if the coal inlet pressure was positive, the flowrate would be restricted. Thus, the coal feedrate was very difficult to control, especially at low feedrates. Fortunately, this test had very high excess air, and a large variation in feedrates could be tolerated for this condition only.

Run 002 Configuration. This configuration was essentially the same as run 001, except that a one-half inch line had been added from the screwfeeder discharge to the screwfeeder coal inlet hopper in an attempt to balance the pressure across the screw. This modification was intended to be an interim change while waiting delivery of rotary airlocks. The pressure balancing lines were marginally successful, and the ability to control the coal feed rate was improved, although not satisfactory for future operation at the nominal value of excess air.

Run 003 Configuration. Rotary airlocks (valves) were added just above the eductor coal inlet to pressure isolate this eductor. The selected airlocks are not leak tight and have a small leakage, although the leakage is small, as compared to the open port arrangement. (These airlocks were selected primarily for their availability.) The airlocks operate at constant speed as coal is metered by the screwfeeder.

Initially, the screwfeeder to airlock inlet was sealed, and this duct pressure would become the same as the coal inlet pressure. Thus, a pressure unbalance across the screwfeeder could occur as on the previous configuration. This connecting duct was then opened to allow venting to the atmosphere.

In this final configuration, no pressure unbalance could exist across the screwfeeder, and control of the coal feed rate was repeatable and reliable. When the coal inlet pressure was negative, a small amount of air would be aspirated through the airlocks. When the coal inlet pressure was positive, a small amount of air would leak back through the airlock, tending to blow coal dust into the area. The final mode of operation was to vary the coal conveying air flowrate

(motive air pressure) during the startup and operation to maintain the coal inlet pressure at a slightly negative valve. This would aspirate a small amount of air, as opposed to blowing coal dust out of the now vented duct between the screwfeeder discharge and the airlock inlet. At nominal conditions of bed height, the coal conveying air flowrate required to achieve this balance was 14%, as compared to the design value of 9%. The 14% value of coal conveying air was acceptable for the planned operation, and there are no further plans to optimize the eductor parameters.

Feedline Plugging. During the early runs, there was no evidence of feedline plugging, with the exception of one system, that would plug under conditions of low conveying air. When the conveying air was about one-half of nominal (40 ft/sec as opposed to 80 ft/sec), the line would plug, but raising the air flow to nominal would clear the line. It was discovered that one fitting was leaking severely, and when this fitting was repaired, this plugging problem did not reoccur.

There were a few occasions of plugging of the 1-1/2-inch feed lines used in the basic feed system, and most cases of plugging were attributed to debris in the coal system such as weld rod, nails, and screws. Such debris was found during post-run inspection and cleaning of the lines. The feed systems were made from straight pipe and plugged crosses that facilitated the tasks of clearing, inspection, and cleaning. Almost all cases of clearing were made without shutdown of the unit. When plugging was detected, the coal feeder would be shut down with the other systems operating at their normal feed rates, and various techniques were developed to clear the lines.

The 1-1/2-inch feedlines appear to operate without plugging over a wide range of conveying velocity and coal moisture up to 10% except in the presence of debris or improperly installed pipe fittings.

The 1-inch lines used in the splitter system for the four-port configuration were more susceptible to plugging and less tolerant of debris. There was several incidences of plugging during many of the runs, and plugging was usually cleared without shutdown of the unit.

Screwfeeder Operation. The vibrascrew feeders were found to be sensitive t pressure unbalance across the screw. When there was a negative pressure on the discharge, the coal would free-flow through the feeder if the feeder was on and vibrating, although the screw was not turning. When there was a positive pressure, the feedrate was inhibited.

However, when there was no pressure unbalance, the screwfeeders performed reasonably well where the feed rate was repeatable and varied linearly with screw speed. There was some effect of coal head on the feed rate, that was noticeable especially when an almost empty bin was filled to capacity. While these screwfeeders did not meet the original design goals with regard to accuracy and sensitivity to pressure unbalance, their operation was satisfactory enough to proceed with the experiment without further modifications.

Nominal Operating Conditions. The original design condition for the coal feed system was an exit conveying velocity of 80 ft/sec, that resulted in a primary air flowrate of 0.085 lb/sec per system, that is 9% of the total combustion air flowrate at nominal conditions. With the latest configuration, the primary air flowrate was increased to 0.134 lb/sec, or 125 ft/sec as this resulted in a slight negative coal inlet pressure.

The feed system and eductor operating conditions are shown in Table 4-101 for a bed height of 90 inches. The eductor for the four-port system required a higher motive air pressure and flowrate to balance the higher discharge pressure that resulted from the higher pressure drop of the splitter system. The eductor motive nozzle was modified for runs 007 and 008 to tune the system so that all feed systems had equal conveying air flow.

The final configuration provided satisfactory operation where coal conveying was reliable over a wide range of conveying air velocities. The coal inlet pressure is a function of the back pressure and conveying air flowrate (motive air), and the back pressure is a function of bed height, conveying air flowrate, and solids feed rate. The selected mode of operation was to adjust the motive air to maintain a slightly negative coal inlet pressure to compensate for variations in solids feed rate and bed height. These changes occurred primarily during startup and, once nominal operation was obtained, the operating conditions remained very stable.

TABLE 4-101. TYPICAL (RUN 006) COAL FEED SYSTEM OPERATING PARAMETERS

System	MOTIVE AIR Flow (lb/sec)	MOTIVE AIR Eductor Pr (psig)	Discharge Pr (psig)	Air Velocity (fps)	
1 Port/Quadrant	0.134	34	4.2	125	
4 Ports/Quadrant	0.172	40	5.5	75	Runs 005 and 006
4 Ports/Quadrant	0.134	55	5.5	50	Runs 007 and 008

Bed Pr. = 2.5 psig

Suction Pressure $\cong$ -0.1 to -0.4 psig

Motive Air Temp $\cong$ 70 F

Four Coal Ports Per Quadrant. Quadrant No. 3 was modified, starting with run 005, to contain four coal feed ports per quadrant. The normal coal feed system through the eductor was used. However, downstream of the eductor, a splitter system was installed consisting of straight lines and plugged crosses as shown in Fig. 4-220. The 1-inch coal lines feed the four 1-inch coal ports with an 8-inch-diameter splash plate. A separate conveying air supply system was installed so that this system could be controlled independently from the other system that fed the other three quadrants.

This system was cold-flow calibrated with coal and air, and the coal was captured and weighed. The results indicated a ±9%. variation in the distribution between the four lines.

The coal feed and splitter system functioned well although the smaller feed lines were more susceptible to plugging problems caused by debris in the system. To monitor and detect plugging, line pressures where installed in each leg as well as temperature measurements in the exit of the coal ports. When a leg started to plug, there would be an increase in the line pressure and the exit temperature would increase toward bed pressure as the conveying air decreased.

Cyclone Operation. The cyclone is a multiclone unit consisting of 36 individual units, that are capable of being mechanically plugged to tune the cyclone pressure drop (inlet velocity) to a given operating condition. Presented are some observations regarding the collection efficiency and flow characteristics. Also, an adverse condition that occurred on run 001 is described, which resulted in minor damage to the unit.

Cyclone Pressure Drop. The cyclone pressure drop characteristic can be expressed as an effective flow area. From the manufacturer's specifications, this area was 125 $in.^2$. During the first two runs, all 36 units were used, and the data indicated a flow area that agreed with the expected 125 $in.^2$. On runs 003 and 007, 12 of the units were mechanically plugged so that the unit operated with about 5 inches W. G. pressure drop, and, the data gave a flow-area of two-thirds, that again agreed with the expected result. Thus, the cyclone unit pressure characteristics were as expected.

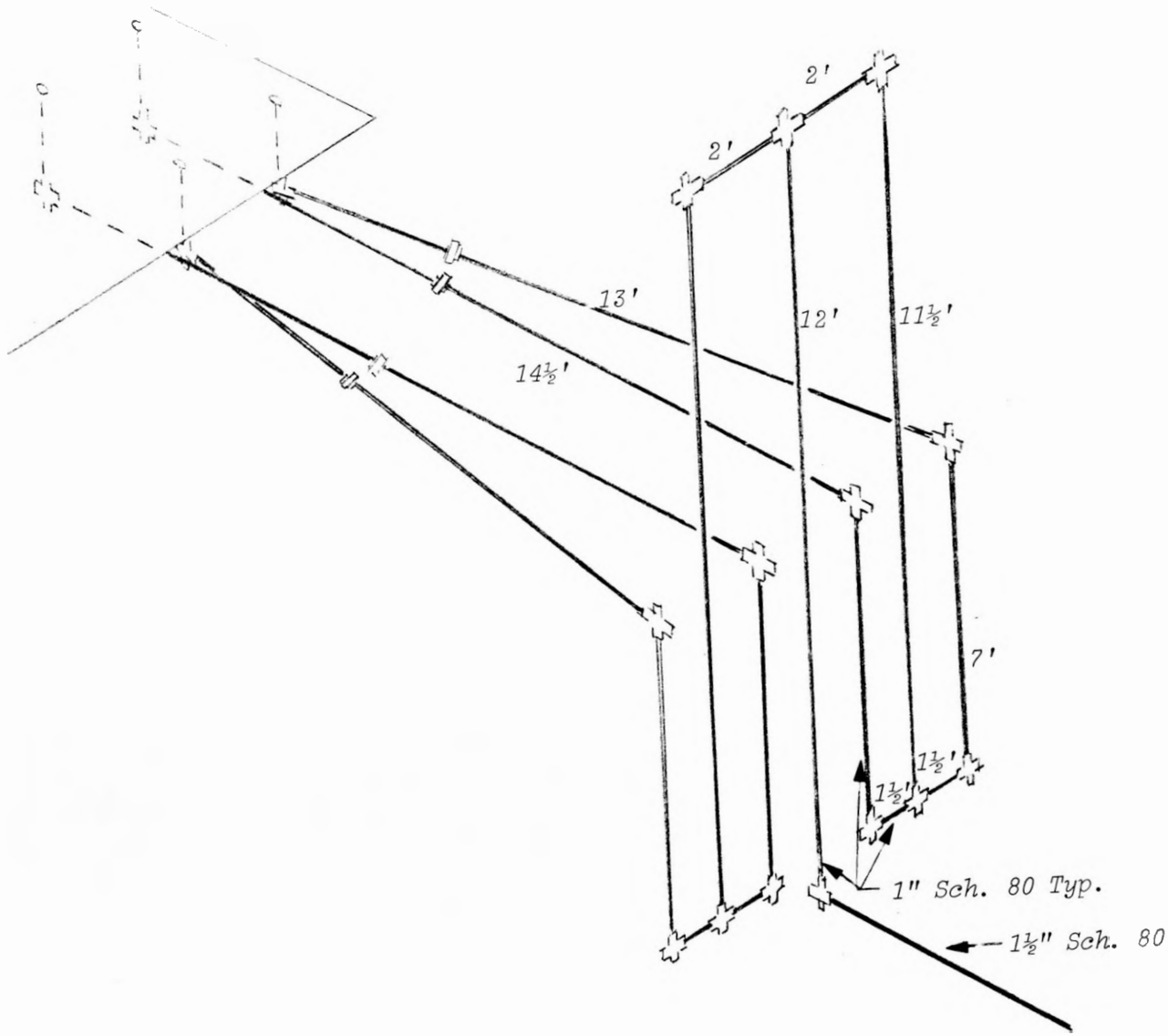


Figure 4-220. Four Coal Ports per Quadrant Configuration (System No. 3)

Cyclone Collection Performance. Ash samples from the recycle system and baghouse were analyzed from run 005 including particle size distribution. The results indicate that the cyclone collection performance was very poor, resulting in larger particle sizes being able to pass through the unit to the baghouse.

The cyclone configuration had 8 of the 36 units plugged, and this should have resulted in a pressure drop in 3.2 inches W.G. with a effective flow area of 97 sq in. The particles collected by the cyclone drain through the cyclone hopper directly into the fill (upper) hopper that is vented to the baghouse through a 3-inch-diameter vent line. Thus, there is a parallel flow path for the flue gas, and a portion of the gas is allowed to flow through the bottom of the cyclone units to the fill hopper to the baghouse. Also, the pressure difference between the fill hopper and baghouse is less than the combination of the cyclone and air preheater. When the parallel flow path and pressure difference are considered in the analysis, the data indicates that 10% of the flue gas goes through the cyclone bottoms and ash vent system.

The cyclone collection efficiency is indicated by the run 005 particle size analysis shown in Fig. 4-221 where the ash samples were analyzed by two different laboratories. A commercial laboratory (Truesdale) used a combination of sieve analysis and Anderson Impactor analysis while a Rockwell Laboratory (ESG) used an L&N Microtrac Particle Size Analyzer. Both approaches gave similar results. The curve labeled cyclone indicates particles collected by the unit while the curve labeled baghouse indicates particles that passed the cyclone unit. This latter curve can be compared to predicted vendor performance that shows that the cyclone performance was actually very poor. For 90% passing and a pressure drop of 3 inches W.G., the particle size should be 7 microns or less instead of 40 microns, that was actually experienced. A possible explanation was that the 10% flue gas bypassing the cyclone unit through the vent line was carrying the larger particles with it to the baghouse.

To improve collection efficiency, modifications were made prior to run 007. The number of plugged cyclone units was increased to twelve to increase the pressure drop to 4 inches W.G. which is at the upper end of the design and optimum value

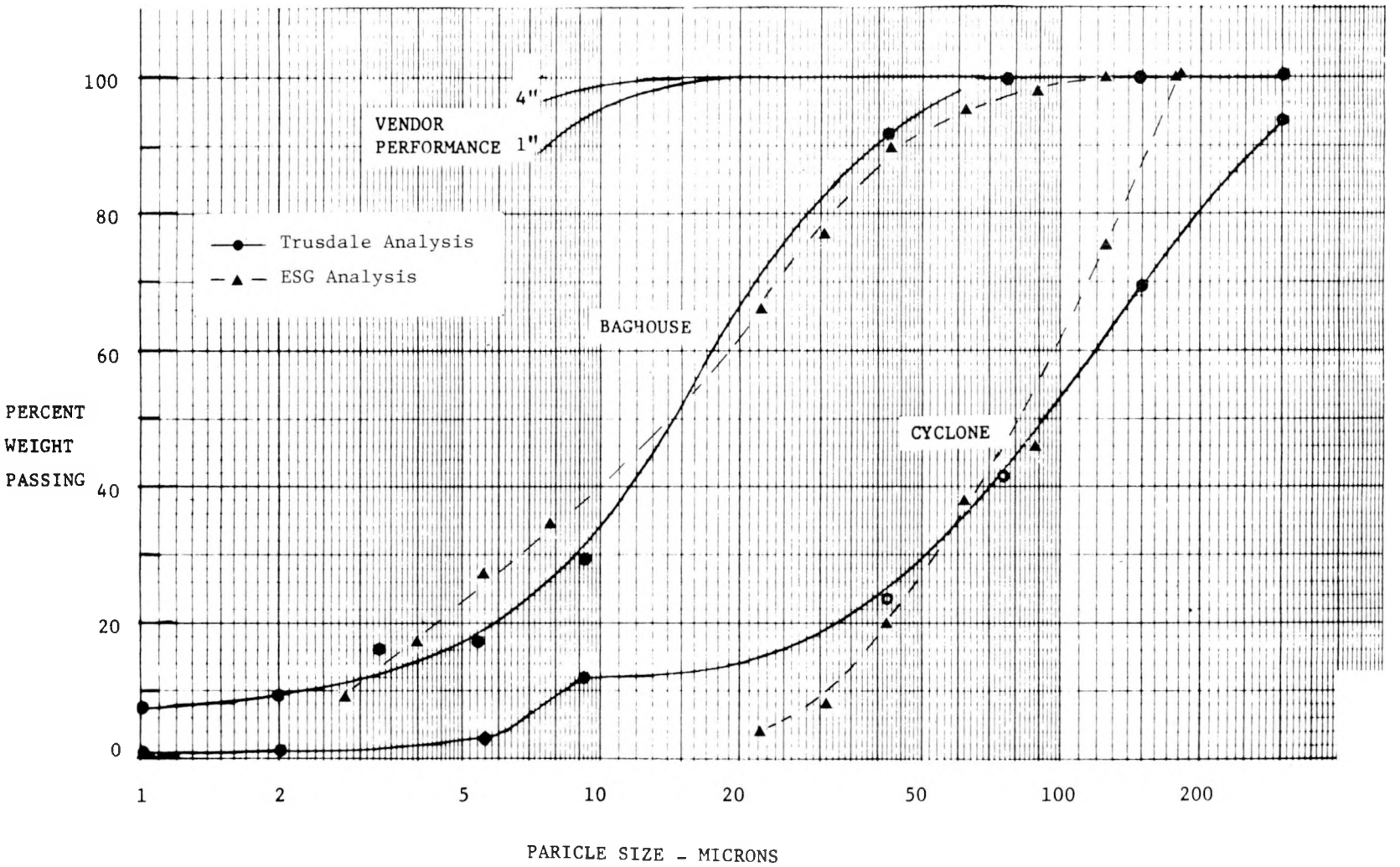


Figure 4-221. Run 005 Ash Size Analysis

of 3 to 4 inches W.G. The orifice plate in the vent line was reduced to reduce the cyclone bypass gas flow from 10 to 1%. (The vent line cannot be closed since venting is required to equalize the cyclone and fill hopper pressures for proper solids flow. This line also vents valve leakage from the run hopper that is pressurized to about 70 inches W.G.). A size distribution analysis of the cyclone ash showed that these modifications did not affect the cyclone performance, and the results were similar to the distribution curves of run 005.

Despite the relatively poor collection efficiency of the cyclone, the objectives of high carbon burnup and limestone utilization of the fly ash appears to have been achieved. Analysis of the baghouse fly ash indicates that the unburned carbon is less than 1% of the total available in the fuel and unreacted CaO is about 4% of the total in the limestone.

Acoustic Soot Blower. Acoustic soot blower devices was installed in both the cyclone unit and air preheater to prevent the buildup of ash deposits in these units. In both cases, the acoustic soot lowers were apparently successful as the deposit problems did not occur after installation of the soot blower. The soot blower, shown in Fig. 4-222, is an acoustic device (foghorn) that provides a periodic sound at a level of 140 db and about 320 Hz. (The sound level external to the unit is sufficiently low that hearing protection is not required.) Both soot blowers were air operated and used for a period of 10 seconds on, each 15 minutes.

Cyclone Unit. Plugging problems had periodically occurred during the first four tests where a somewhat hard ash deposit would form within the individual cyclone units. This deposit would cause the bottom of the units to partically or completely plug with a sometimes significant reduction in collection efficiency. An acoustic soot blower was installed in the cyclone hopper so that the exit of the horn was flush with the hopper wall and the sound was directed across the base of the individual cyclone units. The soot blower was used starting with run 005; there was no buildup of ash after installation and operation of the soot blower.

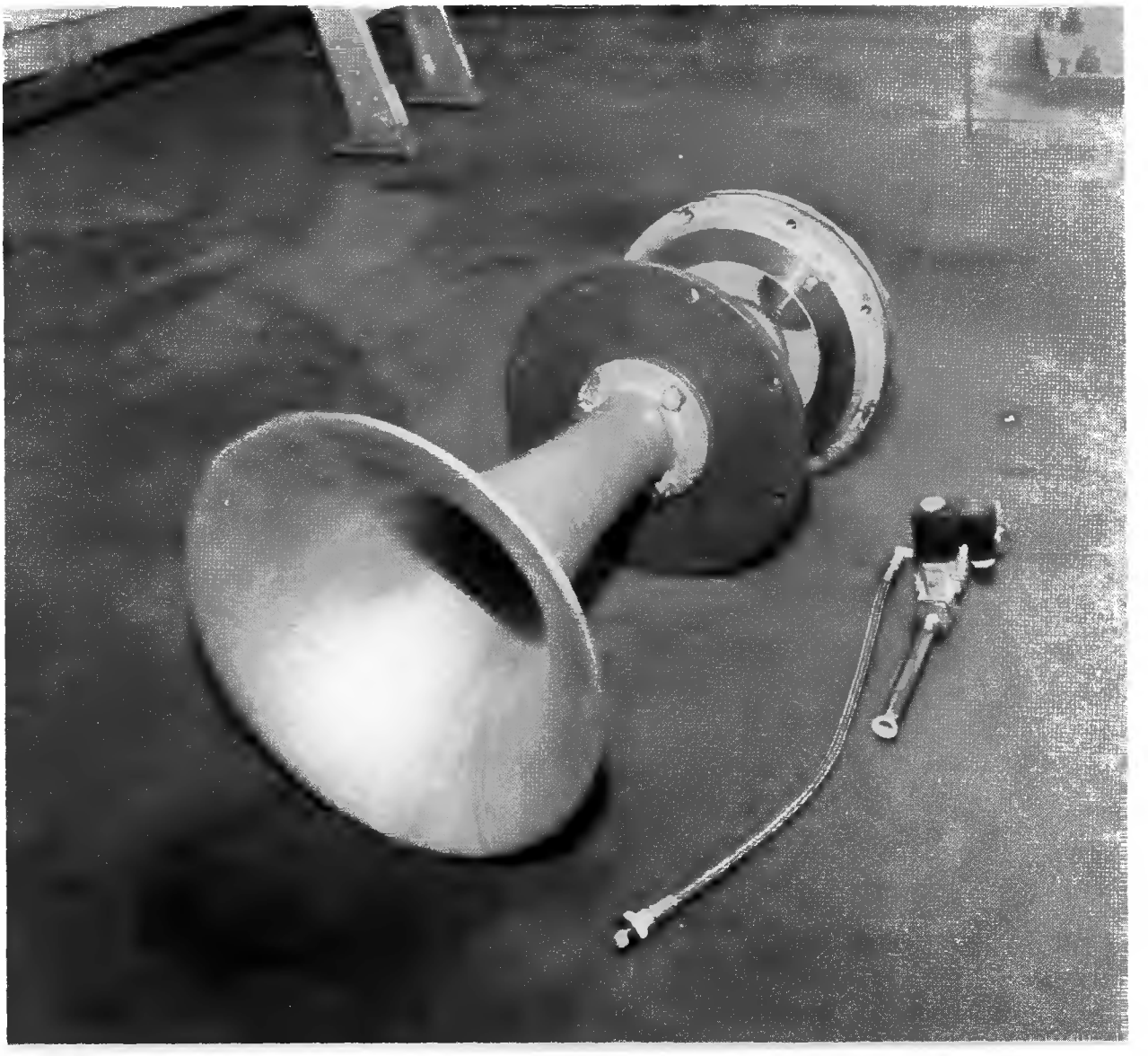


Figure 4-222. Acoustic Soot Blower

Air Preheater. During run 005, an increase in the flue gas system pressure drop was observed as well as a drop in the heat exchange effectiveness, as shown in Fig. 4-223. This occurred during the first test point where a continuous fouling of the unit was taking place. At the planned change from the first to second test point, the unit was slumped, and the air preheater was partially disassembled for inspection and cleaning. A significant amount of ash material was found to have deposited on the inside of the tubes, requring a laborious and messy cleaning task lasting several hours. The unit was restarted and operated at the second test point where both the pressure drop and effectiveness remained essentially constant at the design values. The fouling anomaly did not reoccur as verified by the posttest inspection.

Another acoustic soot blower unit was installed for run 006 at the top (inlet) of the air preheater so that the sound was directed across the tube sheet. Since this is the location of the two in situ oxygen analyzers, the installation of the analyzers was modified by placing the analyzers outside of the ducting with only the sample tube penetrating the flue gas ducting. This was to protect the analyzer sections from direct impingement of the sound wave. Both soot blowers were operated using the same electronic timer with 10 seconds on, each 15 minutes.

Once again, the acoustic soot blower device apparently corrected fouling problems as there was no indication of fouling starting with run 006. The air preheater was inspected after run 006 and found to be clean. The oxygen analyzers performed well with the modified installation where only the sample tube penetrated the flue gas ducting.

Refractory Cure Cycle and Condition. A refractory cure cycle was conducted as part of the run 001 operation. All of the refractory sections had been cured at the fabricator prior to delivery with exception of the two sections holding the heat exchangers. It was planned that these sections be cured on the erected assembly, using the AFBC systems.

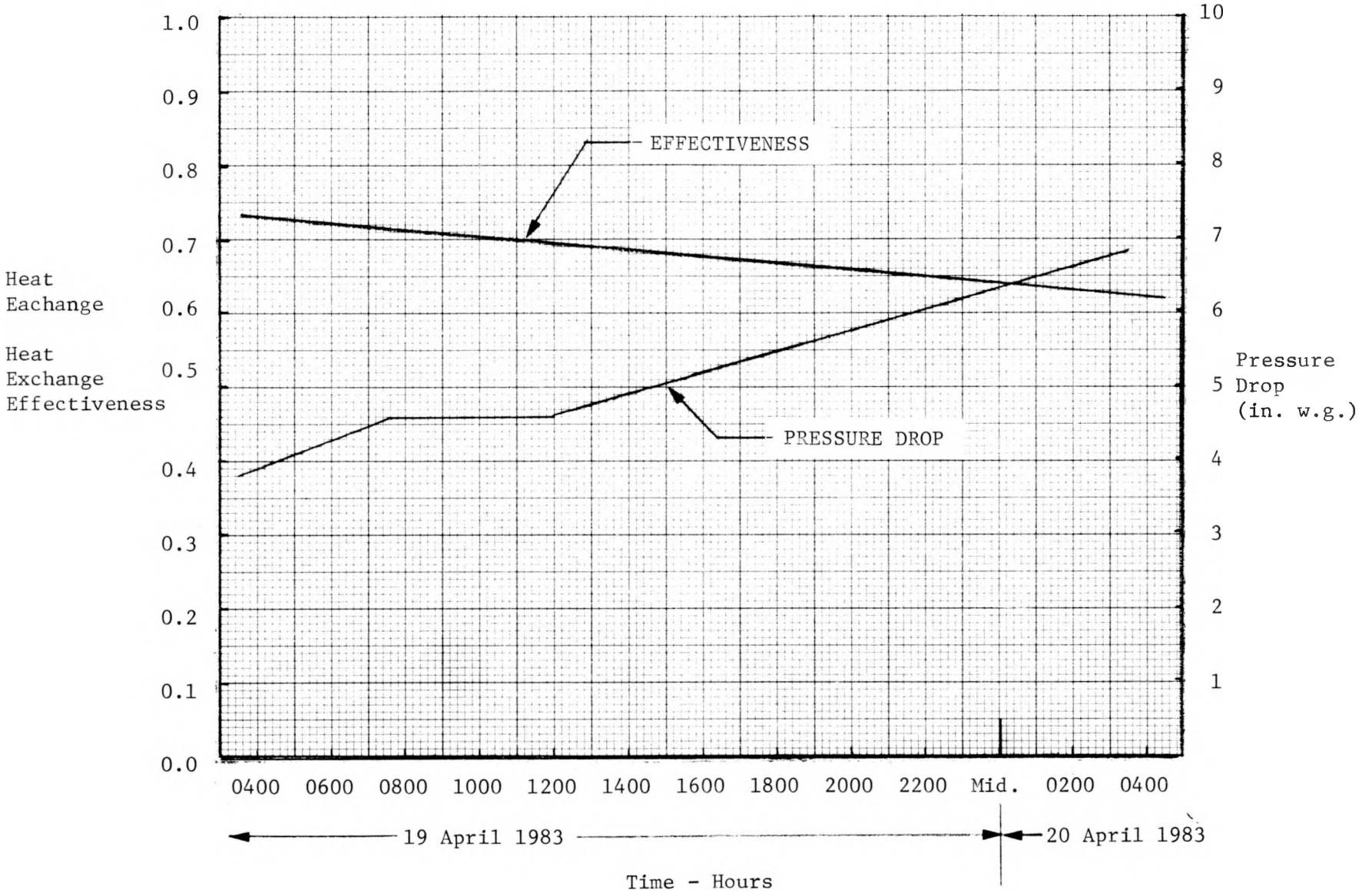


Figure 4-223. Air Heater Characteristics During Fouling - Run 005

The cure schedule recommended by the refractory supplier was incorporated into the run 001 test schedule and is summarized in Table 4-102. The actual test conditions followed the planned profile closely withthe minor exception of extra hold times at several of the temperature plateaus, including a 24-hour hold at 1000 F.

After run 001, the interior of the heater was inspected. In general, the high-temperature hard face material was found to be in excellent condition. Some of the insulating refractory in the manway doors was found to be soft. A representative of the supplier also inspected the unit at that time and concurred that the refractory was in excellent condition. The exception was some minor areas of the freeboard manway door. There was also some minor chipping near ports and other areas of thin sections. All of these discrepancies were considered minor and did not justify any concern other than to monitor the condition of these areas.

TABLE 4-102. REFRACTORY CURE SCHEDULE

(RUN 001)

TEMPERATURE	RAMP AND HOLD TIMES	
	PLANNED	ACTUAL
70 to 250 F	30 F/hr	30 F/hr
250 F	10 hr	10 hr
250 to 350 F	30 F/hr	30 F/hr
350 F	5 hr	5 hr
350 to 450 F	30 F/hr	30 F/hr
450 F	10 hr	10 hr
450 to 1000 F	30 F/hr	30 F/hr
1000 F	12 hr	36 hr
1000 to 1500 F	30 F/hr	30 F/hr
1500 F	10 hr	12 hr

4.5.7 Performance Results

Throughout the test program, the performance of the combustor/heater and system were assessed, and the many areas of performance are discussed in this section. These results indicate that the combustor/heater performance and operation is very satisfactory with the measured values very close to the design analysis. The operation of the supporting systems was also satisfactory with most systems performing close to the design requirements. Discussions are presented on:

Heat Balance
Combustion Efficiency
Heat Exchanger Performance
Air Preheater
Limestone Utilization and Sulfur Dioxide Emissions
Oxides Of Nitrogen Emissions
Material Specimen Probe Experiments
Ash Recycle
Bed Temperature Profiles
Gas Temperature Profiles
Solids Inventory

Oxygen partial pressure characterization for a variety of conditions was a major activity, particularly during runs 005 and 006. Since this activity was extensive and the discussion somewhat lengthy, the results are presented separately in Section 4.5.9.

Heat Balance. An overall system heat balance was made to assess the performance of the system, including combustion performance. For the purposes of this heat balance, the system was considered to be the heater/combustor/air preheater, and connecting ducting. The heat added and removed from this system was estimated, based on direct measurement and analysis.

The heat removed included the following factors:

1. Working Fluid - this is directly measured by the air flowrates ar temperatures.

2. Stack Losses - this is the heat in the flue gas as it leaves the air preheater, and the heat loss was estimated by calculating the quantity of flue gas and assuming that the average temperature of the flue gas constituents entered the system at 100 F. The quantity of flue gas included the windbox air, coal conveying air, ash recycle air, and 90% of the coal feedrate. (Air purges, which are less than 0.5%, were ignored.) Most of the constituents enter the system at ambient temperature, except the windbox air, which enters the air heater at 130 to 150 F. Therefore, the stack temperature loss was approximately the difference in the air heater outlet, temperature and 100 F.
3. Working Fluid Manifold - the working fluid outlet temperature is measured at the exit of the manifold, and there is some heat loss from the heat exchanger tube outlet lines and manifold, even though they are insulated. Thermocouples were located on the outside of some of these tubes under the insulation. While these measurements did not function all of the time during many portions of the testing, they indicated a temperature loss of 30 F at the nominal working fluid conditions. For the purposes of estimating the heat balance, a temperature drop of 30 F was used for all data points.
4. Windbox Duct - there is a measurable temperature loss from the air preheater outlet to the windbox which is a long, large-diameter duct.
5. External - this represents the heat loss through the hard face and insulating refractory, and the loss was estimated based on manufacturer's data. Since all of the test points have approximately the same bed temperature and outside conditions, a constant value of 85 Btu/sec was used for all data points.
6. Recycled Ash - typically, the ash is collected at about 750 F and reinjected at about 600 F where the temperature loss occurs while the ash is being stored in the fill and run bins. (The ash recycle system is not insulated although the ash tends to be a good insulating material. Hot ash collected in a bin will remain at high temperatures of about 600 F even after 10 or 15 hours.) The heat loss was estimated by the recycle rate, cyclone temperature minus reinjection temperature, and estimated specific heat. During the latter runs, a temperature measurement was added to the bottom of the ash run bin to directly measure the injected ash temperature. The typical ash temperature drop was about 130 F.

- Probe Coolant - during the material specimen exposure tests, 10 cool probes were used in the fluidized bed which remove heat from the system. An estimate of the heat removed by the probe coolant was made based on probe experimental results where the probe coolant removes about 73 Btu/sec for the conditions of runs 007 and 008. This amounts to about 4% of the heat removed from the fluidized bed.

These factors represent most of the major sources of heat removed, and there are probably several minor areas of heat losses that are difficult to access. The total heat available was estimated by the averaged coal feedrate and the lower heating value from the coal analysis.

The heat balance for longer duration operations without ash recycle (runs 003 and 004) are presented in Table 4-103. The heat removed is compared to the theoretically available heat (LHV) which represents 100% combustion efficiency. The resultant comparison indicates a "combustion efficiency" of 90% without ash recycle. The scatter of 4% is reasonable considering the number of measured parameters and assumptions used in the analysis.

The heat balance for the condition with ash recycle is presented in Table 4-104 for runs 005 and 006. The run 006 data point 2 is presented as an averaged value for the seven data slices, which is 98%, and the data scatter for these slices was $\pm$2%. While this heat balance technique may not be exact, it does provide a convenient and consistent means of assessing the combustion performance of the unit. The conclusion is that this unit operating with flyash recycle operates at a high combustion efficiency in the range of 96 to 98%.

For runs 007 and 008, an average of the heat balance was determined for each day of operation, and the results are summarized in Table 4-105 where the test average is presented. These results indicate a high combustion efficiency which is consistent with results obtained during the characterization test series. Since the main data acquisition system did not function, there were more assumptions and inaccuracies than in previous tests. Some of the factors were based on similar operating conditions from the characterization test series.

TABLE 4-103. SYSTEM HEAT BALANCE WITHOUT ASH RECYCLE

	003A	003B	003C	003D	004A	004B
TEST CONDITIONS						
SUPERFICIAL VELOCITY, fps	6.3	6.3	6.0	4.2	6.2	6.4
BED TEMPERATURE	1611	1590	1587	1594	1573	1585
HEAT REMOVED (BTU/SEC)						
WORKING FLUID	2620	3004	3258	2124	3349	3152
STOCK LOSSES	327	430	312	202	324	338
WORKING FLUID MANIFOLD	68	81	87	55	92	83
WINDBOX DUCT	22	22	22	6	23	23
EXTERNAL	85	85	85	85	85	85
	3122	3622	3764	2472	3873	3681
HEAT AVAILABLE (BTU/SEC)	3609	3887	4349	2612	4200	4168
HEAT MOVED/AVAILABLE	0.87	0.93	0.87	0.95	0.92	0.88

TABLE 4-104. SYSTEM HEAT BALANCE

	RUN 005		RUN 006	
	A	B	1	2*
TEST CONDITIONS				
SUPERFICIAL VELOCITY, fps	5.7	5.9	7.8	6.2
BED TEMPERATURE, F	1606	1608	1587	1655
HEAT REMOVAL (BTU/SEC)				
WORKING FLUID	3438	2867	4559	3548
STACK LOSSES	371	354	373	357
WORKING FLUID MANIFOLD	94	77	95	86
WINDBOX DUST	29	26	20	20
EXTERNAL	85	85	85	85
RECYCLED ASH	0	33	31	50
TOTAL	4017	3442	5173	4146
HEAT AVAILABLE (BTU/SEC)	4229	3635	5006	4249
REMOVED/AVAILABLE	0.95	0.95	1.03	0.98

*AVERAGE OF SEVEN DATA SLICES

TABLE 4-105. SYSTEM HEAT BALANCE (TEST AVERAGE)

	RUN	
	007	008
TEST CONDITIONS		
SUPERFICIAL VELOCITY, fps	6.0	6.0
BED TEMPERATURE, F	1651	1651
HEAT REMOVAL (BTU/SEC)		
WORKING FLUID	3125	3076
STACK LOSSES	344	360
PROBE COOLANT	73	73
WINDBOX DISTRIBUTION	20	20
EXTERNAL	85	85
RECYCLED ASH	21	21
TOTAL	3668	3635
HEAT AVAILABLE (BTU/SEC)	3671	3637
REMOVED/AVAILABLE	1.00	1.00

Combustion Efficiency. Based on the heat balance approach, the combustion efficiency of the unit was about 90% without ash recycle and 98% with ash recycle.

Another check on combustion performance was made by comparing the actual air/fuel ratio with the value calculated for 100% combustion efficiency based on the coal analysis. This comparison gave the same results as obtained by the heat balance method with combustions efficiencies of about 90 to 98% for the conditions of no ash recycle and with ash recycle.

Another rough assessment of combustion efficiency was made by estimating the carbon burnup. The total amount of coal used was measured as shown in Table 4-106, and the amount of fixed carbon is known by the coal analysis. The quantities of baghouse flyash and bed material were estimated by drum count and typical weights of material in the drums. Solids analysis were used to estimate the quantity of carbon in the waste material where these analyses have shown that the spent bed material has practically no carbon, while the baghouse has a typical carbon content of 4.7%. This approach showed a high carbon burnup of 99% or high combustion efficiency.

TABLE 4-106. ESTIMATED CARBON BURNUP (RUN 008)

TOTAL COAL USED, POUNDS	277,500
FIXED CARBON IN COAL (43.5%), POUNDS	120,700
BAGHOUSE FLYASH, POUNDS	25,200
CARBON IN FLYASH (4.7%), POUNDS	1,180
BED DRAIN, POUNDS	42,900
CARBON IN SPENT BED (0.1%), POUNDS	40
TOTAL CARBON IN WASTE, POUNDS	1,220
CARBON BURNUP, %	0.99

While both of these methods of assessing combustion efficiency have their inaccuracies, they indicate a high combustion efficiency with ash recycle. Even if more conservative assumptions are used, the net result would still be a combustion efficiency of 96% or better.

Heat Exchanger Performance. The heat exchanger performance includes the heat transfer and pressure drop of the convection and bed heat exchangers in the combustor/heater.

An assessment of performance was made for some of the steady-state data points by comparing the measured data from run 003 to the results of the model used to design the unit. The general test conditions were input, such as superficial velocity, bed temperature, and excess air, and the analytical model predicted the working fluid air temperature and pressure profile. The overall heat transfer coefficient for both the convection and bed heat exchangers was calculated from the measured and analytical model temperature profile and working fluid air flowrate. These coefficients are compared in Table 4-107. Within the expected data scatter, the bed heat exchanger performance agrees reasonably well with the predicted performance. The convection heat exchanger appears to be 5 to 10% lower than predicted.

The heat exchanger pressure drop was evaluated by calculating an "effective flo restriction" for both tube bundles, based on average air density in the hea exchangers. (This parameter represents the effective flow area of a nozzle with no pressure recovery with the same pressure drop as the heat exchanger.) These flow restrictions are compared in Table 4-107. The bed heat exchanger had an effective flow resistance, which is 92% of the predicted value, or the actual pressure drop is 85% of the design value. The convection heat exchange had an effective flow resistance which is about 30% higher than predicted, or the measured pressure drop is about 60% higher than design. However, the convection bank comparison is subject to more instrumentation error since the measured pressure drop was only 2 to 5 psid, and this compares to the bed heat exchanger pressure drop, which is on the order of 30 psid. Thus, the bed heat exchanger pressure drop is close to the design value, while the convection heat exchanger (which has a low pressure drop) is somewhat higher than predicted.

TABLE 4-107. HEAT EXCHANGER PERFORMANCE COMPARISON OF RUN 003 DATA TO DESIGN MODEL

	003A	003B	003C	003D
CONDITIONS				
SUPERFICIAL VELOCITY, fps	6.3	6.3	6.0	4.2
BED TEMPERATURE, F	1611	1590	1587	1594
EXCESS AIR, %	53	47	25	30
OVERALL COEFFICIENT, BTU/HR/FT^2/F				
BED, MEASURED	29.9	34.2	35.9	27.8
BED, PREDICTED	31.4	31.9	33.1	28.4
CONVECTION, MEASURED	4.6	5.5	5.4	3.5
CONVECTION, PREDICTED	5.3	5.4	5.8	3.8
PRESSURE DROP PARAMETER, IN.^{2}				
BED, MEASURED	10.4	10.8	11.0	10.2
BED PREDICTED	11.5	11.5	11.5	11.5
CONVECTION, MEASURED	22.1	21.7	22.8	25.9
CONVECTION, PREDICTED	17.4	17.4	17.4	17.4

Air Preheater. The air preheater measured operation was compared to the design condition and was found to be operating reasonably close to design. The measured effectiveness was 76 $\pm$2%, as compared to a design value of 78%. The gas pressure drop across the entire unit, including approach ducting, was 0.5 inch W.G. for both the combustion air and flue gas sides, and this is almost within the accuracy of the measuring system and reasonably agrees with the design pressure drop.

Limestone Utilization and Sulfur Dioxide Emmisions. Obtaining limestone utilization performance requires prolonged operation to stablize the bed chemistry and obtain good measurements of solids feed rates and emissions. The emissions monitoring equipment continued to be a major problem requiring frequent maintenance and repair. During the latter portion of run 006, good measurements of sulfur dioxide were obtained where the meter readings were verified by wet chemical analysis. During the other portions of the tests, the limestone feed rate was maintained at about one-third of the coal feed rate, which should be sufficient to produce the proper emission control based on previous experience.

Prior to run 007, the gas sample system was modified, and the procedure was changed so that samples were not taken during igniter operation to prevent high moisture combustion gases from going to the sulfur dioxide monitor. These changes were successful; the gas analysis console functioned well during both runs 007 and 008.

During the latter tests, the goal was to maintain an average sulfur capture of 90%, and the results shown in Table 4-108 show that this goal was achieved. The limestone use on run 007 was considerably higher than run 008, with a calcium-to-sulfur molar ratio of 4.8 as compared to 3.7. The operating conditions on both runs were the same, and the only difference is that the batch of limestone used on run 007 was delivered at a separate time. The sulfur dioxide emissions were 0.5 $lb/10^6$ Btu which compares to the Federal New Source Standard of 1.2 $lb/10^6$ Btu.

TABLE 4-108. LIMESTONE UTILIZATION

	RUN	
	007	008
BED TEMPERATURE, F	1651	1651
STABILIZED HOURS OF OPERATION, HOURS	148	188
SO_2, PPM	241	220
Ca/S	4.8	3.7
SULFUR CAPTURE, %	0.90	0.90
SO_2/M BTU	0.52	0.52

The limestone utilization was compared to previous results in Fig. 4-224. A general trend of increasing Ca/S molar ratio can be seen as a function of sulfur capture.

Oxides of Nitrogen Emissions. The oxides of nitrogen (NO_x) of this unit are inherently low due to the low combustion temperature that exists in the fluidized bed. Values of NO_x are presented in the Summary Of Data Tables. The test average was 129 and 83 ppm for runs 007 and 008; this results in NO_x levels of 0.09 and 0.14 $lb/10^6$ Btu. The Federal New Source Standard is 0.7 $lb/10^6$ Btu, which means that this AFB unit has an NO_x emission level which is 20% or less of the Federal Standard.

Material Specimen Probe Experiments. During runs 004 and 005, special experiments were conducted on two of the material specimen probes to characterize the probe operating conditions. These probes were installed in the middle of the bed heat exchanger through ports on the West elevation (ports BMUWA amd BMUWB). Experiments were conducted to: (1) characterize the specimen temperature profile versus air coolant flow, (2) investigate the effect of preheating the coolant inlet to achieve a more uniform specimen temperature profile, (3) determine the amount of coolant air leakage into the bed, (4) determine the circumferential temperature profile of the specimens, and (5) determine the effect of bed temperature on the probe specimen temperature. Since this was a checkout of the probe design and operation, the material specimens were limited to 304H and Incoloy 800H materials.

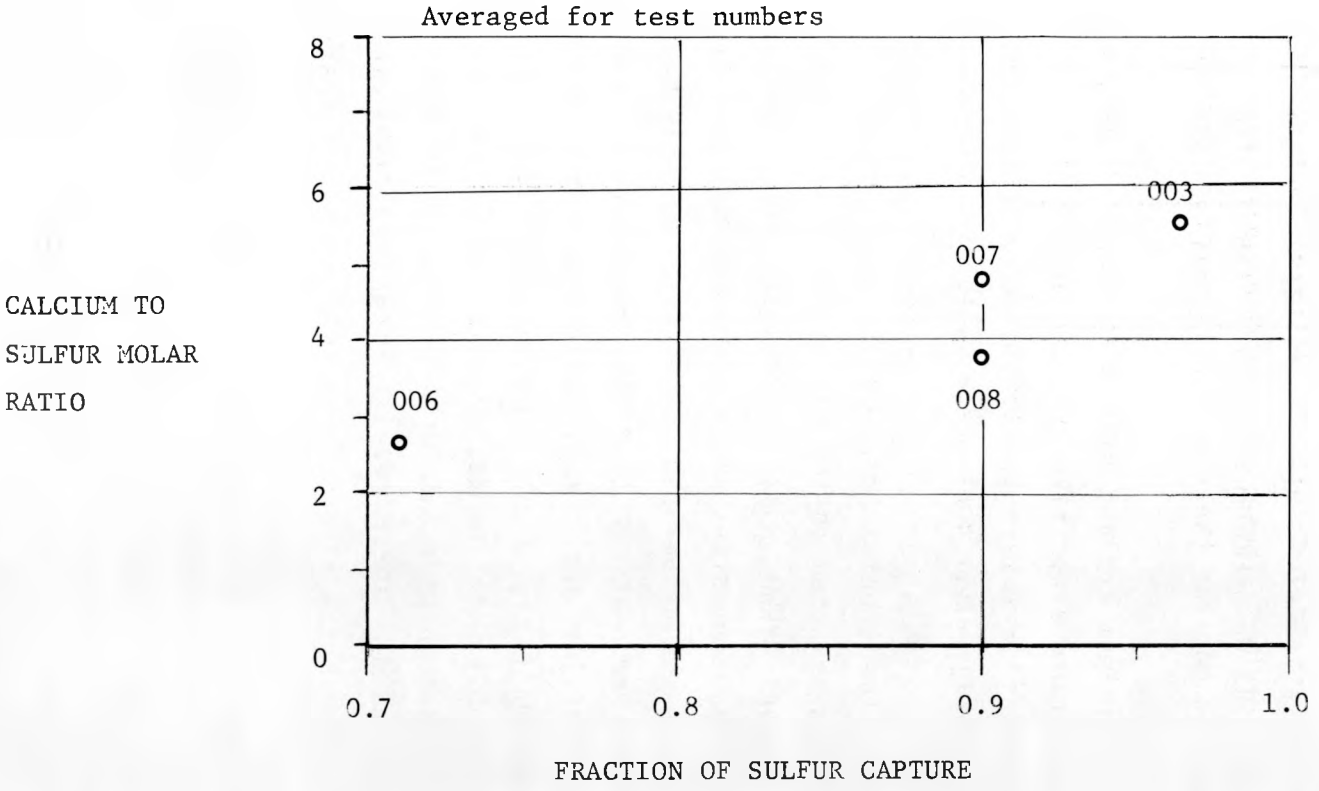


Figure 4-224. Limestone Utilization and Sulfur Capture

The material specimen probe consists of a number of 2-inch-diameter rings with 1-inch length mounted coaxially over a 1.5-inch tube, and the material rings are held in place by a spring. Cooling air flows through the annulus, as shown in Fig. 4-225, to the end of the probe, and flows back through the center of the inner tube. Thermocouples are brazed into the walls of four corrosion specimens equally spaced along the probe. These four thermocouples plus a coolant exit temperature are then used to monitor the specimen temperature profile.

During the operation, a minimum coolant exit pressure of 1 psig was maintained with a throttle valve to ensure a positive pressure inside the probe greater than bed pressure. Air coolant flow was controlled by a calibrated regulating valve in all tests except the leakage experiment where calibrated orifices were used.

Temperature Profile. The specimen temperature profile for various coolant flowrates were measured and compared to the analytical values. This was conducted with Probe A located in port BMUWB. The temperature results were normalized to compensate for varying bed temperatues where the reference bed temperature was 1600 F. As an example, if the actual bed temperature was 1640 F, 40 F was subtracted from the specimen temperatures to arrive at normalized conditions. The analytical temperature profiles are presented in Fig. 4-226 while the experimental values are presented in Fig. 4-227. The specimen temperatures at the end of the probe compare favorably with the design values while the specimen temperatures near the wall are somewhat less. This results in an actual temperature spread greater than predicted. These results were consistent with tests conducted during run 004.

Preheated Coolant Air. A method was devised to flatten the temperature profile by preheating the coolant inlet air using electric band heaters. It was estimated that a heater input of 1500 watts would result in raising the coolant inlet temperature 100 F.

Typical results showed that the coolant inlet temperature increased 23 F and the temperature spread decreased by 18 F. These specimen temperature profiles are presented in Fig. 4-228. Inspection indicated that the heaters were operating at

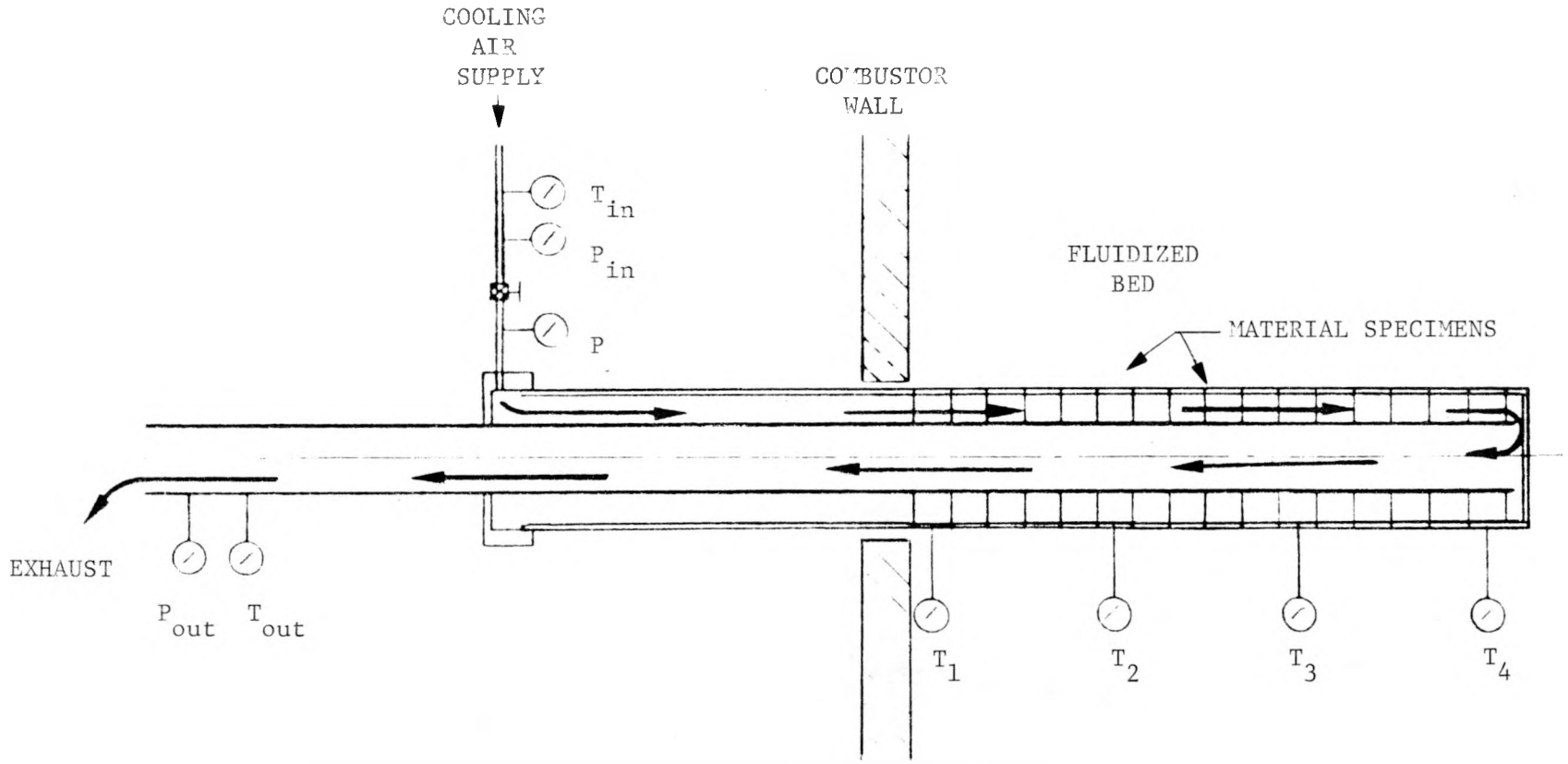


Figure 4-225. Schematic of Material Specimen Probe

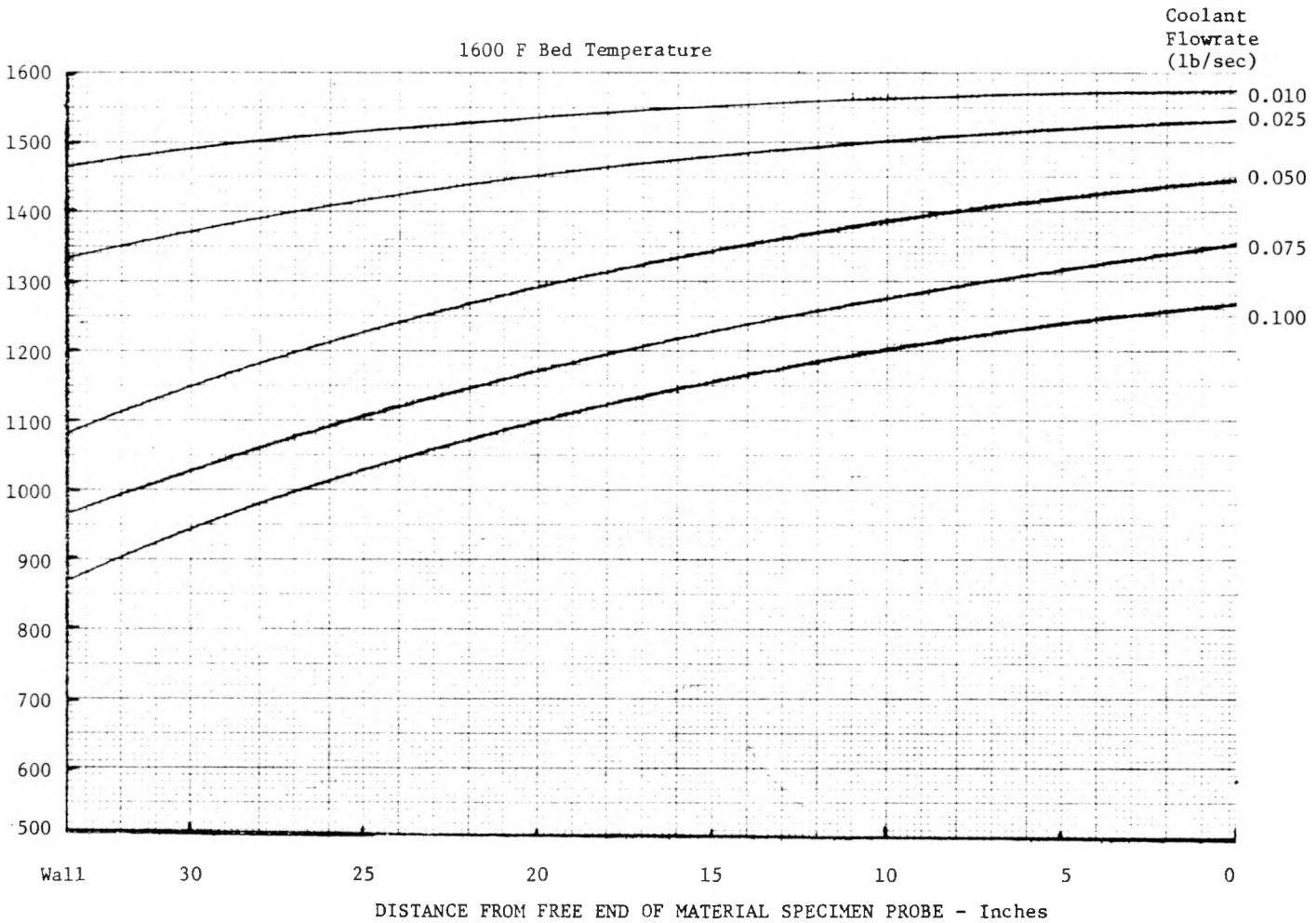


Figure 4-226. Analytical Material Probe Temperature Profile

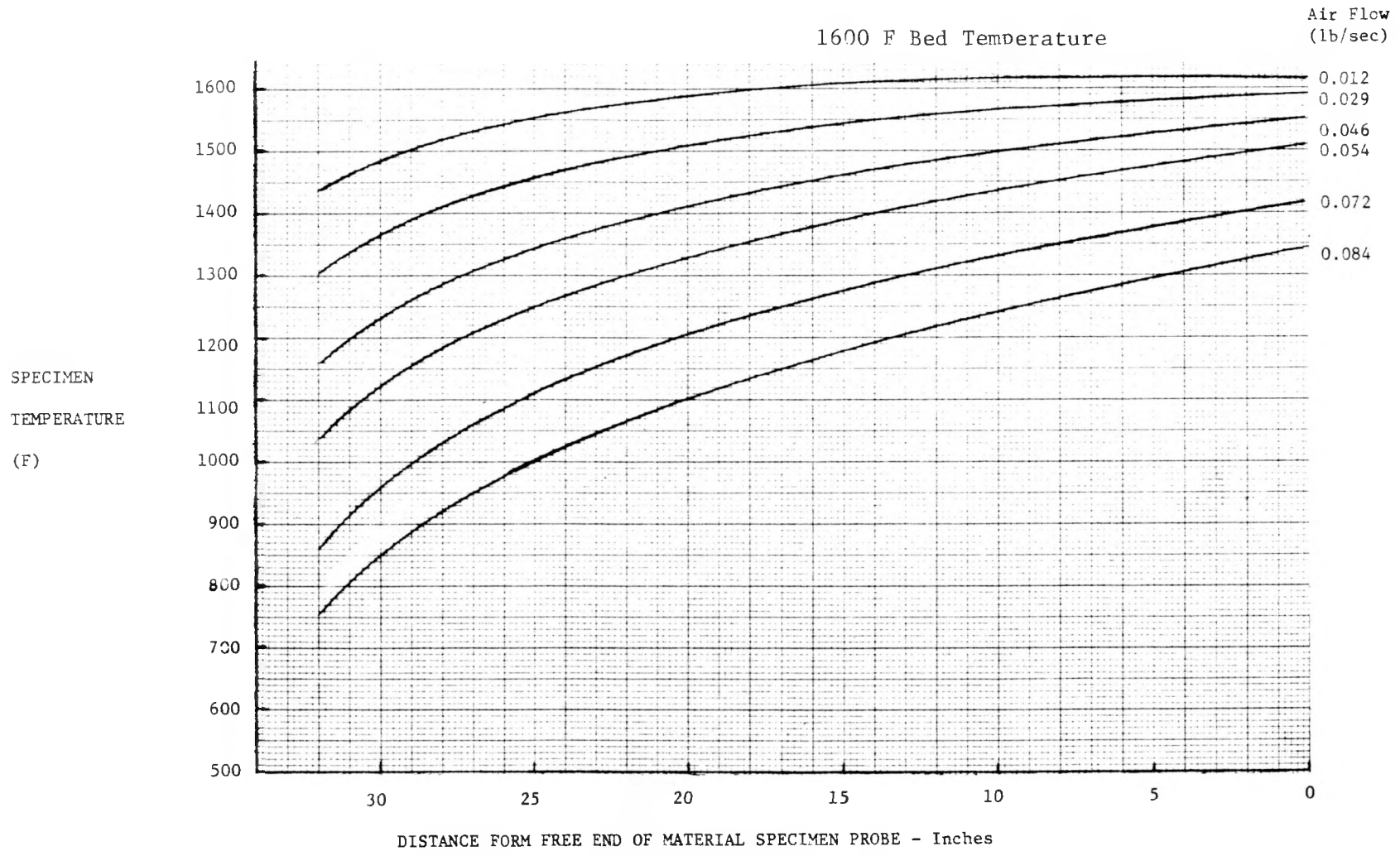


Figure 4-227. Run 005 Material Specimen Probe Temperature Profile

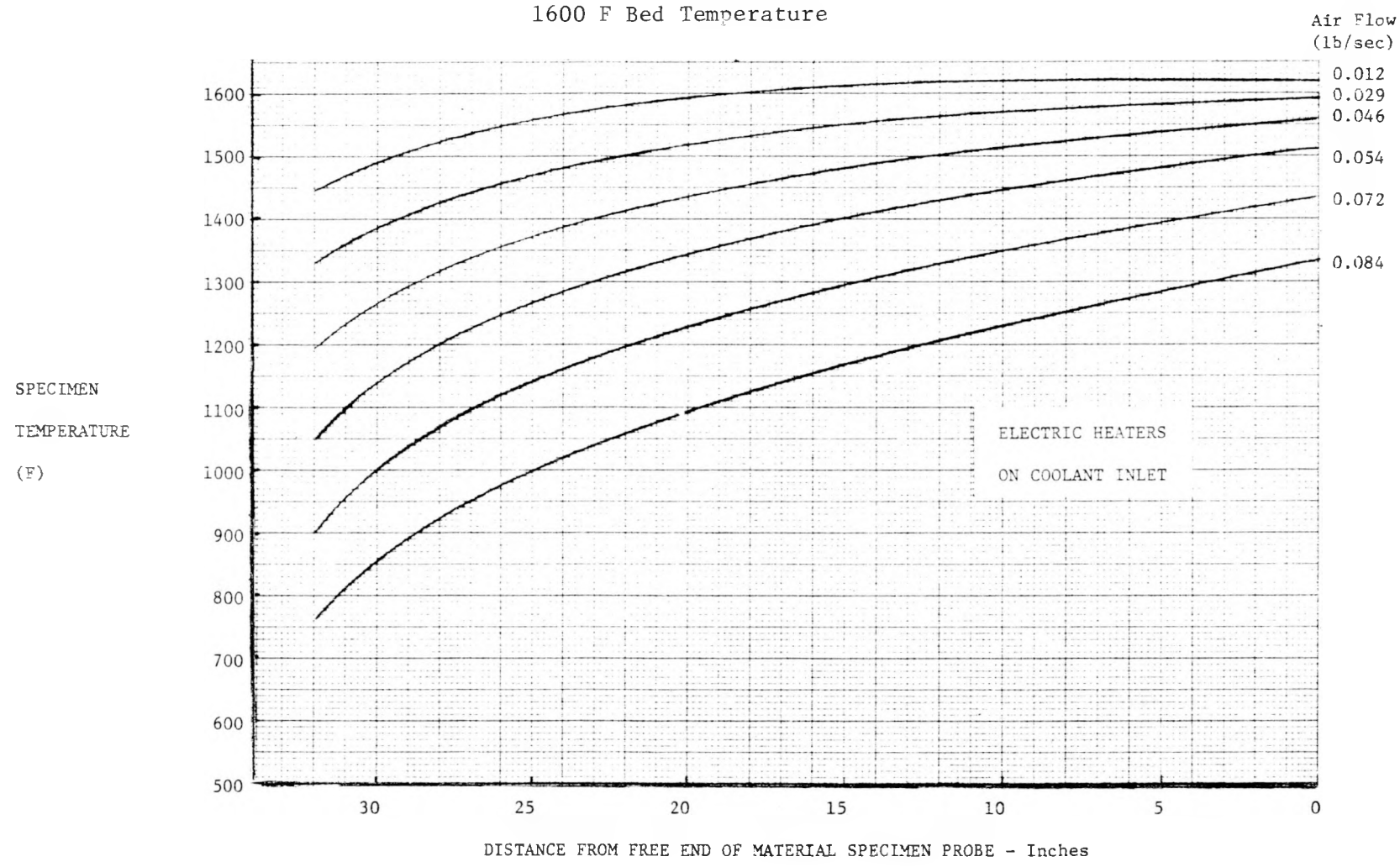


Figure 4-228. Material Specimen Probe Temperature Profile with Heated Coolant

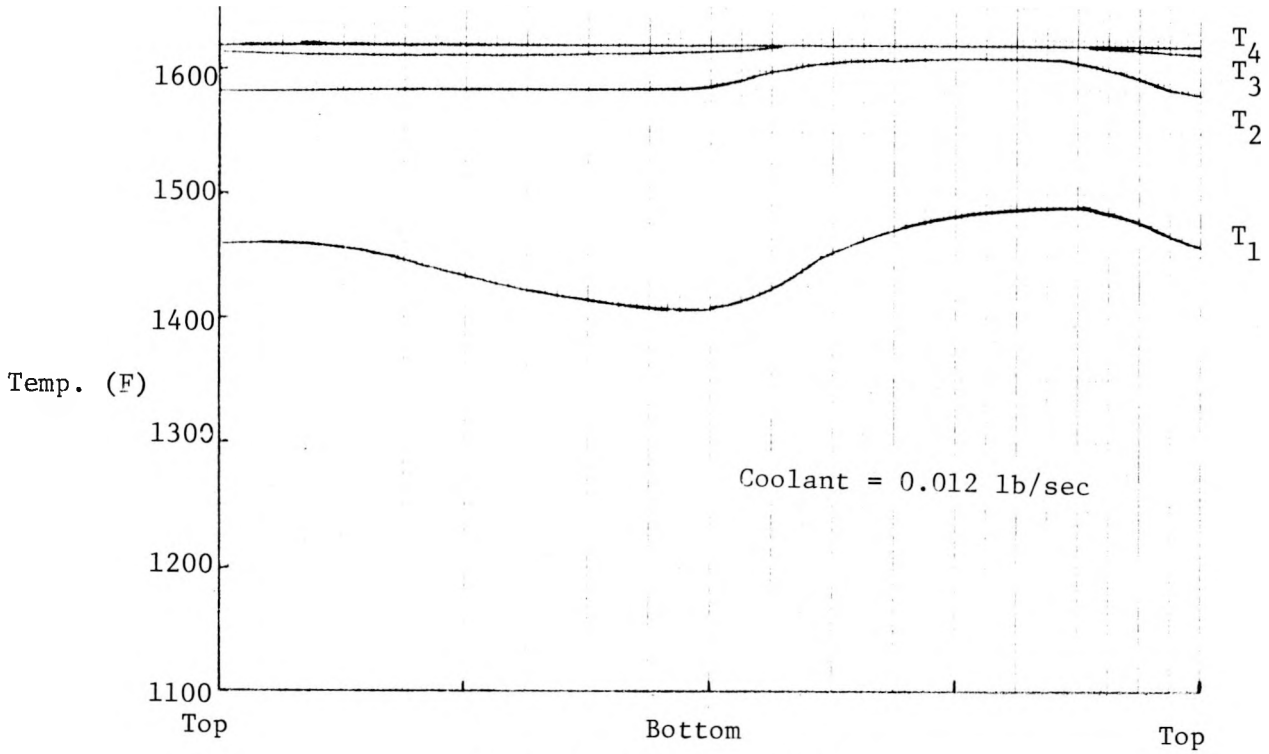
the proper output. The conclusion was that the computer modeling did not accurately represent the entire system. Since there was no significant decrease in the specimen temperature profile, the heaters were not used for the planned material exposure test series.

Coolant Leakage. During material specimen testing on the Battelle Columbus Laboratory 24-inch-diameter unit, the probe coolant leakage between the individual specimens was significant. This leakage had a significant influence on the bed operating conditions. The probes designed for the 6' x 6' AFBC were specifically designed to minimize this leakage through careful fitup and alignment of the probe components and specimens. To verify the probe design, an experiment was conducted to measure the coolant flowrate into and out of the probe. A sonic nozzle was used for the inlet flowrate while a subsonic orifice was used for the downstream outlet flow. Both flow devices were calibrated.

Typically, the average leakage was 0.0057 lb/sec of 0.05 lb/sec inlet flow, which is an average of 11.3% coolant loss. This is significantly less leakage than experienced on the BCL tests. For the planned material exposure test series with eight probes, the estimated leakage is 0.046 lb/sec total, which is 1% of the nominal combustion air.

After run 008, one cooled material specimen probe was removed from the bed and disassembled for metallurgical analysis. It was observed that the specimens were tightly bonded so that there was no evidence of coolant leakage. These probes had been designed to minimize coolant leakage through close fitup and tolerances, and the evidence indicates that the design integrity as well as assembly procedures were successful. Thus, the indication is that under prolonged exposure, the scale deposit seals the specimens so that there is no significant coolant leakage.

Circumferential Temperature Profile. This experiment was conducted where a given flowrate was maintained while the probe was rotated to various positions to obtain circumferential temperature profiles. Two series of experiments were conducted with coolant flowrates of 0.036 lb/sec and 0.012 lb/sec, and the results are shown in Fig. 4-229. The greatest variation was found at T_1 located near the wall of the unit. At the end of the probe, the variation was less than 10 F for both flowrates.



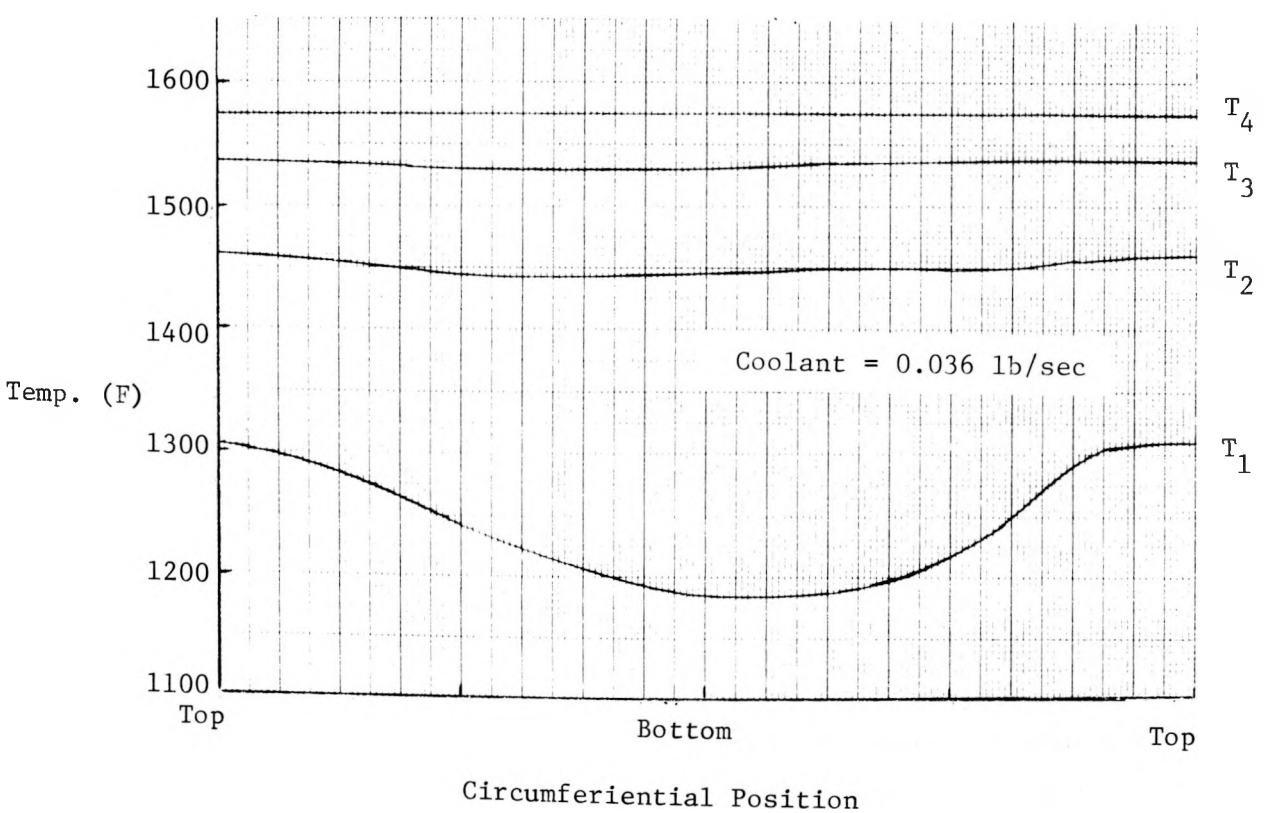


Figure 4-229. Circumferential Temperature Profile

Effect of Bed Temperature. Figure 4-230 presents the history of a given specimen temperature with the bed temperature with a constant coolant flowrate. As expected, the specimen temperature tends to follow variations in the bed temperature.

Ash Recycle. During checkout of the ash recycle system at the start of run 005, the speed of the rotary valve was varied to achieve recycle rates of one to several times the coal feedrate. At the higher rates, the ash hoppers were rapidly depleted, requiring frequent filling operations. The recycle rate selected for most of the subsequent operation was about two times the coal feedrate as this required a filling operation of one time per hour. For steady-state operation, all of the flyash was collected in the baghouse hopper. The effect of ash recycle on limestone utilization could be observed. An almost immediate increase in sulfur dioxide level was observed whenever the ash recycle was stopped, and correspondingly, a decrease in sulfur dioxide was observed when recycle was resumed.

Analysis of the baghouse ash (Section 4.5.8) showed that the calcium carbonate dropped from 9% to about 0.3% when ash recycle was used. The unburned carbon also dropped from about 10% to 5% when ash recycle was used. Thus, ash recycle achieved the expected results of improved limestone utilization and carbon burnup. The unburned carbon is less than 1% of the total available in the fuel and unreacted calcium carbonate is about 4% of the total in the limestone.

The heat loss in the ash recycle system is about 0.7%, which is a small penalty considering the improvements in carbon burnup and limestone utilization. This heat loss could be reduced by insulating the ash recycle system.

Bed Temperature Profiles. A special experiment was conducted during run 006 to measure the bed temperature horizontal profile at various locations in the bed. The bed temperatures are normally monitored by a series of vertical measurements where the thermocouples are inserted about 1 to 2 inches from the wall. During run 006, the oxygen partial pressure probe was used to measure the horizontal temperature profile from the wall to 33-inches insertion at three different bed heights. During these measurements, the normal wall probes were recorded.

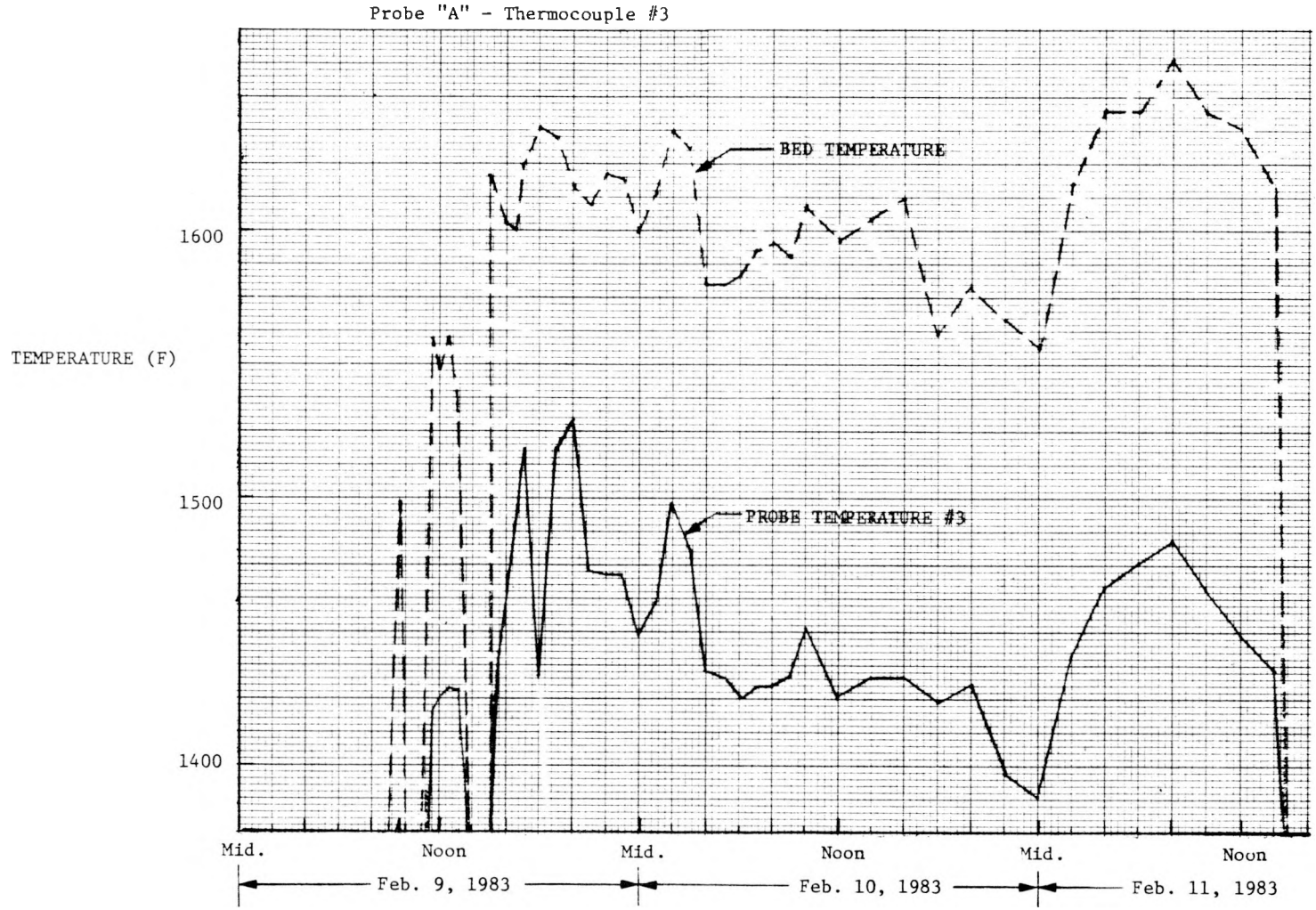


Figure 4-230. Variations in Material Specimen Probe Wall Temperature with Bed Temperature

The results indicate that the bed temperature is very uniform throughout the bed with a temperature variation that is almost within the range of measurement accuracy. The results are presented in Table 4-109 where the mean horizontal temperature is compared to the mean vertical (wall) temperature for each of the three traverses. The standard deviation of the variation in temperatures is shown where the horizontal variation was about 7 F and the vertical variation was about 14 F.

TABLE 4-109. BED TEMPERATURE PROFILE

PROBE HEIGHT, INCHES	MEAN HORIZONTAL TEMPERATURE (3 TO 33-INCH INSERTION), F	MEAN VERTICAL TEMPERATURE (6 TO 103-INCH HEIGHT), F
19	1690 ±7	1679 ±14
49	1659 ±9	1669 ±13
83	1665 ±4	1673 ±14

NOTE: HORIZONTAL TEMPERATURES WERE 11 MEASUREMENTS AT 3-INCH INTERVALS
VERTICAL TEMPERATURES WERE 5 MEASUREMENTS AT ABOUT 24-INCH INTERVALS

Gas Temperature Rakes. Four temperature probes were installed on runs 007 and 008 in the convection heat exchanger region to measure the uniformity of the combustion gas temperature. Probes were installed across the unit below the heat exchanger and half way across the unit in the middle (soot blower cavity) and above the heat exchanger.

Typical results are shown in Fig. 4-231 along with the normally measured wall temperatures. The results show a uniform temperature profile below the heat exchanger, while there is some temperature gradient in the middle and above locations.

Solids Inventory. An inventory of the solids was conducted to monitor the consumables used and determine the amount of disposal material generated. The consumables (coal and limestone) were accurately measured as part of the normal run procedure. The disposal material (bed drain and flyash) was measured on some runs by weighing each drum while on other tests, a simple drum count was made.

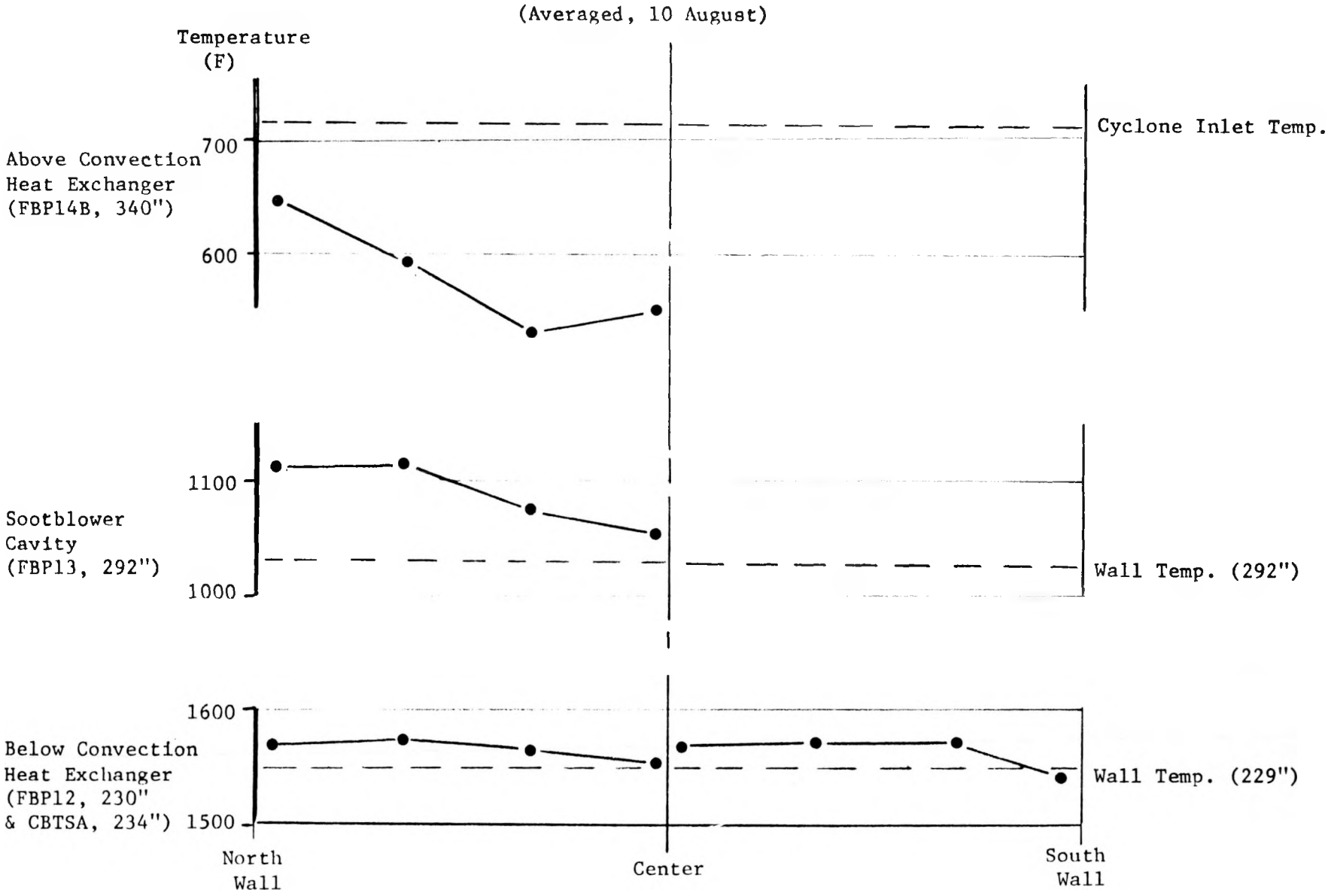


Figure 4-231. Temperature Rake Data - Run 007

An estimate of the net material added to the system was made, which included the coal ash, calcium oxide, initial charge of spent bed material, unburned carbon, and sulfur dioxide (added to solid compounds). The solids inventory and balance is presented in Table 4-110, along with some of the simplified assumptions. While this analysis is not rigorous and some of the material weights are approximate, the inventory balance is sufficiently close to estimate the amount of solid materials generated.

The inventory balance in Table 4-110 provides reasonable agreement between the solids added and removed from the system. Under nominal operating conditions, the amount of bed drain material and flyash material generated are each 20 to 25% of the coal feedrate; this agrees with established rule-of-thumb values for AFB operation.

4.5.8 Solids Analysis

Periodically, samples of the coal, limestone and ash material were taken for analysis. These analysis were then used in some of the results discussed in Section 4.5.7. The analysis were documented in References 1-17, 1-18 and 1-19. This section presents some of the typical results.

Coal Analysis. The coal used for these tests was Illinois No. 6 and, periodically, samples were analyzed for proximate and ultimate analysis plus heat of combustion. Typical analysis of coal used during the latter tests is presented in Table 4-111 along with the analysis of the coal when first received.

The coal was received in the summer of 1982 and used during the test program which was conducted from fall of 1982 until fall of 1983. The as-received coal had a relatively low moisture content. Over the period of 1 year, the moisture content increased where the final product had 10% moisture. Also, there was some aging of the coal as the oxygen content increased and the heating value decreased.

The coal size distribution is shown in Fig. 4-232 for the coal prepared at the coal preparation facility. Initially, the existing crusher produced coal considerable smaller than desired. After several modifications, the size distribution was near the preferred characteristics.

TABLE 4-110. SOLIDS INVENTORY

CONSUMABLE USED - LB	001	002	003	004
Coal	39,000	21,060	44,680	70,660
Limestone	10,220	10,730	17,480	19,175
SOLIDS ADDED - LB				
Coal Ash (1)	4,060	2,110	4,470	6,660
CaO (2)	5,480	5,750	9,370	10,270
Spent Bed Material	-0-	8,990	8,290	12,410
Unburned Carbon, SO_2 (3)	4,875	2,630	5,590	8,830
	14,415	19,480	27,720	38,170
SOLIDS REMOVED - LB				
Bed Drained	-0-	6,400	8,800	12,650
Post Bed Material	9,260	8,290	10,000	10,495
Flyash	4,190	5,340	9,810	11,920
	13,450	20,030	28,610	35,060

(1) Coal ash assumed to be 10.0% for Runs 001 to 003, and 9.4% for Run 004

(2) CaO assumed to be 53.6% of limestone

(3) Carbon in coal assumed to be 65% and carbon utilization was assumed to be 90%. Sulfur in coal was assumed to be 3% while SO_2 removal was 80%. The net material added is approximately 12.5%

TABLE 4-111. COAL ANALYSIS

	AS Received 8/27/82	RUN 007		RUN 008		
		8/11/83	8/15/83	9/21/83	9/26/83	9/27/83
ULTIMATE						
Moisture - %	3.88	8.18	8.39	10.02	10.70	10.76
Carbon - %	65.02	61.17	60.79	58.61	57.22	55.92
Hydrogen - %	4.81	4.65	4.65	4.50	4.38	4.19
Nitrogen - %	1.23	1.04	1.15	1.15	1.15	1.16
Sulfur - %	2.98	3.04	2.88	2.68	2.60	2.60
Ash - %	10.25	10.54	9.71	10.76	10.98	11.61
Oxygen (by difference)	11.83	11.38	12.43	12.28	12.97	13.76
PROXIMATE						
Moisture	3.88	8.18	8.39	10.02	10.70	10.76
Volatile Matter	41.36	37.20	38.96	35.26	34.96	34.47
Ash	10.25	10.54	9.71	10.76	10.98	11.61
Fixed Carbon(by difference)	44.51	44.08	42.94	43.96	43.36	43.16
HEAT OF COMBUSTION						
Gross - Btu/lb.	11,780	10,840	10,980	10,470	10,360	10,090

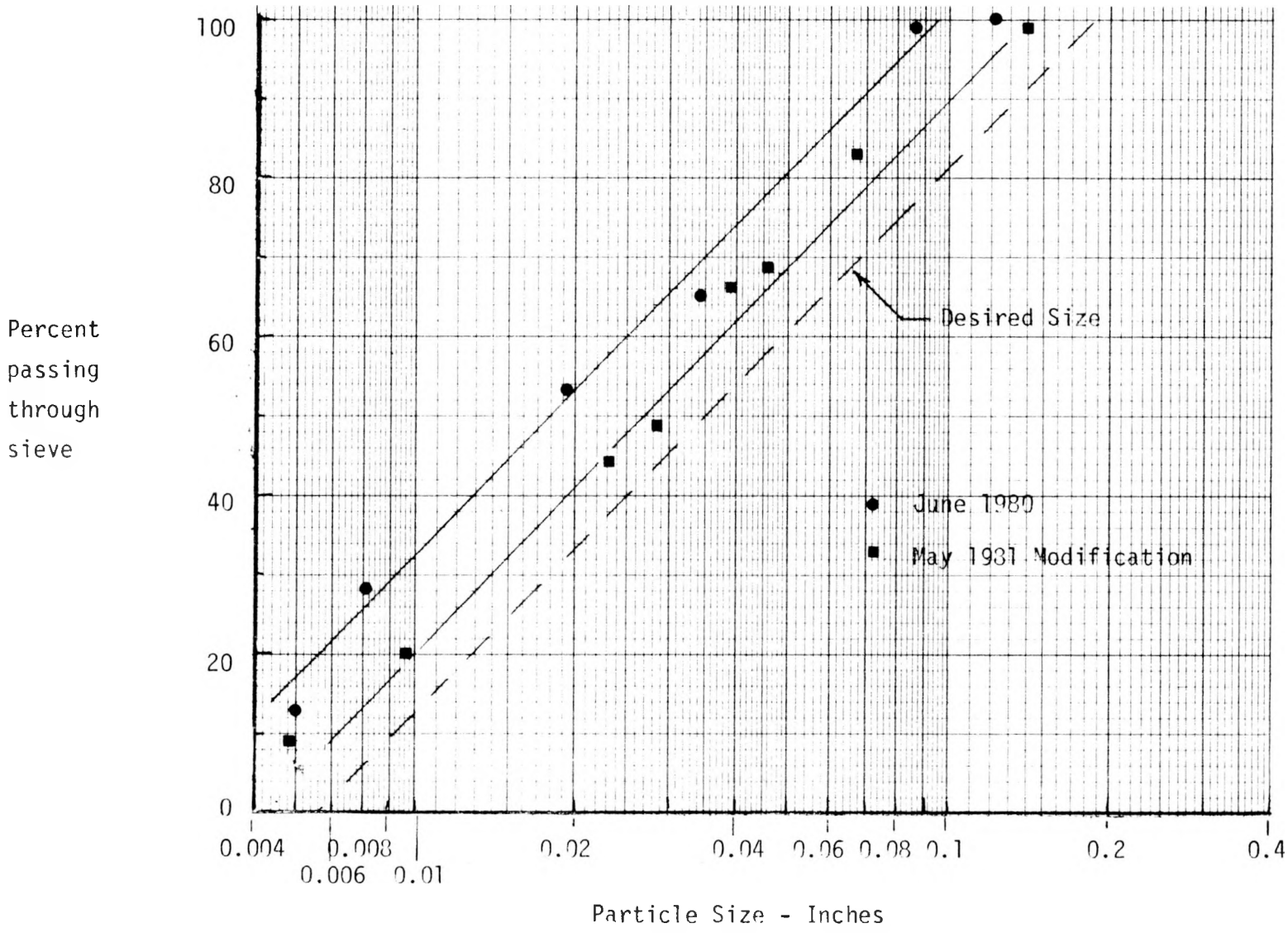


Figure 4-232. ESG Coal Particle Size Distribution

Limestone Analysis. The limestone used in the 6' x 6' AFBC program is referred to as Grove. This type of limestone was selected early in the program to be used by both Battelle and Rocketdyne for consistency of test results. The limestone was purchased in sealed drums from Gemstar Building Materials, Stephens City, VA; the limestone is their standard 6 mesh by 30 mesh product.

At the start of the test program, samples were selected to verify the size and chemical composition. The size distribution was measured at the Rocketdyne Materials and Processes Laboratory, using available sieves and compared to the vendor data. The results shown in Table 4-112 indicate that the sample reasonably matches the vendor's data.

TABLE 4-112. SIZE DISTRIBUTION

	% PASSING SIEVE	
MESH SIZE	SAMPLE RESULTS	VENDOR SPECIFICATION
6	--	99.8
8	94.7	91.1
20	13.8	14.7
30	5.3	4.3
200	4.4	--

A sample was sent to a chemical laboratory. The results were that the calcium (Ca) was 39.0% and carbonate (CO_3) was 59.0%. Thus, the $CaCO_3$ would be 97.5% and 0.5% remaining CO_3 would be in the form of $MgCO_3$. This compared favorably with the vendor's data and results presented in the literature. Grove limestone has been designed by Argonne National Laboratory as ANL-9501; the properties are tabulated in ANL/CEN-FE-80-10, "Sulfur Control in Fluidized Bed Combustors," dated September 1980.

Another sample was taken during the latter portion of the program with a different batch of limestone. The chemical analysis was essentially the same.

Ash Analysis. Samples of the cyclone ash, baghouse ash, and bed drain were periodically taken to assess the performance of the unit. Typical results are presented in Table 4-113, which compares the ash under the conditions of ash recycle and no ash recycle. Ash recycle had a significant reduction in unburned carbon and unreacted calcium carbonate in both the cyclone and baghouse ash samples.

TABLE 4-113. ASH CHEMICAL ANALYSIS

CONSTITUENT, %	RUN 001 BED DRAIN	NO ASH RECYCLE		RUN 007 - ASH RECYCLE			
		RUN 002 CYCLONE	RUN 002 BAGHOUSE	8/11/83 CYCLONE	8/15/83 CYCLONE	8/11/83 BAGHOUSE	8/15/83 BAGHOUSE
CALCIUM	29.1	33.8	31.4	19.8	21.1	10.0	12.5
SULFUR	4.8	4.3	2.7	0.8	0.7	2.3	3.7
CARBON	0.1	17.0	10.7	0.8	0.8	4.3	5.2
CO_3	0.9	9.4	8.6	0.5	0.6	0.2	0.3

4.5.9 Oxygen Partial Pressure Characterization

The results of other AFB development activities on this program, along with interpretation of the results provided by other investigators, lead to the conclusion that many candidate alloys for the bed heat exchanger would provide a much more satisfactory service life in an oxidizing bed environment than in a reducing bed environment. A major objective of the 6' x 6' AFBC characterization test series was to map the oxidizing potential of the fluidized bed and to investigate the influence of the physical and operational parameters on the oxidizing potential. The purpose of this investigation was to develop designs and criteria so as to maintain an oxidizing environment throughout the bed heat exchanger region.

The initial oxygen partial pressure (PO_2) probe activity was conducted on run 004. This probing was essentially repeated during runs 005 and 006 where an extensive amount of PO_2 probe activity was conducted. These results thoroughly characterized the fluidized bed. Verification probing also was conducted during the subsequent material specimen exposure test series (runs 007 and 008).

This section discussed the results from runs 005 and 006 PO_2 probing plus the runs 007 and 008 PO_2 verification activity.

Oxygen Partial Pressure Probe Operation. The oxygen partial pressure had been shown to be an important parameter that can be related to erosion/corrosion phenomenon of tube materials. Reducing zones have been shown to have a severely detrimental effect on tube life, and, therefore, a good fluidized bed design would avoid prolonged operation at reducing conditions in the bed heat exchanger region. The oxygen partial pressure probe was used by Battelle during their 24-inch AFB testing to determine the influence of the bed design and operating conditions on the oxygen environment in various locations. During this test series, the techniques for using the probe were developed and refined.

A probe was designed and fabricated for the 6' x 6' AFBC based on the BCL design, and this probe as well as the BCL probe was used to extensively characterize the bed during runs 005 and 006 for a variety of distributor area configurations and operating conditions.

The 6' x 6' AFBC has a number of ports available for the probe that provide vertical locations to most quadrants at just below, middle, and just above the heat exchanger. Ports are generally provided near the wall, center of the quadrant, and between quadrants in many of the areas.

A series of traverses was made from the wall into the bed, and data were recorded at each location for ~40 seconds. The PO_2 level was recorded at a rate of 100 slices per second and reduced at averaged intervals of 4 slices or 25 intervals per second. At each interval, the PO_2 was analyzed to determine if it was oxidizing, reducing, or in-between. Oxidizing was defined as being greater than $10^{-3.4}$ atm, and reducing was defined as being less than 10^{-12} atm. Over a period of 40 seconds, the fraction of points defined as oxidizing and reducing was determined. The percent of time oxidizing or reducing was then plotted as a function of the distances from the wall to map the conditions in a traverse at the various ports. These traverses were from the wall to 33 inches into the bed in 3-inch increments.

A series of these PO_2 plots was obtained for various configurations and operating conditions to establish criteria for creating a "healthy" bed environment throughout the bed heat exchanger region. An acceptable environment was defined as being predominantly oxidizing and, presumably, the more time that the condition was oxidizing, the better the environment.

The following sections provide a description of the PO_2 results. Typically, for all of the conditions characterized, the bed environment was found to be acceptable in all regions of the heat exchanger with the exception of just over the coal feed port for some of the configurations. Two coal port arrangements did provide acceptable oxidizing environments over the port and met all criteria for a "healthy" combustion environment. The best results were obtained with the four coal ports per quadrant arrangement. Acceptable results also were obtained with the 13% augmented air on the one coal port per quadrant arrangement. This latter configuration has the advantage of being more practical for commercialization from the standpoint of simplicity, maintainability and reliability.

Run 005 Bed Characterization. A summary of the oxygen partial pressure results is presented for run 005 which included both conditions of no recycle and ash recycle. The quadrants had various distributor/coal port configurations which included a plume distributor, four coal ports, reference coal port, and reference coal port with added augmented air. These arrangements have been described in previous sections.

Typical Presentation Of Results. The probe ports used during this test are illustrated in Fig. 4-233 through 4-235 which show the locations and port identifications just below, middle of, and just above the bed heat exchanger. Figure 4-236 is typical of the series of PO_2 plots obtained which indicate the percent of time oxidizing (circles) or reducing (squares) versus the traverse from the wall (0-inch depth) toward the center of the bed (36-inch depth). When the oxidizing and reducing curves cross, the area between is cross hatched for clarity.

A typical arrangement for presenting the data is shown in Fig. 4-236 where the bottom, middle, and top rows of plots represent locations of below, middle, and top of the heat exchanger. The fourth digit in the port identification represents the elevation, as shown in Fig. 4-236 where "W" refers to west elevation. The last digit represents ports going from left to right when viewing the elevation. Thus, "A" is near the left wall, "B" is in the center of a quadrant (generally over a coal port), "C" is between quadrants, "D" is in the center of the next quadrant, and "E" is near the right wall. This can also be observed on the plan view shown in Fig. 4-233.

Another important parameter indicated on the charts is the excess air condition. This is a theoretical number based on the estimated overall air/fuel ratio for each quadrant. While the planned operation was to have all quadrants operating at the same air/fuel ratio (excess air), this was seldom achieved as the fuel feed rate to each quadrant tended to be different. This was because the operators had a good measurement of the overall operation through the excess oxygen measurement; however, monitoring the individual feed systems over a short period was difficult. Also, the air/fuel ratio in a given quadrant could vary with time especially as the operators adjust the coal feeders. Therefore, some of the plots indicate a different excess air for each plot as the PO_2 traverses were all made at different times.

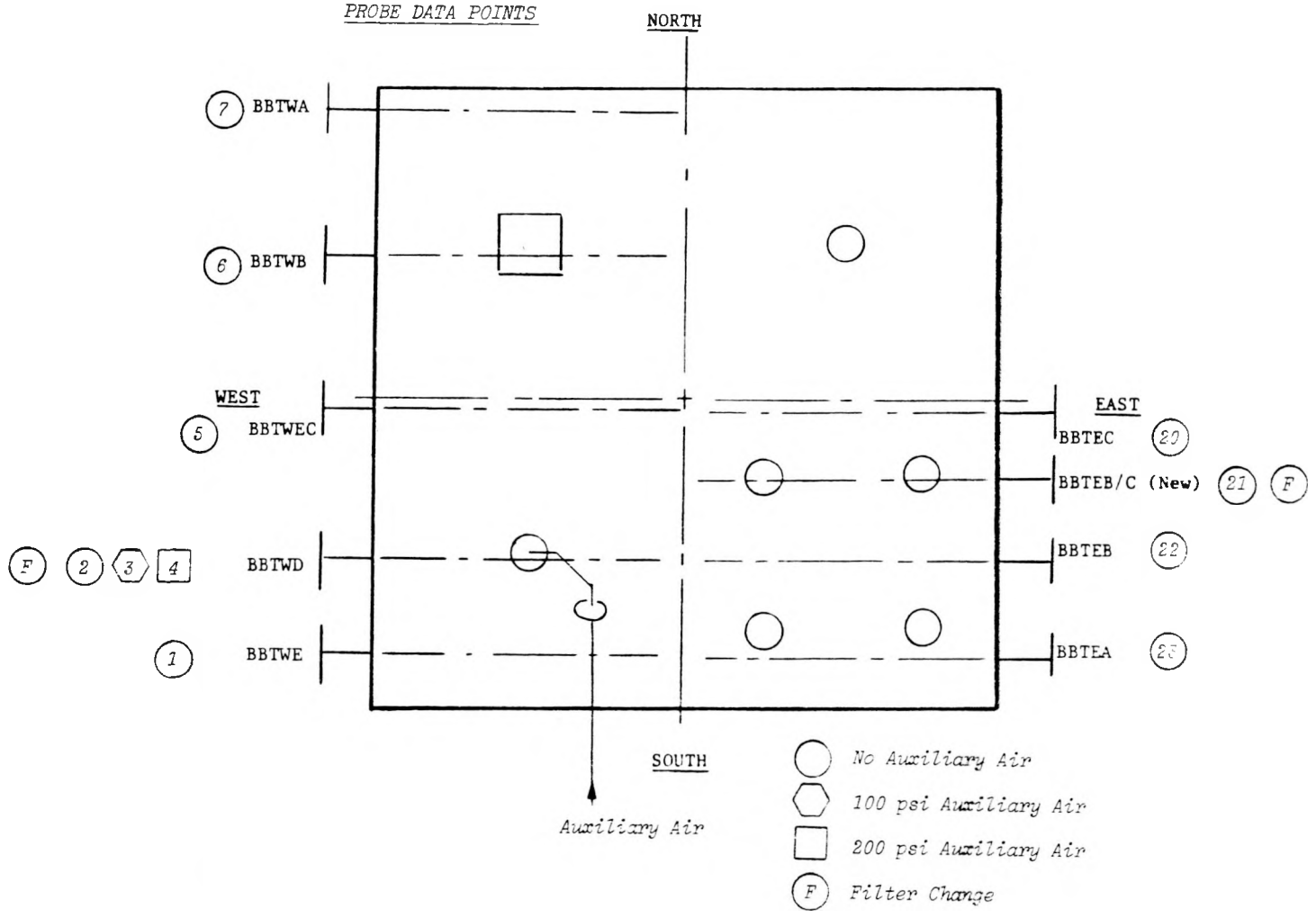


Figure 4-233. PO_2 Probe Locations - Below Bed Heat Exchanger

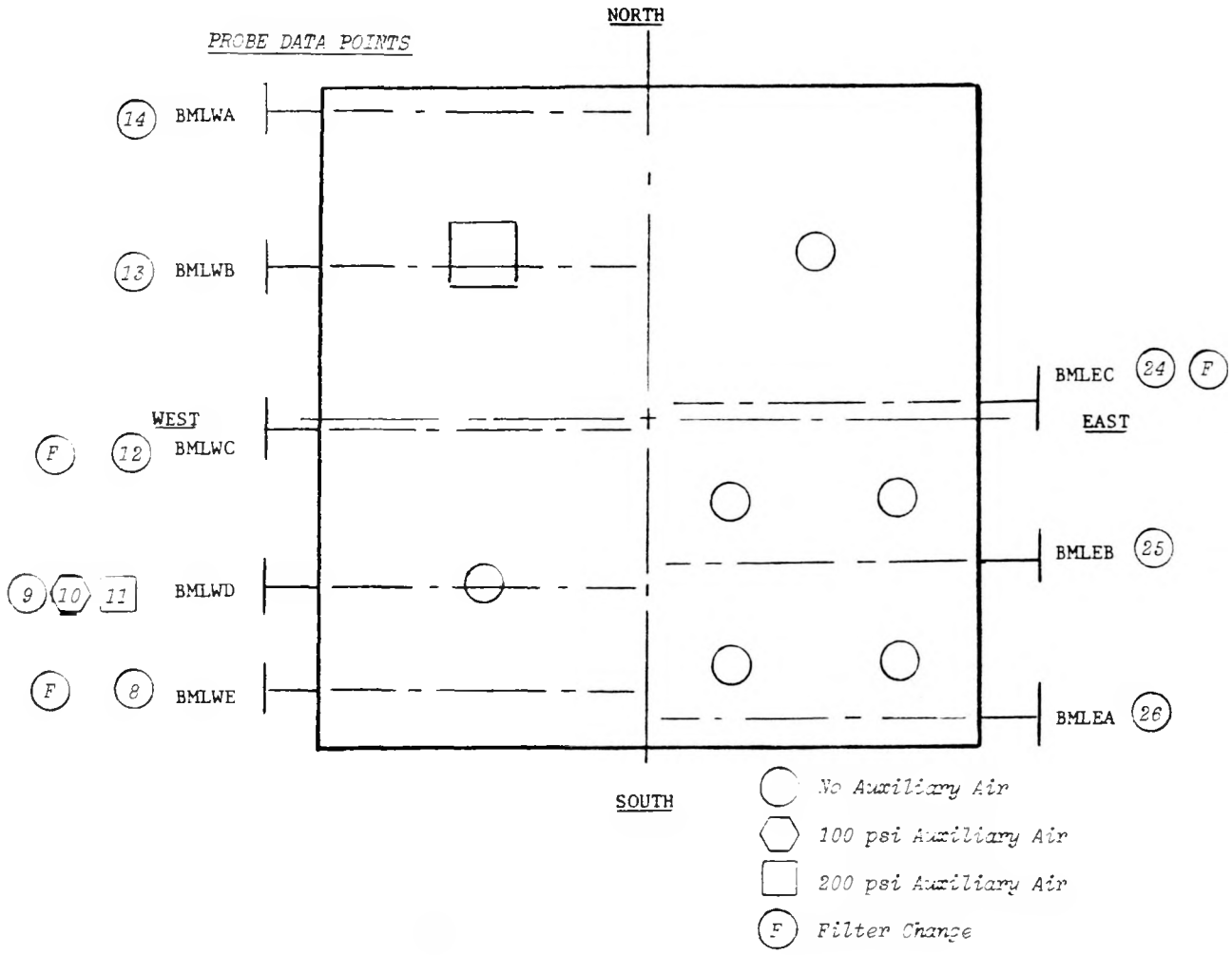


Figure 4-234. PO_2 Probe Locations - Middle Lower Ports of Bed Heat Exchanger

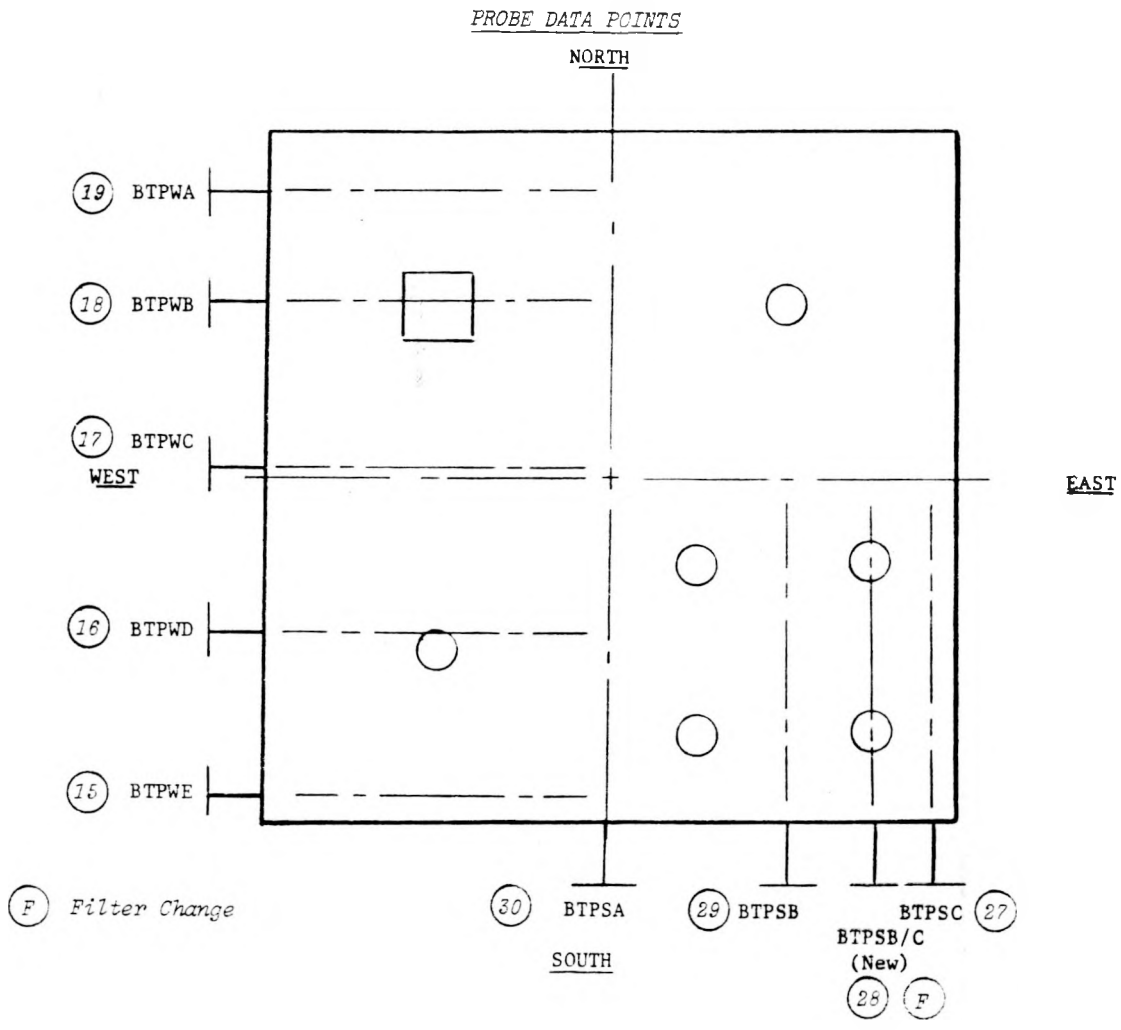
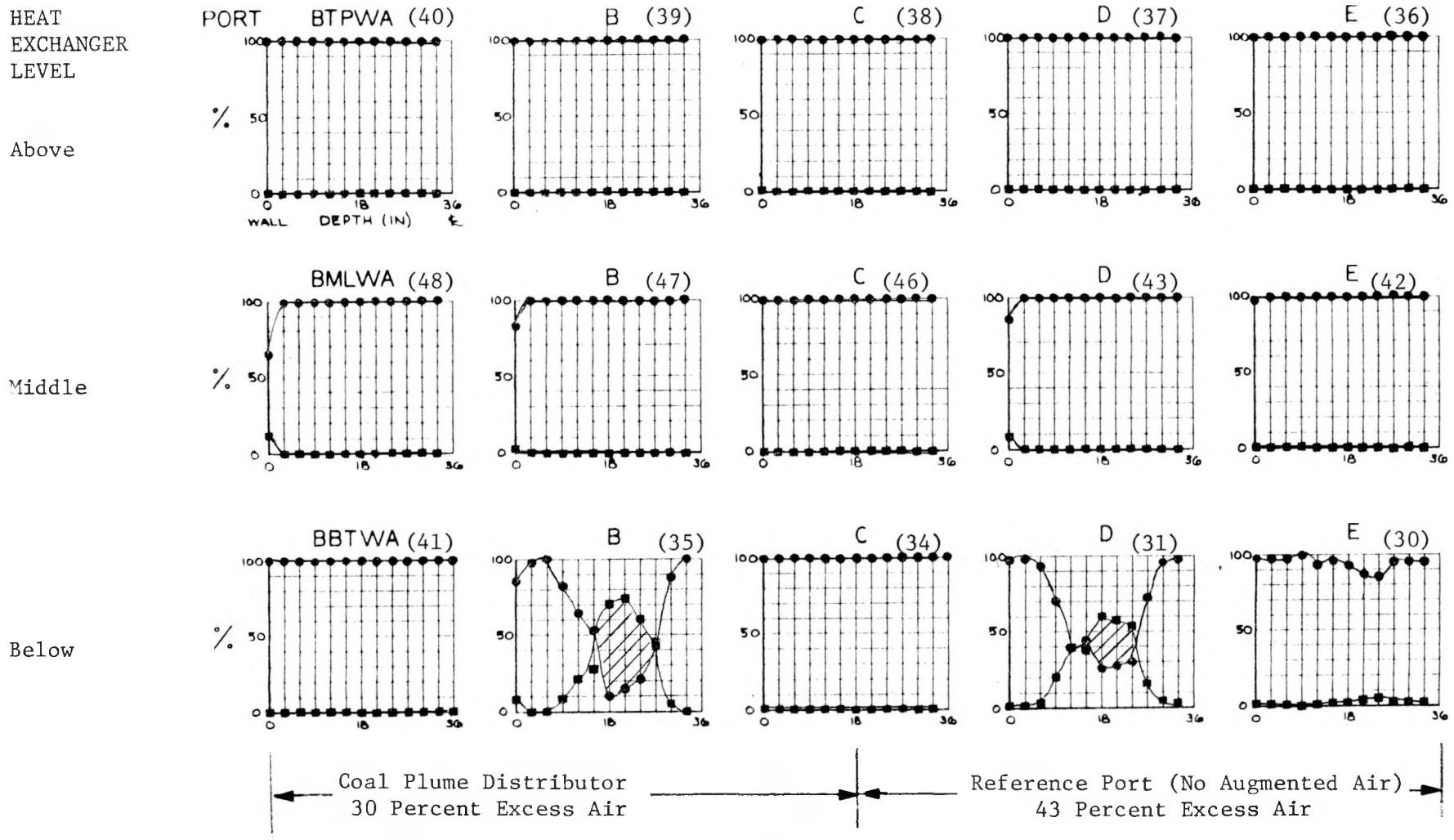


Figure 4-235. PO_2 Probe Locations - Above Bed Heat Exchanger



With Ash Recycle

Figure 4-236. Run 005 PO_2 Data (Coal Plume Distributor and Reference Port)

This estimated air/fuel ratio was based on the averaged coal feed rate fo given quadrant, the coal conveying air, and one-fourth of the ash conveying air and distributor plate air.

Coal Plume Distributor. A complete characterization taken from the west elevation is shown in Fig. 4-236 which covers quadrant No. 1 with the coal plume distributor and quadrant No. 4 with the reference coal port. As previously discussed, ports B (last digit) and D are over the coal ports. All of the plots indicate very good oxidizing enviroments except just above the coal ports. The plot above the reference port has an unacceptable condition, having predominantly reducing conditions, and this trace is very similar to previous test results with this same port arrangement. The trace above the coal plume distributor is also unacceptable, indicating that the distributor as well as adding more distributor air to this region, did not improve the PO_2 characteristics.

Augmented Air. Figure 4-237 presents traverses just above the reference coal port with various amounts of added augmented air from none to 9%. All plots are at the same port location. The no augmented air condition has the unacceptable reducing condition, while 5% augmented air has improved the characteristic to acceptable. A good oxidizing characteristic was obtained when the augmentation was increased to 9%. The conclusion is that adding air directly above the coal port splash plate effectively eliminates the volatiles plume with a reducing environment.

Figure 4-238 is under the same conditions for the location in the middle of the bed heat exchanger, and a very good oxidizing environment is shown for all conditions of augmented air.

Effect Of Ash Recycle. A complete characterization from the west elevation for the condition of no recycle (no ash recycle or conveying air) is shown in Fig. 4-239. These plots can be compared to an identical series which had ash recycle, shown in Fig. 4-236. The curves are very similar, especially over the coal feed ports. The slightly reducing condition noted near the wall on some of the plots was not considered significant as this may be more of a wall effect on the probe reading. Thus, the conclusion is that ash recycle has a small impro ment on the oxygen partial pressure characteristics.

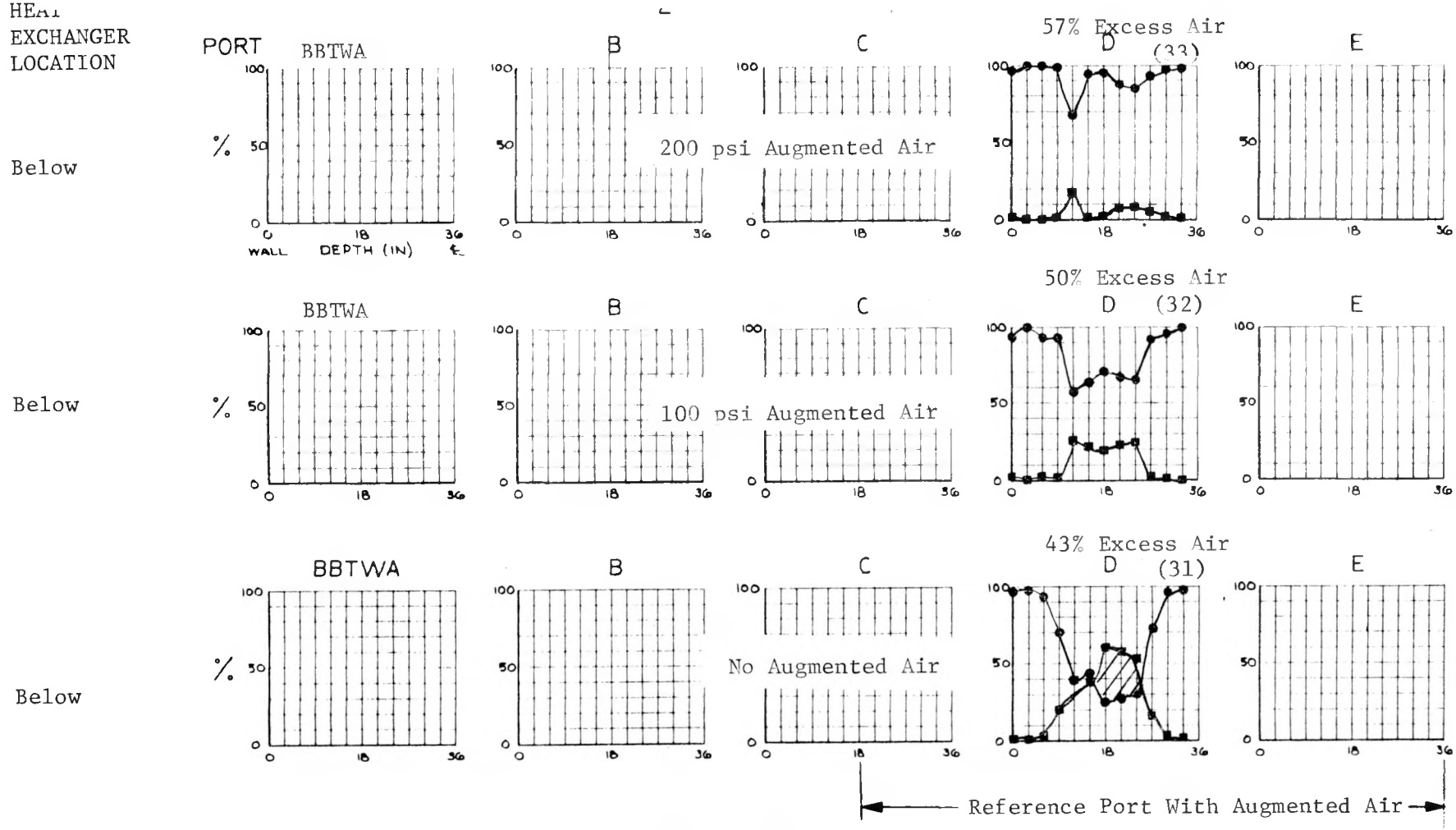
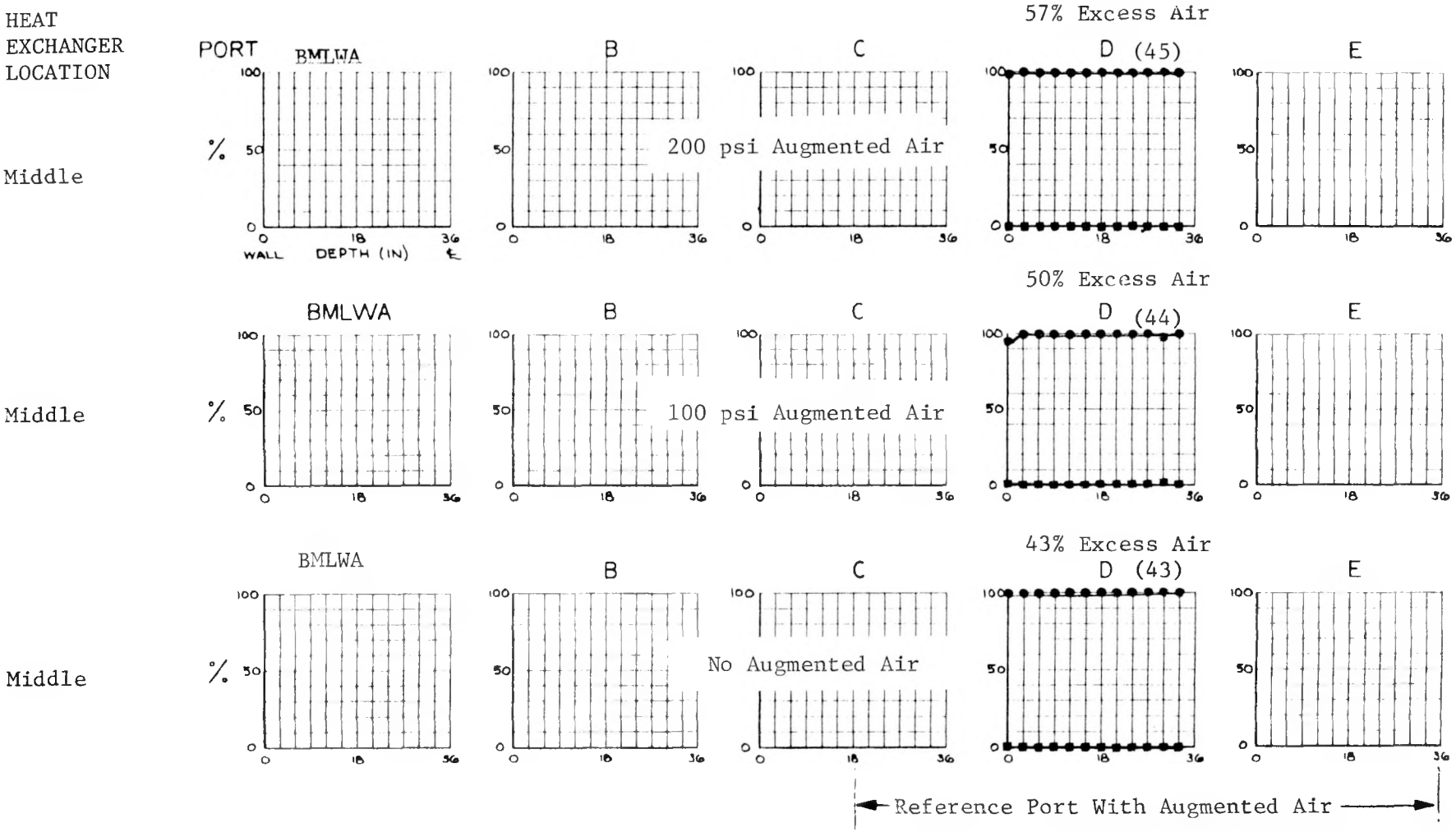


Figure 4-237. Run 005 PO_2 Data (Effect of Augmented Air on Reference Port)



With Ash Recycle

Figure 4-238. Run 005 PO_2 Data (Effect of Augmented Air on Reference Port)

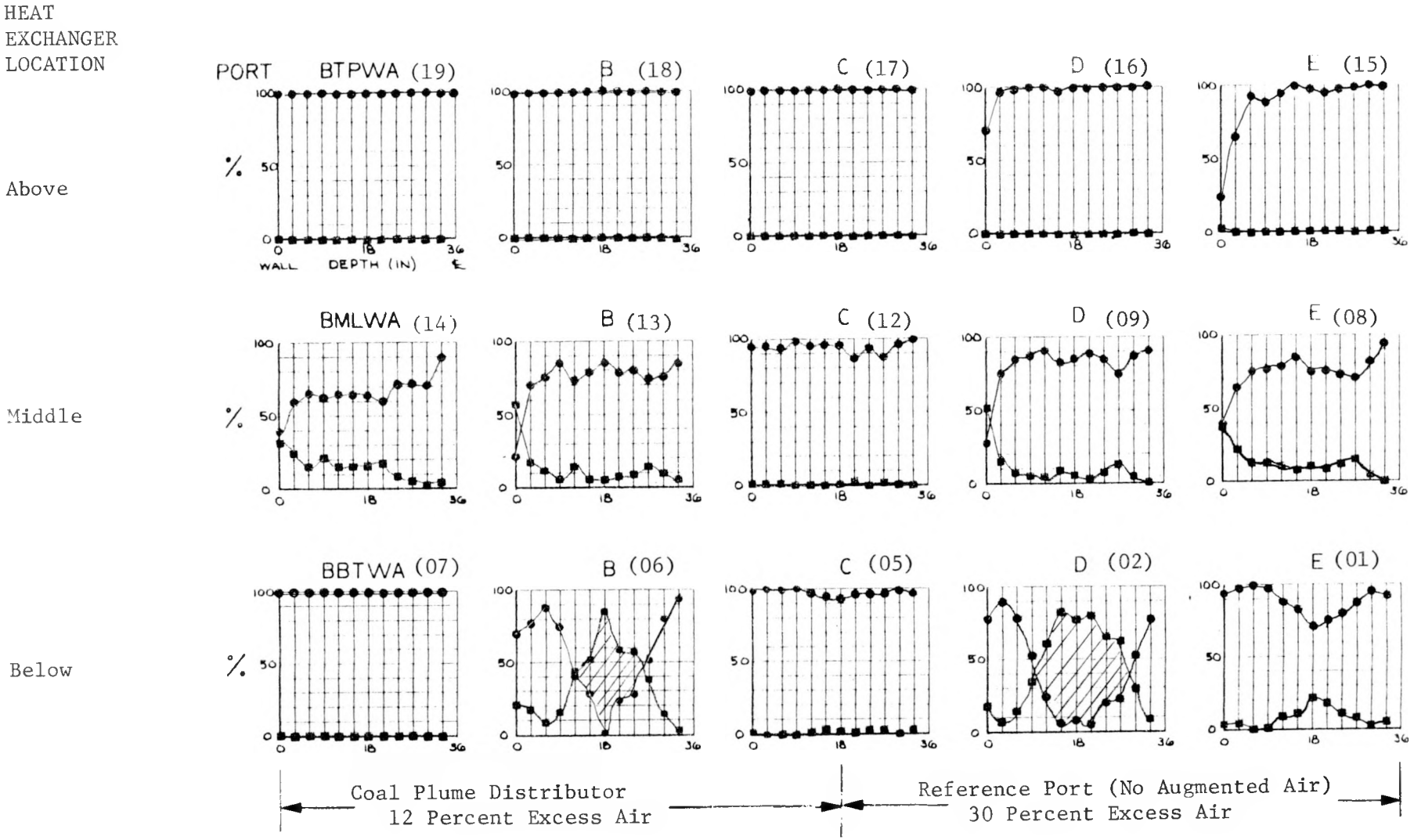


Figure 4-239. Run 005 PO_2 Data (Effect of Ash Recycle on Reference Port and Coal Plume Distributor)

The effect of air augmentation under the condition of no recycle is shown Fig. 4-240 and 4-241. which can be compared to similar plots obtained with recycle, such as shown in Fig. 4-237 and 4-238. The results of the two conditions are again very similar, with no great effect of ash recycle although the recycle plots are somewhat better.

Four Coal Ports Per Quadrant. The characterization of the four coal port arrangements is shown in Fig. 4-242 and 4-243 for the conditions of recycle and no recycle. These figures represent only the one quadrant (No. 3), where Ports A and C represent either near the wall or between the quadrants. Port B/C was added for run 005 so as to be over the coal ports.

Very good oxygen partial pressure measurements were found throughout this quadrant especially over the coal feedports for both conditions of ash recycle. Again, ash recycle had a small but positive effect on the oxidizing environment. The conclusion is that the increased number of coal ports provide the most acceptable environment throughout the heat exchanger region.

Run 006 Bed Characterization. A summary of the oxygen partial pressure results is presented for run 006, which was operated at basically nominal conditions with ash recycle. The quadrants had augmented air, four coal ports, and the reference configuration as described in a previous section. Momentary excursions were made in the amount of augmented air, excess air, and recycle air to investigate these parameters on the bed characteristics. The probe ports used during this test are illustrated in Fig. 4-244 through 4-246, which show the locations and port identifications just below, middle, and just above the bed heat exchanger.

Augmented Air Coal Port. A complete characterization from the west elevation is shown in Fig. 4-247 which covers the augmented air quadrant (No. 1) and the reference quadrant (No. 4). The air/fuel ratio varied during the course of taking the probe data; therefore, excess air values are indicated for each individual plot.

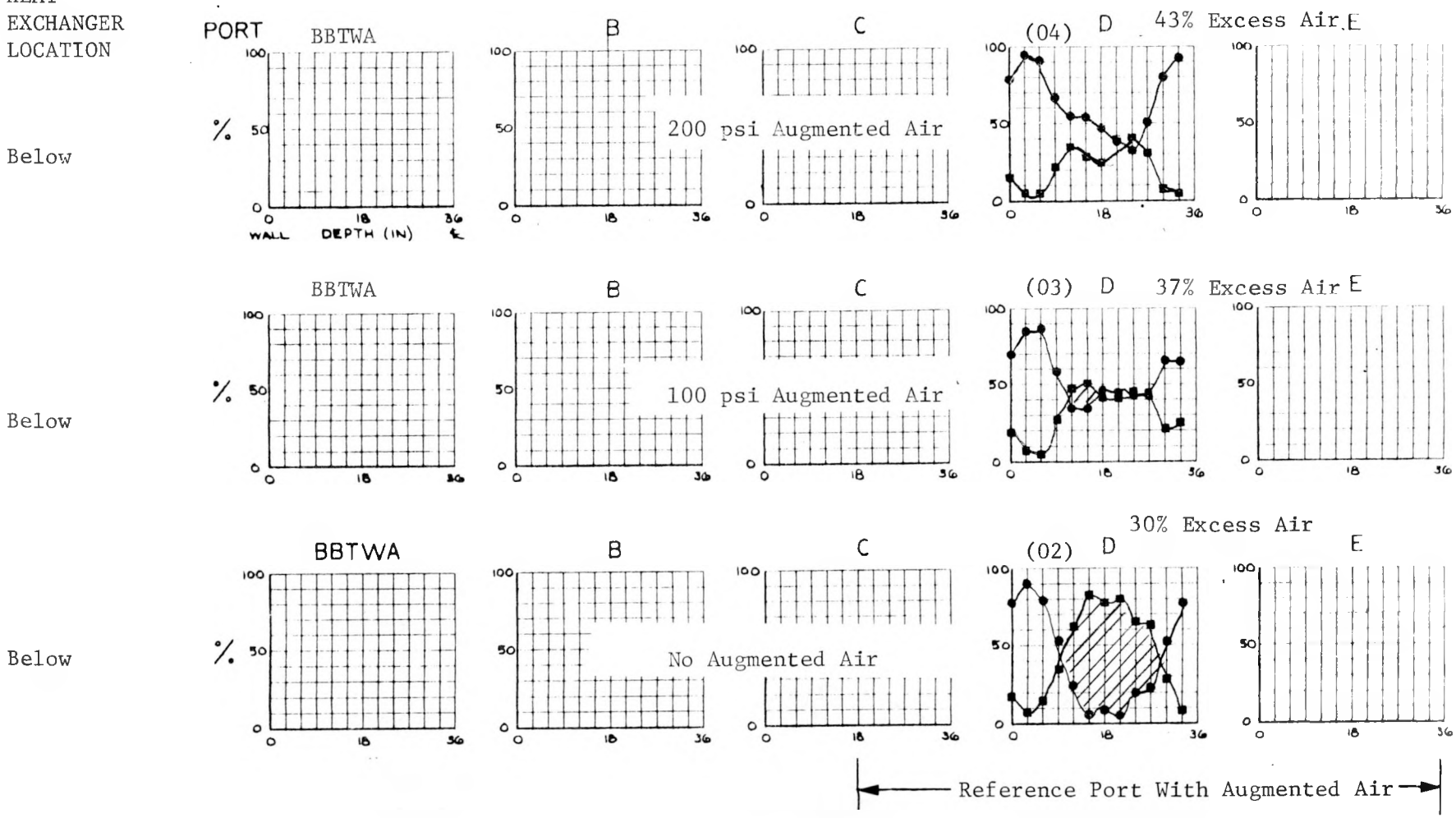


Figure 4-240. Run 005 PO_2 Data (Effect of Ash Recycle on Augmented Air)

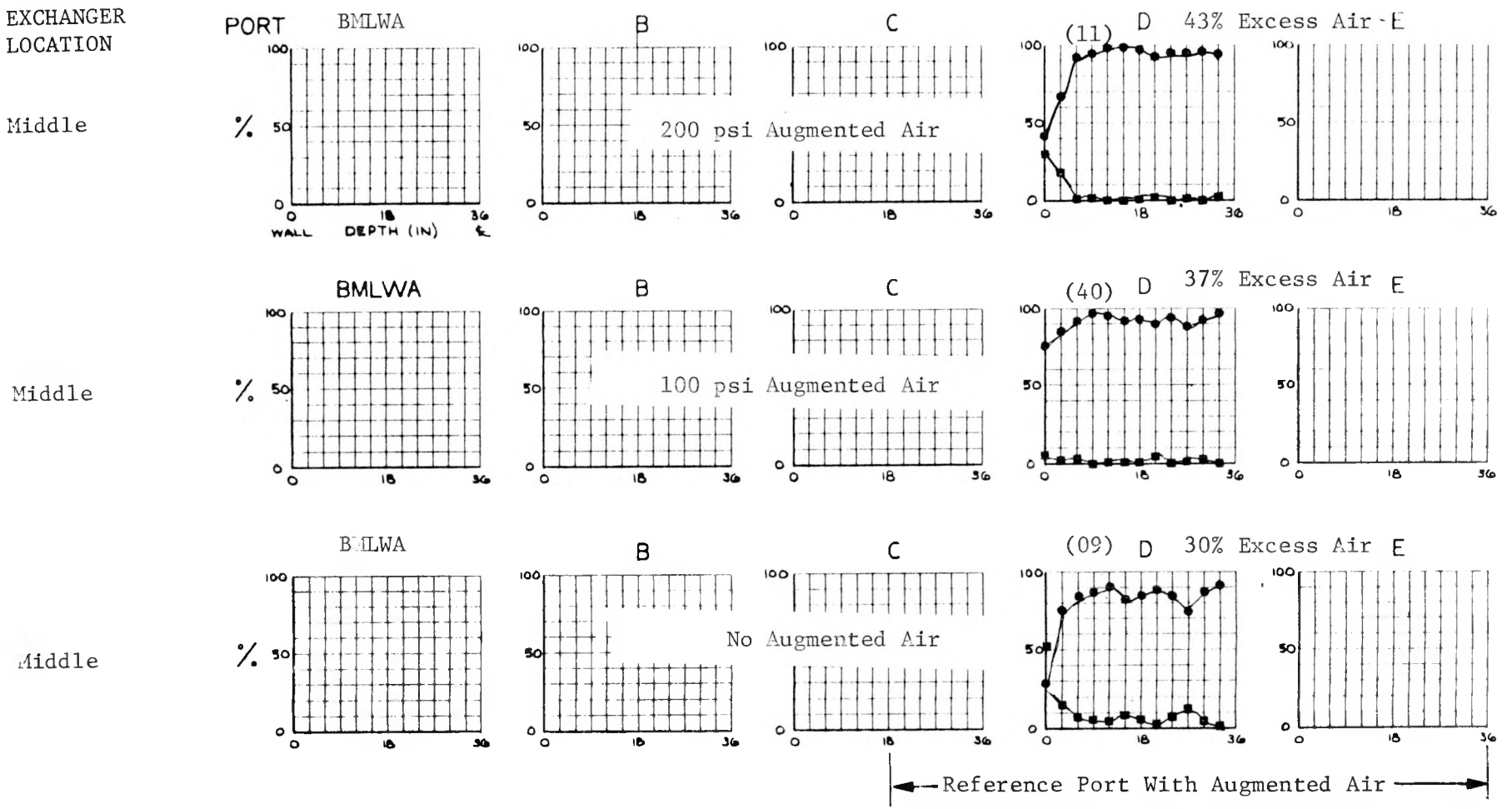


Figure 4-241. Run 005 PO_2 Data (Effect of Ash Recycle on Augmented Air)

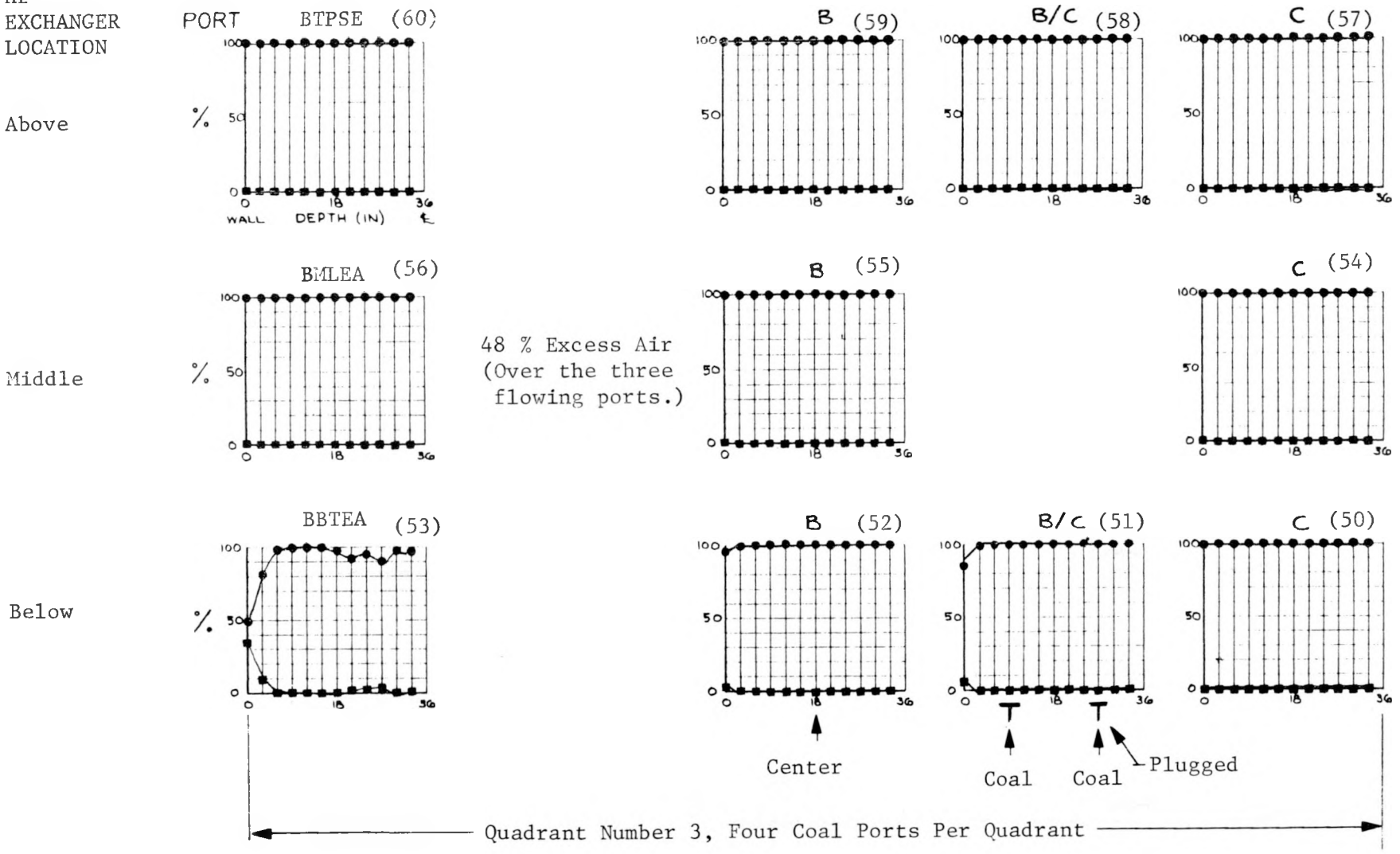


Figure 4-242. Run 005 PO_2 Data (Four Coal Ports Per Quadrant)

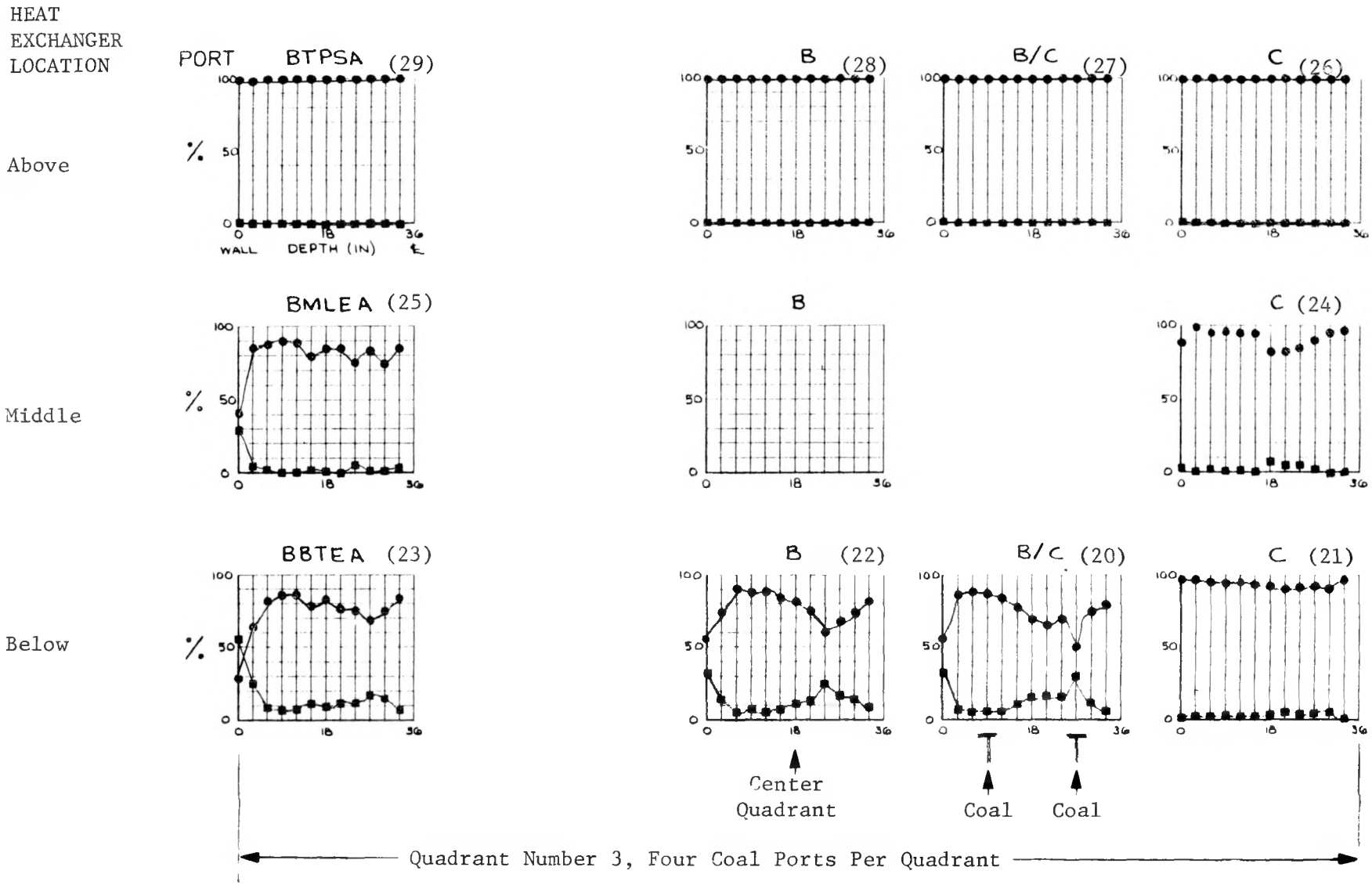
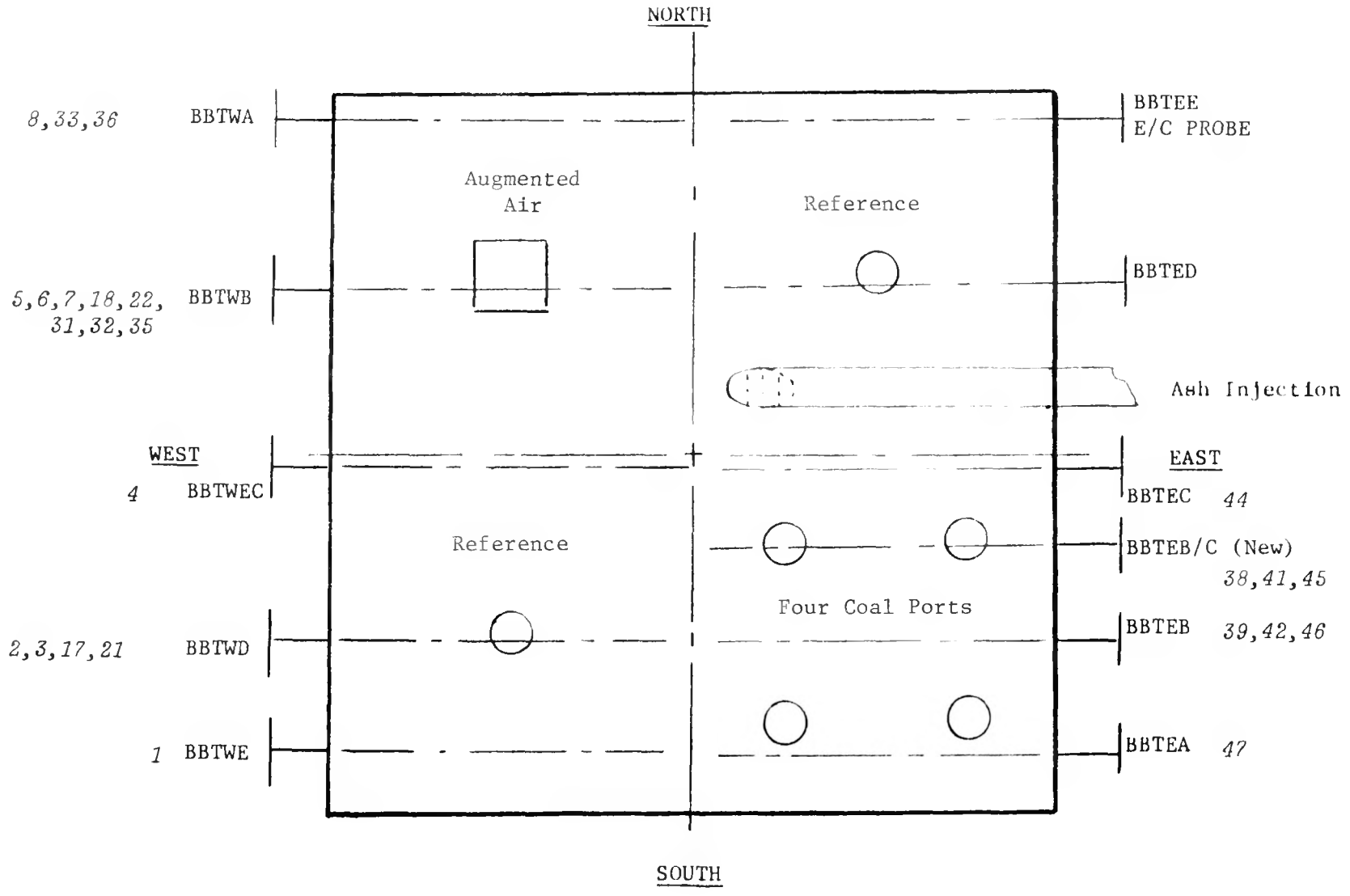
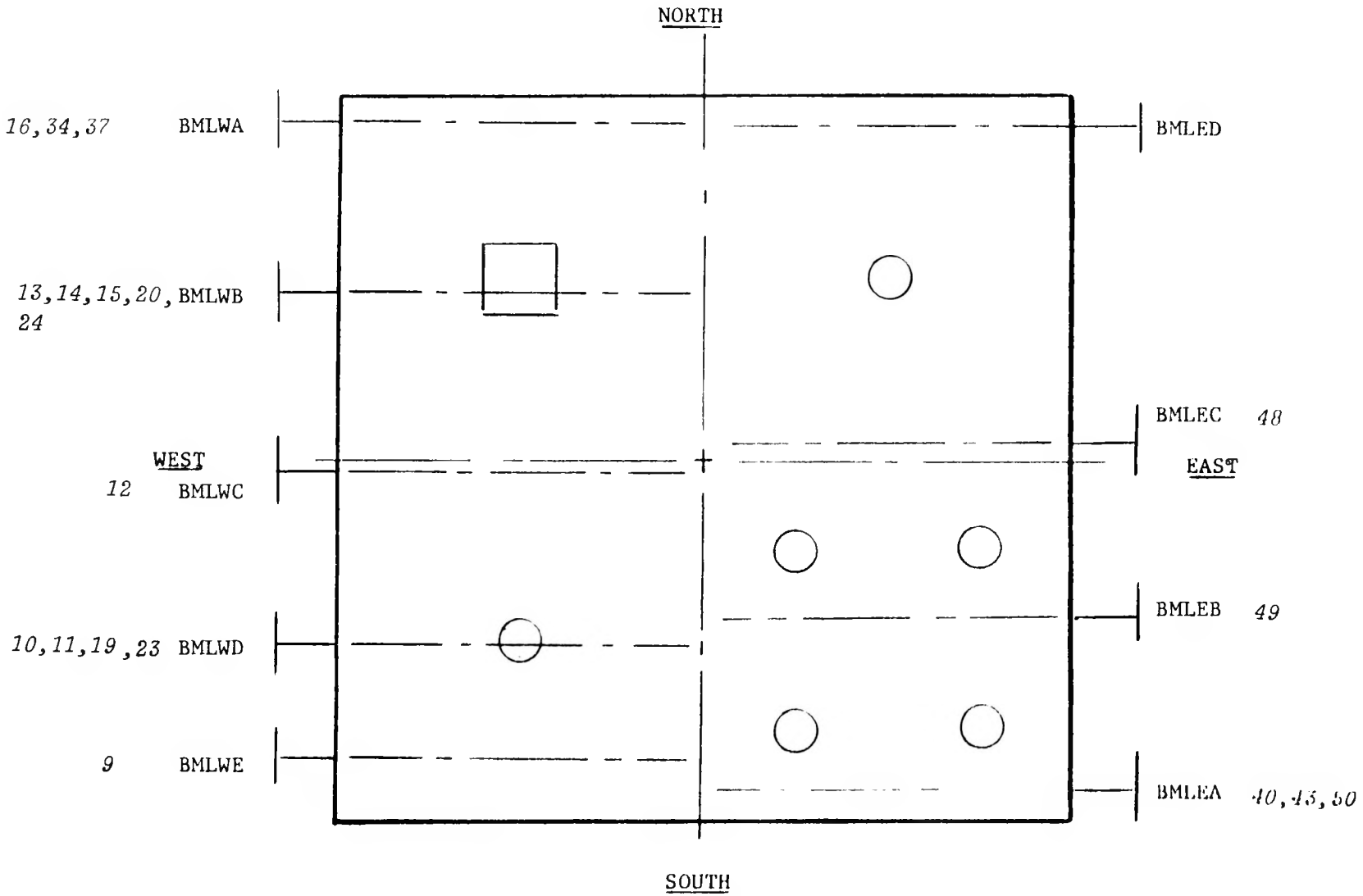


Figure 4-243. Run 005 PO_2 Data (Four Coal Ports Per Quadrant and No Ash Recycle)



NOTE: Numbers are PO_2 data points.

Figure 4-244. Probe Locations - Below Bed Heat Exchanger



NOTE: Numbers are PO_2 data points.

Figure 4-245. Probe Locations - Middle Lower Ports of Bed Heat Exchanger

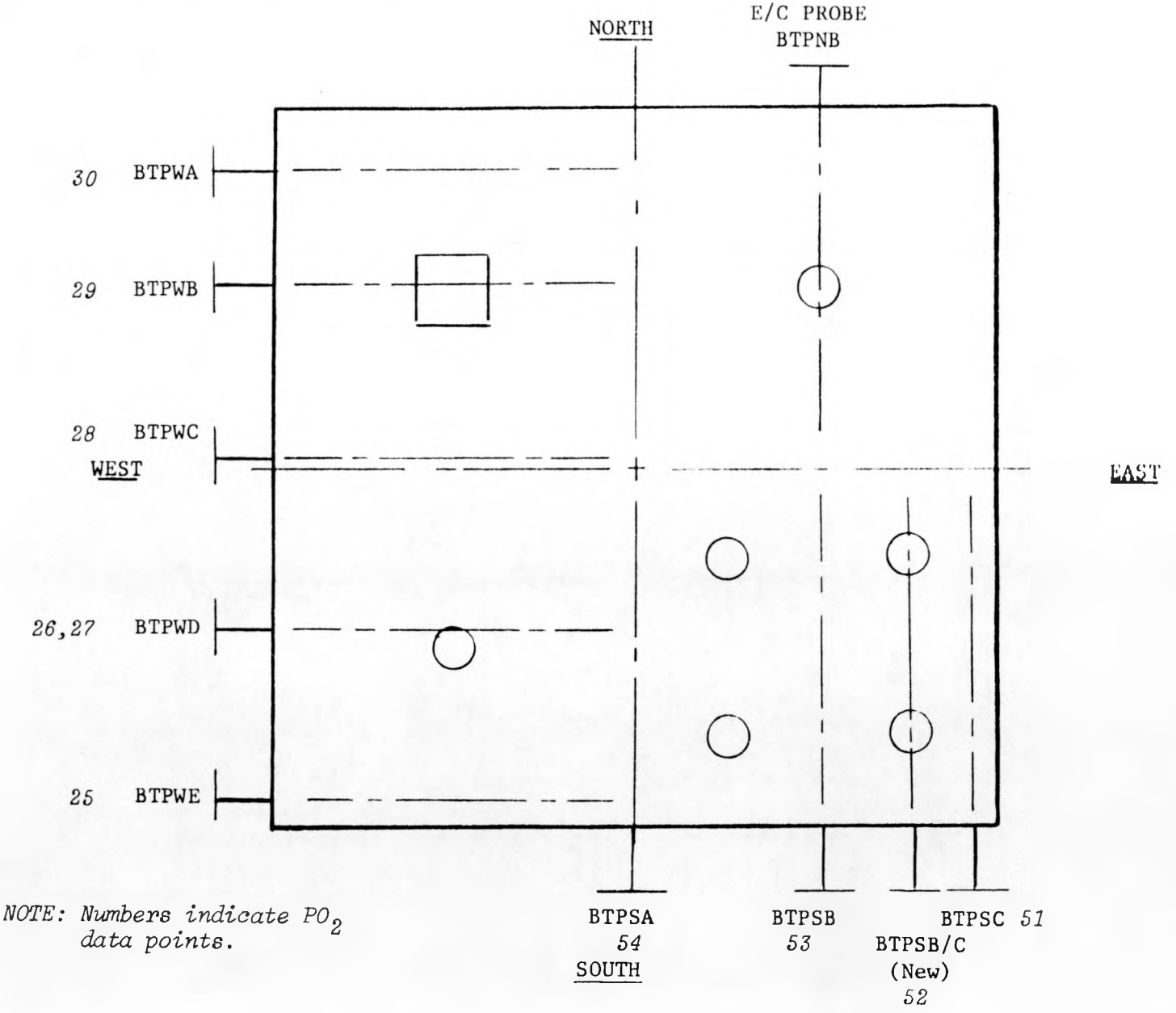


Figure 4-246. Probe Locations - Above Bed Heat Exchanger

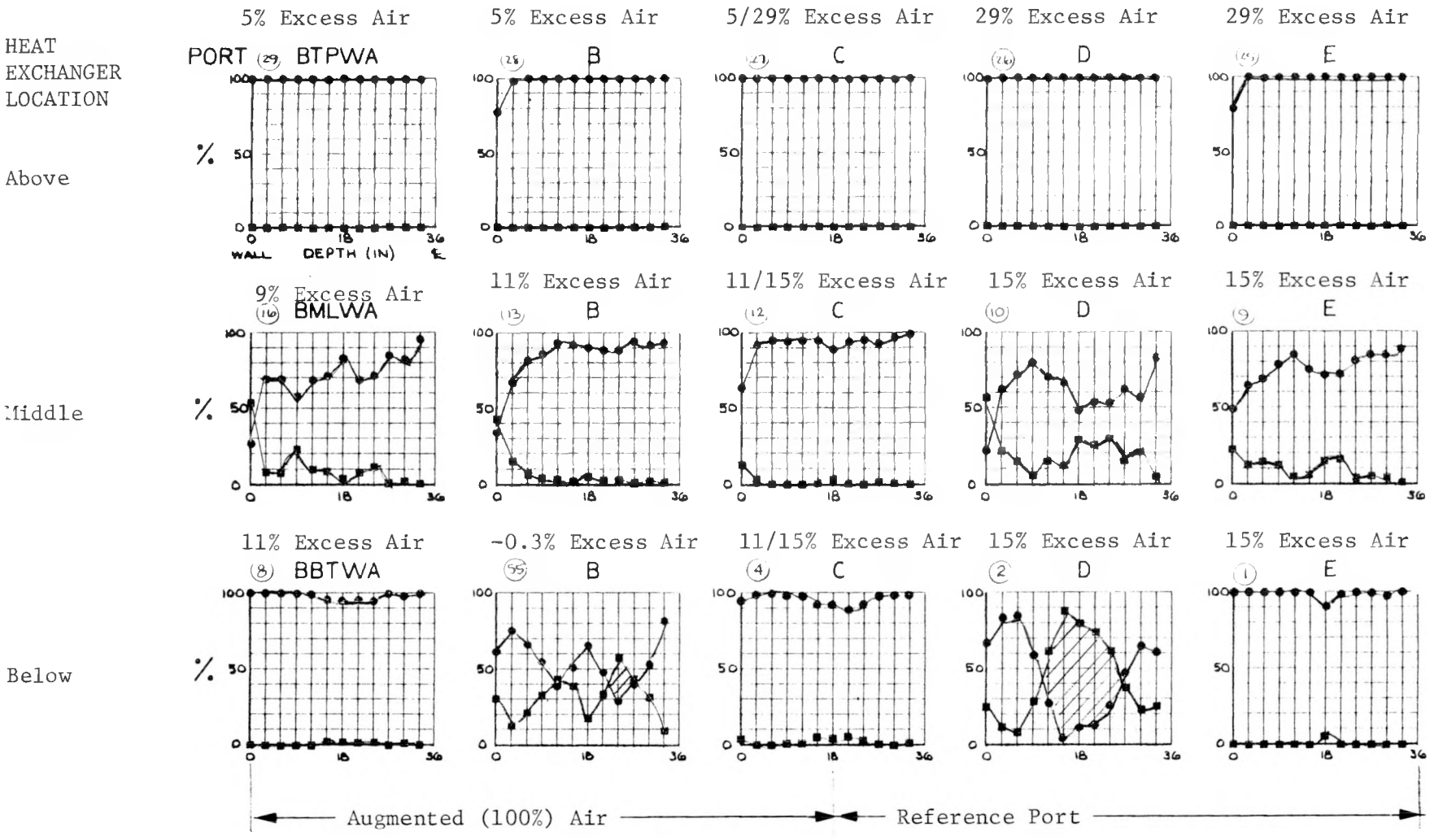


Figure 4-247. Run 006 PO_2 Data (Augmented and Reference Ports)

The reference quadrant (D location) shows the same unacceptable reducing zone just above the coal port as observed during the previous tests. The environment above the augmented air quadrant is almost acceptable except that this traverse was taken when the quadrant was inadvertently being operated in a substoichiometric condition. Under these conditions, the characteristics are very good, and later traverses will show good oxidizing environment under more normal conditions of excess air.

Variation Of Augmented Air. Traverses were made above the augmented air port where the quadrant was operated at nominal conditions except the amount of augmented air was varied from 0 to 150% of nominal. The variation is shown in Fig. 4-248 for the location above the coal port, while the results at the port in the middle of the heat exchanger are shown in Fig. 4-249. The nominal condition of 100% augmented air was shown previously in Fig. 4-247. These results show that without augmented air, the quadrant is the same as the reference quadrant and the characteristic is the same as the reference quadrant. Also, the operating conditions of this quadrant during this test were a somewhat lower air/fuel ratio than desired but, even with as little as 8% excess air, acceptable oxidizing characteristics were achieved.

Variation Of Ash Recycle Air. Traverses above the augmented air and reference coal ports were made for a variation in ash recycle air from zero to 150%. These results are presented in Figures 4-250 and 4-251. The ash recycle air did not have a significant effect on the oxidizing characteristics.

Excess Air Variation - Augmented Air Port. A series of traverses was made at key locations in the augmented air port while the excess air was varied. The method of varying excess air was to change the coal feed rate in the quadrant of interest while compensating for this feed rate in the opposite quadrant. Thus, the overall unit operating condition remained unchanged. It was intended to reduce the excess air from the nominal 20% to near stoichiometric. However, since this quadrant was inadvertently being operated at a low air/fuel ratio, the variation was actually from a small excess air to substoichiometric conditions. These results are shown in Fig. 4-252 and 4-253. Considering the overall condition was reducing, it is not surprising that a reducing condition was observed in the middle of the heat exchanger.

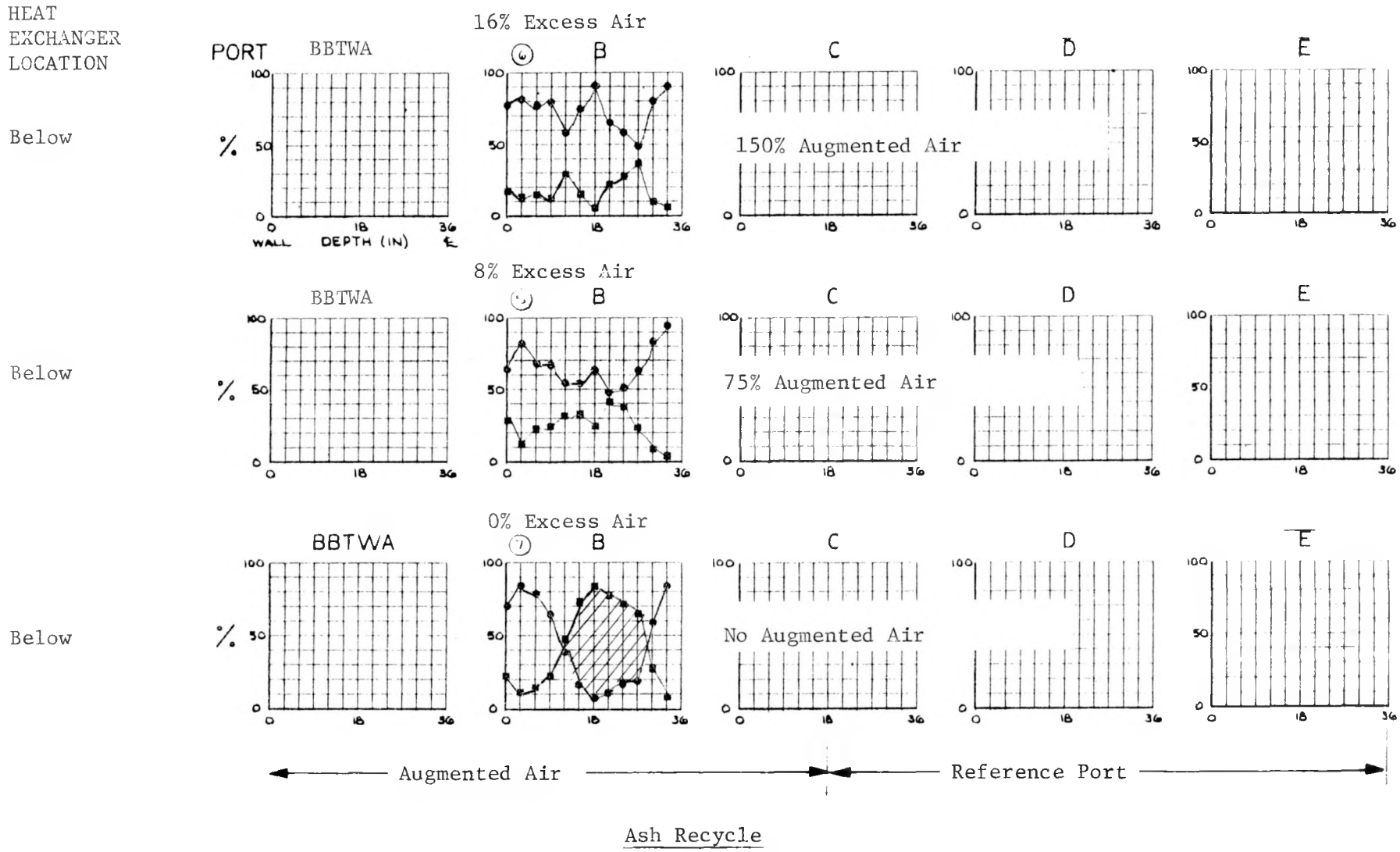
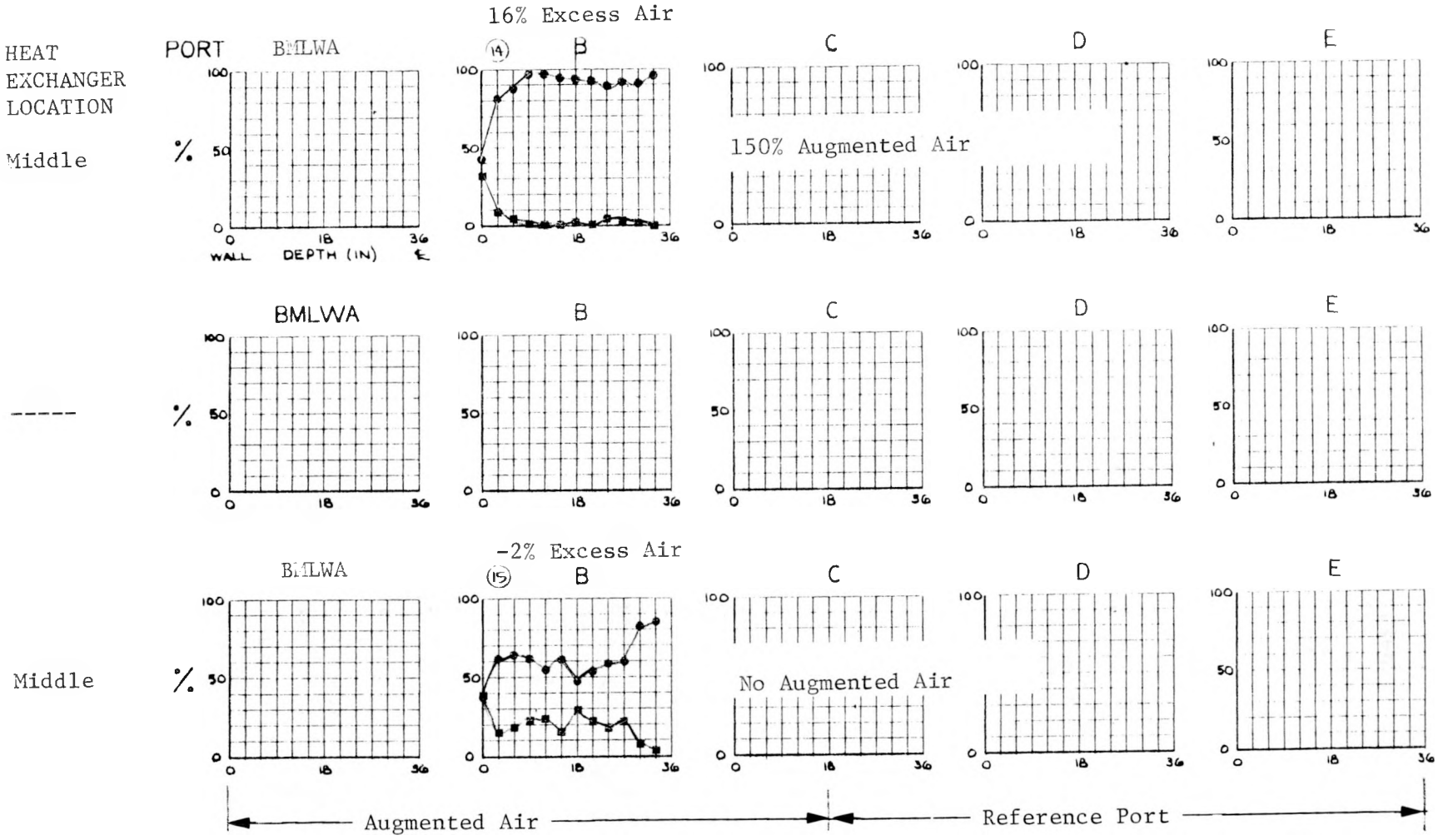
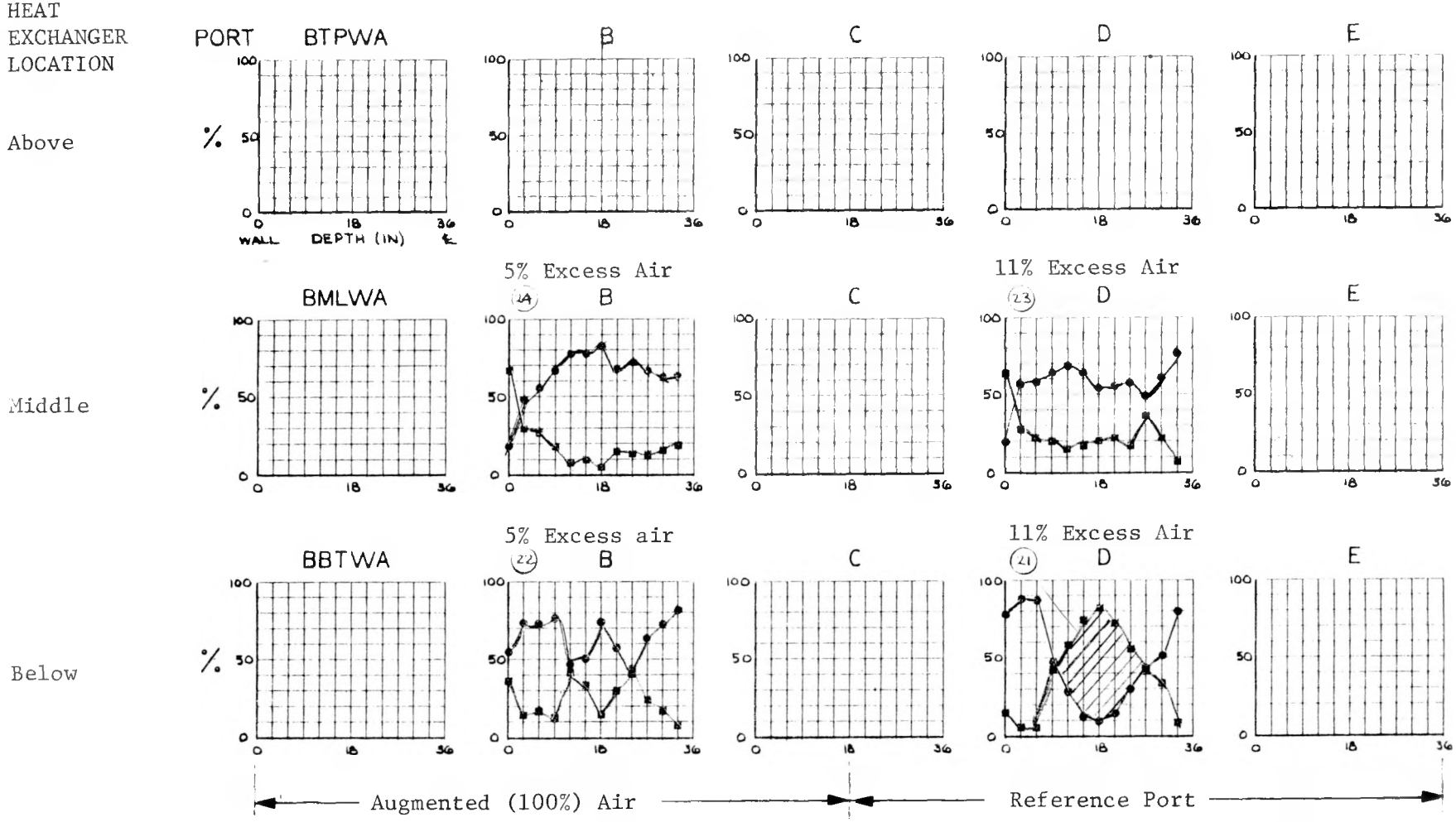


Figure 4-248. Run 006 PO_2 Data (Effect of Various Quantities of Augmented Air)



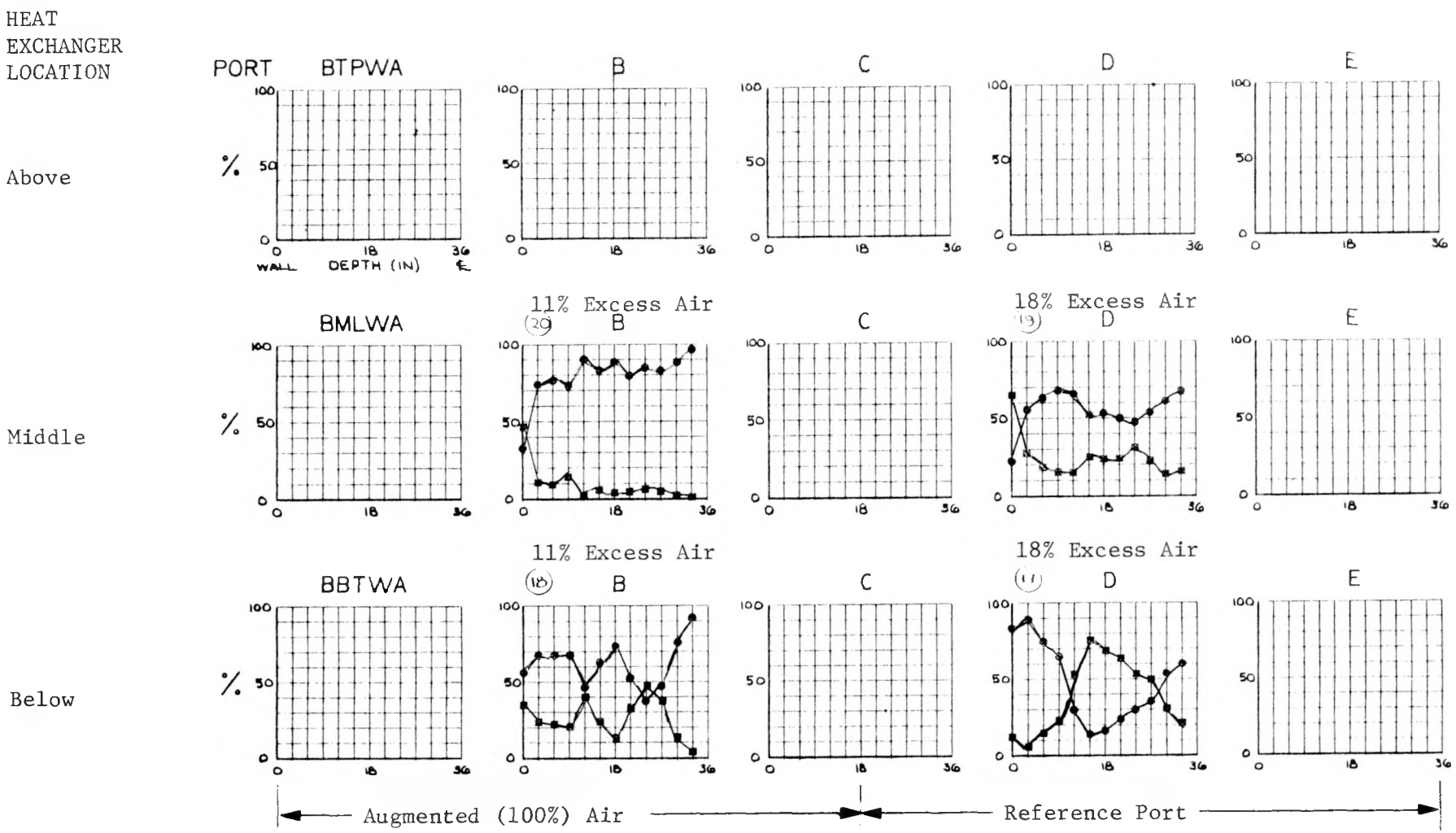
Ash Recycle

Figure 4-249. Run 006 PO_2 Data (Effect of Various Quantities of Augmented Air)



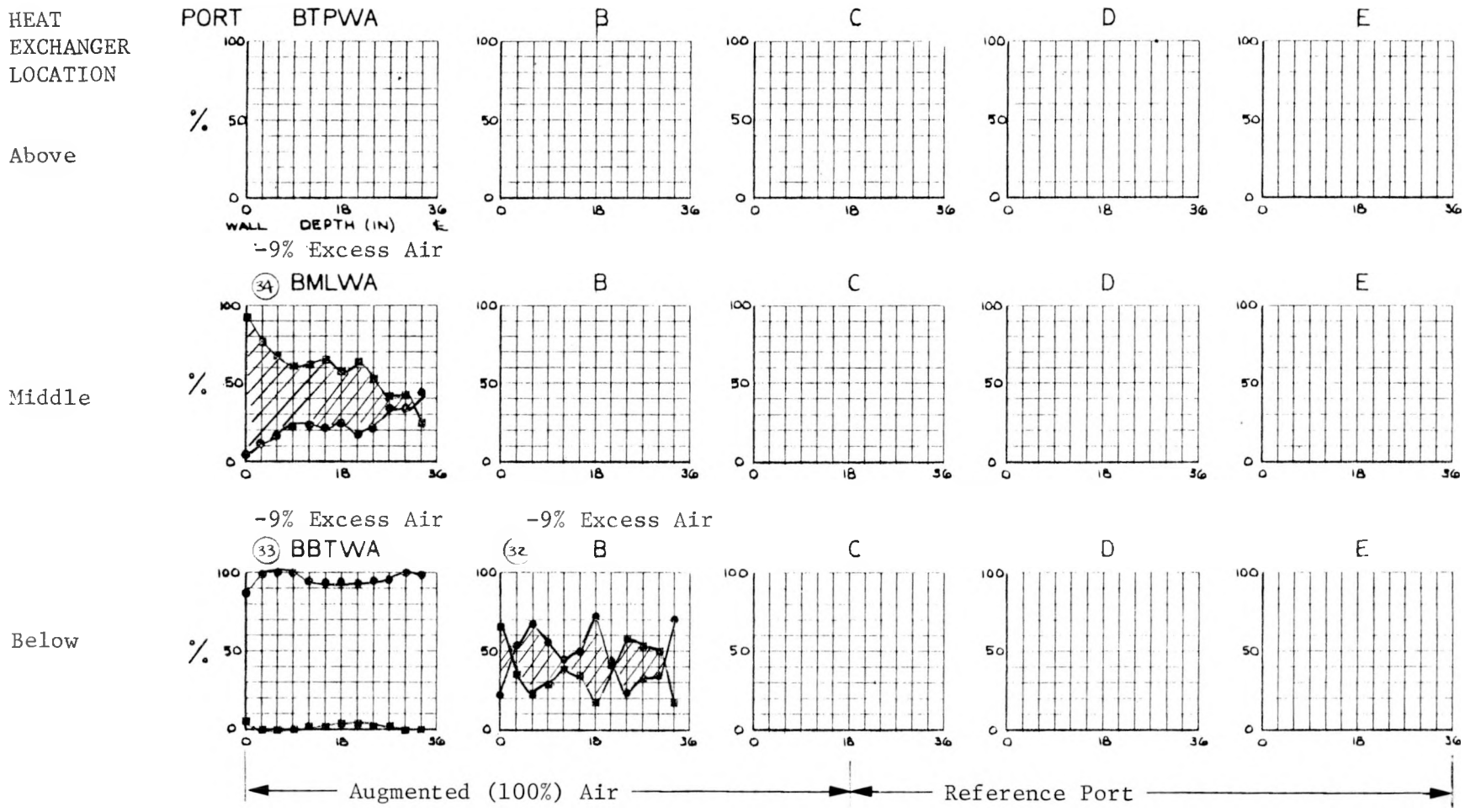
No Ash Recycle Or Air

Figure 4-250. Run 006 PO_2 Data (Effect of No Ash Recycle Air)



Ash Recycle With 150% Conveying Air

Figure 4-251. Run 006 PO_2 Data (Effect of 150% of Nominal Ash Conveying Air)



Ash Recycle

Figure 4-252. Run 006 PO_2 Data (Effect of Low Excess Air)

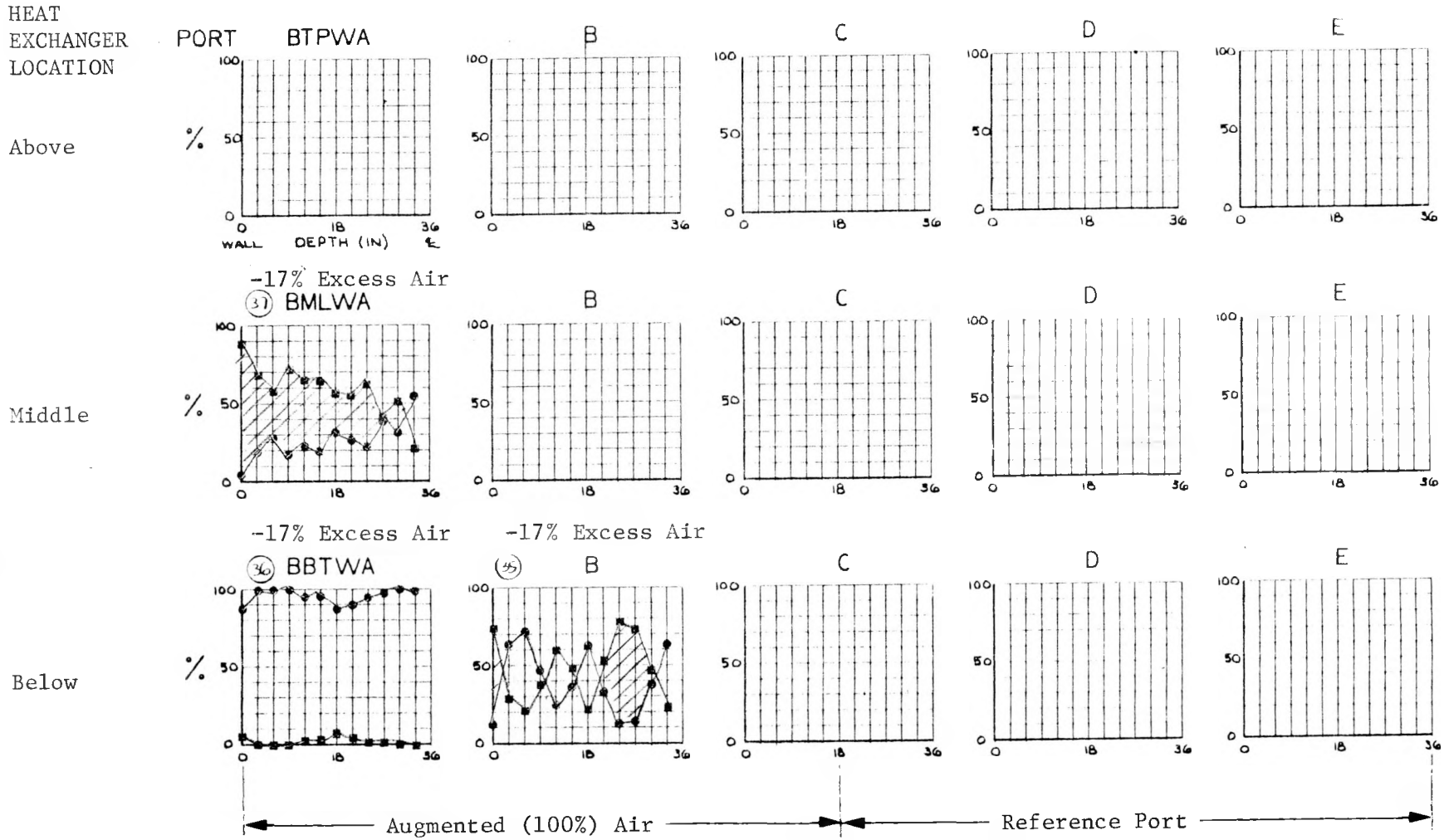


Figure 4-253. Run 006 PO_2 Data (Effect of Low Excess Air)

Probe Filter Effect. To investigate the effect of the probe-sensing element filter on the observed results, one port was selected to be traversed under the same operating condition both with and without the filter. (All probing was conducted with a filter except for this special experiment.) The port was just above the reference coal feed, and the results are shown in Fig. 4-254. There was some effect of the filter, but the difference was not considered significant.

Four Ports Per Quadrant. This port arrangement was the same as run 005, and characterization of this quadrant was repeated at nominal excess air condition plus lower values of excess air. The results for an excess air of 13% are shown in Fig. 4-255, and good oxidizing characteristics can be seen throughout the heat exchanger region. Some reducing zones can be observed near some locations near the wall. This quadrant also was being operated at a slightly lower than planned excess air as the actual excess air was 13% instead of the planned 20%.

Selected traverses were made at an excess air of 4%, which indicates acceptable oxygen partial pressure profiles even at this low value of excess air, as shown in Fig. 4-256. Traverses made at a substoichiometric condition of -5% are shown in Fig. 4-257 which indicates some expected reducing conditions.

PO_2 Verification. Extensive PO_2 probe was conducted during the characterization test series, especially runs 005 and 006. These PO_2 results were used to establish the configuration and operating conditions for the material exposure test series which was essentially the conditions used for the last test of the characterization test series (run 006). The only change was the modification of quadrant No. 2 from a reference port to an augment port configuration. Most of the ports of interest on the material exposure test series now contained a material specimen probe, and there were few ports that could be used for the PO_2 probe. Therefore, the PO_2 probe activity was limited to these few ports to verify that conditions had not changed.

The PO_2 profiles about the reference coal port configuration (quadrant No. 4) are shown in Fig. 4-258 and 4-259 for runs 007 and 008. These are essentially the same as obtained during the previous test series.

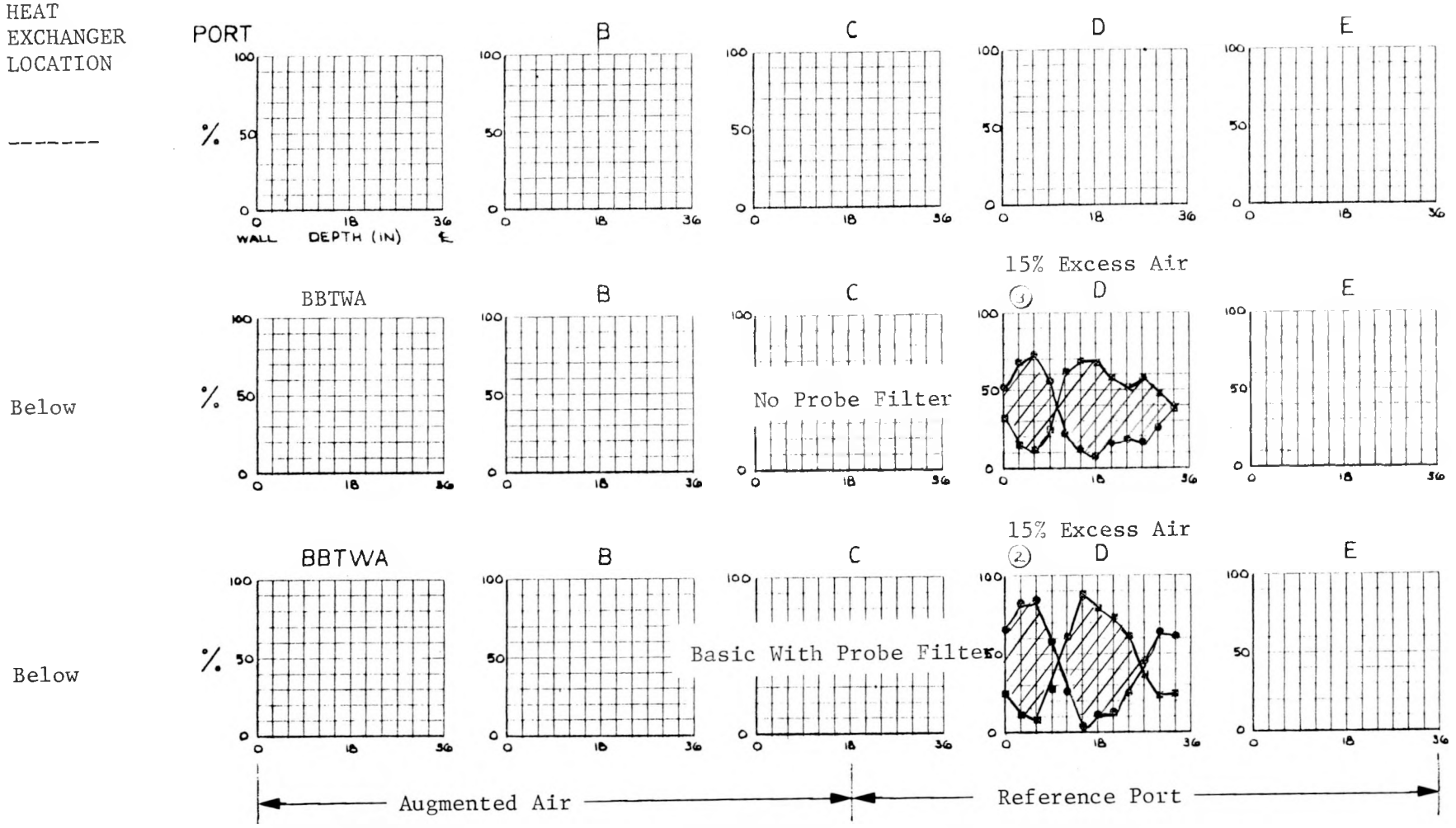


Figure 4-254. Run 006 PO_2 Data (Effect of PO_2 Probe Filter)

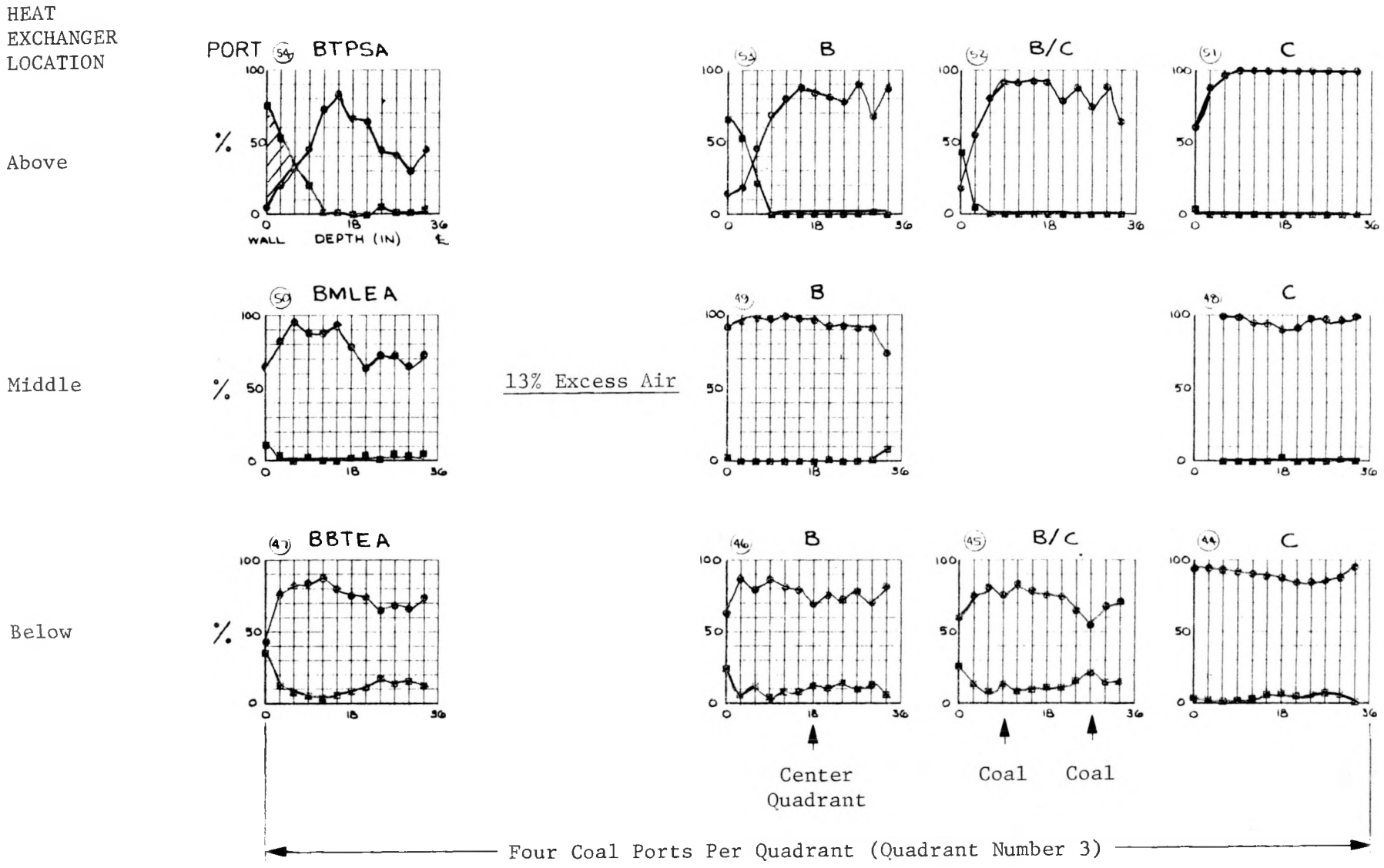


Figure 4-255. Run 006 PO_2 Data (Four Coal Ports Per Quadrant at Nominal Conditions)

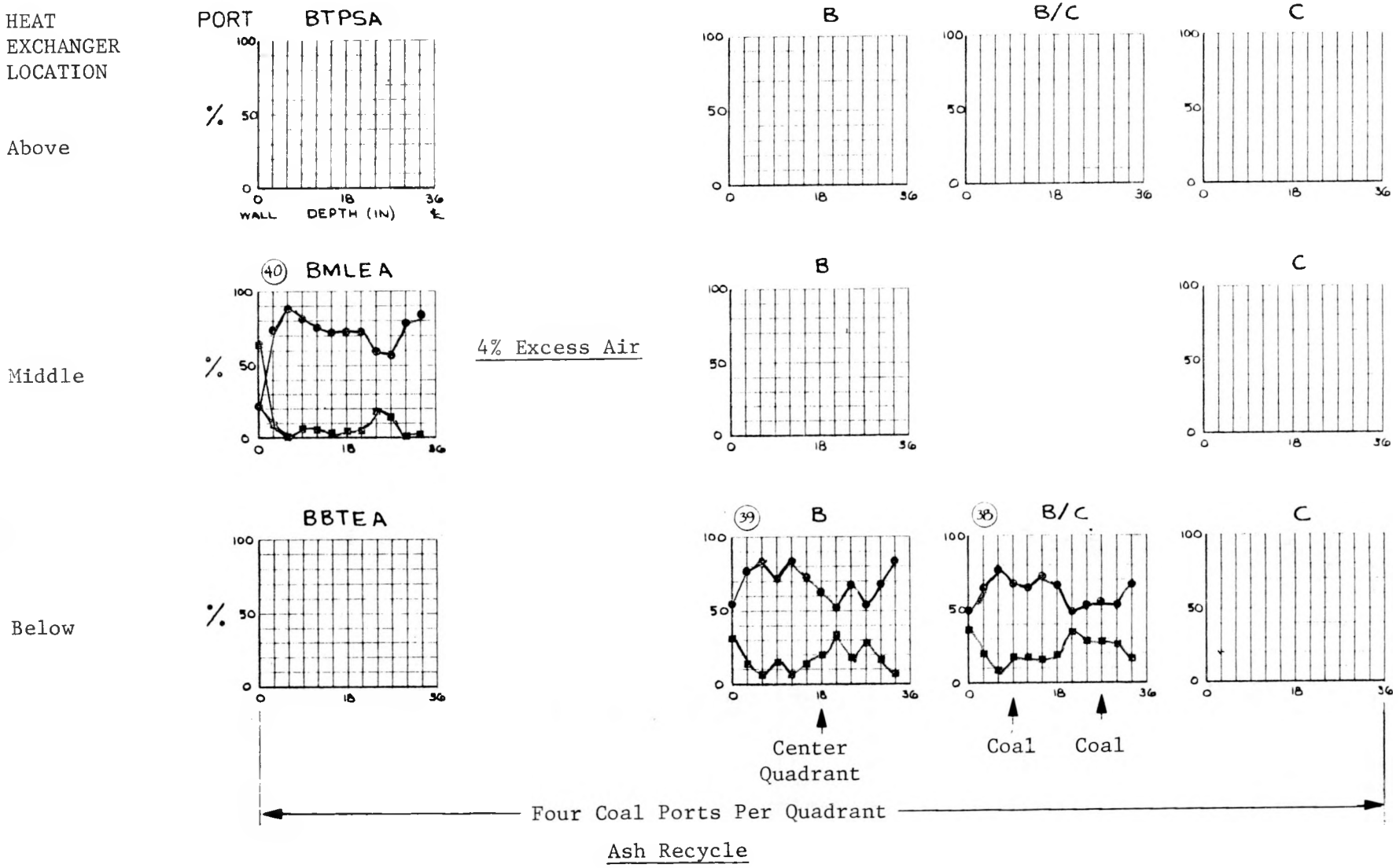


Figure 4-256. Run 006 PO_2 Data (Effect of Low Excess Air (4%) on Four-Port Quadrant)

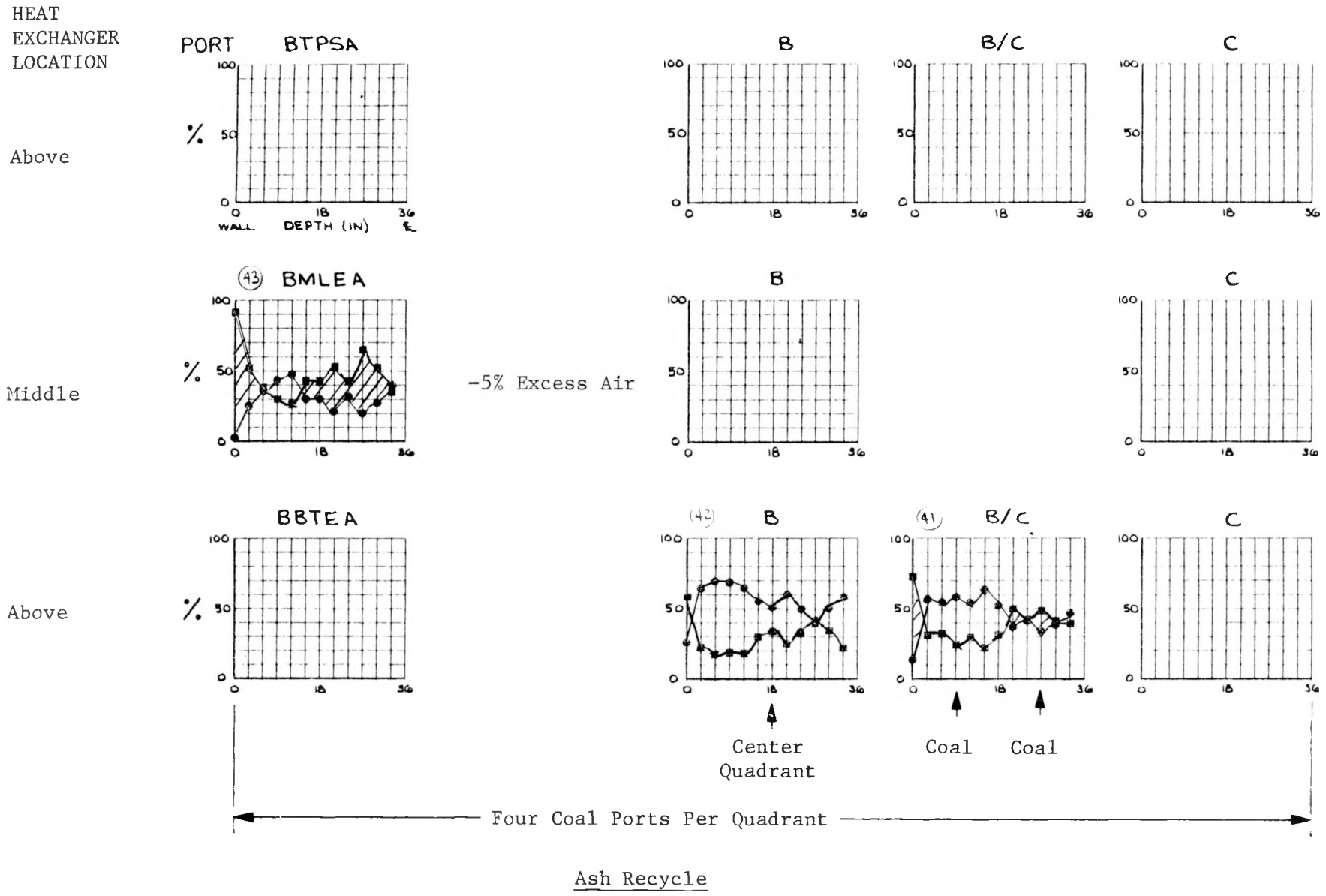


Figure 4-257. Run 006 PO_2 Data (Effect of Low Excess Air (-5%) on Four-Port Quadrant)

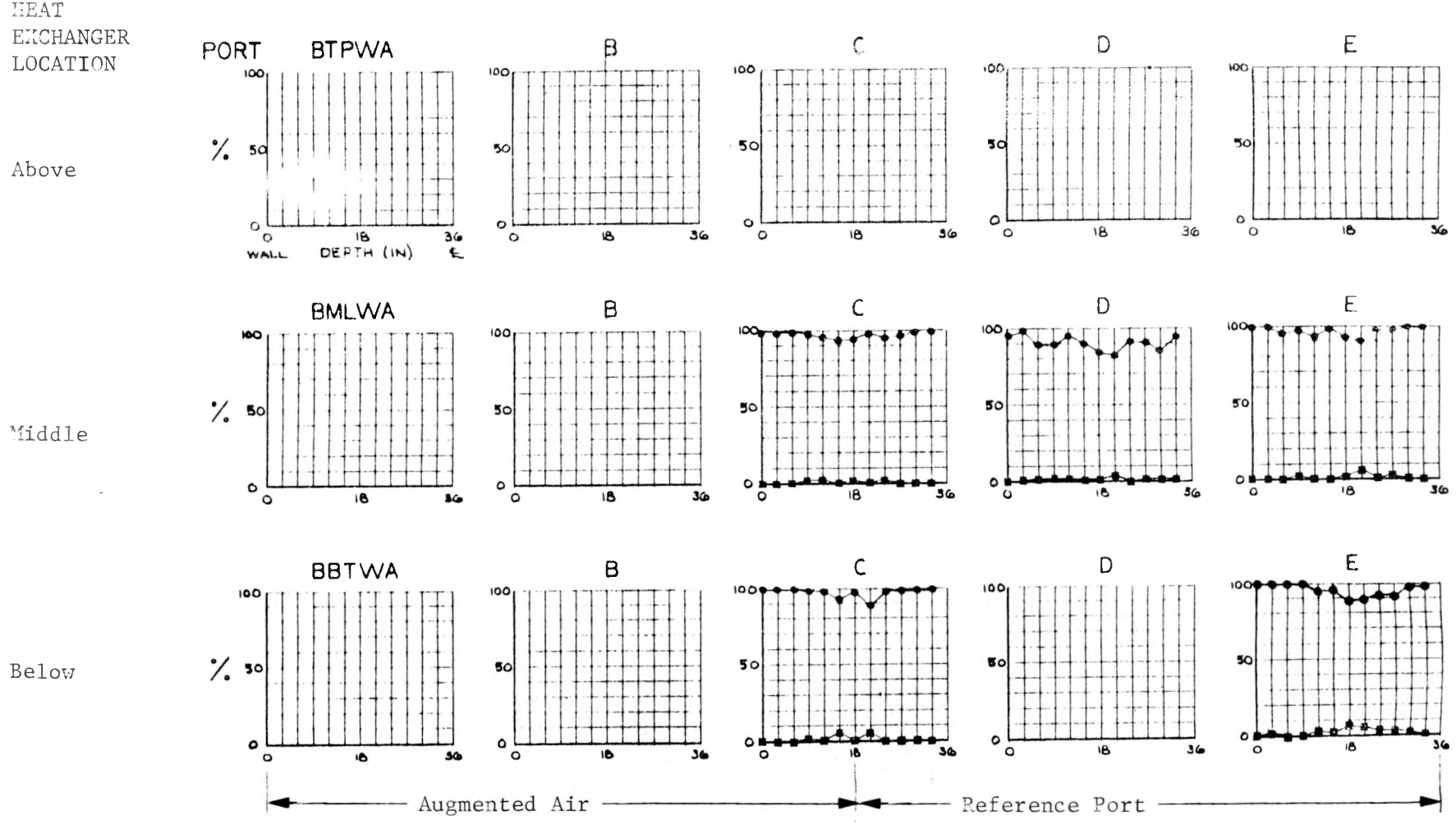


Figure 4-258. Run 007 PO_2 Data (Ash Recycle and 26% Excess Air)

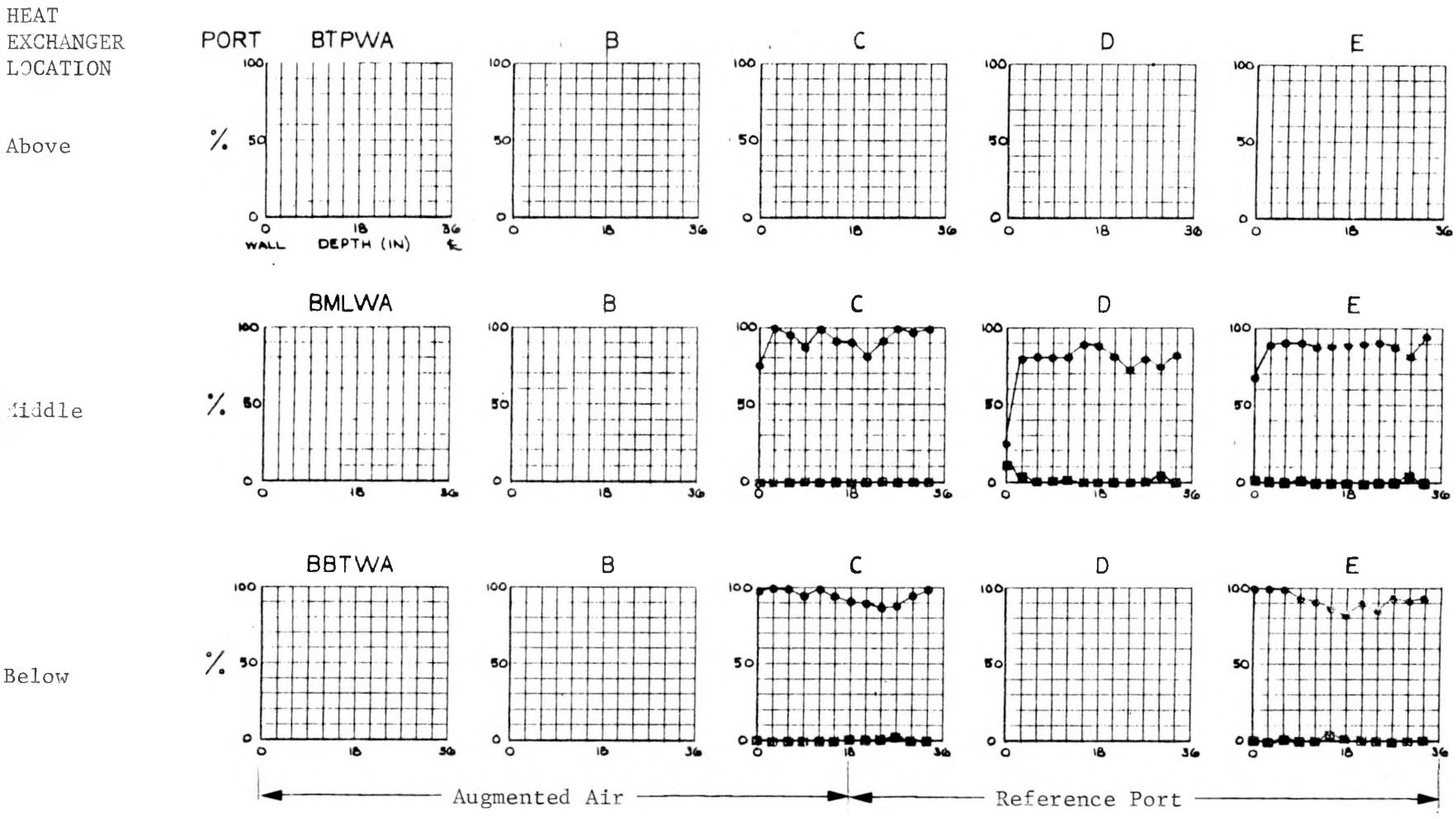


Figure 4-259. Run 008 PO_2 Data (Ash Recycle and 28% Excess Air)

The material specimen probe, located above the coal feed port in quadrant No. 2, was not installed until run 008 so that the addition of augmented air to this quadrant could be PO_2 characterized. This augmented air configuration was very similar to the other quadrant except that the augmented air discharged radially rather than upward. The PO_2 profiles shown in Fig. 4-260 compare favorable with the profile of the other augmented air quadrant which were obtained during the previous test series.

4.10 Hardware Inspection

Throughout the test series, the general practice was to drain the fluidized bed and completely inspect the interior of the combustor/heater. Throughout the series, the combustor/heater and system components were found to be in excellant conditions with a few minor exceptions. The refractory, heat exchangers, and specimen probes were in good condition. The augmented air discharge lines which had been installed for the latter tests had experienced erosive damage, and the ash injection needle discharge deflector had some erosion. These areas requiring repairs are of secondary importance to the experiment and can be easily remedied for the planned 650 additional hours of exposure. Presented is a more detailed discussion, based primarily on the final inspection, of the observations of the various components and systems.

Material Specimen Probes. All material specimen probes were found to be in good condition, and no significant misalignment warpage or attack was noticed on any probes that were accessible for inspection. Varying degrees of scaling, wearing, and appearance were observed.

The material specimen probe located directly over the reference coal port in quadrant No. 4 (BBTWD) showed signs of corrosion on the specimens. Scaling appeared to reach a maximum directly over the coal injection port.

Most of the scale was observed loosely attached to the top side of the probe. The scale was easily broken off, and it can be assumed that a similar scale was present on the lower side of the probe but had fallen off. The probes over the augmented air coal ports (BBTWD and BBTED) appeared to be in better condition, and the scale formation was thinner than compared to the reference port. The

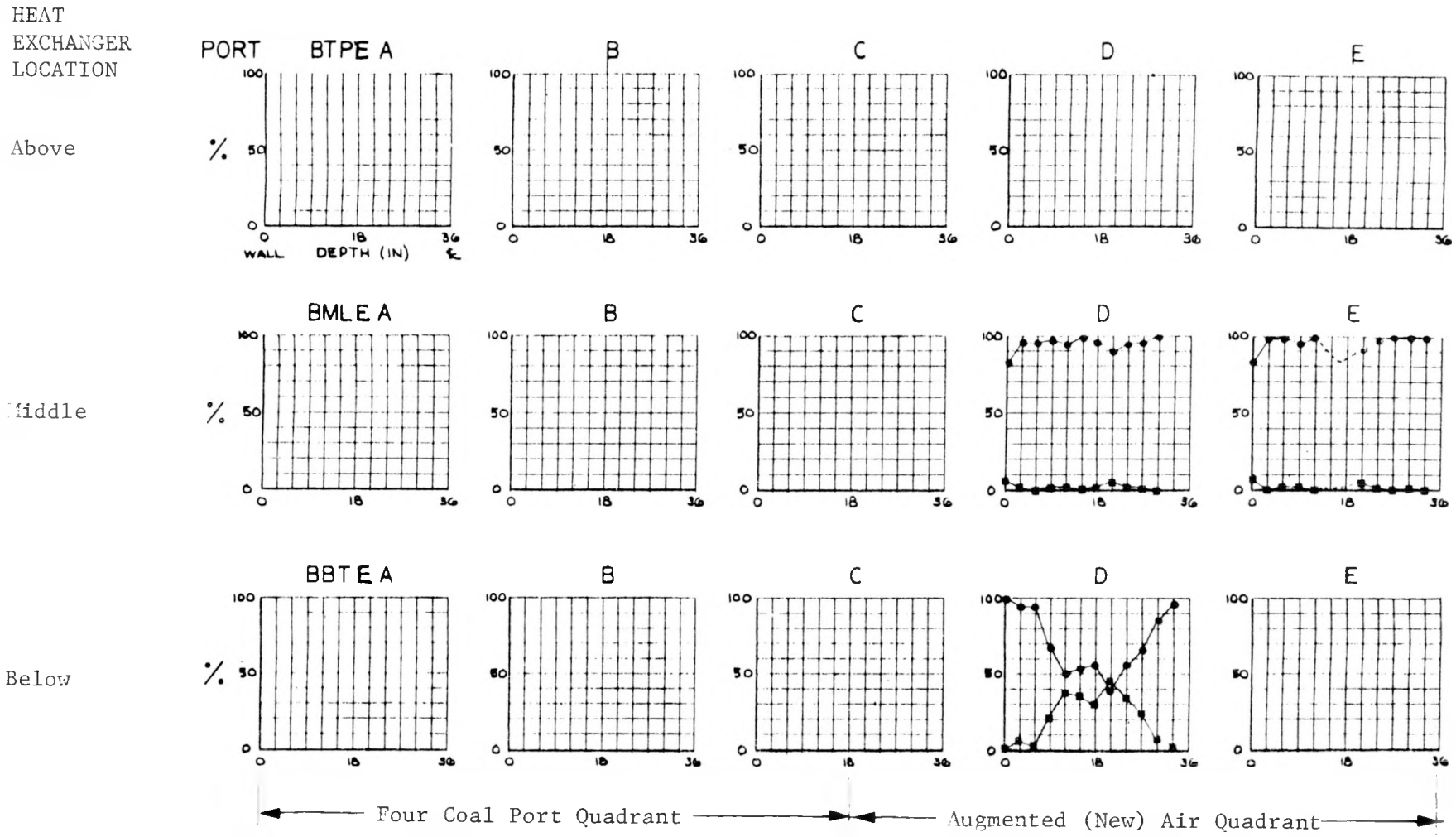


Figure 4-260. Run 007 PO_2 Data (Ash Recycle and 29% Excess Air)

probe over the multiple coal feed ports (BBTED/C) had the best appearance of all of the lower bed probes. The middle of the bed probes was inaccessible for inspection, and the above bed probes appeared to be in good condition. All weld tab probes appeared to be in good condition, and no remarkable material degradation was observed. The tabs appeared to do a good job of trapping stagnant bed material.

All of the other uncooled metallic probes appeared to be in good condition, and nothing remarkable was observed.

One cooled material specimen probe from the bed was removed and disassembled for metallurgical analysis. It was observed that the specimens were tightly bound so that there was no evidence of coolant leakage. These probes had been designed to minimize coolant leakage through close fitup and tolerances, and the evidence indicates that the design integrity as well as assembly procedures were successful. Also, the actual operating conditions did not have any indication of any significant extra air (probe coolant) leakage.

A special inspection of a material specimen probe was conducted after run 005 where the probe was removed in a hot condition to observe the scale deposits. The shut down procedure was modified where the unit was slumped in a hot condition in which the bed temperature was about 1400 F. A team of individuals removed the probe moments later for visual inspection by cognizant metallurgical engineers as well as photographic documentation. This observation of the hot-scale deposits and their cooling may be valuable in interpreting future erosion/corrosion results.

Heat Exchangers. The bed and convection bank heat exchangers were examined visually, and accessible tubes of the bed heat exchanger were measured on the OD in several locations. Though some wear of the lower tubes was apparent in the form of a wavy texture, the measurements indicate that the material loss, if any, was minute. The other regions of the heat exchangers were in good condition.

The bed heat exchanger lower tubes have a dark grey surface with occasional surface deposit flecks. At some points, it appears as though the surface flecks have fallen off, leaving a slight discoloration. The surface has a wavy texture. A dial caliber was used to check thickness at several points, and these measurements were compared against baseline tube thickness data (Table 4-114). A variety of tube hangers was examined visually, and all appeared to be in good condition. The top of the heat appeared to be in good condition. The top of the heat exchanger looked good, and no anomalies were observed. All tubes examined appeared to be a smooth dark grey.

There were no remarkable changes in the convection heat exchanger, and the deposits of the type encountered in the previous runs were observed. Some of these deposits had fallen into the interstices of the tubes.

Refractory. All hard face surfaces were in good condition, with some expected flaking around the bed heat exchanger penetrations. Some injection ports have exposed insulation refractory, i.e., as the limestone and spent bed material injection ports. These ports have unlined holes through the refractory, and significant wear has occurred in the insulating refractory behind the hard face. This had been previously observed in the observation window port where the splashing bed was eroding the insulating refractory. A thin metal liner was then installed to protect the insulating refractory.

Augmented Air Ports. The two augmented air ports both experienced damaging erosion. The discharge of the air (approximately 500 ft/sec) entrains bed material causing erosion in the resultant high-velocity stream. In quadrant No. 1, the augmented air discharged upward, and there was excessive erosion of the augmented air tubing with erosion through the walls of the tubing. Augmented air then discharged through the eroded opening of the tube which was common thin-wall, stainless-steel tubing In the quadrant No. 2 configuration, the discharge is radially outward, which resulted in significant erosion of the top of the coal splash plate as well as erosion of the tube discharge supports.

The ash injection needle was removed and examined, and the turning vanes at the end of the needle had an extensive loss of material. This took the form recession of the upstream surface.

TABLE 4-114. POST RUN 008 COMPARISON OF HEAT EXCHANGER TUBE MEASUREMENTS

MEASUREMENTS BELOW BED BANK

MEAS. LOCATION NUMBER	PLATEN NUMBER*	DISTANCE FROM WEST WALL (in)	OUTSIDE DIAMETER VERTICAL DIRECTION (inches) NEW	BASELINE	DELTA THICK (in)	OUTSIDE DIAMETER HORIZ. DIRECTION (inches) NEW	BASELINE	DELTA THICK (in)
0	13	18	1.998	2.001	-0.003	2	2.003	-0.003
1	7	18	1.998	2.001	-0.003	2	2	0
2	1	19	1.998	2.001	-0.003	1.997	1.998	-0.001
3	13	36	1.998	1.998	0	1.998	2	-0.002
4	7	36	1.999	2	-0.001	1.998	2.002	-0.004
5	1	36	1.999	1.999	0	1.999	2.002	-0.003
6	3	45	2.001	2.002	-0.001	2.001	2.003	-0.002
7	19	54	1.998	1.998	0	2	2.002	-0.002
8	17	54	2	2.001	-0.001	1.999	2.001	-0.002
9	7	54	1.998	2.001	-0.003	1.999	2	-0.001
					AVERAGE -0.0015			AVERAGE -0.002

MEASUREMENTS ABOVE BED BANK

MEAS. LOCATION NUMBER	PLATEN NUMBER*	DISTANCE FROM WEST WALL (in)	OUTSIDE DIAMETER VERTICAL DIRECTION (inches) NEW	BASELINE	DELTA THICK (in)	OUTSIDE DIAMETER HORIZ. DIRECTION (inches) NEW	BASELINE	DELTA THICK (in)
10	12	18	2	2.001	-0.001	2	2	0
11	6	18	2	1.999	0.001	2	1.999	0.001
12	2	18	1.999	1.998	0.001	1.998	1.997	0.001
13	12	36	2	2	0	2	2	0
14	6	36	2	2	0	1.999	1.998	0.001
15	2	36	1.997	1.996	0.001	2	1.999	0.001
16	4	45	2	2	0	2	2	0
17	18	54	1.998	2.001	-0.003	2	2	0
18	16	54	2.001	2.001	0	2	2	0
19	6	54	2	2	0	1.999	1.998	0.001
					AVERAGE -0.0001			AVERAGE 0.0005

*Platen number is determined by counting from the south wall

Conclusion: No material loss has occurred on the top tubes. One to two mils has been lost by the lower bed bank tubes.

All of these areas of erosion will require corrective action prior to the plann 650 additional hours of exposure.

Cyclone. After the first run, inspection of the cyclone showed that it had filled with fly ash because a hard deposit had formed in the ash overflow duct before that system was started. This was undoubtably a result of the unusual conditions of this first test which was a combined checkout, curing, and startup. Apparently, a local fire occurred with the carbon in the fly ash that damaged the bottom of two of the cyclone units. These units were removed, the damaged areas machined off, and the units were reinstalled with plugs.

During early runs, plugging of the bottom of the cyclone units was noted which was attributed to the startup condition and occasional sticky ash deposits. After installation of the acoustic soot blower, there were no ash buildup or plugging of the unit.

Air Preheater. During run 004 and 005, the flue gas pressure drop across the air preheater was abnormally high. During run 005, the run was interrupted while the air heater was opened and cleaned. After installation of another acoustic soot blower, the problem of ash deposit did not reoccur.

Windbox. The windbox was opened and inspected after each run, and a small amount of bed material was found. About a pail of material had accumulated during the course of the first four runs, which included several startups of the bed.

Baghouse. The main baghouse was inspected after some of the runs and was generally found to be in good condition. Dust would drain from the hopper through the rotary valve without difficulty although, occasionally, the flow would be encouraged by rapping on the outside of the hopper. At the start of run 004, dust would not drain; the system was shut down for inspection. A hard deposit of material was found at the bottom of the hopper. It was presumed that this was a result of some rain water getting into the system during the pretest period.

Coal Eductor. After run 004, the coal feed system was completely inspected and some debris was found in each of the feed lines (see Coal Feed System section).

Some of the eductors were removed and disassembled for inspection, and were found to be in excellent condition, with no indication of wear.

4.11. Conclusions

There were a number of conclusions from the 6' x 6' AFB test series, and this section presents conclusions related to the test series, performance aspects, and operational areas.

Test Series.

1. Characterization Test Series. This series has accomplished all of the major objectives including (1) characterizing the bed and system operation, and (2) developing configurations that meet the criteria for maintaining an oxidizing environment for the heat exchanger materials. This series was completed within the planned number of tests and hours of operation.

2. Material Specimen Exposure Test Series. This series has accomplished the major objective of exposing the various material specimen probes to steady-state nominal operation for over 350 hours. The combustor/heater unit and the supporting systems all functioned well and consistent with the previous operation. About 1 to 2 days were required to stabilize the bed chemistry, limestone feed rate, sulfur dioxide level, and ash recycle. After this initial period, the operation was very stable, requiring only minor adjustments. Closer attention by the operators to the coal feed rates resulted in uniform and stable air/fuel ratios to all quadrants.

Performance.

1. Combustion Performance. The combustion performance with an ash recycle rate of two times the coal feed rate is approximately 98%, while the combustion performance without ash recycle is approximately 90%.

2. Heat Exchanger Performance. The overall thermal and pressure drop p formance of the bed and convection heat exchanger agree reasonably wel with the design values.

3. Sulfur Dioxide Emissions. A sulfur dioxide emissions with 90% sulfur capture can easily be obtained using Grove (ANL-9501) limestone and a Ca/S molar ratio of approximately 4:1 and ash recycle. This limestone utilization is somewhat higher than desired, but the rate may be a result of the relatively high bed temperature of 1650 F. The utilization seems to vary with the particular batch of limestone, even though the calcium carbonate contents appears to be the same. For 3% sulfur coal, the limestone feed rate is approximately 38% of the coal feed rate.

4. Oxides Of Nitrogen Emissions. Oxides of nitrogen emissions appear to be well within standards with a level that is about 20% of the Federal New Source Standard.

5. Operating Conditions For Oxidizing Environment. Distributor area configurations and operating conditions were established that met the criteria of having a predominantly oxidizing condition throughout the heat exchanger region. Two acceptable configurations were:

   1. One coal port per quadrant with 13% augmented air
   2. Four coal ports per quadrant.

   An operating condition of 25% excess air will have sufficient margin to account for variations due to coal feed system and operator variations.

   The addition of a second augmented air port produced the expected oxygen partial pressure profile. There was no evidence of change in the oxidizing environment from the previously established characteristics.

System Operation.

1. Oxygen Partial Pressure Probe Operation. The oxygen partial pressure probe has proven to be a reliable and versatile tool for characterizing the bed and measuring the effects of physical and operational parameters.

2. Material Specimen Probe. The design integrity of the probe was verified where the specimen temperatures could be controlled for the range of interest. During early checkouts, a probe coolant leakage of approximately 11% was measured, which will not have a significant effect on the unit operation. During the subsequent material specimen exposure series, all probes functioned well with no evidence of significant coolant leakage from the cooled probes.

3. Startup Procedure. The startup procedure of prewarming the unit without combustion and starting with a small load of limestone resulted in a significant reduction in the hardness and quantity of deposits on the convection heat exchanger.

4. Ash Recycle. An ash recycle rate of two times the coal feed rate was found to be practical for the current system with all fly ash being collected in the baghouse. The objectives of high carbon burnup and limestone utilization of the fly ash appears to have been achieved despite the relatively poor collection efficiency of the cyclone. Analysis of the baghouse fly ash indicates that the unburned carbon is less than 1% of the total available in the fuel and unreacted CaO is about 4% of the total in the limestone.

   The ash reinjection system functioned satisfactorily where the quantity of recycle could be metered and measured. However, the rotary valve shoe clearance has to be relatively large to allow for thermal growth differences between the rotor and housing. This results in a high leakage rate, which can cause plugging of the ash vent system, but this leakage can be negated by equalizing the pressure between the injection line and the run ash bin.

5. Cyclone Performance. The cyclone pressure drop corresponds to an effective flow area of 125 $in.^2$ for all 36 units, which agrees with th vendor specification. The collection efficiency of this unit is very poor in that the 90% passing was 40 microns and larger instead of the expected 7 microns. Nevertheless, the ash recycle system appeared to achieve the objectives of high carbon burnup and limestone utilization.

6. Coal Feed System. The final configuration of coal feed system functioned satisfactorily where rotary airlocks are used to isolate the screwfeeders from the eductor inlets. The coal feed rates were reasonably steady and repeatable, although there was a noticeable effect of run hopper coal head. The operating mode was to adjust the conveying air flowrate so as to maintain a slight negative pressure at the coal inlet. Also, the screwfeeder discharge must be vented to atmosphere as the screwfeeders are very sensitive to pressure unbalances across the screw.

   The two types of coal feed systems operated reliably with a coal moisture level of up to 10%, and these systems were the single port and four ports per quadrant. The four ports per quadrant used a splitter system consisting of straight lines and plugged crosses which had a distribution of $\pm$9%. (No attempt was made to tune this system for better distribution.)

7. Air Preheater. The air preheater performance agrees with the design values with an effectiveness of 76% and a pressure drop of about 0.5 inch W.G. on each side.

8. Solids Inventory. There is reasonable agreement of the amount of permaneni solids added to and removed from the system. The approximate amount of fly ash and bed material generated are each about 20% of the coal feed rate under nominal operating conditions.

9. Bed Temperatures. The bed temperatures tended to be very uniform both in the horizontal and vertical plane.

10. Acoustic Soot Blower. This device appears to be very effective in eliminating the buildup of deposits in the cyclone and air preheater which have occasionally occurred in the past.

11. Augmented Air Systems. The augmented air discharge and ash needle discharge configurations have shown excessive erosion. Corrective action is required for the planned 650 additional hours of exposure.

12. Hardware Condition. The combustor/heater and system components are in excellent condition with a few minor exceptions.

REFERENCES

4-1. Boiarski, A. A., V. Nagarajan, I. G. Wright and H. Carlton, "Oxygen Partial Pressure Measurements Inside a 0.6 m Fluidized Bed Combustor," Submitted to the Journal Institute of Energy (1981).

4-2. Cooke, J. J., A. J. B. Cutler and E. Raask, Journal Institute Fuel, 45 (373), 153, (1972).

4-3. Holt, C. F., A. A. Boiarski and H. E. Carlton, "The Gas Turbine Heat Exchanger in the Fluidized Bed Combustor," Paper Number 82-GT-225, Presented at the International Gas Turbine Conference, London, England, April 1982.

4-4. Nagarajan, V. and I. G. Wright, Unpublished Work (1982).

4-5. Nagarajan, V., I. G. Wright and R. D. Smith, "Mechanics of Sulfidation Attack in a Low Oxygen Partial Pressure/High Sulfur Partial Pressure Environment," Paper Number 160, CORROSION/82, Houston, Texas, 22-26 March 1982.

4-6. Ed Dahsham, M. E., J. Stringer and D. P. Whittle, Oxidation of Metals, Volume 8, p. 179, p. 211 (1974).

4-7. Nagarjan, V., M. A. Rocazella, I. G. Wright and R. D. Smith, "The Morphology of Sulfidation Corrosion in the Oscillating Oxygen/Sulfur Partial Pressure Environments Observed in a Fluidized Bed Coal Combustors," Presented at the Corrosion Coal Conversion Systems Conference, 5-7 May 1982, London, England.

4-8. Rocazella, M. A., I. G. Wright and V. Nagarjan, Unpublished Work (1982).

4-9. Wright, I. G. and A. J. Minchener, "Materials Selection for Metallic Heat Exchangers in Advanced Coal-Fired Heaters," Paper Number 82-GT-226, Presented at the International Gas Turbine Conference, London, England, April 1982.

4-10. Stringer, J., A. J. Minchener, D. M. Lloyd and H. R. Hoy, "In-Bed Corrosion of Alloys in Atmospheric Fluidized Bed Combustors," Paper Presented at the 6th International Conference on Fluidized Bed Combustion, Atlanta, Georgia, 9-11 April 1980.

4-11. Wright, I. G., "Erosion/Corrosion of Components in Coal Conversion Environments," in Proceedings of Conference on Corrosion/Erosion of Coal Conversion System Materials (Ed. A. V. Levy) NACE, P. 103 (1979).

-12. Minchener, A. J. et al., Materials Problems in Fluidized-Bed Combustion Systems, Report Number EPRI CS-1853 (1981).

4-13. DeCoursin, D. G. (private communication), Fluidyne Engineering Corporation.

4-14. Daniel, P. L. and J. Stringer, "Uncooled Alloys in the Bed of an AFBC Boiler," Paper Number 68, Corrosion/81, Toronto, Canada (1981).

4-15. Wright, I. G., Oxidation of Iron., Nickel-, and Cobalt-Base Alloys, MCIC Report Number 71-07 (1972).

4-16. Stringer, J, and D. P. Whittle, "High-Temperature Corrosion of Metals and Alloys in Fluidized-Bed Combustor Environments," VGB Conference on Corrosion and Deposition in Power Plants, Essen (1977).

4-17. Krause, H. H., and V. Nagarajan, Corrosion of High-Chromium Alloys in AFBC Boilers," Final Report to TVA on Contract Number IV 361914 A, 12 March 1982.

4-18. Hall, A. M., et al., Evaluation of Heat Exchanger Materials for Use in Coal-Fired Fluidized-Bed Combustion Environment, Final Report Number FE-2325-19, DOE Contract No. (49-18)-2325, December 1978.

4-19. Stringer, J., Private Communication.

4-20. Perry, Robert H., and Cecil H. Chilton, Chemical Engineers' Handbook, 5th Edition, Equation 10-38, McGraw-Hill, 1973.

4-21. McCarthy, J. R., with W. R. Watner and S. Merrbaum, "Extension of Regenerative Cooling Chamber Pressure Limits," Presented at the 3rd AIAA Propulsion Joint Specialists Conference, National War College, Washington, D.C., 17-21 July 1967.

4-22. McCarthy, J. R., with J. D. Seader and D. M. Trebes, "Heat Transfer of Supercritical Nitrogen Tetroxide at High Heat Fluxes and in Axially Curved Flow Passages," ASME Paper 67-HT-59, Heat Transfer Division, presented at the ASME-AICh Heat Transfer Conference, Seattle, Washington, 6-9 August 1967.

4-23. Modrak, T. M., T. A. Morris and W. C. Lapple, "EPRI/B&W Fluidized-Bed Combustion Development Facility, Initial Test Results," Paper Presented at 86th National AIChE Meeting, 1-5 April 1979.

4-24. Anderson, B. R., and L. R. Glicksman, "Heat Transfer to Horizontal Tubes in Shallow Fluidized Beds," ASME Paper 76-HT-67, 1976.

4-25. Golan, L. P., G. V. LaLonde and S. C. Weiner, "High-Temperat Heat-Transfer Studies in a Tube Filled Bed," Proceedings of the Sixth International Conference on Fluidized-Bed Combustion, Volume III, p. 1173.

4-26. Kiukkola, K. and C. Wagner, J. Electrochem Soc., 104, 373 (1957).

4-27. Cooke, M. J., A. M. Cutler, and E. Raask, J. Inst. Fuel 45, 153 (1972).

4-28. Saari, D. P., in Proceedings from 7th International Conference on Fluidized-Bed Combustion, October 1982.

4-29. Lane, G. J., et al., EPRI Report Number CS-1935, July 1981.

4-30. Weissbart, J., and R. Ruka, Rev. Scien. Inst. 32, 1961, pp 593.

4-31. Eckehardt, H. et al., "Lamda-Sensor with Y_2O_3 - Stabilized ZrO_2 - Ceramic for Application in Automotive Emission Control Systems," SAE Technical Paper 770401.

4-32. Fleming, W. J., "Physical Principles Governing Nonideal Behavior of Zirconia Oxygen Sensor," JECS, 124, 1977, pp. 21.

4-33. Kennedy, Timothy C., "A Study of Forces on Immersed Tubes in Fluidized Beds," Dept. of Mechanical Engineering, Oregon State University, Corvallis, Oregon, EPRI Project No. RP718-2, September, 1980.

4-34. Roark, R. J., and W. C. Young, Formulas for Stress and Strain, Fifth Edition, McGraw Hill Book Company, Copyright 1975.

4-35. Hosny Nasr M., "Forces on Tubes Immersed in a Fluidized Bed," Ph.D. Thesis, University of British Columbia, August 1982.

4-36. Zhang Zu-Yi, "The Progress of Fluidized-Bed Boilers in People's Republic of China," Proceedings from 6th International Conference on Fluidized-Bed Combustion, Vol. 1, p. 36, Atlanta, 1980, US-DOE CONF-800428.

4-37. Yuan Ying, "A Brief Review of Progress of Power-Generating FBC Boilers in China," Proceedings from DOW/WVU Conference on Fluidized-Bed Combustion System Design and Operation, Science Applications, Inc., C.H. Putnam, ed., October 1980, p. 591.

4-38. Tian Ziping, "The 130 T/H Fluidized-Bed Boiler at Di Dao Power Plant," ibid p. 580.

4-39. Boiarski, A. A., Personal Communication on his work on the DOE Phase II Rocketdyne subcontract, 1982 (Presented in Section 4.2.3.).

4-40. Apblett, W. R., Foster-Wheeler Corporation, private communication.

4-41. Godfrey, T. G., and J. M. DeVan, "Corrosion of High-Temperature Materials in an AFBC Environment, Part 2 (4500h Tests)," ORNL/TM-7734/P2, Augu 1981.

4-42. Hall, A. M., et al., Fireside Corrosion Task II: Evaluation of Heat Exchanger Materials for Use in Coal-Fired Fluidized-Bed Combustion Environment," Report on DOE Contract No. E (49-18)-2325, 1977.

4-43. Clark, J. W., and C. J. Spengler, "Fireside Corrosion Task II: Evaluation of Heat Exchanger Materials for Use in a Coal-Fired FBC Environment," Proceedings Fifth Annual Conference on Materials for Coal Conversion and Utilization, Gaithersburg, MD, October 1980.

4-44. Reduction of Atmospheric Pollution, Final Report of NCB to EPA, Ref. No. DHB 060971, September 1971.

4-45. Roberts, A. G., R. V. Wardell, and A. J. Minchener, In-Bed Corrosion Tests of Superheater Alloys in a 10-Square-Foot AFBC, EPRI Report No. CS-2118 (1981).

4-46. Beacham, B. et al., Materials Problems in Fluidized-Bed Combustion Systems, Report No. CS-1449, to EPRI (1980).

4-47. Rocazella, M. A. et al., "In-Situ Oxygen Probe Data From a Fluidized-Bed Coal Combustor," Materials and Components, 40, 3 (1982).

4-48. Rocazella, M. A. et al., "Recent Developments on the Characterization of the Corrosive Environment in the Advanced Fluidized-Bed Heat Exchanger for the CCGT Heater," submitted to ASME for 1983 Gas Turbine Conference.

4-49. Mesko, J. E., Metal Progress, 112(2) 30 (1977).

4-50. Purchased from Robert Bosch Bmbh: Volvo Part No. 464-901-8 Lambdasond Exhaust Gas Oxygen Sensor.

4-51. Rocazella, M. A., "The Use and Limitations of Stabilized Zirconia Oxygen Sensors in Fluidized-Bed Coal Combustors," in the Proceedings Electrochemical Society Symposium on Corrosion in Fossil Fuel Systems, JECS Fall Meeting, October 1982.

4-52. Rogers, W. A., A. J. Poge and R. D. LaNauze, "The Corrosion Performance of Heat Exchanger Tube Alloys in Fluidized Bed Combustion Systems," 6th European Corrosion Congress, London (1977).

4-53. Minchener, A. J. and D. Lloyd, Mechanisms of High-Temperature Corrosion in Coal-Fired Atmospheric Fluidized-Bed Combustors, in Proceedings Conference on Corrosion-Erosion-Wear of Materials in Emerging Fossil Energy Systems, Berkeley, CA, January 27-29 1982 (NACE, in press).

4-54. Gulbransen, E. A.,and S. A. Jansson, "General Concepts of Oxidation a Sulfication Reactions, a Thermochemical Approach," in High-Temperature Metallic Corrosion of Sulfur and Its Compounds, Z. A. Foroulis, ed., The Electrochem. Soc. (1970).

4-55. Wright, I. G., "Erosion/Corrosion of Components in Coal Conversion Environments," Proceedings Conference on Corrosion/Erosion of Coal Conversion System Materials, A. V. Levy, ed., NACE, 1979.

4-56. Minchener, A. J., E. A. Rogers and R. D. LaNauze, Materials Problems in Fluidized-Bed Combustion Systems, Effect of Process Variables on In-Bed Corrosion, EPRI Report CS-1475, August 1980.

4-57. Private Communication with A. J. Minchener, Coal Research Establishment, England, and Stringer, J., and A. J. Minchener, "The Effect of Overall In-Bed Oxygen Concentration on Corrosion in Fluidized-Bed Combustors," Proceedings 7th International Conference on Fluidized-Bed Combustion, Philadelphia, 1982.